GEOLOGICAL SURVEY OF CANADA
COMMISSION GÉOLOGIQUE DU CANADA

CURRENT RESEARCH 1994-E

RECHERCHES EN COURS 1994-E

1994

Natural Resources Canada
Ressources naturelles Canada

Canada

NOTICE TO LIBRARIANS AND INDEXERS

The Geological Survey's Current Research series contains many reports comparable in scope and subject matter to those appearing in scientific journals and other serials. Most contributions to Current Research include an abstract and bibliographic citation. It is hoped that these will assist you in cataloguing and indexing these reports and that this will result in a still wider dissemination of the results of the Geological Survey's research activities.

AVIS AUX BIBLIOTHÉCAIRES ET PRÉPARATEURS D'INDEX

La série Recherches en cours de la Commission géologique contient plusieurs rapports dont la portée et la nature sont comparables à ceux qui paraissent dans les revues scientifiques et autres périodiques. La plupart des articles publiés dans Recherches en cours sont accompagnés d'un résumé et d'une bibliographie, ce qui vous permettra, on l'espère, de cataloguer et d'indexer ces rapports, d'où une meilleure diffusion des résultats de recherche de la Commission géologique.

GEOLOGICAL SURVEY OF CANADA
COMMISSION GÉOLOGIQUE DU CANADA

CURRENT RESEARCH 1994-E

RECHERCHES EN COURS 1994-E

1994

Includes/comprend:

Cordillera and Pacific Margin
Cordillère et marge du Pacifique

Interior Plains and Arctic Canada
Plaines intérieures et région arctique du Canada

Canadian Shield
Bouclier canadien

Eastern Canada and National and General Programs
Est du Canada et programmes nationaux et généraux

Available in Canada through authorized
bookstore agents and other bookstores

or by mail from

Canada Communication Group — Publishing
Ottawa, Canada K1A 0S9

and from

Geological Survey of Canada offices:

601 Booth Street
Ottawa, Canada K1A 0E8

3303-33rd Street N.W.,
Calgary, Alberta T2L 2A7

100 West Pender Street
Vancouver, B.C. V6B 1R8

A deposit copy of this publication is also available for
reference in public libraries across Canada

Cat. No. M44-1994/5
ISBN 0-660-59628-8

Price subject to change without notice

Cover description

Polymictic conglomerate with large load casts and flame structures, Carboniferous Horton Group, Wilkie Brook Formation, near Crystal Cliffs, Nova Scotia. Photo courtesy F.J. Hein. For further information on Horton Group, see paper this volume. GSC 1994-481

Description de la photo couverture

Conglomérat polygénique présentant de grandes empreintes de charge et des moulages de boue, Groupe de Horton (Carbonifère), Formation de Wilkie Brook, près de Crystal Cliffs, Nouvelle-Écosse. Photo gracieuseté de F.J. Hein. Pour plus de renseignements sur le Groupe de Horton, consulter l'étude dans le présent volume. CGC 1994-481

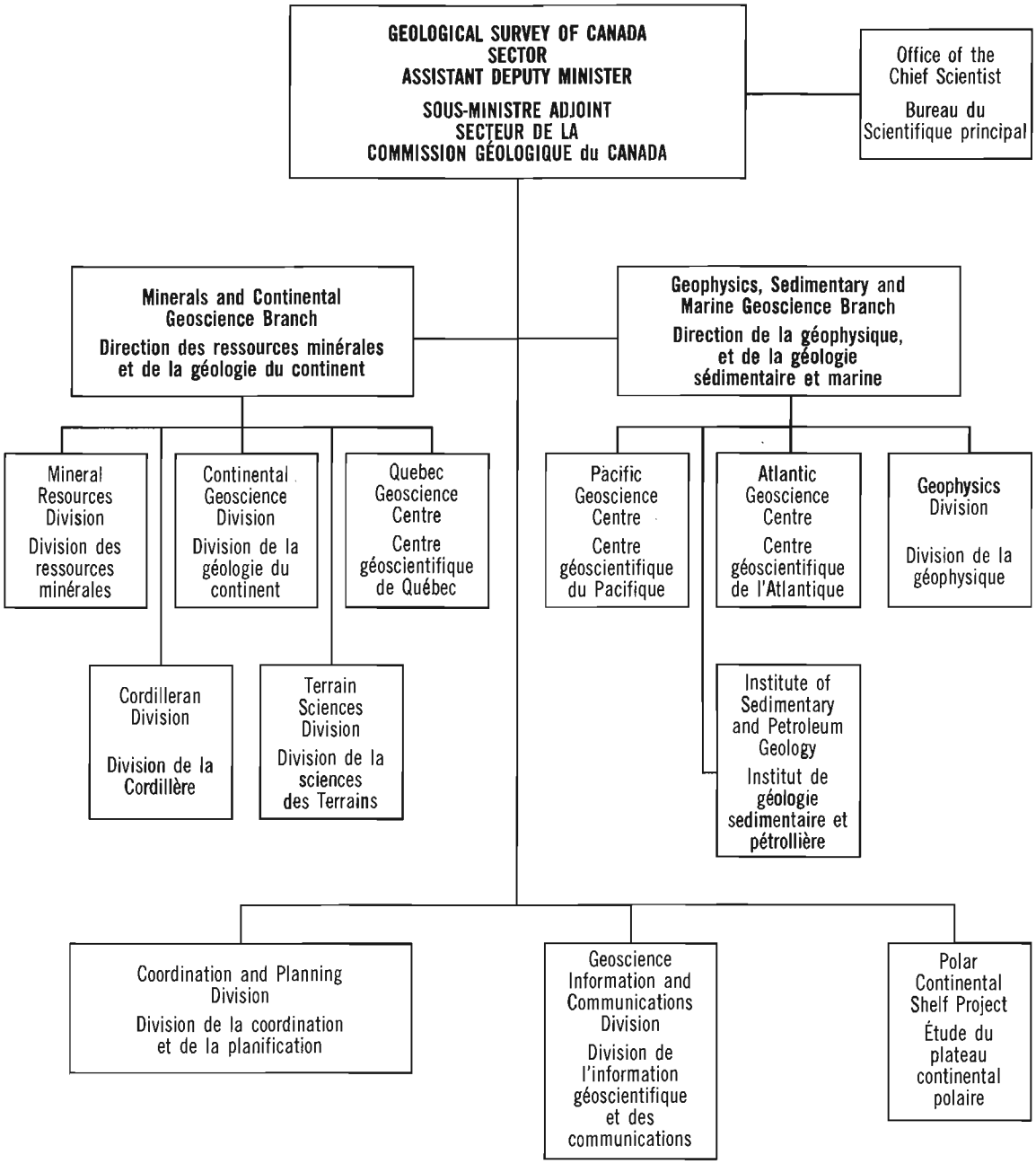
GEOLOGICAL SURVEY OF CANADA
SECTOR
ASSISTANT DEPUTY MINISTER
SOUS-MINISTRE ADJOINT
SECTEUR DE LA
COMMISSION GÉOLOGIQUE du CANADA
Office of the Chief Scientist
Bureau du Scientifique principal
Minerals and Continental Geoscience Branch
Direction des ressources minérales et de la géologie du continent
Geophysics, Sedimentary and Marine Geoscience Branch
Direction de la géophysique, et de la géologie sédimentaire et marine
Mineral Resources Division
Division des ressources minérales
Continental Geoscience Division
Division de la géologie du continent
Quebec Geoscience Centre
Centre géoscientifique de Québec
Pacific Geoscience Centre
Centre géoscientifique du Pacifique
Atlantic Geoscience Centre
Centre géoscientifique de l'Atlantique
Geophysics Division
Division de la géophysique
Cordilleran Division
Division de la Cordillère
Terrain Sciences Division
Division de la sciences des Terrains
Institute of Sedimentary and Petroleum Geology
Institut de géologie sedimentaire et pétrollière
Coordination and Planning Division
Division de la coordination et de la planification
Geoscience Information and Communications Division
Division de l'information géoscientifique et des communications
Polar Continental Shelf Project
Étude du plateau continental polaire

Separates

A limited number of separates of the papers that appear in this volume are available by direct request to the individual authors. The addresses of the Geological Survey of Canada offices follow:

601 Booth Street
OTTAWA, Ontario
K1A 0E8
(FAX: 613-996-9990)

Institute of Sedimentary and Petroleum Geology
3303-33rd Street N.W.
CALGARY, Alberta
T2L 2A7
(FAX: 403-292-5377)

Cordilleran Division
100 West Pender Street
VANCOUVER, B.C.
V6B 1R8
(FAX: 604-666-1124)

Pacific Geoscience Centre
P.O. Box 6000
9860 Saanich Road
SIDNEY, B.C.
V8L 4B2
(Fax: 604-363-6565)

Atlantic Geoscience Centre
Bedford Institute of Oceanography
P.O. Box 1006
DARTMOUTH, N.S.
B2Y 4A2
(FAX: 902-426-2256)

Québec Geoscience Centre
2700, rue Einstein
C.P. 7500
Ste-Foy (Québec)
G1V 4C7
(FAX: 418-654-2615)

When no location accompanies an author's name in the title of a paper, the Ottawa address should be used.

Tirés à part

On peut obtenir un nombre limité de «tirés à part» des articles qui paraissent dans cette publication en s'adressant directement à chaque auteur. Les adresses des différents bureaux de la Commission géologique du Canada sont les suivantes:

601, rue Booth
OTTAWA, Ontario
K1A 0E8
(facsimilé : 613-996-9990)

Institut de géologie sédimentaire et pétrolière
3303-33rd St. N.W.,
CALGARY, Alberta
T2L 2A7
(facsimilé : 403-292-5377)

Division de la Cordillère
100 West Pender Street
VANCOUVER, British Columbia
V6B 1R8
(facsimilé : 604-666-1124)

Centre géoscientifique du Pacifique
P.O. Box 6000
9860 Saanich Road
SIDNEY, British Columbia
V8L 4B2
(facsimilé : 604-363-6565)

Centre géoscientifique de l'Atlantique
Institut océanographique Bedford
B.P. 1006
DARTMOUTH, Nova Scotia
B2Y 4A2
(facsimilé : 902-426-2256)

Centre géoscientifique de Québec
2700, rue Einstein
C.P. 7500
Ste-Foy (Québec)
G1V 4C7
(facsimilé : 418-654-2615)

Lorsque l'adresse de l'auteur ne figure pas sous le titre d'un document, on doit alors utiliser l'adresse d'Ottawa.

CONTENTS

CORDILLERA AND PACIFIC MARGIN
CORDILLÈRE ET MARGE DU PACIFIQUE

INTERIOR PLAINS AND ARCTIC CANADA
PLAINES INTÉRIEURES ET RÉGION ARCTIQUE DU CANADA

CANADIAN SHIELD
BOUCLIER CANADIEN

EASTERN CANADA AND NATIONAL AND GENERAL PROGRANS
EST DU CANADA ET PROGRAMMES NATIONAUX ET GÉNÉRAUX

CORDILLERA AND PACIFIC MARGIN

CORDILLÈRE ET MARGE DU PACIFIQUE

Jurassic stratigraphy in the northwestern Teslin and northeastern Whitehorse map areas, Yukon Territory

G.K. Jakobs
Cordilleran Division, Vancouver

Jakobs, G.K., 1994: Jurassic stratigraphy in the northwestern Teslin and northeastern Whitehorse map areas, Yukon Territory; in Current Research 1994-E; Geological Survey of Canada, p. 1-6.

Abstract: Sediments of the Laberge Group in the northwestern Teslin (105C) and northeastern Whitehorse (105D) map areas have yielded poorly preserved Early Jurassic ammonoids of Sinemurian to possibly Hettangian age. Strata to the west of Swift Lake and southeast of Streak Mountain are comprised of interbedded volcanic-granitic pebble/cobble conglomerate, greywacke, and siltstone, probably representing upper- to mid-fan channel deposits. Strata to the west of Mt. M'Clintock are comprised primarily of interbedded mudstone/siltstone, probably deposited on the lower fan or basinal plain. The mudstone/siltstone sequence overlies a basal volcanic-carbonate pebble/cobble conglomerate, which in turn sharply overlies limestone.

Résumé : Les sédiments du Groupe de Laberge, dans le nord-ouest de la région cartographique de Teslin (105C) et le nord-est de la région cartographique de Whitehorse (105D), ont livré des ammonoïdes mal préservées du Jurassique précoce qui s'échelonnent du Sinémurien à peut-être l'Hettangien. À l'ouest du lac Swift et au sud-est du mont Streak, les strates se composent de conglomérat à galets/cailloux volcaniques-granitiques, de grauwacke et de siltstone interstratifiés, qui représentent probablement des dépôts de chenal formés dans la partie médiane d'un cône alluvial. Les strates à l'ouest du mont M'Clintock sont constituées principalement de mudstone et de siltstone interstratifiés, qui se sont probablement déposés dans la partie inférieure d'un cône alluvial ou dans une plaine de bassin. La séquence de mudstone et siltstone repose sur un conglomérat basal à cailloux/galets volcaniques-carbonatés, qui lui-même repose sur un calcaire avec un contact franc.

INTRODUCTION

Presumed Lower Jurassic sediments of the Laberge Group outcrop in the western half of the Teslin map area (Gordey, 1991, 1992, 1994). Fossil control is absent or poor and the tectonically complex nature of the area has hampered the study and interpretation of these strata. During the 1993 field season, three weeks were spent at three localities to provide fossil control and measured stratigraphic sections. Exposure is generally poor in the study area and structural complications through measured sections are difficult or impossible to identify. The three study areas (Fig. 1) are: the ridge west of Swift Lake (Locality 1), the ridge west of Mt. M'Clintock (Locality 2; Whitehorse map area), and the ridge southeast of Streak Mountain (Locality 3).

STRATIGRAPHY

West of Swift Lake (Locality 1)

The ridge west of Swift Lake (Fig. 1) is composed predominantly of interbedded black siltstone and greenish-grey, fine- to coarse-grained greywacke. The strata generally dip moderately to steeply toward the northeast. Exposure along the measured section (Section 1; Fig. 2, 3, 4) is generally poor although the lower part of the section is well exposed. A thick conglomerate sequence was chosen as the base of the section; below this, exposure was extremely poor and a sharp topographic break may represent a fault. The basal unit is a poorly sorted, clast supported, volcanic-granitic pebble/cobble conglomerate in a fine-grained greywacke matrix. The clasts are generally well rounded and do not show imbrication. Pebble

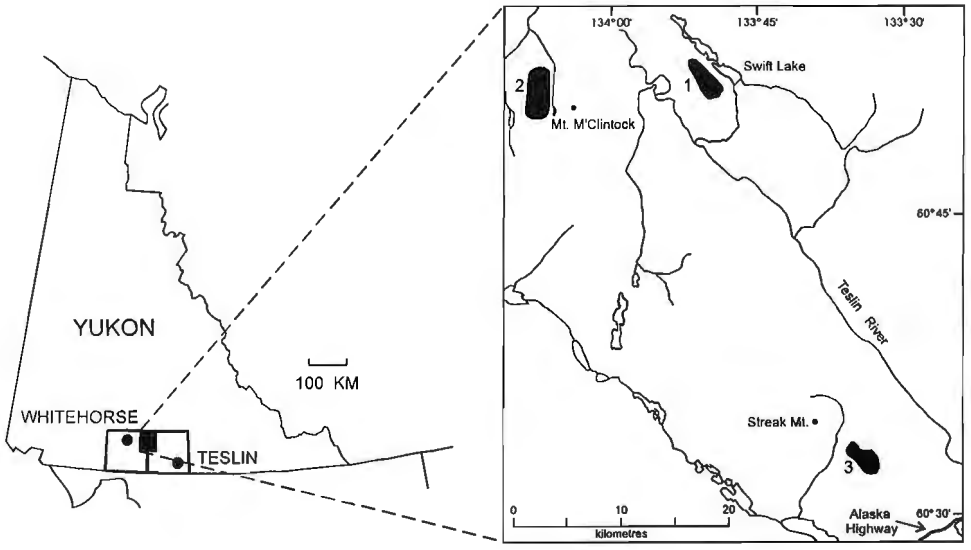

Figure 1. *Location of the study areas in the Teslin and Whitehorse map areas.*

Figure 2. *Section 1 looking north, base of section at left of photo marked by arrow, top of section at right of photo.*

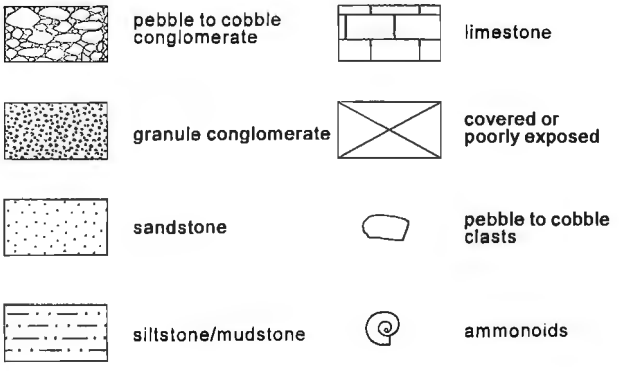

Figure 3. *Lithological legend for Figures 4 and 7.*

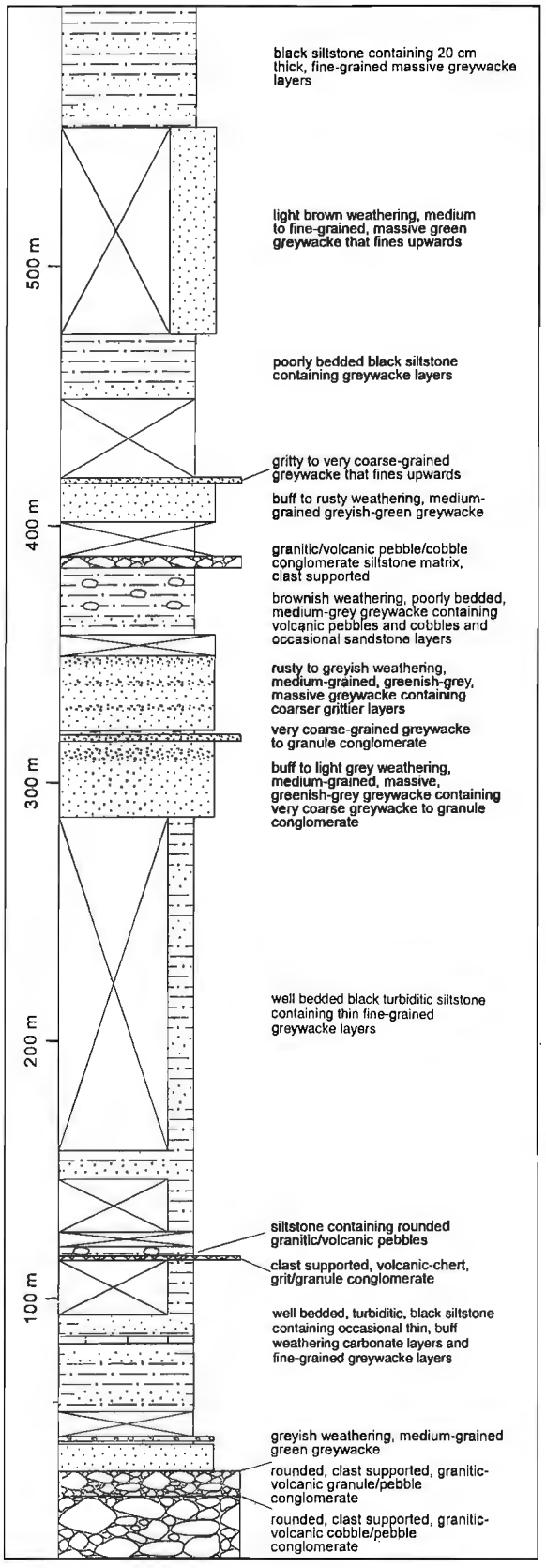

Figure 4. *Section 1 measured at Locality 1, west of Swift Lake. NTS 105C/13, UTM 579300E 6712700N to 578600E 6712600N.*

counts of clasts (3 counts, 25 clasts/count) with a maximum length greater than 1 cm yielded the following results: 15-45% coarse granitoids, 35-65% aphanitic volcanics (generally green), 5-15% chert, 5% carbonate, 5-10% quartzite, and minor greywacke. The majority of clasts had maximum lengths of 3 to 5 cm, although some volcanic and carbonate clasts reached lengths of 45 cm and 150 cm respectively. The largest carbonate clast (150 cm) weathered a light grey and contained corals(?) or algal mounds(?) (Fig. 5). Conglomerate beds were laterally discontinuous (generally reaching a maximum thickness of 5 m) and interbedded with 2-10 m thick medium- to coarse-grained, massive, greenish-grey greywacke and granular conglomerate.

Upsection from the basal conglomerate is a sequence of thinly interbedded siltstone and greywacke. The greyish to rusty weathering black siltstones are generally poorly exposed and commonly contain thin (20 cm) interbeds of fine-grained greywacke or, rarely, thin (5-10 cm) carbonate layers. Sedimentary structures are rare and consist of wavy laminae. Isolated volcanic and granitic pebbles are present in the siltstone at some levels. Trace fossils, represented by worm tracks, are present but macrofossils, such as bivalves, belemnoids, and ammonoids, are absent, with the exception of the figured specimen. The interbedded greywacke is generally fine grained. Distinct greywacke beds are present and are medium to very coarse grained, generally rusty to greyish on weathered surfaces and greenish grey on fresh.

A single poorly preserved ammonite (Plate 1, Fig. 1) was collected from siltstones along the top of the ridge above the limit of measurement. It is an evolute, simply-ribbed specimen, similar to Sinemurian echioceratids. The lack of a preserved venter precludes a more precise identification.

West of Mt. M'Clintock (Locality 2)

The ridge to the west of Mt. M'Clintock (Fig. 1; UTM 546450E 6744500N to 548200E 6744500N) is comprised almost entirely of thinly bedded, black siltstone and mudstone, commonly contact-metamorphosed along intrusive

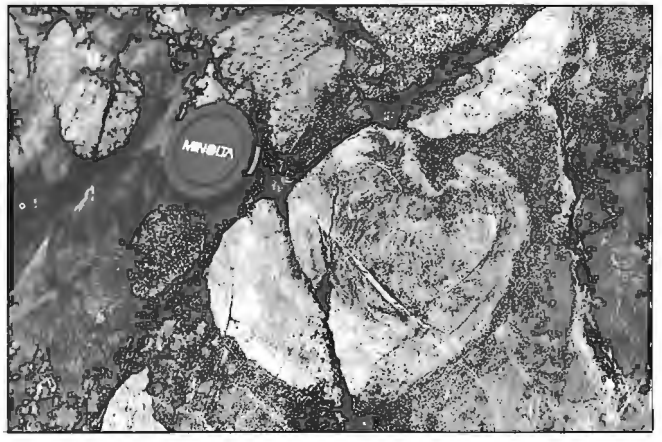

Figure 5. *Fossiliferous limestone clast in basal conglomerate of Section 1 at Locality 1.*

dykes and sills. The western end of the ridge contains an exposure of limestone (Wheeler, 1961; unit 3) that sharply underlies the siltstone/mudstone sequence. A stratigraphic section was not measured due to discontinuous exposure and the possibility of structural complications (faults) throughout the sequence.

The limestone is a massive, medium to dark grey micrite, commonly recrystallized, weathering light grey and cut by numerous coarsely crystalline calcite veins. Fossils are present but are generally replaced by coarse calcite and are poorly preserved. Solitary corals, terebratulid and rhynchonellid brachiopods, thin-shelled bivalves (possibly *Monotis*), and very poorly-preserved ammonoids are present. Exposure above the limestone is poor and cut by intrusives. The limestone is sharply overlain by a brown to greenish-grey weathering, dark grey siltstone.

Approximately 10 m above the limestone is a thick (30 m) sequence of interbedded conglomerate, greywacke, and siltstone. The pebble/cobble conglomerate is poorly sorted and contains rounded limestone and volcanic clasts (Fig. 6). Most of the clasts are 3 to 6 cm in length, although some limestone clasts may reach 29 cm in length. The limestone clasts (50-75%) are generally ovoid or discoidal and the majority are light grey weathering, similar to the underlying carbonate. Some limestone clasts are dark grey to black on fresh surfaces whereas the remainder are medium grey. Volcanic clasts (25-50%) are light to medium green, generally aphanitic but occasionally contain rusty weathering phenocrysts (1-2 mm), possibly hornblende. The conglomerate is clast supported within a matrix of greenish-grey siltstone or fine-grained greywacke. The conglomerate pinches out along strike into a calcareous, medium grey siltstone that contains occasional limestone clasts up to 30 cm in length. The conglomerate was probably deposited as channel fill.

The conglomerate is overlain by a medium-grained, greenish-grey greywacke. The greywacke is separated from the overlying siltstone and mudstone by a topographic depression which may represent a fault.

PLATE 1
All figures are natural size.

Figure 1. Echioceratidae? gen. et sp. indet. GSC 108543. GSC Loc. No. 210101, NTS 105C/13, UTM 564725E, 6746975N. Locality 1, ridge west of Swift Lake, Laberge Group, Sinemurian.

Figure 2. *Juraphyllites* sp. indet. GSC 108544. GSC Loc. No. 210134, NTS 105C/12, UTM 579075E, 6712650N. Locality 3, ridge southeast of Streak Mountain, Laberge Group, Sinemurian.

Figure 6. *Basal carbonate, volcanic pebble conglomerate of the Laberge Group at Locality 2.*

The overlying siltstone/mudstone is well indurated and commonly fractures into shards or blocks perpendicular or at a steep angle to bedding. The medium to dark grey siltstone is commonly found in beds less than 1 cm thick that weather buff to light brown. The dark grey mudstone forms greyish-brown weathering beds, generally greater than 1 cm thick and commonly as thick as 5-10 cm. Wavy mudstone laminae are occasionally present in the siltstone and small scale slump folds may also be present. The siltstone beds, some with a component of fine-grained greywacke at their base, grade upward into the mudstone. Rare medium to dark grey, fine-grained greywacke weathers a rusty, buff or tan colour and is generally parallel laminated, although wavy or ripple laminae are locally present. The greywacke beds are usually 5-10 cm thick. Buff-weathering carbonate layers are locally present but carbonate concretions are rare. Rarely the siltstone/mudstone sequence will display slumping and sediment flow features and cross lamination, generally above a greywacke layer that displays chaotic bedding.

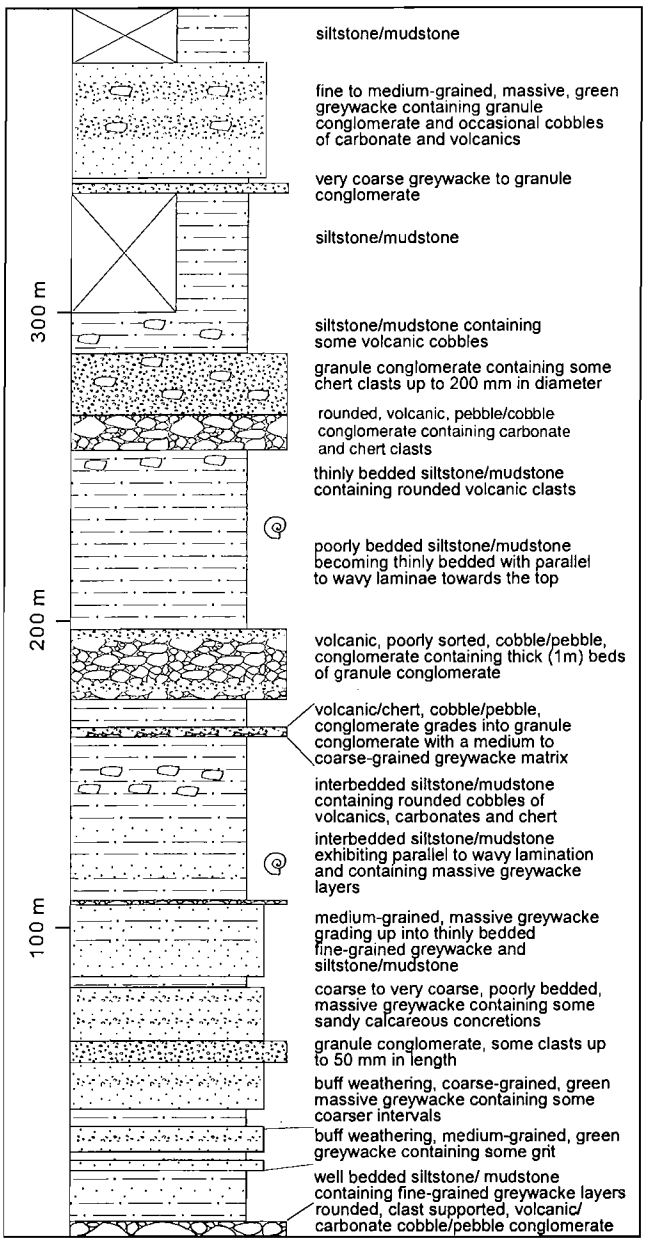

Figure 7. *Section 2 measured at Locality 3, southeast of Streak Mountain. NTS 105C/12, UTM 562700E 6747100N to 563250E 6747650N.*

Macrofossils are extremely rare, and trace fossils are represented only by rare worm burrows. Two poorly preserved ammonites (GSC Loc. C-210111, UTM 547675E 6746900N; GSC Loc. C-210113, UTM 547400E 6745775N) and some small, indeterminate bivalves (GSC Loc. C-210112, UTM 547050E 6747325N) were collected from the siltstone/mudstone sequence. The ammonites are poorly preserved, but are similar to schlotheimids, which are Hettangian to Sinemurian in age.

Southeast of Streak Mountain (Locality 3)

A thick sequence of interbedded siltstone, greywacke, and conglomerate is exposed southeast of Streak Mountain (Fig. 1). Exposure along the ridge crests is good and a section was measured along one ridge spur (Section 2; Fig. 7). The base of the section is marked by the first cliff exposure of conglomerate low along the ridge spur.

Conglomerate outcrops are typically covered with lichen and only rarely are unobscured surfaces exposed. Pebble counts were not possible, but the conglomerates appear to be composed primarily of volcanic, carbonate, and granitic clasts, but also contain rare clasts of chert. Clasts are rounded and generally pebble to cobble sized. Rarely, granitic clasts may reach 50 to 100 cm in diameter. The conglomerate is poorly sorted and generally matrix supported, the matrix ranges from greenish-brown weathering, dark grey siltstone to very coarse-grained greywacke. The conglomerate layers are usually 5-10 m thick and are commonly lensoidal in shape, pinching out laterally along strike within medium- to coarse-grained greywacke.

Most of the sequence is composed of interbedded greywacke and siltstone. Commonly gritty to granular greywacke layers (about 5 m thick) are overlain by medium- to coarse-grained greywacke (5-10 m thick) in turn overlain by siltstone/mudstone units (10-15 m thick). The medium green greywacke weathers grey to tan and is generally massive with no well-defined bedding structures. Very coarse-grained to granular greywacke is common and interbedded with fine-grained greywacke.

The greywacke commonly contains parallel- to wavy-laminated black siltstone/mudstone layers (1-10 cm thick). The medium grey siltstone generally weathers buff, whereas the medium to dark grey mudstone weathers black to dark brown. The siltstone/mudstone units are occasionally very fissile and commonly contain pebble and cobble clasts of carbonate and volcanics.

Macrofossils are rare but several collections were made of poorly preserved ammonoids and coleoids. The ammonoids are generally too poorly preserved to identify with certainty, although one specimen is probably a *Juraphyllites* (Plate 1, Fig. 2), of Sinemurian age. A collection of bivalves from greywacke talus blocks near the top of the ridge have been identified as Late Triassic *Monotis* (E.T. Tozer, pers. comm., 1993) but their relationship to the surrounding strata is not clear.

DISCUSSION

All three study areas appear to be roughly the same age, Hettangian to Sinemurian, but contain slightly different stratigraphies. The Swift Lake locality is comprised predominantly of interbedded greywacke and siltstone, contains occasional conglomerate units, and may represent an upper- to mid-fan deposit. The basal pebble/cobble conglomerate represents an upper fan channel deposit, whereas the overlying, predominantly greywacke/siltstone sequence represents mid-fan channel deposits. The Swift Lake locality is probably Sinemurian in age. Southeast of Streak Mountain a similar sequence is seen, but it differs in that conglomerate units are thinner and more common. This sequence probably represents a braided mid-fan deposit with conglomerates representing channels that migrate across interbedded greywacke/siltstone sequences. The locality to the southeast of Streak Mountain is also probably Sinemurian in age. Lithologically, the two areas are similar and the main clast components in the conglomerates are volcanics with lesser amounts of granitoid material and carbonates. The poorly sorted conglomerate at Swift Lake contains large clasts of limestone (150 cm) and volcanics (40 cm) and is suggestive of deposition in close proximity to the source. A western source is not indicated due to the occurrence to the west of coeval basinal or deep water strata (Mt. M'Clintock area). Wheeler (1961) suggested that the Laberge Group in the eastern half of the Whitehorse map area was derived from an eastern source and the present study suggests the same.

The area to the west of Mt. M'Clintock differs significantly from the other two areas and is Hettangian to Sinemurian in age. Most of the sequence is composed of interbedded siltstone/mudstone containing minor amounts of greywacke overlying a basal conglomerate. The thinly bedded nature of the siltstone/mudstone sequence, the presence of occasional small-scale slump features, and the absence of significant amounts of coarser clastics indicates that the succession was probably deposited on the lower fan or basinal plain. The basal conglomerate, composed exclusively of volcanic and carbonate clasts, may indicate erosion and deposition from an Upper Triassic reef and volcanic complex.

ACKNOWLEDGMENTS

S. Gordey is thanked for providing logistical support and the opportunity to study the Laberge Group rocks of the Teslin map area. Trans North Helicopters and Heli-Dynamix provided helicopter support. The excellent field assistance of Rocio Lopez is greatly appreciated.

REFERENCES

Gordey, S.P.
1991: Teslin map area, a new geological mapping project in southern Yukon; in Current Research, Part A; Geological Survey of Canada, Paper 91-1A, p. 171-178.
1992: Geological fieldwork in Teslin map area, southern Yukon Territory; in Current Research, Part A; Geological Survey of Canada, Paper 92-1A, p. 279-286.
1994: Tectonic framework of the Teslin region, southern Yukon Territory; in Current Research, Part A; Geological Survey of Canada, Paper 94-1A, p. 11-18.

Wheeler, J.O.
1961: Whitehorse map area (105D), Yukon Territory; Geological Survey of Canada, Memoir 312, 156 p.

Geological Survey of Canada Project 900036

Lithochemistry and aqueous metal transport in the Keno Hill mining district, central Yukon Territory

Y.T. John Kwong[1], Charlie Roots[2] and Wayne Kettley[3]
Cordilleran Division

Kwong, Y.T.J., Roots, C., and Kettley, W., 1994: Lithochemistry and aqueous metal transport in the Keno Hill mining district, central Yukon Territory; in Current Research 1994-E; Geological Survey of Canada, p. 7-15.

Abstract: To facilitate remediation and further exploration in the former silver mining camp of the Keno Hill district, this study investigates pertinent water-rock/sediment interactions. Water, rock and sediment samples collected in early and late summer were analyzed to clarify the regional lithochemistry, seasonal change in water chemistry and the impact of mining on the water quality of local streams. Preliminary results indicate that discharge from many mine workings contains elevated metal concentrations, especially Zn and Cd. However, acid rock drainage is not widespread because of galvanic protection of pyrite from oxidative dissolution and neutralization by carbonate in the country rock. Mechanisms apparently operative to limit aqueous metal transport in small streams include cryogenic precipitation, coprecipitation, sorption and rarely dilution. Because Cu, Pb and As are not easily mobilized in the region their occurrence in stream sediments may indicate a nearby source of silver mineralization.

Résumé : Afin de faciliter l'application de mesures correctives et la reprise de travaux d'exploration dans les anciens gisements argentifères du camp minier de Keno Hill, les auteurs ont étudié les interactions pertinentes entre l'eau et les roches ou sédiments. Ils ont analysé des échantillons d'eau, de roches et de sédiments prélevés au début et à la fin de l'été, afin de déterminer la lithochimie régionale, les variations saisonnières de la chimie de l'eau et l'impact de l'exploitation minière sur la qualité de l'eau des cours d'eau de la région. Les résultats préliminaires indiquent que les eaux évacuées par de nombreuses mines renferment des concentrations élevées en métaux, en particulier en Zn et en Cd. Cependant, le drainage minier acide n'est pas très étendu, en raison de la présence de carbonate dans la roche encaissante, qui neutralise les acides et assure une protection galvanique contre la dissolution oxydative de la pyrite. Les mécanismes qui contribuent apparemment à limiter le transport des métaux dans les petits cours d'eau sont la précipitation cryogénique, la coprécipitation, la sorption et, plus rarement, la dilution. Comme Cu, Pb et As ne se laissent pas mobiliser facilement dans la région, leur présence dans des sédiments fluviatiles pourrait indiquer la présence, à proximité, d'une source de minéralisation argentifère.

[1] National Hydrology Research Institute, 11 Innovation Boulevard, Saskatoon, Saskatchewan S7N 3H5
[2] Canada-Yukon Geoscience Office, P.O. Box 2073 (F3), Whitehorse, Yukon Y1A 2C6
[3] Water Resources Division, Northern Affairs Program, 345-300 Main Street, Whitehorse, Yukon Y1A 2B5

INTRODUCTION

The Keno Hill mining district, 350 km by road north of Whitehorse, Yukon, was a major silver producer in Canada for 70 years. Over 14 significant vein deposits have been mined from upper Paleozoic quartzite and schist in a belt about 8 km wide and 22 km long (Fig. 1). Argentiferous galena and silver-containing sulphosalts such as freibergite were the primary ore minerals mined. These minerals, frequently associated with sphalerite and manganiferous siderite, occurred in quartz veins within *en echelon* faults.

Although mining has ceased, there remains active exploration in the area and public concern for continuing environmental degradation resulting from high metal discharge (especially dissolved zinc and cadmium) and potential acidic drainage from some of the abandoned mine workings. To aid finding new ore on the one hand and devising efficient remediation schemes to safeguard the health of the local ecosystem on the other, a study has been conducted to clarify pertinent water-rock/soil interactions occurring in the area. In this report, we present preliminary findings on metal transport and attenuation mechanisms, the effects of prevalent rock types on the stream water chemistry and the potential for acid generation or buffering.

Physiography and glacial geology

Most mining in the district took place on the north slopes of Galena Hill (1444 m) and Keno Hill (1849 m). The relatively smooth northward facing slopes and wide South McQuesten River valley (average elevation 760 m) are underlain by discontinuous permafrost. The two hills are separated by Cristal Creek, with Keno City (elevation 945 m) at its head.

Sampled water courses are intermittent or dry in August-September and frozen from October through April. Stream bottoms generally consist of pebble- to boulder-sized rock fragments from bedrock and lag from overlying glacial deposits. The hill sides are mantled by a hummocky veneer of bouldery sand and clay. On the slopes, black spruce and mountain fir are scattered in a thick mat of sphagnum and Labrador tea bushes, and dense slide alder choke stream courses. Higher elevations are better drained and dwarf birch shrubs predominates above tree line. The glacial deposits in the South McQuesten valley contain many ponds and swamps, but on the slope kame terraces host dry poplar stands.

At least two glaciations have modified the landscape and drainage of the area within the last 120 000 years (Hughes, 1982). The earlier Reid Glaciation covered Galena Hill and reached about 1600 m elevation on Keno Hill. During the later, less extensive McConnell Glaciation an ice lobe occupied the South McQuesten valley and kame terraces are evident at 1300 m on the north side of Galena Hill. The ice lobe also filled the Cristal Creek valley, diverting drainage southward into Duncan Creek (McTaggart, 1960).

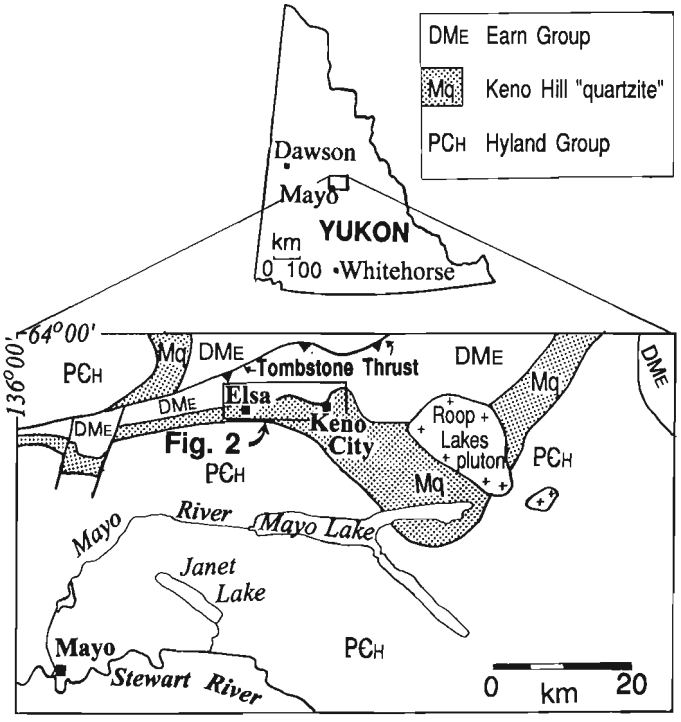

Figure 1. Generalized geological map of northern Mayo map area (105M) adapted from Roots and Murphy (1992).

BEDROCK GEOLOGY

The bedrock geology of the area was described by McTaggart (1960), Boyle (1965) and mapped by Kindle (1962) and Green (1971, 1972). Roots and Murphy (1992) furnished the most recent geological interpretation. Tectonically the district is part of the Tombstone Thrust panel, which underlies both Galena Hill and Keno Hill. The three principal rock units are "Keno Hill quartzite" (Early Mississippian), Earn Group metasedimentary and metavolcanic rocks (Devonian-Mississippian) and metadiorite of Late Triassic age. In the study area bedrock is exposed where open pit mining has taken place, as well as in gullies and glacial meltwater channels. Above treeline are broad areas of frost-fractured rock.

The "Keno Hill quartzite" unit consists mostly of streaky dark grey quartzite with interfoliated carbonaceous and chloritic phyllite, as well as rare limestone pods. A pervasive foliation coupled with pressure solution produces a strong banding in the massive quartzite and sheared lenses within phyllite. Original sedimentary layering and relict grains are rare. In thin section the quartzite is a mosaic of polyhedral quartz grains with interstitial and clusters of calcite, scattered feldspar grains and accessory anhedral tourmaline, chlorite and zircon. The quartzite generally contains 2-10% calcite in addition to the limestone pods.

The underlying Earn Group includes foliated and lineated carbonaceous schist, siliceous carbonaceous phyllite and siltstone, and porphyritic phyllitic felsic metavolcanics. On Galena Hill it varies between grey siliceous phyllite (metasediment) and chloritic phyllite (metavolcanic). In thin section the grey siliceous phyllite is a mosaic of polyhedral

quartz and less abundant albite with thin bands of chlorite and muscovite as well as interstitial calcite. At two sampling sites the chloritic phyllite contains a dense network of recrystallized quartz and calcite micro-veinlets.

The metadiorite is resistant, massive and includes locally unfoliated bodies up to 70 m thick. In thin section the metadiorite is composed of chlorite, actinolite, zoisite and albite after hornblende as well as relict calcic feldspar and rare interstitial pyrite. Carbonate alteration is rarely associated with these intrusions.

SAMPLING AND ANALYTICAL METHODS

To shed light on the regional lithochemistry, representative samples were collected from relatively unweathered outcrops of the four prevalent major rock units (Fig. 2). A small piece of each sample was saved for thin section preparation and the rest submitted for geochemical analyses. To assess the acid rock drainage potential of the major rock units, selected samples were also submitted for acid-base-accounting analyses.

To determine the extent of metal contamination of water courses resulting from mining activities and to assess aqueous metal transport and attenuation mechanisms, both pristine and contaminated streams were sampled during early summer freshet (mid-June) and in late summer (end of August). At each sampling site, pH, Eh, conductivity and temperature were measured and a 1-litre unfiltered water sample collected. At the end of the day, each sample was filtered through a 45 μm cellulose acetate filter and two 100 mL aliquots were saved, one for sulphate analysis and the other, preserved with 2 mL of nitric acid, for dissolved metals. The remainder of the sample was used for determination of alkalinity by titration. The pH of the samples was also remeasured to reveal whether or not significant change in aqueous chemistry had taken place during transport from the sampling site to the camp.

To evaluate the role of sediments in attenuating metal transport and to determine the mobility of metal contaminants, stream sediments and tailings were sampled at selected sites for examination and analyses. Grab samples of about 1 kg in weight were taken with a plastic scoop and cores 2.5 cm and 10 cm in diameter were sampled using a stainless steel coring tube with a plastic sleeve and a steel hand auger, respectively. Because fine grained sediments usually dominate water-mineral interaction occurring at a site, only the -180 μm portion of each sample was analyzed. Parameters measured include trace element content, mineralogy (by powder x-ray diffractometry) and fractionation pattern of five heavy metals (As, Cd, Cu, Pb and Zn) commonly found in the mining district by sequential extraction analysis. The procedure in the sequential extraction analysis is summarized in Figure 3.

RESULTS

Rock geochemistry

Table 1 shows the major oxide and selected trace element composition of the five dominant rock units occurring in the Keno Hill mining district as well as the net neutralization potential of selected rock samples.

The "Keno Hill quartzite" samples vary from pure quartzite (JK-11) to impure limestone (JK-2). Only one sample with a graphitic schist component (JK-7) contains anomalous Pb (31 ppm). The samples are generally low in Zn content. The two Earn Group metavolcanic samples greatly differ in Fe, Ca, Mg, K, Na, Ti and Si concentrations. Sample JK-21, with relatively high loss on ignition (LOI) and CaO, has undergone pervasive carbonate replacement. It also has the highest Cu content in the entire sample suite. Although still heterogeneous, the three Earn Group phyllites show less variation in rock geochemistry. The differing amounts of sericite present may explain the differences in major element composition. This

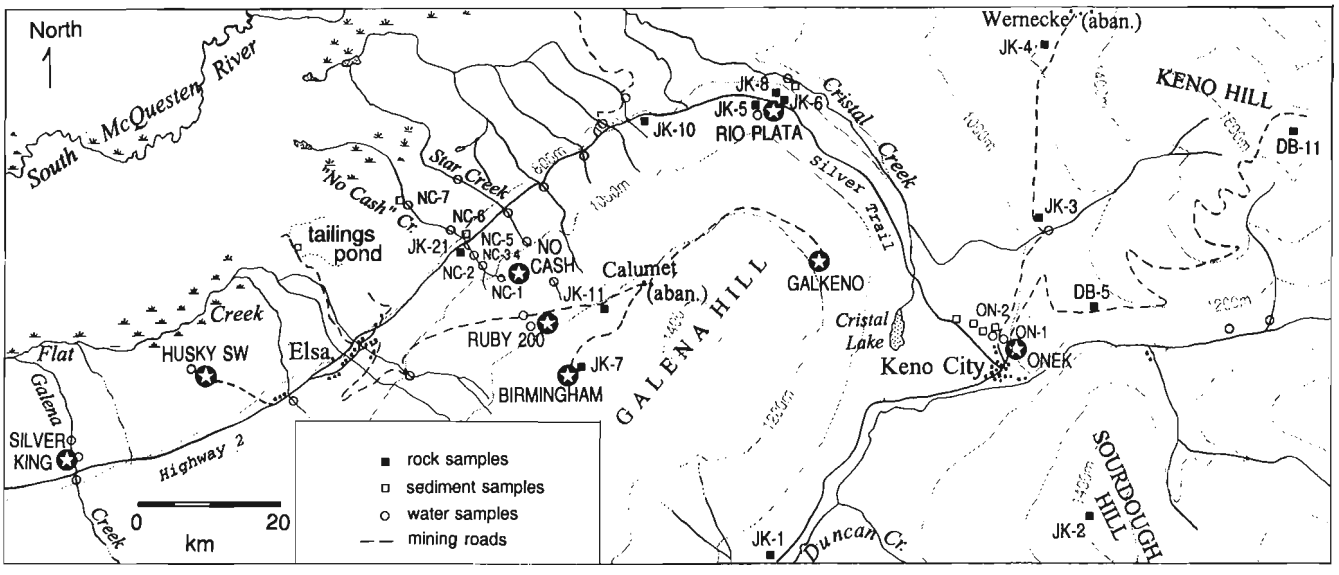

Figure 2. Location of rock, sediment and water samples.

rock unit contains the highest As content among the five prevalent lithologies and one sample (JK-8) also contains anomalous Pb (21 ppm).

The Triassic metadiorite shows only minor variations in major oxide and trace element content. On the average, it contains the highest Cu and Ni content among all rock types present. One Precambrian Hyland Group graphitic phyllite, analyzed for comparison, is relatively siliceous and not anomalous in any trace element. The net neutralization potential of selected samples is shown in the last column of Table 1. Largely controlled by their carbonate content (reflected by the LOI and %C analyses), the acid buffering capacity of these rocks ranges by nearly three orders of magnitude.

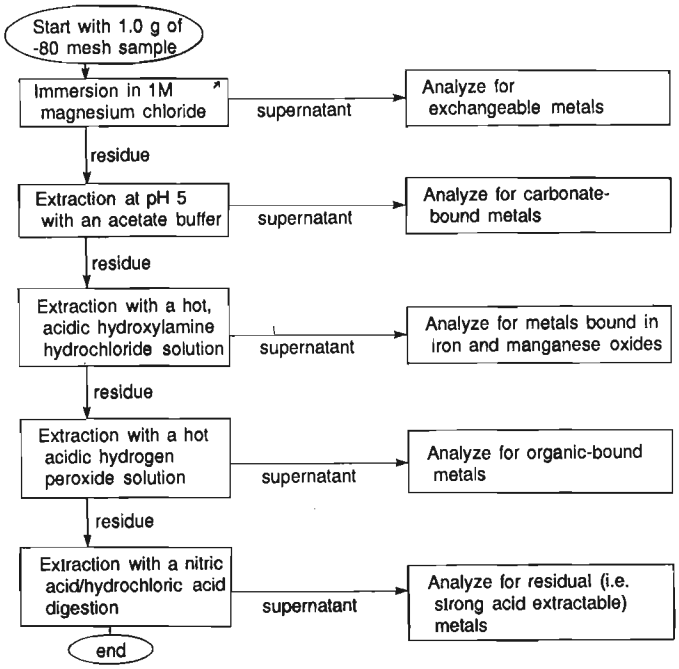

Figure 3. Flow chart of sequential extraction analysis.

Water chemistry

Although acidic drainage occurs very locally in the mining district, elevated levels of dissolved Zn, Mn and occasionally Cd are common in drainage from many abandoned mine workings. Table 2 shows the water chemistry of discharge during freshet (mid-June) from the Onek, No Cash and Silver King mines, and a standing pool of water in the Rio Plata workings. The data amply illustrate the nature and concentration of metal contaminants released into the environment as a result of mining in the district. In June, seeps with a pH of about 5 were found at the toe of the Ruby mine waste rock dump and the discharge from Silver King mine also had a pH of <7 (Table 2).

Two examples will illustrate the seasonal variation of water chemistry and metal attenuation along small streams. Figure 4 compares the water chemistry of No Cash Creek in mid-June and in late August, and depicts the changes in selected parameters along the flow path. No Cash Creek flows through boreal forest on till and Earn Group phyllite. Drainage from No Cash mine enters the stream immediately above Station NC-2. During freshet, the dissolved Zn and Cd concentrations were nearly twice those in late August. Although the pH of the stream was lower during freshet, the dissolved

Table 1. Major and trace element composition of major rock units in the Keno Hill mining district and net neutralization potential of selected samples.

Field #	SiO_2	Al_2O_3	Fe_2O_3	CaO	MgO	K_2O	Na_2O	TiO_2	MnO	P_2O_5	LOI	Total	Cu	Zn	Cd	As	Pb	Ag	Ni	Co	Bi	Mo	%C	NNP*
	%												ppm											
Hyland Group																								
JK-1	88.7	5.67	2.54	0.09	0.66	0.8	0.38	0.22	0.032	0.06	1.5	100.65	33	37	3	1	1	0.2	12	2	2	1	0.3	2
Keno Hill Quartzite																								
DB-5	94.6	0.28	1.36	1.47	0.40	0.1	0.04	0.14	0.012	0.02	1.9	100.32	2	2	1	1	2	0.1	6	1	31	1	0.56	-
JK-2	4.5	0.27	0.40	54.67	0.41	0.2	0.01	0.04	0.007	0.01	40.4	100.91	2	3	1	1	3	0.1	1	1	2	2	12.56	934
JK-7	88.6	4.88	0.66	0.01	0.26	1.6	0.06	0.24	0.001	0.03	4.0	100.34	4	14	1	1	31	0.3	7	1	2	9	2.86	-
JK-11	99.7	0.01	0.69	0.01	0.01	0.1	0.02	0.16	0.001	0.01	0.1	100.81	1	2	1	3	1	0.1	4	1	2	1	0.02	-
Earn Group metavolcanics																								
JK-3	71.8	13.37	6.09	0.28	2.13	3.1	0.71	0.59	0.121	0.12	2.4	100.71	30	86	1	1	2	0.1	35	14	2	1	0.08	6
JK-21	44.7	13.55	12.22	10.49	5.15	0.1	2.83	1.65	0.176	0.10	9.5	100.46	230	76	3	20	13	0.3	30	24	2	1	nd	162
Earn Group metasediments																								
JK-6	74.2	6.36	3.02	8.80	2.26	1.7	0.14	0.39	0.084	0.38	1.2	98.53	9	87	1	87	6	0.1	13	5	2	1	2.85	182
JK-8	74.4	7.72	2.47	7.20	2.05	1.8	0.18	0.53	0.075	0.30	3.4	100.12	9	66	1	19	21	0.3	15	4	2	2	2.41	-
JK-10	62.6	11.7	4.01	5.15	2.51	3.0	0.84	0.66	0.056	0.24	8.3	99.06	16	52	1	6	9	0.1	21	8	2	3	2.31	105
Triassic metadiorite																								
DB-11	47.7	14.19	12.38	11.69	7.66	0.4	2.10	1.54	0.178	0.15	2.1	100.08	154	52	1	1	1	0.1	36	15	2	1	0.03	-
JK-4	48.3	16.20	10.91	11.92	7.45	0.3	2.11	1.26	0.153	0.10	2.2	100.90	75	26	1	1	1	0.1	40	13	2	1	0.11	-
JK-5	48.2	15.15	11.31	12.38	7.83	0.1	2.49	1.39	0.169	0.07	2.3	101.38	137	93	1	6	1	0.1	31	14	2	1	0.16	18

* Net neutralization potential in kg $CaCO_3$/tonne

sulphate content showed little variation. The dissolved Zn introduced by mine water is dissipated downstream but the relatively constant dissolved sulphate concentrations suggest that dilution is not the cause. Precipitation and/or sorption of the metallic ion onto solid matter along the stream bed and banks are probably predominant.

Figure 5 depicts the change in water chemistry along the Onek drainage. Station ON-1 is located at the entrance to the old mine portal and ON-2 about 150 m downstream where the surface drainage disappears into ground. During freshet, the drainage was also characterized by a lower pH and higher concentrations of dissolved Zn, Cd and sulphate. In late summer, both dissolved Zn and Cd dropped significantly whereas dissolved sulphate only slightly decreased. This again demonstrates that dilution is an insignificant metal attenuation mechanism in these small streams.

Soil and tailings geochemistry

The dispersion of trace elements released during mining is commonly revealed by vertical concentration profiles in sediments. Figure 6 compares the concentration of selected trace elements in sediment cores sampled at the lowest locations where the Onek drainage, No Cash Creek and Star Creek can still be identified. In contrast to the Onek and No Cash systems, Star Creek has not been affected by any mine drainage and its sediment trace element content does not vary with depth. The Pb, Cu, Zn and As concentrations in the stream sediment of Star Creek can thus be taken as baseline values for pristine streams in the study area.

Near the surface (<41 cm), the Onek sediment shows elevated concentrations of Zn, Cd, As, Pb and Cu. Whereas the last three metals rapidly drop to background level at a

Table 2. Water chemistry at selected old mine workings in mid-June, 1993.

mg/L	Onek	No Cash	Silver King	Rio Plata
Al	<0.005	<0.005	0.018	<0.005
Sb	0.18	<0.02	<0.02	<0.02
As	0.1	0.08	<0.04	<0.04
Ba	0.009	0.004	0.017	0.018
Be	<0.0002	<0.0002	<0.0002	<0.0002
Bi	<0.02	<0.02	<0.02	<0.02
Cd	2.34	0.239	0.0486	2.07
Ca	212	125	152	440
Cr	0.003	0.002	<0.001	0.007
Co	0.020	0.015	0.044	0.096
Cu	<0.001	<0.001	0.222	<0.001
Fe	<0.003	<0.003	25.5	<0.003
Pb	0.026	0.005	<0.004	0.013
Li	<0.05	<0.05	<0.05	<0.05
Mg	63.6	16.7	41.0	161
Mn	160	18.4	6.60	51.7
Mo	0.028	0.012	0.013	0.028
Ni	0.621	0.081	0.153	0.276
P	0.13	<0.02	<0.02	<0.02
K	1.85	0.79	1.75	2.82
Se	<0.02	<0.02	<0.02	<0.02
Si	13.6	4.38	12.0	9.76
Ag	<0.001	<0.001	<0.001	<0.001
Na	3.55	0.96	2.16	1.69
Sr	0.17	0.14	0.25	0.69
Th	<0.01	<0.01	<0.01	<0.01
Ti	0.012	0.005	<0.001	0.006
U	<0.02	<0.02	<0.02	<0.02
V	<0.001	<0.001	<0.001	<0.001
Zn	80.6	25.7	3.97	109
Sulphate	590	409	571	1886
pH	7.2	7.2	6.2	7.3
Alkalinity	159	70	15	108
Conductivity (µS/cm)	838	543	674	1730

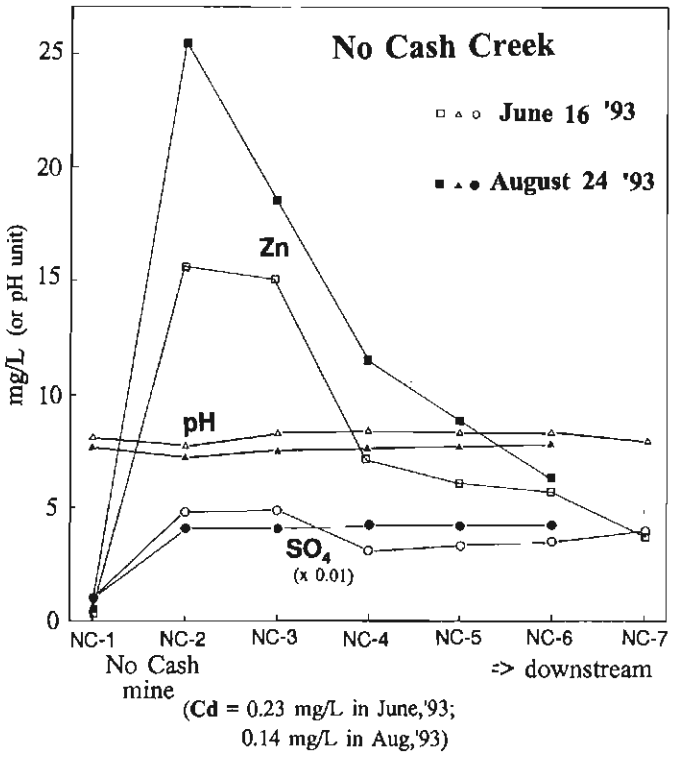

Figure 4. Comparison of selected water chemistry along No Cash Creek during freshet and late summer.

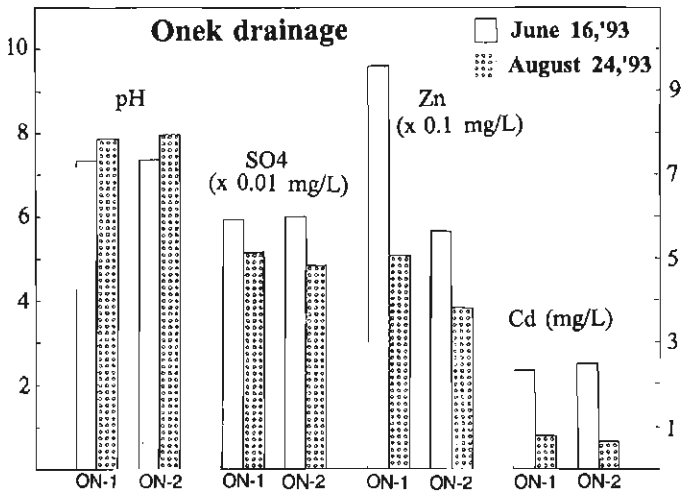

Figure 5. Change in water chemistry along the Onek drainage during freshet and late summer.

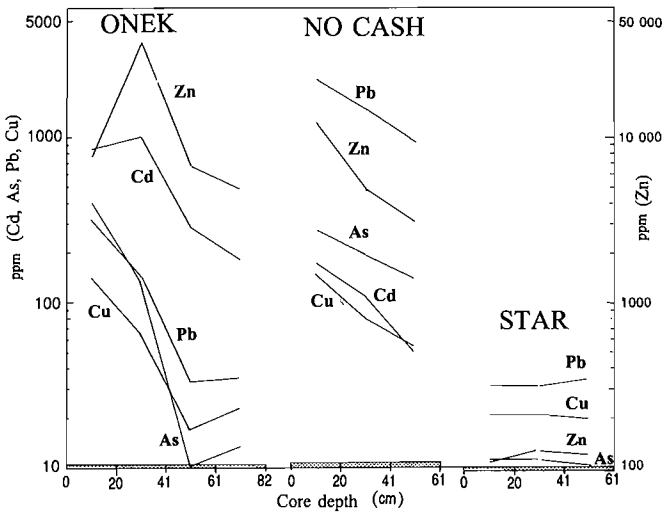

Figure 6. Comparison of selected trace metal content in sediments at terminations of Onek drainage, No Cash Creek, and Star Creek.

depth of greater than about 41 cm, the first two elements are significantly above the background levels even at the coring depth of 82 cm. This suggests that Zn and Cd are more mobile (i.e., they travel farther with infiltrating waters) than As, Pb and Cu in the Onek drainage system. Furthermore, both the Zn and Cd concentrations peak not at the surface but 20 to 30 cm below it. Along the stream bed, a light yellow precipitate was found coating organic litter and less commonly rock fragments. X-ray diffraction and chemical analyses indicate that the precipitate consists mainly of hydrozincite mixed with poorly crystalline ferric hydroxide. A possible mechanism for the formation of hydrozincite and an explanation for the Zn and Cd profile in the Onek sediment will be discussed later.

The No Cash sediment core was sampled deep in South McQuesten valley where saturated conditions prevail throughout the year and the sediment may not have been completely frozen in the winter. The concentration of all five elements depicted decreases rapidly with depth. However, at the coring depth of 61 cm, these elements are significantly above the background concentrations for the region. Upstream from the coring site, reddish ferric hydroxide can occasionally be seen coating the stream bed, particularly where the No Cash mine drainage enters the creek system, but hydrozincite has not been identified.

During mining a large tailings pond was constructed in the South McQuesten valley (Fig. 2). Each spring, controlled addition of lime is still practised to control the amount of zinc released from the tailings pond. During the dry season, a prominent phenomenon is the formation of a widespread whitish coating on the exposed tailings. X-ray diffraction analysis indicates that gypsum is the major component of the coating but bianchite (an iron and zinc sulphate) is also common. Figure 7 shows the Zn and Cd profile in a breached tailings deposit below the last containment dam. The two elements are more concentrated towards the surface, regardless of the nature and redox conditions prevailing at various depths of the tailings deposit.

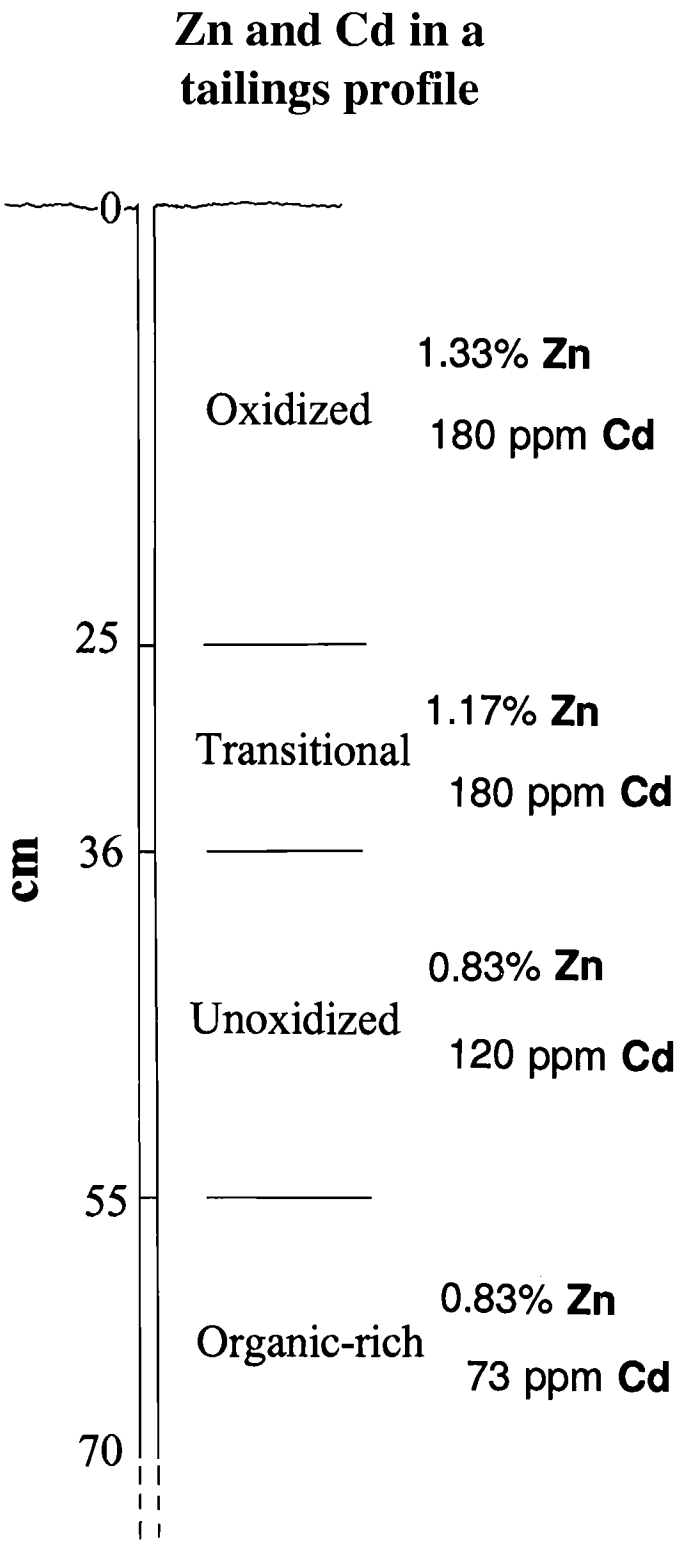

Figure 7. Variation of Zn and Cd content with depth in a tailings deposit at Elsa, Yukon.

Sequential extraction analyses on sediments

Sequential extraction analyses on sediments are used to assess trace element mobility in the surface environment. In the Keno Hill mining district, ore mineralization contains varying amounts of Pb, Ag, Zn, Cd, Cu, As and Sb. The generally low levels of Ag and Sb in soils and sediments in the area preclude accurate determination of these elements in the sequential extraction procedure and they are not analyzed.

Figure 8 depicts the partition of Cd, Zn, Pb, Cu and As among five major components of the sampled sediments. The diagram is constructed by averaging the results of sequential extraction analyses performed on 9 individual sediments collected at different sites. Over 40% of Cd occurs as exchangeable ions loosely adsorbed onto sediment particles. It can readily be remobilized upon subtle changes in pore fluid composition. The majority of Zn is associated with the carbonate (about 42%) and iron plus manganese oxide (about 30%) fractions. This agrees with the mineralogy and chemical analyses of secondary precipitates found along the Onek drainage. Zn associated with carbonates can readily be remobilized under even mildly acidic conditions. The bulk of Pb (60%) found in the sediments is strongly sorbed onto iron and manganese oxides. It can be removed upon destruction of the oxides under highly reducing conditions or in a highly acidic environment (e.g., pH <3 for the dissolution of ferric hydroxide).

Organic material in the sediments plays a significant role in attenuating aqueous transport of Cu in the region. Given the extreme climatic conditions of the mining district (especially in the presence of discontinuous permafrost), organic matter in the sediments is not easily oxidized to release the bound Cu. As shown in Figure 8, a great proportion of Cu (30%) is also associated with the residual fraction. The detailed form of Cu in this fraction is unknown but it can be remobilized only by a strong acid leach, which does not occur in a natural environment. Most of the As in the sediments (65%) is also associated with the residual fraction. As noted by Kwong and Whitley (1992), As is strongly sorbed onto precipitating ferric hydroxide on stream beds or banks. Mineralogical transformation subsequently renders the As immobile as a stable ferric arsenate.

DISCUSSION

The problem of acidic drainage and aqueous transport of metals that may adversely affect the local ecosystem is often confronted during the closing of extensively worked mining districts. Although mines are no longer operating in the Keno Hill mining district, sporadic exploration for new deposits and remediation of contaminated mine discharges continues. Both endeavours can benefit from a better understanding of water-rock/mineral interaction occurring in the area. The water chemistry data here presented clearly indicate that discharge from old mine workings contains elevated concentrations of trace metals, especially Zn and Cd, but acidic drainage occurs only locally. Moreover, aqueous transport of metal contaminants are apparently attenuated along some streams (e.g., Fig. 4, 5). In this section we briefly

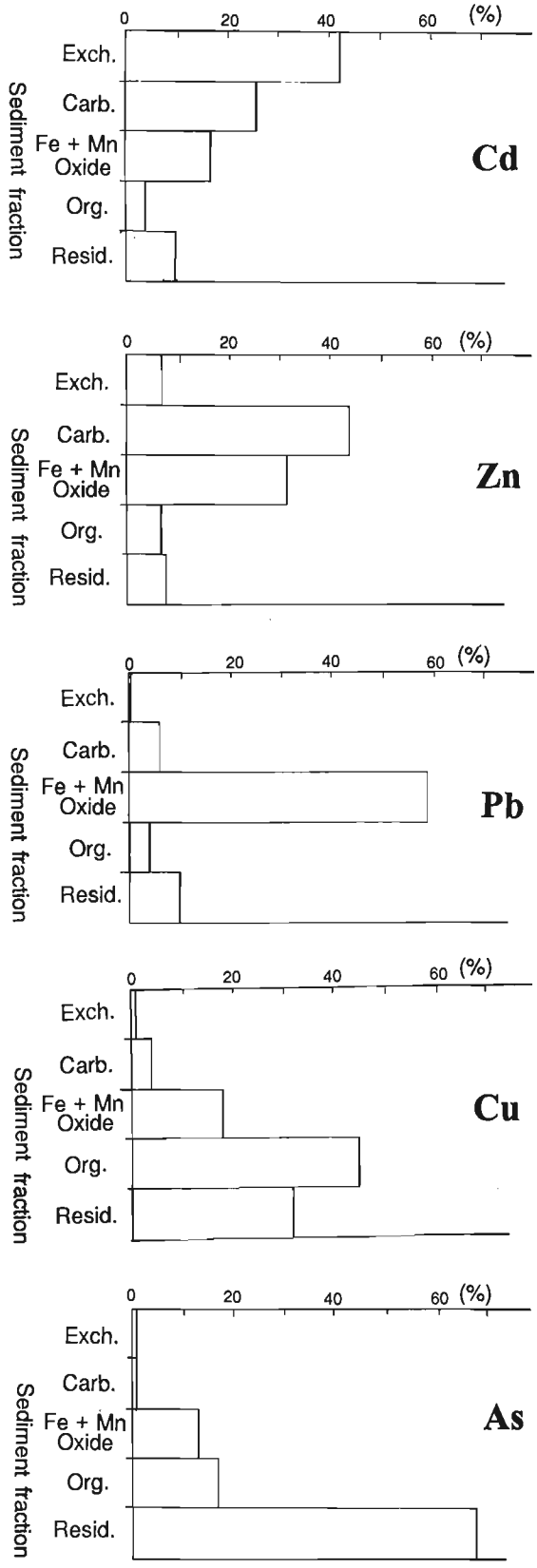

Figure 8. Partition of Cd, Zn, Pb, Cu and As in five fractions of a sediment as revealed by sequential extraction analysis.

discuss the apparent metal transport and attenuation mechanisms, as well as reasons for limited acid rock drainage occurrences and lithological controls of water chemistry.

Metal transport and attenuation mechanisms

The water chemistry data, especially dissolved sulphate concentrations, indicate that mere dilution is not significant in attenuating metal transport in small streams like the Onek drainage and No Cash Creek. However, the seasonal differences in metal concentrations in mine discharges and receiving streams suggest the formation of soluble secondary minerals during the dry season (including winter) as temporary storage of trace metals. The identification of hydrozincite along the Onek drainage attests to the plausibility of such a temporary metal attenuation mechanism. The formation of hydrozincite through cryogenic precipitation is described below.

Microbial growth is unhindered in small streams like the Onek drainage that flow from early summer through fall. Dissolved metals like Zn are sorbed onto the body walls of bacteria which form a microbial mat on organic litter lying on the stream bed. With the onset of winter, progressive freezing results in increasingly concentrated dissolved constituents in the stream water. Metal ions already sorbed onto the microbial mat provide convenient sites of initial nucleation once the solubility product of a secondary mineral like hydrozincite is exceeded. The precipitation of these secondary minerals may also lead to coprecipitation of other metals. For example, the geochemical behaviour of Cd is very similar to that of Zn. Thus, precipitation of hydrozincite will certainly result in coprecipitation of Cd. Results of sequential extraction analyses are compatible with coprecipitation because about 22% of Cd in the sediments is associated with the carbonate fraction (Fig. 8). However, hydrozincite formed by cryogenic precipitation is likely to redissolve during freshet unless it is rapidly buried by new sediment. This accounts for the peaking of Zn and Cd concentrations at shallow depth in the Onek sediment core (Fig. 4).

Ferrous ion sorbed onto sediments along the stream bed will undergo oxidation to precipitate ferric hydroxide, especially under open water conditions. Extensive iron oxide coatings (presumably ferric hydroxide) occur along the Onek drainage and No Cash Creek. Based on the results of sequential extraction analyses, iron oxide is an efficient scavenger for all five trace metals investigated. Thus sorption onto precipitating ferric hydroxide is an important metal attenuation mechanism operative in these small streams. Once these small streams drain into larger tributaries (like the South McQuesten River), dilution will inevitably become more significant. In these larger water courses, a greater volume of water is involved and efflorescent minerals cannot form.

In the tailings pond, large amounts of metal-rich sediments are deposited and an unsaturated condition prevails for at least part of the year due to high evaporation rates. Here, translocation processes are apparently operative to redistribute mobile metals. These are exemplified by the deposition of gypsum and bianchite on the surface of the United Keno Hill mine tailings. In summer when the evaporation rate is high, water lost from the surface of the tailings deposit is continuously replenished by water from the saturated zone through capillary action. On its upward journey the replenishing water carries with it dissolved constituents including Ca, Fe, Zn, Cd and sulphate. The latter precipitate as secondary sulphate minerals at or near the surface as water is evaporated, which accounts for the concentration of Zn and Cd towards the surface (Fig. 5).

Reasons for limited acid rock drainage occurrences

Although sulphide minerals abound in numerous old mine workings and waste rock dumps in the mining district, acid rock drainage rarely fully develops. For instance, at the oxidized Rio Plata prospect, copiapite (an efflorescent iron sulphate hydrate stable only under acidic conditions) has formed locally on siliceous phyllite enriched in fine grained pyrite. Water in a pond 5 m from the outcrop has a pH of 7.3 and is highly enriched in Zn, Cd and sulphate (Table 2). High dissolved metals and sulphate indicate sulphide oxidation but acidic drainage is not effected. We suggest two probable causes below.

First, any acidic drainage generated locally by sulphide oxidation is neutralized in the immediate vicinity by carbonate minerals. This is supported by the widespread occurrence of carbonate in Keno Hill quartzite and Earn Group rocks, as well as high net neutralization potential of many non-mineralized samples (Table 1).

Second, in the Keno Hill mining district galena and sphalerite commonly accompany pyrite. In the weathering of a sulphide mineral assemblage, the sulphide with a higher electrode potential is galvanically protected from oxidative dissolution while weathering of the mineral with a lower electrode potential is enhanced (Sato, 1992; Kwong, 1993b). Among pyrite, galena and sphalerite, pyrite has the highest and sphalerite the lowest electrode potential (Sato, 1992). When these minerals are in contact with each other, sphalerite will be preferentially weathered while oxidative dissolution of pyrite will not occur until all the sphalerite and galena have disappeared. With a metal-to-sulphur ratio of 1:1, however, the oxidative dissolution of either galena or sphalerite will not generate acid (Kwong, 1993a). The onset of acid drainage is therefore delayed. The galvanic weathering process readily explains the near-neutral pH and high dissolved metal and sulphate concentrations in the ponded water at Rio Plata. It is also supported by two other field observations: 1) acidic drainage is present at the toe of the Ruby mine waste rock dump in early summer which consists of siliceous phyllite with abundant pyrite and no carbonate or sphalerite; and 2) the low grade ore stockpile at the Husky SW Mine contains melanterite, which coats fine grained bands of pyrite. Like copiapite, melanterite is indicative of an acidic environment. In this rock sphalerite and galena are rare and not associated with pyrite. The stockpile has been exposed to the atmosphere for about four years. The appearance of melanterite in such a short period indicates that the pyrite is highly reactive.

The possible delay in occurrence of acid rock drainage resulting from galvanic protection of pyrite from oxidative dissolution has important implications to the remediation of

old mine workings in the mining district. To avoid intensive leaching of trace metals presently concentrated in shallow sediments by acidic drainage, highly reactive rocks with little buffering capacity should be identified and properly disposed prior to potential onset of intense acid generation.

Lithological control of water chemistry

Largely dictated by the local climate (northern continental with discontinuous permafrost), the rate of silicate weathering is extremely slow. Water chemistry is thus dominated by carbonate equilibria, which is reflected in pH values of >7 in most water courses draining the district. Although calcite is a minor constituent of all rock units, only a small amount of calcite or dolomite is required to effect carbonate equilibria in surface and ground waters in a cold region (Freeze and Cherry, 1979). It is therefore not surprising to find a lack of correlation between water chemistry and specific rock units in the study area. In portions of a drainage system that receive discharge from old mine workings, the pH of the water is frequently lower than a value of about 8, which is characteristic of carbonate equilibria. This probably reflects consumption of carbonate alkalinity by reacting sulphides. The oxidation of sulphides also produces dissolved metals and sulphate, which increase the electrical conductivity of the water and may affect its redox potential. Using subtle differences in field pH, Eh and conductivity along water courses can expedite the search for more mineralization in poorly exposed areas in the mining district. Once an area of interest is identified, however, sediment geochemistry is likely a better tool to locate potential ore. Based on the sequential extraction results, Zn and Cd are highly mobile along water courses in the district; their presence in a sediment sample does not necessarily indicate a nearby source. In contrast, Pb, Cu and As are less likely to be transported far from their source area and would serve better as pathfinders towards silver mineralization.

CONCLUSIONS

Based upon field observations and the results of an array of water, rock and sediment analyses, we conclude that:

1. Discharge from many old mine workings contain elevated concentrations of dissolved metals, especially Zn and sometimes Cd. Metal loadings are especially high during freshet resulting from dissolution of efflorescent minerals formed during the dry seasons including winter.
2. Prominent metal attenuation mechanisms operative in small streams include cryogenic precipitation, coprecipitation, sorption and rarely dilution.
3. Despite evidence of active sulphide oxidation, acid mine drainage is not widespread (yet) due to neutralization by carbonates in the country rock and galvanic protection of pyrite from oxidative dissolution.
4. Largely affected by the local climate, water chemistry in non-mineralized areas is dominated by carbonate equilibria and show little relationship with lithochemistry.
5. Because Cu, Pb and As are less mobile than Zn and Cd, the former are better pathfinders for blind silver mineralization.

To protect a healthy ecosystem in the district, further work is required to quantify field sulphide oxidation rates so as to facilitate timely disposal of reactive mine waste and prevent a potential onset of intense acid generation and metal leaching.

ACKNOWLEDGMENTS

This study is jointly funded by the National Hydrology Research Institute, the Cordilleran Division of the Geological Survey of Canada and the Water Resources Division of the Northern Affairs Program, Whitehorse. We are grateful to our respective management for their support of the collaborative project. Victor Enns of the Environmental Protection Service, Whitehorse kindly provided background information on environmental monitoring in the area and Diane Brent of the Canada-Yukon Geoscience Office ably assisted with rock sampling.

REFERENCES

Boyle, R.W.
1965: Geology, geochemistry and origin of the lead-zinc-silver deposits of the Keno Hill-Galena Hill area, Yukon Territory; Geological Survey of Canada, Bulletin 111.

Freeze, R.A. and Cherry, J.A.
1979: Groundwater; Prentice-Hall, Englewood Cliffs, New Jersey.

Green, L.H.
1971: Geology of Mayo Lake, Scougale Creek and McQuesten Lake map areas, Yukon Territory; Geological Survey of Canada, Memoir 357.
1972: Dawson, Larsen Creek and Nash Creek map areas, Yukon Territory; Geological Survey of Canada, Memoir 364.

Hughes, O.L.
1982: Surficial geology and geomorphology, Janet Lake; Geological Survey of Canada, Map 4-1982.

Kindle, E.D.
1962: Geology, Keno Hill, Yukon Territory; Geological Survey of Canada, Map 1105A.

Kwong, Y.T.J.
1993a: Minesite acid rock drainage assessment and prevention - a new challenge for a mining geologist; in International Mining Geology Conference Kalgoorlie WA, 5-8 July 1993; The Australasian Institute of Mining and Metallurgy Publication Series No. 5/93, p. 213-217.
1993b: Prediction and prevention of acid rock drainage from a geological and mineralogical perspective; Canada Centre for Mineral and Energy Technology, MEND Report 1.32.1.

Kwong, Y.T.J. and Whitley, W.G.
1993: Heavy metal attenuation in northern drainage systems; in Proceedings, 9th International Northern Research Basin Symposium/Workshop, Canada, 1992; National Hydrology Research Institute Symposium No. 10, p. 305-322.

McTaggart, K.C.
1960: The geology of Keno and Galena hills, Yukon Territory (105M); Geological Survey of Canada, Bulletin 58.

Roots, C.F. and Murphy, D.C.
1992: New developments in the geology of Mayo map area, Yukon Territory; in Current Research, Part A; Geological Survey of Canada, Paper 92-1A, p. 163-171.

Sato, M.
1992: Persistency-field Eh-pH diagrams for sulphides and their application to supergene oxidation and enrichment of sulphide orebodies; Geochimica et Cosmochimica Acta, v. 56, p. 1202-1231.

Geological Survey of Canada Project 900035

Upper Triassic to Middle Jurassic biostratigraphic and facies studies in the Iskut River map area, northwestern British Columbia

G.K. Jakobs and J. Pálfy[1]
Cordilleran Division, Vancouver

Jakobs, G.K. and Pálfy, J., 1994: Upper Triassic to Middle Jurassic biostratigraphic and facies studies in the Iskut River map area, northwestern British Columbia; in Current Research 1994-E; Geological Survey of Canada, p. 17-28.

Abstract: New ammonite and other macrofossil collections improve or confirm the biostratigraphy of Norian, possible Rhaetian, uppermost Hettangian to lowermost Sinemurian, Upper Pliensbachian, upper Aalenian, Lower Bajocian, Upper Bathonian, and Lower Callovian strata in the Iskut River map area (104B). Sedimentary facies within the Hazelton Group record diverse and laterally variable depositional environments controlled by their tectonic setting and relation to volcanic sources. Oolitic limestone in the Jack formation and laminated algal limestone in the Betty Creek Formation are locally significant. The basal member (bioclastic unit) of the Salmon River Formation, which overlies felsic volcanic strata, is interpreted as a transgressive lag deposit that is laterally extensive. In the Treaty Ridge section two bioclastic units overlie felsic pyroclastic rocks. The lower unit is probably Toarcian in age and the upper is Early Bajocian, but their biostratigraphic correlation with the similar successions east of the Bowser River is ambiguous.

Résumé : De nouvelles collections d'ammonites et d'autres macrofossiles sont venues améliorer ou confirmer la biostratigraphie des strates du Norien, peut-être du Rhétien, de l'intervalle Hettangien sommital-Sinémurien basal, du Pliensbachien supérieur, de l'Aalénien supérieur, du Bajocien inférieur, du Bathonien supérieur et du Callovien inférieur dans la région cartographique de la rivière Iskut (104B). Les faciès sédimentaires à l'intérieur du Groupe de Hazelton représentent des milieux de sédimentation divers et latéralement variables, contrôlés par leur environnement tectonique et par leur relation avec les sources volcaniques. Un calcaire oolitique dans la formation de Jack et un calcaire algaire laminé dans la Formation de Betty Creek sont localement importants. Le membre basal (unité bioclastique) de la Formation de Salmon River, qui recouvre des strates volcaniques felsiques, est interprété comme un résidu de déflation transgressif de grande étendue latérale. Dans la section du massif Treaty, deux unités bioclastiques reposent sur des roches pyroclastiques felsiques. La plus basse date probablement du Toarcien, et l'autre du Bajocien précoce, mais leur relation biostratigraphique avec les successions semblables observées à l'est de la rivière Bowser est ambiguë.

[1] Department of Geological Sciences, University of British Columbia, 6339 Stores Road, Vancouver, British Columbia V6T 1Z4

INTRODUCTION

During the 1993 field season several Jurassic sections were examined in the eastern part of the Iskut River map area (Fig. 1, 2) to augment the biostratigraphic database from the area and to document various sedimentary facies and their lateral variations which bear upon the reconstruction of paleoenvironments and paleogeography. New and recollected fossil localities from these stratigraphic sections are presented to illustrate the vertical distribution of ammonoids and other macrofauna. Our observations and discussions follow the stratigraphic framework of Anderson (1993).

Isotopic dating of intercalated volcanic rocks in biochronologically well-constrained intervals will help better calibrate the Jurassic numerical time scale. Paleomagnetic studies on Triassic and Jurassic rocks by C. Palmer and M. Gala (University of Western Ontario) also benefit from this improved chronostratigraphic framework.

STUHINI GROUP

Although this study focuses on the Jurassic system of the area, the age range of the Upper Triassic Stuhini Group is important in assessing the duration of the hiatus separating it from the overlying Lower and Middle Jurassic Hazelton Group. Stuhini Group sedimentary rocks have previously been known to range from the Carnian to the Norian. Collections of *Monotis* suggested the presence of the Cordilleranus Zone of Tozer (1979), whereas ammonoids collected from still higher levels indicated the undivided Amoenum/Crickmayi zones (Nadaraju, 1993).

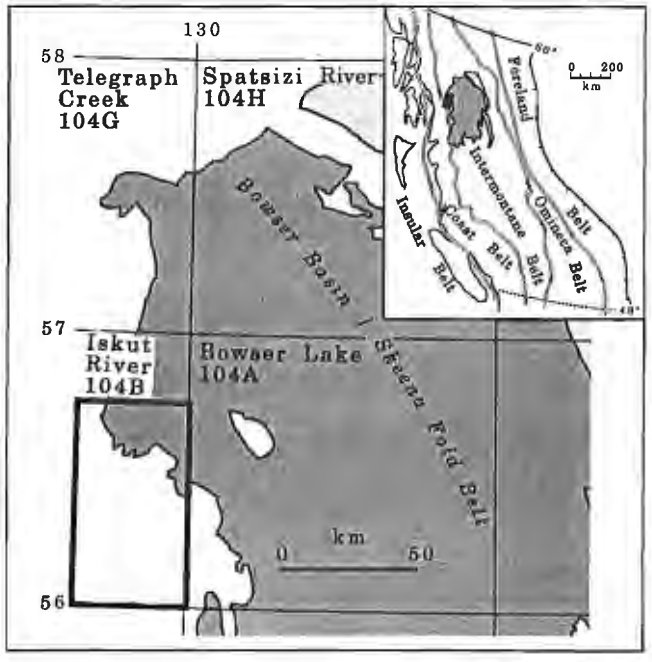

Figure 1. *Location of the Iskut River (104B) map area in northwestern British Columbia showing distribution of Sustut (light pattern) and Bowser (dark pattern) basins.*

Monotis beds to the north of the Forest Kerr Creek area (GSC Loc. No. C-201504) have, for the first time, yielded *Heterastridium conglobatum* (Pl. 1, fig. 1). This hydrozoan is restricted to the Norian but occurs at numerous localities world-wide, in many cases together with *Monotis* (Campbell, 1974). In North America, it has previously only been recorded from the Wrangell Mountains in Alaska (Silberling and Tozer, 1968) and the Queen Charlotte Islands (Carter et al., 1989).

A thick sequence (several hundred metres) of Stuhini Group strata occurs west of Atkins Glacier (Fig. 2). The uppermost part of the succession underlies Atkins ridge. A few tens of metres below the contact with the Hazelton Group (GSC Loc. No. C-210856), a brownish greywacke yielded a specimen of *Choristoceras*? sp. (Pl. 1, fig. 2). The identification is tentative, inasmuch as the crushed external mould does not allow the full characterization of the venter, where the interruption of ribs would serve as a basis of distinction from the related genus *Peripleurites*. If our specimen is *Choristoceras*, it would unequivocally indicate the presence of the latest Triassic Crickmayi Zone, and the youngest Triassic strata from Stikinia. *Peripleurites*, on the other hand, is known in British Columbia from the underlying Cordilleranus and Amoenum zones.

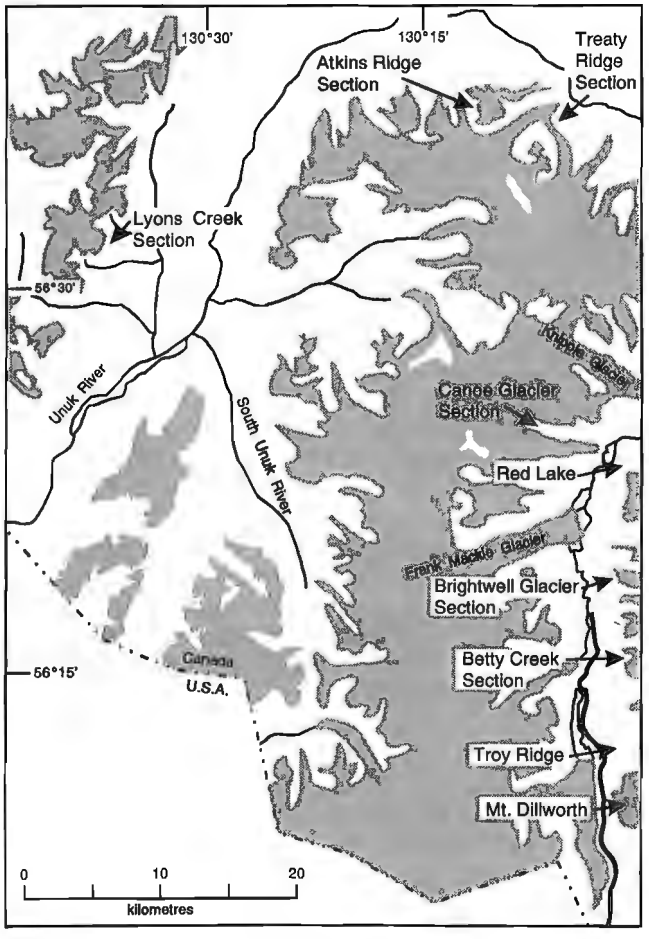

Figure 2. *Location of study areas in the Iskut River (104B) map area.*

JACK FORMATION

The Jack formation *sensu* Henderson et al. (1992) is the basal unit of the Hazelton Group separated from the Stuhini Group by an unconformity exposed along the northern and northwestern limbs of the McTagg anticlinorium. Our observations are restricted to a single but richly fossiliferous section exposed on Atkins ridge (Fig. 3, 4). A minor angular unconformity and a basal conglomerate were also noted here. The bulk of the Jack formation comprises buff weathering, fossiliferous calcareous sandstone. A 3-4 m thick limestone unit occurs near the top of the formation and contains abundant bivalves at its base. It appears to be a well-sorted oolitic grainstone with sparry calcite cement. Deposition may have occurred in a short-lived oolite shoal with further shell enrichment and winnowing enhanced by storm activity.

Some layers of the calcareous sandstone are rich in limy concretions which yielded a well-preserved ammonoid fauna (Fig. 4). The entire assemblage is characteristic to the Canadensis Zone which is thought to straddle the Hettangian/Sinemurian boundary (Pálfy et al., in press). In addition to the ammonoids, a diverse assemblage of other macroinvertebrates was also recovered (GSC Loc. No. C-210857, C-210859) and is listed below (bivalve identifications by M. Aberhan, pers. comm., 1994):

Gastropods:	*Ptychomphalus* sp.
	Neritopsis sp.
	Pleurotomariacea gen. et sp. indet.
	Amberleyidae gen. et sp. indet.
	Nerinacea? gen. et sp. indet.
Bivalves:	*Weyla (Lywea)* sp.
	Chlamys sp.
	Bakevellia sp.
	Pholadomya sp.
	Pleuromya sp.
	Antiquilima? sp.
	"Cardinia" sp.
Corals:	*Isastrea?* sp.
	indeterminate solitary scleractinian coral

BETTY CREEK FORMATION

At Lyons Creek (Fig. 2, 5) a thick succession of silicified, laminated algal-microbial limestone is present (Fig. 6) indicative of a peritidal environment and the absence of a terrigenous volcanogenic sediment supply. Besides the common stromatolitic lithotype (Fig. 7), brecciated horizons with storm-generated rip-up clasts of semi-lithified limestone (Fig. 8), and oncoidal limestone layers also occur (Fig. 9). The primary algal structures are obliterated by recrystallization and pervasive fibrous calcite cement growth. Cyclical carbonate sedimentation may record sealevel oscillations during a period of subdued local tectonic activity. The Betty Creek Formation at Troy Ridge and Betty Creek (Fig. 2) includes an algal limestone of variable thickness that, compared with the Lyons Creek locality, is much thinner (40 m) and interbedded with fluvial epiclastic sandstone and siltstone (Fig. 10), and suggests deposition near the mouth of a paleoriver. If correlative, these limestone facies changes indicate a paleogeography with subdued relief.

The limestones at Lyons Creek, Troy Ridge, and Betty Creek have not yielded any age-diagnostic fossils. Microfossil collections were made and are currently being processed. The contact with the overlying dark mudrocks at Lyons Creek is gradational, with no indication of disconformity, and we therefore favour the assignment of this package to the Betty Creek Formation rather than the Triassic as suggested by Alldrick et al. (1989).

The algal limestone at Lyons Creek is conformably overlain by a sequence of black to dark-grey weathering siltstone containing occasional fine- to medium-grained sandstone layers and rare tuffaceous intervals. Load casts and cross-lamination were occasionally observed in the sandier layers. The siltstones are fractured and cleaved and commonly cut

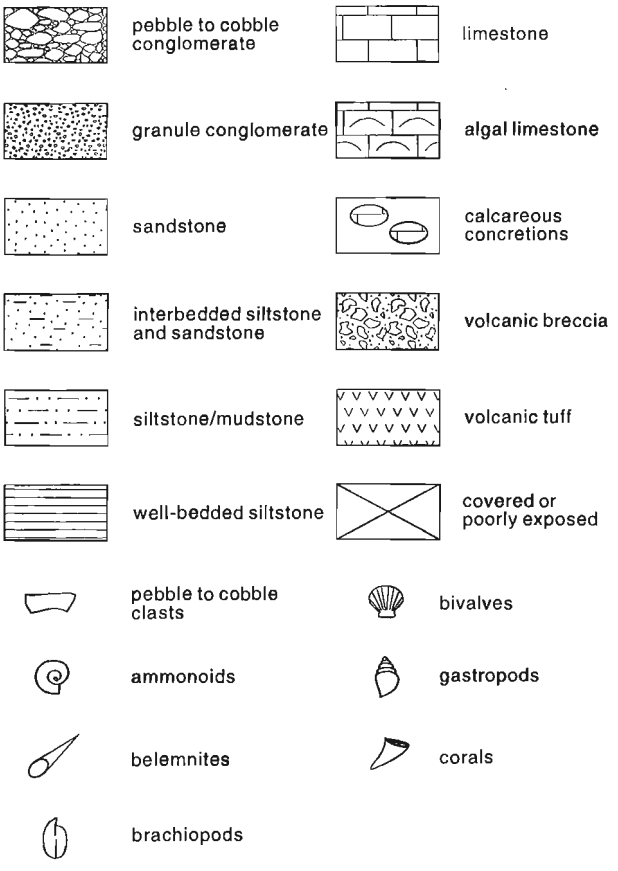

Figure 3. Legend for Figures 4, 5, 11, 13, 14.

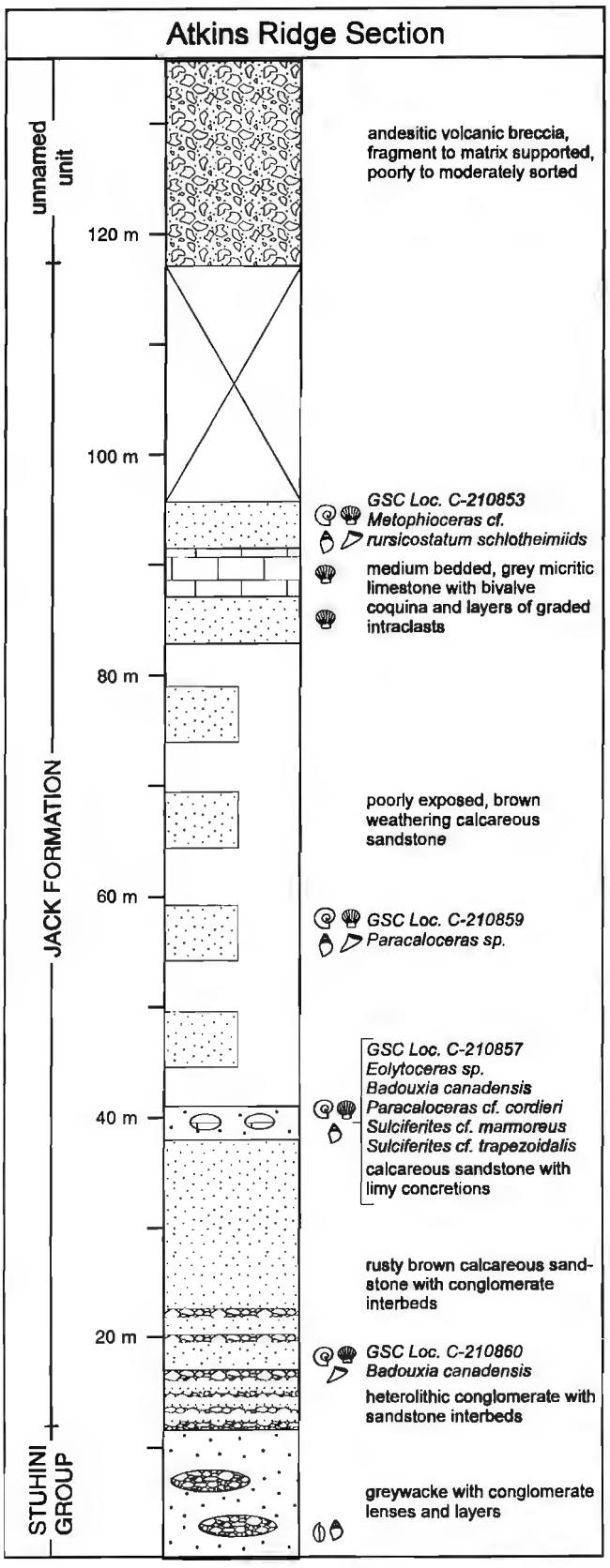

Figure 4. Lithostratigraphy and biostratigraphy of the Atkins ridge section. See Figure 3 for legend.

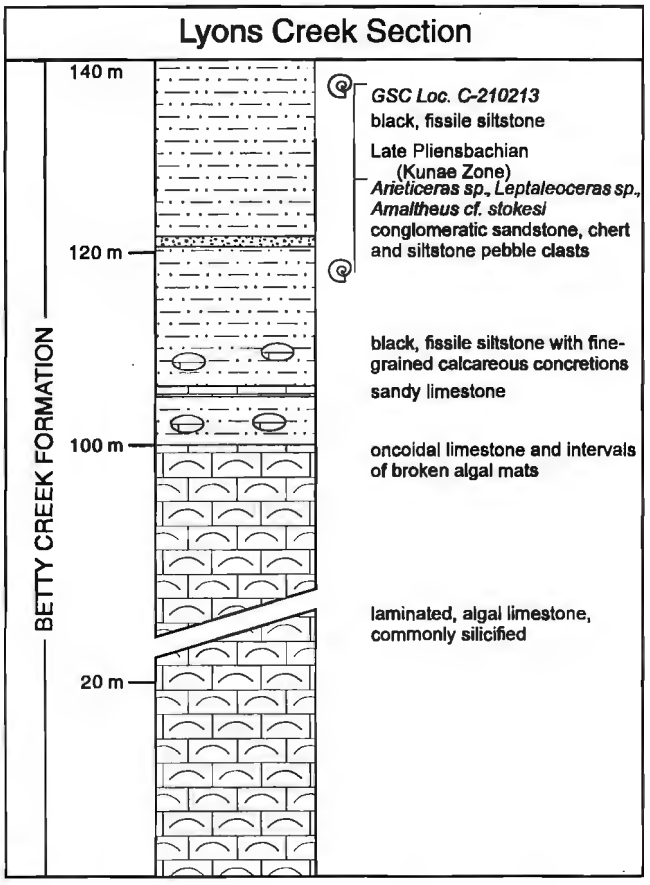

Figure 5. Lithostratigraphy and biostratigraphy of the Lyons Creek section. See Figure 3 for legend.

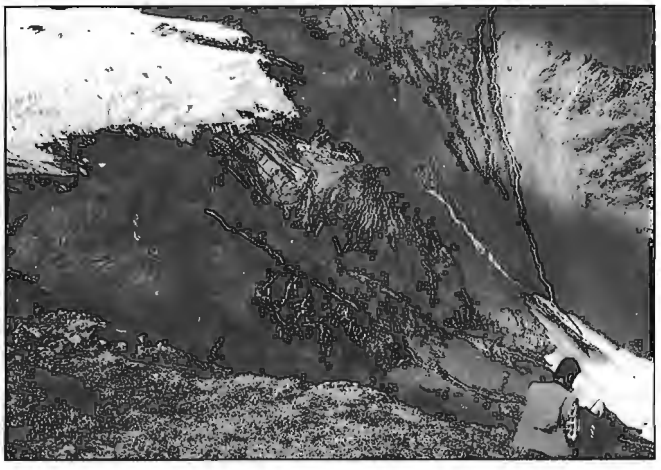

Figure 6. View of well-bedded algal limestone section in the Betty Creek Formation at the headwaters of Lyons Creek.

by buff to light green weathering dykes. Calcareous concretions are locally present, particularly near the base of the siltstones and were collected for microfossils.

Poorly preserved ammonite fragments are common in the siltstones and include: *Arieticeras* spp., *Leptaleoceras* spp., and *Amaltheus stokesi* (Pl. 1, fig. 8, 9) from the Late Pliensbachian Kunae Zone (Smith and Carter, 1990).

SALMON RIVER FORMATION

Lower part (Bioclastic unit)

The basal member of the Salmon River Formation is a fossiliferous, calcareous sandstone unit that has been recognized over much of the eastern half of the Iskut River map area. It has been previously dated as Toarcian based on the reported co-occurrence of doubly grooved belemnites and *Weyla*. Dicoelitid belemnites are Toarcian to Kimmeridgian in age (Jeletzky, 1980), whereas *Weyla* is restricted to the Early Jurassic in North America (Damborenea and Manceñido, 1979). The co-occurrence of *Weyla* and doubly grooved belemnites has therefore been used as an indicator of the Toarcian (Nadaraju, 1993).

The bioclastic unit exposed from Mt. Dilworth to Red Lake is a buff to rusty weathering, medium grey, medium- to coarse-grained calcareous sandstone that commonly contains whitish to rusty weathering volcanic clasts (5-20 mm in length). At Troy Ridge, the thickness of the unit varies along strike (500 m) from 2 to 4 m and two fining upwards sequences were recognized, capped by a clast-rich, coarse sandstone. Fossils are common at Troy Ridge and include a diverse collection of solitary and colonial corals, high-spired gastropods, trigoniid bivalves, coarsely ribbed pectinid

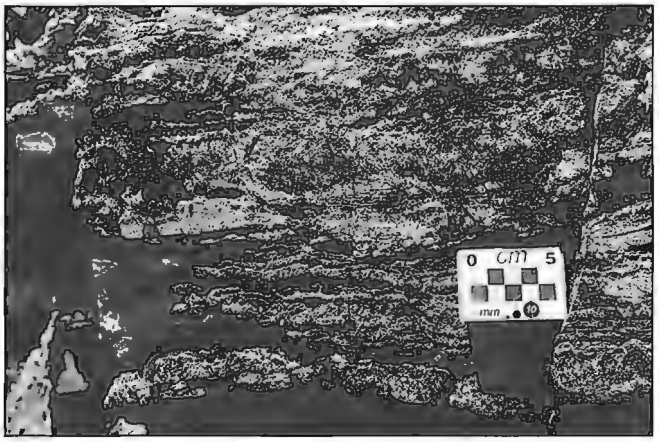

Figure 7. *Typical laminated algal limestone in the Betty Creek Formation, Lyons Creek.*

Figure 9. *Oncoidal lithofacies, limestone in the Betty Creek Formation, Lyons Creek.*

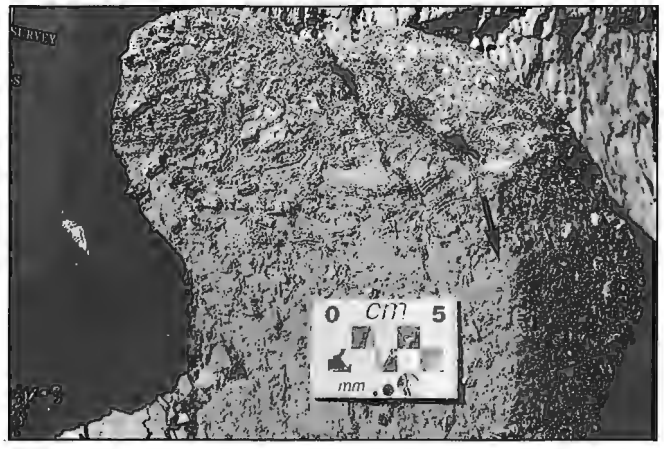

Figure 8. *Brecciated limestone with rip-up clasts of algal mats, Betty Creek Formation, Lyons Creek. Note grading of clasts, interpreted here as a storm-generated feature. Talus block, stratigraphic top is indicated by an arrow.*

Figure 10. *View of interbedded limestone and epiclastic fluvial sediments from the Betty Creek Formation, north of Betty Creek.*

bivalves, and singly grooved belemnites. The bioclastic unit at Troy Ridge is overlain by thinly bedded tuffaceous siltstones of the upper part of the Salmon River Formation.

The bioclastic unit exposed near Brightwell Glacier is almost identical to that at Troy Ridge, but is thinner (1 m) and contains only vertebrate fragments (Fig. 11).

At Red Lake the bioclastic unit is composed of a medium grey, fine- to coarse-grained sandstone and reaches about 2-3 m in thickness. The basal unit of the bioclastic unit is a coarse grained sandstone containing large (5 cm long) volcanic clasts. The bioclastic unit is overlain by the upper part of the Salmon River Formation, represented by thickly bedded (20-30 cm) siltstones, with rare tuff layers, that grade into more thinly bedded (5 cm) tuffaceous siltstones. Belemnites and bivalves are occasionally seen in the bioclastic unit.

A poorly exposed outcrop of the bioclastic unit at Canoe Glacier is similar to those described above and is composed of a rusty weathering, medium grey, coarse-grained sandstone that contains volcanic clasts (up to 10 mm in length).

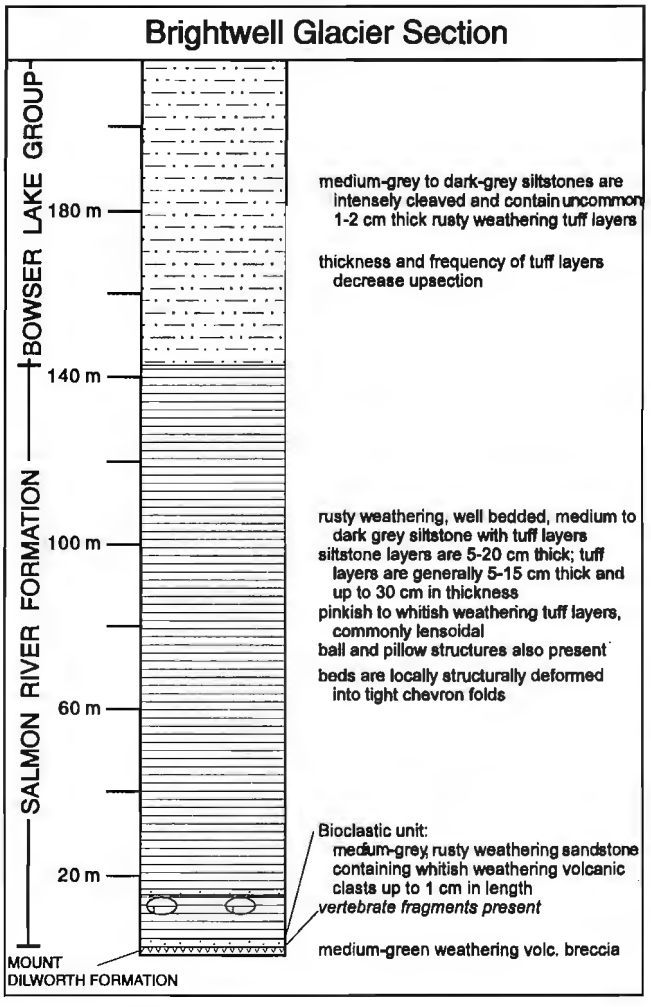

Figure 11. *Lithostratigraphic section measured along ridge to the south of Brightwell Glacier, see Figure 3 for legend.*

The unit is approximately 4 m thick and grades up into finer sandstone and siltstone. It is overlain by siltstones of the Salmon River Formation. Vertebrate fragments and belemnites are present.

The condensed beds from Troy Ridge to Canoe Glacier and Red Lake are interpreted as the result of onlap onto the erosional surface of the Mt. Dilworth Formation. The age of the bioclastic unit at these localities has not been unequivocally determined. Coarsely ribbed pectinid bivalves are too poorly preserved to identify with certainty.

At Treaty Ridge previous studies have identified two bioclastic units (units 2a and 5a of Lewis et al., 1993) that both overlie felsic volcanic strata (units 1b and 4b-c of Lewis et al., 1993). The lower bioclastic unit contains doubly grooved belemnites and coarsely ribbed pectinid bivalves and underlies well-dated dark mudstones and siltstones (unit 2d of Lewis et al., 1993) which yielded *Pseudolioceras* cf. *whiteavesi* (Pl. 1, fig. 10), *Tmetoceras* cf. *kirki* (Pl. 1, fig. 12), and *Leioceras*? sp. (Pl. 1, fig. 11), indicative of the Upper Aalenian. In the lower bioclastic unit thick-shelled bivalves are abundant in coquinoid layers and show diverse orientation (Fig. 12). Intraformational breccias and conglomerates, scour marks, and rip-up clasts also indicate reworking of sediment and downslope movement. Ferromanganese encrustation of clasts is conspicuous at some layers. The inferred depositional environment is a slope receiving gravity flows from shallow marine areas in a tectonically active area.

The upper bioclastic unit (above the upper felsic unit) is approximately 15 m thick and contains belemnites, bivalves, bryozoans, and gastropods. Some of the bivalves are coarsely ribbed and thick-shelled, thus they can be easily confused with *Weyla*. The oldest ammonites from the overlying rusty weathering shale (unit 5b of Lewis et al., 1993) include *Sonninia*? sp. (Pl. 1, fig. 14), followed upsection by *Stephanoceras*? sp. (Pl. 1, fig. 13). Fragments of large specimens of *Zemistephanus* also occur. This faunal succession suggests an Early Bajocian age, but zonal assignment is hampered by poor preservation of fossils which makes specific identifications difficult.

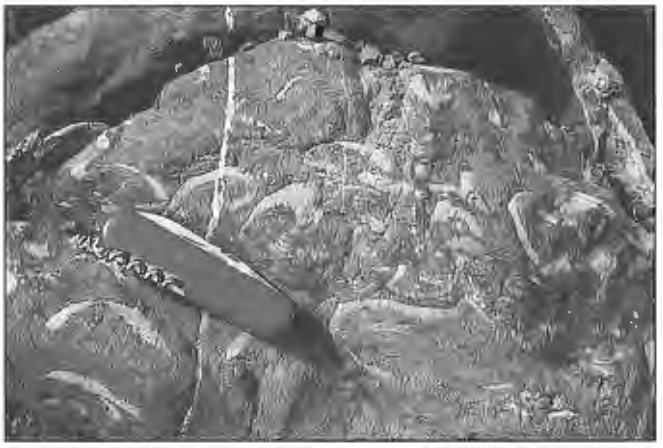

Figure 12. *Thick-shelled bivalves in the lower bioclastic unit at Treaty Ridge. Note poor sorting and variable orientation of bioclasts, interpreted to indicate sediment gravity flow origin.*

Stratigraphic evidence and the lack of precise paleontological constraints permit the bioclastic unit exposed at Troy Ridge and to the east of the Bowser River to be correlated with either the lower or the upper bioclastic sandstone units exposed at Treaty Ridge. Within the common facies succession of subaerial volcanics and local fluvial epiclastic sediments overlain by a transgressive marine sequence, the bioclastic units indicate nearshore, high-energy environment. For paleoecological and taphonomic reasons, thick-shelled, coarsely ribbed pectinid bivalves and belemnoids are the most common fossils in this facies. Both groups range throughout the Jurassic and a more precise age determination requires identification of genera. Ammonoids are rare or absent, as they have not been found in the basal member of the Salmon River Formation in its type area. Lithologically, the thin bioclastic unit exposed at Troy Ridge and to the east of the Bowser River is more similar to the upper bioclastic unit at Treaty Ridge, than it is to the 45 m thick lower bioclastic unit at Treaty Ridge. The base of the Salmon River Formation at Treaty Ridge may then be represented by the base of the upper bioclastic unit. The formational assignment of strata underlying the upper felsic unit, however, remains unclear.

Upper part

The upper part of the Salmon River Formation is represented by a sequence of thinly bedded, tuffaceous siltstones informally known as "pyjama beds", the Troy Ridge facies along the eastern edge of the map area, from Troy Ridge to Canoe Glacier (Fig. 11, 13).

The pyjama beds exposed from Troy Ridge to Canoe Glacier are typically rusty weathering, but the siltstone strata commonly weather medium to dark grey and the tuff layers weather whitish to pink. Siltstone strata are commonly 5-20 cm thick whereas the tuff layers are typically 5-15 cm thick but reach 30-40 cm in thickness. Bedding thicknesses vary throughout the sequence. Load casts are common at contacts between tuff and overlying siltstone, and other sedimentary structures such as normally graded bedding, small scale slump features, sole marks, and ripples are also present. Tuff layers commonly pinch out along strike. Upsection, tuff layers become thinner and less frequent and the sequence grades into the overlying Bowser Lake Group. Calcareous concretions are generally rare, except at Red Lake. The pyjama beds commonly display tight chevron folds and are generally fractured perpendicular to bedding. Trace fossils were observed on bedding surfaces at Red Lake. Fossils, such as belemnoids, are rare and not well preserved.

BOWSER LAKE GROUP

Bowser Lake Group strata were examined from Mt. Dilworth to Canoe Glacier. Siltstones of the lower Bowser Lake Group are most common and overlain by a thick, coarser interval of interbedded siltstone, sandstone, and conglomerate.

Lower Bowser Lake Group conformably overlies thinly bedded, tuffaceous siltstones of the Salmon River Formation. The contact is generally gradational, marked by a decrease in the frequency and thickness of tuffaceous layers. The lower siltstones are commonly intensely cleaved at a high angle to bedding and generally do not yield well-preserved fossils. Late Bathonian to Early Callovian ammonites, represented by *Iniskinites* (Pl. 1, fig. 16) and *Lilloettia* (Pl. 1, fig. 15), were collected from the lower siltstones and shales in the Canoe Glacier and Treaty Ridge sections (Nadaraju, 1993).

The upper, coarser interval of the Bowser Lake Group occurs at Mt. Dilworth, Troy Ridge, and Canoe Glacier. At Mt. Dilworth, a massive, buff to rusty weathering, medium grey, medium- to coarse-grained sandstone is interbedded with siltstone and conglomerate. The siltstone or mudstone

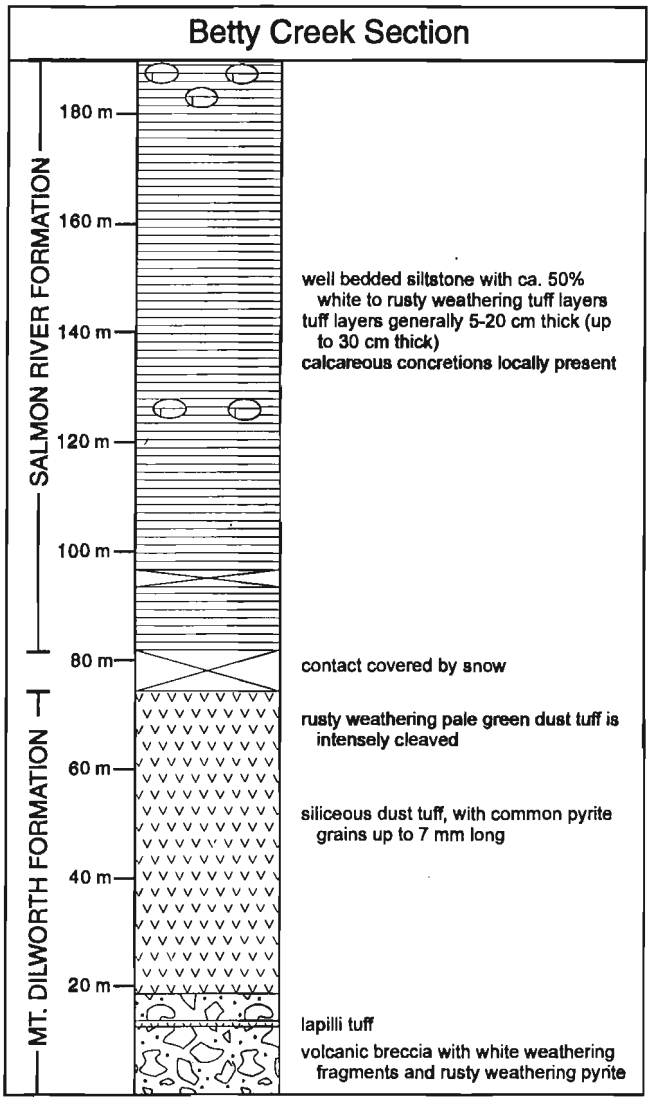

Figure 13. *Lithostratigraphic section measured along the ridge to the north of Betty Creek, see Figure 3 for legend.*

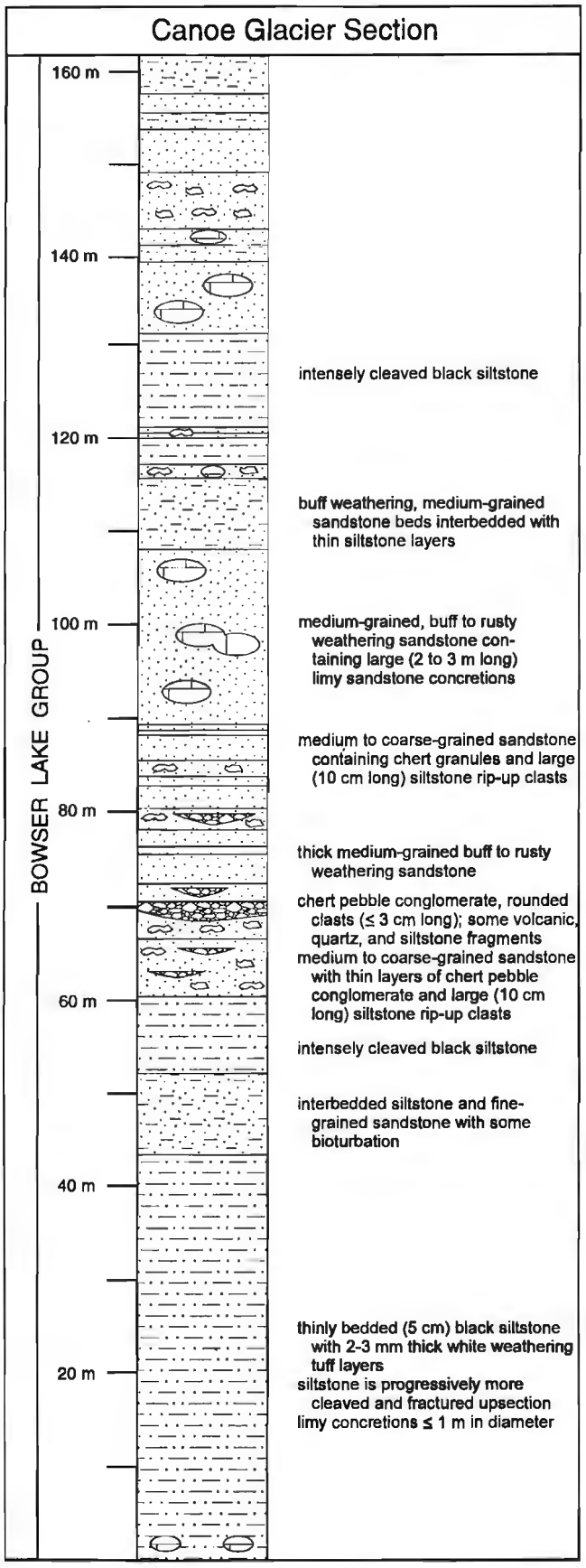

Figure 14. *Lithostratigraphic section measured along the ridge flank to the north of Canoe Glacier, see Figure 3 for legend.*

layers are thin (about 20 cm). The poorly sorted, chert, pebble to cobble conglomerate contains subrounded black siltstone clasts.

At Troy Ridge, the upper Bowser Lake Group is well exposed and is composed of a sequence of interbedded siltstone, sandstone, and chert pebble conglomerate. Large black siltstone rip-up clasts (up to 30 cm long) are common in the coarser intervals. Load casts, crossbedding, and fining upwards sequences are common in the sandstone members.

A thick sequence of the Salmon River Formation and Bowser Lake Group is exposed along the northern flank of Canoe Glacier (Fig. 14). Cleaved siltstone of the lower Bowser Lake Group are overlain by an upper succession of interbedded siltstone and sandstone containing lenses of conglomerate and large, calcareous, sandstone concretions. The base of the upper succession (60 m to 80 m above base of section) is represented by a buff-weathering, medium- to very coarse-grained sandstone that is interbedded with thin siltstone laminae and commonly contains large (50 mm long) siltstone rip-up clasts (Fig. 15). Lens-shaped channel-fill deposits within the sandstone are represented by a rounded, clast-supported, chert pebble conglomerate which is inversely to normally graded. About 80 m from its base the sequence comprises interbedded siltstone and sandstone containing large (2-3 m long, 1 m thick) calcareous sandstone concretions. The concretions are buff to rusty weathering and commonly join to form larger pods. The buff weathering, medium green medium- to coarse-grained sandstone is commonly massive, although thinly bedded sandstone to siltstone

Figure 15. *Large siltstone rip-up clasts contained in a matrix-supported chert pebble conglomerate, Bowser Lake Group, Canoe Glacier section.*

intervals are also present. Large (up to 1 m long) siltstone rip-up clasts are common and chert pebbles are also present in some layers. The presence of the siltstone clasts and inversely to normally graded channel conglomerates in the lower part of the coarse sequence, suggests deposition in a high energy environment, probably on an upper fan. The upper part of the sequence, which comprises interbedded siltstones and massive sandstones, were probably deposited on the mid-fan.

CONCLUSIONS

A single specimen of *Choristoceras*? sp. recovered from the uppermost part of the Stuhini Group suggests that deposition of this unit persisted to the latest Triassic. The unconformably overlying Jack formation at Atkins ridge yielded a rich fauna from the uppermost Hettangian–lowermost Sinemurian. The hiatus between the Stuhini and Hazelton groups, which represents a regionally important tectonic event, thus approximately corresponds to the Hettangian time. The Betty Creek Formation is generally unfossiliferous. An algal limestone unit is interbedded with fluvial epiclastic sediments at Betty Creek and Troy Ridge and, at Lyons Creek, a thick limestone sequence is conformably overlain by Upper Pliensbachian mudstones. The occurrence of peritidal carbonates is important for paleogeographic reconstructions. The bioclastic unit of the basal Salmon River Formation has not yielded age-diagnostic fossils in its type area. At Treaty Ridge, where biostratigraphy is better understood, a lower bioclastic unit is probably Toarcian in age, an upper bioclastic unit is Early Bajocian in age. Biostratigraphic correlation between the two bioclastic units at Treaty Ridge and the basal member of the Salmon River Formation in its type area is unresolved. The thinly bedded "pyjama beds" of the upper part of the Salmon River Formation (Troy Ridge facies) have not yielded any age-diagnostic fossils. Siltstones of the basal Bowser Lake Group at Canoe Glacier are Late Bathonian to Early Callovian in age and contain *Iniskinites* and *Lilloettia*.

ACKNOWLEDGMENTS

Bob Anderson is thanked for initiating this project, introducing us to field aspects of local Mesozoic strata, and providing generous and carefully planned logistical assistance. His thoughtful review improved the manuscript. Vancouver Island Helicopters pilots from the bases at Stewart, Bob Quinn, and Brucejack Lake, moved us safely and cheerfully around the Iskut River map area. Discussions with Tim Tozer on Triassic ammonoid identification were helpful. Paul L. Smith (UBC) confirmed our Pliensbachian ammonoid identifications. Bivalves were studied by Martin Aberhan (Institut für Paläontologie der Universität, Würzburg). One fossil specimen was collected by M. Gunning (University of Western Ontario) and K. Patterson. Cheerful and able field assistance was provided by R. Lopez, S. Galway, D. Green, K. Patterson, and Y. Zuidema. Biostratigraphic research at UBC was funded through an NSERC operating grant to Paul L. Smith.

REFERENCES

Alldrick, D.J., Britton, J.M., Webster, I.C.L., and Russell, C.W.P.
1989: Geology and mineral deposits of the Unuk area; British Columbia Ministry of Energy, Mines, and Petroleum Resources, Open File Map 1989-10.

Anderson, R.G.
1993: A Mesozoic stratigraphic and plutonic framework for northwestern Stikinia (Iskut River area), northwestern British Columbia, Canada; in Mesozoic Paleogeography of the Western United States – II; G. Dunne and K. McDougall (ed.); Society of Economic Paleontologists and Mineralogists, Pacific Section, v. 71, p. 477-494.

Campbell, J.D.
1974: Heterastridium (Hydrozoa) from Norian sequences in New Caledonia and New Zealand; Journal of the Royal Society of New Zealand, v. 4, p. 447-453.

Carter, E.S., Orchard, M.J., and Tozer, E.T.
1989: Integrated ammonoid-conodont-radiolarian biostratigraphy, Late Triassic Kunga Group, Queen Charlotte Islands, British Columbia; in Current Research, Part H; Geological Survey of Canada, Paper 89-1H, p. 23-30.

Damborenea, S.E. and Manceñido, M.O.
1979: On the paleogeographical distribution of the Pectinid genus *Weyla* (Bivalvia, Lower Jurassic); Palaeogeography, Palaeoclimatology, Palaeoecology, v. 27, p. 85-102.

Jeletzky, J.A.
1980: Dicoelitid belemnites from the Toarcian - Middle Bajocian of Western and Arctic Canada; Geological Survey of Canada, Bulletin 338, 71 p.

Lewis, P.D., Thompson, J.F.H., Nadaraju, G., Anderson, R.G., and Johannson, G.G.
1993: Lower and Middle Jurassic stratigraphy in the Treaty Glacier area and geological setting of the Treaty Glacier alteration system, northwestern British Columbia; in Current Research, Part A; Geological Survey of Canada, Paper 93-1A, p. 75-86.

Nadaraju, G.T.
1993: Triassic-Jurassic biochronology of the eastern Iskut River map area, northwestern British Columbia; M.Sc. thesis, University of British Columbia, Vancouver, 223 p.

Pálfy, J., Smith, P.L., and Tipper, H.W.
in press: Sinemurian (Lower Jurassic) ammonite biostratigraphy of the Queen Charlotte Islands, British Columbia; Geobios Mémoirs.

Poulton, T.P. and Tipper, H.W.
1991: Aalenian ammonites and strata of western Canada; Geological Survey of Canada, Bulletin 411, 71 p.

Silberling, N.J. and Tozer, E.T.
1968: Biostratigraphic classification of the marine Triassic in North America; Geological Society of America, Special Paper 110, 63 p.

Smith, P.L. and Carter, E.S.
1990: Jurassic correlation in the Iskut River map area, British Columbia, and the age of the Eskay Creek deposit; in Current Research, Part E; Geological Survey of Canada, Paper 90-1E, p. 149-151.

Tozer, E.T.
1980: Latest Triassic (Upper Norian) ammonoid and Monotis faunas and correlations; Rivista Italiana di Paleontologia e Stratigrafia, v. 85, p. 843-846.

Geological Survey of Canada Project 840046

PLATE 1

All figures are natural size.

Figure 1. *Heterastridium conglobatum* Reuss; GSC 108520; GSC Loc. No. C-201504; Stuhini Group; Upper Norian.

Figure 2. *Choristoceras?* sp.; GSC 108521; GSC Loc. No. C-210856; Stuhini Group; Crickmayi Zone?, Rhaetian?

Figure 3. *Badouxia canadensis* (Frebold); GSC 108522; GSC Loc. No. C-210857; Jack fm.; Canadensis Zone; Hettangian/Sinemurian.

Figure 4. *Sulciferites* cf. *marmoreus* (Oppel); GSC 108523; GSC Loc. No. C-210857; Jack fm.; Canadensis Zone; Hettangian/Sinemurian.

Figure 5. *Sulciferites* cf. *trapezoidalis* (Sowerby); GSC 108524; GSC Loc. No. C-210857; Jack fm.; Canadensis Zone; Hettangian/Sinemurian.

Figure 6. *Eolytoceras* sp.; GSC 108525; GSC Loc. No. C-210857; Jack fm.; Canadensis Zone; Hettangian/Sinemurian.

Figure 7. *Paracaloceras* cf. *cordieri* (Canavari); GSC 108526; GSC Loc. No. C-210857; Jack fm.; Canadensis Zone; Hettangian/Sinemurian.

Figure 8. *Amaltheus stokesi* (Sowerby); GSC 108527; GSC Loc. No. C-210213; Betty Creek Fm.; Kunae Zone, Upper Pliensbachian.

Figure 9. *Amaltheus stokesi* (Sowerby); GSC 108528; GSC Loc. No. C-210213; Betty Creek Fm.; Kunae Zone, Upper Pliensbachian.

Figure 10. *Pseudolioceras* cf. *whiteavesi* (White); GSC 108529; GSC Loc. No. C-210869; Salmon River Fm.?; Upper Aalenian.

Figure 11. *Leioceras*? sp.; GSC 108530; GSC Loc. No. C-210869; Salmon River Fm.?; Upper Aalenian.

Figure 12. *Tmetoceras* cf. *kirki* Westermann; GSC 108531; GSC Loc. No. C-210869; Salmon River Fm.?; Upper Aalenian.

Figure 13. *Stephanoceras*? sp.; GSC 108532; GSC Loc. No. C-210866; Salmon River Fm.; Lower Bajocian.

Figure 14. *Sonninia*? sp.; GSC 108533; GSC Loc. No. C-210864; Salmon River Fm.; Lower Bajocian.

Figure 15. *Lilloettia* sp.; GSC 108534; GSC Loc. No. C-210217; Bowser Lake Group; Lower Callovian.

Figure 16. *Iniskinites* cf. *intermedius* (Imlay); GSC 108535; GSC Loc. No. C-210216; Bowser Lake Group; Upper Bathonian.

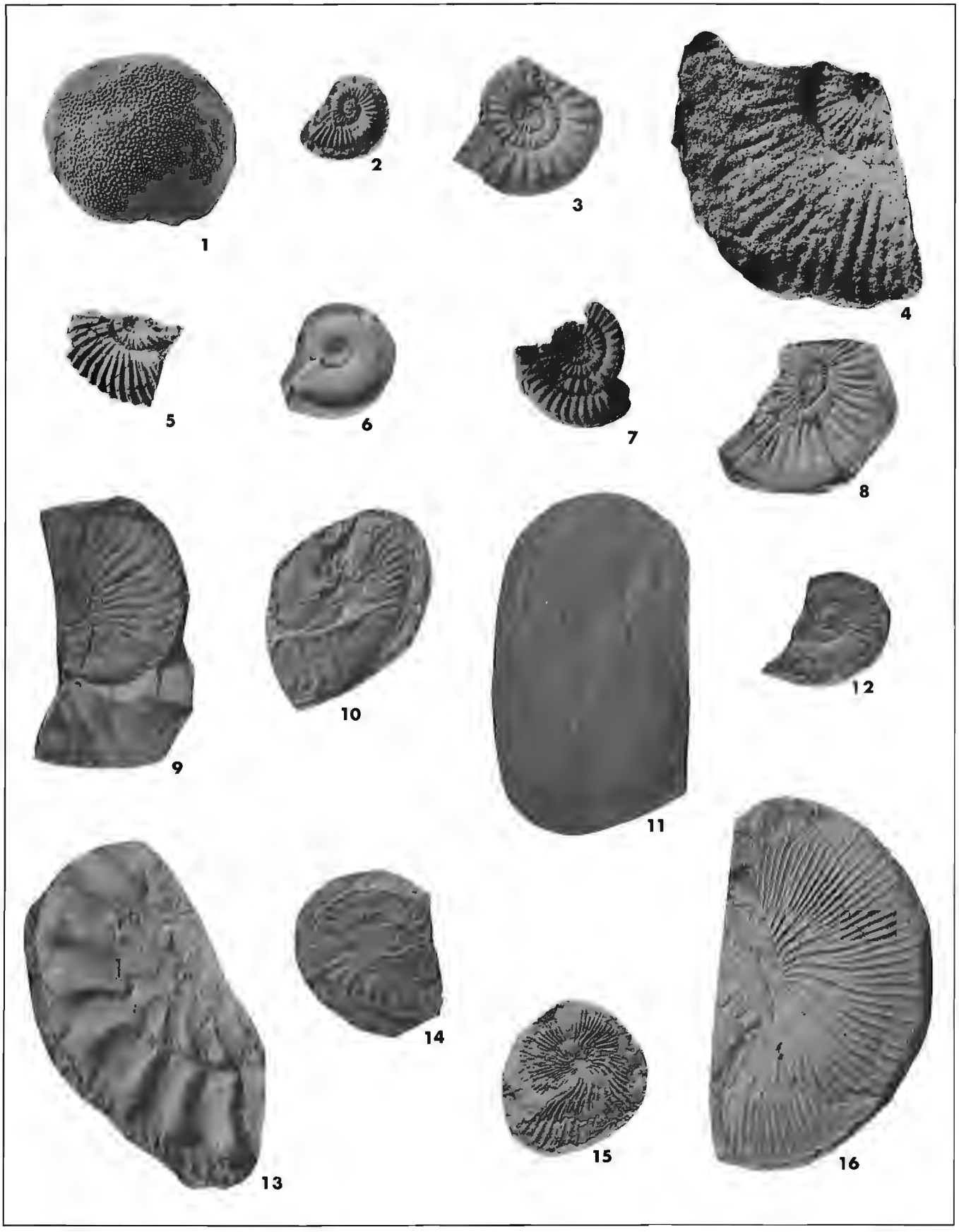

Plate 1

APPENDIX

Locality Register (by GSC Locality No.)

GSC Loc. No. C-201504. 93-ATG-59, NTS 104G/2, UTM 386440E 6341620N. South of Arctic Lake, Stuhini Group; Upper Norian.

GSC Loc. No. C-210213. 93-ATJ-65, NTS 104B/7, UTM 400350E 6265575N. Lyons Creek, Hazelton Group, Betty Creek Formation; Upper Pliensbachian, Kunae Zone.

GSC Loc. No. C-210216. 93-ATJ-71, NTS 104B/8, UTM 431875E 6251440N. Canoe Glacier, Bowser Lake Group, Upper Bathonian.

GSC Loc. No. C-210217. 93-ATJ-73, NTS 104B/8, UTM 431810E 6251550N. Canoe Glacier, Bowser Lake Group, Lower Callovian.

GSC Loc. No. C-210853. 93-ATP-4, NTS 104B/9, UTM 427100E 6275050N. Atkins ridge, Hazelton Group, Jack formation; Hettangian/Sinemurian.

GSC Loc. No. C-210856. 93-ATP-7, NTS 104B/9, UTM 426760E 6275375N. Atkins ridge, Stuhini Group; Rhaetian?, Crickmayi Zone?

GSC Loc. No. C-210857. 93-ATP-8, NTS 104B/9, UTM 426950E 6274950N. Atkins ridge, Hazelton Group, Jack formation; Hettangian/Sinemurian.

GSC Loc. No. C-210859. 93-ATP-10, NTS 104B/9, UTM 426950E 6275030N. Atkins ridge, Hazelton Group, Jack formation; Hettangian/Sinemurian.

GSC Loc. No. C-210860. 93-ATP-11, NTS 104B/9, UTM 426940E 6274920N. Atkins ridge, Hazelton Group, Jack formation; Hettangian/Sinemurian.

GSC Loc. No. C-210864. 93-ATP-18, NTS 104B/9, UTM 433050E 6273350N. Treaty Ridge, Hazelton Group, Salmon River Formation; Lower Bajocian.

GSC Loc. No. C-210866. 93-ATP-20, NTS 104B/9, UTM 433060E 6273250N. Treaty Ridge, Hazelton Group, Salmon River Formation; Lower Bajocian.

GSC Loc. No. C-210869. 93-ATP-23, NTS 104B/9, UTM 432620E 6273570N. Treaty Ridge, Hazelton Group, Salmon River Formation?; Upper Aalenian.

Biostratigraphic and facies studies of the Telkwa Formation (Lower Jurassic), Smithers map area, British Columbia

J. Pálfy[1] and K.L. Schmidt[2]
Cordilleran Division

Pálfy, J. and Schmidt, K.L., 1994: Biostratigraphic and facies studies of the Telkwa Formation (Lower Jurassic), Smithers map area, British Columbia; in Current Research 1994-E; Geological Survey of Canada, p. 29-38.

Abstract: Observations on four sections of Upper Sinemurian sedimentary units within the Telkwa Formation show that they were formed in two distinct stratigraphic intervals. Ammonite biostratigraphy suggests that two of these sections should be assigned to the Varians Assemblage (lower Upper Sinemurian), and the other two to the upper part of the Harbledownense Assemblage (upper Upper Sinemurian). Carbonate accumulation, locally attaining 200 m in thickness, is documented from both intervals. Lithofacies and biofacies characteristics indicate predominantly onshore, shallow subtidal depositional environments subjected to storms and controlled by local paleogeography restricting volcaniclastic input.

Résumé : Des observations effectuées sur quatre coupes d'unités sédimentaires du Sinémurien supérieur à l'intérieur de la Formation de Telkwa mettent en évidence deux intervalles stratigraphiques distincts. La biostratigraphie des ammonites suggère que deux des coupes devraient être assignées à l'Assemblage de Varians (partie inférieure du Sinémurien supérieur), et les deux autres à la partie supérieure de l'Assemblage de Harbledownense (partie supérieure du Sinémurien supérieur). Les deux intervalles renferment une accumulation de carbonates qui atteint localement 200 m d'épaisseur. Les lithofaciès et biofaciès indiquent que la sédimentation s'est opérée principalement sur la terre ferme, dans des milieux subtidaux peu profonds exposés à des tempêtes et contrôlés par la paléogéographie locale, qui a limité les apports volcanoclastiques.

[1] Department of Geological Sciences, University of British Columbia, 6339 Stores Road, Vancouver, British Columbia V6T 1Z4
[2] Department of Geology, Idaho State University, Pocatello, Idaho 83209, U.S.A.

INTRODUCTION

The Lower Jurassic strata of Stikinia form part of the Hazelton Group, a thick succession of calc-alkaline volcanic and volcanosedimentary rocks deposited in an island-arc setting. The Telkwa Formation is the basal unit of the Hazelton Group in north-central British Columbia. It is composed of mostly volcanic and volcaniclastic rocks with local fossiliferous sediments which yielded a Sinemurian fauna (Tipper and Richards, 1976). One such sedimentary member was identified on Ashman Ridge by Tipper and Richards (1976); others

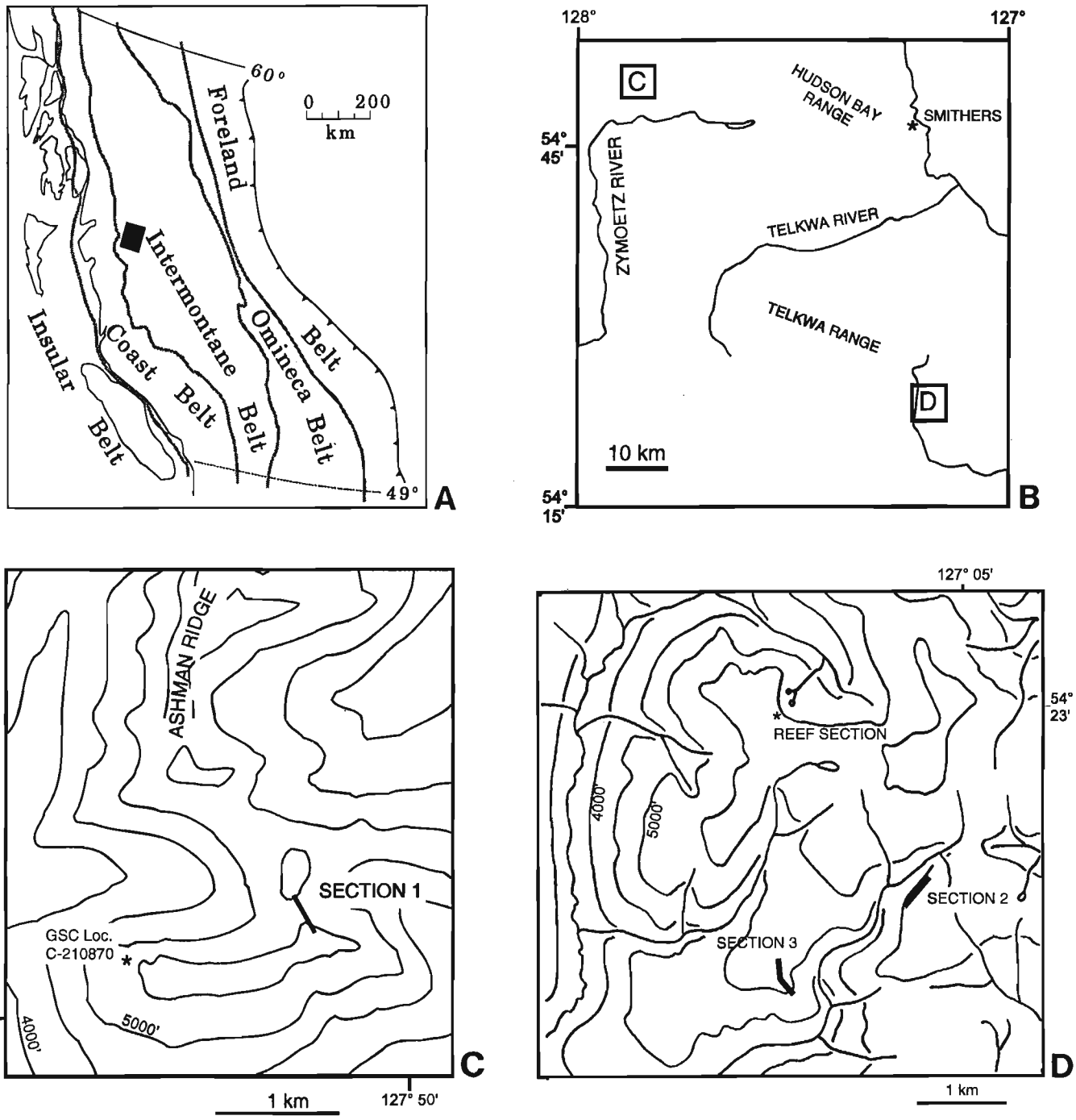

Figure 1.

A. Location of the Smithers map area.

B. Location of the study areas within the western half of the Smithers map area.

C. Location of the measured section 1 on Ashman Ridge.

D. Location of the measured sections referred to in the text from the southern Telkwa Range.

were identified in the Telkwa Range by MacIntyre et al. (1989) and Desjardins et al. (1990a) and include a well-preserved coral reef described in detail by Poulton (1989) and Stanley and McRoberts (1993).

In 1993 sections of the Telkwa Formation were studied as part of a project to recalibrate the Jurassic absolute time scale. Sites were selected where volcanic (pyroclastic or flow) horizons dateable by U-Pb methods can be biochronologically constrained at a zonal level using ammonites. Field work at these localities (Fig. 1) involved measuring three stratigraphic sections and collecting macrofossils and zircon samples for U-Pb dating. The coral reef was revisited to assess its stratigraphic relationship to other carbonate units. Samples for reconnaissance paleomagnetic work undertaken by R. Enkin (GSC Pacific Geoscience Centre) were also collected. Processing of samples for geochronology is underway. Preliminary biostratigraphic results are reported here together with evaluation of the facies and stratigraphic relationships of the marine sedimentary units.

SECTION 1: ASHMAN RIDGE

The Ashman Ridge section was reported by Tipper and Richards (1976) who interpreted its lower part as thick subaerial volcanics belonging to the Howson facies of Telkwa Formation and noted the presence of fossiliferous sediments. Fossils were collected and some 300 m of the underlying volcanic sequence was studied in detail to select the most suitable sampling sites for U-Pb geochronology. The measured section is shown in Figures 2 and 3; the base was not seen. The bulk of the sequence consists of diverse pyroclastic rocks composed of non-welded to moderately and densely welded crystal, crystal-lithic, and lapilli tuffs and tuff breccias that vary in composition from andesite to rhyolite.

A 10 m thick, grey, medium- to thick-bedded limestone body varies in thickness laterally but is traceable to the southwest limb of the ridge, a distance of about 2 km. It contains several, thin tuffaceous sandstone interbeds; plagioclase, quartz, and mafic crystals occur in the micritic matrix. The abundance of volcanogenic material decreases upsection. Intraclasts, chert nodules, and algal oncoids nucleated around shell debris or volcanogenic clasts also occur. The macrofauna is sparse, only zeilleriid brachiopods, indeterminate corals, and uncommon bivalves were observed. The faunal assemblage and lithofacies suggest a shallow subtidal depositional environment. The top of the limestone is an irregular surface, perhaps due to emergence and karstic erosion.

Overlying the limestone is a 4-5 m thick rusty weathering, bluish grey, very fossiliferous, calcareous cemented, tuffaceous arkosic lithic sandstone containing angular limestone and volcanic fragments up to 1 cm in size. Bioclast-supported beds and lenses occur in the unit. These are composed of fragmented shells comprising an unsorted, stacked and nested biofabric, indicative of sedimentological skeletal concentration (Kidwell et al., 1986). In the measured section asteroceratid ammonite shells are the most common large bioclasts; the smaller ones are typically indeterminate bivalves. This deposit is interpreted as proximal tempestite onlapping the

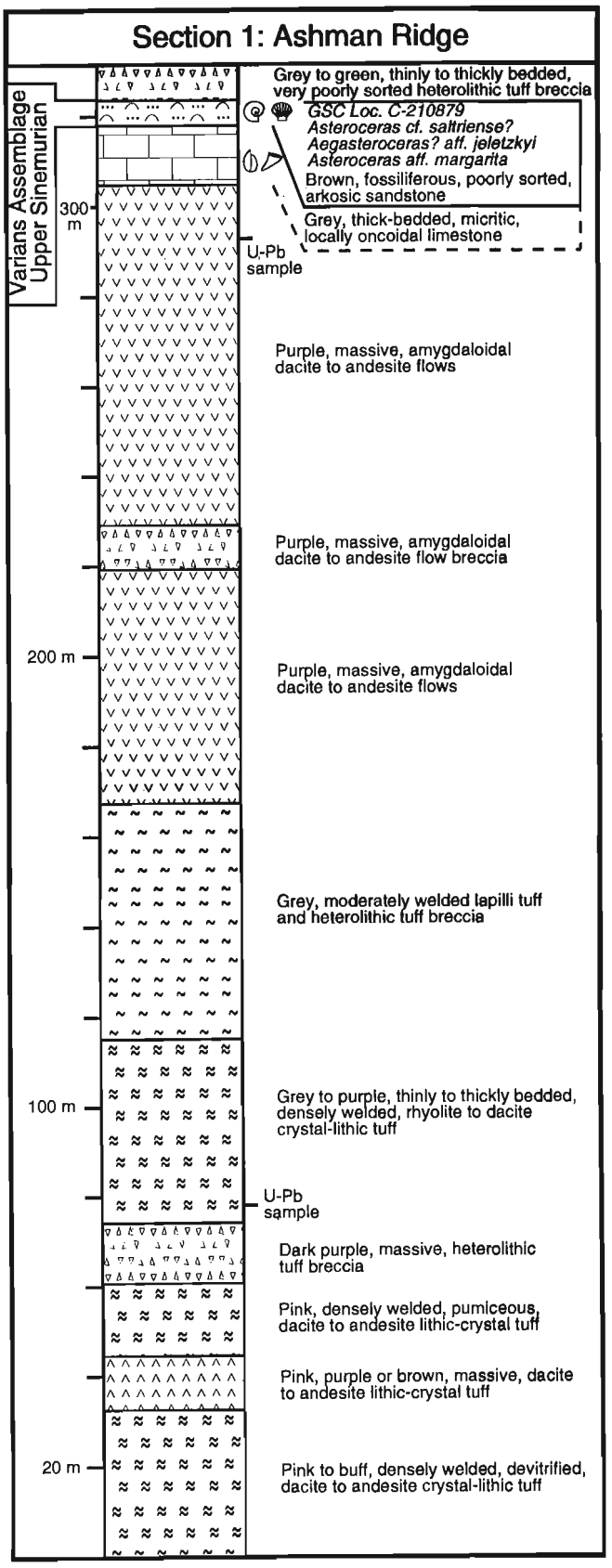

Figure 2. *Lithostratigraphy and biostratigraphy of Section 1 on Ashman Ridge. See Figure 3 for legend.*

karstic erosional surface of the underlying limestone. Correlative tuffaceous arkosic lithic sandstone occurs on the southwestern limb of Ashman Ridge (GSC Loc. C- 210870), and contains a different fauna, dominated by large, thick-shelled *Weyla alata*. Asteroceratid ammonites (*Eparietites*?, *Asteroceras*, *Aegasteroceras*?) are common. Other epifaunal and infaunal bivalves occur together with a large, smooth, turbiniform gastropod.

These marine sediments are overlain by coarse pyroclastic rocks, marking a sudden influx of volcaniclastics terminating the short episode of marine sedimentation.

SECTION 2: SOUTHERN TELKWA RANGE

The measured section 2 is located approximately 4.4 km northeast of the confluence between a tributary and Houston Tommy Creek, along the steep edge of a broad, flat ridge that forms the east side of the tributary valley (Fig. 1D). This section contains the greatest thickness, nearly 200 m, of limestone known within the Telkwa Formation (Fig. 4). The limestone at this location can be divided into three parts. The lower part consists of dark grey, bioclastic and micritic limestone including abundant coquinoid beds. The middle part is composed of interbedded fine- and coarse-grained calcarenite containing some coquinoid beds. The upper part consists of dark grey, thick bedded to massive, sparsely fossiliferous limestone. In each of the three parts, some beds contain significant amounts of quartz, plagioclase, and biotite crystals.

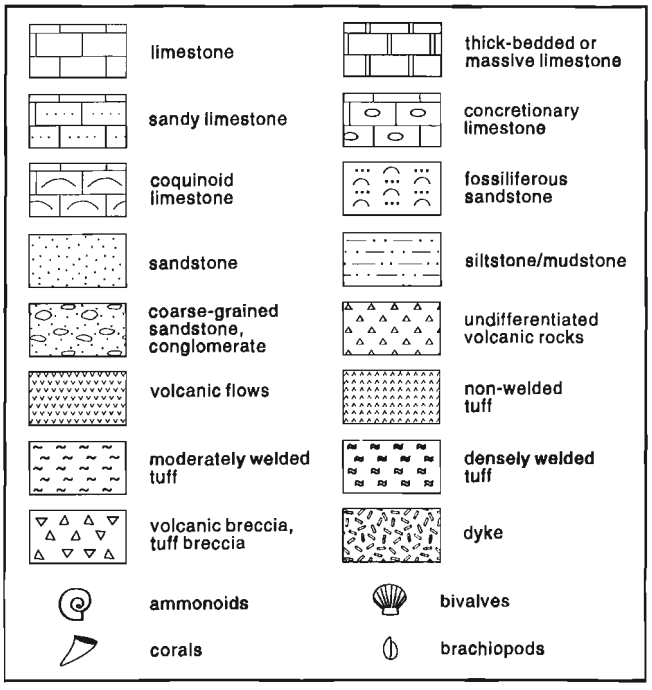

Figure 3. *Legend for Figures 2, 4, and 5.*

The contact between the limestone and underlying green, aphyric, medium- to thick-bedded volcanic rocks is partly covered, but thin beds of volcanics are interbedded with the limestone near the covered interval, suggesting that the base is nearby and has not been removed by faulting. The lowermost few metres of the dark grey limestone comprise a mono- or oligospecific terebratulid coquina. Most specimens are articulated valves with partial sparry calcite infilling. In places geopetal structures were observed. Subordinate epifaunal

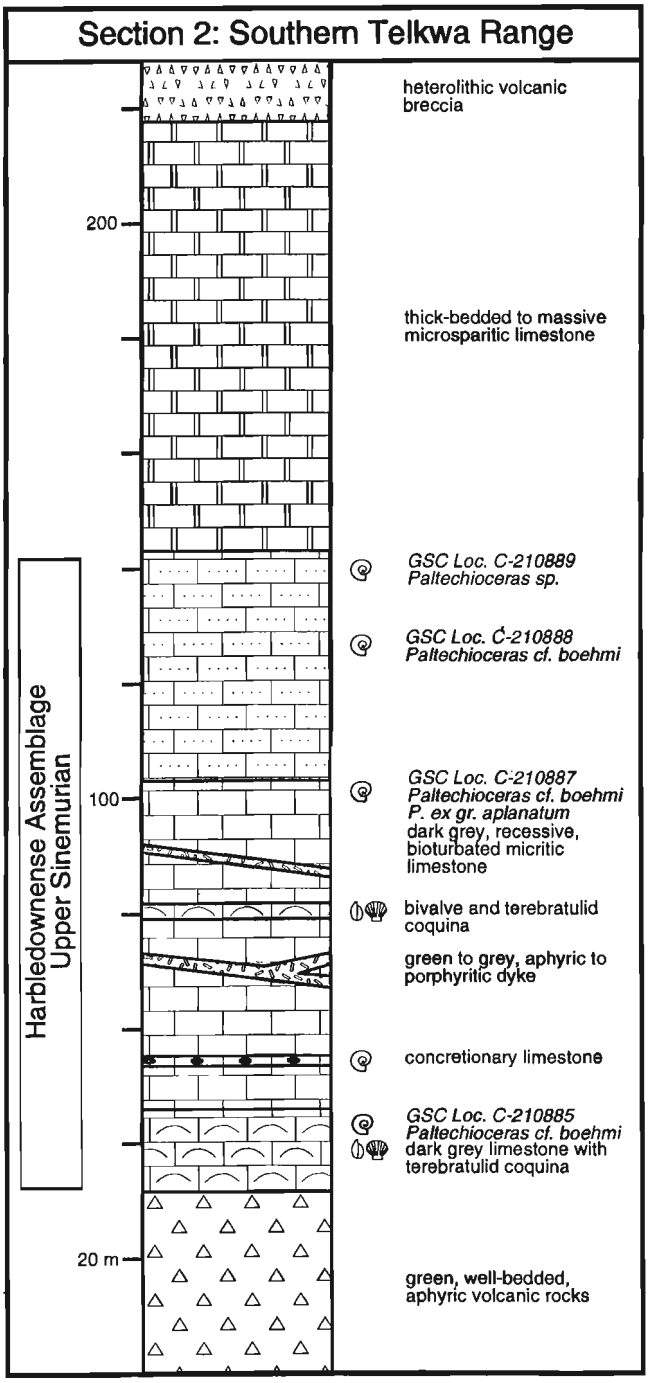

Figure 4. *Lithostratigraphy and biostratigraphy of section 2 in the southern Telkwa Range. See Figure 3 for legend.*

bivalves occur with large specimens of thick-shelled *Weyla*. Rapid episodic sedimentation and limited transportation of shells is indicated in a shallow subtidal depositional environment. Shells from a low-diversity paleocommunity dominated by gregarious terebratulids were subjected to storm-induced reworking.

Upward in the section the brachiopodal biofacies is replaced by a less fossiliferous association with common *Weyla*. Thin terebratulid or occasionally bivalve coquinas recur at several levels. Apart from the lowermost beds, sporadic ammonites (*Paltechioceras*) occur throughout the section. The middle part of the section is characterized by rhythmic alternation of finer and coarser grained calcarenite beds. The upper part comprises resistant, cliff-forming beds of thick bedded to massive, sparsely fossiliferous limestone.

Overlying the limestone is a heterolithic tuff breccia unit. Green to grey, aphyric to strongly porphyritic dykes containing plagioclase, hornblende, biotite, quartz, and K-feldspar cut the limestone. A similar intrusive unit occurs farther upsection from the limestone.

SECTION 3: SOUTHERN TELKWA RANGE

Another section containing thick Upper Sinemurian carbonates was measured on the west side of the same tributary that section 2 is located, 2.7 km northeast of the confluence with Houston Tommy Creek (Fig. 1D, 5). The carbonate is micritic to bioclastic and contains more volcanogenic material than the limestone in section 2. It is sparsely to moderately fossiliferous, yielding ammonites (*Paltechioceras* spp.), infaunal and epifaunal bivalves (*Weyla* cf. *alata*, *Antiquilima*?, *Pholadomya*, *Machomya*), terebratulid and rhynchonellid brachiopods, gastropods, and small colonial corals. The interpreted depositional environment is comparable to that of section 2. The greater abundance of infaunal bivalves suggest prevailing carbonate sand and mud substrate in a shallow marine setting. The lowest limestone beds in the carbonate rest on red and green plagioclase, biotite, quartz-bearing crystal-lithic tuff. Similar tuff intercalations occur within the limestone sequence and are several metres thick. The first maroon tuff bed within the limestone section was sampled for U-Pb dating. The carbonate unit is overlain by coarse grained, volcanogenic, epiclastic(?) breccia and sandstone, further red tuff beds, and a rhyolite flow(?) unit, which was also sampled for U-Pb dating. Green to grey, aphyric to porphyritic dykes similar to those described from section 2 cut the limestone in several locations.

REEF SECTION

The best documented example of carbonate sedimentation on the Telkwa Formation is the coral reef in the southern Telkwa Range. A detailed description of the lithology and fauna of the biohermal limestone is given by Poulton (1989) and Stanley and McRoberts (1993). The section was revisited to compare its stratigraphy with other sedimentary sequences. The bioherm is underlain by well-bedded, welded, siliceous crystal-lithic lapilli tuff, broadly comparable to that encountered on Ashman Ridge. Interbedded, thin pyroxene basalt flows and volcaniclastic sediments also occur below the reef. The rusty weathering bioclastic calcareous sandstone which appears to onlap the bioherm on the northwest side is similar in litho- and biofacies to the more shell-rich unit overlying the micritic limestone on Ashman Ridge. However, the relationship between the reef and fossiliferous sandstone is

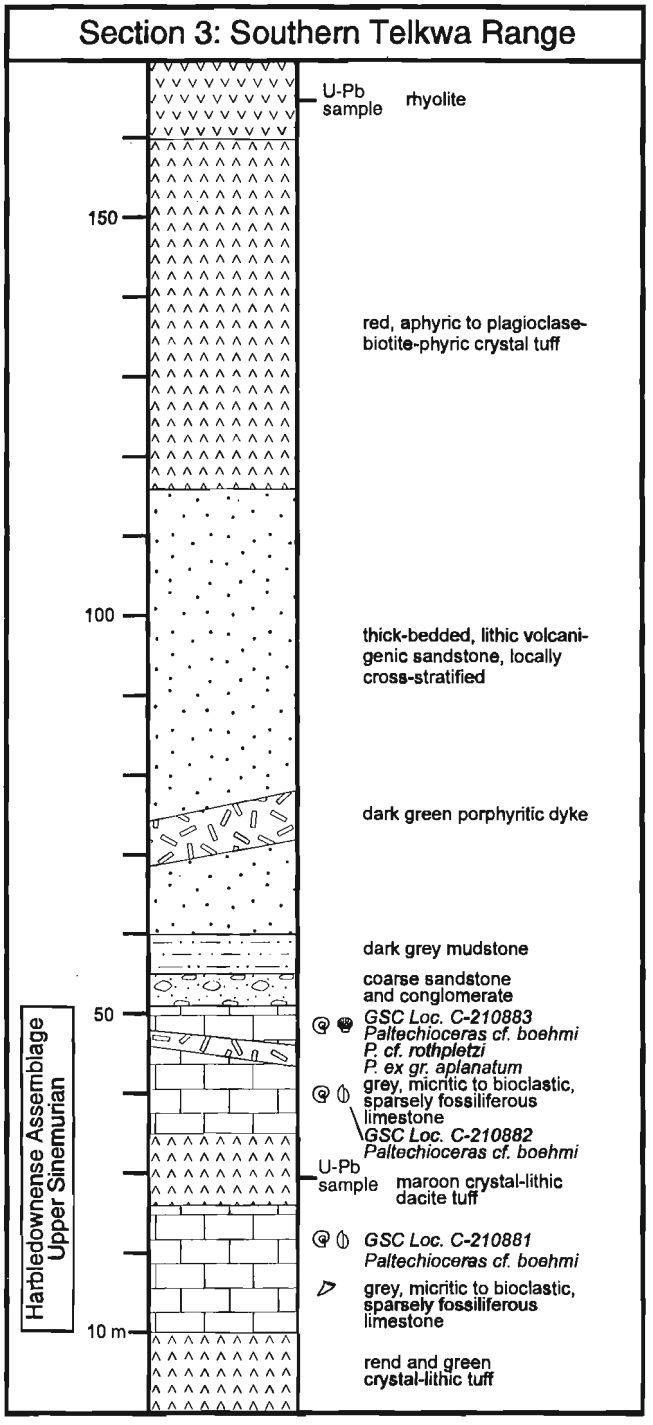

Figure 5. Lithostratigraphy and biostratigraphy of section 3 in the southern Telkwa Range. See Figure 3 for legend.

PLATE 1

All figures are natural size. Figured specimens are housed in the type collection of the Geological Survey of Canada, Ottawa.

Figure 1. *Asteroceras* cf. *saltriense*? Parona; GSC 108536; GSC Loc. No. C-210879; Varians Assemblage; Upper Sinemurian.

Figure 2. *Aegasteroceras*? aff. *jeletzkyi* (Frebold); GSC 108537; GSC Loc. No. C-210879; Varians Assemblage; Upper Sinemurian.

Figure 3. *Eparietites*? sp.; GSC 108538; GSC Loc. No. C-210870; Varians Assemblage; Upper Sinemurian.

Figure 4. *Asteroceras* aff. *margarita* Parona; GSC 108539; GSC Loc. No. C-210879; Varians Assemblage; Upper Sinemurian.

Figure 5. *Paltechioceras* cf. *rothpletzi* (Böse); GSC 108540; GSC Loc. No. C-210883; Harbledownense Assemblage; Upper Sinemurian.

Figure 6. *Paltechioceras* cf. *boehmi* (Hug); GSC 108541; GSC Loc. No. C-210887; Harbledownense Assemblage; Upper Sinemurian.

Figure 7. *Asteroceras* sp.; GSC 108542; GSC Loc. No. C-210879; Varians Assemblage; Upper Sinemurian.

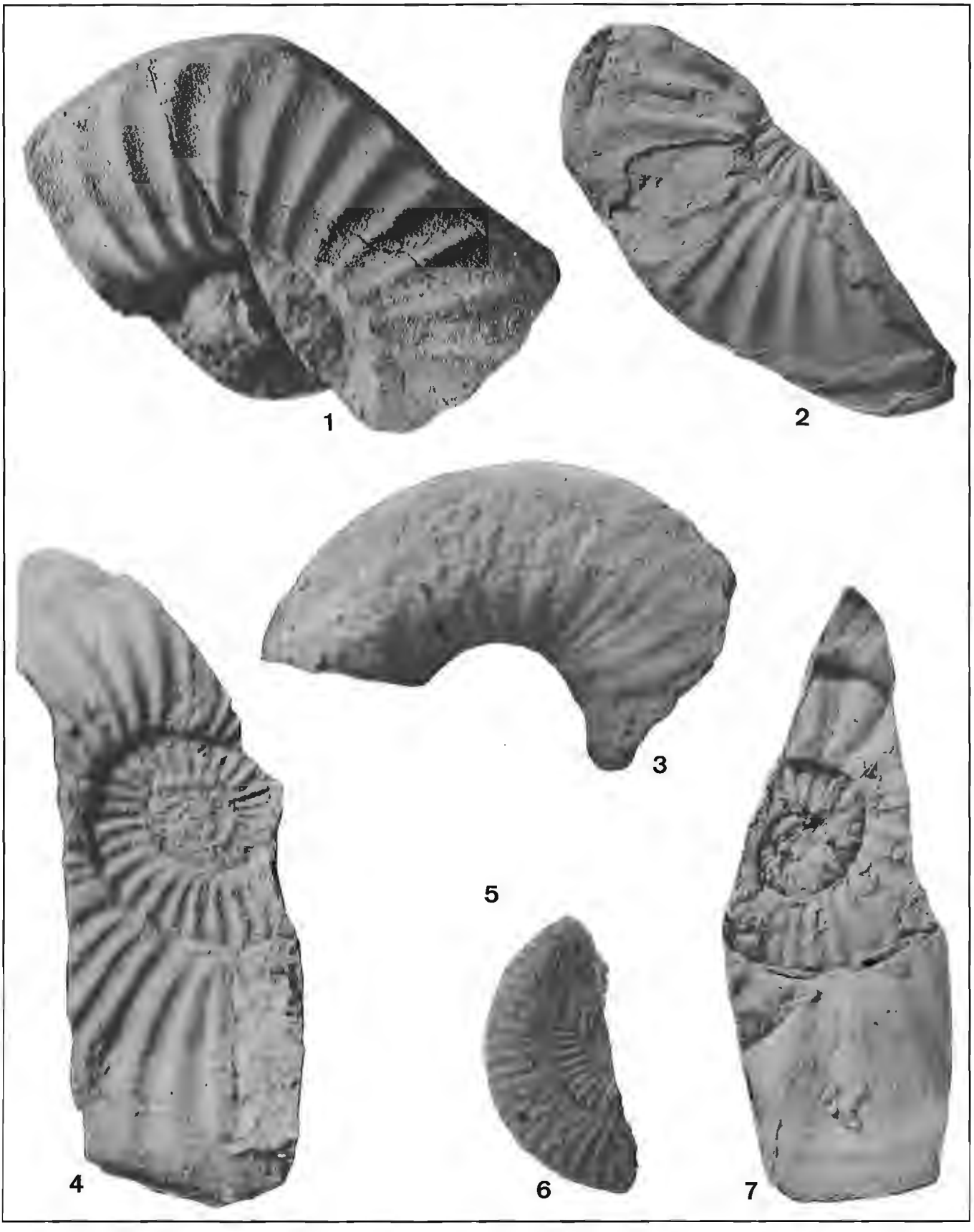
1
2
3
4
5
6
7

obscured by a normal fault and talus. Correlation between the reef and sedimentary rocks on Ashman Ridge is somewhat uncertain because we were unable to find asteroceratid ammonites at the reef, which were reported by Poulton (1989). At both localities the heterolithic tuff breccia capping the sedimentary sequence may have resulted from an explosive volcanic episode which effectively halted the carbonate sedimentation.

BIOSTRATIGRAPHY

The development of a regionally applicable standard ammonite zonation for the Sinemurian of western North America is in progress. A local ammonite biostratigraphy established in the relatively complete succession of the Queen Charlotte Islands (Pálfy et al., in press) is used here as a reference. The informal units referred to as assemblages may be formalized later as regional standard assemblage zones. As Late Sinemurian faunas are generally cosmopolitan, correlation can be made with the northwest European standard zones (e.g., Dean et al., 1961).

The ammonite faunas from the Telkwa Formation represent two distinct stratigraphic intervals in the Upper Sinemurian: the Varians Assemblage and the upper part of the Harbledownense Assemblage of Pálfy et al. (in press). The numerous specimens collected from the Ashman Ridge section all came from a few metres thick, very fossiliferous calcareous sandstone unit. They are assignable to the following asteroceratid taxa: *Asteroceras* cf. *saltriense*? (Pl. 1, fig. 1), *Asteroceras* aff. *margarita* (Pl. 1, fig. 4), *Asteroceras* sp. (Pl. 1, fig. 7), *Aegasteroceras*? aff. *jeletzkyi* (Pl. 1, fig. 2), and *Eparietites*? sp. (Pl. 1, fig. 3). Only the first two forms occur in the Queen Charlotte Islands, where they are known from the middle part of the Varians Assemblage. *Aegasteroceras*? *jeletzkyi* in its type area, the Richardson Mountains (Northwest Territories), is associated with oxynoticeratids including the zonal index *Oxynoticeras oxynotum* (Frebold, 1960, 1975; Poulton, 1991). This is an anomalously high occurrence for the genus. Asteroceratids and *Oxynoticeras* are mutually exclusive elsewhere and there is no indication of early Late Sinemurian faunas from northern Canada. It is therefore possible that *Aegasteroceras*? *jeletzkyi* is not restricted to the Oxynotum Zone but only ranges to that level in northern Canada. Another occurrence of *Arctoasteroceras jeletzkyi* is reported from Alaska by Imlay (1981), in association with a single specimen of *Paltechioceras* (*Orthechioceras*?) sp. If it were a true *Paltechioceras*, it would represent an even higher stratigraphic horizon, so correlation with the standard Raricostatum Zone was suggested. The serpenticone specimen bears a resemblance to certain *Epophioceras*, except the venter is unusually sulcate for that genus. Such revised identification would justify a reassignment of the Alaskan collection to the Varians Assemblage (standard Obtusum Zone). *Eparietites* is imperfectly known in North America; in Europe, the genus is restricted to the Obtusum Zone.

The higher ammonite fauna known from the southern Telkwa Range (sections 2 and 3) is also not diverse. Several species of *Paltechioceras* were distinguished: *P.* cf. *boehmi* (Pl. 1, fig. 6), *P.* cf. *rothpletzi* (Pl. 1, fig. 5), *P.* ex gr. *aplanatum*, and *P.* sp. No succession of species is apparent, hence these taxa are used together to characterize this level. In the Queen Charlotte Islands the first two species and *P.* cf. *romanicum* (which shows close affinity to *P. aplanatum* and included here in this species group) are restricted to the upper part of the Harbledownense Assemblage, i.e. they occur at the top of the range and above *Plesechioceras*? *harbledownense*. The only other areas in North America where a succession of echioceratids has been established are Nevada and Oregon (Smith, 1981). There, too, *Plesechioceras*? *harbledownense* appears to occur below diverse *Paltechioceras* spp. This level is also correlatable with the upper part of the standard Raricostatum Zone in Europe.

DISCUSSION

Our biostratigraphic data together with geological mapping (Desjardins et al., 1990b) indicate that sedimentary facies within the Telkwa Formation have limited extent both temporally and laterally and are correlated with two well constrained intervals, the Varians Assemblage (lower Upper Sinemurian) and the upper part of the Harbledownense Assemblage (upper Upper Sinemurian). Therefore the marine sediments cannot be used as a single marker horizon, as suggested by Desjardins et al. (1990a). Although distinctive within the predominantly volcanic Telkwa Formation, their inclusion in a single lithostratigraphic unit based on their sedimentary nature poses problems for assignment of volcanic rocks stratigraphically above the lower unit or below the upper unit. Assignment of the sedimentary strata to the Nilkitkwa Formation, as indicated by Stanley and McRoberts (1993) based on as yet unpublished work by MacIntyre and Desjardins (in press), cannot be reconciled with the original definition of this formation (Tipper and Richards, 1976). The Nilkitkwa Formation, according to Tipper and Richards (1976), consists of predominantly interbedded shale and greywacke and is Early Pliensbachian to Middle Toarcian in age.

A common feature of the studied sections is that carbonate sedimentation was rapidly established on volcanic basement with some transition zone of interfingering sedimentary and volcanic layers. In all cases termination of carbonate deposition was brought about by overwhelming volcaniclastic (either pyro- or epiclastic) input. That these episodes of marine sedimentation were short-lived is attested by the lack of distinguishable faunal replacement in the ammonoids of any given section. Storm deposition played an important role in producing shell-rich beds, both proximal and distal tempestites were observed. Tipper and Richards (1976) noted that the distribution of carbonate bodies delineates a facies belt which they interpreted as a transition zone between the subaerial and shelfal areas. Our facies interpretation confirms that in the studied sections nearshore, shallow subtidal depositional environments prevailed. The discontinuous lateral distribution is accounted for by local topographic control on sedimentation, as carbonate deposition could only occur in

areas where volcaniclastic input was reduced. The limited areal extent and rapid lateral changes of facies are in accordance with the postulated island-arc setting.

ACKNOWLEDGMENTS

We wish to thank Howard W. Tipper for initiating this project, providing support, and useful advise. His critical review greatly improved the manuscript. Field work was funded by the Geological Survey of Canada and we are especially grateful to Robert G. Anderson for his logistical assistance. Biostratigraphic research at UBC was funded through an NSERC operating grant to Paul L. Smith. Martin Aberhan (Universität Würzburg) provided bivalve identifications.

REFERENCES

Dean, W.T., Donovan, D.T., and Howarth M.K.
1961: The Liassic ammonite zones and subzones of the northwest European province; Bulletin of the British Museum (Natural History), Series A, Geology, v. 4, p. 438-505.

Desjardins, P., MacIntyre, D.G., Hunt, J., Lyons, L., and Pattenden, S.
1990a: Geology of the Thautil River map area (93L/6); in Geological Fieldwork 1989; British Columbia Ministry of Energy, Mines, and Petroleum Resources, Paper 1990-1, p. 91-99.
1990b: Geology of the Thautil River area; British Columbia Ministry of Energy, Mines, and Petroleum Resources, Open File Map 1990-5.

Frebold, H.
1960: The Jurassic faunas of the Canadian Arctic (Lower Jurassic and lowermost Middle Jurassic ammonites); Geological Survey of Canada, Bulletin 59, 33 p.
1975: The Jurassic faunas of the Canadian Arctic (Lower Jurassic ammonites, biostratigraphy and correlation); Geological Survey of Canada, Bulletin 243, 24 p.

Imlay, R.W.
1981: Early Jurassic ammonites from Alaska; United States Geological Survey, Professional Paper 1148, 49 p.

Kidwell, S.M., Fürsich, F.T., and Aigner, T.
1986: Conceptual framework for the analysis and classification of fossil concentrations; Palaios, v. 1, p. 228-238.

MacIntyre, D.G. and Desjardins, P.
in press: Geology and mineral deposits of the Smithers map area; British Columbia Ministry of Energy, Mines, and Petroleum Resources, Bulletin.

MacIntyre, D.G., Desjardins, P., and Tercier, P.
1989: Jurassic stratigraphic relationships in the Babine and Telkwa ranges (93L/10, 11, 14, 15); in Geological Fieldwork 1988; British Columbia Ministry of Energy, Mines, and Petroleum Resources, Paper 1989-1, p. 195-208.

Pálfy, J., Smith, P.L., and Tipper, H.W.
in press: Sinemurian (Lower Jurassic) ammonite biostratigraphy of the Queen Charlotte Islands, British Columbia; Geobios Mémoirs.

Poulton, T.P.
1989: A Lower Jurassic coral reef, Telkwa Range, British Columbia; in Reefs, Canada and Adjacent Area, H.H.J. Geldsetzer, N.P. James, and G.E. Tebbutt (ed.); Canadian Society of Petroleum Geologists Memoir, v. 13, p. 754-757.
1991: Hettangian through Aalenian (Jurassic) guide fossils and biostratigraphy, northern Yukon and adjacent Northwest Territories; Geological Survey of Canada, Bulletin 410, 71 p.

Smith, P.L.
1981: Biostratigraphy and ammonoid fauna of the Lower Jurassic (Sinemurian, Pliensbachian and lowest Toarcian) of Eastern Oregon and Western Nevada; Ph.D. thesis, McMaster University, Hamilton, Ontario, 368 p.

Stanley, G.D., Jr. and McRoberts, C.A.
1993: A coral reef in the Telkwa Range, British Columbia: the earliest Jurassic example; Canadian Journal of Earth Sciences, v. 30, p. 819-831.

Tipper, H.W. and Richards, T.A.
1976: Jurassic stratigraphy and history of north-central British Columbia; Geological Survey of Canada, Bulletin 270, 73 p.

Geological Survey of Canada Project 750035

APPENDIX 1

Locality Register

GSC Loc. No. C-210870; 93-TDP-24; NTS 93L/13; UTM 572870E 6076920N; 1.5 km W of section 1, Ashman Ridge southwest limb; Telkwa Fm.; Varians Assemblage; Upper Sinemurian.

GSC Loc. No. C-210879; 93-TDP-363; NTS 93L/13; UTM 574310E 6077250N; section 1, S saddle on Ashman Ridge; Telkwa Fm.; Varians Assemblage; Upper Sinemurian.

GSC Loc. No. C-210881; 93-TDP-38; NTS 93L/6; UTM 622290E 6024670N; section 3, E of Houston Tommy Creek, E side of tributary; Telkwa Fm.; Harbledownense Assemblage; Upper Sinemurian.

GSC Loc. No. C-210882; 93-TDP-39; NTS 93L/6; UTM 622240E 6024730N; section 3, E of Houston Tommy Creek, E side of tributary; Telkwa Fm.; Harbledownense Assemblage; Upper Sinemurian.

GSC Loc. No. C-210883; 93-TDP-40; NTS 93L/6; UTM 622220E 6024770N; section 3, E of Houston Tommy Creek, E side of tributary; Telkwa Fm.; Harbledownense Assemblage; Upper Sinemurian.

GSC Loc. No. C-210885; 93-TDP-42; NTS 93L/6; UTM 623830E 6025830N; section 2, E of Houston Tommy Creek, ridge on W side of tributary; Telkwa Fm.; Harbledownense Assemblage; Upper Sinemurian.

GSC Loc. No. C-210887; 93-TDP-44; NTS 93L/6; UTM 623715E 6025740N; section 2, E of Houston Tommy Creek, ridge on W side of tributary; Telkwa Fm.; Harbledownense Assemblage; Upper Sinemurian.

GSC Loc. No. C-210888; 93-TDP-45; NTS 93L/6; UTM 623695E 6025700N; section 2, E of Houston Tommy Creek, ridge on W side of tributary; Telkwa Fm.; Harbledownense Assemblage; Upper Sinemurian.

GSC Loc. No. C-210889; 93-TDP-46; NTS 93L/6; UTM 623690E 6025690N; section 2, E of Houston Tommy Creek, ridge on W side of tributary; Telkwa Fm.; Harbledownense Assemblage; Upper Sinemurian.

Notes on Cretaceous calcareous nannofloral biostratigraphy and paleobiogeography, Queen Charlotte Islands, British Columbia

James W. Haggart, Jackie A. Burnett[1], and Paul R. Bown[1]
Cordilleran Division, Vancouver

Haggart, J.W., Burnett, J.A., and Bown, P.R., 1994: Notes on Cretaceous calcareous nannofloral biostratigraphy and paleobiogeography, Queen Charlotte Islands, British Columbia; in Current Research 1994-E; Geological Survey of Canada, p. 39-44.

Abstract: To aid in correlation of poorly macrofossiliferous fine clastic strata of Queen Charlotte Islands, British Columbia (NTS 103 C, F, K), we collected shale samples of Cretaceous and Jurassic (?) age, and processed and examined them for nannofossils. The ages of some collections are well defined by ammonites, particularly in the Albian interval, but macrofossil age constraints for most of the collections are poor.

The collections provided a number of poorly preserved nannofloras. Possible nannofloral ages represented in the collections range from Albian to Maastrichtian, but most probably are within the Albian/Cenomanian interval. No pre-Albian nannofloras were identified. Nannofossil biostratigraphical zones are given and some correlation with the macrofossils is achieved. The presence of *Seribiscutum primitivum* in several samples suggests a high latitude site of deposition.

Résumé : Aux fins de la corrélation des strates clastiques à grain fin pauvres en macrofossiles dans les îles de la Reine-Charlotte, en Colombie-Britannique (cartes 103 C, F, K du SNRC), les auteurs ont prélevé des échantillons de shale du Crétacé et du Jurassique(?) et, après traitement, en ont examiné les nannofossiles. Les âges de certaines collections sont bien définis par les ammonites, en particulier dans l'intervalle albien, mais dans la plupart des collections, les âges déterminés au moyen des macrofossiles sont mal encadrés.

Les collections ont livré un certain nombre de nannoflores mal préservées. Les âges possibles des nannoflores présentes s'échelonnent de l'Albien au Maastrichtien, mais se situent très probablement dans l'intervalle Albien-Cénomanien. Aucune nannoflore antérieure à l'Albien n'a été identifiée. Les zones biostratigraphiques des nannofossiles sont indiquées et mises en corrélation, dans une certain mesure, avec les macrofossiles. La présence de *Seribiscutum primitivum* dans plusieurs échantillons suggère un dépôt sous de hautes latitudes.

[1] Postgraduate Micropalaeontology Unit, Research School of Geological and Geophysical Sciences, Birkbeck College and University College London, Gower Street, London WC1E 6BT, United Kingdom

INTRODUCTION

The Queen Charlotte Islands form part of the Insular Belt of British Columbia, the most outboard of the morphogeological belts which comprise the western Canadian Cordillera (Fig. 1). Cretaceous strata are widespread across the Queen Charlotte Islands and various fossil faunas, principally ammonites and buchiid and inoceramid bivalves, have been used to demonstrate that almost every stage of the Cretaceous is present in the islands (Fig. 2). The Cretaceous rocks are altered to low metamorphic grade, if at all, and structural disruption is minimal in most exposures. Thus, the Queen Charlotte Islands are a natural laboratory for Cretaceous paleontological studies and, in fact, a significant number of biostratigraphic and biochronological studies have been undertaken previously on the older Mesozoic rocks there (see various papers in Woodsworth, 1991).

To date, correlation of Cretaceous rocks of the Queen Charlotte Islands has relied exclusively on macrofossils (cf. McLearn, 1972; Riccardi, 1981; Haggart, 1991). Abundant and diverse mollusc faunas are found only at certain stratigraphic levels (i.e., Albian), however, and mostly in specific lithofacies (e.g., shallow marine coarse clastics). Some levels of the Cretaceous, particularly the Aptian and post-Lower Turonian, are mostly lacking in macrofauna, due to ubiquitous deep-water deposition in much of the islands region at those times (Haggart, 1991; Haggart and Carter, 1993). Few macrofossils are found in these areally widespread mudstones, thus, local and regional correlation of these rocks is problematic. To address this issue, we sampled mudstones from the Queen Charlotte Islands for their nannofossil content.

The development of an integrated microfossil and macrofossil biochronology for the Canadian Cordillera is a long-term objective of paleontological research at the Geological Survey of Canada. Nannofossil biostratigraphy complements ongoing studies of molluscs, foraminifera, and radiolarians.

NANNOFOSSIL RESULTS

One hundred and seventy-eight shale samples were collected by one of us (JWH) from the Queen Charlotte Islands; smears of these were processed and examined subsequently for nannofossils in the Micropalaeontology Unit at University College London. The samples comprised a suite of Cretaceous and Jurassic(?), indurated black and dark grey shales and siltstones (see Appendix), much of which appeared to contain varying amounts of volcanogenic material.

Only 24 of the samples yielded calcareous nannofossils. All nannofossils were badly etched and exhibited low abundance and assemblage diversity. Such characteristics indicate that nannofossils were present at the time of shale deposition but that post-depositional/diagenetic activity has removed the majority of the nannofossils, leaving only the more solution-resistant species. These robust forms are, for the most part, stratigraphically long-ranging and consequently are of limited value for biostratigraphical correlation and resolution. The most robust Mesozoic nannofossil species present, *Watznaueria barnesae*, was the only species found in 11 of the samples (GSC locs. C-173869, C-185037, C-185042, C-187409, C-187582, C-208717, C-208721, C-208723 rare; C-196865, C-208725 few; C-208733 questionable occurrence). GSC loc. C-187301 contained very rare *Watznaueria fossacincta*; C-173857 contained *W. barnesae* and *Zeugrhabdotus* sp. and C-196959 contained *Retecapsa* sp.

The species found in the remaining samples are detailed below. Ages are based primarily on the *presence* of species in the samples, the *absence* of species probably being unreliable as age-indicative with material in this state of preservation. The nannofossil zones (CC) are based on Sissingh's (1977, 1978) and Perch-Nielsen's (1985) cosmopolitan biozonation schemes.

Longarm Formation samples

Sample C-184976 was collected on northern Burnaby Island (Fig. 1), from strata mapped previously as Longarm Formation (Lewis, 1991). Exposure in the vicinity of this locality consists of mudstone with minor, 2-4 cm-thick intercalated sandstone beds. The sample had a relatively diverse nannoflora comprising *Eiffellithus turriseiffelii?*, *Manivitella pemmatoidea*, *Prediscosphaera cretacea?*, *Retecapsa* sp., and *Watznaueria barnesae*.

The age suggested by the assemblage is Late Albian/Early Cenomanian to Maastrichtian, or CC9-26. This is the first recognition of strata of latest Early Cretaceous age or younger in the southern Queen Charlotte Islands, most Cretaceous rocks in the area being of Hauterivian-Barremian age (Haggart, 1991). Haggart (1991) suggested that fine clastic facies of this age might be present locally in the southern islands, as offshore, deeper-water equivalents of Haida Formation sandstones preserved in the offshore to the north and east. Identification of an Albian or younger nannofossil assemblage on Burnaby Island seems to support this hypothesis.

Haida Formation samples

Samples collected from the Haida Formation on northwestern Graham Island provided minimal constraining stratigraphic data. Sample C-208724, from Lepas Bay (Fig. 1), contained *Tranolithus orionatus*, *Watznaueria barnesae*, and *Zeugrhabdotus* sp. The suggested age is Albian to Early Maastrichtian, or CC8-23. Macrofossils collected from this vicinity suggest an Albian to Cenomanian age.

Sample C-208722, from the tidal bench north of Newcombe Hill (Fig. 1), contained a diverse nannoflora of *Biscutum ellipticum*, *Chiastozygus* sp., *Discorhabdus ignotus*,

Figure 1. *Map of Queen Charlotte Islands, British Columbia, showing locations of nannofossil localities discussed in text. Inset shows position of islands within the Insular Belt of the Canadian Cordillera (after Monger et al., 1982).*

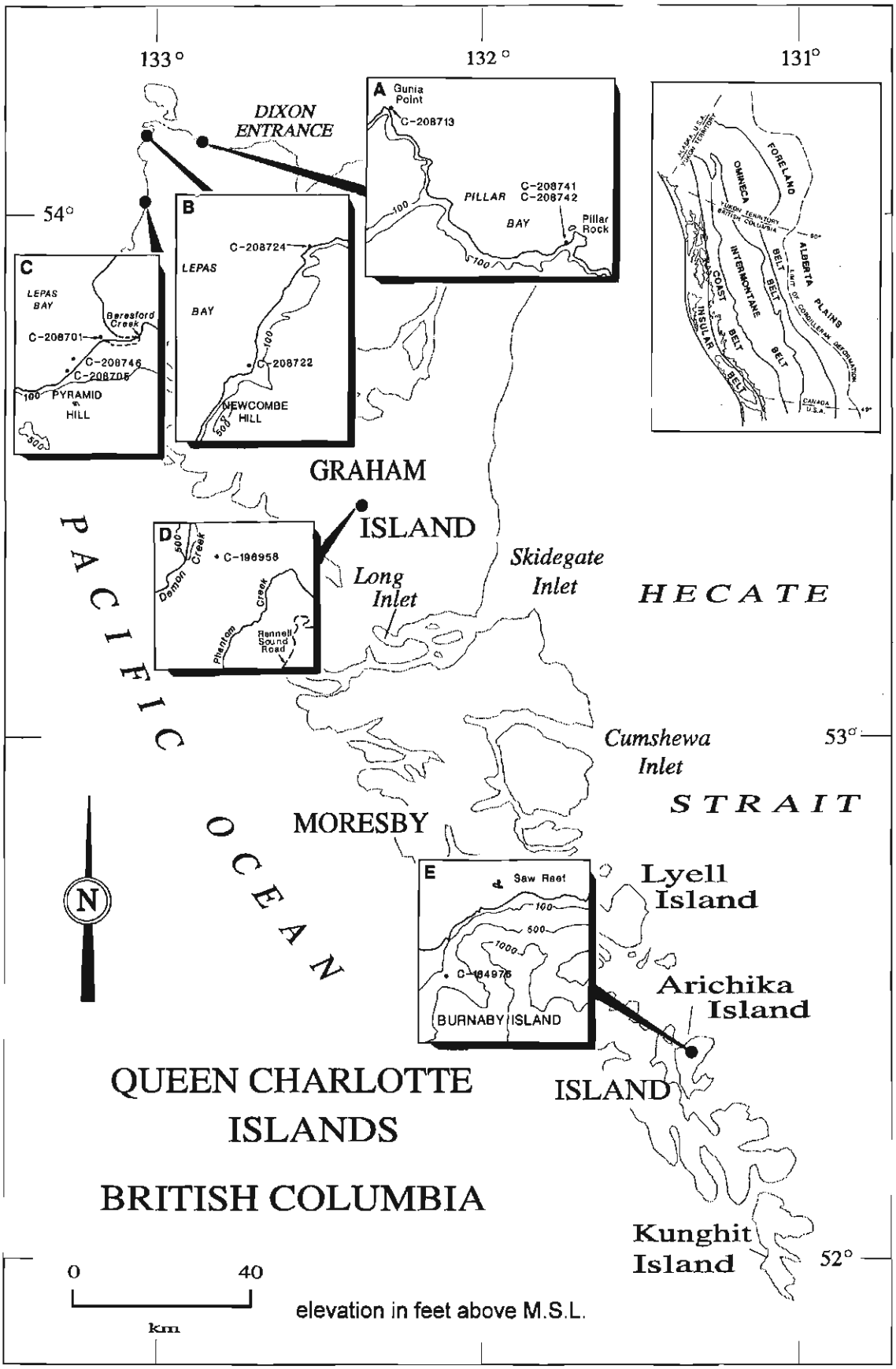
133°
132°
131°
54°
53°
52°
DIXON ENTRANCE
A
Gunia Point
C-208713
PILLAR BAY
C-208741
C-208742
Pillar Rock
B
C-208724
LEPAS BAY
C-208722
NEWCOMBE HILL
C
LEPAS BAY
Beresford Creek
C-208701
C-208746
C-208705
PYRAMID HILL
FORELAND
OMINECA
INTERMONTANE BELT
COAST PLUTONIC BELT
INSULAR BELT
ALBERTA PLAINS
GRAHAM ISLAND
D
C-196958
Denon Creek
Phantom Creek
Rennell Sound Road
Long Inlet
Skidegate Inlet
HECATE STRAIT
PACIFIC OCEAN
Cumshewa Inlet
MORESBY
E
Saw Reef
C-184976
BURNABY ISLAND
Lyell Island
Arichika Island
QUEEN CHARLOTTE ISLANDS
BRITISH COLUMBIA
Kunghit Island
N
0
40
km
elevation in feet above M.S.L.

Eiffellithus turriseiffelii, Eprolithus floralis, Manivitella pemmatoidea, Prediscosphaera columnata, Prediscosphaera cretacea?, Radiolithus planus, Retecapsa sp., *Staurolithites laffittei, Tranolithus orionatus, Watznaueria barnesae*, and *Zeugrhabdotus* sp. The general age suggested by this assemblage is Late Albian/Early Cenomanian to Late Santonian, or CC9-16; however, it can probably be restricted to Late Albian/Early Cenomanian to Turonian, or CC9-12, which is in agreement with macrofossil data suggesting an Albian-Cenomanian age.

Three collections from the thick section exposed in Beresford Bay (Fig. 1) provided nannofloras. From ammonite-poor strata at the base of the section, along Beresford Creek, sample C-208701 produced *Eprolithus floralis, Tranolithus orionatus*, and *Watznaueria fossacincta*, suggesting an Albian to Late Santonian age (CC8-16), probably Albian (CC8). Macrofossils collected from somewhat higher in this section are of Late Albian age (Haggart, 1986).

Sample C-208746, from the approximate middle of the Beresford Bay succession, contained a nannoflora with *Eiffellithus turriseiffelii, Eprolithus floralis, Retecapsa* sp., *Seribiscutum primitivum, Tranolithus orionatus, Watznaueria barnesae, Zeugrhabdotus diplogrammus*, and *Z. elegans*, suggesting an Albian/Cenomanian to Late Santonian age (CC9-16), also probably Late Albian (CC9).

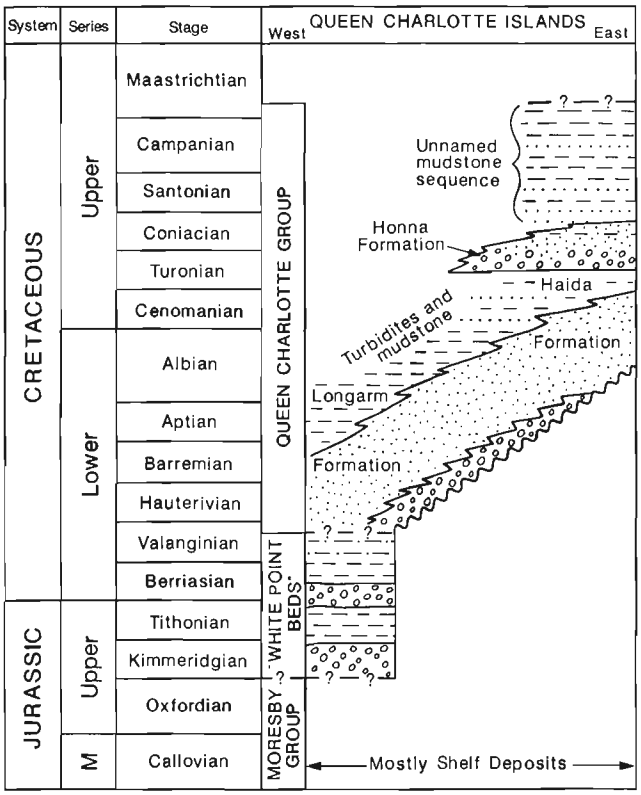

Figure 2. *Stratigraphic framework for Cretaceous rocks, Queen Charlotte Islands (after Haggart, 1991, 1993).*

The stratigraphically highest fossiliferous sample from the Beresford Bay region, C-208705, yielded a diverse nannoflora containing *Discorhabdus ignotus, Eiffellithus turriseiffelii, Eprolithus floralis, Manivitella pemmatoidea, Radiolithus planus, Rhagodiscus asper?, Tranolithus orionatus, Watznaueria barnesae, W. fossacincta, Zeugrhabdotus elegans*, and *Zeugrhabdotus* sp. Again, a Late Albian/Early Cenomanian to Late Santonian age is suggested (CC9-16), probably Late Albian/Early Cenomanian to Turonian (CC9-12). Ammonite data reported by Haggart (1986) from this part of the section also indicate a Late Albian to Early Cenomanian age.

Several samples from the Haida Formation exposed on central Graham Island yielded nannofossils but only one, locality C-196958, from just east of Demon Creek (Fig. 1), yielded a stratigraphically useful nannoflora. Identified in this assemblage are *Biscutum ellipticum, Discorhabdus ignotus, Eiffellithus turriseiffelii, Eprolithus floralis, Flabellites oblonga, Manivitella pemmatoidea, Microstaurus chiastius, Retecapsa surirella, Rhagodiscus angustus, Seribiscutum primitivum, Tranolithus orionatus, Watznaueria barnesae, W. britannica, Zeugrhabdotus elegans?*, and *Zeugrhabdotus* sp.

The age suggested by the assemblage is Late Albian/Early Cenomanian (CC9A-B). Macrofossils are rare in the belt of fine clastic Cretaceous rocks which trends through central Graham Island, thus identification of highest Lower Cretaceous to low Upper Cretaceous strata in this region confirms mapping based on lithological correlations (Hesthammer et al., 1991).

Honna Formation samples

The age of strata assigned to the Honna Formation is problematic. A few macrofossil collections have indicated a general post-Cenomanian age for the formation (Haggart, 1991). Most of the formation consists of conglomerate and sandstone but fine clastic interbeds are present locally in the unit.

Three collections provided nannofossils from the Honna Formation, all from northwest Graham Island, in the vicinity of Pillar Bay (Fig. 1). Sample C-208713 contained the following nannofloral elements: *Cretarhabdus striatus, Eiffellithus turriseiffelii, Eprolithus floralis?, Helicolithus trabeculatus, Prediscosphaera columnata?, Prediscosphaera cretacea, Rectapontis compactus, Tranolithus orionatus, Watznaueria barnesae*, and *Zeugrhabdotus elegans?*. The suggested age is Late Albian/Early Cenomanian to Late Santonian (CC9-16).

Samples C-208741 and C-208742 were collected from the section of the upper Honna Formation exposed in the east side of Pillar Bay. The stratigraphically lower collection, C-208741, yielded *Gartnerago obliquum, Rectapontis compactus, Staurolithites laffittei, Tranolithus orionatus*, and *Watznaueria barnesae*, giving a possible age range of Albian to Early Maastrichtian (CC8-23), but more likely Cenomanian at the oldest. The stratigraphically higher collection, C-208742, yielded *Chiastozygus* sp., *Eiffellithus turriseiffelii?, Eprolithus floralis?, Prediscosphaera columnata?, Rotelapillus laffittei, Retecapsa* sp., *Tranolithus orionatus*,

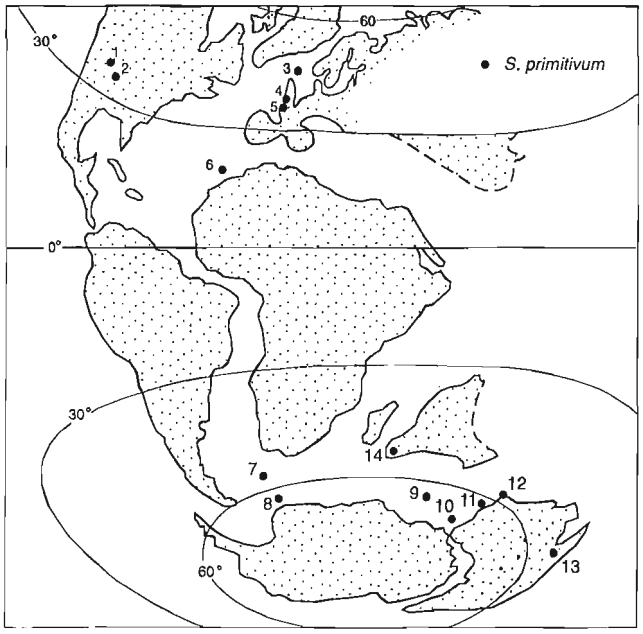

Figure 3. Bipolar distribution of Seribiscutum primitivum, *shown by black dots, during late Early to Late Cretaceous time (modified after Mutterlose and Wise, 1990: fig. 5). The species is not present in numerous ODP cores from the central Atlantic and Pacific Ocean regions.*

Watznaueria barnesae, Zeugrhabdotus elegans, Z. embergeri, and *Zeugrhabdotus* sp. The suggested age of this second collection is Late Albian/Early Cenomanian to Late Santonian (CC9-16).

DISCUSSION

Given their poor preservation, it is not possible to develop any significant paleoecological interpretations from the nannofloral assemblages; similarly, paleobiogeographical observations are also limited. One taxon is common in many of the samples, however, and it does appear to have important biogeographical implications: the species *Seribiscutum primitivum* is present in the collections from GSC localities C-196958 and C-208746. This species has previously been identified from high latitude deposits of both northern and southern hemispheres (Fig. 3) and is considered indicative of a high latitude of deposition (Thierstein, 1976; Mutterlose and Wise, 1990). This observation is in agreement with the molluscan and radiolarian faunas of the Queen Charlotte Islands, which also suggest high-latitude origins for the strata (Haggart and Carter, 1994).

ACKNOWLEDGMENTS

Many persons have collected samples for microfossil analysis from mudstones of uncertain age throughout Queen Charlotte Islands – we particularly thank Jonny Hesthammer and Charle Gamba for submitting several of the samples used in this study. Mike Orchard provided efficient and inexpensive courier service to London. T. Williams drafted the figures. J.A.B. was funded by a NERC/ODP Fellowship.

REFERENCES

Haggart, J.W.
1986: Stratigraphic investigations of the Cretaceous Queen Charlotte Group, Queen Charlotte Islands, British Columbia; Geological Survey of Canada, Paper 86-20, 24 p., 1 pl.
1991: A synthesis of Cretaceous stratigraphy, Queen Charlotte Islands, British Columbia; in Evolution and Hydrocarbon Potential of the Queen Charlotte Basin, British Columbia, G.J. Woodsworth (ed.); Geological Survey of Canada, Paper 90-10, p. 253-277.
1993: Latest Jurassic and Cretaceous paleogeography of the northern Insular Belt, British Columbia; in Mesozoic Paleogeography of the Western United States - II, G.C. Dunne and K.A. McDougall (ed.); Society of Economic Paleontologists and Mineralogists, Pacific Section, Book 71, p. 463-475.

Haggart, J.W. and Carter, E.S.
1993: Cretaceous (Barremian-Aptian) radiolaria from Queen Charlotte Islands, British Columbia: newly recognized faunas and stratigraphic implications; in Current Research, Part E; Geological Survey of Canada, Paper 93-1E, p. 55-65.
1994: Radiolarians: new biostratigraphic tools for dating Early Cretaceous strata of Queen Charlotte Islands, British Columbia; Geological Society of America, Abstracts with Programs, v. 26, no. 2, p. 56.

Hesthammer, J., Indrelid, J., Lewis, P.D., and Haggart, J.W.
1991: Geology of southern Graham Island, Queen Charlotte Islands, British Columbia; Geological Survey of Canada, Open File 2319, 2 sheets, scale 1:50 000.

Lewis, P.D.
1991: Geology of the Burnaby Island/Ramsay Island map area, Queen Charlotte Islands, British Columbia; Geological Survey of Canada, Open File 2316, 2 sheets, scale 1:25 000.

McLearn, F.H.
1972: Ammonoids of the Lower Cretaceous Sandstone member of the Haida Formation, Skidegate Inlet, Queen Charlotte Islands, western British Columbia; Geological Survey of Canada, Bulletin 188, 78 p., 45 pls.

Monger, J.W.H., Price, R.A., and Tempelman-Kluit, D.J.
1982: Tectonic accretion and the origin of the two metamorphic and plutonic welts in the Canadian Cordillera; Geology, v. 10, p. 70-75.

Mutterlose, J. and Wise, S.W., Jr.
1990: Lower Cretaceous nannofossil biostratigraphy of ODP Leg 113 Holes 692B and 693A, continental slope off east Antarctica, Weddell Sea; Proceedings of the Ocean Drilling Program, Scientific Results, v. 113, p. 325-351.

Perch-Nielsen, K.
1985: Mesozoic calcareous nannofossils; in Plankton Stratigraphy, H.M. Bolli, J.B. Saunders, and K. Perch-Nielsen (ed.); Cambridge University Press, v. 1, p. 329-426.

Riccardi, A.
1981: An Upper Cretaceous ammonite and inoceramids from the Honna Formation, Queen Charlotte Islands, British Columbia; in Current Research, Part C; Geological Survey of Canada, Paper 81-1C, p. 1-8, 1 pl.

Sissingh, W.
1977: Biostratigraphy of Cretaceous calcareous nannoplankton; Geologie en Mijnbouw, v. 56, no. 1, p. 37-65.
1978: Microfossil biostratigraphy and stage-stratotypes of the Cretaceous; Geologie en Mijnbouw, v. 57, no. 3, p. 433-440.

Thierstein, H.R.
1976: Mesozoic calcareous nannoplankton biostratigraphy of marine sediments; Marine Micropaleontology, v. 1, p. 325-362.

Woodsworth, G.J. (ed.)
1991: Evolution and hydrocarbon potential of the Queen Charlotte Basin, British Columbia; Geological Survey of Canada, Paper 90-10, 569 p.

Geological Survey of Canada Project 880038

APPENDIX A

Brief sample descriptions

1. Indurated, black shale: samples C-173869; C-185037; C-187301; C-187409; C-187582; C-196865; C-196958; C-208733.
2. Indurated, dark grey/green shale: samples C-184976 (crumbly), C-185042.
3. Indurated, dark grey shale: samples C-208701; C-208705; C-208713; C-208717; C-208721; C-208722; C-208723; C-208724; C-208725; C-208741; C-208742; C-208746.

APPENDIX B

Sample Localities

C-173857: 103 F/8; UTM = 678300E, 5916800N; central Graham Island, bed of Phantom Creek. Mapped as undifferentiated Cretaceous shale by Hesthammer et al. (1991).

C-173869: 103 F/8; UTM = 690400E, 5904300N; southern Graham Island, quarry on east side of logging road. Haida Formation shale.

C-184976: 103 B/6; UTM = 343500, 5811850; Burnaby Island, in bed of creek draining northeast side of island, approximately 1 km southeast of Alder Island. Mapped as Longarm Formation by Lewis (1991).

C-185037: 103 F/14; UTM = 623200E, 5983300N; northwest Graham Island, intertidal platform 3 km SW of White Point. 'White Point beds' of Haggart (1993).

C-185042: 103 F/14; UTM = 623100E, 5983450N; northwest Graham Island, intertidal platform 3 km SW of White Point. 'White Point beds' of Haggart (1993).

C-187301: 103 F/14; UTM = 623250E, 5983175N; northwest Graham Island, intertidal platform 3 km SW of White Point. Longarm Formation.

C-187409: 103 F/1; UTM = 689900E, 5890050N; northern Moresby Island, quarry adjacent to logging road. Yakoun Group?

C-187582: 103 G/4; UTM = 307200E, 5888300N; northern Moresby Island, quarry on north side of Skidegate Lake logging road. Haida Formation shale.

C-196865: 103 B/12; UTM = 328350E, 5840925N; Lyell Island, cut along logging road. Yakoun Group?

C-196958: 103 F/8; UTM = 677775E, 5918025N; central Graham Island, hillside east of Demon Creek. Mapped as undifferentiated Cretaceous shale by Hesthammer et al. (1991)

C-196959: 103 F/8; UTM = 678100E, 5918150N; central Graham Island, quarry along logging road, hillside east of Demon Creek. Haida Formation shale.

C-208701: 103 K/3; UTM = 627550E, 5988450N; northwest Graham Island, Beresford Bay. Haida Formation shale.

C-208705: 103 K/3; UTM = 626950E, 5987900N; northwest Graham Island, Beresford Bay. Haida Formation shale.

C-208713: 103 K/2; UTM = 634450E, 6004200N; northern Graham Island, Gunia Point. Honna Formation.

C-208717: 103 K/2; UTM = 632120E, 6006100N; Langara Island, Holland Point. Shales overlying Honna Formation.

C-208721: 103 K/2; UTM = 631700E, 6006000N; Langara Island, shoreline on north side of Solide Passage. Upper Honna Formation.

C-208722: 103 K/3; UTM = 626350E, 6000850N; northwest Graham Island, tidal bench north of Newcombe Hill. Haida Formation shale.

C-208723: 103 K/3; UTM = 626400E, 6000800NE; northwest Graham Island, intertidal terrace north of Newcombe Hill. Haida Formation shale.

C-208724: 103 K/3; UTM = 627400E, 6002900N; northwest Graham Island, Lepas Bay. Haida Formation shale.

C-208725: 103 K/3; UTM = 627400E, 6003100N; northwest Graham Island, south side of Lepas Bay. Haida Formation shale.

C-208733: 103 K/2; UTM = 635790E, 6002100N; northern Graham Island, Pillar Bay. Shales overlying Honna Formation.

C-208741: 103 K/2; UTM = 637650E, 6001900N; northern Graham Island, Pillar Bay. Shales overlying Honna Formation.

C-208742: 103 K/2; UTM = 637700E, 6001950N; northern Graham Island, Pillar Bay. Shales overlying Honna Formation.

C-208746: 103 K/3; UTM = 627000E, 5988100N; northwest Graham Island, Beresford Bay. Haida Formation.

Magnetostratigraphic potential of Longarm Formation (Lower Cretaceous) strata, Queen Charlotte Islands, British Columbia

James W. Haggart and Kenneth L. Verosub[1]
Cordilleran Division, Vancouver

Haggart, J.W. and Verosub, K.L., 1994: Magnetostratigraphic potential of Longarm Formation (Lower Cretaceous) strata, Queen Charlotte Islands, British Columbia; in Current Research 1994-E; Geological Survey of Canada, p. 45-52.

Abstract: A new magnetostratigraphic study of Cretaceous rocks of the Queen Charlotte Islands should improve the resolution of local and regional correlations and help assess possible latitudinal displacements. Preliminary sampling of Longarm Formation strata was done at three widely spaced localities in the islands (NTS 103C, F) to test the preserved magnetic signal. Biostratigraphic data suggest the sections include Hauterivian, Barremian, and Aptian strata.

All samples have magnetizations of moderate intensity and almost all reached stable endpoints during alternating field demagnetization. Stable endpoint inclinations are generally negative and commonly quite steep. Declinations are somewhat scattered but tend to fall in the southwest quadrant. Rock magnetic studies indicate that the principal magnetic carrier is very fine-grained magnetite. On the basis of this pilot study, we conclude that Longarm Formation strata contain a primary remanent magnetization suitable for magnetostratigraphic and tectonic studies.

Résumé : Une nouvelle étude magnétostratigraphique des roches crétacées des îles de la Reine-Charlotte devrait améliorer la précision des corrélations locales et régionales et faciliter l'évaluation des éventuels déplacements latitudinaux. Un échantillonnage préliminaire des strates de la Formation de Longarm a été exécuté dans trois localités largement espacées dans les îles (cartes 103 C, F du SNRC), afin de vérifier le signal magnétique préservé. Les données biostratigraphiques suggèrent que les coupes échantillonnées renferment des strates du Hauterivien, du Barrémien et de l'Aptien.

Tous les échantillons présentent des aimantations modérées et presque tous ont atteint des points extrêmes stables lors de la désaimantation du champ alternatif. Les inclinaisons des points extrêmes stables sont généralement négatives et souvent assez raides. Les déclinaisons affichent une certaine dispersion, mais elles ont tendance à chuter dans le quadrant sud-ouest. Les études magnétiques des roches indiquent que le principal porteur magnétique est une magnétite à grain très fin. À la lumière des résultats de cette étude pilote, les auteurs concluent que les strates de la Formation de Longarm renferment une aimantation rémanente primaire qui convient à des études magnétostratigraphiques et tectoniques.

[1] Department of Geology, University of California at Davis, Davis, California 95616 USA

INTRODUCTION

Cretaceous rocks form a significant part of the Mesozoic succession of Queen Charlotte Islands, western British Columbia (Fig. 1). The basement to the Cretaceous rocks of Queen Charlotte Islands is the classic Wrangellia Terrane sequence (summarized in Thompson et al., 1991 and Lewis et al., 1991) and includes Triassic pillow basalts and massive flows of the Karmutsen Formation and a conformably overlying succession of marine carbonates and clastics of Late Triassic to Early Jurassic age. Subsequent Middle to Late Jurassic arc volcanism is reflected in widespread pluton emplacement, and coeval andesitic volcanic rocks and associated epiclastic strata (Anderson and Reichenbach, 1991; Cameron and Tipper, 1985; Haggart, 1992).

The latitudinal position of Wrangellia during the Cretaceous is unclear. Various workers, citing paleomagnetic data, have inferred that Wrangellia Terrane occupied a low paleolatitude during Cretaceous time (Monger et al., 1982; Cowan, 1993; Wynne and Irving, 1993). Others cite geological evidence to suggest that the terrane arrived at its approximate position relative to North America by Middle Jurassic time (Thompson et al., 1991; van der Heyden, 1992; McClelland et al., 1992). The present study may resolve the problem.

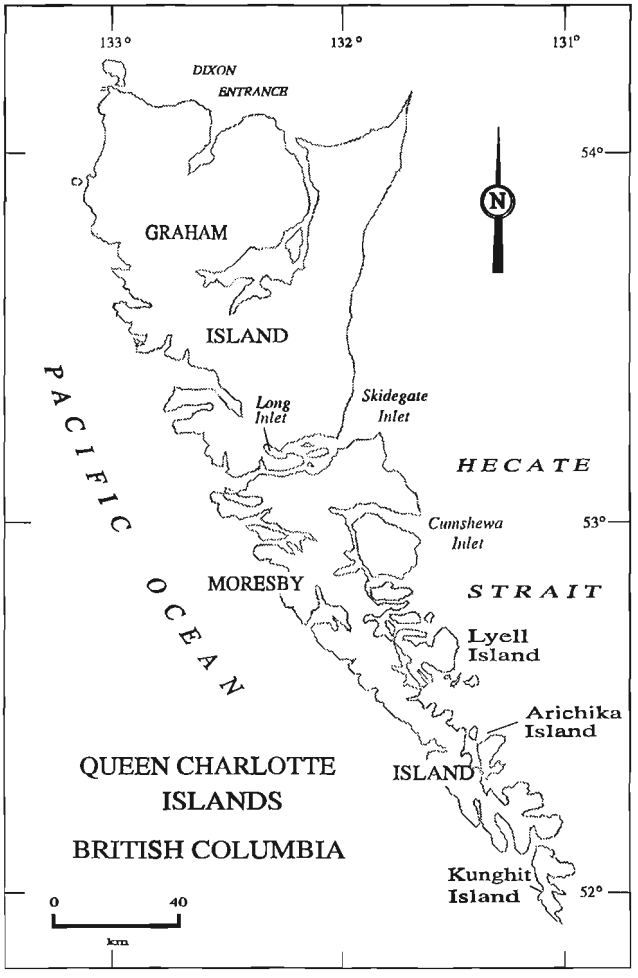

Figure 1. *Location map of Queen Charlotte Islands, British Columbia.*

The Cretaceous sequence of the islands records a history of essentially uninterrupted sedimentation through Cretaceous time. Strata of all stages are known with the exception of Berriasian and Maastrichtian, although there is a suggestion that at least the Berriasian may also be present (Haggart, 1991, 1992). Volcanic strata are uncommon in the Cretaceous succession and are known from only one geographically and temporally restricted Late Cretaceous locale. Most sections of Cretaceous strata exhibit an overall fining-upward trend and reflect initial transgression upon pre-Cretaceous basement and subsequent basin deepening. Stratigraphic analysis and paleocurrent and provenance studies indicate the basin was mostly open to the west (Yagishita, 1985; Haggart, 1991; Haggart and Carter, 1993; Gamba, 1993).

To date, correlation of Cretaceous strata of Queen Charlotte Islands has relied principally on molluscan biostratigraphy. However, difficulties exist in correlating poorly fossiliferous sections, especially in finer-grained facies. In addition, the endemic nature of much of the Cretaceous macrofauna of the islands restricts their utility in long distance, global correlations. Typically, microfauna are poorly preserved, although recent work suggests that some microfaunal groups may have promise in this area (e.g., Haggart and Carter, 1993).

As a potential correlation tool, we have initiated a magnetostratigraphic sampling program of Cretaceous strata of the Queen Charlotte Islands. The goals of this program are: 1) to improve the resolution of local stratigraphic correlations; 2) to increase the precision of regional and global correlations; 3) to integrate bio- and magnetostratigraphy for Cretaceous strata of the Northeast Pacific region; and 4) to assess various models of the Cretaceous tectonic history of the region.

PALEOMAGNETIC SAMPLING

To assess the suitability of Lower Cretaceous rocks for paleomagnetic studies, we sampled strata of the Valanginian to Aptian Longarm Formation in four sections at three widely separated localities in the islands: at Long Inlet in western Skidegate Inlet; at Cumshewa Inlet; and at Arichika Island (Fig. 1). The Longarm Formation at each of these localities consists of clastic sedimentary strata, variably rich in macrofossils. Although biostratigraphic control in each of the sections is limited, molluscan fossils indicate that the four sections include strata of at least Hauterivian-Barremian age (Fig. 2).

Section 89-1, in Cumshewa Inlet, was sampled using a portable, gasoline-powered diamond core drill. Three oriented cores were collected at each sample site. This section consists of medium- to coarse-grained, cross-stratified silty sandstone at the bottom, locally with pebble stringers. Several covered intervals characterize the lower part of the section and basalt sills, 0.5 to 3 m thick, are found near the base and

top. The section fines upward into massive to cross-stratified, silty fine-grained sandstone and sandy siltstone. Fossils collected from Section 89-1 include *Inoceramus* cf. *paraketzovi* EFIMOVA and *Simbirskites* in the lower part, indicating the presence of Hauterivian strata (Jeletzky, 1970), and the ammonites *Shasticrioceras, Lytoceras,* and *Shastoceras* in the middle part, indicating the presence of Barremian and possibly Aptian as well (Anderson, 1938; Murphy, 1975). Nine sites were sampled from this section, for an average sample interval of 15 m.

Sections 89-2 and 89-3, both in Long Inlet, do not include the base of the Cretaceous section, although facies and age relationships suggest that our paleomagnetic sampling included strata near the base of the stratigraphic succession in this region. Section 89-2 dips gently (30°NE) while Section 89-3 dips vertically (also NE). Several 0.5 to 1 m thick sills were noted in the upper part of Section 89-3. Lower strata in Section 89-3 and all strata in Section 89-2 consist of strongly indurated, silty, fine- to medium-grained, cross-stratified sandstone to granule sandstone, of lithic-arenite composition. Higher strata in Section 89-3 are more massive and consist of fine-grained sandstone to sandy siltstone. Fossils from the middle of Section 89-3 include the bivalve *Inoceramus* cf. *paraketzovi*, suggesting a general Hauterivian age. Fossils from Section 89-2 include the ammonite *Simbirskites* spp., also indicating a Hauterivian age, probably early (Jeletzky, 1970). Paleomagnetic samples were collected from each section following the procedure outlined above. Two sites were sampled from Section 89-2, for an average sample interval of 20 m. Five sites were sampled from Section 89-3, for an average sample interval of 30 m.

On Arichika Island, the last sampled locality (Section 89-4), the section consists of a basal conglomerate that fines upward through coarse-grained sandstone to fine-grained sandstone in its upper limits. The bivalve *I.* cf. *paraketzovi* and small belemnites were collected from the lower part of the section, indicating a Hauterivian age for those beds. We collected four oriented hand samples from Section 89-4, for an average sample interval of 46 m (Fig. 2).

All samples were measured on a cryogenic magnetometer at the Paleomagnetics Laboratory, University of California, at Davis.

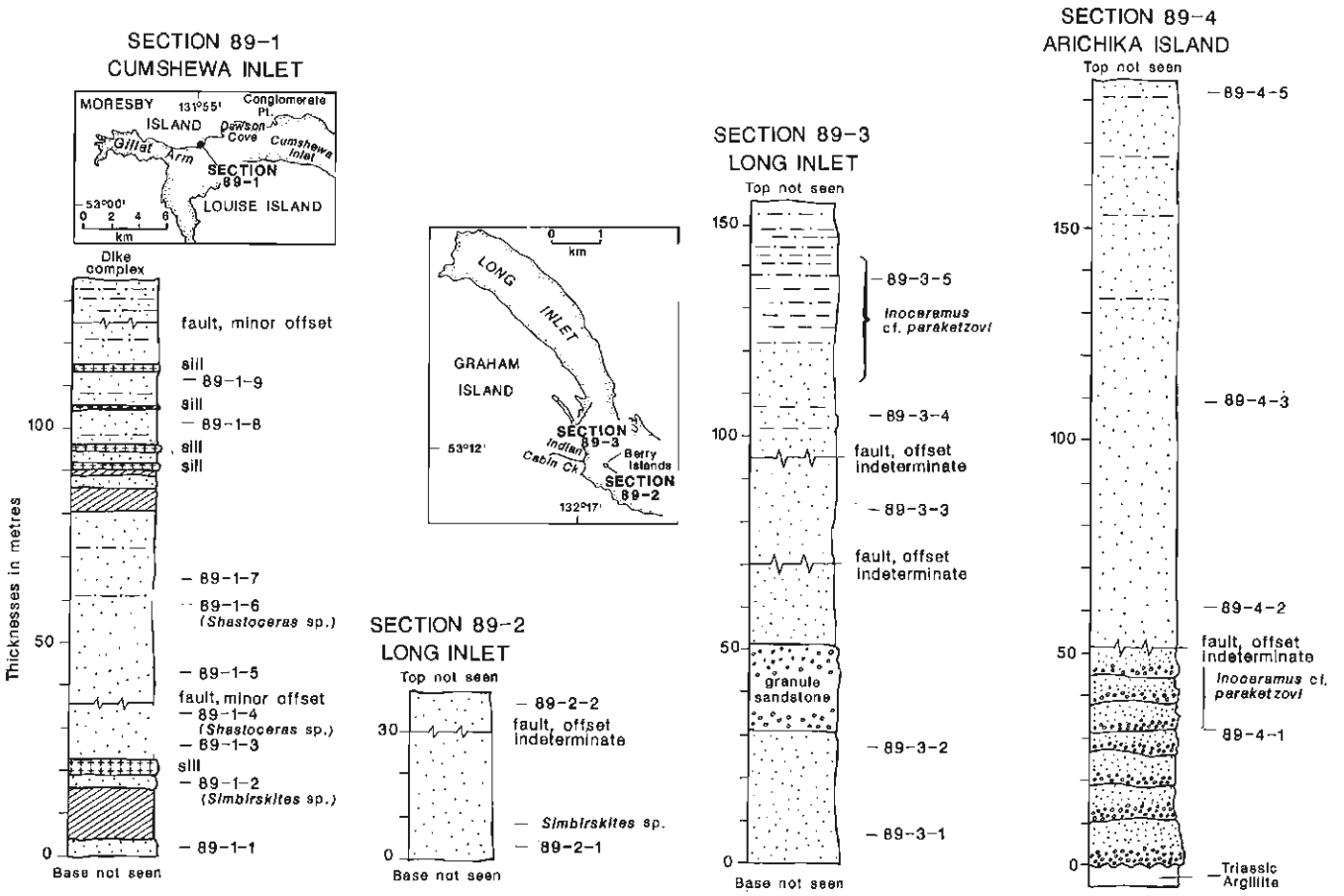

Figure 2. *Stratigraphy of sampled Longarm Formation sections, Queen Charlotte Islands. No correlation of sections implied.*

ROCK MAGNETIC ANALYSIS

We determined the nature of the magnetic carriers by studying the acquisition and demagnetization of anhysteretic remanent magnetization (ARM) and isothermal remanent magnetization (IRM). ARM is the magnetization acquired by a sample exposed to a weak direct field in the presence of a decreasing alternating magnetic field. IRM is the magnetization acquired in the presence of a strong direct field. Figure 3 shows typical curves for IRM acquisition. In these examples, the magnetization levels off and becomes saturated at about 100-200 milliTesla, which suggests that magnetite, rather than hematite, is the magnetic carrier.

Comparisons of alternating field demagnetization of the ARM and the saturated IRM (SIRM) of typical samples are shown in Figure 4. The SIRM curve is consistently below the ARM curve, which implies that the strata contain fine-grained magnetic carriers in either a single domain or pseudo-single domain state. Together with IRM acquisition data, these results indicate that the magnetic mineralogy of the Longarm Formation consists primarily of fine-grained magnetite.

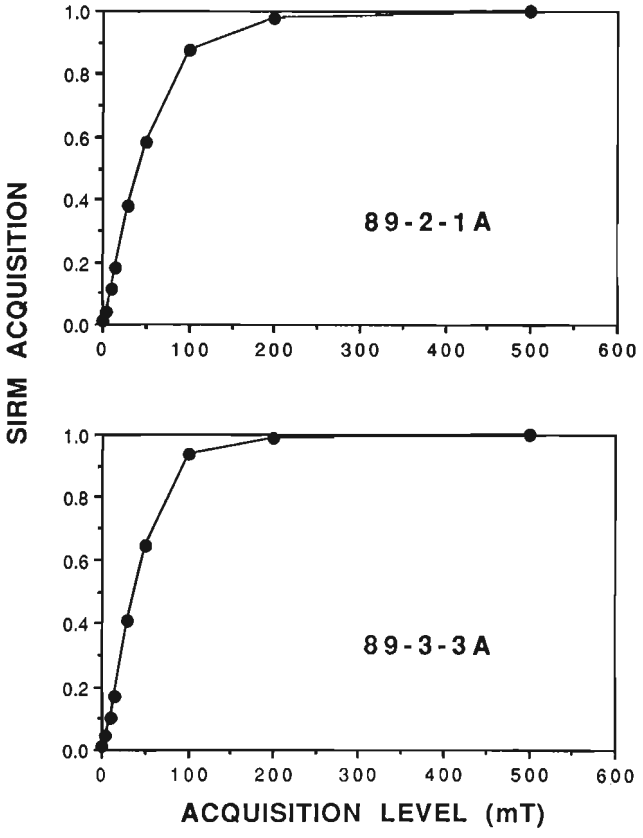

Figure 3. Typical SIRM acquisition curve obtained after demagnetization. Induced magnetization on the vertical axis and acquisition level (milliTesla) on the horizontal. The curve levels off, or becomes saturated, at ~100-200 milliTesla.

PALEOMAGNETIC ANALYSIS

Samples from all four sections were subjected to both alternating field and thermal demagnetization. Figure 5 shows typical curves of the decrease in intensity during alternating field demagnetization. The curves have median destructive fields of about 20-35 milliTesla, which is consistent with our inference about the nature of the magnetic carriers. Figure 6 shows typical curves of directional changes during alternating field demagnetization of samples from Long Inlet. Closed squares are plotted on north-south and east-west axes, and represent the declinations at each demagnetization level. Open squares are plotted on vertical and horizontal axes, and represent the inclinations at each demagnetization level. The initial direction (zero demagnetization level) is shown by the enlarged box.

Paleomagnetic results from Arichika Island and the two sites on Long Inlet are quite promising. In each case, the alternating field demagnetization quickly removed any viscous secondary components and thereafter the magnetization decayed univectorially toward the origin. Thus, these samples appear to have stable primary directions with well-defined endpoints. The samples from Cumshewa Inlet are more difficult to interpret, and it is not always clear that a stable endpoint was reached in the demagnetization process.

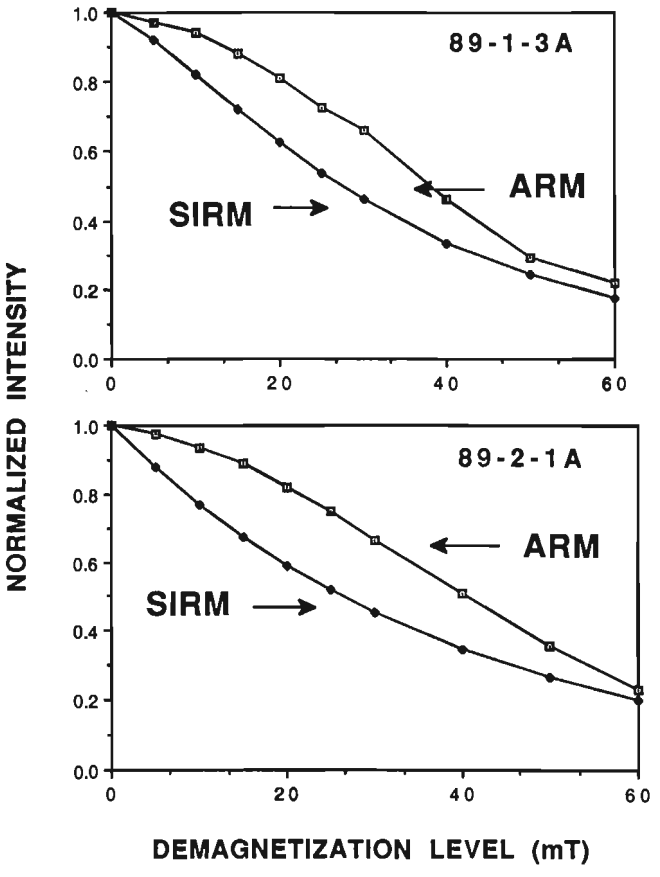

Figure 4. Typical ARM-SIRM curves.

The results of thermal demagnetizations are problematical. At about 400°C several of the samples showed large and erratic changes in direction, associated with moderate increases in magnetic susceptibility. We believe that these directional changes reflect chemical alteration of magnetic minerals caused by heating. Paleomagnetic data obtained below 400°C generally showed univectorial decay toward the origin and, more importantly, for paired samples there was very good agreement between the results obtained by alternating field demagnetization and those obtained by thermal demagnetization.

The alternating field or thermal demagnetization curve for each sample was analyzed using the least-squares approach of Kirschvinck (1980). For alternating field demagnetization, the 16 samples from Long Inlet and Cumshewa Inlet yielded 12 good directions. All of these directions had upward inclinations and southerly declinations that indicate a reversed magnetic polarity. These results are shown in Figure 7a. The four samples from Arichika Island yielded three good directions, all of which had the downward inclinations and northerly declinations of a normal magnetic polarity. As noted above, thermally demagnetized samples generally yielded directions that were consistent with directions obtained from paired samples that had been thermally demagnetized. The thermally demagnetized directions from samples from Long Inlet and Cumshewa Inlet are shown in Figure 7b.

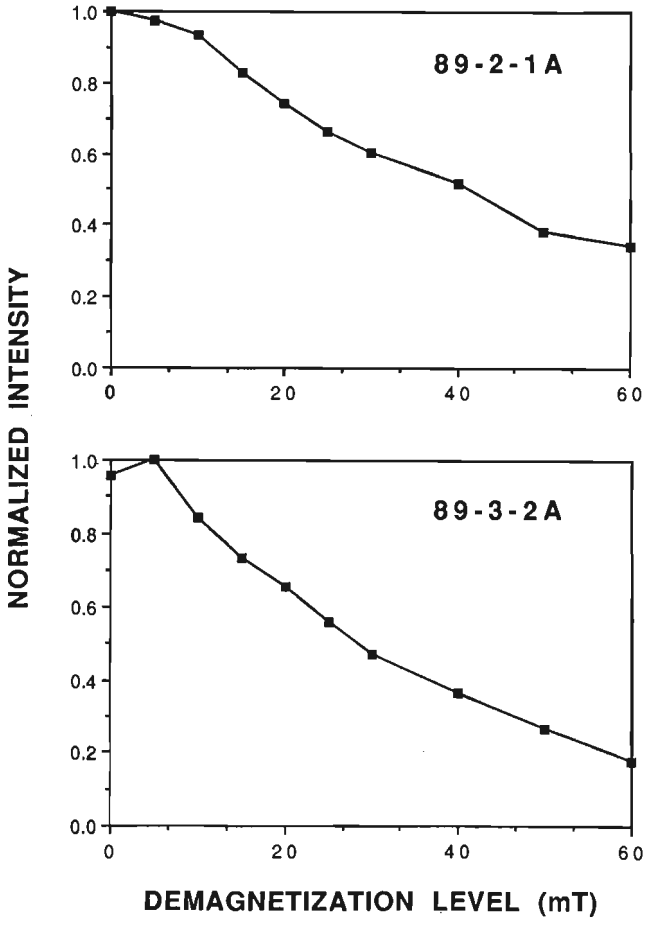

Figure 5. Typical curves of intensity decrease during demagnetization. The curves fall off with median destructive fields of about 30-35 milliTesla, consistent with our inferences about the nature of the magnetic carrier.

DISCUSSION

Subsequent remagnetization possibilities

Structural disruption of Mesozoic strata on Queen Charlotte Islands is concentrated in discrete zones (Thompson et al., 1991) and most rocks exhibit low metamorphic grade (Sutherland Brown, 1968). Most sections of Cretaceous rocks outside the principal deformation zones are flat lying to gently dipping, show minimal deformation and alteration, and, at a few sites, contain mollusc fossils that retain their original aragonite component (Haggart, 1991).

Conodont Colour Alteration work on Triassic rocks and organic maturation studies on Mesozoic strata indicate a systematic diagenetic alteration pattern across the islands, increasing towards the southern part of Queen Charlotte Islands and likely reflecting proximity to plutonism (Orchard and Forster, 1991; Vellutini and Bustin, 1991). Our sampled sections were selected to avoid as much as possible structural disruption and effects of intrusion. It appears that this strategy

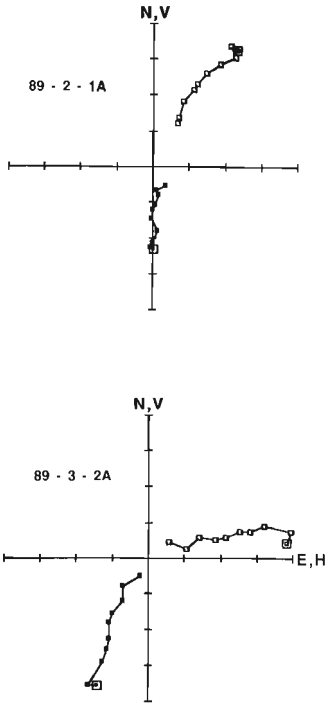

Figure 6. Typical curves of directional change during demagnetization of Longarm Formation samples. Closed squares refer to sample declination and are related to north and east axes. Open squares refer to vertical and horizontal axes and give sample's magnetic inclination. The start of each curve is shown by the enlarged boxes.

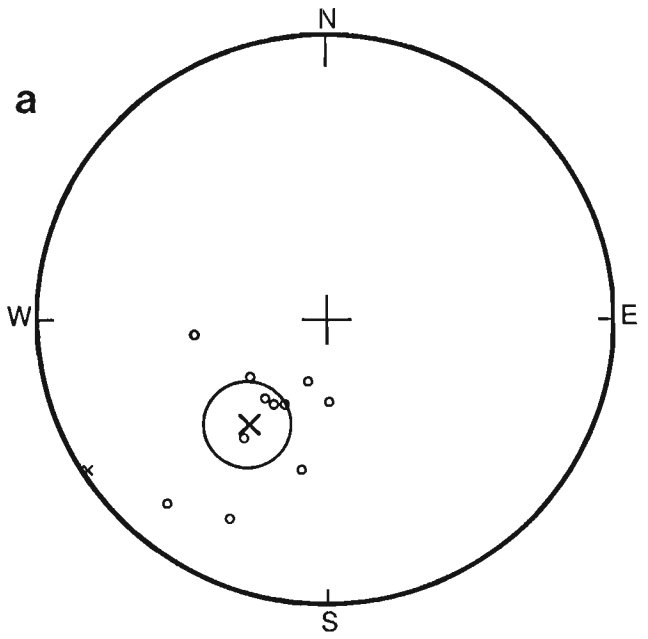

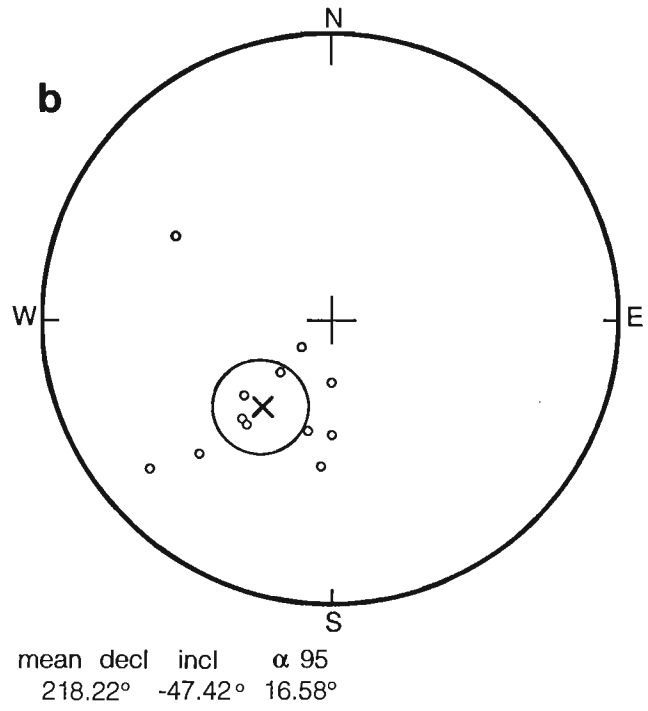

Figure 7. *Stereonet of final directions for the 12 samples with stable endpoints.* ***(a)*** *shows mean direction for alternating field demagnetized samples;* ***(b)*** *shows mean direction for thermally demagnetized samples.*

can guide us in future sampling. The fact that good magnetic signals were obtained from the vertically dipping Section 89-3 in Long Inlet suggests that structural disruption has affected the magnetic signature minimally or not at all.

The question of whether a normal overprint has been fully removed is relevant to magnetostratigraphic studies of the Longarm Formation. The recovery of almost antipodal normal and reversed directions is strong evidence that we are dealing with a primary detrital remanent magnetization that has not been subsequently remagnetized. In fact, the two most likely sources of remagnetization are the Recent and the Cretaceous Long Normal Intervals. The fact that most of the polarities measured are reversed is additional evidence against the remagnetization hypothesis.

Magnetostratigraphy

The magnetic polarity time scale for the Lower Cretaceous is shown in Figure 8. The Hauterivian-Aptian interval is a period characterized by both normal and reversed magnetic polarity zones of varying length. Above Chron M0, however,

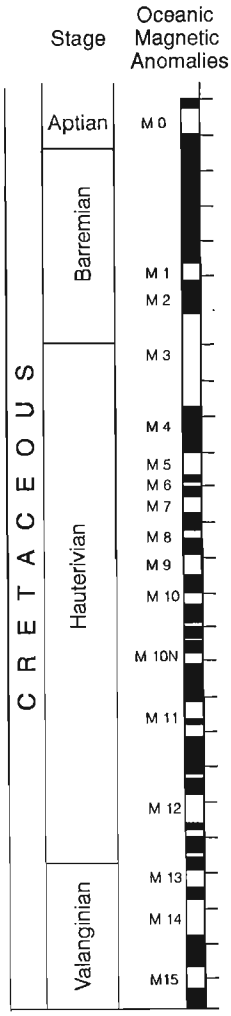

Figure 8. *Lower Cretaceous magnetostratigraphic time scale (after Lowrie and Alvarez, 1984).*

found within the lower part of the Aptian (Lowrie and Alvarez, 1984; Lowrie and Ogg, 1986), an extended period of normal polarity, termed the Cretaceous Long Normal Interval, characterizes the time scale until the lower Campanian.

The biostratigraphic data we have for our four sections suggest that Aptian strata are present only in the Cumshewa Inlet section (Section 89-1). This is based on the occurrence of the ammonite *Shastoceras* at several levels in this section. The genus *Shastoceras* is endemic to the western coast of North America, and was previously recognized in the lower Aptian of northern California (Anderson, 1938; Wright, 1957). Thus, we infer that all strata sampled in Section 89-1 in Cumshewa Inlet, spanning some 135 m, are contained within Chron M0 or below. It is interesting to note that to date, our sampling of this section has only detected reversed polarity zones. However, we consider this fortuitous and due to the sparse sampling density undertaken for our preliminary study. We also note that six of the sampled horizons in Section 89-1 are within the zone of *Shastoceras* and thus are likely within the lower Aptian reversed zone. Given that the absolute time represented by both normal and reversed polarity periods is approximately equal for the Hauterivian-lower Aptian interval (Lowrie and Ogg, 1986), it is not surprising that the three sampled horizons lower in the Cumshewa Inlet section are also of reversed polarity.

Unfortunately, with the low sampling density that characterizes our preliminary study it is not possible to confidently correlate the bulk of our sampled sections with the magnetic polarity time scale. We are confident, however, that a complete magnetostratigraphic study of the Longarm Formation, integrated with available biostratigraphic control, will ultimately allow us to make an unambiguous correlation with the time scale.

Displacement and rotation?

The mean direction for alternating field demagnetized samples in Figure 7a has an inclination of -41.0° and a declination of 216.5° with an α_{95} of 14.9°. For thermally demagnetized samples in Figure 7b the inclination is -47.4°, the declination is 218.2°, and the α_{95} is 16.6°. On first assessment, these data seem to suggest that strata of the Longarm Formation may have been deposited at a latitude of about 25°, and that they have been subsequently rotated clockwise about 15-20°.

Although tectonic rotations of parts of northern Queen Charlotte Islands have been inferred previously, based on paleomagnetic data (Yorath and Chase, 1981; Higgs, 1990), these interpretations have been questioned on the grounds of geologic evidence (Lewis et al., 1992). At present, we feel there are too few samples in our data set to allow us to draw any firm conclusions from the data regarding possible displacements or rotations. In addition, we note that the three good (normal) directions from Arichika Island are significantly steeper than the reversed directions shown in Figure 7. This suggests that we may not have removed all the normal overprint in the samples with reversed directions. Clearly, additional sampling and additional paleomagnetic and rock magnetic studies are needed before the questions of translation and rotation can be resolved. However, our preliminary results indicate that these studies are certainly worth pursuing.

CONCLUSIONS

We emphasize that our study to date has been preliminary in scope, with the goal of assessing the suitability of Cretaceous strata of Queen Charlotte Islands for detailed paleomagnetic study. We have found that the principal magnetic carrier appears to be fine-grained magnetite and that the rocks carry a strong and stable magnetic signal. Primary directions with stable endpoints have been recovered using both alternating field and thermal demagnetization methods, and these directions represent both normal and reversed polarities. With additional work, it should be possible to develop a detailed magnetostratigraphy of Cretaceous strata and possibly to determine the extent of tectonic translations and rotations.

REFERENCES

Anderson, F.M.
1938: Lower Cretaceous deposits in California and Oregon; Geological Society of America, Special Paper 16, 339 p.

Anderson, R.G. and Reichenbach, I.
1991: U-Pb and K-Ar framework for Middle to Late Jurassic (172≥158 Ma) and Tertiary (46-27 Ma) plutons in Queen Charlotte Islands, British Columbia; in Evolution and Hydrocarbon Potential of the Queen Charlotte Basin, British Columbia, (ed.) G.J. Woodsworth; Geological Survey of Canada, Paper 90-10, p. 59-87.

Cameron, B.E.B. and Tipper, H.W.
1985: Jurassic stratigraphy of the Queen Charlotte Islands, British Columbia; Geological Survey of Canada, Bulletin 365, 49 p.

Cowan, D.S.
1993: Alternative models for Late Jurassic and Early Cretaceous paleogeography of the western Cordillera, California to SE Alaska; Geological Society of America, Abstracts with Programs, v. 25, no. 5, p. 24.

Gamba, C.A.
1993: Stratigraphy and sedimentology of the Late Jurassic to Early Cretaceous Longarm Formation, Queen Charlotte Islands, British Columbia; in Current Research, Part A; Geological Survey of Canada, Paper 93-1A, p. 139-148.

Haggart, J.W.
1991: A synthesis of Cretaceous stratigraphy, Queen Charlotte Islands, British Columbia; in Evolution and Hydrocarbon Potential of the Queen Charlotte Basin, British Columbia, (ed.) G.J. Woodsworth; Geological Survey of Canada, Paper 90-10, p. 253-277.
1992: Progress in Jurassic and Cretaceous stratigraphy, Queen Charlotte Islands, British Columbia; in Current Research, Part A; Geological Survey of Canada, Paper 92-1A, p. 361-365.

Haggart, J.W. and Carter, E.S.
1993: Cretaceous (Barremian-Aptian) radiolaria from Queen Charlotte Islands, British Columbia: newly recognized faunas and stratigraphic implications; in Current Research, Part E; Geological Survey of Canada, Paper 93-1E, p. 55-65.

Higgs, R.
1990: Sedimentology and tectonic implications of Cretaceous fan-delta conglomerates, Queen Charlotte Islands, Canada; Sedimentology, v. 37, p. 83-103.

Jeletzky, J.A.
1970: Cretaceous macrofaunas; in Biochronology: Standard of Phanerozoic Time, E.W. Bamber, et al. (ed.); Geological Survey of Canada, Economic Geology Report No. 1, pt. B, p. 649-662.

Kirschvinck, J.L.
1980: The least-squares line and plane and the analysis of palaeomagnetic data; The Geophysical Journal of the Royal Astronomical Society, v. 62, p. 699-718.

Lewis, P.D., Haggart, J.W., Anderson, R.G., Hickson, C.J., Thompson, R.I., Dietrich, J.R., and Rohr, K.M.M.
1991: Triassic to Neogene geologic evolution of the Queen Charlotte region; Canadian Journal of Earth Sciences, v. 28, p. 854-869.

Lewis, P.D., Thompson, R.I., Haggart, J.W., and Hickson, C.J.
1992: Discussion: Sedimentology and tectonic implications of Cretaceous fan-delta conglomerates, Queen Charlotte Islands, Canada; Sedimentology, v. 38, p. 1173-1182.

Lowrie, W. and Alvarez, W.
1984: Lower Cretaceous magnetic stratigraphy in Umbrian pelagic limestone sections; Earth and Planetary Science Letters, v. 71, p. 315-328.

Lowrie, W. and Ogg, J.G.
1986: A magnetic polarity time scale for the Early Cretaceous and Late Jurassic; Earth and Planetary Science Letters, v. 76, p. 341-349.

McClelland, W.C., Gehrels, G.E., and Saleeby, J.B.
1992: Upper Jurassic-Lower Cretaceous basinal strata along the Cordilleran margin: implications for the accretionary history of the Alexander-Wrangellia-Peninsular terrane; Tectonics, v. 11, p. 823-835.

Monger, J.W.H., Price, R.A., and Tempelman-Kluit, D.J.
1982: Tectonic accretion and the origin of the two metamorphic and plutonic welts in the Canadian Cordillera; Geology, v. 10, p. 70-75.

Murphy, M.A.
1975: Paleontology and stratigraphy of the lower Chickabally Mudstone Member (Barrenian-Aptian) in the Ono Quadrangle, northern California; University of California Publications in Geological Sciences, v. 113, 52 p.

Orchard, M.J. and Forster, P.J.L.
1991: Conodont colour and thermal maturity of the Late Triassic Kunga Group, Queen Charlotte Islands, British Columbia; in Evolution and Hydrocarbon Potential of the Queen Charlotte Basin, British Columbia, (ed.) G.J. Woodsworth; Geological Survey of Canada, Paper 90-10, p. 453-464.

Sutherland Brown, A.
1968: Geology of the Queen Charlotte Islands, British Columbia; British Columbia Department of Mines and Petroleum Resources, Bulletin 54, 226 p.

Thompson, R.I., Haggart, J.W., and Lewis, P.D.
1991: Late Triassic through early Tertiary evolution of the Queen Charlotte Basin, British Columbia, with a perspective on hydrocarbon potential; in Evolution and Hydrocarbon Potential of the Queen Charlotte Basin, British Columbia, (ed.) G.J. Woodsworth; Geological Survey of Canada, Paper 90-10, p. 3-29.

van der Heyden, P.
1992: A Middle Jurassic to Early Tertiary Andean-Sierran arc model for the Coast Belt of British Columbia; Tectonics, v. 11, p. 82-97.

Vellutini, D. and Bustin, R.M.
1991: Organic maturation of Mesozoic and Tertiary strata of the Queen Charlotte Islands, British Columbia; in Evolution and Hydrocarbon Potential of the Queen Charlotte Basin, British Columbia, (ed.) G.J. Woodsworth; Geological Survey of Canada, Paper 90-10, p. 411-451.

Wright, C.W.
1957: Systematic descriptions; in Mesozoic Ammonoidea, W.J. Arkell, B. Kummel, and C.W. Wright; in Treatise on Invertebrate Paleontology Part L (*Mollusca IV, Cephalopoda, Ammonoidea*), (ed.) R.C. Moore; Geological Society of America and University of Kansas Press, Lawrence, Kansas, p. 129-437.

Wynne, P.J., Irving, E., Maxson, J., and Kleinspehn, K.
1993: Paleomagnetic results from the middle Cretaceous Silverquick and Powell Creek formations and northward displacement of the western Intermontane Belt, British Columbia; Geological Association of Canada, Mineralogical Association of Canada, Joint Annual Meeting, 1993, Program and Abstracts, p. A-112.

Yagishita, K.
1985: Evolution of a provenance as revealed by petrographic analyses of Cretaceous formations in the Queen Charlotte Islands, British Columbia, Canada; Sedimentology, v. 32, p. 671-684.

Yorath, C.J. and Chase, R.L.
1981: Tectonic history of the Queen Charlotte Islands and adjacent areas - a model; Canadian Journal of Earth Sciences, v. 18, p. 1717-1739.

Geological Survey of Canada Project 870070

Coastal erosion on the east coast of Graham Island, Queen Charlotte Islands, British Columbia

Kim W. Conway and J. Vaughn Barrie
Pacific Geoscience Centre, Sidney

Conway, K.W. and Barrie, J.V., 1994: Coastal erosion on the east coast of Graham Island, Queen Charlotte Islands, British Columbia; in Current Research 1994-E; Geological Survey of Canada, p. 53-58

Abstract: The coastal zone of eastern Graham Island, the largest of the Queen Charlotte Islands, is subject to severe erosional events during winter storms. Over 11 m of land was lost over a one year period (1992-1993) at one monitoring site (Cape Fife) and 1.5 m was measured to have eroded at the same location in a 24 hour period following a storm (Feb. 8, 1994). Analysis of airphotos indicate that a rate of erosion of about 1 m per annum is indicated in the northern part of the study area.

Slumping of oversteepened Holocene dunes and Pleistocene cliffs during and shortly after southeasterly winter storms combined with strong longshore transport to the north are the dominant processes observed. Shore-attached bars may also play an important role in sediment storage and transport of eroded sediments on the east coast of Graham Island.

Résumé : La zone côtière de la partie est de l'île Graham, la plus vaste des îles de la Reine-Charlotte, a été soumise à des épisodes d'érosion intense pendant les tempêtes hivernales. Pendant une période d'une année (1992-1993), plus de 11 m de terrain ont été perdus à un site de surveillance (Cap Fife); selon les mesures effectuées au même endroit, 1,5 m a été enlevé par l'érosion pendant une période de 24 heures, à la suite d'une tempête (8 février 1994). L'analyse de photographies aériennes indique une vitesse d'érosion d'environ 1 m par an dans la partie nord de la région étudiée.

Les glissements subis par les dunes fortement pentées d'âge holocène et par les falaises d'âge pléistocène pendant et peu après les tempêtes hivernales de direction sud-est, combinés à une longue dérive littorale vers le nord, sont les principaux processus observés. Les cordons littoraux rattachés au rivage peuvent aussi jouer un rôle important du point de vue du stockage et du transport des sédiments érodés sur la côte est de l'île Graham.

INTRODUCTION

Erosion of the eastern coast of Graham Island, the northern main island of the Queen Charlotte Islands, has been noted by residents and B.C. Parks personnel over several years. Residents of Tlell report losing as much as 2 m of land during a single storm in 1992 (Jennifer Davies, pers. comm.). Harper (1980) suggested that this coast has been eroding throughout the Holocene, and that the shallow portion of Dogfish Bank was the remnant of a more extensive Graham Island. The east coast is sparsely populated; a large provincial park (Naikoon Park) forms about 60% of the coastline and the area is relatively undeveloped.

Erosion along the southern part of the east side of Graham Island (south of Tlell) has been of some concern to the British Columbia Ministry of Highways for over 35 years due to coastal erosion affecting the highway (Hwy.16) which follows the coastline from Tlell to Skidegate (Fig.1). Sections of this highway have been relocated due to coastal erosion prior to 1970 (Nyland, 1981). The Ministry has recently constructed armour riprap blankets to protect the roadbed in this area (Alexander, 1993). Clasts 250 to 500 kg have been effective in stabilizing the intertidal zone and adjacent roadbed.

Given the dynamic nature of the eastern Graham Island coastline the Geological Survey of Canada began an erosion monitoring program at three selected sites in the area between Rose Spit and Cape Fife in 1990. A further three monitoring sites were established on the accretionary north coast of Graham Island. The purpose of this paper is to review what is known about the erosion on the east coast of Graham Island to date, from our monitoring work in a restricted study area, and more generally along the entire coastline.

REGIONAL SETTING

The eastern coast of Graham Island forms part of the Argonaut Plain, a poorly drained, lowland area bordered by Dogfish Bank in Hecate Strait (Fig.1). The plain is underlain by Neogene clastic sediments up to 1500 m thick, the Skonun Formation (Sutherland Brown, 1968; Higgs, 1991). A few outcrops of volcanic rocks occur in the area (Woodsworth, 1991). The plain is largely covered by a thick sand deposit, thought to have developed as an outwash deposit (Clague et al, 1982) formed when peidmont glaciers from the last glaciation receded from the area. The Tertiary sediments are also mantled by tills, stiff marine silt and clay, fluvial and marine sediments and dunes locally (Clague and Bornhold, 1980; Clague et al., 1982). The narrow (average <150 m) intertidal zone is backed by cliffs cut into Pleistocene sediments and Holocene sand dunes.

The predominant wind direction is from the southeast during the winter and storms can be frequent and intense from this quarter. The tides are mixed semidiurnal and the tidal range is large, with higher high water often 5 m above datum. Southeast winds can quickly blow up and marine conditions deteriorate rapidly during the winter months in Hecate Strait (Thomson, 1981). The summer wind pattern is from the northwest and is the wind direction during fair weather conditions.

METHODS

The sites were selected based on criteria to provide an even distribution of observation sites within the study area as well as being representative of the beach/shoreline conditions. A total of six stations, three on the north coast and three on the east, have been monitored on an annual basis since 1990. Standard survey techniques were used to establish local benchmarks against which erosion could be measured and beach profiles run. Vertical air photos (1937 and 1980), oblique air photos (February 1994) and a SPOT satellite image (May 1992) were used to obtain estimates of erosion south of Cape Fife and north of Tlell. The lack of good reference points on the ground inhibits continuous measurement of erosion by photogrammetry along the entire east coast of Graham Island. Selected areas with good morphological reference features were chosen (lakes, meanders in streams, scarps) to provide a relative reference for point measurements.

RESULTS

Measured amounts of erosion are given for two monitoring sites on East Beach in Table 1. It is noteworthy that the erosion occurring in a one day period in February 1994 at the Cape Fife site (site 2) is greater than the measured erosion during all of 1993 at that location. At Kumara Lake (Fig. 2), south of Cape Fife, comparison of 1980 vertical air photos and 1994 oblique air photos coupled with ground truthing traverses indicate that about 60 m has been lost in this area between 1980 and 1994. The seaward shore of Kumara Lake was breached by the ocean in 1988 and since that time has become a lagoon or embayment. Coarse marine sediments (sands and gravels) which are storm washover deposits, are rapidly infilling the seaward side of the former lake basin.

Just north of Eagle Hill a small unnamed lake has drained in a similar fashion to Kumara, erosion at this site appears to be roughly 80 m over the period 1937-1980.

Erosion at certain locations is estimated at between 10 and 70 m over the period from 1937 to 1980 by comparing vertical air photos for different sites in the area between Eagle Hill and the Oeanda River mouth. The mean erosion for the measurements made was 36 m, or slightly less than a metre per year.

Between Cape Ball and Eagle Hill estimates of erosion between 1937 and 1980 were also obtained by comparing air photos. The measurements varied from 0 to 70 m. The mean erosion over the period here was 48 m. These mean values are included for discussion only, as erosion may occur in short time intervals separated by relatively inactive periods.

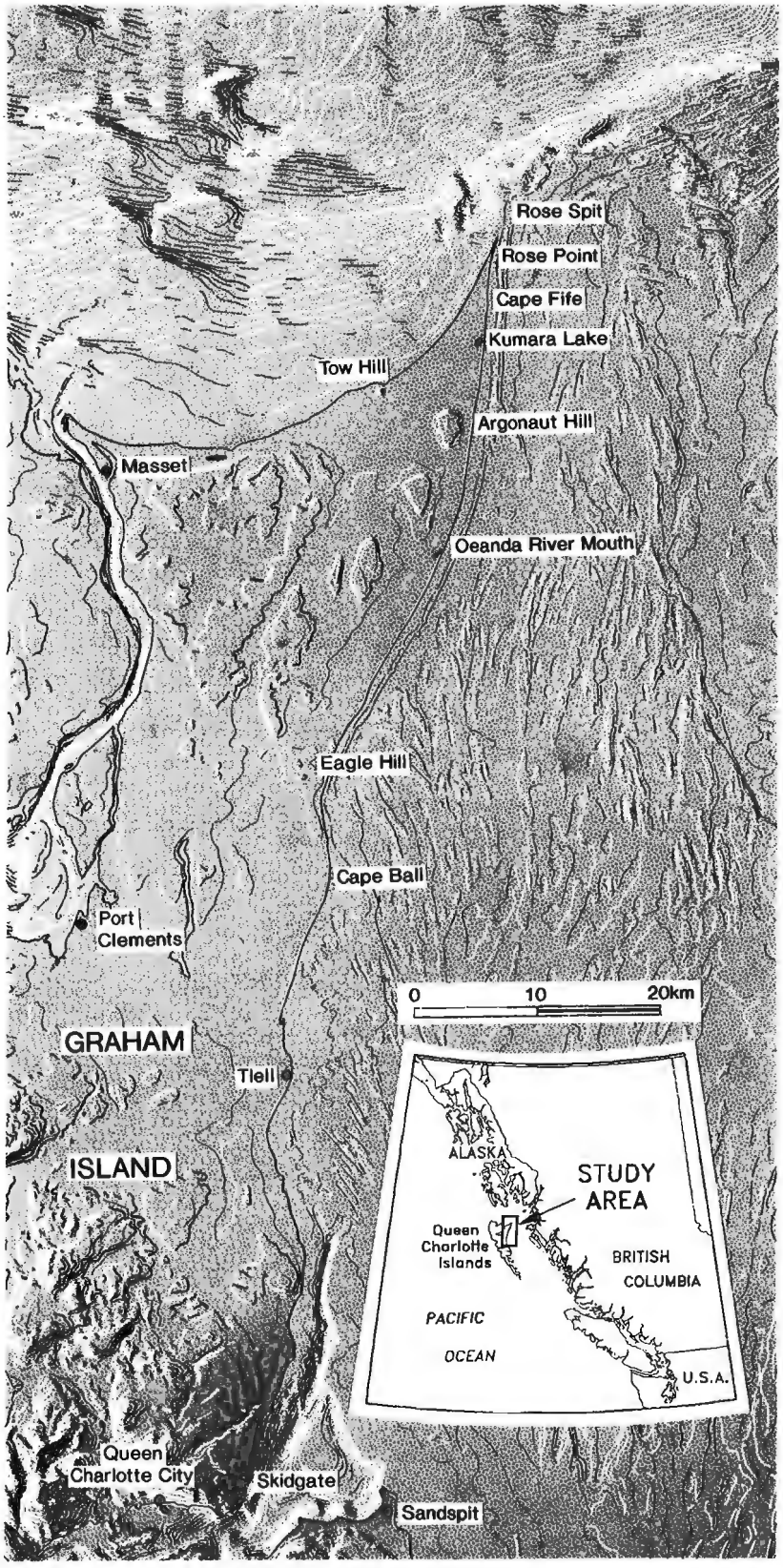

Figure 1. *Study area. On land contour interval 25 m; isobaths contoured at 5 m intervals. Erosion monitoring sites described are at Cape Fife (Site 2) and 1676 m north of Cape Fife (Site 1).*

Table 1. Erosion at two sites on the northeast Graham Island coast. Erosion measured in metres change (lost) normal to cliff scarp. Site 2 is at Cape Fife (Fig.1) and site 1 is 1676 m north of the cape.

Date d/m	23/08/90	24/03/91	14/09/92	17/03/93	01/03/94	08/03/94	09/03/94
Site 1	start	≈18	>26	1.4	0.1	0.0	0.0
Site 2	start	0.0	0.2	11.1	1.4	0.0	1.5

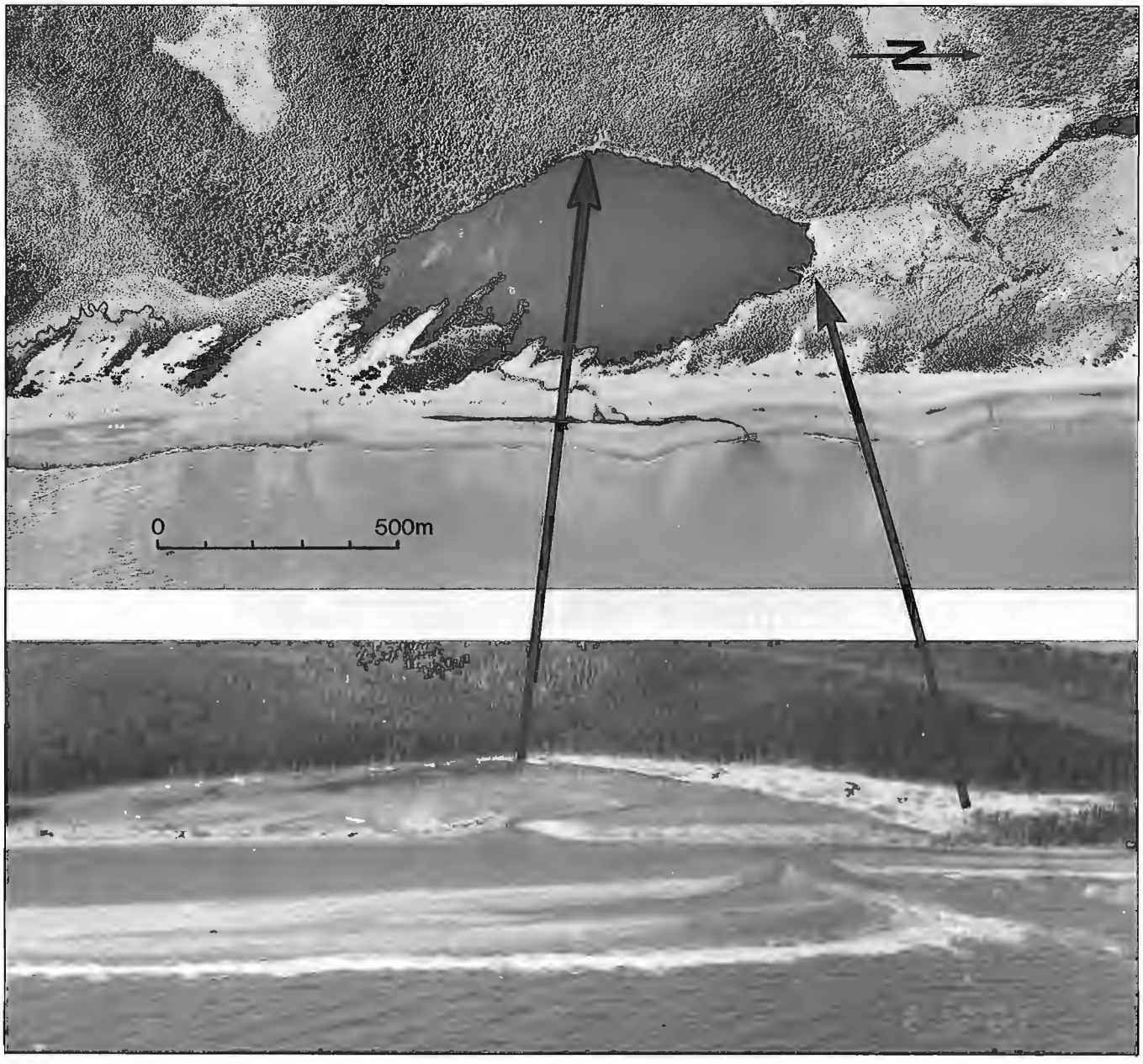

Figure 2. Oblique air photo of Kumara Lake bed taken in February 1994 compared to a 1980 B.C. Government air photo. Note that most of the seaward forested margin of the lake has been removed. Erosion is estimated to be about 60 m since 1980.

Shore attached bars, evident on air photos and in the SPOT image, occur from Cape Ball to Rose Spit along the entire length of the coastline. The bars are attached at their southern end and indicate the strong northwards longshore drift prevalent. There are at least 9 bars, the longest of which is more than 8 km, along the Cape Ball-Rose Spit coast. Where the bars attach to the coast the beach may be more than 1 km wide.

DISCUSSION

The erosion in the Cape Fife area appears to be episodic and to affect discrete segments of the coastline during different periods. While our data only encompass a few sites and represent a limited number of observations the rate of retreat measured is significant. For example during the period from the start of monitoring on 23 August 1980 until 14 September 1992 more than 44 m of erosion occurred at site 1. The shoreline at this station began as a slight bulge of the coastline or broad point of land. After the erosion period mentioned there was a noticable change in the orientation and shape of the coast at the site, the shoreline having essentially been "straightened", and the broad point removed.

In the 24 hour period after the 8 February 1994 storm, 1.5 m of erosion was measured at the Cape Fife site. Winds at Rose Spit gusted 45-52 knots from the southeast during the peak of the storm. Winds were from the southeast and over 30 knots for an eight hour period, and dropped off completely within one hour (Environment Canada, pers. comm., 1994). Wave height normally approaches 4 m under these wind conditions in Hecate Strait. The time (04:00-16:00 local time) during which the storm occurred covered one high water (11:35) in a period of spring tides, causing a storm set up situation. Wind conditions similar to or more extreme than these are expected to occur several times a year (Nyland, 1981). At site 1, 1676 m to the north, no erosion was measured during and after the storm, suggesting that the erosion is site specific.

While the erosion does affect the coastline as a whole, the pattern appears to reflect a punctuated assault on different sections of the coast which vary from year to year. The net retreat of the coast may be moderate but the effect on any given segment of the coast in one year (or one storm) may be severe. Qualitative observations made during field work support this inference.

Figure 3. Retrogressive failures in unconsolidated dunes in the Cape Fife area. The cliff is about 12 m high.

Observations made during and after the 8 February 1994 storm indicate that the mechanism by which the shoreline retreats within the study area is by failure of oversteepened cliffs as retrogressive, small land slips or slumps (Fig.3). These slumps vary in size from 20 to 1000 m^3 of material. The oversteepening of the cliff face probably occurs during the storm as the wave runup removes material from the foot of the slope. Following slope failure the material is then reworked and washed away in the surf zone. A series of linear cracks were found at the top of the scarp at the Cape Fife site on the day following the storm. Extensive cracks up to 5 mm wide and 3-5 m long, subparallel to the crest of the cliff to about 5 m back of the present scarp were noted (9 February 1994). These cracks, which are probably crown cracks of incipient failures, suggest more slumping will occur at the Cape Fife site before the slope temporarily stabilizes. At Cape Fife the material underlying the dune deposits consists of Holocene lacustrine muds, which are in turn underlain by early Holocene indurated gravels. These sediments appear to be broken up during storms by wave impact on the shoreface and on cliff sections, and excavated as large (20-50 cm) clasts.

Nyland (1981) gave a minimum annual erosion rate for the area between Tlell and Skidegate of between 0 and 0.8 m per year between the years 1936 and 1980. His study concluded that erosion of the shoreline was caused by washout from wave runup and overtopping. Damage was also seen to be secondarily caused by waves breaking on the upper portions of the shoreline.

The development and migration of large shore attached bars may play a role in storing the large volume of material eroded from eastern Graham Island. The shore attached bars, visible in the SPOT satellite image, almost continuously bar the coast from Cape Ball to Rose Spit. The bar adjacent to Kumara Lake appears to have grown and migrated extensively in a six or seven year period.

The evolution of the eastern Graham Island coastline has involved significant erosion over the last several hundred and probably thousands of years. The longshore transport to the north of the eroded material has contributed to the growth of the Rose spit and the spit platform (Barrie and Conway, 1993).

SUMMARY AND FUTURE WORK

Erosion on eastern Graham Island is ongoing from the area south of Rose Spit to Tlell. The rate of erosion varies from year to year and from site to site. The pattern discernible from the present study and from previous work indicates that most of the erosion occurs during the winter storms combined with spring tides and storm set up conditions from the southeast. Our work indicates that more than one metre and possibly several metres of coastline may be lost during, or as a result of, one storm. The eroded material is probably reworked into an extensive system of shore attached bars and transported north in the prevailing longshore drift, though this has yet to be demonstrated.

A program of annual or biannual oblique and vertical aerial photography combined with ground truthing by erosion monitoring surveying will be continued and expanded to include areas between Cape Fife and Tlell. With a longer time series of observations a better estimate of erosion rates and determination of the critical mechanisms controlling erosion will be possible.

ACKNOWLEDGMENTS

Earl Coatta of Environment Canada provided the meteorological data. Tanis Purcell of the British Columbia Ministry of Highways and Transportation in Terrace kindly provided reports and information as did Dave Byng of the Skeena Division of Highways and Transportation. R.D. McDonald provided field support. Residents of Tlell are thanked for their co-operation and information. Jerry Ferguson of the B.C. Ministry of Lands and Parks is also acknowledged for his assistance. Ralph Currie kindly reviewed this report.

REFERENCES

Alexander, S.
1993: Queen Charlotte Islands erosion control report; British Columbia Ministry of Transportation and Highways (internal report).

Barrie, J.V. and K.W. Conway
1993: Modern evolution of a nearshore and coastal macrotidal sand transport system, Queen Charlotte Islands; Canadian Quaternary Association Biennial Meeting, Program with Abstracts. p. A2

Clague, J.J., Mathewes, R.W., and Warner, B.G.
1982: Late Quaternary geology of eastern Graham Island, Queen Charlotte Islands, British Columbia; Canadian Journal of Earth Sciences, v. 19, p. 1786-1795.

Clague, J.J. and Bornhold, B.D.
1980: Morphology and littoral processes of the Pacific coast of Canada; in The Coastline of Canada, S.B. McCann (ed.); Geological Survey of Canada, Paper 80-10, p. 339-380.

Harper, J.R.
1980: Coastal processes on Graham Island, Queen Charlotte Islands, British Columbia; in Current Research, Part A; Geological Survey of Canada, Paper 80-1A, p. 13-18.

Higgs, R.
1991: Sedimentology, basin-fill architecture and petroleum geology of the Tertiary Queen Charlotte Basin, British Columbia; in Evolution and Hydrocarbon Potential of the Queen Charlotte Basin, British Columbia; Geological Survey of Canada, Paper 90-10, p. 337-371.

Nyland, D.
1981: Report on Queen Charlotte erosion from Skidegate to Tlell; to British Columbia Ministry of Highways (internal report).

Sutherland Brown, A.
1968: Geology of the Queen Charlotte Islands, British Columbia; British Columbia Department of Energy, Mines and Petroleum Resources, Bulletin 54, 226 p.

Thomson, R.E.
1981: Oceanography of the British Columbia Coast; Canadian Special Publication of Fisheries and Aquatic Sciences, 56, 291 p.

Woodsworth, G.J.
1991: Neogene to Recent volcanism along the east side of Hecate Strait, British Columbia; in Evolution and Hydrocarbon Potential of the Queen Charlotte Basin, British Columbia; Geological Survey of Canada, Paper 90-10, p. 325-335.

Geological Survey of Canada Project 890052

New results in Jura-Cretaceous stratigraphy, northern Vancouver Island, British Columbia

James W. Haggart and Howard W. Tipper
Cordilleran Division, Vancouver

Haggart, J.W. and Tipper, H.W., 1994: New results in Jura-Cretaceous stratigraphy, northern Vancouver Island, British Columbia; in Current Research 1994-E; Geological Survey of Canada, p. 59-66.

Abstract: Jurassic-Cretaceous strata were studied on northern Vancouver Island. Early Sinemurian fossils were collected from an isolated outcrop consisting of interstratified thin sandstone and shale, and thin tuffaceous beds. We correlate these strata with the Harbledown Formation. Probable Pliensbachian ammonites were collected from a section of volcanic lithic-rich sandstone just south of central Holberg Inlet and are probably correlative with ?Pliensbachian rocks recognized in western Quatsino Sound.

Similar Cretaceous rocks occur on Queen Charlotte Islands. However, there are important dissimilarities in the successions of the two regions and the stratigraphic nomenclature of northern Vancouver Island requires revision. The Blumberg Formation conglomerate sequence represents a submarine fan complex which prograded into a marine basin during Late Cretaceous (post-Cenomanian to Coniacian?) time. This unit is lithologically similar to, and probably equivalent with, Late Cretaceous Honna Formation fan complexes of Queen Charlotte Islands.

Résumé : Les chercheurs ont étudié les strates du Jurassique-Crétacé dans le nord de l'île de Vancouver. Ils ont extrait des fossiles du Sinémurien précoce d'un affleurement isolé qui se compose de minces interstratifications de grès et de shale et de minces couches tufacées. Ces strates sont mises en corrélation avec la Formation de Harbledown. Des ammonites datant probablement du Pliensbachien ont été prélevées dans une section de grès lithique volcanique juste au sud de la partie centrale de l'inlet Holberg; elles sont probablement corrélatives des roches du Pliensbachien? qui ont été reconnues dans l'ouest du détroit de Quatsino.

Des roches semblables du Crétacé sont présentes dans les îles de la Reine-Charlotte. Cependant, des différences importantes s'observent entre les successions des deux régions, et la nomenclature stratigraphique du nord de l'île de Vancouver a besoin de révision. La séquence de conglomérat de la Formation de Blumberg représente un complexe de cônes sous-marins qui ont avancé par progradation dans un bassin marin au cours du Crétacé tardif (entre le post-Cénomanien et le Coniacien?). Cette unité est lithologiquement semblable, et probablement équivalente, aux complexes de cônes de la Formation de Honna (Crétacé tardif) dans les îles de la Reine-Charlotte.

INTRODUCTION

Mesozoic rocks are widespread on northern Vancouver Island, part of British Columbia's Insular Belt (Fig. 1). To date, rocks of Late Triassic, Early Jurassic, Late Jurassic, and Early and Late Cretaceous ages have been identified there (Fig. 2). In fact, the stratigraphic succession of northern Vancouver Island is, in many respects, similar to that preserved on Queen Charlotte Islands, to the north. This similarity of rock types over a wide geographic region suggests that both regions experienced broadly similar geological histories. In essence, Triassic to lowermost Jurassic strata of the Insular Belt comprise the classical Wrangellia sequence, whereas younger Jurassic and Cretaceous rocks form an overlap sequence to Wrangellia.

The Mesozoic rocks of northern Vancouver Island have been the focus of previous regional studies by Jeletzky (1976) and Muller et al. (1974). Recent and continuing mapping by the British Columbia Geological Survey Branch is examining the Lower Jurassic Bonanza Volcanics unit, to assess the regional potential of this unit for economic mineralization (Nixon et al., 1993, 1994).

One of us (J.W.H) recently examined exposures of Mesozoic strata on northern Vancouver Island, in reconnaissance for a new project on the Upper Jurassic-Cretaceous stratigraphy of this region. Our investigations to date have centred on the Quatsino Sound-Holberg Inlet region (Fig. 1). In this paper we describe results of this work and present some preliminary ideas on the Jurassic-Cretaceous stratigraphy.

LOWER JURASSIC STRATA

New exposures of Lower Jurassic strata were studied at a quarry east of Rupert Inlet and along recent logging road cuts near Hathaway Creek on the south side of Holberg Inlet.

Lower Sinemurian strata

A large quarry located approximately 3.5 km east of the head of Rupert Inlet (Fig. 1, loc. A) includes a thick succession of sedimentary and volcanic rocks, dipping moderately to the south. The succession in the quarry consists of several tens of metres of interstratified thin sandstone, shale and mudstone, and thin tuffaceous beds (Fig. 3). The stratigraphically highest part of the quarry is characterized by multiple, thick beds of intermediate-composition igneous rock, possibly extrusive volcanics, although thick (0.5 to 1.5 m) dykes and sills of similar composition are also present.

Macrofossils were collected from strata at the middle part of the quarry, at GSC loc. C-300899. Identified fossils include *Arnioceras* spp. and *Weyla* sp., of middle Early Sinemurian age. The sedimentary facies present in the quarry, interstratified thin sandstone, mudstone, and tuffaceous beds, are typical of the Harbledown Formation, the type section of which is found on Harbledown Island, 50 km to the east, and which ranges in age from late Early to Late Sinemurian (Crickmay, 1928). Temporally-equivalent rocks in western Quatsino Sound, the Matthews Island Formation of Jeletzky (1976), appear to be dissimilar lithologically. Given the temporal and lithological similarities between the quarry strata and the Harbledown Formation, it seems reasonable to correlate the quarry outcrops with that unit. Harbledown Formation strata are also known on Nigei and nearby islands just north of Vancouver Island, and on Cox Island off Cape Scott; the unit has not previously been recognized on northern Vancouver Island proper. Jeletzky (1976) recognized the widespread distribution of Harbledown Formation equivalents across the northern Insular Belt.

Upper Pliensbachian? strata

Good exposures of sedimentary strata are present along logging roadcuts between Hathaway Creek and the south shore of Holberg Inlet (Fig. 1, loc. B). These strata are found topographically overlying mafic volcanic rocks of the Karmutsen Formation and overlying calcareous strata of the Quatsino Formation and were previously mapped as Parson Bay Formation by Muller and Roddick (1983). The strata dip moderately to the southwest and consist of thin- to thick-bedded, friable to well-indurated, lithic-rich arkosic sandstone, locally with thin pebble stringers. No interstratified volcanic rocks were identified in the exposures studied during our cursory visit. Intermediate-composition volcanic rocks were noted at nearby quarry exposures, however, suggesting that the full succession may include such strata. Plant material is common in the sedimentary strata, as are molluscan fossils. The strata are lithologically similar to the ?Pliensbachian-?Toarcian greywacke unit of Jeletzky (1976), which outcrops in the Browning Inlet area west of Winter Harbour.

Fossils collected from GSC loc. C-300918 include a large oxyconic ammonite form strongly suggestive of the Late Pliensbachian genus *Fanninoceras*. A second fossil locality, GSC loc. C-300919, produced several gastropod taxa, including *Pleurotomaria* sp. Although age-indeterminate, such gastropods are common in the Lower Jurassic. Although some morphological similarities exist between the ammonites at loc. C-300918 and Bajocian sonniniid ammonites, Bajocian rocks are presently unknown on Vancouver Island and we prefer a correlation with the Pliensbachian. Late Pliensbachian ammonites were collected in 1950 by J.A. Jeletzky on the west coast of Vancouver Island and identified by H. Frebold (GSC internal palentological report J-10-1977-HF).

OTHER JURASSIC? STRATA, HOLBERG INLET

Upper Clesklagh Creek

Recent logging roadcuts along the hillside east of Clesklagh Creek, north of Holberg Inlet (Fig. 1, loc. C), expose good sections of clastic strata. This section was previously noted in Nixon et al. (1994: fig. 3, loc. 4). Strata are structurally disrupted but, in general, dip moderately to steeply to the northeast. Assuming the constant dips reflect minimal structural repetition, a rough schematic section can be established for the sequence exposed on the hillside.

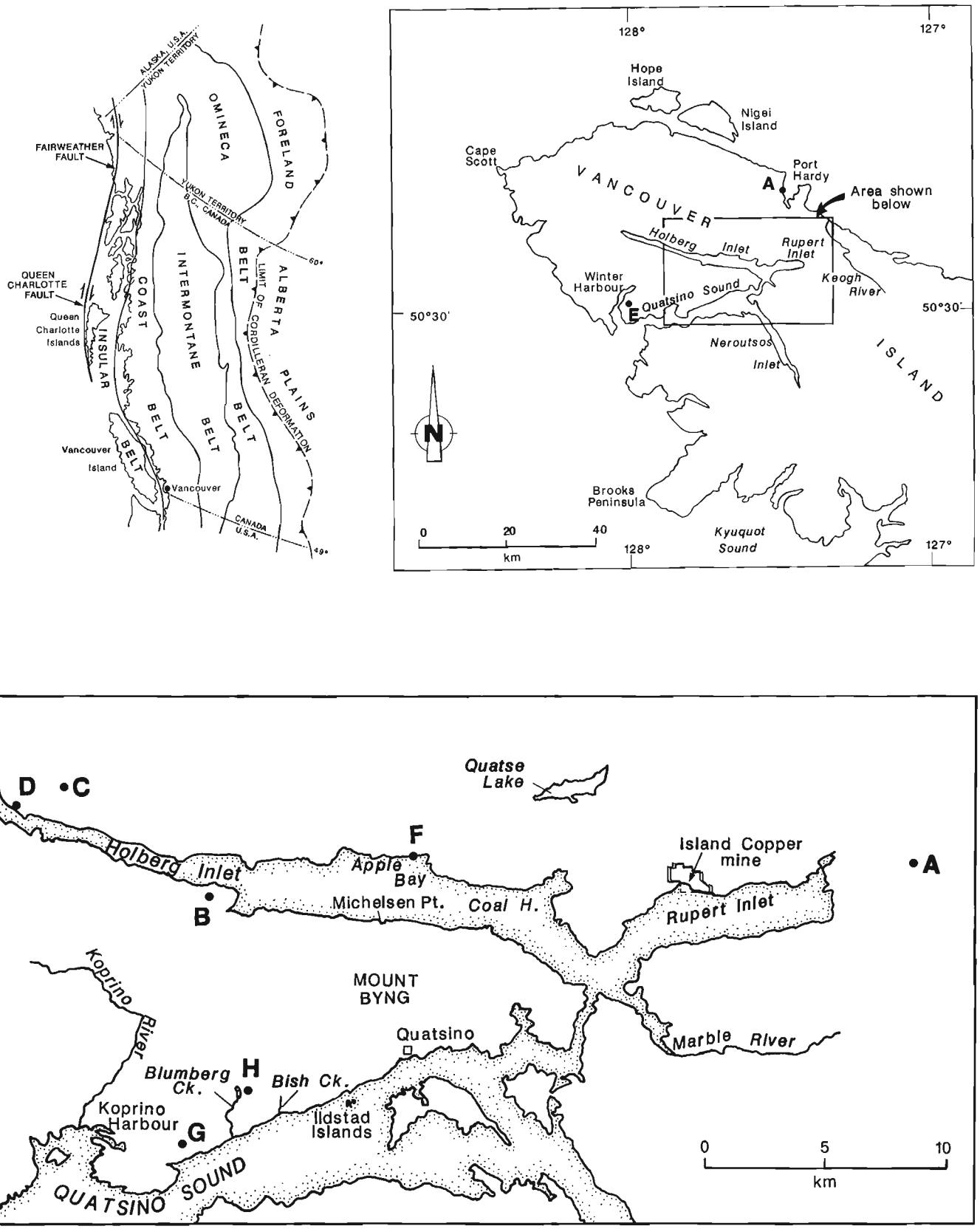

Figure 1. Location map of northern Vancouver Island showing important localities mentioned in text.

Topographically lowest exposures consist of thick-bedded, medium- to coarse-grained arkosic sandstone and pebble conglomerate, interstratified with thick-bedded volcanic strata of intermediate composition. The base of the sequence was not observed. Fossils collected from sandstone beds within this basal sequence include common rhynchonelliform brachiopods, similar to Early to Middle Jurassic brachiopods found elsewhere in the Insular Belt.

Topographically and stratigraphically(?) overlying the basal sandstone and volcanic rock sequence is a thick succession of mudstone, strongly oxidized locally. Minor, thin (2-6 cm) sandstone interbeds are found within the sequence and, locally, calcareous concretions are found. No interstratified volcanic strata were noted. The mudstones contain rare moulds of indeterminate belemnites but are otherwise lacking in fossils.

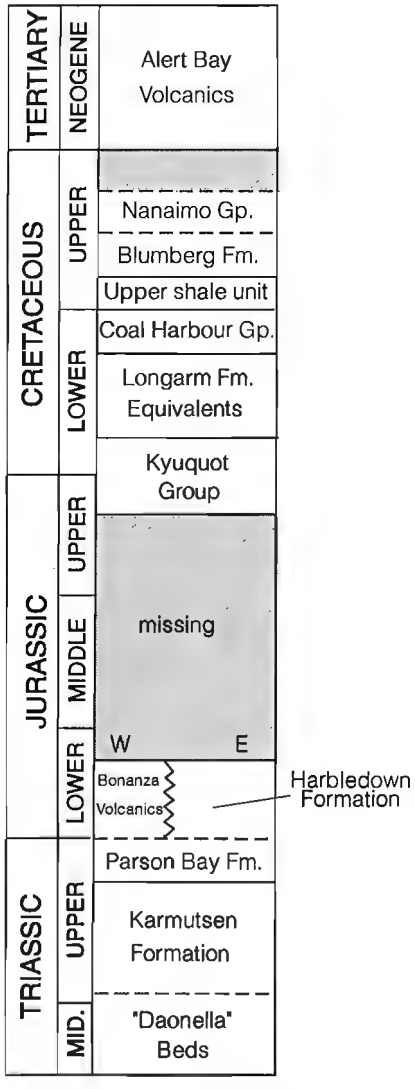

Figure 2. *Simplified Mesozoic-Cenozoic stratigraphy for northern Vancouver Island, modified after Muller et al. (1974), Haggart (1993), and Nixon et al. (1994).*

The topographically and stratigraphically highest(?) unit is found along the highest logging roads on the hillside, where a good section was measured. Strata in this section consist of interstratified fine- to coarse-grained, planar- to trough-cross-stratified, lithic-rich sandstone, siltstone, and minor mudstone. Plant debris is abundant throughout the section. The single marine fossil, a belemnite mould, was found in the basal part. Volcanic strata were not noted in this unit. The higher strata in this section are interpreted as nonmarine in origin.

Given the probable Early-Middle Jurassic age of the brachiopods in the lowermost exposures, as well as the presence in those strata of intercalated volcanic strata, we consider the age of the entire upper Clesklagh Creek succession to be of Early-Middle Jurassic age, possibly coeval with the Bonanza Volcanics of earliest? Jurassic to Pliensbachian age (Muller et al., 1974; Nixon et al., 1994). The succession may represent marine transgression upon the Bonanza near the end of significant volcanic activity. Subsequent basin deepening is indicated by the transition to a deeper-water mudstone facies with belemnites. Finally, marine deposition was succeeded

Figure 3. *Quarry exposure of thin bedded sandstone, argillite, and tuffaceous beds (lighter colour) correlated with Harbledown Formation, locality A in Figure 1.*

by nonmarine deposits in the region, perhaps reflecting the onset of renewed volcanism. It is uncertain whether the nonmarine strata are succeeded by further volcanic strata, but such rocks form the hillside topographically and apparently stratigraphically above the sedimentary section (Nixon et al., 1994).

Lower Clesklagh Creek

Poor exposures of volcanic rocks are found along the north shore of Holberg Inlet just east of the mouth of Clesklagh Creek (Fig. 1, loc. D). These exposures were previously mapped as Cretaceous Longarm Formation by Muller and Roddick (1983).

No significant stratigraphic section is preserved as most of the shoreline is a cobble beach. Exposed strata dip steeply to vertically southwards and consist of volcanic-lithic-rich, thin- to medium-bedded, locally trough cross-stratified, medium- to coarse-grained tuffaceous and volcanic-rich sandstone with minor thin (2-6 cm), discontinuous coal seams, and andesitic breccias and flow breccias up to 2 m in thickness (Fig. 4).

No fossils have yet been found in these strata. Because the outcrops include interstratified volcanic deposits, we place them provisionally within the Lower Jurassic Bonanza Volcanics. Correlation of the strata with the Cretaceous Longarm Formation, or with any Cretaceous unit, is considered unlikely as no definite volcanic deposits have yet been recognized in the Cretaceous sequence of northern Vancouver Island (Jeletzky, 1976; Muller et al., 1974). Indeed, volcanic strata of Cretaceous age appear rare throughout the Insular Belt (Haggart, 1993).

LONGARM FORMATION EQUIVALENTS

Many workers have recognized the lithological and temporal similarity of particular Lower Cretaceous stratal units of northern Vancouver Island with the Longarm Formation of Queen Charlotte Islands. Muller et al. (1974) and Muller (1977) correlated these strata directly with that unit whereas Jeletzky (1976) preferred to treat them as 'Longarm Formation Equivalents'. Although the northern Vancouver Island outcrops may at one time have been more closely associated with their equivalents on Queen Charlotte Islands (Yorath and Chase, 1981; but see Lyatsky et al., 1990 for an alternate view), there is still uncertainty in correlating strata over such large geographic distances lacking intermediate exposures. As well, regional studies of the Longarm Formation of Queen Charlotte Islands have recognized a more heterogeneous assemblage within that succession than previously interpreted (see Haggart, 1991, 1993). Thus, for the present, we follow Jeletzky (1976) in interpreting all Cretaceous strata of northern Vancouver Island as equivalents, rather than direct correlatives, of Queen Charlotte Islands rocks.

Longarm Formation Equivalent strata were studied briefly on logging roads east of Winter Harbour (Fig. 1, loc. E). Lithologically, the succession appears typical to that seen on Queen Charlotte Islands and, indeed, our study does not add significant new data to the extensive study of this unit in this region by Jeletzky (1976). An unconformity of shallow-marine, coarse grained sandstone of Longarm Formation Equivalent strata upon the Lower Jurassic Bonanza Volcanics was observed east of Winter Harbour. Buchiid fossils from these strata include *Buchia crassicollis*, indicative of a Late Valanginian age. Successive strata are finer grained and also rich in buchiids, reflecting continued marine transgression in the region. No top was seen to the succession east of Winter Harbour.

Longarm Formation Equivalent strata have also been mapped at Apple Bay, Holberg Inlet (Jeletzky, 1976; Muller and Roddick, 1983) (Fig. 1, loc. F). Strata here dip very gently to southwards and include an 8 cm-thick, discontinuous coal seam just above the contact with Bonanza Volcanics. Stratigraphically higher rocks consist of cross-stratified sandstone with abundant examples of the trigoniid bivalve *Quoiecchia aliciae*, indicative of a general Barremian age. Highest strata in the section at Apple Bay appear rich in siltstone and, locally, mudstone: much of the shoreline exposure is covered with fine shale chips obscuring the underlying geology but suggesting that a significant thickness of mudstone is likely present in the upper part of the section. No Valanginian age strata are presently known from the Holberg Inlet area. The relationship of Barremian and younger(?) strata at Apple Bay with Hauterivian and early Barremian? strata farther west in Holberg Inlet is presently unclear.

COAL HARBOUR GROUP

Jeletzky (1976) named the Coal Harbour Group for strata which outcrop in the vicinity of Coal Harbour in Holberg Inlet. In this region, the group forms an east-west-trending outcrop belt extending eastward to the vicinity of the Island Copper mine and westward to Apple Bay. The predominant unit within the group is the Blumberg Formation, named by Jeletzky (1976) for extensive exposures of conglomerate found to the south along Quatsino Sound near Blumberg Creek.

Figure 4. *Interstratified tuffaceous sandstone (hammer) and andesitic flow deposit (left of photo), Clesklagh Creek shoreline section, locality D in Figure 1.*

In the vicinity of Coal Harbour the group consists of conglomerate, sandstone, and minor coal, siltstone, and shale. No basal contact of the unit with underlying strata has yet been noted, although earlier mapping by personnel at Island Copper documented conglomerate resting on volcanic strata, presumably Bonanza Volcanics, at one locality at the mine site; this locality has subsequently been incorporated into the milling facilities of the mine. Jeletzky (1976: p. 96), citing Dawson (1887), suggested the group may overlie older Cretaceous rocks in the vicinity of Coal Harbour.

At Coal Harbour, exposures of the group dip gently southward and, in general, the stratigraphic succession fines upward. A similar trend is seen in the section just west of Island Copper mine (Section 37 of Jeletzky, 1976). Lower strata of the unit in this region consist predominantly of framework-supported conglomerate, typically unbedded, massive and poorly sorted, and locally with lenses of medium- to coarse-grained sandstone. Such lenses range from several decimetres to several metres in thickness. Clasts within the conglomerate are typically sub- to well-rounded and are principally of volcanic compositions; plutonic compositions are uncommon. In the Coal Harbour area, flow-banded rhyolite clasts are common in the conglomerate, presumably derived from similar rhyolites recognized in the Bonanza Volcanics (Nixon et al., 1994).

The upper part of the section at Coal Harbour, as well as at Island Copper, becomes increasingly dominated by medium- to coarse-grained, trough cross-stratified sandstone, although conglomerate lenses and interbeds are also common. Paleocurrent measurements on cross-stratification in both the Coal Harbour and Island Copper sections indicate a southward to southwestward transport direction. Thin (4-20 cm) coal seams, laterally discontinuous over several tens of metres, outcrop in the upper part of the sections at both Coal Harbour and at Island Copper, commonly associated with poorly consolidated mudstone and siltstone. Shoreline exposures of coal and mudstone are typically found within extensive covered intervals, interpreted as probably underlain by additional fine clastics.

Available evidence suggests the Coal Harbour Group in the Coal Harbour and Rupert Inlet region is principally nonmarine to marginal marine in nature. A few oyster and other bivalve fragments have been found within the coarse sandstones and conglomerates in the middle part of the succession at Coal Harbour, in stratigraphic association with the coal seams. The age of the group is poorly constrained. Hopkins (in Jeletzky, 1976) identified Albian palynomorphs in the section just west of Island Copper mine. Strata of the group appear to overlie older Cretaceous (?Hauterivian-Barremian) Longarm Formation Equivalent strata at Apple Bay in central Holberg Inlet.

Jeletzky (1976) established his unfossiliferous Coarse Arenite Unit for a widespread but discontinuous, medium- to coarse-grained lithic arenite facies which outcrops locally in association with conglomerates of the Coal Harbour Group, and was assumed to underlie them. However, because of its discontinuous nature and its lack of stratigraphic integrity in relation to associated units, we treat it variously as a lithofacies of the Coal Harbour Group or the Blumberg Formation (see below).

BLUMBERG FORMATION

Strata of the Blumberg Formation outcrop extensively along the north shore of Quatsino Sound from Koprino Harbour eastward to near Quatsino townsite. Jeletzky (1976) included these strata within his Coal Harbour Group, based on similarity of the conglomerates in the two regions. For reasons outlined below, we treat the Blumberg Formation conglomerate package as distinct from the Coal Harbour Group.

Details of lithologies present in the Blumberg Formation are provided in Jeletzky (1976), whose study assessed shoreline exposures in Quatsino Sound. In addition to these, our study also examined inland exposures, newly accessible by logging roads. In these areas, we recognize two principal lithofacies within the Blumberg Formation: a conglomerate facies, which makes up the vast bulk of the formation; and a volumetrically minor, fine grained sandstone and mudstone facies. No coal bearing facies were recognized anywhere within the large area of exposure on the peninsula between Holberg Inlet and Quatsino Sound.

Blumberg Formation conglomerate is typically moderately well-sorted and thickly bedded. Clasts are typically very well rounded to subrounded and include common volcanic and plutonic lithologies; however, plutonic clasts are much more abundant in the Blumberg Formation conglomerates than in the Coal Harbour Group conglomerates in the vicinity of Coal Harbour. Minor, thin sandstone lenses are noted locally, as is rare imbrication of clasts (Fig. 5). Blumberg Formation conglomerates comprise a very thick succession, much thicker than the conglomerates to the north at Coal Harbour.

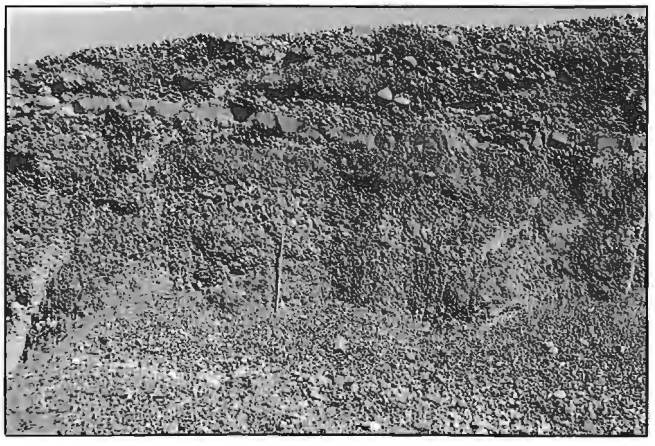

Figure 5. *Massive conglomerate of Blumberg Formation, south flank of Mount Byng.*

Outcrops of mudstone with thin (5-20 cm), graded sandstone beds (Fig. 6) are found within the Blumberg conglomerate succession at several localities several kilometres west of the mouth of Blumberg Creek (Fig. 1, loc. G). Syndepositional slump features are locally present in the mudstone facies. Small, inoceramid bivalves of possible Coniacian age were collected from the mudstone at one locality (GSC loc. C-300908), indicating the marine nature of the rocks. The total thickness of these strata are unknown; at one locality, a few tens of metres of mudstone outcrop beneath conformably overlying conglomerate.

An upper limit to the Blumberg Formation has not yet been identified. Conglomerates are apparently found on the summit of Mount Byng, as well as on the high peak 5 km north-northwest of the mouth of the Koprino River. The flat-lying nature of the Blumberg Formation throughout this region suggests that some 600 m of strata are present, at least locally, within the unit.

The base of the formation also has not yet been located. However, we identified restricted outcrops of shale in shoreline exposures stratigraphically beneath the Blumberg Formation in the area just west of Quatsino townsite. Here, although the underlying geology is mostly obscured by a mantle of beach cobbles, we identified strongly-indurated shale clearly intruded by mafic to felsic dykes, previously mapped by Jeletzky (1976) as ?Sooke Intrusions. The resistant dyke rocks stand above the beach cobbles and the intruded shale can clearly be seen on the dyke margins and lateral to them. Several small, calcareous concretions suggest the shales are likely of marine origin. We suggest the flat-lying Blumberg Formation conglomerates which outcrop several tens of metres to the west conformably overlie the mudstones present in the beach sequence.

Similarly, we suggest that the shales which outcrop several kilometres to the southwest, between Bish Creek and Hawisnakwi Creek, also conformably underlie the Blumberg Formation conglomerates. These strata were assigned by Jeletzky (1976) to his Upper shale unit (after Dawson, 1887) and contain marine fossils of Cenomanian and possibly Turonian age. Jeletzky considered the shales to overlie the Blumberg Formation conglomerate, requiring a significant fault in the vicinity of Ildstad Islands with at least 600 m of offset (the total thickness of Blumberg conglomerate present in the region). Our mapping on Ildstad Islands failed to reveal any deformation of Blumberg Formation strata, other than a localized, near-vertical jointing pattern. Given the lack of significant deformation of the flat-lying Blumberg Formation throughout this entire region, we consider it highly probable that the shales which underlie the conglomerates west of Quatsino townsite are equivalent to Jeletzky's Cenomanian-Turonian? Upper shale unit found to the west.

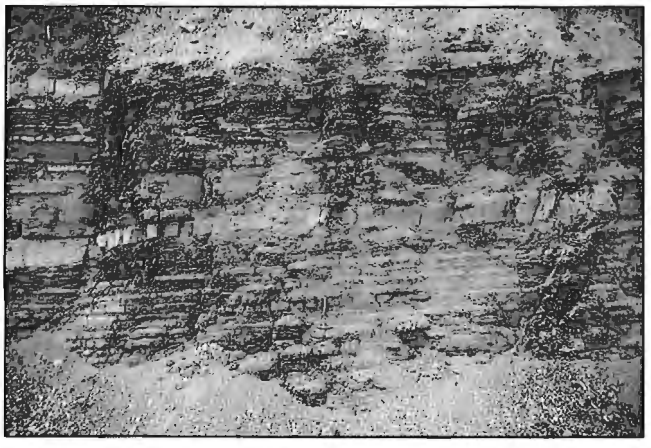

Figure 6. Mudstone with interstratified, thin bedded sandstone, locally graded, locality G in Figure 1.

Thus, it seems likely that the lowest Blumberg Formation conglomerates were deposited in a marine basin; the presence of marine fossils higher in the Blumberg Formation within the mudstone facies indicates that much of the Blumberg itself is also of probable marine origin, and likely intertongued with marine shales in a southward direction.

We consider the Blumberg Formation to be a submarine fan-delta complex which prograded rapidly into a marine basin. This interpretation is in contrast to that of Jeletzky (1976), who considered the Blumberg to be a nonmarine, alluvial fan deposit, based on his correlation of the unit with the conglomerates and sandstones of the coal-bearing Coal Harbour Group. However, we argue that the age of the Blumberg fan-complex is post-Cenomanian, based on its position overlying the Cenomanian-Turonian? Upper shale unit, rather than Albian as proposed by Jeletzky (1976). The Blumberg Formation is lithologically and temporally distinct from the conglomerates of the Coal Harbour Group and should not be included within that unit.

The Blumberg Formation fan complex is approximately the same age as lithologically similar fan-delta deposits of the Honna Formation in Queen Charlotte Islands. Best-dated exposures of the Honna Formation are dated as post-Early Turonian to Santonian in age, although possible Cenomanian rocks may also be present in the unit locally (Haggart, 1991; F. Clark, pers. comm., 1994). We thus consider it likely that the Blumberg Formation is equivalent to the Honna Formation and represents one of several fan-complexes which developed along the British Columbia coast during early Late Cretaceous time (Haggart, 1993).

LATE CRETACEOUS?-TERTIARY DYKES

Exposures of the Blumberg Formation approximately 2 km west-northwest of the mouth of Bish Creek (Fig. 1, loc. H) are intruded by rhyolite dykes. The dykes form an anastomosing complex up to 200 m in width which is responsible for the topographic expression of several ridges in the area. Dykes can be seen to clearly intrude the conglomerate at several localities (Fig. 7). The dyke complex is on trend with, and appears to occupy the axis of, a large-scale, northeast-trending anticlinal flexure developed in the Blumberg Formation which can be traced northward from the vicinity of Bish Creek to Michelsen Point on Holberg Inlet.

Figure 7. Rhyolite dyke (light-coloured) intruding conglomerate and pebble- and cobble-rich mudstone and siltstone of the Blumberg Formation, locality H in Figure 1.

At Apple Bay, in Holberg Inlet, both felsic and mafic dykes intrude Cretaceous rocks and a single mafic dyke was noted in exposures in Coal Harbour. Although a Late Cretaceous age for dyke emplacement can not be ruled out at present, we consider all of these occurrences to be associated with the early Oligocene event documented by Muller et al. (1974).

ACKNOWLEDGMENTS

We thank Graham Nixon of the British Columbia Geological Survey Branch for providing a boat, shelter from the storm, a plug for the computer, and never-ending good cheer at his Marble River camp, the base for our investigations. Graham is also thanked for pointing us to the upper Clesklagh Creek sections. Gary Payie showed J.W.H. the Lower Sinemurian Harbledown quarry. Doug Archibald provided insightful discussion regarding Tertiary dykes and is thanked also for his commanding boatmanship.

REFERENCES

Crickmay, C.H.
1928: The stratigraphy of Parson Bay, British Columbia; University of California Publications, Bulletin of the Department of Geological Sciences, v. 18, no. 2, p. 51-70, 4 pls.

Dawson, G.M.
1887: Report on a geological examination of the northern part of Vancouver Island and adjacent areas; Geological Survey of Canada, Annual Report, 1886, Part B, 129 p.

Haggart, J.W.
1991: A synthesis of Cretaceous stratigraphy, Queen Charlotte Islands, British Columbia; in Evolution and Hydrocarbon Potential of the Queen Charlotte Basin, British Columbia, (ed.) G.J. Woodsworth; Geological Survey of Canada, Paper 90-10, p. 253-277.

1993: Latest Jurassic and Cretaceous paleogeography of the northern Insular Belt, British Columbia; in Mesozoic Paleogeography of the Western Unites States - II, (ed.) G.C. Dunne and K.A. McDougall; Society of Economic Paleontologists and Mineralogists, Pacific Section, Book 71, p. 463-475.

Jeletzky, J.A.
1976: Mesozoic and ?Tertiary rocks of Quatsino Sound, Vancouver Island, British Columbia; Geological Survey of Canada, Bulletin 242, 243 p., 12 pls.

Lyatsky, H.V., Chase, R.L., Lewis, P.D., Thompson, R.I., and Woodsworth, G.J.
1990: Block faulting and evolution of the Queen Charlotte (QC) Basin, west coast of Canada; EOS, Transactions of the American Geophysical Union, v. 71, p. 1581 [abs.].

Muller, J.E.
1977: Evolution of the Pacific margin, Vancouver Island, and adjacent regions; Canadian Journal of Earth Sciences, v. 14, p. 2062-2085.

Muller, J.E. and Roddick, J.A.
1983: Geology, Alert Bay - Cape Scott, British Columbia; Geological Survey of Canada, Map 1552A, scale 1:250 000.

Muller, J.E., Northcote, K.E., and Carlisle, D.
1974: Geology and mineral deposits of Alert Bay-Cape Scott map-area, Vancouver Island, British Columbia (92L, 102I); Geological Survey of Canada, Paper 74-8, 77 p.

Nixon, G.T., Hammack, J.L., Hamilton, J.V., and Jennings, H.
1993: Preliminary geology of the Mahatta Creek area, northern Vancouver Island (92L/5); in Geological Fieldwork 1992; British Columbia Ministry of Energy, Mines and Petroleum Resources, Paper 1993-1, p. 17-35.

Nixon, G.T., Hammack, J.L., Koyanagi, V.M., Payie, G.J., Panteleyev, A., Massey, N.W.D., Hamilton, J.V., and Haggart, J.W.
1994: Preliminary geology of the Quatsino-Port McNeill map areas, northern Vancouver Island (92L/12, 11); in Geological Fieldwork 1993; British Columbia Ministry of Energy, Mines and Petroleum Resources, Paper 1994-1, p. 63-85.

Yorath, C.J. and Chase, R.L.
1981: Tectonic history of the Queen Charlotte Islands and adjacent areas - a model; Canadian Journal of Earth Sciences, v. 18, p. 1717-1739.

Geological Survey of Canada Project 880038

APPENDIX:

GSC fossil localities

C-300899: NTS 92L/11; UTM 615350E, 5606850N; quarry along logging roads north of Rupert Main. Harbledown Formation.

C-300908: NTS 92L/5; UTM 584450E, 5594625N; road cut along logging road, approximately 2 km west of mouth of Blumberg Creek. Blumberg Formation.

C-300918: NTS 92L/12; UTM 584970E, 5604770N; road cut along logging road, north side Hathaway Creek. ?Pliensbachian sandstone.

C-300919: NTS 92L/12; UTM 584475E, 5604625N; road cut along logging road, north side Hathaway Creek. ?Pliensbachian sandstone.

Results of a survey of clients for a proposed geoscience atlas of Georgia Basin, British Columbia

N. Hussain, P.S. Mustard, L.C. Struik, J.L.L. Luternauer, P. Matysek[1], S. Sibbick[1], P. Bobrowsky[1], and W.P. Noble[1]
Cordilleran Division, Vancouver

Hussain, N., Mustard, P.S., Struik, L.C., Luternauer, J.L.L., Matysek, P., Sibbick, S., Bobrowsky, P., and Noble, W.P., 1994: Results of a survey of clients for a proposed geoscience atlas of Georgia Basin, British Columbia; in Current Research 1994-E; Geological Survey of Canada, p. 67-75.

Abstract: The Georgia Basin is one of the fastest growing urban regions in Canada. The Geological Survey of Canada and the Geological Survey Branch, British Columbia Ministry of Energy, Mines, and Petroleum Resources, have explored the potential growing need for geoscience information in the area through a telephone and mail survey of educational institutions, government agencies, geoscience consulting firms, and community organizations. Existing and potential clients were surveyed about the types of geoscience information they currently use and/or have used, in what format the data were used, and what topics may be required in the future. This survey confirms four points: 1) traditional geoscience topics remain popular; 2) a digital atlas of geoscience data is desired; 3) there is an eager audience for educational material on geological sciences; and, 4) geoscience information is increasingly being requested and used in digital formats.

Résumé : Le bassin de Georgia est une région urbaine qui connaît un des plus hauts taux de croissance au Canada. La Commission géologique du Canada et la *Geological Survey Branch* du ministère de l'Énergie, des Mines et des Ressources pétrolières de la Colombie-Britannique ont étudié les besoins de cette région en information géoscientifique, en procédant à un sondage téléphonique et postal auprès d'établissements d'enseignement, d'organismes gouvernementaux, de firmes d'experts-conseils en sciences de la Terre et d'organisations communautaires. On a demandé à des clients actuels et potentiels quels types d'information géoscientifique ils utilisaient actuellement ou avaient utilisés par le passé, sous quelle forme et quels sujets d'intérêt ils sentaient le besoin d'approfondir. Ce sondage confirme que : 1) les thèmes traditionnels des sciences de la Terre demeurent populaires; 2) les clients aimeraient disposer d'un atlas numérique des données géoscientifiques; 3) il y a une très forte demande de matériel éducatif sur les sciences géologiques; et 4) l'information géoscientifique est de plus en plus demandée et utilisée sous forme numérique.

[1] British Columbia Ministry of Energy, Mines, and Petroleum Resources, Geological Survey Branch, Fifth Floor, 1810 Blanshard Street, Victoria, B.C. V8V 1X4

INTRODUCTION

From November, 1993 to January, 1994, the Vancouver office of the Geological Survey of Canada (GSC) and the Victoria office of the B.C. Geological Survey Branch (GSB) conducted a joint telephone and mail survey of various individuals and organizations in the Georgia Basin area (Lower Mainland and Vancouver Island) in an effort to understand: 1) what type of geoscience information was being used; 2) how it was being used; 3) who was using it; 4) in what format it was being used; and 5) what information was lacking.

This client survey was part of an attempt by the GSC and GSB to incorporate the views of its geoscience information users and potential users into the design of future publications on the Georgia Basin area (Fig. 1). The 1993 B.C. Round Table on the Environment and the Economy described this area:

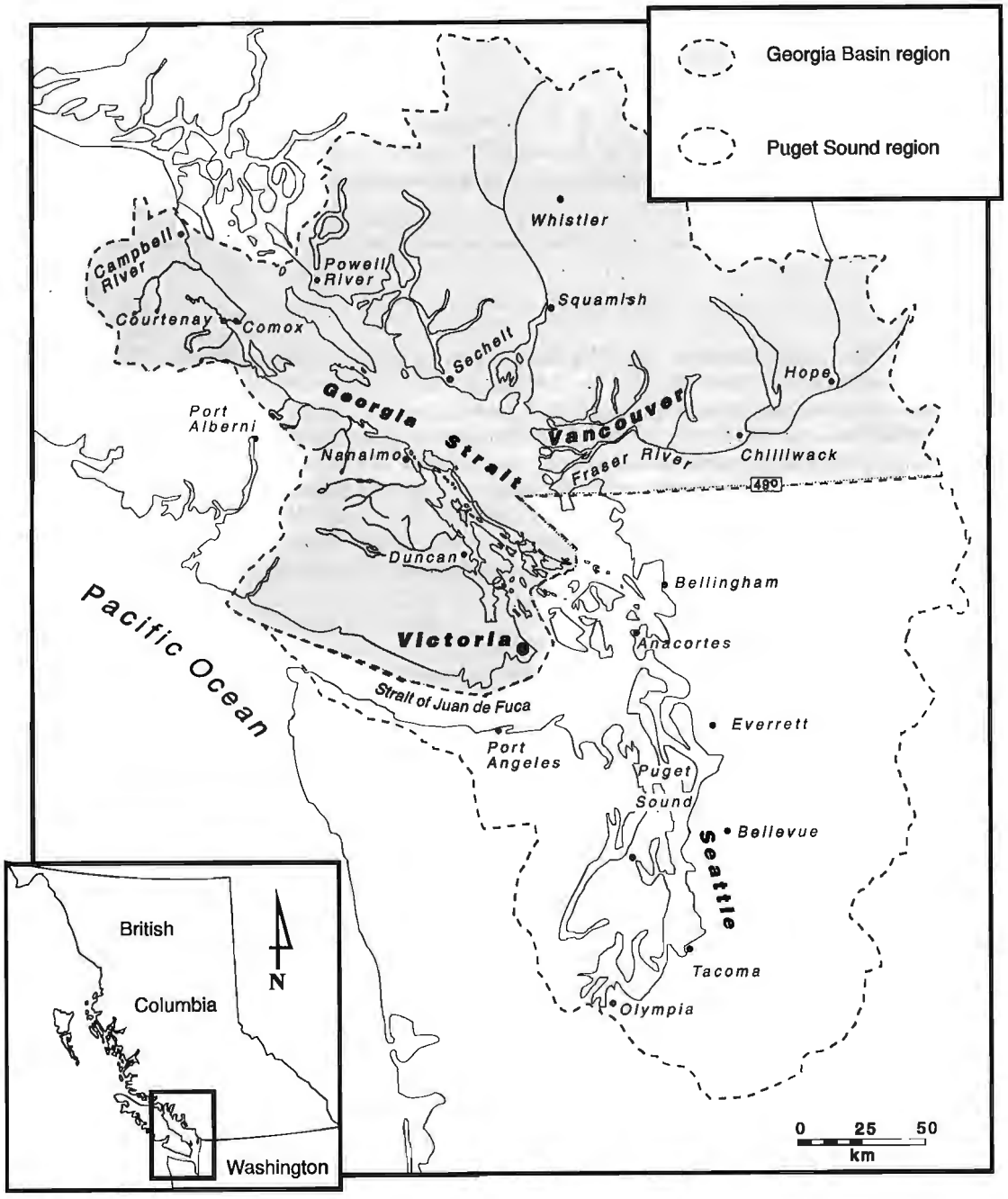

Figure 1. *Location of the Georgia Basin region and related Puget Sound region, southwestern British Columbia and northwestern Washington State. Areal extent of regions as defined by the British Columbia Table on the Environment and the Economy (1993).*

"The Georgia Basin region runs along a coastal corridor, stretching from Campbell River and Powell River, south to the U.S. border and as far east as Hope, British Columbia (p. 3). Narrow hills, box canyons, and countless bays and headlands provide shelter and habitat for a wide array of marine, terrestrial, and avian wildlife (p. 3). The region's temperate climate, spectacular natural setting, and quality of life have made it one of the fastest growing areas in North America (p. 6)."

With increasing population, major issues and challenges facing regional authorities include how to protect air quality, water quality and quantity, biodiversity and habitat and manage waste, urban development, and soil erosion in a region with many potential geohazards (volcanic eruptions, earthquakes, and landslides).

The following are some examples of the issues and challenges of the Georgia Basin area identified by the B.C. Round Table on the Environment and the Economy (1993): 1) it includes the fastest expanding metropolitan centre in Canada, 2) it contains about 300 water discharge outfalls (includes sewage) draining into Georgia Strait, 3) 63 000 barrels of oil are spilt in Georgia and Juan de Fuca straits annually, 4) it is prone to frequent minor earthquakes and is part of an area possibly susceptible to a major (> magnitude 8) earthquake, 5) it lies near Mount Baker, an active volcano, and, 6) it is the site of increasing groundwater aquifer depletion and contamination.

For this client survey, contacts were made with representatives of assorted special interest groups (environmental, historical, archaeological, outdoors, fisheries, etc.), educators at high school and university levels, engineers in local and provincial governments, regional park managers, as well as geotechnical engineering consultants. Telephone contacts were divided geographically between the two agencies. The GSC contacted all clients in the Lower Mainland and the GSB contacted those on Vancouver Island. Of the 178 organizations and individuals we attempted to contact collectively, we managed to reach 128; the GSC reached 109 and the GSB surveyed 19. This contact list consisted of: a) individuals and organizations who had taken part in earlier surveys, b) individuals known to be regular users of geoscience information, c) consulting firms that advertised their geotechnical services in various technical and scientific journals, d) a variety of engineers in government, and e) private groups that, from reading their profiles in the Vancouver and Victoria Public Library's Community Organizations Directory, we felt could be using or might be interested in using geoscience information. Of the 128 groups represented in the survey, 6% were park managers, 12% were educators, 21% were employees of consulting firms, 23% were local and provincial government engineers, and 38% were representatives of special interest groups. The special interest groups were made up of various organizations such as environmental advocacy groups, natural history preservation groups, recreational associations, nature clubs, and representatives from certain industries (mining, forestry, construction, etc.). Although representatives of special interest groups formed a large percentage of the individuals contacted for the survey, many had not used geoscience information (as shown in the answers to Question 1 of the survey). Employees of consulting firms and government engineers had the highest positive response rate to Question 1 and the results for the survey reflect this high response rate.

QUESTIONNAIRE AND TREATMENT OF DATA

The questionnaire used for this survey is provided in Table 1. It should be noted that this survey was a subjective exercise aimed at known and potential clients and thus no rigid polling methods or statistical analysis tools were employed or implied. During the survey, some questions were amended and responses recorded in a different manner than initially structured. For instance, the possible answers to Question 1 were either yes or no, but the actual answers were much more diverse (Fig. 2). Accordingly, four main types of answers were recorded for Question 1: 1) respondent has used geoscience information before and would like to continue using it; 2) respondent has not used geoscience information before and is not interested in using any in the future; 3) respondent has not used geoscience information before but would like to; and, 4) respondent is not sure whether the information he used could be classified as geoscience and is unsure about its application to his specific needs.

Question 3 – "What topics did you find useful and not useful?" – failed to provide constructive insight. Nearly all respondents found the information they used "useful" and thus this question was dropped from the survey. Similarly, Questions 12 and 13 did not produce useful responses. The only individuals who were asked these questions were those people who had not used any geoscience information and, because they had no previous experience in using geoscience information, it was difficult for respondents to adequately answer Questions 12 and 13. Most people who did reply to these two questions answered yes to all the categories listed, but with noticeable ambivalence.

Another difficulty encountered during the survey was that respondents could not realistically list their preferences or answers in numerical order over the telephone for questions such as 2, 3, and 9. It became impractical to note choices in numerical order and for this reason tick marks were employed instead to indicate selections.

Changes to the questionnaire were also implemented in the statistical analysis of some questions. For instance, the results for Questions 5 and 10 were combined since both questions were essentially asking for the same information, but from different audiences. The responses for Questions 7 and 11 were also combined for the same reasons, as were responses for Questions 8 and 14 and Questions 6 and 9.

Another notable change in our statistical analysis was the combination and rewording of certain answers. For example, in Question 2, answers number 11, 18, 19, and 20 were combined as "Geohazards". In addition, answers 7 and 10 as well as answers 5 and 6 were assessed collectively. It should be noted that in Figure 2, there are categories that were not

Table 1. Client Survey Questionaire.

1. Have you used any geoscience information before ? Yes ____, No ____. *IF NO GO TO QUESTION 9*

2. What kind of geoscience information have you used? *INDICATE CHOICES IN NUMERICAL ORDER*

1) bedrock	___	12) surficial deposits	___
2) rock collecting	___	13) river and marine sediments	___
3) fossil collecting	___	14) marine geology	___
4) mineral exploration	___	15) geophysical properties	___
5) hiking guides to the geology of certain areas	___	16) geotechnical studies	___
6) descriptions of the geology of parks	___	17) groundwater	___
7) geochemistry	___	18) landslides	___
8) chemical contamination	___	19) volcanic activity	___
9) radioactivity	___	20) natural hazards	___
10) soil chemistry	___	21) geoscience publication indices	___
11) earthquake hazards	___	Others	_____

3. Which topic(s) did you find useful? _____ *CHOOSE FROM ABOVE NUMBERS*
Which topic(s) did you find *not* useful? _____ *CHOOSE FROM ABOVE NUMBERS*

4. What type of source(s) did you use?

A) maps	___	G) videos	___
B) scientific reports (Memoirs, Bulletins, Papers)	___	H) telephone enquiries	___
C) brochures	___	I) public talks or lectures	___
D) pamphlets	___	J) posters	___
E) computer databases or computer bulletin boards	___	K) cassette tapes	___
F) computer disks	___	Others	_____

5. Did you want this source(s) in a different format? No ____ *IF NO GO TO QUESTION 6.*
Yes ____ *IF YES WHAT FORMAT DO YOU PREFER?*

___ ▸ ___ *(This ▸ symbol indicates the format you would have preferred the source to be in; ie. if you used*
___ ▸ ___ *a pamphlet, but would have liked the information as a video then you would indicate D ▸ F)*

Others_____

6. What information did you want that was not available? None ____ Others _____

7. From where should our geoscience publications be accessible?

Government sales offices	___	Private book stores	___
Computer bulletin boards	___	Libraries	___
Scientific journals	___	Mail order	___
Newspapers	___	Others	_____

8. What type of computers do you use? None ____
IBM Compatible ___ Amiga ___ Unix workstation ___ Apple ___ Others _____

Table 1. (cont.)

9. What geoscience topic(s) would you want information on? None ____

PLEASE LIST IN ORDER OF PREFERENCE

A) topographic maps	___	J) fault ages	___
B) rock types	___	K) volcanic activity	___
C) rock ages	___	L) radioactivity	___
D) mineralogy	___	M) rock collecting	___
E) groundwater maps	___	N) fossil collecting	___
F) publication indexes	___	O) rock chemistry	___
G) geology of parks	___	P) soil chemistry	___
H) earthquake hazards	___	Q) water chemistry	___
I) landslides	___	R) hiking guides to geology of parks...	___

Others_____

10. In what format would you prefer the above geoscience information?

Indicate which format you would prefer your chosen topic(s) in. (For example, if you would like hiking guides of certain parks or other areas in poster format then you would indicate R ▸ I)

A) maps	___	G) computer databases or bulletin boards	___
B) scientific reports	___	H) public talks or lectures	___
C) brochures	___	I) posters	___
D) pamphlets	___	J) displays	___
E) computer disks	___	K) cassette tapes	___
F) videos	___	Others _____	

___ ▸ ___ ___ ▸ ___ ___ ▸ ___ ___ ▸ ___

11. From where should our geoscience information be accessible?

Government sales offices	___	Private book stores	___
Computer bulletin boards	___	Libraries	___
Scientific journals	___	Mail order	___
Newspapers	___	Others _____	

12. For what purposes would you use the geoscience information?

Education ___ Recreation ___ Business ___ Community Issues ___

13. Would you use the geoscience information yourself or transfer it to others?

Self ___ Others ___

14. What type of computers do you use? None ____

IBM Compatible ___ Amiga ___ Unix workstation ___ Apple ___ Others_____

15. Do you access computer Bulletin Boards? Yes ____ No ____

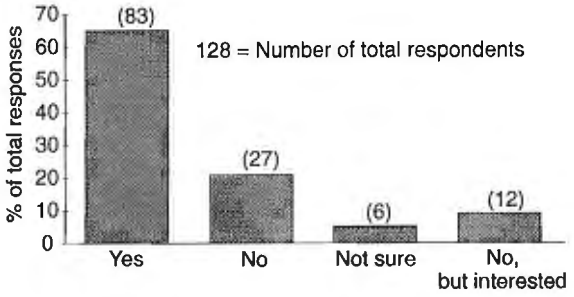

Figure 2. *Graph illustrating response to Question 1, "Have you used any geoscience information before?" The bars show percentage of total positive responses (623) normalized to 100%. Numbers at the top of each bar show the number of respondents (out of 128) who have used each type of geoscience information.*

part of our original selection list, but were chosen by a significant number of respondents. In contrast, some sources in Question 4 were never chosen (Fig. 4).

SURVEY RESULTS

Figures 2 to 9 graphically summarize the responses to each question in the survey. The production of a traditional paper-format atlas of geoscience information for the Georgia Basin had been discussed during planning meetings for a proposed Vancouver-Victoria integrated project. However, the survey clearly indicates that such a geoscience atlas is not warranted for this area. Respondents felt that such an atlas would be too general and inflexible for their site-specific requirements. There was also concern that the price would be too high and the publication too cumbersome.

This survey has provided useful data to guide production of our future publications. It was encouraging to see that most respondents were receptive to using geoscience information. Individuals and organizations in areas not traditionally associated with the geological sciences were interested in geoscience information provided the content and format were relevant, accessible, and understandable to them.

Have you used any geoscience information before? (Fig. 2)

We found that respondents who have used geoscience information are regular and committed consumers of our information. It was encouraging to note that many respondents who have not used geoscience information before would be interested in acquiring such data. Some of our results may have been skewed due to the relatively large number of special interest groups contacted. In retrospect, we could have tried to balance the percentage of each group more evenly. However, it was an important learning exercise to assess the views of non-traditional geoscience users.

The "Not Sure" block represents respondents who may have used geoscience data, but were uncertain of the source or of the fact that it was geoscience information. A large part of this category consists of administrators who have used individual consultants for geotechnical studies. The use of geotechnical consultants was most noticeable among local government engineering departments, but is also common practice among some consulting firms. Unfortunately, we could not always contact the actual geotechnical consultants who had done the work because consultants would vary from project to project depending on the nature of information needed in each situation.

The individuals in the "No, but interested" category represent respondents who have not used any geoscience information before, but would be interested in using such information if it was made relevant and responsive to their needs.

What kind of geoscience information have you used? (Fig. 3)

Publications on conventional geoscience topics are the most popular and widely used publications among our clients. Most interest currently centres around the assessment of geohazards (e.g., liquefaction potential, earthquakes, dam safety reports, volcanic activity, etc). However, there is a notable demand for natural history maps, satellite imagery data, and information about the geology of parks. There is less demand in the Vancouver area for bedrock mapping information than for data on geohazards and surficial geochemistry.

In what format have you used the information? (Fig. 4)

Conventional geoscience maps and reports continue to be the most extensively used formats. Modems and bulletin board subscriptions are increasingly affordable options, and the ability to download information through a modem is now perceived as a necessary business tool. Most respondents also

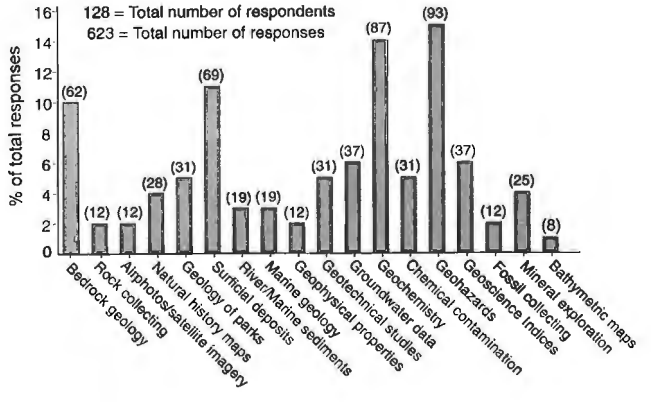

Figure 3. *Graph illustrating response to Question 2, "What type(s) of geoscience information have you used?"*

indicated that the acquisition of digital mapping technology, modems, databases, and related software was part of their future objectives.

In what format would you have preferred the information? (Fig. 5)

Although demand for traditional paper maps continues, a strong preference for both maps and non-graphical data in digital format is clearly apparent. Moreover, there is a noticeable demand for future geoscience information to be available through computer databases and bulletin boards. It is interesting to note that no respondents indicated that they would have preferred current geoscience information in written reports.

What geoscience topics would you like information on? (Fig. 6)

High demand remains for traditional geoscience topics such as bedrock geology, geochemistry, geohazards, etc. Educators and certain interest groups wanted more educational materials concerning natural history and earth sciences. Local and provincial government engineers, park managers, and geotechnical consultants all expressed an interest in groundwater maps, publications on geohazards risk assessments, and more site-specific geotechnical studies.

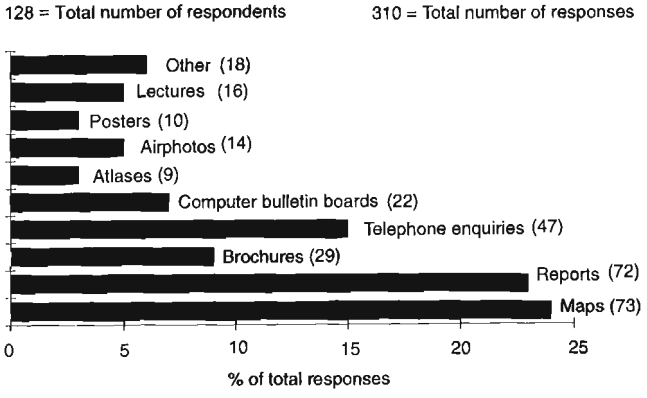

Figure 4. Graph illustrating response to Question 4, "What type of source(s) did you use?"

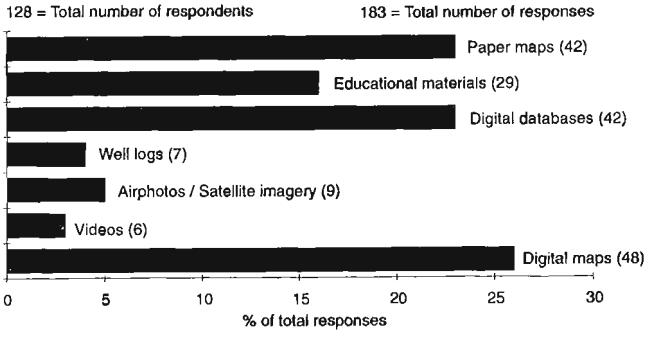

Figure 5. Graph illustrating combined response to Questions 5 and 10, "Did you want the geoscience information in a different format?"

From where should the information be available? (Fig. 7)

Government sales offices and libraries are still the preferred source for government publications. It is notable that the third highest demand was for modem access through computer bulletin board systems.

What type of computers do you use? (Fig. 8)

A large majority of respondents are DOS-based IBM-type computer users. The surprisingly high percentage of UNIX workstation users reflects the use of sophisticated GIS

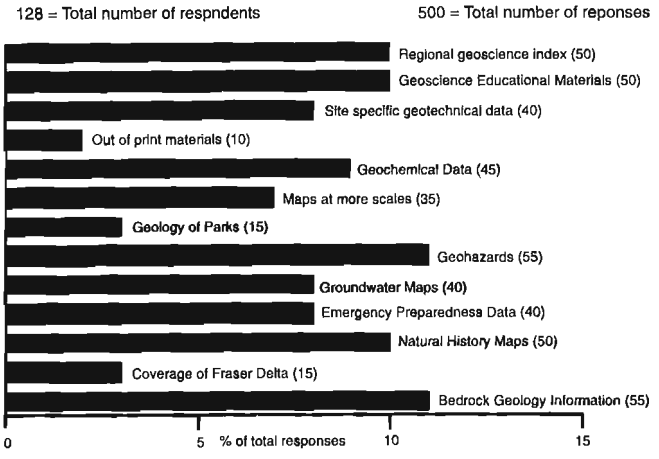

Figure 6. Graph illustrating combined response to Questions 6 and 9, "What type(s) of geoscience information did you want?"

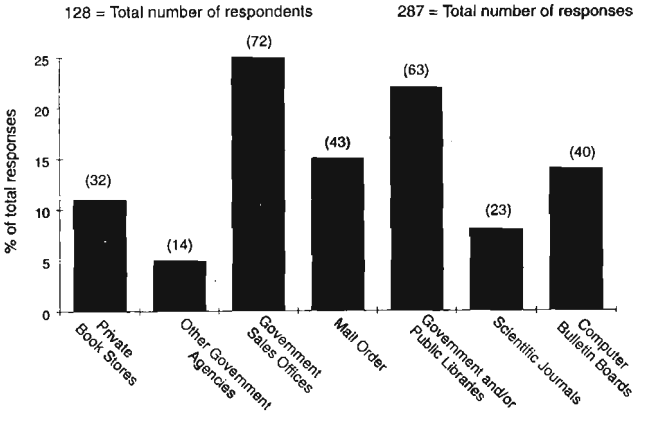

Figure 7. Graph illustrating combined response to Questions 7 and 11, "From where should our information be accessible?"

applications by several large geotechnical and engineering firms. However, the speed, storage capacity, and range of applications offered by IBM compatibles seem to be more than adequate for the needs of most users. Apple computers appear to be used less often for geotechnical applications.

Do you use computer bulletin boards? (Fig. 9)

Although not all respondents were asked Question 15 due to the layout of the questionnaire, more than half of the respondents who did answer this question indicated that they do use computer bulletin boards. Computer bulletin boards may have been used other than for accessing geoscience-related information (Fig. 9).

MAIN FINDINGS

Our main findings from this survey were:

1. A traditional paper atlas of geoscience information on the Georgia Basin area is not a widely used or preferred format (Fig. 4, 5). However, a geoscience atlas in digital format for the Georgia Basin area had appeal. Respondents reported that they would be much easier to manipulate and customize the information to meet their specific needs if it was available in digital format.
2. Geoscience information in GIS format was frequently requested. Individuals and organizations in all fields clearly feel that the ability to manipulate digital information is essential to their future needs. The flexibility a digital product offers, for example for choosing the scale of a map to be plotted and its combination of both attribute and spatial data in one package, is one of the main reasons for its popularity (Fig. 5).

   However, there is real concern among regular GIS users about the compatibility of various GIS programs, such as ArcInfo, Spans-Tydec, Terrasoft, MapInfo and so on. Respondents have reported difficulties and frustrations with using digital maps produced by various government departments using different program formats. This format inconsistency makes the integration of data from different sources very difficult and an unnecessary waste of client resources. Respondents are looking to the GSC and the GSB to use their authority and influence within the geoscience community and to take a leadership role in the adoption of an industry-wide GIS system or to establish common formats that simplify data integration. Survey respondents stated that any positive effort by the GSC/GSB to solve this problem would be welcomed.
3. Those who have used GSC and GSB maps before are pleased with the quality but would like these maps to be updated more frequently and available in a greater variety of scales. These requests are not easily manageable when dealing with traditional paper maps. However, with the increasing sophistication of digital mapping technology, these obstacles can be more easily overcome. This is reflected in the popularity of GIS format maps (Fig. 5, 6, and 8).
4. Publications on geohazards, surficial deposits, geochemistry, and bedrock geology were the most widely used geoscience topics (Fig. 3). This indicates a continuing high demand for traditional geoscience topics. However, a demand for educational materials on earth sciences is emerging. The public and educators are becoming more aware of the interconnected nature of all sciences: environmental, geological, etc. General interest in the environment is being translated into an interest in the role of geology in our global ecosystem.

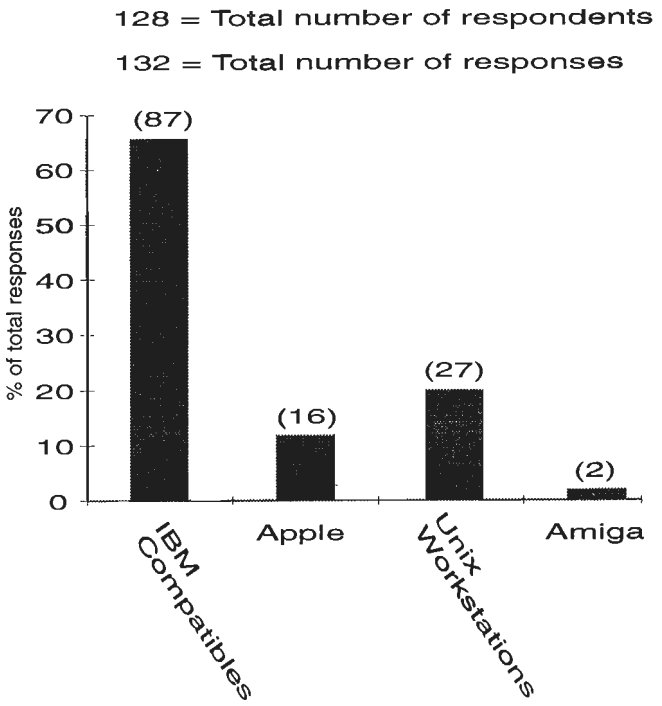

Figure 8. Graph illustrating combined response to Questions 8 and 14, "What type of computers do you use?"

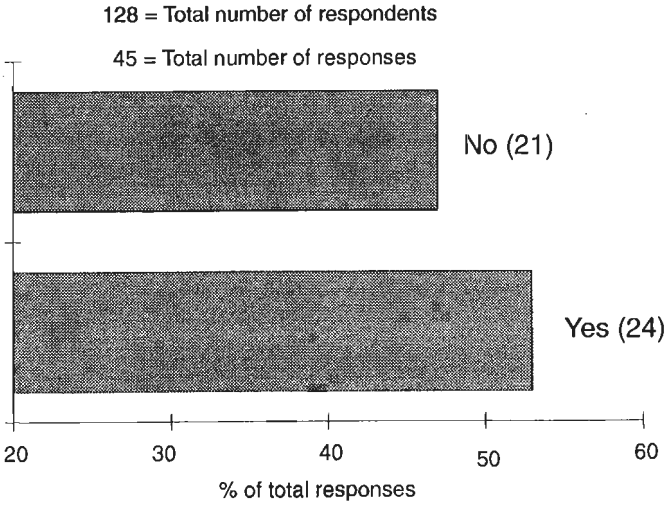

Figure 9. Graph illustrating response to Questions 15, "Do you use Computer Bulletin Boards?"

5. The main geoscience topic of interest to local government engineering departments is related to emergency preparedness and geohazards risk assessments (i.e. liquefaction potential, dam safety reports, volcanic activity, etc.) (Fig. 3 and 6).
6. Site-specific geoscience data for civil engineering, local government planning, and park management purposes was in demand (Fig. 6). Urban planners and park managers would like this type of data to be more site specific than is currently feasible for the GSB or GSC to produce. For example, local planners requested borehole logs for very specific future development sites.
7. Respondents noted a marked lack of educational material on geological sciences and the functions of the GSC and GSB that are suitable for teaching at university and high school levels as well as for educating the general public (Fig. 3 and 6).
8. Survey respondents who regularly use the GSC Library see a need to simplify and rearrange our current publication cataloguing and indexing system. An index of all GSC and GSB maps for B.C. organized by subject/title and/or year would be of interest. An "on-line" modem system for accessing publications as well as publication indices available in both our sales offices and/or libraries was also requested. Respondents would also like all GSC publications on the Cordilleran region to be available from local sales offices rather than from Ottawa (Fig. 7). In addition, quite a few respondents requested that their names be added to our mailing list for currently available publications.
9. The majority of special interest groups were unaware of the existence of the GSC and/or the GSB. Moreover, it was difficult for many of these groups to visualize the potential applications of geoscience information to their specific interests. The special interest groups we surveyed that have used geoscience information before were less interested in the finer details of geotechnical studies and more interested in the broad conclusions of these reports.
10. Topographic maps with natural history features were of interest to all contact groups surveyed (Fig. 6). These respondents requested maps with topographic features such as locations of old mining sites, migration routes, gold sites, lines of communications, former logging sites, old trails, previous place names, and so on. These maps would serve a variety of functions, such as park management, urban planning, public education, and emergency preparedness.

WHAT NEXT

The proposed integration of geoscience information for the Georgia Basin is still in its formative stage. This client survey has provided us with some very practical data to guide decisions on the types of publications the project should produce. A clear desire from clients for geoscience information in computer format is apparent. Moreover, the rapidly expanding and changing technologies of GIS systems, digital databases, computer bulletin boards, etc. are not only being embraced by the geotechnical community and urban planners, but also by non-traditional geoscience users. A strong desire was also expressed for more earth science educational material on the Lower Mainland and Vancouver Island, in forms suitable for educational institutions, for the many parks in the area, and for the general non-scientist population.

ACKNOWLEDGMENTS

This project has evolved thanks to the participation of many individuals from the GSC and the GSB, who have offered their advice at the most critical points during the course of the project. Without their instructive support, this exercise would not have been possible.

REFERENCES

British Columbia Round Table on the Environment and the Economy 1993: Creating a sustainable future - Georgia Basin Initiative. British Columbia Government Publications; 54 p.

Geological Survey of Canada Project 860022

Downhole logging measurements in the Fraser Delta, British Columbia

C.J. Mwenifumbo, P.G. Killeen, and B. Elliott
Mineral Resources Division

Mwenifumbo, C.J., Killeen, P.G., and Elliott, B., 1994: Downhole logging measurements in the Fraser Delta, British Columbia; in Current Research 1994-E, Geological Survey of Canada, p. 77-84.

Abstract: Downhole geophysical logging measurements have been made on the Fraser River Delta to construct a more precise lithostratigraphy of the area. The parameters measured include gamma ray, density, magnetic susceptibility, and temperature. Lithological identifications were made through the use of gamma-ray logs. Sands, silts, and clayey silts are characterized by very low, medium, and high radioactivity, respectively. Most of the sediments show a progressive consolidation with depth due to compaction, which can be easily determined from the geophysical logging data. Because of the good correlation between texture and natural radioactivity, the gamma ray logs were used to determine the depositional environments of the drilled sediments.

Gamma ray data correlate well with geotechnical data obtained with a cone penetrometer. Cohesive, clayey/silty soils are associated with increased radioactivity. The natural gamma-ray data may, therefore, be used to characterize soil types in the Fraser River Delta.

Résumé : Des diagraphies géophysiques de fond ont été réalisées dans le delta du fleuve Fraser pour établir avec plus de précision la lithostratigraphie de la région. Les paramètres mesurés ont été notamment les rayons gamma, la masse volumique, la susceptibilité magnétique et la température. Les identifications lithologiques ont été faites en utilisant des diagraphies par rayons gamma. Les sables, les silts et les silts argileux sont caractérisés par une radioactivité respectivement faible, moyenne et élevée. La plupart des sédiments indiquent une consolidation progressive avec la profondeur due à la compaction, que l'on peut facilement déterminer à partir des données de diagraphie géophysique. En raison de la bonne corrélation qui peut être établie entre la texture et la radioactivité naturelle, les diagraphies par rayons gamma ont servi à déterminer les milieux dans lesquels se sont déposés les sédiments forés.

Les données sur les rayons gamma correspondent bien aux données géotechniques obtenues avec un pénétromètre à cône. Les sols argileux/silteux cohésifs sont associés à une radioactivité accrue. Les données sur les rayons gammas naturels, peuvent, par conséquent, servir à caractériser les types de sol dans le delta du fleuve Fraser.

INTRODUCTION

Downhole logging measurements were made on the Fraser River Delta as part of a detailed study aimed at understanding the evolution and structure of the delta. Seven holes were drilled on the southern delta in Delta, B.C., in 1986 and 1987, and cased for later geophysical logging (Fig. 1). Only four of the seven holes were open at the time geophysical field work was conducted (September, 1987). Three of these (FD86C-DH3, FD86C-DH4, and FD86C-DH5) had been cased with plastic casing and the fourth (FD87A-DH1) with steel. All four holes were logged with natural gamma-ray spectrometry, gamma-gamma density, magnetic susceptibility (MS), and temperature, except for the steel-cased hole in which MS was not done. Holes FD86C-DH3, FD86C-DH4, and FD86C-DH5 were logged to depths of 50, 117, and 88 m, respectively. Hole FD87A-DH1 was drilled to a depth of 365 m, but logged only to 72 m due to a blockage.

Another hole (FD88A1) was drilled in 1988 on the northern Fraser Delta in Richmond, B.C. (lat. 49°09′20″, long. 123°11′40″) to a depth of 120 m. Self potential and single-point resistance measurements were made in this hole before casing was installed in 1988. Gamma ray, density, magnetic susceptibility, and temperature were logged later through plastic casing. Although this hole is far from those on the southern delta, the results are presented here to provide a complete report covering the logging done in the Fraser Delta area.

The main objectives of the borehole logging measurements were to obtain a continuous record of the changes in the physical and chemical properties of the sediments and to utilize this information to elucidate depositional environments. The logging was also done to provide data that might be of help in interpreting seismic reflectors observed in shallow seismic reflection records.

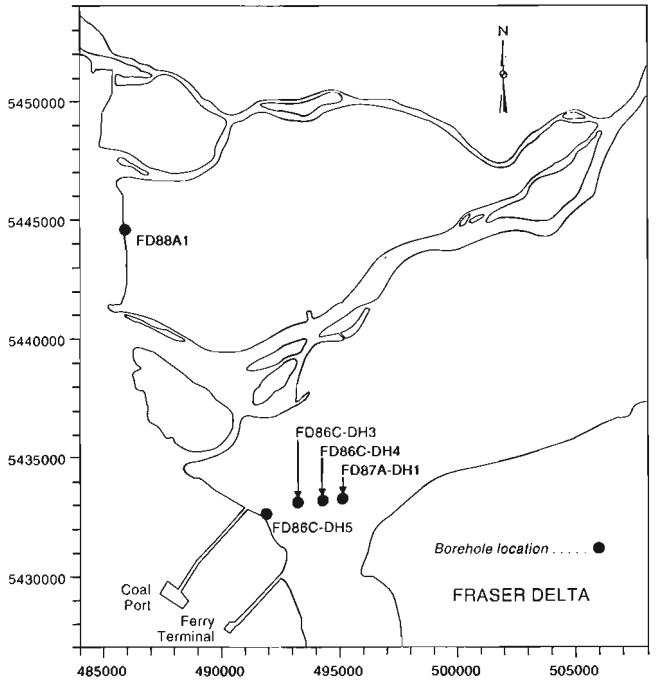

Figure 1. *Location of boreholes on the southern Fraser River Delta.*

LOG DESCRIPTION AND DATA ACQUISITION

Downhole logging measurements are direct indicators of the in-situ physical and chemical properties of sediments along the length of a borehole. The following is a summary description of the parameters measured on the Fraser River Delta.

Natural gamma ray

Gamma-ray measurements are used to detect variations in natural radioactivity due to changes in the concentrations of the trace elements uranium and thorium, and the major element potassium. The principal source of natural gamma radiation in sedimentary environments is ^{40}K, found in clay minerals such as illite and mixed-layer illite-montmorillonite. In sands, high concentrations of K-feldspar minerals may contribute significantly to the natural gamma radioactivity.

Full gamma-ray energy spectra are recorded in 256 channels covering an energy range from approximately 0.1 to 3.0 MeV. Four standard windows provide information on total count (0.03 to 3.0 MeV), potassium, uranium, and thorium. A 32 mm by 127 mm sodium iodide (NaI(Tl)) scintillation detector was used and logging was done at a speed of 1 m/minute in the plastic-cased holes and 0.5 m/minute in the steel-cased hole. The gamma-ray data were accumulated every 3 seconds, giving a measurement every 5 cm for the 1 m/minute logging speed and every 2.5 cm for the 0.5 m/minute logging speed. Only the total count gamma-ray logs, which monitor the total gamma radioactivity, are presented in this report. The low count rates observed in this environment (plus gamma-ray attenuation by the casing) produced count rates in the K, U, and Th windows with extremely poor statistics, making it impossible to convert the raw count rates to radioelement concentrations.

Density

The density probe consists of a gamma-ray source and a gamma-ray detector. The density probe response is primarily a function of the sediment bulk density. Gamma rays emitted by the source are scattered by the enclosing sediments. Density information is determined from the back-scattered gamma rays in the 180-500 keV energy window. The number of back-scattered gamma rays is inversely proportional to the electron density of the sediment. The electron density is related to bulk sediment density and to secondary physical properties, including porosity, water content, and chemical composition.

The acquisition system for the density data is the same as that for natural gamma-ray spectral logging. The density probe contains a 10 mCi ^{60}Co source and a 25 mm by 76 mm NaI(Tl) scintillation detector. The source-detector spacing

for the logging data presented in this paper was 17.5 cm. All data were acquired at a logging speed of 6.0 m/minute with a sample time of 1 second, giving a measurement every 10 cm. The density data presented in this paper are in arbitrary units because the tool was not calibrated for the cased hole.

Magnetic susceptibility

Magnetic susceptibility (MS) measurements provide an indication of the amount of ferromagnetic minerals, primarily magnetite and hematite/ilmenite, in sediments and rock. Variations in these measurements may be interpreted to reflect lithological changes and, possibly, the presence of alteration zones within rock units.

The data from the Fraser River delta were acquired with a Geo Instruments Ky probe interfaced to the GSC digital signal processing unit (Bristow, 1985). This system has four sensitivity ranges (20, 80, 320, and 1280×10^{-3} SI units), with the most sensitive setting giving a measurement resolution of approximately 0.005×10^{-3} SI. Susceptibility data are acquired continuously at a rate of 3 samples per second. All the holes were logged at 6 m/minute, providing a measurement approximately every 3 cm along the length of the hole.

Temperature

Four major factors affect the temperature profile in a borehole: 1) drilling fluid circulation; 2) seasonal and longer term temperature variations; 3) groundwater flow; and 4) lithological changes. The effects of drilling fluid circulation are transient and decay with time after completion of the hole. Even though these effects are considered noise in most studies, useful information on the location of fractures and permeable zones may be derived from temperature data acquired immediately after drilling. Seasonal and longer term climatic changes in surface temperatures usually affect only the top few tens of metres of the sediment column. Paleoclimatic information may be derived by studying these shallow geothermal gradient perturbations (Beck, 1982). The location of water flow zones and the direction of movement of water within a borehole may provide useful information in understanding the groundwater flow regime within an area. The use of temperature gradient measurements for lithostratigraphic mapping assumes a fairly stable geothermal environment and requires a good thermal conductivity contrast between the different sediments intersected by the drill hole.

The temperature probe consists of a 10-cm long tip of thermistor beads with a sensitivity of 0.0001°C. Changes in the borehole fluid temperatures are recorded as changes in the thermistor resistance and then converted into true temperatures, using an inverse operator and appropriate probe time constants. The temperature gradients are derived from the temperature data by means of a combined gradient and smoothing operator. All temperature data were acquired during a down hole run at a logging speed of 6 m/minute with data sampled every 0.2 second, giving a measurement every 2 cm. This high spatial resolution is necessary for the determination of accurate temperature gradients with the use of numerical derivative operators.

RESULTS

Drillhole FD87A-DH1

Figure 2 shows the gamma-ray, density, temperature, and temperature gradient logs for hole FD87A-DH1. Based on the gamma ray data, the logged interval may be divided into three major lithological zones: (1) an upper, dominantly sandy unit between 5 and 61 m, characterized by low radioactivity; there are several thin (< 3 m), clayey/silty layers with higher radioactivity in this unit; (2) a middle clayey or silty unit from 61 to 68 m of high radioactivity; and (3) a lower sandy unit from 68 to 72 m. The relationship between texture of these sediments and gamma radioactivity will be discussed in a later section.

The upper 30 m of the hole show a lower density that increases with depth. There are some changes in density that do not correlate with either the gamma-ray or temperature data. These variations in the upper portion of the hole may be due to changes in porosity, but more likely are due to changes in the hole diameter (similar to the illustration in Figure 3) outside the casing. Between 30 and 65 m there is a gradual increase in density that may be attributed to increasing sediment compaction with depth. The low densities at the bottom of the logged interval are probably caused by a washout.

The temperature and temperature gradient logs show no abnormal changes. The temperature gradient reversal (temperature minimum) is at approximately 31 m depth. The temperature minimum is due to past climatic changes. The

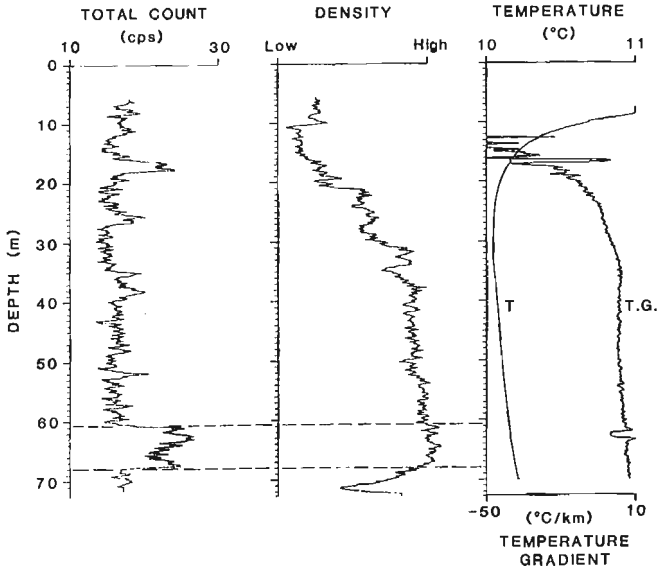

Figure 2. Natural gamma-ray, gamma-gamma density, and temperature logs acquired in the 10 cm steel-cased hole FD87A-DH1 (Fig. 1). The temperature (T) and temperature gradient (TG) logs are presented on the same track with the top axis representing the T-log and bottom axis the TG-log. The density is in arbitrary units and the gamma-ray log, in counts per second (cps).

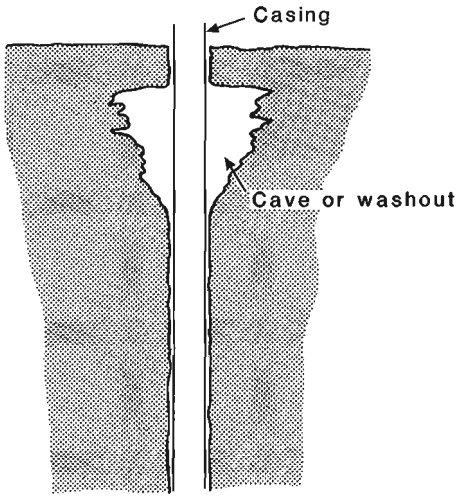

Figure 3. Illustration of the hole conditions that may be present outside the casing within unconsolidated sediments. Caves or washouts commonly exist in water-saturated sediments and may change the response characteristics of geophysical parameters.

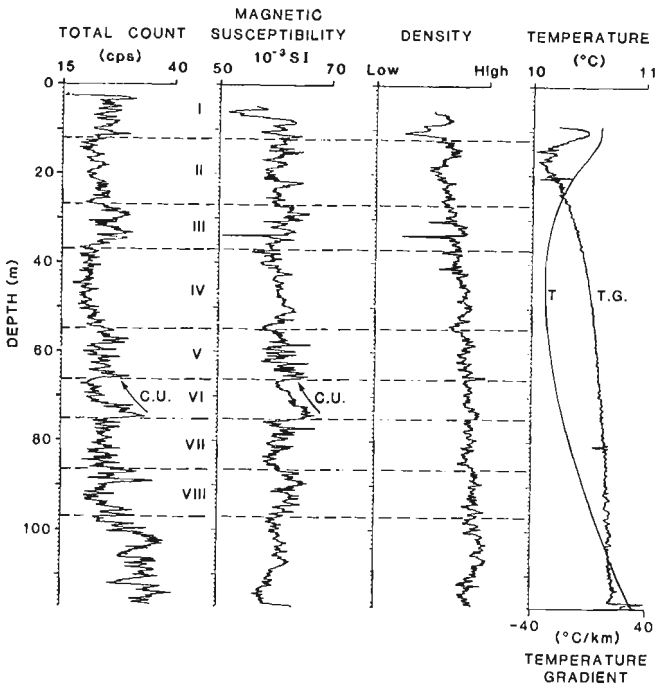

***Figure 4.** Natural gamma-ray, magnetic susceptibility, gamma-gamma density, and temperature logs acquired in plastic-cased hole FD86C-DH4. The temperature (T) and temperature gradient (TG) logs are presented on the same track with the top axis representing the T-log and bottom axis the TG-log. The log-derived units are indicated by roman numerals. C.U. stands for "coarsening upward".*

increase in temperature uphole from 30 m is due the warming of average surface temperatures since the last glaciation period (Beck, 1982).

Drillhole FD86C-DH4

Figure 4 shows the gamma-ray, MS, density, and temperature logs acquired in hole FD86C-DH4. A number of units (indicated by roman numerals in the figure) are recognized in the gamma-ray and MS logs. Sandy units are characterized by low radioactivity, whereas silty and clayey units have high radioactivity as well as high magnetic susceptibility. The correlation between radioactivity and susceptibility suggests that the magnetic minerals are associated with clay-rich units. This relationship, however, is not observed in all the drillholes. Some of the units show high-frequency, high-amplitude variations in gamma ray and MS (i.e., III, V, VIII), presumably reflecting the lithological heterogeneity of the sediments. The gamma-ray and susceptibility logs indicate that unit VI coarsens upward from clay through silty sand to clean sand. Detailed discussion on the use of gamma logs for determining depositional environments will be given in a later section.

There is a gradual increase in density with depth due to compaction. The temperature log shows a decrease in temperature down to the zero-gradient point at approximately 50 m and an increase below this depth. The temperature gradient is approximately 20°C/km near the bottom of the hole.

Drillhole FD86C-DH3

Figure 5 shows the gamma-ray, MS, density, and temperature logs acquired in plastic-cased hole FD86C-DH3. Five units are recognized on the basis of gamma-ray and MS data. The sands of unit II and upper part of unit V are indicated by low radioactivity and MS. The low density and susceptibility measurements in unit V indicate that the sand probably has a high porosity. In contrast, unit II does not show a corresponding low density, suggesting that it is less porous than unit V.

There are no significant changes in the temperature log that can be related to either groundwater flow or lithology. Temperature, however, decreases with depth, and the zero-gradient point is below 50 m, which is the bottom of the hole.

Drillhole FD86C-DH5

Figure 6 shows gamma-ray, MS, density, and temperature logs acquired in plastic-cased hole FD86C-DH5. Units I - V are inferred mainly from the gamma-ray and MS logs. Units I, III, and IV consist mainly of sand. Units III and IV have similar natural radiation characteristics, but can be distinguished on the basis of MS and slight density differences. The gamma-ray log suggests that unit III is a fining-upwards sequence, whereas unit IV is a coarsening-upwards sequence. Unit II is finer than either unit I or unit III and has higher levels of radioactivity. Unit V is very heterogeneous, with large-amplitude variations in gamma ray, MS, and density. It consists of sand and gravel interlayered with silt and clay. The density log shows a gradual increase in density with depth down to 60 m.

The temperature-depth profile is very different from those observed in FD87A-DH1 (Figure 2), FD86C-DH4 (Figure 4), and FD86C-DH3 (Figure 5). The temperature increases from

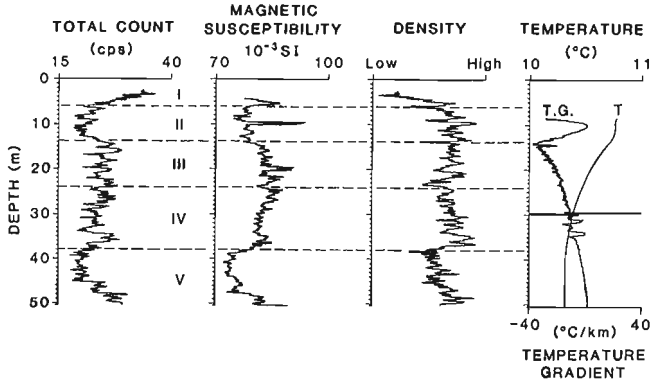

Figure 5. *Natural gamma-ray, magnetic susceptibility, gamma-gamma density, and temperature logs acquired in plastic-cased hole FD86C-DH3.*

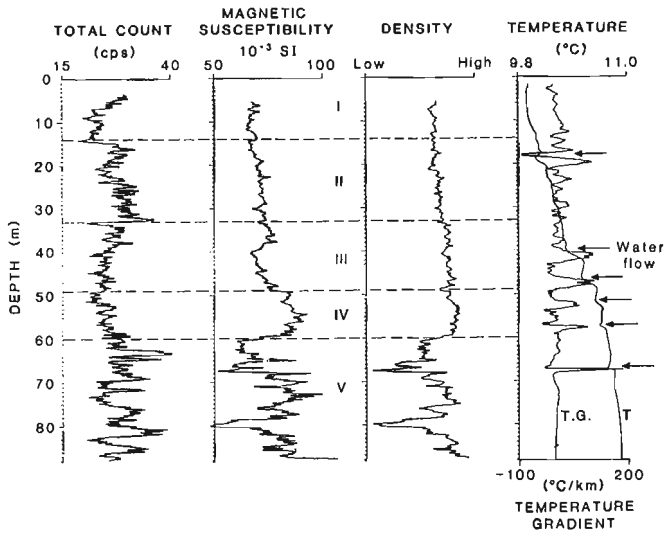

Figure 6. *Natural gamma-ray, magnetic susceptibility, gamma-gamma density, and temperature logs acquired in plastic-cased hole FD86C-DH5. Arrows indicate zones of water flow.*

the surface down to 90 m and there is no zero-gradient point. The temperature and temperature gradient logs show a number of anomalies that indicate water movement behind the casing. Hole FD86C-DH5 is located very close to the shore line and therefore, may be highly influenced by sea level changes. The temperature and temperature gradient logs show large-amplitude anomalies, indicating fluid circulation behind the casing.

Drillhole FD88A1

Figure 7 shows the logging data from hole FD88A1 in Richmond. The hole intersects fine to medium sand, silty sand, silt, and silty clay. These sediment types are easily identified on the gamma-ray log; the highest radioactivity is associated with silty clay and the lowest with sand. Density increases gradually with depth to the bottom of the medium sand layer at 103 m, where it increases abruptly. The gamma-ray log does not indicate any difference in the silty clay layers above and below this sand, but the change in density suggests that the lower layer is more consolidated than the upper. This may indicate the presence of an unconformity at approximately 103 m.

The MS log shows variations in susceptibility that generally correlate with the gamma-ray log and lithology. The SP and single point resistance logs clearly identify the sand layers, higher resistances being observed within the sand units. Temperature generally decreases, but there are temperature gradient anomalies between 40 and 70 m. These anomalies may be due to ground water flow or to the circulation of drilling fluids.

RELATIONSHIP BETWEEN SEDIMENT TEXTURE AND GAMMA RADIOACTIVITY

The silt- and clay- size fractions contain substantial amounts of potassium-rich clay minerals such as illite and mixed-layer clays (illite-montmorillonite). These minerals are responsible for much of the gamma radioactivity in the sediments.

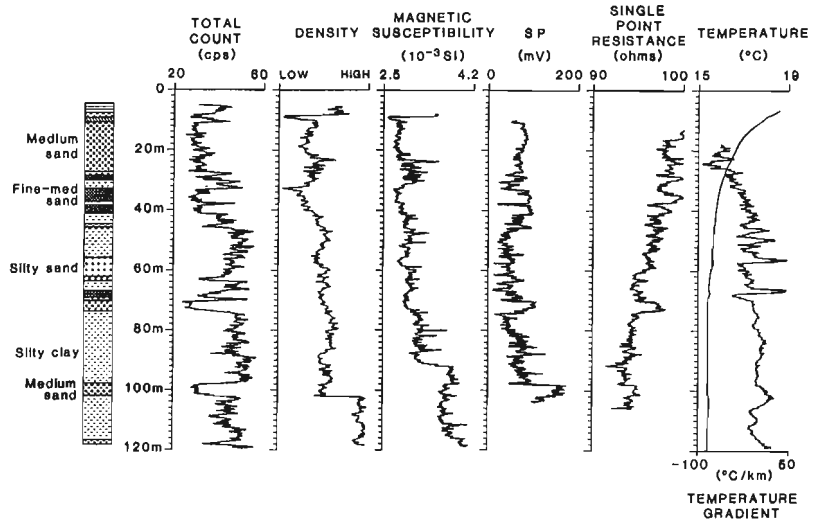

Figure 7.

Lithological, natural gamma-ray, density, magnetic susceptibility, SP, single-point resistance, and temperature logs in plastic-cased hole FD88A1. The lithological log is based on samples and geophysical logs.

The relationship between radioactivity and grain size is illustrated by data from borehole FD87A-DH1, shown in Figure 8. In this figure, radioactivity shows a good positive correlation with the percentage of mud (silt + clay). Figure 9 shows gamma-ray logs for four holes on the southern Fraser Delta. There is good hole-to-hole correlation between the gamma-ray logs, indicating their usefulness for stratigraphic correlation.

LOGGING MEASUREMENTS AND DEPOSITIONAL ENVIRONMENT

Downhole measurements provide continuous high spatial resolution data. By analyzing the shape of the borehole log responses and the bedding contacts, it may be possible to infer the sedimentological process at the time of deposition. Log responses are interpreted in terms of geological parameters such as mineralogy (clay type and abundance), texture, and porosity. These parameters provide some insight into the depositional environments of the sediments.

Natural gamma-ray data have been frequently used in the analysis of depositional environments (Serra, 1986; Serra and Abbott, 1982; Pirson, 1983). Since radioactivity is generally low in sands, increases in gamma radioactivity may be associated with increases in clay content. Clay-rich sediments generally indicate low-energy depositional environments.

Figure 10 is an expanded section of unit VI in hole FD86C-DH4 (see figure 4), showing the use of gamma-ray, MS, and density data in determining depositional environments. The logs indicate a coarsening-upwards sequence with sharp upper and lower contacts. The high gamma, MS, and density at the bottom of the sequence suggest the presence of clay-rich zones, whereas the decrease in gamma, MS, and density towards the top indicates an increase in sand content. The gamma ray response has a serrated character indicating an oscillatory, high/low energy, depositional environment.

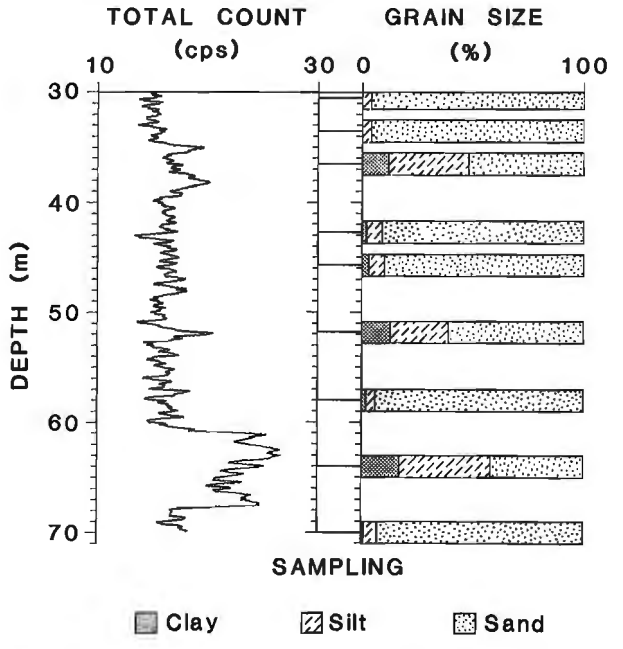

Figure 8. Relationship between the texture of sediments from borehole FD87A-DH1 and the total count gamma ray. Sandy zones with little silt and clay are characterized by low radioactivity. Increases in radioactivity are associated with increases in clay and silt content.

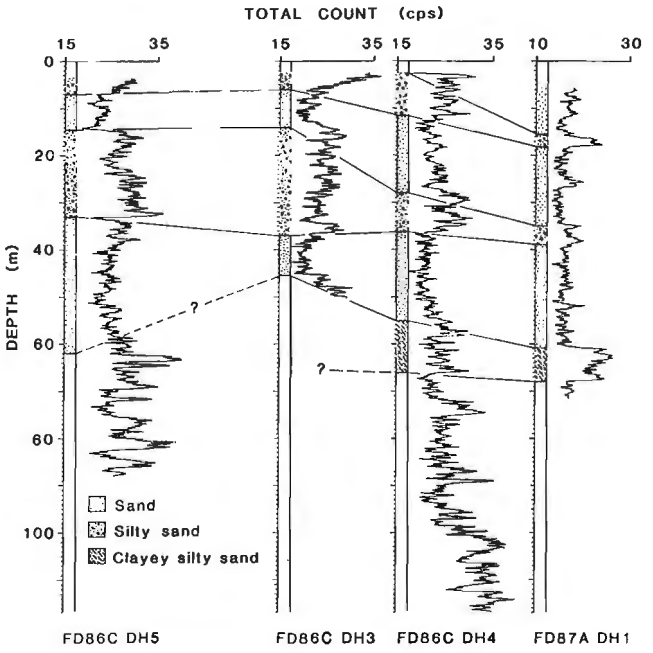

Figure 9. Stratigraphic correlations among four boreholes using natural gamma-ray logs. Lithology is derived from the logs and is based on the relative amplitudes of gamma-ray count rates.

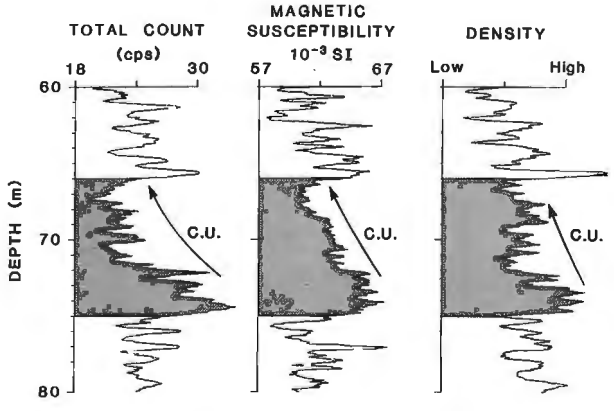

Figure 10. Use of geophysical logs in determining depositional environments. Identification of a coarsening-upwards (C.U.) sequence in hole FD86C-DH4 from gamma-ray, susceptibility, and density data. Fine-grained sediments at the bottom of the sequence are suggested by the higher radioactivity (high clay content - low energy depositional environment), higher susceptibility, and higher density (low porosity clayey layers).

Figure 11 shows gamma-ray responses from holes FD86C-DH5 and FD86C-DH3, indicating fining-upwards sequences, one with an abrupt lower contact and the other with a gradational lower contact.

Natural gamma-ray logs should be used with caution in determining the clay content of sediments and in interpreting depositional environments. High gamma radioactivity is not always associated with clay minerals. Minerals rich in uranium or thorium (zircon, allanite, thorite, uraninite, monazite, phosphates, etc.) may be present in coarse sediments and can strongly influence the gamma-ray response. Their presence may completely mask variations in clay content and hence render any textural interpretation erroneous. However, gamma-ray spectral logs (K, U, and Th) and other geophysical logs such as density and electrical resistivity may be used to differentiate high gamma anomalies resulting from clay minerals from those due to other causes.

CORRELATION OF GEOPHYSICAL AND GEOTECHNICAL DATA

Cone penetration test data were acquired to a depth of 45 m in hole SCPT-1, 6.5 m from hole FD87A-DH1 (ConTec Investigations Ltd., unpub. report, Cordilleran Division, 1987). Among the measurements made were tip resistance (Qc), sleeve friction (Fs), and friction ratio (Rf = Fs/Qc). These are used to determine the soil behaviour type and to interpret the stratigraphy of the penetrated sediments. Cohesive soils have low tip resistance and high friction ratios whereas soils with low cohesion, such as sands, have lower friction ratios and higher tip resistance.

Figure 12 shows the tip resistance and friction ratio for hole SCPT-1 and the gamma-ray log for FD87A-DH1. Natural gamma-ray data show a good correlation with tip resistance and friction ratios. Qc is inversely correlated with the total gamma-ray count rate (clay content), whereas Rf is positively correlated. The low Qc values, high Rf, and TC at 16-18 m indicate the presence of cohesive clayey to silty sand.

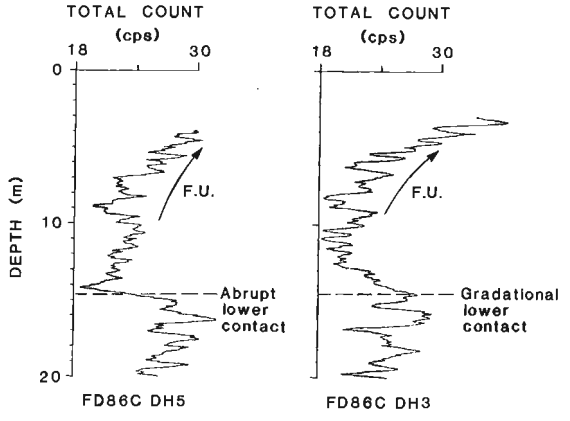

Figure 11. *Natural gamma-ray response to fining upward (F.U.) sequences, holes FD86C-DH5 and FD86C-DH3. The increase in gamma-ray count rate corresponds to an increase in clay or silt content.*

Figure 13 is a crossplot of total count gamma-ray (TC) and friction ratio (Rf). The regression equation is TC = 5.53Rf + 11.61, with a correlation coefficient of 0.87. A properly calibrated gamma-ray log may, therefore, be used to determine soil cohesiveness, which may remove the necessity for cone penetrometer tests on every hole.

CONCLUSION

The natural gamma-ray data provide a good indication of the relative proportions of sand and fines in the Fraser River Delta sedimentary sequence. Silty or clayey sediments exhibit higher levels of radioactivity than sands. Radioactivity is mainly associated with clay minerals containing potassium,

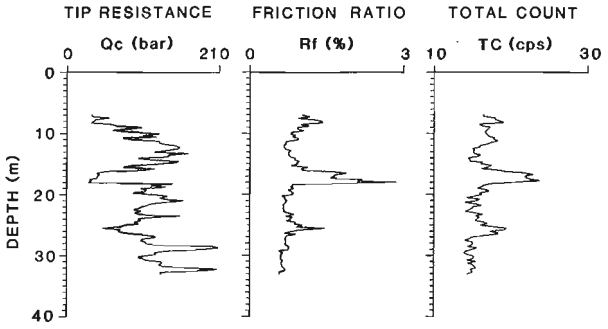

Figure 12. *Cone penetrometer tip resistance (Qc) and friction ratio (Rf) from hole SCPT-1 and total count gamma-ray log (TC) from hole FD87A-DH1, 6.5 m from SCPT-1.*

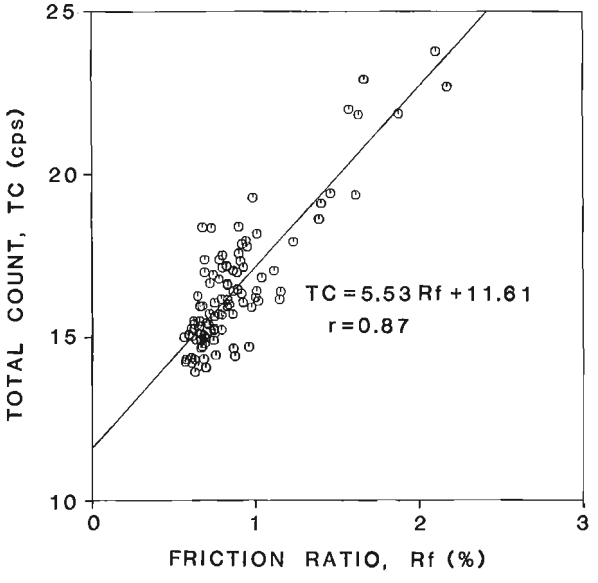

Figure 13. *Crossplot of total count gamma ray (TC) versus friction ratio (Rf) between 7 and 33 m in hole FD87A-DH1, illustrating the degree of correlation between these parameters.*

although some non-clay minerals are also sources of radioactivity. Density logs show a gradual increase in density with depth due to progressive consolidation of the sediments.

The cone penetrometer friction ratio correlates well with natural gamma-ray data. Sediments with high natural gamma radioactivity (i.e., clay) tend to be cohesive, whereas sediments with low radioactivity (sand) are less cohesive.

Continuous logging measurements in the Fraser Delta area have shown that logging data may provide useful information on the texture of sediments, soil types, and lithostratigraphy of the area.

REFERENCES

Beck, A.E.
1982: Precision logging of temperature gradients and the extraction of past climate; Tectonophysics, v. 83, p. 1-11.

Bristow, Q.
1985: A digital signal processing unit for the Geo Instruments magnetic susceptibility sensors, with analogue and RS-232C outputs; in Current Research, Part B; Geological Survey of Canada, Paper 85-1B, p. 463-466.

Pirson, S.J.
1983: Geologic Well Log Analysis; Gulf Publishing Company, Houston.

Serra, O.
1986: Fundamentals of Well Log Interpretation: Volume 2; in The Interpretation of Logging Data; Elsevier, Amsterdam.

Serra, O. and Abbott, H.T.
1982: The contribution of logging data to sedimentology and stratigraphy; 55th Annual Fall Technical Conference, Society of Petroleum Engineers of the American Institute of Mining Engineers, paper SPE 9270, p. 117-131.

Geological Survey of Canada Project 880030

Greater Vancouver Geotechnical Database (British Columbia): Richmond Pilot Project

Patrick A. Monahan[1] and John L. Luternauer
Cordilleran Division, Vancouver

Monahan, P.A. and Luternauer, J.L., 1994: Greater Vancouver Geotechnical Database (British Columbia): Richmond Pilot Project; in Current Research 1994-E; Geological Survey of Canada, p. 85-91.

Abstract: The Richmond Pilot Project was initiated to determine the extent and availability of geotechnical data in western Richmond and to serve as a model for a public geotechnical database in Greater Vancouver. A large volume of data acquired directly by public agencies is available for the database and is concentrated along highways and at the airport. Data acquired for public buildings by consultants are not available to the database, but are available to individual researchers. These data are widely distributed throughout western Richmond. Private data, not currently available to the database, are concentrated in the downtown and commercial areas of Richmond and include less useful data than those in the other categories. We suggest the database include a record of significant data that are not generally available, particularly those acquired for public buildings, and contain copies of original borehole logs.

Résumé : Le projet pilote de Richmond a pour objectif de déterminer l'étendue et la disponibilité des données géotechniques dans l'ouest de Richmond et d'établir un modèle en vue de la mise sur pied d'une base de données géotechniques à usage public dans le grand Vancouver. Des organismes publics ont déjà recueilli quantité de données, en particulier le long des autoroutes et à l'aéroport, qui sont prêtes à verser dans la base de données. Quant aux données que des consultants ont obtenues pour des édifices publics, elles ne sont pas versées dans la base de données, mais elles sont mises à la disposition des chercheurs. Elles couvrent un large territoire dans l'ouest de Richmond. Les données privées, qui ne sont pas encore disponibles, concernent surtout le centre-ville et les zones commerciales de Richmond, et sont moins utiles que les données dans d'autres catégories. Nous proposons que la base de données contienne les données importantes qui ne sont pas autrement disponibles, en particulier celles qui concernent les édifices publics, et aussi des copies de diagraphies de sondage originales.

[1] School of Earth and Ocean Sciences, University of Victoria, P.O. Box 1700, Victoria, British Columbia V8W 2Y2

INTRODUCTION

The steering committee of the Greater Vancouver Geotechnical Database was established in order to develop a public database of geotechnical and subsurface geological data for Greater Vancouver. This committee is chaired by the Geological Survey of Canada and includes representatives of other public agencies that obtain geotechnical data, including the British Columbia Ministry of Transportation and Highways and B.C. Hydro, municipal governments, universities, and geotechnical consulting companies. The geotechnical database would be used for regional geological mapping, land use planning, geological hazard assessment, ground water resource assessment, and planning geotechnical investigations. However, it is not intended to replace site specific geotechnical investigations for new construction.

In the summer of 1992, the steering committee decided to proceed with a pilot project for the City of Richmond, in the southern part of Greater Vancouver. The objectives of the pilot project were to determine the extent and availability of geotechnical data in the area and to identify potential data entry problems. This paper summarizes the results of our data search to the end of 1992 and makes recommendations on the structure that a public geotechnical database should take.

The study area includes all of Richmond west of No. 6 Road (Fig. 1). This area comprises the northwestern part of the modern Fraser River delta and was chosen for the pilot project because the authors were already acquiring subsurface geological data in the delta for other research (Monahan et al., 1993, in press).

PREVIOUS WORK

A database of subsurface geological data in the Greater Vancouver area for the period from 1913 to 1972 was compiled by Bélanger and Harrison (1976) and re-released in a DOS database format by Mustard and Roddick (1992). This database was compiled primarily from borehole logs in the files of geotechnical consulting companies and government agencies and consists of 4421 records. Each record includes the location, elevation, depth, and a lithologic summary of a borehole, but does not identify the source of the data.

DATA COLLECTION AND AVAILABILITY

The following public agencies either collect geotechnical and subsurface geological data directly or manage public domain data files: the British Columbia Ministry of Transportation and Highways and B.C. Hydro, both of which collect their own data and are subject to the British Columbia Freedom of Information Act; the Vancouver International Airport Authority, which now controls data acquired by Public Works and Transport Canada for the Airport; the Geological Survey of Canada, which has been studying the seismic hazard to the Fraser River Delta region; the Civil Engineering Department of the University of British Columbia (UBC), which has been acquiring geotechnical data to be used in graduate theses; and the Groundwater Section of the British Columbia Ministry of Environment, Lands, and Parks and the Petroleum Geology Branch of the British Columbia Ministry of Energy, Mines, and Petroleum Resources, both of which maintain public files on the results of drilling for water and petroleum. We went directly to these organizations to obtain their geological and geotechnical data. These data are available to the geotechnical database.

Other public agencies cause geotechnical data to be acquired in support of their construction activities. Those in the pilot project area include the City of Richmond, the Richmond School Board, and the Greater Vancouver Regional District, all of whom consented to the release of their geotechnical data to us for our research and the database. The commonly expressed opinion was that these data were acquired at public expense and should be available to the public. We were then directed to the geotechnical consultants who had acquired the data. The consultants readily provided us with the data for our research because it would benefit the geotechnical community as well as the public. However, they were reluctant to provide data that they had acquired, for both public and private clients, to a public geotechnical database. Most consultants are not prepared to spend time extracting data from their files and some consider that their data give them a competitive advantage. The most significant concern among larger consulting firms was about legal liability due to misuse of their data by other parties. A liability disclaimer on the database was not regarded as providing sufficient protection, and any lawsuit, no matter how frivolous it may seem, would be costly to fight. Furthermore, those firms that indicated it was the clients' decision to release data would object if theirs were the only data released to the geotechnical database. Consequently, most of these data are unlikely to be made publicly available.

In order to assess the extent of data collected for private organizations by geotechnical consultants, the Director of the Permits and Licences Department of the City of Richmond granted us permission to examine geotechnical reports in the City building permit files. Geotechnical reports are now required for all new building permit applications in Richmond. To help us identify significant data, we were provided with a computer listing of all new building permit applications with a value in excess of $1 000 000 since 1985, when their computer file was initiated. From approximately 200 building projects, we selected approximately 80 files to examine, including all projects with a value greater than $3 000 000, and some projects with a lesser value. Although data in these files could not be copied, the number, types, depths, and locations of test holes, the identities of building owners and consultants, and the file numbers were recorded. As with data acquired for public buildings by consultants, these data are not likely to be released to the geotechnical database. Not all municipalities in the Greater Vancouver area require that geotechnical data be provided with all building permit applications or would be able to provide the same level of support to identify significant geotechnical data within their boundaries.

Three types of subsurface geological data were recognized:

1. boreholes, drilled primarily to obtain sample material, including standard penetration tests;

2. cone penetration tests (CPTs), in which a cone-tipped rod is pushed into unlithified sediment and the resistance to penetration and other physical properties are recorded at the cone tip. CPTs were introduced into the Fraser Delta region in the 1980s and are particularly useful for stratigraphic investigations (Campanella et al., 1983; Monahan et al., 1993, in press). They are recorded in digital format; and
3. dynamic cone penetration tests (DCPTs), in which a cone-tipped rod is hammered into the ground and the number of hammer blows required to advance the cone every 300 mm is recorded.

In the following discussion a "site" refers to an individual building project or an isolated borehole.

RESULTS

The total volume of test hole data collected and identified for the database consists of 1648 boreholes, 274 CPTs and 162 DCPTs from 279 sites. The data can be grouped into three categories - available data, data collected for public buildings by consultants, and private data (Fig. 1; Table 1).

AVAILABLE DATA

The total amount of data available for the database includes 911 boreholes, 106 CPTs, and 53 DCPTs from 189 sites (Fig. 1; Table 1). The largest data sets are those acquired by the British Columbia Ministry of Transportation and Highways (MOTH) and by Transport Canada for the Vancouver Airport. Both data sets include data acquired by consultants and available to the database. MOTH considers itself the sole owner of all data it commissioned and believes that consultant data are subject to the Freedom of Information Act as much as data acquired by its own staff. Similarly, data acquired for Transport Canada by consultants is considered the property of the Crown.

MOTH data have been acquired over the past 40 years and are located along the principal highways and river crossings. This is an excellent data set with numerous deep CPTs and boreholes.

Transport Canada data at the Vancouver Airport have been acquired over the past 30 years. At 55 of the sites at the Airport there are 546 logs, none of which are deeper than 6 m. The remaining 26 sites include 51 boreholes deeper than 10 m that are an excellent data set with a full set of grain size analyses.

Table 1. Distribution of data by type and depth range.

		Number of Boreholes, including SPTs — Total depth (m)							Number of Cone Penetration Tests — Total depth (m)							Number of Dynamic Cone Penetration Tests — Total depth (m)					
Source	# of sites	total #	0-10	10-20	20-30	30-40	>40	max depth (m)	total #	0-10	10-20	20-30	30-40	>40	max depth (m)	total #	0-10	10-20	20-30	30-40	max depth (m)
AVAILABLE DATA																					
B.C. Ministry of Environment - Groundwater	3	3					3	127													
B.C. Energy, Mines and Petroleum Resources - Petroleum Geology	4	4					4	565													
B.C. Hydro	4	9	5	1	1		2	43	5		3	1	1		37						
B.C. Ministry of Transport and Highways	55	172	93	22	4	21	32	115	58	2	14	17	12	13	82	38	17	5	12	4	38
Geological Survey of Canada	8	6		1		1	4	120	17		1	4	9	3	49						
Published	3	1					1	107	3			2	1		31						
University of B.C.	4	2			2			25	18		3	12		3	64						
Vancouver International Airport	108	714	641	37	25	9	2	63	5			3	2		34	15		2	8	5	35
TOTAL AVAILABLE DATA	189	911	739	61	32	31	48	565	106	2	21	39	25	19	82	53	17	7	20	9	38
PUBLIC BUILDINGS, COLLECTED BY CONSULTANTS																					
City and School	27	133	116	12	1	2	2	160	88	1	24	47	16		31	44	29	15			15
GVRD	2	102	86	4	4	6	2	109	15		1	11	3		31	7	6	1			15
other	6	51	42	6	1	2		36	6		1	5			29.8	9		9			18
TOTAL	35	286	244	22	6	10	4	160	109	1	26	63	19		31	60	35	25			18
PRIVATE BUILDINGS																					
TOTAL	55	451	369	56	12	9	5	61	59		10	21	21	7	62	49	6	38	2	3	39
TOTAL ALL SOURCES	279	1648	1352	139	50	50	57	565	274	3	57	123	65	26	82	162	58	70	22	12	39

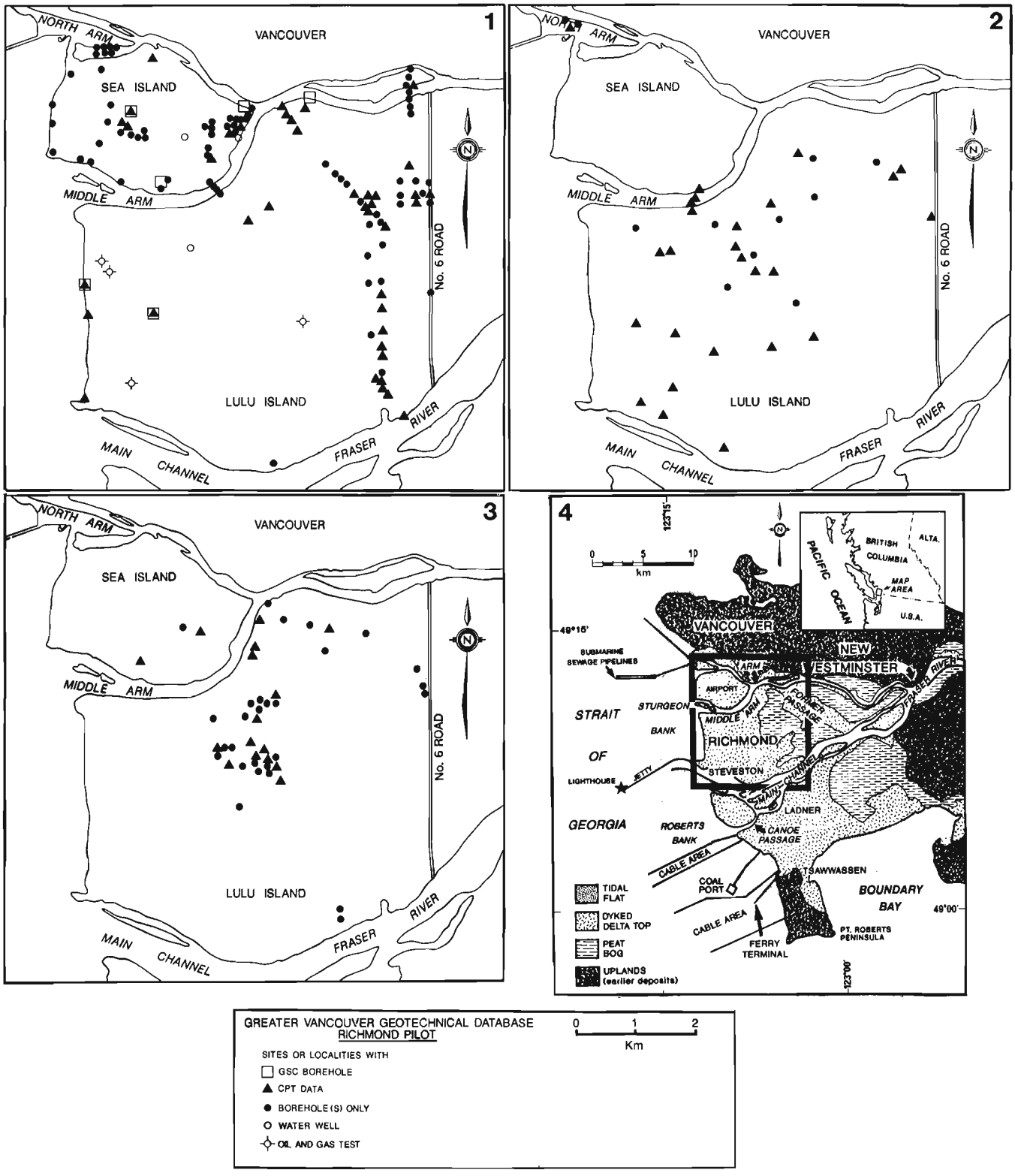

Figure 1. *Map 1: Locations of sites with data available to a database. Map 2: Locations of sites with data acquired for public buildings but which are not available to a database. Map 3: Locations of selected sites for which private data were collected. Map 4: General surficial geology and location of the pilot project area (bold rectangle).*

To the end of 1992, the Geological Survey of Canada (GSC) has drilled six boreholes in the study area. Five of these have been continuously cored and five have been cased and logged by wireline logs (Hunter et al., 1994). All CPTs acquired by the GSC include shear wave data (SCPTs), and four include resistivity data (RCPTs; Finn et al., 1989; Woeller et al., 1993b). In 1993 and 1994, the GSC acquired additional borehole and SCPT data in the area that are not included in these totals (Woeller et al., 1993a; Hunter et al., 1994).

B.C. Hydro has a modest data set, most of which was acquired by B.C. Hydro staff since 1989, although some of boreholes were acquired by consultants earlier. The CPTs include two SCPTs.

U.B.C. Civil Engineering graduate theses contain numerous CPTs and boreholes acquired at four research sites. From these sources, 18 CPTs were selected, including 5 RCPTs and 3 SCPTs (Gillespie, 1981; Robertson, 1982; Campanella et al., 1983; Laing, 1985; Leclair, 1988; Weemees, 1990; Kokan, 1992). In addition, dilatometer data are available from one site (Robertson, 1982; Tsang, 1987).

Only three water wells are recorded in the files of the Groundwater Section of the British Columbia Ministry of Environment, Lands, and Parks, primarily because water in the sand of the Fraser River delta is brackish to salty. Furthermore the descriptions are sketchy and inconsistent with more recent adjoining data. Elsewhere in the Lower Mainland, however, over 10 000 wells have been drilled for water, and these are on a computer database maintained by the Groundwater Section (A. Kohut, pers. comm.).

At least 13 petroleum exploration wells have been drilled in this area between 1906 and 1949 (British Columbia Ministry of Energy, Mines, and Petroleum Resources, Well Location Map of the Lower Mainland Area; Hume, 1933; Crickmay, 1947). Because this activity occurred prior to the implementation of the modern provincial reporting requirements, data could only be located on four of these tests in the files of the Petroleum Geology Branch of the Ministry of Energy, Mines, and Petroleum Resources and in GSC publications. The data are sketchy and ambiguous.

Borehole data have also been identified in published sources (Terzaghi, 1962; Byrne et al., 1992; Naesgaard et al., 1992). Almost certainly more data exist in the literature.

DATA ACQUIRED FOR PUBLIC BUILDINGS BY CONSULTANTS

Although data acquired for public buildings by consultants are unlikely to be released to the database, they are likely to be available to individual researchers, because consent to obtain the data is readily granted by public agencies. Data in this category amount to 286 boreholes, 109 CPTs, and 60 DCPTs from 35 sites (Table 1). CPTs are present at 66% of the sites and boreholes deeper than 10 m are present at 91% of the sites. The data, particularly school board data, are widely distributed throughout the study area (Fig. 1).

City and school board data comprise most of the data acquired for public buildings by consultants. The two sources are grouped together because they frequently collaborate on investigations on adjoining properties. All these data were acquired in the last eight years.

Greater Vancouver Regional District (GVRD) data, for two sewage treatment plants, were acquired during original site investigations over 20 years ago and during more recent investigations.

Other public buildings with significant data were identified by examining the city building permit files. These include the Richmond General Hospital, Kwantlen College, and buildings owned by other provincial and federal agencies.

PRIVATE DATA

A large volume of private data exists but is difficult to obtain because of the large number of building owners who must consent to the release of the data. Private data identified include 451 boreholes, 59 CPTs, and 49 DCPTs from 55 sites (Table 1). Most were acquired since 1985. CPTs are present at 29% of the sites (vs. 66% in the case of public buildings), and data identified are concentrated in the central and commercial portions of the city (Fig. 1). Proportionately more significant data have been acquired at higher-cost building sites: 86% of the projects valued at over $3 000 000 have boreholes deeper than 10 m, compared to 56% of the projects valued at less than $3 000 000. However, significant data have been acquired for a few of lower cost projects as well (e.g., a 24-m borehole in a $1 300 000 building project).

SURFACE GEOPHYSICAL DATA

Some publicly available surface geophysical data that are relevant to geotechnical investigations were identified during the data search. Surface shear-wave data have been acquired by the GSC at 32 sites in this area (Hunter et al., 1992) and gravity data have been acquired at 103 stations (Jensen, 1959).

DISCUSSION

A large volume of high quality data currently available to the public geotechnical database is concentrated along highways and at the Airport. A significant volume of data unlikely to be released to the geotechnical database particularly data acquired for public buildings by consultants is potentially available to researchers. Such data are not only easier for researchers to obtain than private data, because the owners are public agencies and fewer in number, but also provide better regional coverage and are proportionately more useful. Consequently, the geotechnical database should not only include data that have been released, but should also record the existence of significant data that have not been released, focusing on data collected for public buildings by consultants. Records of unreleased data should include the locations of

building sites, depths and types of test holes, and identities of building owners and consultants, so that an investigator could approach owners of unreleased data directly.

An alternative approach would be to summarize unreleased borehole data and not identify the source. We do not recommend such an approach. It would be time-consuming and costly, and would result in a product of limited value because summaries are subjective, subject to error, and data could not be easily verified. These points can be demonstrated by reference to the previous subsurface database (Bélanger and Harrison, 1976; Mustard and Roddick, 1992). The deepest boreholes reported are part of a series of boreholes 100 m apart at the eastern end of Sea Island and dated November, 1968: #4410 (depth 760 ft) and #4411 (depth 730 ft). In the latter borehole, the lithological summary records sand at 10 ft, clay-silt at 70 ft, and till at 719 ft. The reported locations for these boreholes are within 25 m of boreholes #4192 (depth 160.5 ft) and #4191 (depth 130.5 ft) respectively, which are dated August 1968 and must be the logs by R.C. Thurber and Associates for the Arthur Lang Bridge investigation: #68-17 (depth 160.5 ft) and #68-16 (depth 130.5 ft) respectively, drilled in August 1968. Thurber's log of test hole 68-16 reports sand at 10 ft, clay at 70 ft, and till at 119 ft. Thus, boreholes #4410 and #4411 of the previous database are erroneous duplications of boreholes #4192 and #4191. The discrepancy in the dates is due to the fact that one set of records was compiled from the geotechnical report (which is not in error), dated November, 1968, and the other, from the original logs, which record the August 1968 drilling date. Furthermore, the lithological summary of borehole #4191 is simply "sand-silt-gravel-till-grey-loose", a poor summary of Thurber's original log.

Because lithological summaries are inadequate, as discussed above, the geotechnical database should include copies of the original logs of released non-digital data, in addition to digital listing of boreholes. These copies should be in either hard copy or scanned image form.

Building owners and consultants who own significant unreleased data should be approached for consent to release data to the geotechnical database. If only one of the two parties consents to release data, this information should also be recorded in the database to further simplify the researcher's task of obtaining unreleased data.

Depending on resources that are available to compile the geotechnical database, criteria may have to be established to limit the amount of data included. For example, need we include all 546 logs at 55 sites at the airport with no logs deeper than 6 m? Similarly, when screening municipal files to record the existence of private geotechnical data, should sites with boreholes under a certain depth (e.g., 10 m) be recorded or should the objectives be to record the most significant data and provide regional coverage? In the Netherlands, the national geotechnical database is restricted to boreholes deeper than 10 m (de Mulder and Westerhoff, 1985). A geotechnical database for Greater Vancouver limited to the deeper data would still be a valuable asset. Such criteria need not be uniform throughout the region.

Elevation control is not widely reported in Richmond, most of which is between 1 and 2 m above mean sea level. However, many holes are located on preloads or embankments. Furthermore, when they are reported, elevations are referenced to a bewildering variety of datum elevations (e.g., geodetic survey, mean sea level (msl)=0 ft; hydrographic survey, msl=+9.85 ft; City of Vancouver, msl=+91.37 ft). Care must be taken during data entry.

RECOMMENDATIONS AND CONCLUSIONS

1. The geotechnical database should not only include released data, but should also record location, depth, and ownership (building owner and consultant) of significant unreleased data, particularly data acquired at public expense. Data currently available to the database and data acquired for public buildings by consultants together provide a body of high quality data that is well distributed regionally for geological investigations, land use planning, and hazard assessment.
2. For non-digital data that have been released to the database, in addition to digital listing of boreholes, copies of original logs should be available in hard copy or as scanned images.
3. Criteria for the inclusion of data into the database need to be developed for each area of Greater Vancouver.

ACKNOWLEDGMENTS

The authors gratefully acknowledge the assistance of R. Switzer and his staff at the Permits and Licences Department of the City of Richmond, R. Campanella of the Civil Engineering Department of the University of British Columbia, and the other members of the steering committee of the Greater Vancouver Geotechnical Database for their support: D. Tempelman-Kluit, D. Lister, J. Psutka, J. Meeks, J. Jorgenson, I. Morrison, and G. Rawlings. The authors also acknowledge the following organizations for their support and cooperation: British Columbia Ministry of Transportation and Highways Geotechnical and Materials Engineering Branch, British Columbia Ministry of Environment, Lands, and Parks Groundwater Section, British Columbia Ministry of Energy, Mines, and Petroleum Resources Petroleum Geology Branch, B.C. Hydro, Vancouver International Airport Authority, Public Works Canada, Greater Vancouver Regional District, City of Richmond, School District 38 (Richmond), ConeTec Investigations Ltd., Klohn Crippen Ltd., Geopacific Consultants Ltd., Macleod Geotechnical Ltd., Cook Pickering and Doyle Ltd., HBT Agra Ltd., Golder Associates, Thurber Engineering Ltd., and PBK Engineering Ltd. The figures were drafted by T. Oliveric. This paper was reviewed by B. Groulx, D. Lister, and J. Psutka, whose comments are greatly appreciated. P.A. Monahan is receiving scholarship support from NSERC and the University of Victoria.

REFERENCES

Bélanger, J.R. and Harrison, J.E.
1976: Vancouver subsurface information data bank; Geological Survey of Canada, Open File 382.

Byrne, P., Clague, J.J., Luternauer, J.L., and Naesgaard, E.
1992: Fraser River delta, Technical Tour No. 3; in Technical Tours Guidebook, May 7, 1992; Geotechnique and Natural Hazards, A Symposium Sponsored by the Canadian Geotechnical Society and the Vancouver Geotechnical Society, p. 101-119.

Campanella, R.G., Robertson, P.K., and Gillespie, D.
1983: Cone penetration testing in deltaic soils; Canadian Geotechnical Journal, v. 20, p. 23-35.

Crickmay, C.H.
1947: Report on the geology and natural gas and petroleum possibilities of the Terra Nova area, Lulu Island, British Columbia; British Columbia Ministry of Energy, Mines, and Petroleum Resources, Energy Resources Division, Geological and Geophysical Report 34.

de Mulder, E.F.J. and Westerhoff, W.E.
1985: Geology; in The Netherlands Commemorative Volume, Eleventh International Conference on Soil Mechanics and Foundation Engineering, San Francisco, 12-18 August 1985, (ed.) E.H. de Leeuw; The Netherlands Member Society, p. 19-28.

Finn, W.D.L., Woeller, D.J., Davies, M.P., Luternauer, J.L., Hunter, J.A., and Pullan, S.E.
1989: New approaches for assessing liquefaction potential of the Fraser River Delta, British Columbia; in Current Research, Part E; Geological Survey of Canada, Paper 89-1E, p. 221-231.

Gillespie, D.G.
1981: The piezometer cone penetration test; M.A.Sc. thesis, University of British Columbia, Vancouver, British Columbia.

Hume, G.S.
1933: Oil and gas in western Canada; Geological Survey of Canada, Geology Series no. 5, second edition.

Hunter, J.A., Luternauer, J.L., Neave, K.G., Pullan, S.E., Good, R.L., Burns, R.A., and Douma, M.
1992: Shallow shear wave velocity-depth data in the Fraser River Delta from surface refraction measurements, 1989, 1990, 1991; Geological Survey of Canada, Open File 2504.

Hunter, J.A., Luternauer, J.L., Roberts, M.C., Monahan, P.A., and Douma, M.
1994: Borehole geophysical logs, Fraser River Delta (92G), British Columbia; Geological Survey of Canada, Open File 2841.

Jensen, W.R.
1959: Gravity meter survey, Fraser River Valley; British Columbia Ministry of Energy, Mines, and Petroleum Resources, Energy Resources Division, Geological and Geophysical Report 823.

Kokan, M.
1992: Dilatancy characterization of sands using the resistivity cone penetration test; M.A.Sc. thesis, University of British Columbia, Vancouver, British Columbia.

Laing, N.
1985: Sources and receivers with the CPT; M.A.Sc. thesis, University of British Columbia, Vancouver, British Columbia.

Leclair, D.G.
1988: Prediction of embankment performance using in-situ tests; M.A.Sc. thesis, University of British Columbia, Vancouver, B.C.

Monahan, P.A., Luternauer, J.L., and Barrie, J.V.
1993: A delta topset sheet sand and modern sedimentary processes in the Fraser River Delta, British Columbia; in Current Research, Part A; Geological Survey of Canada, Paper 93-1A, p. 263-272.
in press: A delta plain sheet sand in the Fraser River Delta, British Columbia, Canada; Quaternary International.

Mustard, P.S. and Roddick, J.A.
1992: Vancouver subsurface information data bank for the period 1913 to 1972. A re-release of Open File 382 (1976, J.R. Belanger and J.E. Harrison) in a DOS database format; Geological Survey of Canada, Open File 2532.

Naesgaard, E., Sy, A., and Clague, J.J.
1992: Liquefaction dykes at Kwantlen College, Richmond B.C.; in Geotechnique and Natural Hazards. A symposium sponsored by the Vancouver Geotechnical Society and the Canadian Geotechnical Society, May 6-9, 1992, p. 159-166.

Robertson, P.K.
1982: In-situ testing of soil with emphasis on its application to liquefaction assessment; Ph.D. thesis, University of British Columbia, Vancouver, British Columbia.

Terzaghi, K.
1962: Discussion of Sedimentation of Fraser River Delta by W.H. Mathews and F.P. Shepard; Bulletin of the American Association of Petroleum Geologists, v. 46, p. 1438-1443.

Tsang, C.
1987: Research dilatometer testing in sands and clayey deposits; M.A.Sc. thesis, University of British Columbia, Vancouver, British Columbia.

Weemees, I.
1990: A resistivity cone penetrometer for groundwater studies; M.A.Sc. thesis, University of British Columbia, Vancouver, British Columbia.

Woeller, D.J., Hunter, J.A., and Luternauer, J.L.
1993a: Results of SCPT and SASW Testing of the Fraser River Delta sediments, British Columbia (92 G/2,3); Geological Survey of Canada, Open File 2714.

Woeller, D.J., Luternauer, J.L., and Hunter, J.A.
1993b: Presentation and interpretation of seismic cone penetration test data, Fraser River Delta, British Columbia (92 G/2,3); Geological Survey of Canada, Open File 2715.

Geological Survey of Canada Project 860022

Interior Plains and Arctic Canada

Plaines intérieures et région arctique du Canada

Significance of the Pakowki Formation to mapping in the deformed belt of the southern Canadian Cordillera, Alberta[1]

Tomasz Jerzykiewicz
Institute of Sedimentary and Petroleum Geology, Calgary

Jerzykiewicz, T., 1994: Significance of the Pakowki Formation to mapping in the deformed belt of the southern Canadian Cordillera, Alberta; in Current Research 1994-E; Geological Survey of Canada, p. 95-100.

Abstract: A shale unit in the footwall of the Coleman thrust plate at Coleman, Alberta, possesses foraminiferal, palynological, and lithological characteristics of the Pakowki/Nomad marine cycle. The Pakowki transgression of the Plains of southern Alberta correlates with the Claggett transgression which began in western Montana at approximately 80 Ma. Recognition of the Pakowki marine shale in the deformed belt permits separation of the uppermost formations of the Alberta Group (Burmis and Lees Lake formations) from the Belly River strata. A new stratigraphic classification of the upper, Campanian part of the Alberta Group, and the Belly River Group, recommended for the NATMAP projects, allows a refinement of sedimentological and structural interpretations of the thrust and fold belt of the southern Canadian Cordillera.

Résumé : Une unité de shale dans le mur de la nappe de charriage de Coleman (Coleman, Alberta) possède des caractéristiques du cycle marin de Pakowki/Nomad (contenu en foraminifères, palynologie et lithologie). La transgression de Pakowki qui a envahi les Plaines du sud de l'Alberta est en corrélation avec la transgression de Claggett qui a pris naissance dans la partie ouest du Montana il y a environ 80 Ma. La reconnaissance du shale marin de Pakowki dans la zone déformée permet de séparer les formations sommitales du Groupe d'Alberta (formations de Burmis et de Lees Lake) des strates de Belly River. Une nouvelle classification stratigraphique de la partie supérieure du Groupe d'Alberta (Campanien) et du Groupe de Belly River, recommandée pour les projets du CARTNAT, permet de raffiner les interprétations sédimentologiques et structurales de la zone de plissement et de charriage dans la partie sud de la Cordillère canadienne.

[1] Contribution to the NATMAP Southeastern Cordillera project

INTRODUCTION

The Pakowki/Nomad marine cycle of Campanian age consists of the Pakowki Formation in southern Alberta and the Nomad Member of the Wapiabi Formation in the northern part of the Alberta Basin. The cycle underlies the predominantly nonmarine Belly River Group and correlative strata over the entire Alberta Basin. The Pakowki Formation was described by Dowling (1917) from Pakowki Coulee, southeast of Lethbridge, and subsequently investigated and mapped in the entire southern Plains (Williams and Dyer, 1930; Russell, 1970; Lerbekmo, 1961; McLean, 1971).

The lack of positive identification of Pakowki marine shale in the southern Foothills to date precluded the possibility of distinguishing between uppermost Alberta Group strata and the overlying Belly River Group within the deformed belt of the southern Canadian Cordillera. Recent recognition of the Pakowki shale near Lundbreck allows a revision of stratigraphic classification of the Campanian strata in the southern Foothills by making a correct separation of the Alberta and Belly River groups (Jerzykiewicz and Norris, in press). The purpose of this paper is to extend this classification westward into the footwall of the Coleman thrust plate on the basis of the newly discovered Pakowki section at Coleman.

STRATIGRAPHIC POSITION

The biostratigraphic position of the Pakowki Formation is defined by the presence of *Baculites obtusus* Meek and *B. mclearni* Landes (Landes, 1940). The Pakowki/Nomad transgression correlates with the Claggett transgression which began in western Montana in the *zone* of *Baculites obtusus* (at approximately 80 Ma) and culminated in the *zone* of *Baculites mclearni* (at approximately 79 Ma) (Gill and Cobban, 1973; Obradovich and Cobban, 1975). During this brief transgression, the shoreline in northwestern Montana moved westward as much as 225 km – about 150 m per thousand years (Gill and Cobban, 1973). In Alberta, the Pakowki sea flooded the Burmis delta in the southern Foothills (Jerzykiewicz and Norris, in press), and the Virgille/Chungo shoreface in the southern Plains and central/northern Foothills.

PAKOWKI FORMATION AT COLEMAN

The Pakowki shales occur in a roadcut in the eastern part of Coleman in Lsd. 11, Sec. 9, Twp. 8, Rge. 4 W5 Mer. (Fig. 1). The shales are underlain by the Burmis, Lees Lake, and Wapiabi formations in a normal succession similar to that described from the vicinity of Lundbreck (Jerzykiewicz and Norris, 1993, in press). At Coleman, the Pakowki shales occur in the footwall of the Coleman thrust plate (Fig. 2).

There are other outcrops of the Lees Lake and Burmis formations in the footwall of the Coleman plate in the vicinity of Coleman (Fig. 2, secs. 2, 3; Fig. 3) that were mapped erroneously as the Belly River Formation (Price, 1962; Norris, 1993).

The Pakowki Formation at Section 1 (Fig. 1, 2) consists of up to 25 m of shale interstratified with thin, hummocky cross-stratified sandstone beds. Marine trace fossils and foraminifera and pollen occur in abundance.

According to J.H. Wall (Appendix) the foraminiferal assemblage found in the shale fully supports recognition of the Pakowki Formation at Coleman. The same conclusion has been reached independently by D. Braman (written comm., 1993) on the basis of a palynological assemblage from the same outcrop.

Figure 1. *The Pakowki shale at Coleman, designated Section 1 on Figure 2. View toward the north from above Section 2.*

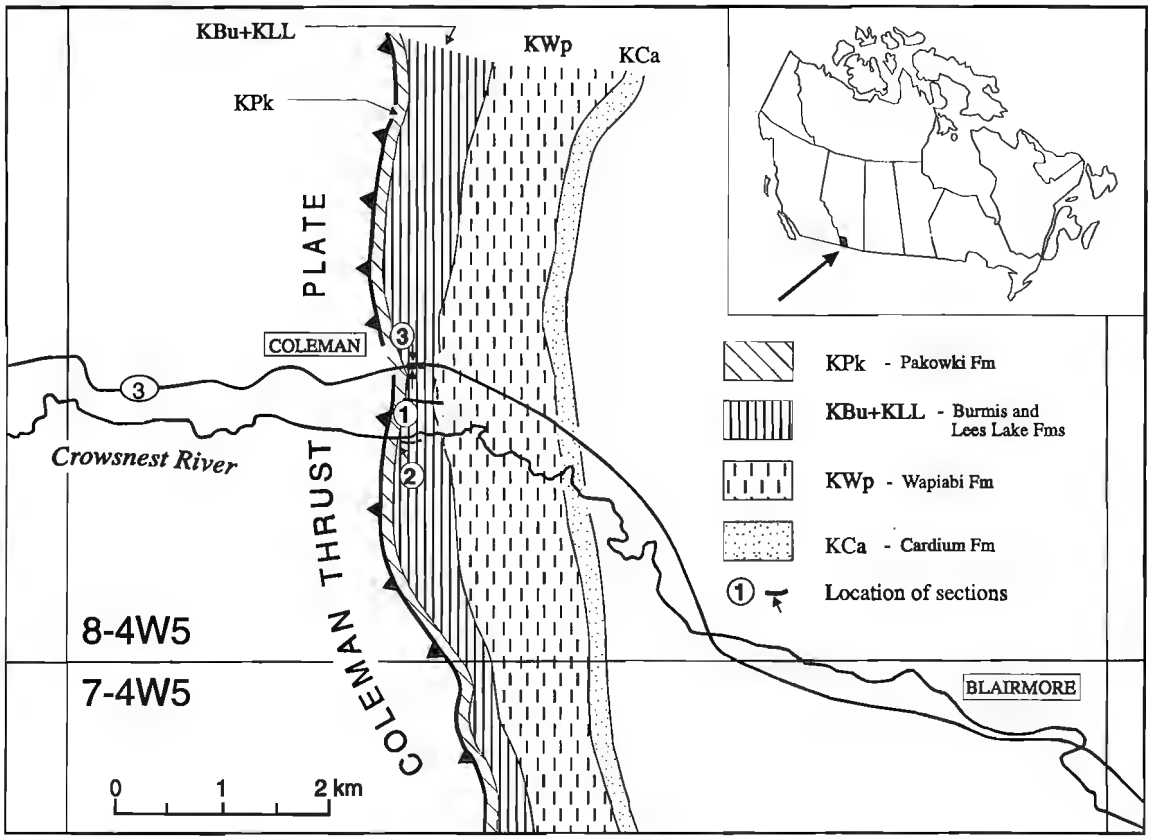

Figure 2. *The structural setting of the Pakowki Formation in the vicinity of Coleman.*

Figure 3. *Uppermost Alberta Group formations exposed along Highway 3 at Coleman. View toward the southwest from the Forestry Trunk Road.*

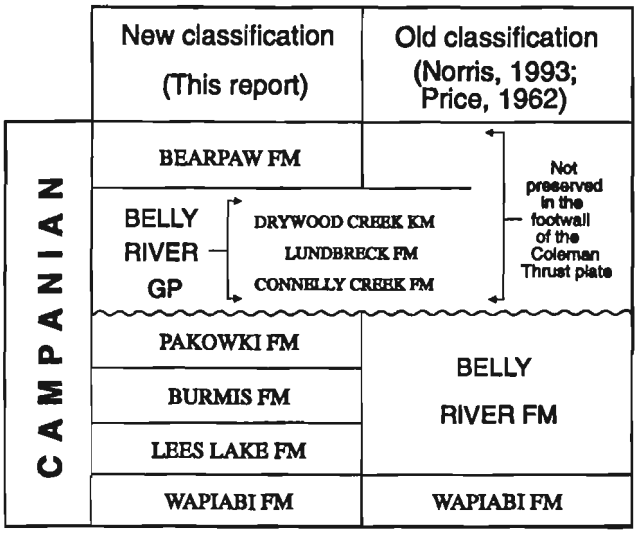

Figure 4. New and old stratigraphic classifications of the Campanian, post-Wapiabi strata of the deformed belt of southern Canadian Cordillera. The Belly River formations, capped by Bearpaw shale, which are not present in the study area, were recognized farther west in the footwall of the Lewis Thrust, and east of the Livingstone Thrust (cf. Jerzykiewicz and Norris, in press).

CONCLUSIONS

The shales that occur in the footwall of the Coleman plate, in the vicinity of Coleman, overlie Wapiabi, Lees Lake and Burmis formations and possess foraminiferal, palynological, and lithological characteristics of the Pakowki Formation.

Previously mapped as the Belly River Formation (Price, 1962; Norris, 1993), the Pakowki shale at Coleman correlates with the Pakowki Formation of the southern Alberta Plains and Montana.

The Belly River Formation is not preserved in the footwall of the Coleman thrust plate. It occurs farther west of the study area in the footwall of the Lewis thrust, and within the imbrication zone east of the Livingston thrust (Jerzykiewicz and Norris, in press).

A new stratigraphic classification of the upper part of the Alberta Group presented in this report (Fig. 4) permits a refinement of the sedimentological and structural interpretations of the deformed belt in the southern Canadian Cordillera, and is recommended for the Southern Alberta NATMAP projects.

ACKNOWLEDGMENTS

An introduction to the structural geology of the study area by D.K. Norris during a field trip in 1992, and the palynological expertise of D. Braman (Royal Tyrrell Museum) are gratefully acknowledged.

REFERENCES

Dowling, D.B.
1917: The southern plains of Alberta; Geological Survey of Canada, Memoir 93, 200 p.

Gill, J.R. and Cobban, W.A.
1973: Stratigraphy and geologic history of the Montana Group and equivalent rocks, Montana, Wyoming, and North and South Dakota; U.S. Geological Survey, Professional Paper 776, 37 p.

Jerzykiewicz, T. and Norris, D.K.
1993: Evolution of the Laramide foredeep and adjacent thrust belt in southern Alberta; Geological Survey of Canada, Open File 2663, 96 p.
in press: Stratigraphy, structure and syntectonic sedimentation of the Campanian "Belly River" clastic wedge in the southern Canadian Cordillera; Cretaceous Research.

Landes, R.W.
1940: Part II: Paleontology of the marine formations of the Montana Group; in Geology of the Southern Alberta Plains, L.S. Russell and R.W. Landes; Geological Survey of Canada, Memoir 221, p. 129-217.

Lerbekmo, J.F.
1961: Stratigraphic relationship between the Milk River Formation of the southern Plains and the Belly River Formation of the southern Foothills of Alberta; Journal of the Alberta Society of Petroleum Geologists, v. 9, p. 273-276.

McLean, J.R.
1971: Stratigraphy of the Upper Cretaceous Judith River Formation in the Canadian Great Plains; Saskatchewan Research Council, Geology Division Report, v. 11, 96 p.

Norris, D.K.
1993: Blairmore, Alberta; Geological Survey of Canada, Map 1829A.

Obradovich, J.D. and Cobban, W.A.
1975: A time-scale for the Late Cretaceous of the Western Interior of North America; in The Cretaceous System in the Western Interior of North America, (ed.) W.G.E. Caldwell; Geological Association of Canada, Special Paper 13, p. 31-54.

Price, R.A.
1962: Fernie map-area, east half, Alberta and British Columbia 82G E 1/2; Geological Survey of Canada, Paper 61-24, 65 p.

Russell, L.S.
1970: Correlation of the Upper Cretaceous Montana Group between southern Alberta and Montana; Canadian Journal of Earth Sciences, v. 7, p. 1099-1108.

Wall, J.H.
1967: Cretaceous foraminifera of the Rocky Mountain Foothills, Alberta; Research Council of Alberta, Bulletin 20, 185 p.

Wall, J.H. and Rosene, R.K.
1977: Upper Cretaceous stratigraphy and micropalaeontology of the Crowsnest Pass-Waterton area, southern Alberta Foothills; in Cordilleran Geology of Southern Alberta and Adjacent Areas, (ed.) M.S. Shawa; Canadian Society of Petroleum Geology, Special Publication 25, p. 842-867.

Williams, M.Y. and Dyer, W.S.
1930: Geology of southern Alberta and southwestern Saskatchewan; Geological Survey of Canada, Memoir 163, 160 p.

Geological Survey of Canada Project 930005

APPENDIX

by J.H. Wall

This is part of Report No. 3-JHW-1993 concerning Pakowki shale at Coleman

Field no. and stratigraphy	Locality, microfossils, age and environment	GSC loc. no.
BR-3/1a Pakowki(?) Fm.	Coleman, NTS 82G/9 Lsd. 11, Sec. 9, Twp. 8, Rge. 4 W5 Mer. Foraminifera: *Saccammina*? sp., very large thick forms *Reophax* sp. 4 Wall 1967, Pl. 11, figs. 9, 10 *Haplophragmoides* sp. 2 Wall 1967, Pl. 11, figs. 14-16 - abundant *Ammobaculites* sp.-spp. *Trochammina* sp. 2 Wall 1967, Pl. 11, figs. 1-8 - abundant *Uvigerinammina*? sp. 1 Wall 1967, Pl. 14, figs. 19, 20 - one *U.*? sp., very large - one Age: Late Cretaceous, middle Santonian to early Campanian indicated through comparison of the microfauna with the so-called "southern assemblage" of Wall (1967, p. 32), later referred to as "Wapiabi unnamed agglutinated microfauna" by Wall and Rosene (1977, p. 862). This assemblage occurs in the "Hanson Member" (upper Thistle Member of Wapiabi Formation in updated terminology) and overlying transition beds to the Belly River Formation (old terminology) on Mill and Dungarvan creeks in the Crowsnest-Waterton area. Although the composition of this Foothills microfauna differs somewhat from that of the Pakowki Formation in the Plains, correlation of the host rocks seems reasonable when changes in depositional environment between these areas are taken into account. Environment: Marine, shallow, inner shelf to nearshore, possibly with below normal salinity. Assemblage is entirely arenaceous and dominated by two species with large populations.	C-208409
BR-3/1c same unit	Same locality Foraminifera: *Saccammina* spp. - one large thick and one small thin species with one specimen each *Haplophragmoides* sp. 2 Wall 1967 - abundant *Ammobaculites* sp. *Trochammina* sp. 2 Wall 1967 - abundant *Verneuilinoides bearpawensis* (Wickenden), poorly preserved Age and Environment: As for previous entry.	C-208410
BR-3/3-3 same unit	Same locality Foraminifera: *Haplophragmoides* sp. 2 Wall 1967, including forms transitional or referable to *H.* sp. cf. *H. rota* Nauss *Ammobaculites* sp., small, compressed - one *Pseudobolivina* sp., small - one *Trochammina* sp. 2 Wall 1967 Age and Environment: As for previous entries. There is a considerable reduction in population.	C-208411
BR-3/4 bottom same unit	Same locality Foraminifera: *Saccammina* sp. - two *Ammodiscus* sp., small, siliceous - one *Haplophragmoides* sp. cf. *H. rota* Nauss *H.* sp. 2 Wall 1967 *Trochammina* sp. 2 Wall 1967 Age and Environment: As for previous entries. There is a resurgence of the microfauna with *Haplophragmoides* spp. being dominant.	C-208412
BR-3/4 top	Same locality Foraminifera: *Saccammina* sp. - one *Haplophragmoides* sp. cf. *H. rota* Nauss *H.* sp. 2 Wall 1967 *Ammobaculites* sp. *Trochammina* sp. 2 Wall 1967 taxonomic assignment uncertain - large, siliceous, biscuit-shaped forms, possibly related to *Saccammina* or may not be foraminifera Bivalvia (Pelecypoda): presence of *Inoceramus* or similar bivalve indicated by strong occurrence of aragonite prisms Age and Environment: As for previous entries. Assemblage is dominated by *Haplophragmoides* spp.	C-208413

Summary

The object of this investigation was to acquire microfossil data which would either support or question the collector's designation of the Pakowki Formation at various localities in the study area.

The best development of the Pakowki Formation equivalent is in the Coleman section which yielded a substantial arenaceous foraminiferal assemblage similar to that from the higher Wapiabi and transition beds to the Belly River Formation (old terminology) in outcrop sections studied by the author (Wall, 1967) in the Crowsnest Pass-Waterton area. The microfaunal evidence for recognition of the Pakowki equivalent in the Lundbreck-Burmis railway section is not nearly as strong as at Coleman, but the limited foraminiferal recovery, together with the collector's observations of the sedimentological features, support the interpretation of a marine environment.

Triangle zone and foothills structures along and adjacent to the Oldman River, southwestern Alberta[1]

Glen S. Stockmal and Paul A. MacKay[2]
Institute of Sedimentary and Petroleum Geology, Calgary

Stockmal, G.S. and MacKay, P.A., 1994: Triangle zone and foothills structures along and adjacent to the Oldman River, southwestern Alberta; in Current Research 1994-E; Geological Survey of Canada, p. 101-108.

Abstract: New mapping and interpretation of triangle zone and foothills structures along and adjacent to the Oldman River, southwestern Alberta, utilizes proprietary industry seismic reflection data as well as a recently proposed subdivision of the former Belly River Formation. A newly recognized fault is interpreted to form the upper detachment of a triangle zone, above which significant deformation occurs in the form of west-vergent thrusts and kilometre-scale folds. This structural configuration, considerably more complex than often ascribed to triangle zones, may reflect mechanical consequences of increasing dip on the upper detachment or zones of overlap and linkage between propagating thrusts within the hanging wall of the upper detachment. East-vergent thrusts west of the upper detachment are seen on the seismic data to flatten abruptly with depth, within 3 to 5 km of the surface, a geometry nowhere suggested by steep surface dips.

Résumé : Dans le sud-ouest de l'Alberta, une nouvelle cartographie et une réinterprétation d'une zone triangulaire et de structures de contreforts, le long de la rivière Oldman et en position adjacente par rapport à celle-ci, fait appel à des données de sismique réflexion (propriétés de l'industrie) ainsi qu'à une subdivision récemment proposée de l'ancienne Formation de Belly River. On interprète qu'une faille nouvellement reconnue forme le décollement supérieur d'une zone triangulaire, au-dessus de laquelle une importante déformation s'observe (chevauchements à vergence ouest et plis à l'échelle du kilomètre). Cette configuration structurale, considérablement plus complexe que celle qu'on attribue souvent aux zones triangulaires, peut traduire les effets mécaniques d'un pendage de plus en plus prononcé sur le décollement supérieur ou encore l'existence de zones de recouvrement et de liens entre les chevauchements en progression dans le mur du décollement supérieur. Les données sismiques font apparaître que les chevauchements à l'ouest du décollement supérieur (qui convergent vers l'est) s'affaissent de façon abrupte avec la profondeur, à moins de 3 ou 5 km de la surface; cette géométrie n'est nulle part suggérée, de forts pendages étant observés en surface.

[1] Contribution to the NATMAP Southeastern Cordillera project
[2] Morrison Petroleums Limited, Suite 2900, 400-3rd Avenue S.W., Calgary, Alberta T2P 4H2

INTRODUCTION

The structural geology along and adjacent to the Oldman River, southwestern Alberta, was described and mapped by Douglas (1950, 1:63 360 scale), whose foothills studies are exemplary of careful, detailed fieldwork. Existing GSC maps of the southern Alberta foothills are now quite dated however, having stemmed from field mapping conducted primarily in the 1940s and 1950s. Knowledge of Upper Cretaceous and Tertiary stratigraphy has advanced (e.g., Jerzykiewicz, 1994, in press), and the proprietary seismic data bases of petroleum exploration companies have vastly expanded with significant improvements in acquisition and processing techniques. These factors have lead to the initiation of a new NATMAP program to remap the southern Alberta foothills at 1:50 000 scale from the international border to just south of Calgary (Fig. 1; see Lebel, 1994).

Exposures of triangle zone and associated foothills structures along and adjacent to the Oldman River occur in the east half of the Maycroft map sheet (82G/16), in the middle of the Southern Alberta NATMAP Program field area (Fig. 1). This eastern half-sheet was called Callum Creek (GSC Map 982A) in Douglas (1950); the western half-sheet is well known as Gap (GSC Map 978A). Preliminary field mapping, co-ordinated through the NATMAP program, was undertaken by the GSC (G.S. Stockmal) in the summer and fall of 1993. It indicated that previously published interpretations of the structural framework underlying the triangle zone and eastern foothills at this latitude required re-evaluation. Proprietary seismic reflection data, in the form of a detailed line drawing of depth-migrated reflections[1], not only corroborated the field observations, but provided a unique view of structural details at depth (Stockmal and MacKay, 1994).

Structures exposed at the surface and imaged in the seismic data clearly show that the triangle zone is a highly complex feature exhibiting substantial deformation above the west-vergent upper detachment. Preliminary interpretation of structures along strike to the north indicates similar complexity between Oldman River and the Turner Valley area (see MacKay, 1991), probably involving overlap zones between thrusts linked within the triangle zone.

STRATIGRAPHY

Within the portion of the Maycroft map sheet examined in 1993, only Upper Cretaceous (post-Cenomanian) and Tertiary rocks are exposed. The Belly River Formation (now elevated to group status) and the uppermost Wapiabi Formation have been subdivided according to Jerzykiewicz and Norris (1993, in press) and Jerzykiewicz (1994, in press; also see Lebel, 1994). In this new subdivision, the upper Alberta Group comprises the Wapiabi, Lees Lake, Burmis, and Pakowki formations, and the overlying Belly River Group comprises the Connelly Creek, Lundbreck, and Drywood Creek formations (Fig. 2). Previously, the Belly River "Formation" had been mapped by Douglas (1950) to include what are now defined as the Lees Lake through Drywood Creek formations (Fig. 2). Overlying the Belly River Group are, in ascending order, the Bearpaw, St. Mary River, Willow Creek, and Porcupine Hills formations (Fig. 2).

The latest Turonian to latest Santonian Wapiabi Formation (Stott, 1963) is composed of thin bedded, dark grey, marine shale, and minor thin bedded, fine grained sandstone and dark grey limestone and concretions. Its thickness is poorly constrained, mainly because exposures are almost always faulted and folded. Douglas (1950) suggested a local thickness of about 330 m, based on an early exploration well in the Langford Creek map area (immediately to the north). For this study, a nominal value of 330 m, increasing modestly to 350 m in the west, was used.

The latest Santonian to Campanian(?) Lees Lake Formation is a coarsening- and thickening-upward succession of interstratified, generally dark grey, marine mudstone, siltstone, and fine grained sandstone, in transitional contact with the Wapiabi Formation. Sedimentary structures in the lower

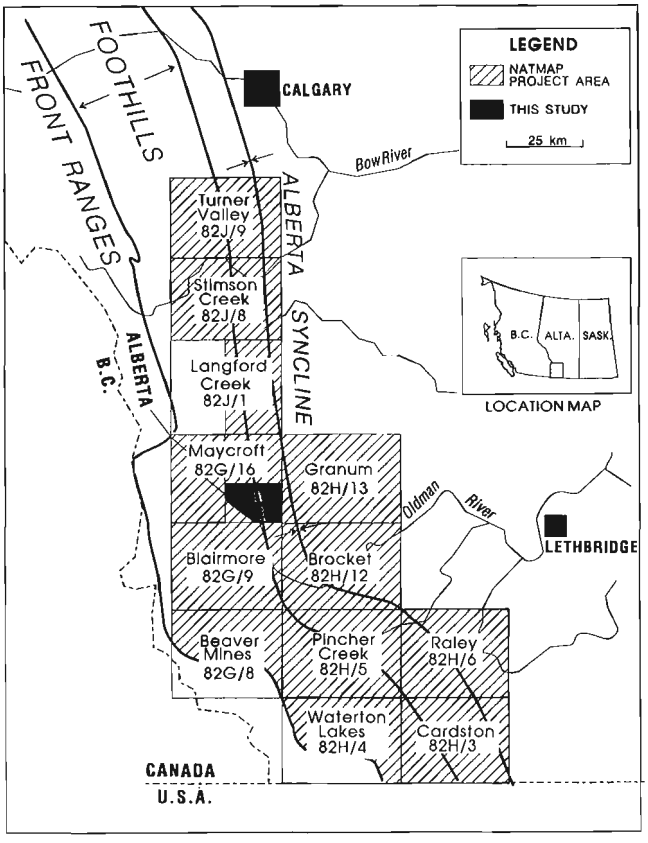

Figure 1. *Location map of southern Alberta, showing locations of 1:50 000 scale map sheets encompassed by the Southern Alberta NATMAP program, and the location of this study (see Fig. 3). Modified after Lebel (1994).*

[1] Amoco Canada Petroleum Company Limited has kindly permitted the use of proprietary seismic data for the production of this paper.

portion are typical of tempestites (Jerzykiewicz, in press), whereas hummocky cross-stratification is observed in the upper portion. The Lees Lake Formation is generally recessive.

The Campanian Burmis Formation is generally coarser (fine- to medium-grained sandstone) and substantially better sorted than the Lees Lake Formation, which it overlies abruptly. Stratification within the Burmis Formation characteristically varies from swaley cross-stratification in the lower portion, to herringbone cross-stratification passing upward into trough crossbedding in the upper portion. When present, magnetite-bearing sandstone is diagnostic. The unit is a persistent cliff and ridge former.

The outcrop of thin (<10 m), recessive, dark greenish grey marine shale and siltstone of the Pakowki Formation, immediately overlying the Burmis Formation, in the Maycroft area, is similar to that in the Blairmore (east half) sheet to the south (Jerzykiewicz, 1994). For preliminary mapping purposes, the Pakowki, Burmis, and Lees Lake formations were grouped in a single unit; combined thickness is about 150 m in the hanging wall of the Chimney Rock Fault (Fig. 3).

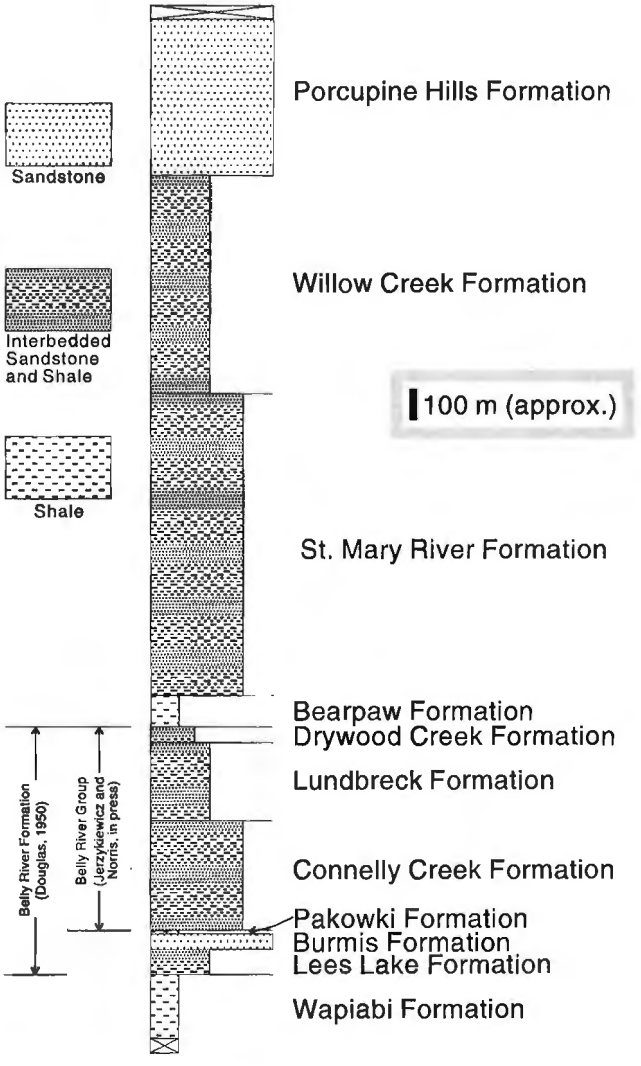

Figure 2. *Schematic stratigraphic column corresponding to the mapped portion of Maycroft (east half) (Fig. 3). Thicknesses are approximate. Those units encompassed by the new definition (Jerzykiewicz and Norris, 1993, in press) of the Belly River Group and those encompassed by the usage of Douglas (1950) are indicated.*

The dominantly fluvial Connelly Creek Formation consists of fine- to medium-grained, often channelized sandstone interstratified with siltstone and mudstone on the scale of a few to ten or more metres. Fragments of wood, coal, and freshwater bivalves are common. The dark to greenish grey (olive) colour of the fine grained components contrasts markedly with the lighter and brighter yellowish green colour of the overlying Lundbreck Formation. The Connelly Creek Formation is relatively resistant, and underlies many of the prominent ridges in the area. Its thickness is about 430 m in the hanging wall of the Chimney Rock Fault (Fig. 3).

The Lundbreck Formation is characterized by concretions and limestone layers of pedogenic origin (caliche) within greyish green to yellowish green mudstone and siltstone. Fining-upward, medium- to coarse-grained sandstone layers, generally a few metres thick with sharp bases, are embedded within the caliche-bearing mudstone and siltstone. The depositional environment is envisaged as a semi-arid distal alluvial fan with ephemeral channels and intermittent playa lakes (Jerzykiewicz, in press). The Lundbreck Formation is generally recessive.

The overlying Drywood Creek Formation, as exposed along the Oldman River, contains significantly less organic-rich, carbonaceous material than that at the type section along Drywood Creek, about 60 km to the southeast (Jerzykiewicz and Norris, in press; Jerzykiewicz, in press). The transitional contact with the underlying Lundbreck Formation occurs where caliche concretions and limestone give way to redeposited freshwater to brackish water bivalve shells, and the sand/shale ratio decreases. Due to their generally recessive nature and the scale of the map for this preliminary report, the Lundbreck and Drywood Creek formations are shown as a single mapped unit; they will be separated in the future wherever possible. Their combined thickness in the hanging wall of the Whaleback Fault (Fig. 3) is about 360 m.

The total thickness of Lees Lake Formation through Drywood Creek Formation strata appears to vary considerably across the map area. The total thickness in the 6-30-8-1-W5 well is given by Jerzykiewicz and Norris (1993) as 640 m. To the west, this appears to increase to about 950 m, although minor thickening by small faults may occur.

The Campanian Bearpaw Formation consists predominantly of rubbly, dark grey, marine shale, interbedded with minor thin, fine- to very-fine grained sandstone beds. A few isolated resistant sandstones, up to 5 m thick, occur within the mapped interval of Bearpaw strata. Contacts with the underlying Drywood Creek Formation and the overlying St. Mary River Formation are faulted, although displacement between the Bearpaw and St. Mary River formations may be as little as a few tens of metres, as suggested by the preservation of the marine to nonmarine transition between them. The thickness of the Bearpaw Formation, in an equivalent structural position near Crowsnest River to the south, is about 100 m or

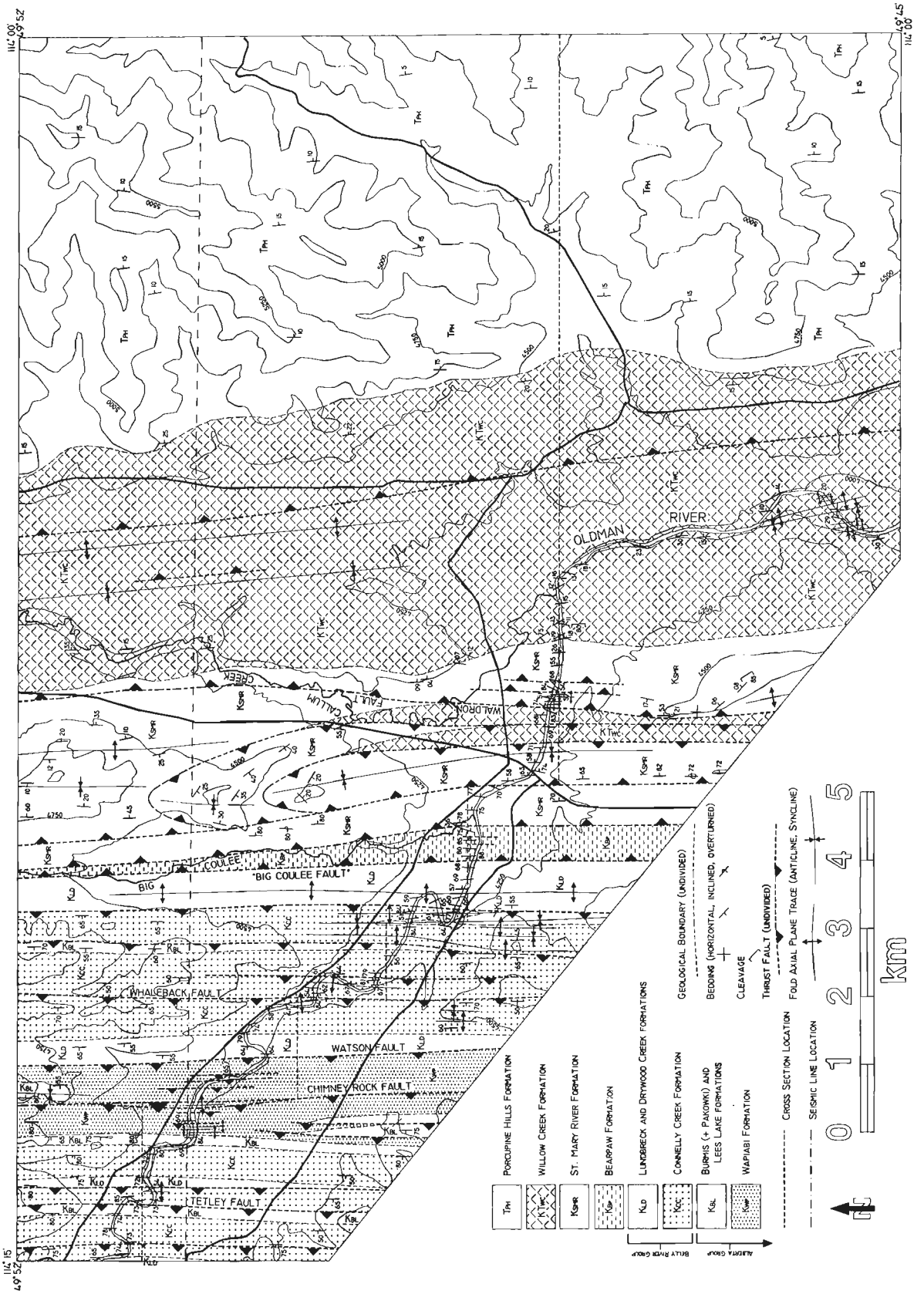

Figure 3. *Geological map of a portion of Maycroft (east half), 82G/16.*

less (Jerzykiewicz and Norris, 1993). The apparent thickness along the Oldman River, however, is substantially greater (Fig. 3), probably due to tight folding and faulting associated with displacement on the "Big Coulee Fault" (see below).

The Campanian to earliest Maastrichtian St. Mary River Formation is relatively resistant, and well-exposed along the Oldman River. It consists of fine grained, hard to soft, grey to greenish grey sandstone interbedded with grey to greenish grey mudstone with occasional thin lacustrine limestone ("ironstone" of Douglas, 1950). The sandstone/shale ratio is about 1:1, similar to that in the Connelly Creek Formation. However, the St. Mary River Formation is generally finer grained, more finely interbedded, and lacks the characteristic olive green colour of the Connelly Creek Formation. Total thickness measured by Douglas (1950), using a lithological correlation between two structurally separated segments of outcrop, was 970 m; this value was used in this study (Fig. 4). Jerzykiewicz and Norris (1993) report a thickness of about 900 m in the 3-25-10-29-W4 well to the east.

The contact between the St. Mary River and Willow Creek formations is placed at the base of the first soft, massive, grey sandstone typical of the recessive Willow Creek Formation (Douglas, 1950). The sandstones of the St. Mary River Formation, although similar, are generally less quartzose, darker weathering, and harder. The predominant lithologies of the Maastrichtian to early Paleocene Willow Creek Formation are recessive green, red, pink, and grey mudstones, often bearing caliche nodules. Jerzykiewicz and Norris (1993) report a thickness of about 625 m in the 3-25-10-29-W4 well to the east. A nominal thickness of 700 m was used in the cross-section (Fig. 4), consistent with outcrop positions of the thick basal sandstone of the Porcupine Hills Formation.

The resistant sandstones of the Paleocene Porcupine Hills Formation underlie the topographically high Porcupine Hills along the eastern third of the mapped area (Fig. 3). The formation consists of fine- to coarse-grained massive to cross-bedded sandstone interbedded with massive, rubbly shale. The base of the formation is marked by a coarse grained, commonly conglomeratic sandstone, which may unconformably overlie the Willow Creek Formation (Douglas, 1950). Maximum preserved thickness probably exceeds one kilometre.

Thicknesses of units appearing in the cross-section (Fig. 4) but not at the surface, and their sources, are as follows. The nominal thickness for the cross-section representation of the Upper Cretaceous Cardium Formation is 50 m (Norris, 1993a, b). The Upper Cretaceous Blackstone Formation is 200 to 220 m thick (Douglas, 1950; Norris, 1993a, b). Total thickness of the Wapiabi, Cardium, and Blackstone formations in the 6-30-8-1-W5 well is 637 m, according to the Energy Resources Conservation Board (ERCB) log (probably slightly thickened tectonically). The Lower Cretaceous Blairmore Group is 480 to 500 m thick (6-30-8-1-W5 and 8-36-11-2-W5 wells, ERCB logs; Norris, 1993a, b). And the Jurassic-Cretaceous Kootenay Group plus the Jurassic Fernie Formation are 150 to 300 m thick (8-36-11-2-W5 and 6-30-8-1-W5 wells, ERCB logs; Norris, 1993a, b).

STRUCTURAL GEOLOGY FROM MAPPING AND SEISMIC INTERPRETATION

Preliminary mapping undertaken in 1993 was concentrated along and adjacent to the Oldman River. Figure 3 incorporates these new observations, interpretation of aerial photographs (1:20 000 scale), and compilation of selected observations from Douglas (1950).

Mapping demonstrated the viability and usefulness of the stratigraphic subdivision of the upper Alberta Group and the Belly River Group (Fig. 2), proposed by Jerzykiewicz and Norris (1993, in press) and Jerzykiewicz (in press), north of the Crowsnest Pass area. It also indicated the existence of the "Big Coulee Fault" (Fig. 3), a west-verging fault interpreted to form the upper detachment of a foreland propagating tectonic wedge. The geological basis for this interpretation is two-fold. First, there appears to be relatively little offset (perhaps a few hundred metres) along the Waldron Fault (Fig. 3), which was previously considered the primary candidate for the upper detachment (cf. Price, 1981, 1986; see "Discussion" below). Second, the sense of vergence of minor structures, as discussed and used by MacKay (1991) in his analysis of the triangle zone at Turner Valley, switches from predominantly eastward vergence west of the Bearpaw Formation exposures to predominantly westward vergence to the east.

The offset on the Waldron Fault estimated by Douglas (1950, his structure section C-D) is less than 300 m, and is constrained by the attitudes and interpreted stratigraphic levels of the St. Mary River and Willow Creek formations in its hanging wall and footwall, respectively. A number of small (<20 m wavelength), west-vergent folds occur within the St. Mary River Formation between the Waldron Fault and the second west-vergent thrust splay to the east (Fig. 3, 4). These folds and splay faults collectively outline an antiformal shape which suggests, from cross-section construction (Fig. 4), that the stratigraphic level of the St. Mary River Formation in the immediate hanging wall of the Waldron Fault is only a few hundred metres or less below the contact with the Willow Creek Formation. The steeply west-dipping Willow Creek strata in the immediate footwall are characteristic of the lower portion of the formation, and the soft massive sandstone considered to define the base of the Willow Creek Formation may be present. Total displacement on the Waldron Fault and associated hanging wall splays may be on the order of 1 km (Fig. 4).

MacKay (1991) demonstrated that the upper detachment of the triangle zone at Turner Valley forms a structural domain boundary with respect to the sense of vergence of structures above and below the detachment. There, the dominant sense of vergence in the footwall of the upper detachment is to the east (foreland-directed), whereas in the hanging wall it is to the west (orogen-directed). A similar general pattern is observed along the Oldman River, where the vergence domain boundary coincides with the mapped belt of Bearpaw Formation strata and the interpreted trace of the "Big Coulee Fault" (Fig. 3).

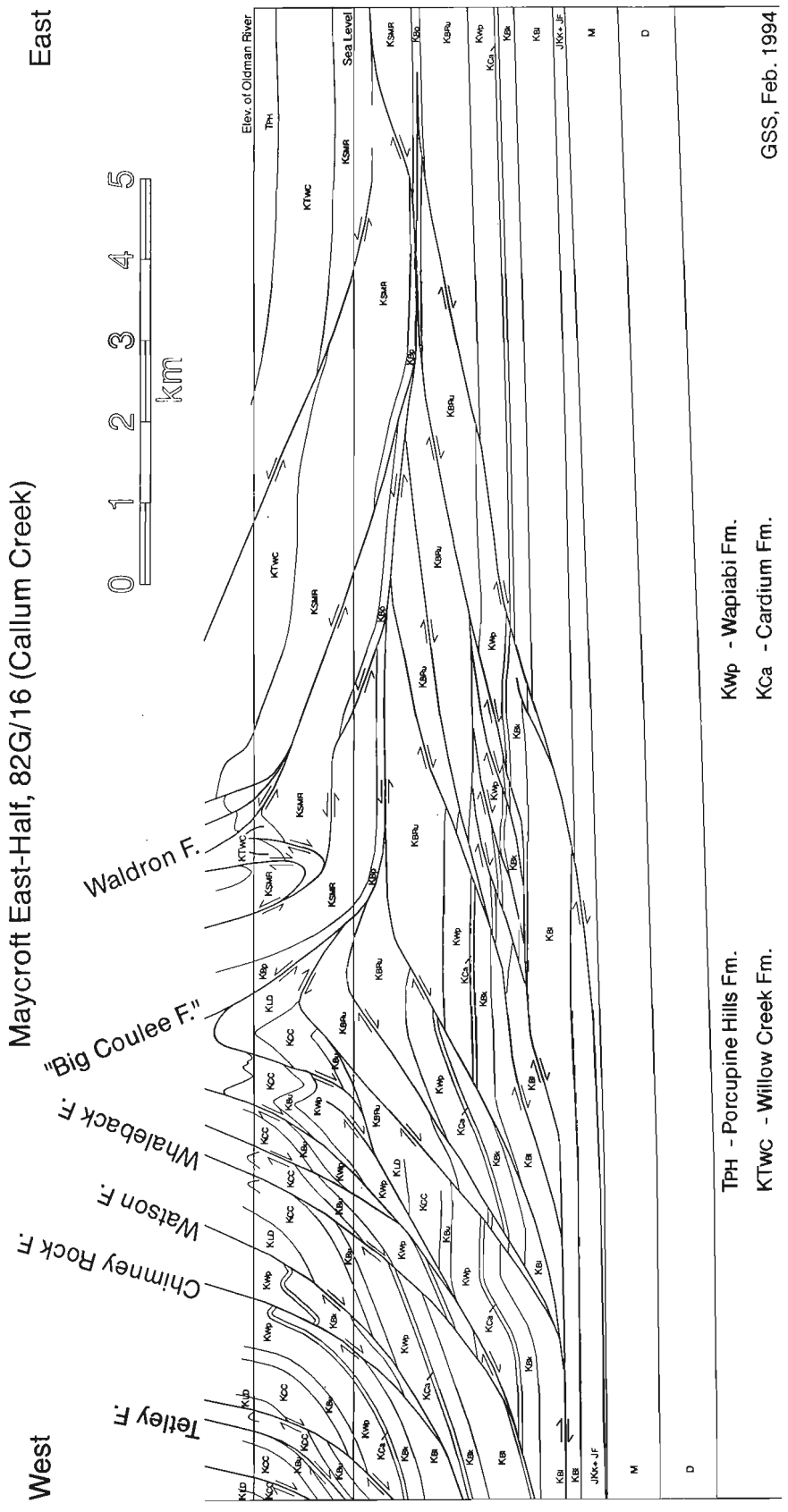

Figure 4. *Preliminary geological cross-section along and adjacent to the Oldman River, based on new mapping and interpretation of proprietary seismic data. Locations of cross-section and seismic line indicated in Figure 3.*

This simple vergence pattern is disrupted by two east-vergent thrusts, the traces of which cross the Oldman River between the trace of the Waldron Fault and the bridge over the river (Fig. 3). However, these are interpreted to be out-of-syncline faults, originating from a south-plunging syncline in the St. Mary River Formation (Fig. 3). In cross-section (Fig. 4), the St. Mary River/Willow Creek contact is seen to trace out a large west-vergent anticline-syncline fold pair, cut by a number of small-displacement thrusts which include the Waldron Fault. The near-surface portion of the cross-section (Fig. 4) is quite similar to that of Douglas (1950, his structure section C-D) who named the anticline the Waldron Anticline.

West of the belt of Bearpaw Formation strata, new mapping using the stratigraphic subdivision discussed above significantly enhanced the map scale representation of east-vergent fault repetitions within the upper Alberta Group and the Belly River Group (Fig. 3, compare with Douglas, 1950). Without the aid of seismic data, however, their extrapolation to depth (Fig. 4) is conjectural.

The location of the seismic line (see MacKay et al., 1994, p. 25) used to construct the cross-section (Fig. 4), and the location of the cross-section, are shown on Figure 3. The line of cross-section is segmented, to minimize projection distances from exposures along the Oldman River.

Seismic data quality is exceptional, clearly showing the change in overall structural vergence, and indicates that the interpreted "Big Coulee Fault" forms the upper detachment of the triangle zone in the vicinity of Oldman River. The interpretation of the two faults immediately west of the Waldron Fault (Fig. 3, 4) as out-of-syncline features is supported by the seismic data in that east-vergent thrusts are not observed to offset the upper detachment or the panel of St. Mary River strata. Thrusts confined to the Mesozoic section are seen to flatten rapidly to subhorizontal attitudes within 3 to 5 km of the surface, a configuration nowhere suggested by the nearly ubiquitous 60° and greater surface dips. Note that subdivision of the upper Alberta Group and the Belly River Group is shown in Figure 4 wherever thrust sheets are contiguous with mapped exposures; elsewhere it is shown as "Belly River (undivided)".

DISCUSSION

The triangle zone structure portrayed in Figure 4 is significantly more complex than that interpreted for some triangle zones elsewhere (e.g., Teal, 1983; Banks and Warburton, 1986), although other workers have noted multiple orogen-vergent thrusts associated with the triangle zone (e.g., Jones, 1982; MacKay, 1991). Clearly, the description of such a structure as a "passive roof duplex" is not applicable in this case, since substantial orogen-vergent deformation, in the form of kilometre-scale folds and associated faults, occurs above the upper detachment. These west-vergent thrusts could have formed in response to the progressive steepening of the "Big Coulee Fault", or they may represent a kinematic process involving overlap zones and linkage between thrusts associated with the upper detachment. In either case, had deformation continued, one of them could have later developed into a newer, more easterly upper detachment.

The cross-section (Fig. 4) across the triangle zone differs in a number of ways from that of Price (1981, 1986), which was constructed at the southern edge of the map sheet along 49°45′N. Figure 4 is in agreement with Douglas (1950) in that the Waldron Fault has limited displacement (<1 km), whereas Price (1981, 1986) interpreted about 5 km of total displacement, to accommodate its role as the upper detachment of the triangle zone. Furthermore, the partial palinspastic restoration of Price's (1981, 1986) section apparently implies that prior to initiation of displacement along the Waldron Fault, a triangle zone did not exist at this latitude. However, removal of all displacement on the "Big Coulee Fault" (Fig. 4) does not preclude the existence of the triangle zone prior to development of the "Big Coulee Fault". No clear test is available to determine whether or not the triangle zone was a nearly ubiquitous feature of the leading edge of the thrust and fold belt in time as well as in space. However, multiple west-vergent thrusts above the upper detachment favour the triangle zone being sustained and modified in a nearly continuous fashion for a substantial period of time.

The west-verging "Big Coulee Fault" may be interpreted northward to Langford Creek (MacKay et al., 1994). At this location a large south-plunging fold representing the southern termination of the Highwood Structure dominates the structural style. A new upper detachment is developed to the east that outcrops along the east flank of the Highwood Structure (MacKay and Theriault, 1994). It is unclear whether this fault (the "Chain Lakes Fault") is a continuation of the "Big Coulee Fault" or the two faults acted to jointly accommodate consistent shortening along the deformation front.

Future NATMAP related fieldwork in the area and access to additional proprietary seismic data should give insight into the relationship between the triangle zone developed along the Oldman River and that to the north associated with the Highwood Structure. Tracing the nature of the triangle zone to the south should prove especially interesting, in that there appears to be little expression of the zone at the surface in the Cardston area (Lebel, 1994; Fig. 1).

ACKNOWLEDGMENTS

G.S. Stockmal thanks Tom Jerzykiewicz for his patient assistance with Upper Cretaceous and Tertiary stratigraphy, Daniel Lebel for discussions in and out of the field, and Andrew Harries for assistance during fieldwork. P.A. MacKay thanks Robert Brady for assistance in the field. We both thank Amoco Canada Petroleum Company Limited for making proprietary seismic data available for this study, and Tom Jerzykiewicz, Margot McMechan, and Daniel Lebel for helpful reviews.

REFERENCES

Banks, C.J. and Warburton, J.
1986: "Passive-roof" duplex geometry in the frontal structures of the Kirthar and Sulaiman mountain belts, Pakistan; Journal of Structural Geology, v. 8, p. 229-237.

Douglas, R.J.W.
1950: Callum Creek, Langford Creek, and Gap map-areas, Alberta; Geological Survey of Canada, Memoir 255, 124 p.

Jerzykiewicz, T.
1994: Significance of the Pakowki Formation to mapping in the deformed belt of the southern Canadian Cordillera, Alberta; in Current Research 1994-E; Geological Survey of Canada.
in press: Stratigraphic framework of the uppermost Cretaceous to Paleocene strata of the Alberta basin; Geological Survey of Canada, Bulletin.

Jerzykiewicz, T. and Norris, D.K.
1993: Evolution of the Laramide foredeep and adjacent thrust belt in southern Alberta; Geological Survey of Canada, Open File 2663, 96 p.
in press: Stratigraphy, structure and syntectonic sedimentation of the Campanian "Belly River" clastic wedge in the southern Canadian Cordillera; Cretaceous Research.

Jones, P.B.
1982: Oil and gas beneath east-dipping underthrust faults in the Alberta foothills; in Geological Studies in the Cordilleran Thrust Belt, (ed.) R.B. Powers; Rocky Mountain Association of Geologists, v. 1, p. 61-74.

Lebel, D.
1994: Regional geology of the Cardston map area, Alberta; in Current Research 1994-A; Geological Survey of Canada, p. 231-236.

MacKay, P.A.
1991: A geometric, kinematic and dynamic analysis of the structural geology at Turner Valley, Alberta; Ph.D. thesis, University of Calgary, Calgary, Alberta, 138 p.

MacKay, P.A. and Theriault, J.T.
1994: The triangle zone at Willow Creek, a re-interpretation of the Highwood Structure in the Chain Lakes area of the Southern Alberta Foothills in Program, Expanded Abstracts and Biographies; Canadian Society of Exploration Geophysicists/ Canadian Society of Petroleum Geologists, 1994 Joint National Convention, Calgary, Alberta, p. 76.

MacKay, P.A., Spratt, D.A., Soule, G., and Lawton, D.C.
1994: The triangle zone of southern Alberta - geometry, lateral variations and associated oil and gas fields; Field-Trip Guidebook, (PR-2), Canadian Society of Exploration Geophysicists/Canadian Society of Petroleum Geologists, 1994 Joint National Convention, Calgary, Alberta, 105 p.

Norris, D.K.
1993a: Geology and structure cross-sections, Blairmore (West Half), Alberta; Geological Survey of Canada, Map 1829A, scale 1:50 000.
1993b: Geology and structure cross-sections, Langford Creek (West Half), Alberta; Geological Survey of Canada, Map 1837A, scale 1:50 000.

Price, R.A.
1981: The Cordilleran foreland thrust and fold belt in the southern Canadian Rocky Mountains; in Thrust and Nappe Tectonics, (ed.) N.J. Price and K.R. McClay; Geological Society of London, Special Publication No. 9, p. 427-448.
1986: The southeastern Canadian Cordillera: thrust faulting, tectonic wedging, and delamination of the lithosphere; Journal of Structural Geology, v. 8, p. 239-254.

Stockmal, G.S. and MacKay, P.A.
1994: The triangle zone and foothills structures adjacent to Oldman River, southern Alberta: a reappraisal based on seismic data and new structural and stratigraphic observations in Program, Expanded Abstracts and Biographies; Canadian Society of Exploration Geophysicists/Canadian Society of Petroleum Geologists, 1994 Joint National Convention, Calgary, Alberta, p. 74.

Stott, D.F.
1963: The Cretaceous Alberta Group and equivalent rocks, Rocky Mountain Foothills, Alberta; Geological Survey of Canada, Memoir 317, 306 p.

Teal, P.R.
1983: The triangle zone at Cabin Creek, Alberta; in Seismic Expression of Structural Styles, (ed.) A.W. Bally; American Association of Petroleum Geologists, Studies in Geology No. 15, v. 3, p. 3.4.1-48 - 3.4.1-53.

Geological Survey of Canada Project 930012

Seismic definition of the triangle zone east of Maycroft, Alberta[1]

Don C. Lawton[2], Glen S. Stockmal, and Deborah A. Spratt[2]
Institute of Sedimentary and Petroleum Geology, Calgary

Lawton, D.C., Stockmal, G.S., and Spratt, D.A., 1994: Seismic definition of the triangle zone east of Maycroft, Alberta; in Current Research 1994-E; Geological Survey of Canada, p. 109-116.

Abstract: Interpreted seismic reflection data from the Oldman River area of the southern Alberta Foothills reveals the progressive eastward advancement of triangle zone deformation into the Alberta Foreland Basin. Seismic data, of mid-1970s vintage, along an east-west transect across the triangle zone were reprocessed in order to enhance images of shallow reflectors and provide linkage between surface and subsurface structural interpretations. Interpretation was assisted by the analysis of velocity anomalies caused by lateral changes in thicknesses of rocks with relatively low seismic velocities. It was found that deep structures are not tightly folded or overturned, and a sequence of successively younger backthrusts developed progressively toward the foreland. Important detachment horizons are within the St. Mary River and Bearpaw formations, and near the base of the Belly River Group. Ramps in the deeper thrusts have developed above normal faults that cut Paleozoic and basement rocks.

Résumé : L'interprétation de données de sismique réflexion sur la région de la rivière Oldman, dans les Foothills de l'Alberta méridionale, révèle le mouvement progressif vers l'est de la zone triangulaire, dans le bassin d'avant-pays de l'Alberta. Des données sismiques, version du milieu des années soixante-dix, le long d'un transect est-ouest à travers la zone triangulaire, a fait l'objet d'un deuxième traitement afin d'améliorer les images des réflecteurs peu profonds de même que d'assurer le lien entre les interprétations des structures de surface et de subsurface. Cette interprétation a bénéficié de l'analyse des anomalies dues à des changements latéraux dans l'épaisseur de roches aux vitesses sismiques relativement faibles. On a constaté que les structures profondes ne sont pas très plissées ou déversées et qu'une séquence de rétrochevauchements à tour de rôle plus jeunes s'est développée de façon progressive vers l'avant-pays. D'importants horizons de décollement s'observent dans les formations de St. Mary River et de Bearpaw, ainsi qu'à proximité de la base du Groupe de Belly River. Des rampes dans les chevauchements plus profonds se sont formées au-dessus des failles normales qui recoupent les roches du Paléozoïque et le substratum rocheux.

[1] Contribution to the NATMAP Southeastern Cordillera project
[2] Department of Geology and Geophysics, University of Calgary, Calgary, Alberta T2N 1N4

INTRODUCTION

In recent years, the interpretation of seismic reflection data has provided new insights into structural relationships within the triangle zone along the eastern margin of the Rocky Mountain fold and thrust belt (e.g., Jones, 1982; Teal, 1983; MacKay, 1991; Skuce et al., 1992; Slotboom, 1992; Sukaramongkol, 1993; Spratt et al., 1993; Stockmal and MacKay, 1994; Lawton et al., in press). Along most of the triangle zone in Alberta, only Upper Cretaceous and Tertiary rocks are exposed at the surface; subsurface data are required to delineate the geometry of the triangle zone at depth. Also, structures within the eastern flank of the triangle zone often have no expression at the present erosional surface and their existence has been detected only from seismic images (Lawton et al., in press). Seismic data have been critical for mapping trajectories of blind thrusts and significant backthrusts in the subsurface of the foreland basin.

As part of the NATMAP program in the Maycroft area of southwestern Alberta (for location, see Figure 1 of Stockmal and MacKay, 1994), seismic data were incorporated to assist in mapping and in the construction of a cross-section through the triangle zone in this region. Proprietary seismic data were available in the northern part of the study area and the interpretation of these data is described by Stockmal and MacKay (1994). However, it was necessary to obtain additional seismic data close to the Oldman River to facilitate a more direct linkage between surface and subsurface structural interpretations. Costs for acquiring and processing new seismic data were found to be prohibitive and an approach was made to the petroleum industry to gain access to existing data from the area. This investigation resulted in over 100 km of data being made available to the project, including copies of original field data and observers' logs from lines in key locations. This paper describes the processing and interpretation of data from a sinuous east-west line across the triangle zone near the Oldman River. The location of the line (Line O-1) is shown in Figure 1.

GEOLOGY AND REGIONAL REFLECTION SEISMIC SIGNATURE

The stratigraphy of Upper Cretaceous and Tertiary rocks that outcrop along the Oldman River in the study area, based on new subdivisions proposed by Jerzykiewicz and Norris (1993) and Jerzykiewicz (1994, in press), is described elsewhere in this volume (Stockmal and MacKay, 1994). These rocks include sandstones and shales of both marine and nonmarine origin, as well as coals that occur in the lower part of the St. Mary River Formation. Subdivisions of Lower Cretaceous and older rocks are based on mapping by Douglas (1950). A geological map of the area, based on the work of Stockmal and MacKay (1994), is presented in Figure 1.

Structure sections in the area were first drawn by Douglas (1950) and showed steeply west-dipping thrust faults (Willow Creek and Bridge faults) emerging from an asymmetric, east-facing anticline (Whaleback), juxtaposed against a west-facing anticline (Waldron) breached by the steeply east-dipping Waldron Fault. Price (1981, 1986) interpreted the Waldron Fault as a backthrust rising out of a bedding-parallel detachment in the Bearpaw Formation and cutting up-section to the west through strata of the St. Mary River and Willow Creek formations.

Figure 2 shows correlations between major stratigraphic units and key seismic markers in the area. Major picks in Mesozoic rocks identified in Figure 2 are the tops of the St. Mary River Formation (KSMR), Bearpaw Formation (KBp), Belly River Group (undifferentiated; KBRu), and Wapiabi Formation (KWp). The top of the Mississippian (M) is also identified. Other Lower Cretaceous formations were not identified because these rocks are not involved significantly in deformation associated with the eastern part of the triangle zone in this area.

A synthetic seismogram was computed using sonic and density logs from well 3-25-10-29W4, located about 6 km east of seismic line O-1 (Fig. 1). This well reached a depth of over 4000 m and penetrated rocks of Devonian age at its bottom. The synthetic seismogram (Fig. 2) has close ties with a portion of processed seismic data from a profile about 1.5 km from the location of the well, and this correlation enabled seismic events to be positively identified in the data that were reprocessed for this study. The character of both the sonic and density logs from well 3-25-10-29W4 clearly shows the variation in stratigraphy of the formations intersected, with generally high sonic velocities (>3500 m/s) and high densities (>2400 kg/m^3) over intervals of competent sandstones (e.g., upper St. Mary River Formation), and lower sonic velocities (<3500 m/s) and lower densities (<2400 kg/m^3) in shale-dominated intervals (e.g., Bearpaw Formation).

The reflectivity sequence and the synthetic seismogram (Fig. 2) show high-amplitude events associated with coals and interbedded sandstones and shales near the base of the St. Mary River Formation, and low-amplitude events associated with marine shales of the Wapiabi Formation. The top of the Bearpaw Formation is characterized by a high-amplitude peak which proved to be very important for interpreting seismic data. Note, however, that the interval between the KBp and KBRu picks may in fact be occupied by uppermost Belly River Group strata such as the Drywood Creek Formation (Jerzykiewicz and Norris, 1993; Jerzykiewicz, in press), as well as strata of the Bearpaw Formation.

SEISMIC DATA REPROCESSING

Seismic data used in this study were acquired by Sefel Geophysical in 1975 along the line shown in Figure 1. Vibrator sources were used and data were recorded using 48-channel instruments and field parameters that were industry standard at the time; acquisition parameters used are listed in Table 1. During data acquisition, the seismic source was located at the centre of the active spread (split-spread geometry), with a near-trace offset of 253.8 m (825 ft.) and a far-trace offset of 1408.5 m (4620 ft.) to each side of the source position (Table 1). Resolution was limited by the relatively low-bandwidth source sweep (14-56 Hz) and the large group interval (≈50 m) used. However, inspection of the original

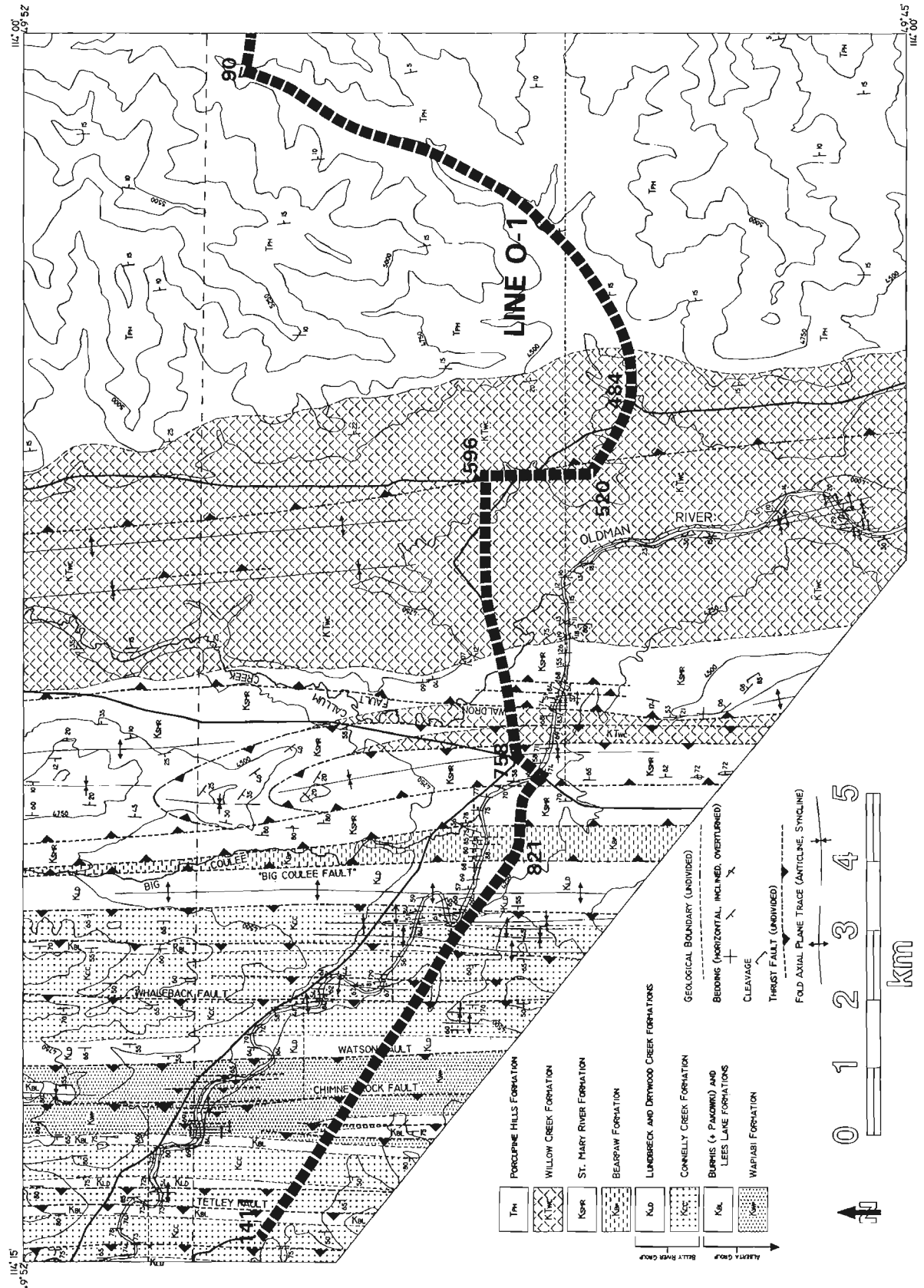

Figure 1. *Geological map of a portion of Maycroft (east half), 82G/16, also showing the location of seismic line O-1 (after Stockmal and MacKay, 1994).*

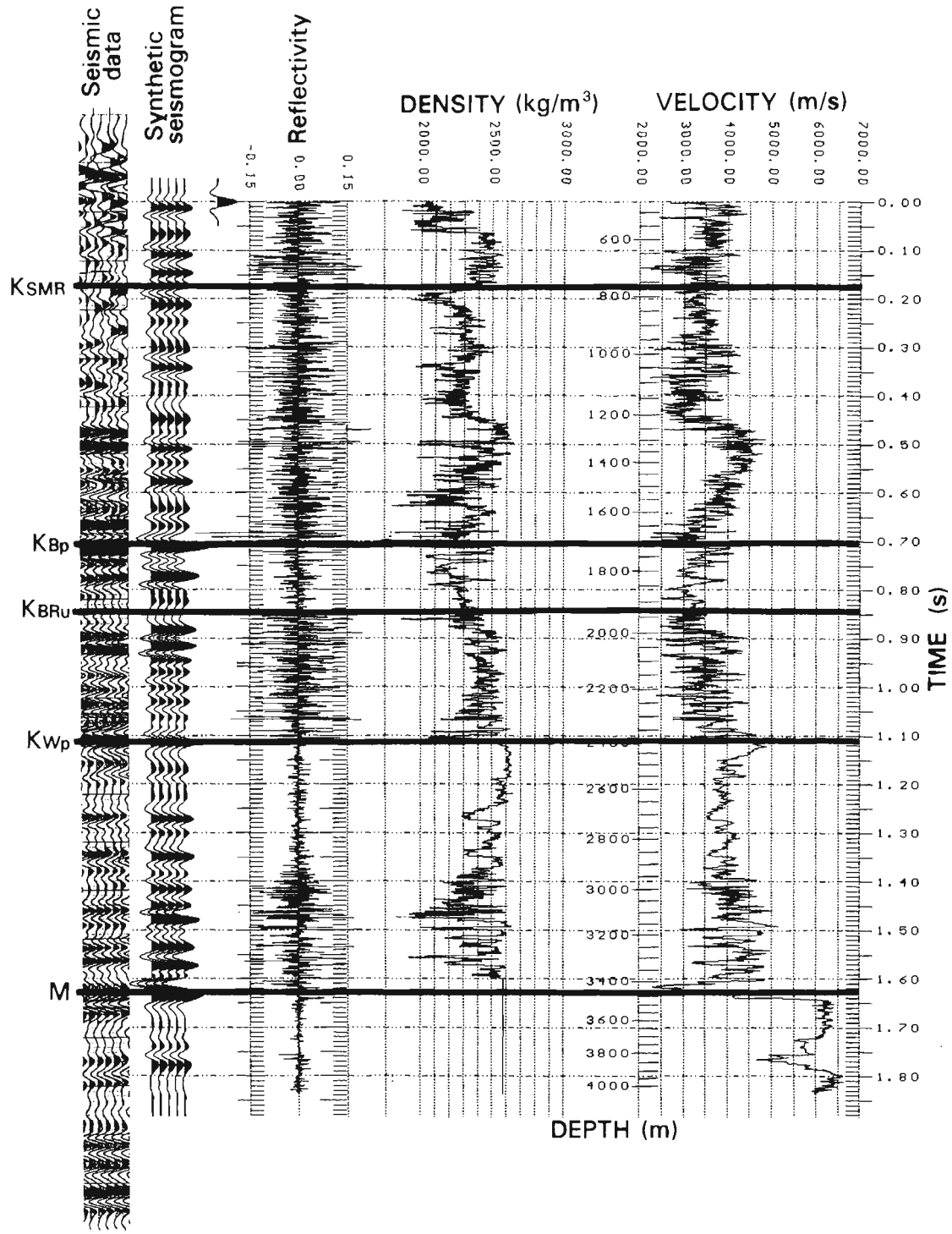

Figure 2. Sonic and density logs from well 3-25-10-29W4, reflectivity sequence, and a synthetic seismogram computed using a 22 Hz Ricker wavelet. Correlation of the synthetic seismogram with seismic data shown on the left hand side of the figure was assisted by the stratigraphic picks indicated. KSMR=St. Mary River Formation; KBp=Bearpaw Formation; KBRu=Belly River Group (undifferentiated); KWp=Wapiabi Formation; M=Mississippian. Picks represent the tops of the stratigraphic units.

Table 1. Seismic Data Acquisition Parameters.

Source parameters	
Source type	Vibroseis™
Source effort	3 vibrators x 16 sweeps
Source interval	330 ft (100.6 m)
Sweep	14 - 56 Hz
Sweep length	9 s
Spread parameters	
Geophone frequency	10 Hz
Group length	10 geophones over 330 ft. (100.6 m)
Group interval	165 ft. (50.3 m)
Spread geometry	4620 - 825 - SP - 825 - 4620 ft. (1408.5 - 253.8 - SP - 253.8 - 1408.5 m)
Coverage	1200 %
Instrument	
Model	SUM-IT 7
Channels	48
Gain	Binary
Sample interval	4 ms
Record length	14 s
Field filter	0 - 62 Hz

seismic sections showed that the signal to noise ratio in data over the triangle zone was quite good and it was expected that the quality of the sections in this area would be improved significantly using modern processing techniques.

Reprocessing of the seismic data was undertaken by Veritas Seismic Ltd. of Calgary, from January to March, 1994. A summary of the processing flow is presented in Table 2. Some initial problems were encountered due to large noise spikes present in the uncorrelated data, but these were removed using a customized despiking filter prior to correlation (Table 2, step 2). The remainder of the processing flow followed a standard sequence, including several iterations of velocity analysis and surface-consistent static corrections. Post-stack time migration tests were undertaken, using a finite-difference method, for a range of migration velocities from 80 to 110 per cent of the stacking velocities determined from velocity analysis. It was found that the optimum migrated section was obtained using migration velocities that were 90 per cent of the stacking velocity values. This is expected since, in areas of dipping reflectors, stacking velocities are always higher than true root-mean-square velocities, which should be used to migrate the data. Coherency of reflections in migrated data was further improved using an *f-x* deconvolution filter, which enhances curvilinear events and discriminates against random noise, followed by a 4-point filter with a passband of 15 to 40 Hz. The final, migrated seismic section from Line O-1 is shown in Figure 3a. Data between common depth points (CDP) 520 and 596 were cut from the display in Figure 3 (note "splice") because this part of the seismic line trended in the strike direction and it was desired that the section represent a dip line as closely as possible.

Table 2. Seismic Processing Flow.

1. Demultiplex uncorrelated data
2. Despike uncorrelated data
3. Correlate data:
   - Processing length: 5 s
   - Sample interval: 4 ms
4. Exponential gain function
5. Crooked line geometry
6. Minimum phase spiking deconvolution:
   - Operator length: 100 ms
   - Prewhitening: 0.1%
7. Structure statics - generalized linear inversion method
   - Final datum elevation: 1700 m
   - Replacement velocity: 4000 m/s
8. Manual trace edits
9. Trace gather - 1200 % subsurface multiplicity
10. Preliminary velocity analysis:
    - Referenced to surface
    - Constant velocity stacks
11. Surface consistent statics - 1st pass
    - Processing window: 800 - 3400 ms
    - Passband: 10/15 - 50/60 Hz
    - Maximum allowable static: ±42 ms
12. Final velocity analysis
13. Normal moveout correction
14. Surface consistent statics - 2nd pass
    - Processing window: 800 - 3400 ms
    - Passband: 10/15 - 50/60 Hz
    - Maximum allowable static: ±32 ms
15. First break mutes
16. CDP trim statics
    - Processing window: 800 - 3400 ms
    - Passband: 10/15 - 50/60 Hz
    - Maximum allowable static: ±12 ms
17. Amplitude equalization:
    - AGC window length: 500 ms
18. Stack (12 fold)
19. Finite difference migration
20. *f-x* noise deconvolution filter
21. Bandpass filter: 10/15 - 40/50 Hz
22. Amplitude equalization:
    - AGC window length: 500 ms

INTERPRETATION

The seismic interpretation (Fig. 3b) shows deformed upper Mesozoic and Tertiary strata underlain by autochthonous Paleozoic rocks. The sections in Figure 3 have been plotted at a 1:1 scale for an assumed average velocity of 3600 m/s, and the marker horizons (Fig. 3b) were identified from the correlations shown in Figure 2. The surface geology mapped by Stockmal and MacKay (1994) was used to constrain the locations of faults and formation boundaries in the shallow part of the interpreted seismic section. Structural complexity

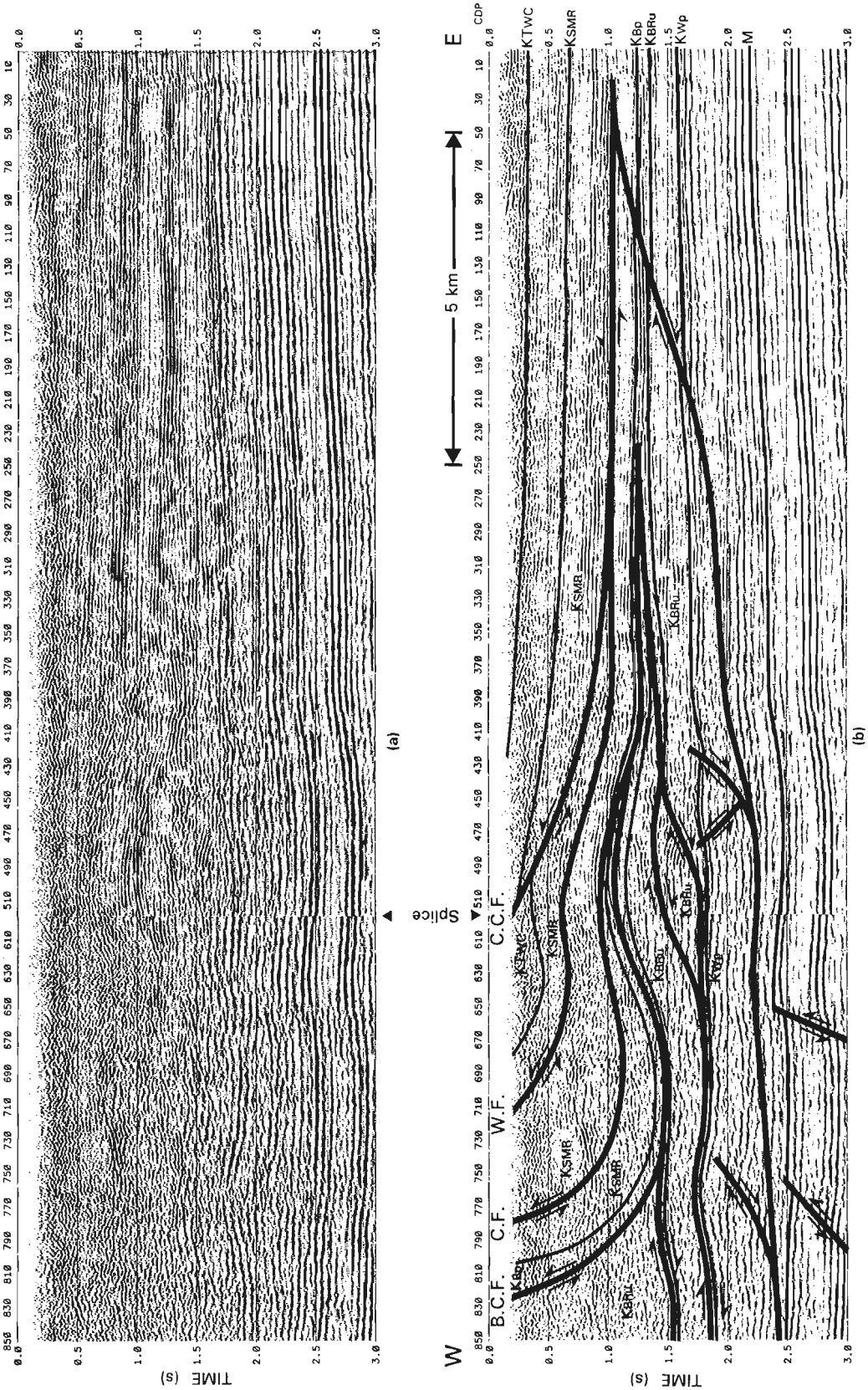

Figure 3. *Seismic section from Line O-1: (**a**) Migrated uninterpreted section; (**b**) Interpreted section. B.C.F.=Big Coulee Fault; C.F.=Co-op Fault; W.F.=Waldron Fault; C.C.F.=Callum Creek Fault.*

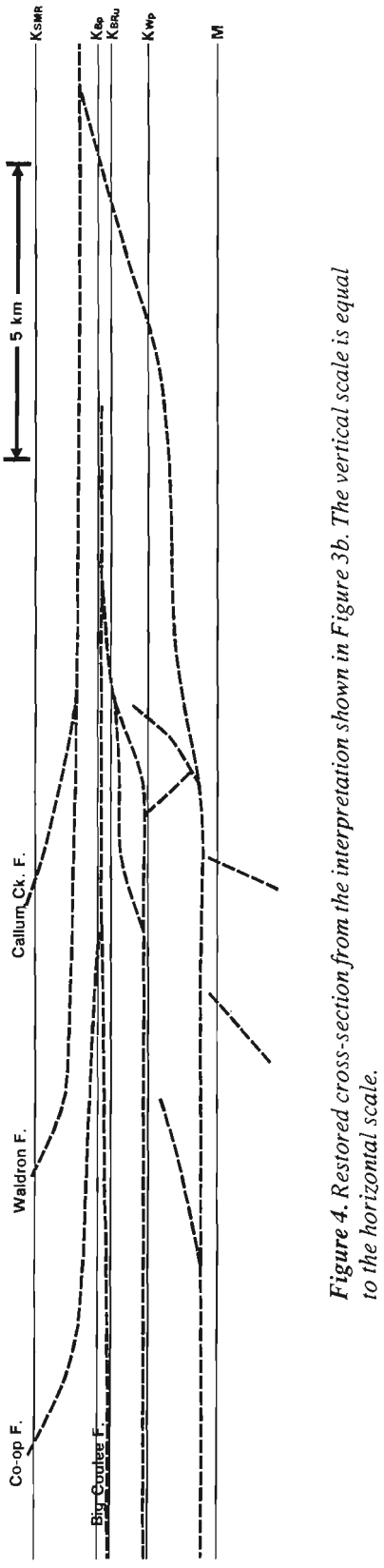

Figure 4. Restored cross-section from the interpretation shown in Figure 3b. The vertical scale is equal to the horizontal scale.

increases from east to west, to the extent that events in the early part of the seismic section essentially become uninterpretable west of about CDP 800.

Reflections from Paleozoic rocks are continuous across the section and show the gentle westward dip of the underlying craton. Short-wavelength undulations (<3 km) in these events are interpreted to be velocity anomalies caused by lateral velocity variations in deformed rocks shallower in the section. However, vertical offsets of nearly 100 ms in Paleozoic events at CDP 665 and CDP 760 are interpreted to be normal faults, downthrown to the west. The throw of each of these faults is calculated to be about 250 m.

The structural style of the interpreted seismic section is similar to that seen elsewhere along the triangle zone of the Rocky Mountain Foothills (MacKay, 1991; Lawton et al., in press). The westward divergence of reflections at the eastern end of the line supports the model of tectonic wedging discussed by Price (1981, 1986). However, our interpretation (Fig. 3b) shows that the Waldron Fault becomes a bedding-parallel detachment within rocks of the St. Mary River Formation, rather than in shales of the Bearpaw Formation, and that it is not the only significant backthrust in the triangle zone at this location. The Big Coulee, Co-op (named herein), and Waldron faults are interpreted to be successively younger backthrusts that developed progressively toward the foreland because each one is folded less than the backthrust in its footwall. They are folded over the horse and pop-up structures between CDP 410 and CDP 660 in such a manner that portions of these faults dip west (Fig. 3b), even though the thrust sheets are entirely west-vergent (Fig. 3b, 4). Another fault, herein named the Callum Creek Fault, outcrops near CDP 520, and is interpreted to be the youngest of the backthrusts because it has not been folded.

Thickening of the Bearpaw Formation is interpreted to be caused by a low-angle ramp in the Big Coulee Fault, which merges with the Co-op Fault at a branch point below CDP 233. The geometry of these thrusts is shown in the restored section (Fig. 4) and it is clear that the Bearpaw Formation is a major detachment horizon followed by the Big Coulee Fault. The blind thrust sheets in its footwall are east-vergent, whereas the Co-op Fault and other structures in its hanging wall are west-vergent. In addition to detachments within the St. Mary River and Bearpaw formations, detachments are interpreted to occur near the base of the Belly River Group and within Lower Cretaceous rocks (Figs. 3b, 4).

The primary differences between our interpretation and those of Douglas (1950) and Price (1981, 1986) are that the deep structures are not tightly folded or overturned, and that the Waldron thrust sheet is not the only west-vergent structure.

DISCUSSION

The interpretation of seismic data (Fig. 3b, 4) illustrates the progressive advancement of triangle zone deformation into the foreland basin. The emplacement of a horse of Belly River Group strata has successively folded the Big Coulee, Co-op,

and Waldron faults, forming an anticline not recognized at the surface due to limited exposure. The Callum Creek fault is interpreted to have developed in response to folding of the underlying Co-op and Waldron thrust sheets. Thickening of low-velocity rocks of the Belly River Group in the horse is evidenced by a "push-down" velocity anomaly in reflections from older strata between CDP 410 and CDP 650.

During deformation, tectonic wedging occurred along detachment horizons, and the tip of the wedge stepped toward the foreland and upsection from the Bearpaw Formation to the St. Mary River Formation. In its undeformed state (Fig. 4) the Big Coulee Fault cuts upsection to the east through the Bearpaw Formation, suggesting that the Big Coulee and Co-op faults, respectively, once formed the base and roof of an east-vergent wedge.

Backthrusting along the Big Coulee Fault presumably began as it was tilted eastward during emplacement of the underlying thrust sheets. The youngest wedge in the triangle zone was emplaced along the detachment in the St. Mary River Formation. This wedge is bounded below by the basal thrust of the triangle zone and above by the Waldron Fault initially and later by the Callum Creek Fault. Significantly, ramps in the deeper thrust faults appear to be associated with the locations of normal faults that cut Paleozoic and basement rocks.

ACKNOWLEDGMENTS

We thank Mike Kary of Kary Data Consultants for kindly arranging access to the reflection seismic data from Shapco Resources Ltd., and Home Oil Ltd. "Move On Fault" software, used to restore the cross-section, was donated to The University of Calgary by Midland Valley Exploration Limited. The synthetic seismograms and displays in Figure 2 were generated using GMA LOGM software. We thank Margot McMechan for helpful discussions.

REFERENCES

Douglas, R.J.W.
1950: Callum Creek, Langford Creek, and Gap map areas, Alberta; Geological Survey of Canada, Memoir 255, 124 p.

Jerzykiewicz, T.
1994: Significance of the Pakowki Formation to mapping in the deformed belt of the southern Canadian Cordillera, Alberta; in Current Research 1994-E; Geological Survey of Canada.
in press: Stratigraphic framework of the uppermost Cretaceous to Paleocene strata of the Alberta basin; Geological Survey of Canada, Bulletin.

Jerzykiewicz, T. and Norris, D.K.
1993: Evolution of the Laramide foredeep and adjacent thrust belt in southern Alberta; Geological Survey of Canada, Open File 2663, 96 p.

Jones, P.B.
1982: Oil and gas beneath east-dipping underthrust faults in the Alberta foothills; in Geological studies of the Cordilleran thrust belt, (ed.) R.B. Powers; Rocky Mountain Association of Geologists, Bulletin, v. 1, p. 61-74.

Lawton, D.C., Spratt, D.A., and Hopkins, J.C.
in press: Tectonic wedging beneath the Rocky Mountain foreland basin, Alberta, Canada; Geology.

MacKay, P.A.
1991: A geometric, kinematic and dynamic analysis of the structural geology at Turner Valley, Alberta; Ph.D. thesis, University of Calgary, Alberta, 138 p.

Price, R.A.
1981: The Cordilleran foreland thrust and fold belt in the southern Canadian Rocky Mountains; in Thrust and Nappe Tectonics, (ed.) N.J. Price and K.R. McClay; Geological Society of London, Special Publication 9, p. 427-448.
1986: The southeastern Canadian Cordillera: thrust faulting, tectonic wedging, and delamination of the lithosphere; Journal of Structural Geology, v. 8, p. 239-254.

Skuce, A.G., Goody, N.P., and Maloney, J.
1992: Passive-roof duplexes under the Rocky Mountain foreland basin, Alberta; American Association of Petroleum Geologists, Bulletin, v. 76, p. 67-80.

Slotboom, R.T.
1992: Geophysical investigation of the triangle zone structure in the Jumpingpound-Wildcat Hills area, southern Alberta Foothills; M.Sc. thesis, University of Calgary, Alberta, 136 p.

Spratt, D.A., Lawton, D.C., and MacKay, P.A.
1993: The triangle zone and Turner Valley Structure west of Calgary; Geological Association of Canada/Mineralogical Association of Canada, Field Trip A-1 Guidebook, 41 p.

Stockmal, G.S. and MacKay, P.A.
1994: Triangle zone and foothills structures along and adjacent to the Oldman River, southwestern Alberta; in Current Research 1994-E; Geological Survey of Canada.

Sukaramongkol, C.
1993: Seismic imaging of a non-emergent thrust front in the Fallen Timber Creek area, southern Alberta Foothills; M.Sc. thesis, University of Calgary, Alberta, 140 p.

Teal, P.R.
1983: The triangle zone at Cabin Creek, Alberta; in Seismic expression of structural styles, (ed.) A.W. Bally; American Association of Petroleum Geologists, Studies in Geology No. 15, v. 3, p. 3.4.1-48-3.4.1.-53.

Geological Survey of Canada Project 930012

Hydrochemical and hydrogeological investigation of a potential coalbed methane area, southeastern British Columbia

S.M. Harrison[1], H.J. Abercrombie, and J.F. Barker[1]
Institute of Sedimentary and Petroleum Geology, Calgary

Harrison, S.M., Abercrombie, H.J., and Barker, J.F., 1994: Hydrochemical and hydrogeological investigation of a potential coalbed methane area, southeastern British Columbia; in Current Research 1994-E; Geological Survey of Canada, p. 117-120.

Abstract: Field sampling and inorganic and organic chemical and isotopic analyses of surface and subsurface waters in the Elk River and Fording River valleys have been done as part of a hydrochemical and hydrogeological examination of potential coalbed methane development in southeastern British Columbia. The waters sampled are characterized by low total dissolved solids and, except where contamination of production test facilities is indicated, are essentially devoid of BTEX and PAH compounds. Isotopic analysis of aqueous carbonate species indicates that methane is probably being actively produced by microbial reactions. Tritium analyses of subsurface waters indicate that the area is characterized by active flow systems.

Résumé : Les eaux de surface et souterraines dans les vallées des rivières Elk et Fording ont fait l'objet d'un échantillonnage de terrain ainsi que d'analyses chimiques (organiques et inorganiques) et isotopiques, dans le cadre d'une évaluation hydrochimique et hydrogéologique du potentiel de mise en valeur du méthane dans les couches de charbon de la partie sud-est de la Colombie-Britannique. Les eaux échantillonnées sont caractérisées par de faibles quantités de matières totales dissoutes et, sauf lorsqu'on spécifie la contamination des installations d'essai de production, sont exemptes de BTEX et d'HAP. L'analyse isotopique des espèces carbonatées aqueuses indique que du méthane est sans doute activement produit par des réactions microbiennes. Des analyses (tritium) des eaux souterraines permettent de conclure que la région est caractérisée par des systèmes d'écoulement actifs.

[1] Waterloo Centre for Groundwater Research, University of Waterloo, Waterloo, Ontario N2L 3G1

INTRODUCTION

Interest in coalbed methane potential in the Western Canada Sedimentary Basin (WCSB) has increased recently and southeastern British Columbia may be the site of the first development of coalbed methane in western Canada. Identification of key aspects of coalbed methane development and production is needed to assure that the resource is developed in an environmentally sound manner. The Institute of Sedimentary and Petroleum Geology (ISPG), the Waterloo Center for Groundwater Research (University of Waterloo), Norcen Energy Resources Limited, and Fording Coal Limited have jointly undertaken a program to investigate the environmental geochemistry and hydrogeology of coalbed methane exploration and development, with particular reference to coalbed methane resources in southeastern British Columbia.

The impact of water production associated with reservoir depressuring is one of several important environmental issues in assessing the impact of development of coalbed methane resources. The principle risks include how much water will be produced and the quality of the water produced (Table 1). A water sampling program was carried out in the spring and summer of 1993 within the Elk River and Fording River valleys at Norcen Energy Resources' Weary Creek exploration block and Fording Coal's Fording River operation.

a. Weary Creek, Elk River valley: Twenty-seven water samples were collected from a 10 km^2 area within the Elk River Valley, near Weary Creek, approximately 45 km north of the end of the paved portion of Highway 43 at Elkford, British Columbia. The sampling points lie within areas of outcrop and subcrop of the Mist Mountain Formation, which contains coals targeted for coalbed methane development.

b. Fording River valley production test: Twenty-four water samples were collected during the coalbed methane production test on the Fording River production test site. The samples were collected at various stages during the drawdown of the production well.

Standard methods were used to sample and preserve the waters. Routine field analyses included pH, conductivity, temperature measurements, and acid/base neutralizing capacity. The waters collected in both sampling programs were analyzed for the parameters listed in Table 2.

The analyses for organics - benzene, toluene, ethylbenzene, and xylene (BTEX) and polycyclic aromatic hydrocarbons (PAHs) - and isotopic signatures were carried out at the Waterloo Centre for Groundwater Research. The inorganic (cation/anion) and organic acid analyses were carried out at ISPG, Calgary.

RESULTS

Weary Creek, Elk River valley

The waters collected within the Elk River valley study area are characterized by consistent pH ranging from 6.50 to 8.36 and relatively low conductivities ranging from 0.258 to 1.988 mS/cm suggesting relatively low total dissolved solids. The waters were collected from three general sampling points:

i. wells,

ii. near surface waters, and

iii. flowing waters from streams and the Elk River.

Table 1. Principle risks to the hydrogeological regime from coalbed methane production.

Principle Impact	Mechanism	Determinant
Production of groundwater and potentially large volumes of groundwater	Drawdown	i) Hydraulic characteristics of the geological medium (transmissivity, storativity) ii) Annual aquifer or groundwater recharge
Water quality - modification of groundwater quality - modification of surface water quality		i) Deep water quality. ii) Vertical extent of zone of influence iii) Recharge iv) Discharge
Surface hydrology (base flow in surface streams)	Change in flow system	i) Groundwater-surface water interaction (hydraulically connected or isolated) ii) Cone of influence and vertical distribution of drawdown
Others - land subsidence - modification of hydraulic parameters by depressuring pore fluids	Pressure reduction leading to an increase in effective stress (consolidation)	i) Compressiblity of media

Organics

Analysis of the three groups for hydrocarbons indicated undetectable amounts of BTEX and PAHs in each.

C_1 to C_4 gases

Methane was detected in all samples analysed for C_1 to C_4 gases. Concentrations ranged from 46.5 ppm collected from an open well to trace amounts in stream waters. Ethene, ethane, and propene concentrations were generally below 0.01 ppm.

Inorganics

The waters are comparatively dilute. However, the inorganic data suggest that the concentrations of major cations tend to increase with sample depth. As might be expected, metals show an increase in concentration with depth. Anions are dominated by bicarbonate.

Table 2. Parameters analyzed for samples from the Elk River and Fording River valleys.

Analyte	Measured Parameters
Inorganic Species	·dissolved inorganic carbon ·anions ·cations
Organic Species	·polycyclic aromatic hydrocarbons (PAH) ·monocyclic aromatic hydrocarbons (BTEX) ·organic acids ·DOC
Gases	·C_1 - C_4 hydrocarbon gases
Isotopes	·$\delta^{18}O$, δD, $\delta^{13}C$, ^3H

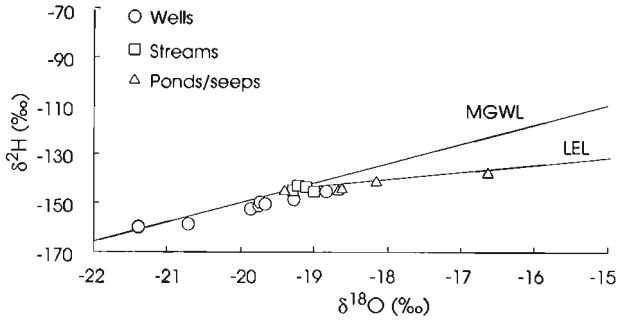

Figure 1. δ^{18} *O and* ^{2} *H for surface and subsurface waters from the Elk River valley, southeastern British Columbia. MGWL=mean global water line; LEL=local evaporation line. Results reported using standard mean ocean water (SMOW) standard.*

Isotopes

The ^{18}O-^2H isotopic signatures generally trend along the mean global water line (MGWL; Fig. 1). Differences in the ^{18}O-^2H isotopic signatures of waters collected may suggest different recharge sources. An evaporative trend is evident for some pond waters. Concentrations of ^3H ranged from <0.8 (±0.3) to 20.3 TU (±1.4) and from <0.8 to 16.0 TU in samples of well waters, suggesting that at least part of the flow system is relatively active. Enriched ^{13}C (+32.6‰) dissolved inorganic carbon signature in some samples, which is characteristic of microbial reduction of CO_2, suggests that a biological substrate may actively be producing methane in parts of the Elk River valley study area.

Fording River valley production test

The waters collected at the Fording production test represent comparatively deep groundwaters within the Fording River valley. The pH of the waters were consistent ranging from 6.69 to 7.54. Conductivity measurements ranged from 0.570 to 1.124 mS/cm, suggesting relatively low total dissolved solids. The water sample points included:

i. the production test well, sampled at the wellhead (bottom-hole temperature 22°C, wellhead 10°C);

ii. storage tanks; and

iii. the water/gas separator.

Organics

Results of the organic analyses indicate that the wellhead production waters do not contain detectable concentrations of polycyclic or aromatic hydrocarbons. Only one sample collected from the wellhead contained 7.46 ppb toluene. Detected concentrations of BTEX and PAH in samples collected from the tanks and separator probably represent, in part, contamination from previous use in other oil field settings. The first waters removed from the completion may have also been partly contaminated by workover, completion, and drilling fluids used onsite and these cannot be ruled out as potential sources.

C_1 to C_4 gases

Gas-cuts were detected in all samples collected and analyzed for gas. Methane, ethane, and propane were detected in all the samples analyzed for C_1 to C_4 gases. Methane concentrations were the highest among the gases analyzed ranging from 13.5 to 23.8 ppm. Samples analyzed for ethane and propane indicated concentrations of less than 1.0 ppm.

Inorganics

Inorganic analyses show that the Fording production waters are characterized by comparatively high concentrations of Fe, Ca, and Mg. Anions are dominated by bicarbonate (HCO_3-) and sulphate (SO_4-).

Isotopes

^{18}O-^{2}H isotopic signatures for groundwaters lie on or near the mean global water line with little deviation from approximately -21.0 ‰ ^{18}O and -156.0‰ ^{2}H. ^{3}H ranged from ≤0.8 (±0.3) to 1.3 TU (±0.3).

DISCUSSION

The preliminary data suggest the following conclusions may be drawn for the region of the Elk River and Fording River study areas:

1. The waters sampled are generally dilute and devoid of organic compounds. The dominant cations include Ca, Mg, K, Fe, and Na. The dominant anions are sulphate and bicarbonate.
2. The concentrations of major cations, in particular Ca and Fe, tend to increase with depth; the deeper groundwaters (Fording River production test and selected waters from wells in the Elk River valley) are characterized by markedly higher concentrations of the major cations compared to stream and river waters. Iron and barium are among regulated compounds that generally exceed acceptable drinking water or aquatic life criteria. Selected samples also indicated elevated concentrations of Ni, Cu, Se, and Pb.
3. Distribution of ^{2}H and ^{18}O suggest different sources for the various well waters. ^{3}H isotopic signatures in the samples collected from wells suggest that the flow system in this region may be relatively active.
4. Enriched (heavy) ^{13}C signatures in dissolved inorganic carbon suggest that an active biological substrate is likely producing methane as a metabolic product in parts of the Elk River valley study area.

FURTHER WORK

Field sampling, including sampling of C_1 to C_4 gases, dissolved inorganic carbon, and routine inorganic sampling of selected locations and the Fording River during low flow stage are planned. The additional sampling data are needed to refine the existing hydrochemical database and will be included as part of a more detailed assessment and interpretation of the water chemistry (hydrochemical modeling).

An assessment of the physical hydrogeological database to establish the flow system within a physical context has been initiated. As a final step in assessing the region, available hydrogeological and hydrochemical databases will be synthesized and an environmental analysis completed.

Geological Survey of Canada Project 890060-XP

Disseminated Au-Ag-Cu mineralization in the Western Canadian Sedimentary Basin, Fort MacKay, northeastern Alberta: a new gold deposit type[1]

Rui Feng and Hugh J. Abercrombie
Institute of Sedimentary and Petroleum Geology, Calgary

Feng, R. and Abercrombie, H.J., 1994: Disseminated Au-Ag-Cu mineralization in the Western Canadian Sedimentary Basin, Fort MacKay, northeastern Alberta: a new gold deposit type; in Current Research 1994-E; Geological Survey of Canada, p. 121-132.

Abstract: Disseminated Au-Ag-Cu mineralization has been discovered in the Western Canadian Sedimentary Basin (WCSB) at Fort MacKay, Alberta, Canada. Host rocks are basement granitoids, Devonian limestones, and Cretaceous sandstones. Dominant gold forms (mostly 0.5-2 μm) are Au+Si and native Au in granitoids, and Au+Ca, Au+Al, Au, Au+Ag, Au+Cd, Au+Si, and Au+salts mixtures in sediments. Alteration includes calcite, quartz, salts, clay, and Ce-bearing minerals with abundant hematite and little pyrite. Other metallic elements occur as alloys, oxides, chlorides, and carbonates. The occurrence of Au-Ag-Cu mineralization is explained by a genetic model in which oxidized brines leach metals from basal redbed sandstone, paleosols, and basement, which are later precipitated by reducing agents and by brine mixing. The discovery of Au-Ag-Cu mineralization signifies a great opportunity for Au and other metal exploration in the WCSB.

Résumé : On a découvert une minéralisation disséminée en Au-Ag-Cu dans le bassin sédimentaire de l'Ouest canadien, à Fort MacKay (Alberta, Canada). Les roches hôtes sont des granitoïdes du substratum, des calcaires du Dévonien et des grès du Crétacé. Les formes dominantes de l'or (surtout de 0,5 à 2 μm) sont du type Au+Si et Au natif dans les granitoïdes; Au+Ca, Au+Al, Au, Au+Ag, Au+Cd, Au+Si et mélanges de sels et d'or dans les roches sédimentaires. Les minéraux d'altération incluent la calcite, le quartz, les sels, l'argile et les composés de Ce; l'hématite est abondante, au contraire de la pyrite. On trouve d'autres éléments métalliques sous forme d'alliages, d'oxydes, de chlorures et de carbonates. La minéralisation en Au-Ag-Cu s'explique par un modèle génétique dans lequel la saumure oxydée lessive les métaux du grès basal (couches rouges), des paléosols et du substratum, lesquels sont ultérieurement précipités par des agents réducteurs et par le mélange de la saumure. La découverte de la minéralisation en Au-Ag-Cu revêt une grande importance pour l'exploration de l'or et d'autres métaux dans le bassin sédimentaire de l'Ouest canadien.

[1] Contribution to Canada-Alberta Agreement on Mineral Development (1992-1995), a subsidiary agreement under the Canada-Alberta Economic and Regional Development Agreement.

INTRODUCTION

The Western Canadian Sedimentary Basin (WCSB), especially the Alberta portion, contains abundant petroleum resources and is the largest petroleum-producing province in Canada. However, except for the Pine Point Pb-Zn deposits (Anderson and Macqueen, 1982) and Ca, Li, and Mg potential from high salinity brines, no metallic mineral deposits have been reported in the basin (Edwards, 1988). Gold has been recovered from rivers in Alberta and Saskatchewan for over a century, but on a very small scale (Giusti, 1986; Edwards, 1988). The lack of known large-scale metallic mineralization in the basin may indicate an underdeveloped opportunity rather than a lack of geological potential because most geological studies have focused on energy resources.

Recently, elevated abundances of Au, Ag, and platinum-group elements (PGE) have been reported in Phanerozoic sedimentary rocks of the WCSB from Fort MacKay, northeastern Alberta, indicating possible mineralization. However, different assay methods have produced contrasting Au results, and there has been confusion over the existence of significant Au mineralization in the area (see Abercrombie and Feng (1994) and a series of reports in the Northern Miner, 1993). In this study, 32 rock chips, polished thin sections, and rock slabs from altered basement granitoids, redbed sandstone, and Beaverhill Lake Formation (drill core and surface) near Fort MacKay were examined using a scanning electron microscope (SEM) and a backscatter image and energy dispersion X-ray spectrometer (EDS). More than half the samples examined contain various amounts of Au and other metallic phases. This paper presents these results.

GEOLOGICAL BACKGROUND

Fort MacKay, Alberta, lies near the southwestern edge of the Proterozoic Trans-Hudson basement outcrop (Fig. 1, 2). Three broad rock sequences are identified: basement; a Devonian sequence dominated by redbed sandstone, evaporite, and carbonate formations; and a Cretaceous sequence of predominantly sandstones containing heavy oils (Carrigy, 1959; Fig. 1, 2). Basement rocks buried underneath Fort MacKay are Proterozoic granitoids forming part of a 1.8 to 2.0 Ma magmatic belt (Ross et al., 1991). Paleosols developed on basement granitoids are preserved and are called "Granite Wash" (Fig. 2). The northwest-striking Middle Devonian sequences (Lower and Upper Elk Point groups) in this region unconformably overlie the basement. The Lower Elk Point Group comprises basal units of interbedded red sandstone, reddish-green mudstone, and evaporites which change upward into limestone and evaporites, forming a typical redbed sequence (Meijer Drees, 1986; Fig. 2). The Upper Elk Point Group includes Winnipegosis Formation carbonates and Prairie Formation salt-evaporates. The edge or "solution front" of the Prairie Formation salts parallels the basin-basement boundary (Hamilton 1971; Fig. 2). The Beaverhill Lake Formation is the basal unit of the Upper Devonian and consists of a sequence of alternating limestones and shales (Fig. 1). Other Upper Devonian rocks, including the Woodbend and Nisku carbonate formations, are absent in the study area (Fig. 2).

The Cretaceous Mannville Group (sandstones) was deposited on eroded Devonian rocks and contains the largest reserve of heavy oil in the world (Fig. 2). Between the contact of Devonian and Cretaceous rocks, there is a unique sequence of quartz-cemented sandstones (Beaver River sandstones),

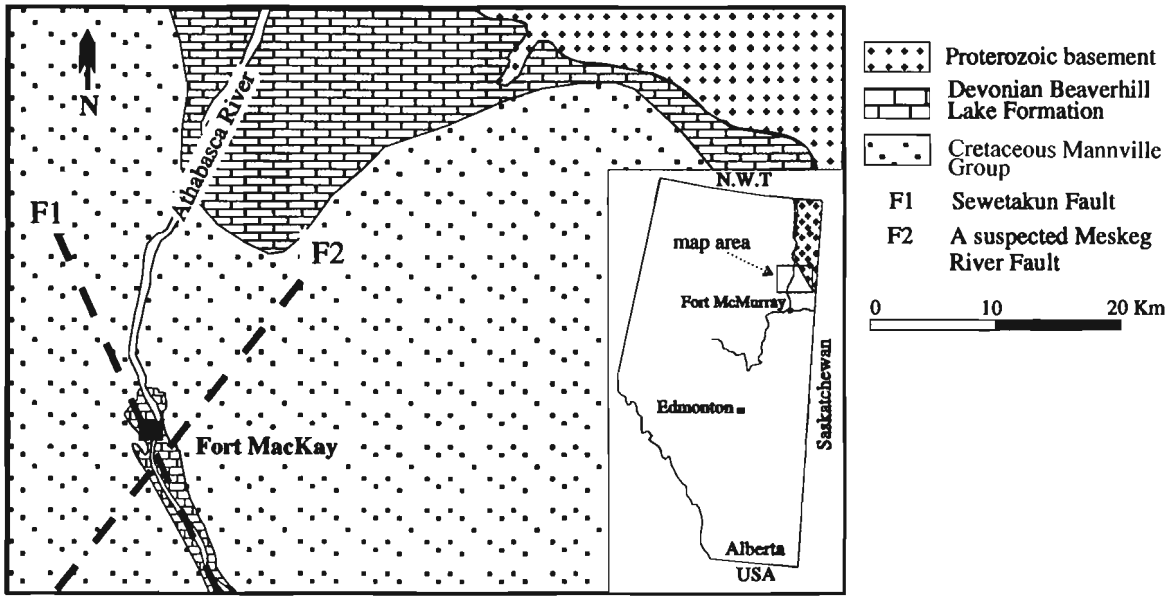

Figure 1. Bedrock geology of the Fort MacKay area, Alberta, Canada (after Carrigy, 1959). The Sewetakun Fault was identified by Hackbarth and Nastasa (1979), the Muskeg River Fault was inferred from topographic features and offset of magnetic anomalies.

which also outcrops in the area (Carrigy, 1959; Martin and Jamin, 1963). A northwest-southeast fault (Sewetakun Fault), which may have affected rock units as young as Devonian, was identified by Hackbarth and Nastasa (1979) based on geological, geophysical, and hydrogeological evidence (Fig. 2).

Bachu and Underschultz (1993) have documented the regional hydrogeology of formation waters in the northeastern Alberta basin. Pre-Prairie Formation aquifers, beneath the regionally extensive, impermeable Prairie salt aquiclude, are characterized by regional topographically-driven flow along stratigraphic layers and updip migration (Fig. 2). At the edge of the Prairie Formation salt, along the trace of the Sewetakun Fault, vertical cross-formational flow occurs (Fig. 2). Post-Prairie Formation aquifers are characterized by transitional flow regimes between regional and localized flows (Fig. 2).

ANALYTICAL RESULT

Basement granitoids

Ten granitoid samples from Athabasca Oil Ltd. well No. 1 and Scurry-Rainbow Oil Ltd. well CD-1, drilled within the Sewetakun Fault zone near Fort MacKay, were examined and found to show extensive deformation and alteration. The deformation is mainly high-angle ductile-brittle shear. Well developed foliation and fractures are present in the high-strain zone, accompanied by K-feldspar, chlorite, Fe-epidote, and quartz veining. Hematite is the predominant metallic mineral, occurring as nodules and veins, or as thin films on fracture surfaces. Pyrite is less abundant and also occurs as veins and nodules. Minor native sulphur is associated with hematite and pyrite. Monazite and $CeCO_3$ microveining are widespread and locally associated with calcite. Alteration and mineralization in the granitoids are zoned. Granitoids are reddish brown near the upper contact with the "Granite Wash", and grade downward into a pale red zone about 40 m deeper, due to reduced hematite abundance and increased quartz veining with depth. From cross-cutting relationships, at least two generations of alteration were observed: an older K-feldspar +chlorite+disseminated hematite association possibly with Fe-epidote; and younger alteration of Ce-bearing minerals, carbonates, and quartz, hematite, and pyrite veins. The older generation of alteration may be Proterozoic.

Pb-bearing minerals, including $PbCl_2$, Pb-carbonate (Pb+O EDS peak), Pb silicate (Pb+Si EDS peaks), and PbSb (Pb+Sb EDS peaks), are widespread. $PbCl_2$ is the most abundant (Fig. 3A). AgCl and native Ag are also widely distributed and associated with Pb minerals, $CePO_4$ and $CaCO_3$, and Fe-epidote nodules (Fig. 3A, B, C, D). Some Ag minerals display complex EDS peaks (e.g., Ag+Si, Ag+P+Ce, Ag+Si+Al+Mg+P+Ca). It is not clear whether they are actual minerals or fine mixtures. Less abundant metallic phases include Cu, Cu+Zn, Sb_2O_3, SnO_2, CuSb, scheelite, and Bi+Cl.

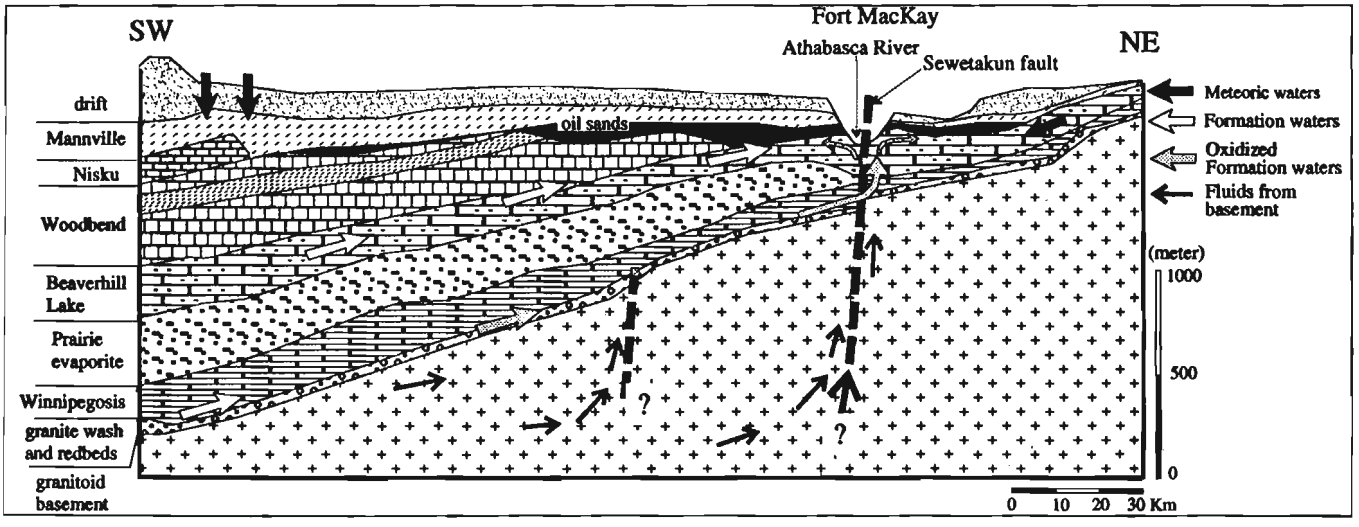

Figure 2. Schematic stratigraphic cross-section of the Fort MacKay area, Alberta, Canada, showing geology and hydrology of the formation waters or brines in the basin (after Carrigy, 1959; Hackbarth and Nastasa, 1979; Bachu and Underschultz, 1993). Fluid flow in the basement is inferred from observed alterations of granitoids. Because of impermeability of the Prairie Formation, brines in aquifers beneath the Prairie Formation are characterized by regional, updip flow and can only be discharged at the solution front of the Prairie Formation. When passing through evaporites, redbed sandstones, and "Granite Wash", these brines were oxidized, which would leach Au, Ag, Cu, and other metals in the redbed sequences and basement rocks. Eventually, these ore-bearing brines discharge at the solution front of the Prairie salts, facilitated by major structures. Brine mixing at two major boundaries, the contacts between basement and redbed sequences and between oil-sand and Devonian Beaverhill Lake Formation carbonates, together with reducing agents (hydrocarbon and organic matter) in the sediments were major causes for metal precipitation.

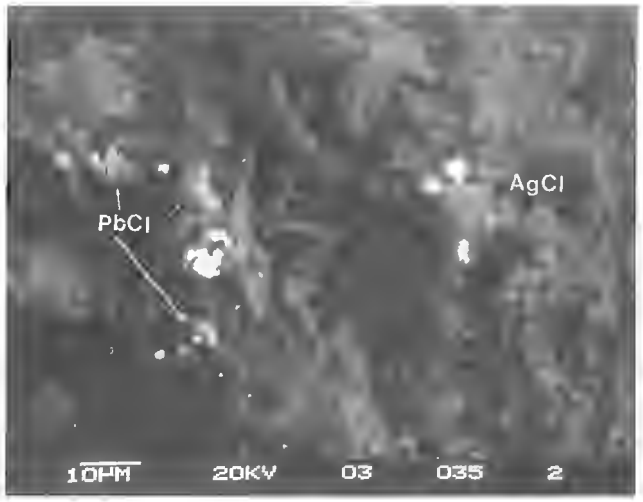
AgCl
PbCl
10PM 20KV 03 035 2

A

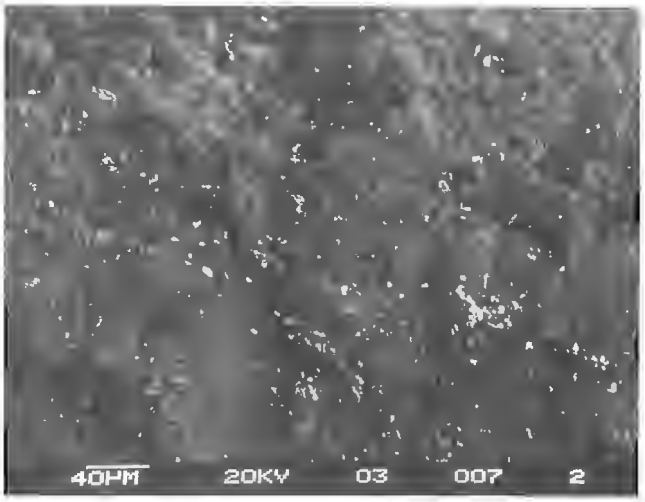
40PM 20KV 03 007 2

B


2PM 20KV 03 034 2

C

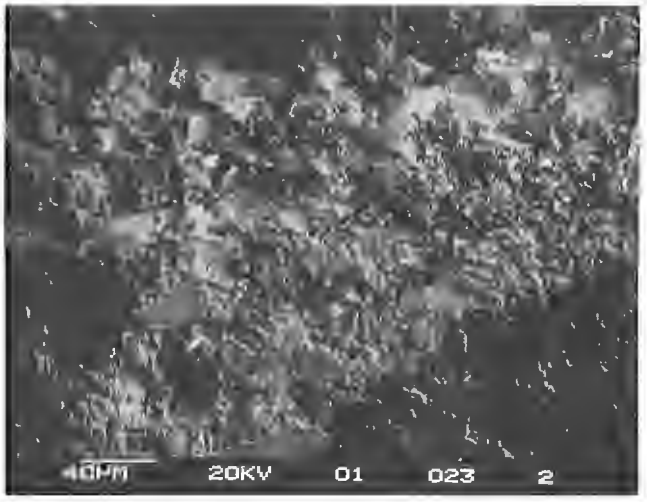
40PM 20KV 01 023 2

D

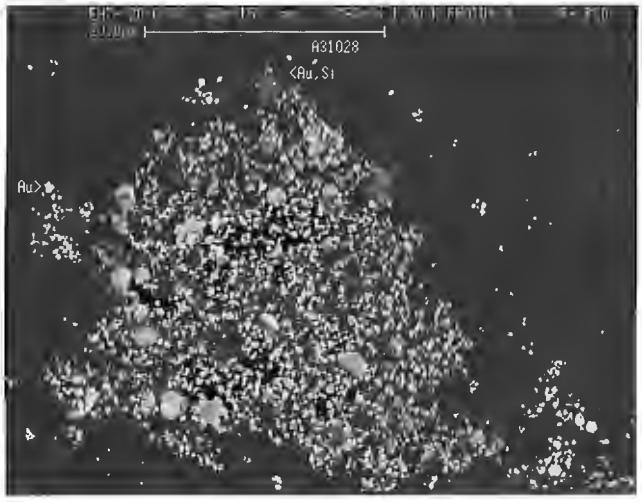
A31028
<Au,Si
Au>

E

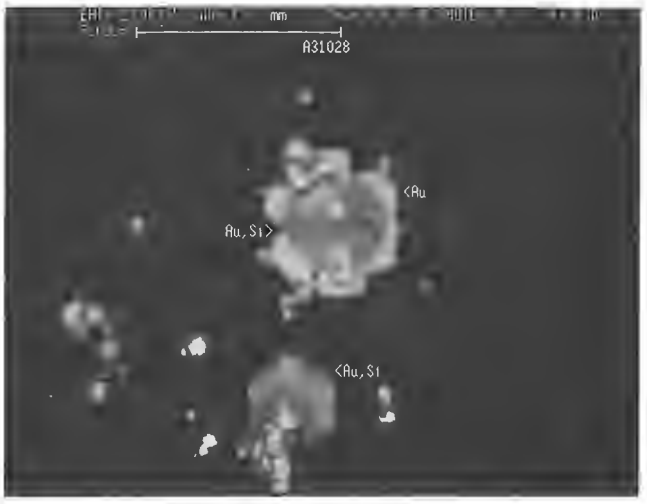
A31028
<Au
Au,Si>
<Au,Si

F

Abundant native Au was also observed in two samples as aggregates (Fig. 3E) or as small disseminated grains. Close examination of Au aggregates in Figure 3E shows zoning: hexagonal Au+Si grains (Ai+Si EDS peaks) are rimmed by pure Au (Fig. 3F). Au appears to be associated with native Cu, and less commonly with Ag-bearing minerals. Generally, Au, Ag, and Pb minerals are more abundant in the upper reddish-brown granitoid zone than in the lower pale red zone.

"Granite Wash" and redbed sandstones

"Granite Wash" consists of coarse-grained K-feldspar, quartz, biotite, salt, gypsum, and hematite. It changes gradually upward into red sandstones and reddish-green mudstones with some thin gypsum or anhydrite beds. Dominant minerals in the red sandstones and mudstones are quartz, K-feldspar, clay, biotite, salt, calcite, Fe-oxide, zircon, and apatite. The $CeCO_3$ and $CePO_4$ that are widespread in altered granitoids also occur in the "Granite Wash" and red sandstone sequences. Native S grains were also observed.

A variety of metallic phases were found on freshly broken sandstone and mudstone surfaces, including relatively abundant Cu and Cu+Zn alloys (0.2%), and lesser amounts of AgCl, native Ag, $PbCl_2$, Pb carbonate, (Cu, Zn)Cl_2, $FeCl_3$, (Cu, Fe)S, and trace SnO_2, Sb_2O_3, PbSb, and native Au (Fig. 4A). Some Pb carbonate and native Ag grains were observed in the thin gypsum beds (veins).

Several complex mixtures of Au-bearing aggregates were found at the edge of one red mudstone thin section (T4-312.5), indicating that they are not in situ. As shown in Figure 4B, Au+minor Cl+K+Al+Na grains of <1 to >10 μm occur on top of (Na+K)Cl+clay mixture. Figure 4C shows that Cd+Au+Zn+Pd grains grow on aggregates of quartz+(Na, K)Cl+Au+Ag+Zn. Similar Au-bearing aggregates were observed on freshly broken surfaces of limestone outcrop samples (RR-43A, RR-09, and F-02). This illustrates the importance of handling these samples with care, since Au-bearing grains may be easily scraped off the surfaces of porous limestones during polishing.

Beaverhill Lake Formation fine-grained carbonates

Most limestones examined contain some amount of detrital clay, quartz, and trace amounts of zircon and apatite. Oil staining is widespread with bitumen occurring in pores and fractures. In some rocks, the bitumen can be as high as 5 per cent by volume. Core logging reveals many high-angle faults and fracture zones 0.5 to 1 m wide in the Beaverhill Lake Formation, which may have resulted from movement on the Sewetakun Fault and/or karst development. The fractures contain gouge consisting of relatively coarse-grained mixtures of quartz, K-feldspar, calcite, and fine-grained illite, chlorite, biotite, and pyrite. Microscopic examination reveals compaction- and/or deformation-related structures, including calcite grains showing undulatory extinction. Relatively widespread but fine-grained secondary alteration minerals include quartz, hematite, calcite, illite, K-feldspar, chlorite, apatite, $CePO_4$, $CeCO_3$, rutile, Fe-Ni-Cr oxides, and pyrite. All are microcrystalline and are not obvious in hand specimens. Silicification is abundant in some samples and occurs as quartz microveining and hardening of limestones by microcrystalline quartz. Hematite veins about 1 cm wide associated with quartz, calcite, and illite often occur along microfracture zones, replacing host limestones. Secondary calcite forms microveins in association with illite, chlorite, apatite, monazite, rutile, and less commonly with hematite, which is also widespread as nodules and microveining, and replaces pyrite. In the only dolostone examined (T3-116), a calcite+illite+apatite+chlorite+rutile+pyrite association has replaced dolomite along fractures and cavities. Pyrite, which occurs in spherical and irregular shapes in the matrix, is probably biogenic. Elsewhere, secondary pyrite is associated with calcite microveining.

Gold is most abundant in the Beaverhill Lake Formation samples and is found in many different forms, associations, and compositions. On freshly broken limestone surfaces, Au, Au+Ca, and Au+Al were commonly found as very small grains, ranging from <0.1 to ~2 μm. Commonly, a larger grain (e.g., ~2 μm) will be surrounded by a cloud of submicron grains (Fig. 4D). Such small Au grains were rarely found on polished surfaces of rock slabs, but rather on unpolished, broken surfaces at the edges of rock slabs. In a typical limestone sample (F18), ≥300 such grains were found on the broken surface while only a few grains were observed on the polished surface of the same slab. This indicates that the polishing process has removed gold grains from the rock. Native Au and Au alloys may also coalesce into large grains with irregular shape, surface, and edges (Fig. 4E, F). Clay is found in the larger grains (Fig. 4E). Au minerals show a close relationship with other metallic minerals and may occur as different alloys. In Figure 5A, several Au grains occur with Cu-Zn alloys within pores in the limestone. Figure 5B shows the association between Ag+Ca+Au, Au, Ag+Au, Si+Au+Ca,

Figure 3.

A. Association of $PbCl_2$ and AgCl grains on a fresh broken surface of an altered granitoid sample (B-1, core).

B. Disseminated AgCl grains on a fresh broken surface of a granitoid sample (AgCl grains <1000; B-1).

C. Enlargement of AgCl crystals in (B).

D. Ag+Si (Ag+Si EDS peaks) grains occur inside of an Fe-epidote nodule in the altered granitoids (WS-1, core).

E. An aggregate of Au and Au+Si grains on a newly sawed granitoid surface, more than five such aggregates and more than 100 Au grains were found in the sample (A31028).

F. A hexagonal Au+Si core is rimmed by pure Au (A31028). All photomicrographs shown are backscattered electron images. The element sequence is arranged in declining EDS peak intensity in all the figures.

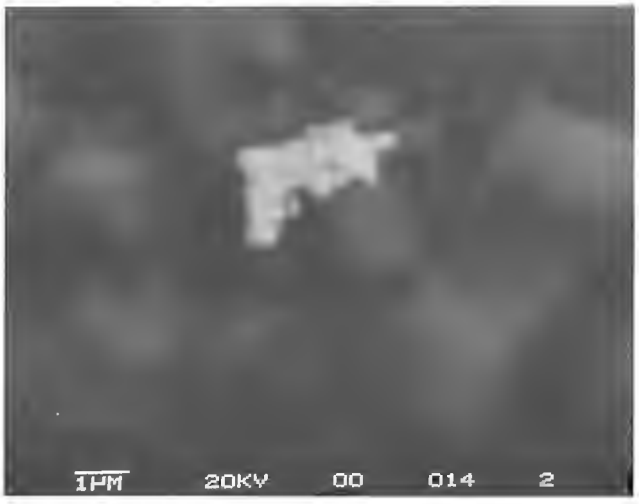
1μM 20KV 00 014 2

A

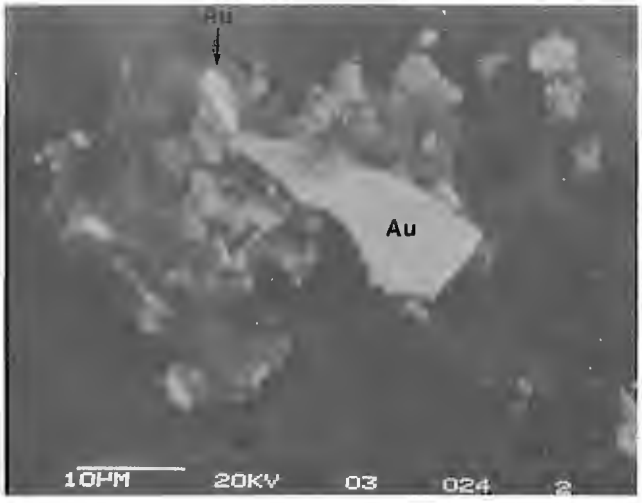
Au
Au
10μM 20KV 03 024 2

B

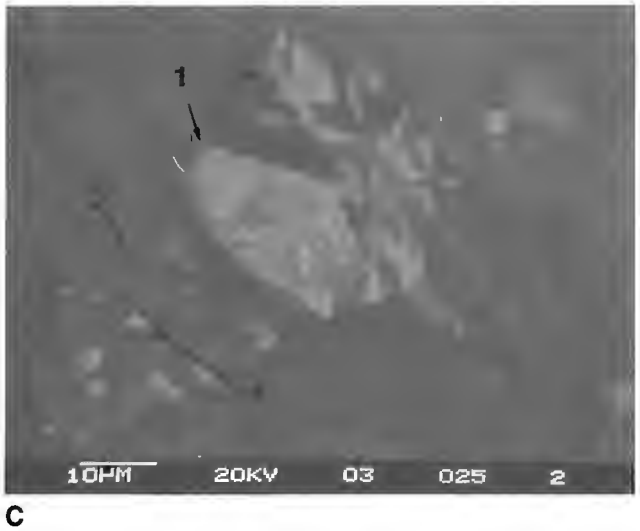
1
10μM 20KV 03 025 2

C

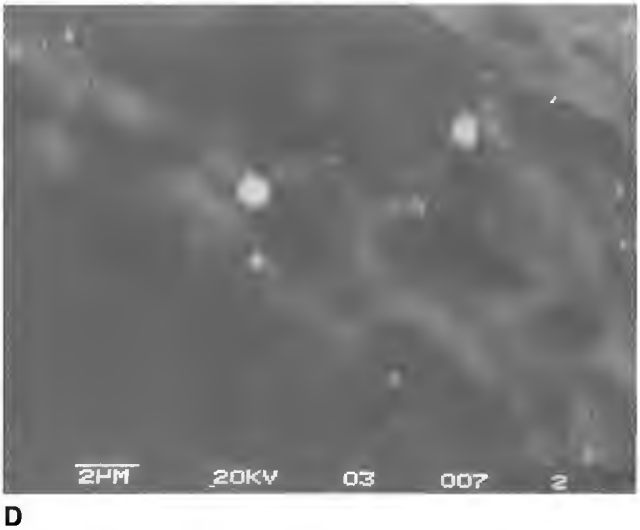
2μM 20KV 03 007 2

D

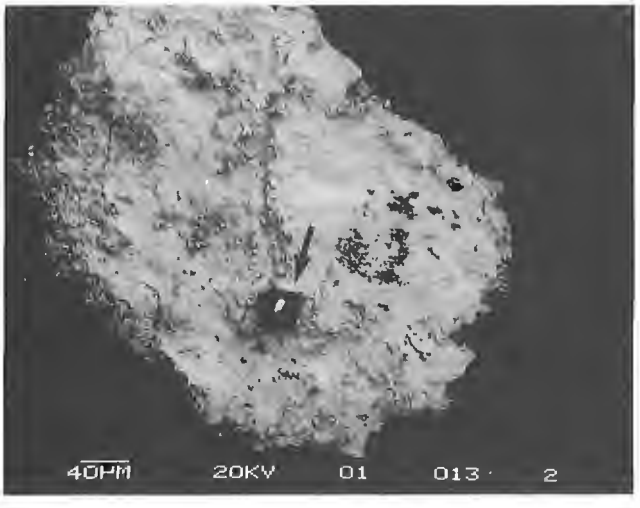
40μM 20KV 01 013 2

E

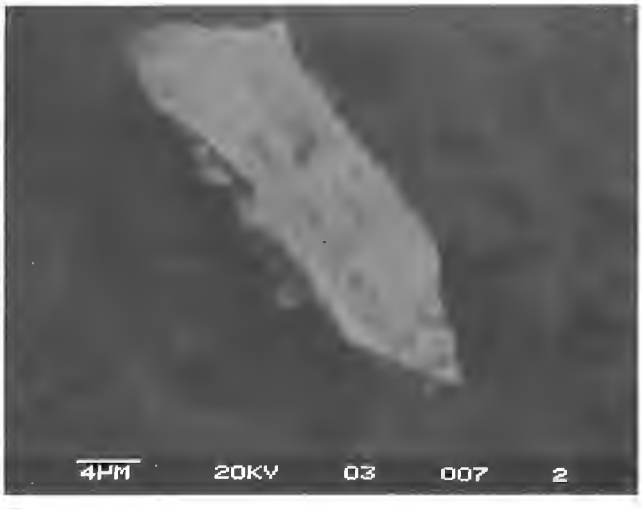
4μM 20KV 03 007 2

F

and Au+Cd alloys, and other smaller bright Au alloy grains. In Figure 5C, Au and Au+Fe+Cd+Cu+Cr+Ni alloy mixtures occur in limestone pores, but were plucked out during polishing.

Au-bearing minerals may be zoned, as shown in Figure 3F. In Figure 5D, a Au+Si rim surrounds a Au+Al core, whereas in Figure 5E, areas with Au+Ca+Al+K+Cl EDS peaks (bright) are irregularly intergrown with zones containing less Au. Figure 5F shows a Au-bearing mineral with regular zoning, where a Ca-rich, Au-bearing rim surrounds a Au-rich, Ca-bearing core.

Au minerals also show a relationship to alteration. In Figure 6A, a Au-Cd alloy with illite+chlorite and calcite+clay aggregates occurs within the same pore system in limestone. In Figure 6B, a Au+Ca grain occurs in the calcite veining network. As mentioned above, Au-bearing minerals are found associated with salts in sample T4-312.5 (Fig. 4B, C). Figure 6C is taken from a fresh broken limestone surface (RR-43A), where a Au-salt grain (with minor K+Cl EDS peaks) and KCl cubes are embedded in a NaCl+KCl+calcite matrix, confirming the Au-salt relationship. In most of the polished thin sections examined, Au-bearing grains were found to be located above the polished surface and may be explained by the evidence shown in Figure 6D, where three Au+Ag alloy grains occur on the top of salt+gypsum+organic matter mixtures. The entire aggregate appears to have erupted out of the polished surface of the matrix, which in this case is organic matter. The disturbed area in the organic matrix surrounding the aggregates clearly indicates that the eruption occurred after polishing. A possible cause for this phenomenon may be expansion due to absorption of water from the atmosphere by salts after polishing.

In summary, the most commonly observed Au-bearing minerals in the Beaverhill Lake carbonates are small, disseminated Au, Au+Ca, Au+Al grains within limestone pores in association with calcite, clay, and other mineral veining. The remaining Au is alloyed with other metals (e.g., Ag, Cd, and Cu) or associated with salts (NaCl+KCl). Although Au-salt association is less common than Au, Au+Ca, and Au+Al, it signifies an important Au form. It is not clear whether Au in Au+K+Na+Cl+Ca mineral grains occurs as Au-chloride or as an independent Au metal mixed with KCl+NaCl. A striking feature worth mentioning is that none of these Au-bearing rocks show any visible signs of alteration in hand specimens.

Ag minerals are relatively less common and not as widely distributed as Au-bearing minerals. Although Ag is locally associated with Au or found as Au-Ag or Ag-Au alloys (e.g., Fig. 6D), it appears that Ag- and Au-bearing minerals are not associated. Sample RR-43A is the only limestone examined that contains abundant Ag and AgCl (>500 grains) with a few Au grains (Fig. 6E).

Native Cu and Cu+Zn alloys are the most common metallic minerals in the Beaverhill Lake Formation limestones. They occur as disseminated particles or aggregates of flakes (Fig. 6F), or in association with Au grains (Fig. 5A), with calcite+clay, and with salts. In some cases, native Cu may be as abundant as about 0.1 per cent, which is potentially economic. Pb-carbonate and $PbCl_2$ are also widely distributed but less abundant than Cu and Cu+Zn alloys. Minerals found in very low abundance include Zn, Ni+Co+Cr oxide, SnO_2, Sb_2O_3, Bi, BiCl, and WCO_3.

Figure 4.

A. A native Au grain on the freshly broken surface of a redbed sandstone sample (A1-RR).

B. Intergrowth of Au-bearing grains with salts (NaCl+KCl), calcite, and clay on the edge of the thin section (not in-situ). EDS peaks are Au+minor Cl+K+Al+Na for Au (T4-312.5, core).

C. Cd+Au+Zn+Pd alloys (1) grow on top of (2), a mixture of quartz+(Na,K)Cl+Au+Ag+Zn. EDS peaks are Si+Cl+Na+K+minor Au+Ag+Zn (T4-312.5, core).

D. A group of fine Au grains (<2 μm bright spots) in a fresh broken limestone surface. EDS peaks include Au+minor Ca+Al (Au grains >200; F20).

E. A large Au+Ag (9:1) grain (400 μm), the dark inclusion is a mixture of clay and calcite. More than 30 grains of Au between 0.5 and 400 μm were found in the sample (T2-25.75).

F. A tongue-shaped Au grain on a fresh limestone surface. EDS peaks include Au+minor Al+Ca (F20).

Cretaceous Beaver River sandstones and quartzites

Beaver River sandstones and quartzites are oil stained and porous. Calcite and salts may be secondary. $CePO_4$ and $CeCO_3$ occurs as micronodules and are probably alteration products. There are also some hematite and pyrite. In some parts of the sandstone sequence, Fe oxy-hydroxides may be as high as 10 per cent, giving the rocks a brown colour.

Au-bearing minerals were identified in the Beaver River sandstones and quartzites, both in polished thin sections and on freshly broken surfaces. Au phases, including native Au (1-5 μm), Au+Ag, and Au+Cd alloys, are less abundant than in the Beaverhill Lake limestones. Other metallic minerals observed include Ag, Cd+Pb, Cu, Cu+Zn, Sb_2O_3, and SnO_2.

DISCUSSION OF SEM OBSERVATION

Similarities of mineralization in the different rock units

Alteration and metallic mineralization of the four different rock units show some similarities. They all contain Ce-bearing minerals, salts (NaCl and KCl), calcite, quartz, and clay. A unique metallic element association, including Au, Ag, Cu,

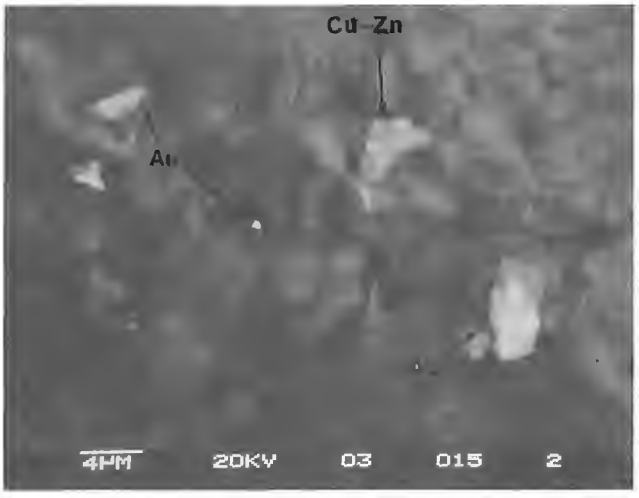
Cu-Zn
Au
4PM 20KV 03 015 2

A

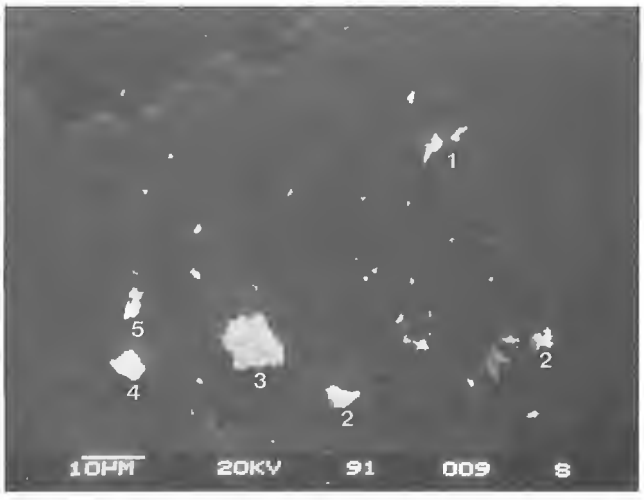
1
5
4
3
2
2
10PM 20KV 91 009 S

B

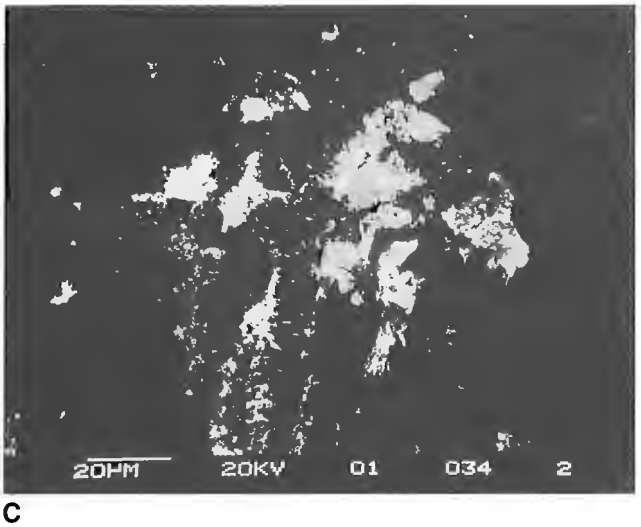
20PM 20KV 01 034 2

C

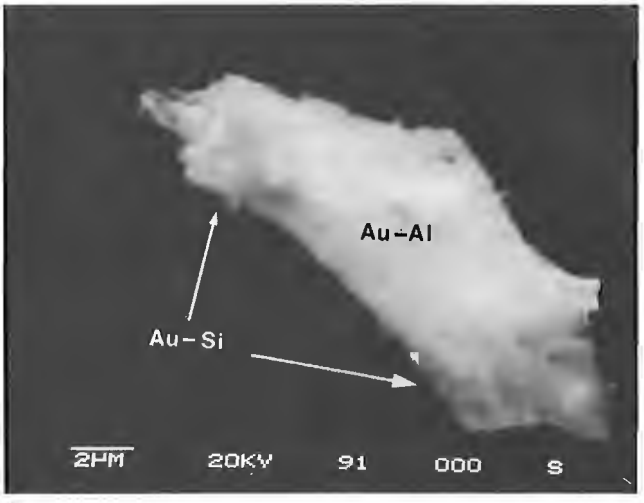
Au-Al
Au-Si
2PM 20KV 91 000 S

D

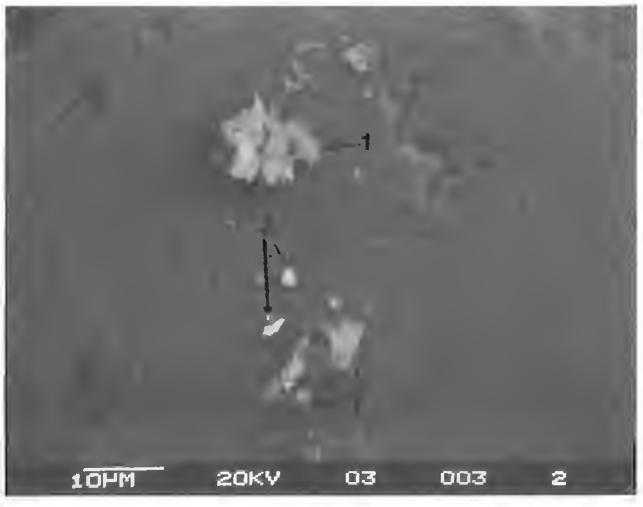
1
10PM 20KV 03 003 2

E

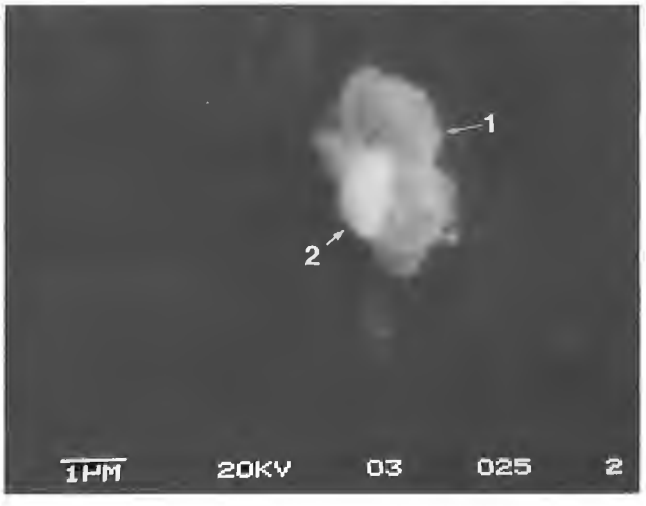
1
2
1PM 20KV 03 025 2

F

Zn, Pb, Sb, Sn, Cd, Bi, and W, occurs in finely disseminated form in all four rock units. All rock units lack sulphide except for some pyrite. Metallic minerals mainly occur as alloys (e.g., Cu and Cu+Zn), oxides (e.g., Sb_2O_3), chlorides (e.g., AgCl and $PbCl_2$), and carbonates (e.g., Pb-carbonate). Au, Ag, and Cu mineralization is related to calcite, clay, quartz, hematite, and salt alteration. All these features suggest that alteration and mineralization in the different rock units may have been caused by similar fluid processes.

The slight difference in the degree of alteration and mineralization in the various rock units may reflect different physical-chemical conditions in the different host rocks. Pb and Ag chlorides and pyrite are relatively more abundant in altered granitoids near the "Granite Wash" than in the sedimentary rocks above. The form of Au minerals is also slightly different among the different rock units. In the altered granitoids, Au+Si is associated with native Au, while in the limestone, Au+Ca and Au+Al are associated with native Au, probably reflecting host-rock composition.

Forms of Au-bearing minerals

Detailed EDS study indicates that Au+Ca, Au+Al, and Al+Si grains in granitoids and sediments have little or no oxygen, which rules out the possibility that these mixtures are oxides or carbonates. Instead, Au may alloy with Ca, Al, and Si. These types of Au alloys do not appear to have been previously reported in the literature, and their chemical properties are unknown. Another important Au form is related to halide salts. Au in the sediments shows associations with salts, and Au-bearing grains were found to have Au+Cl+K+Na EDS peaks, suggesting that they may be in the form of chlorides. However, the proportion of Au-chlorides to total Au is unknown, since some Au-chlorides may be submicron in size and not detected by SEM. Au-chlorides are soluble even in cold water and may be volatile at less than 300°C. This form of Au could easily be lost because of inapproprite assay methods. The combined effects of novel forms of Au mineralization and the presence of hydrocarbons and salts in the sediments may in part account for the non- reproducible assay results for gold.

Figure 5.

A. Association of Au and Cu-Zn grains on a fresh broken limestone surface (F20).

B. A group of Au-bearing grains: (1) Ag+Ca+Au; (2) Au; (3) Ag+Au; (4) Si+Au+Ca; and (5) Au+Cd in a polished thin section of limestone (Au grains >15; RR-40).

C. Au and Au-Fe-Cd-Cu-Cr-Ni alloys occur near a cavity in the limestone and in fractures (T2-25.75, core). The left corner shows a Au scratch mark during polishing.

D. Zoned Au-bearing grain. At the two ends, the shaded parts are Au+Si, the bright centre is Au+Al (RR-40).

E. Au-bearing aggregate consisting of two parts on a polished limestone surface. Less bright part (1) is Ca+Al+Si+K+Cl+Au (less Au) and bright part (2) is Au+Ca+Al+Si+K+Cl (more Au) (Au grains >200; F18).

F. A zoned Au-bearing grain in limestone: the less bright rim (1) is Ca+Au, the bright core is Au+Ca (Au grains >200; F02).

Physical-chemical conditions of ore-forming solution

A unique alteration feature is the widespread occurrence of Ce-bearing minerals in all rocks. Ce can only be decoupled from other rare-earth elements (REE) under relatively oxidizing conditions when it is removed as Ce^{4+}. This is consistent with abundant hematite and Fe-Ni-Cr oxide minerals, both of which are indicators of high Eh conditions. Calcite, salt, clay, and quartz as the main alteration minerals suggests that ore-forming solutions were enriched in Cl, CO_3^{2-}, Si, Na, and K. The presence of Au-, Ag-, Pb-, Bi-, Cu-, and Fe-chlorides, and the Au-salt association indicate that Cl is a major agent in the ore-forming solutions, indicating Cl-rich formation waters or brines as the mineralizing solution. The fact that most metallic minerals do not occur as sulphides, except for some pyrite, indicates that either S was not abundant in the ore-forming solution or ore-forming conditions were oxidized so that S existed in forms other than sulphide, or a combination of both. This is supported by the occurrence of a small amount of native S and barite.

The small grain size of the metallic and alteration minerals, their disseminated distribution, the alteration mineral associations, the wide distribution of soluble bitumen within host rocks, and burial reconstruction together indicate that the temperature of mineralization was probably not greater than 120°C. In the altered granitoids, alteration minerals associated with Ag, Pb, and probably Au mineralization are larger, probably indicating somewhat higher temperatures in the basement. The mineralization may be Cretaceous or younger, since Cretaceous Beaver River sandstones and quartzites were also mineralized, but conditions for transportation of metals by oxidized Cl-rich brines may have existed since the Middle Devonian and continue to the present day.

Au-Ag-Cu transportation and precipitation in the WCSB

Au, Ag, and Cu must have been enriched by some process to form a deposit. Therefore, the source, mobility, transport, and precipitation mechanisms of the metals must be addressed. The solubility of these metals in natural waters is mainly a function of Eh and fluid compositions (Maynard, 1983; Jaireth, 1992; Thornber, 1992, and references therein). According to these authors, Au, Ag, and Cu chloride, bromide, and iodide complexes are the most stable species in oxidized, neutral to acidic waters at low temperature. In the


EHT= 20.0 KV WD= 26 mm MAG= X 2.80 K PHOTO= 16
10.0µm
calcite+clay
Au,Cd
illite
chlorite

A

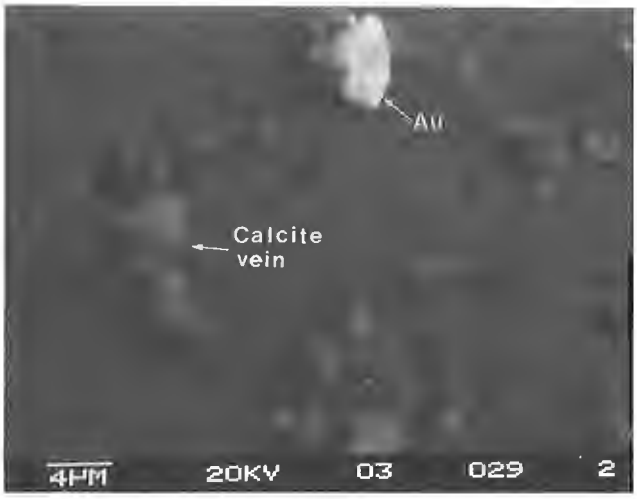
Au
Calcite
vein
4µM 20KV 03 029 2

B

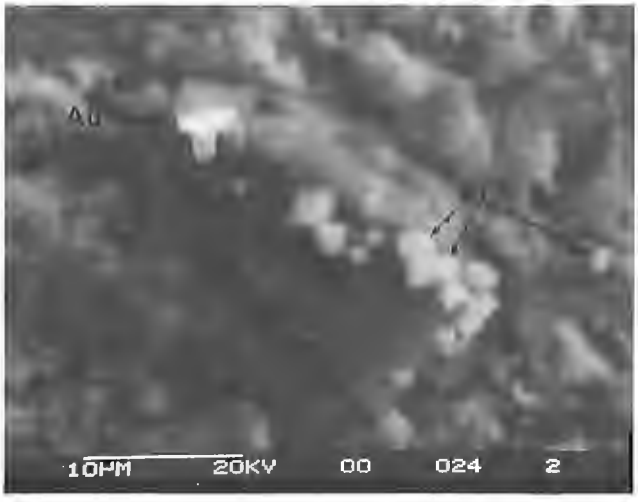
Au
10µM 20KV 00 024 2

C

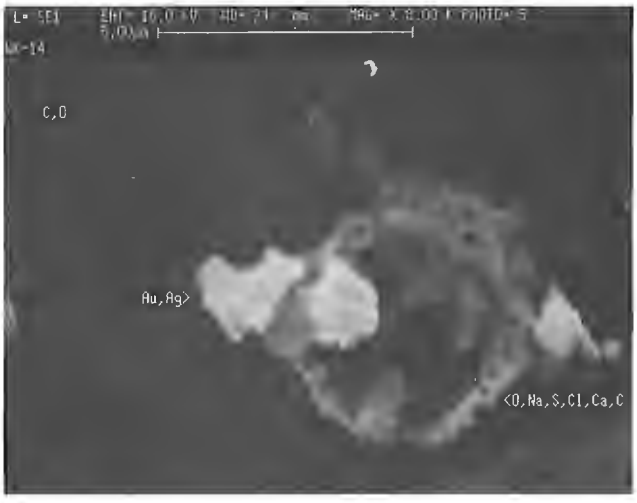
C,O
Au,Ag>
<O,Na,S,Cl,Ca,C

D

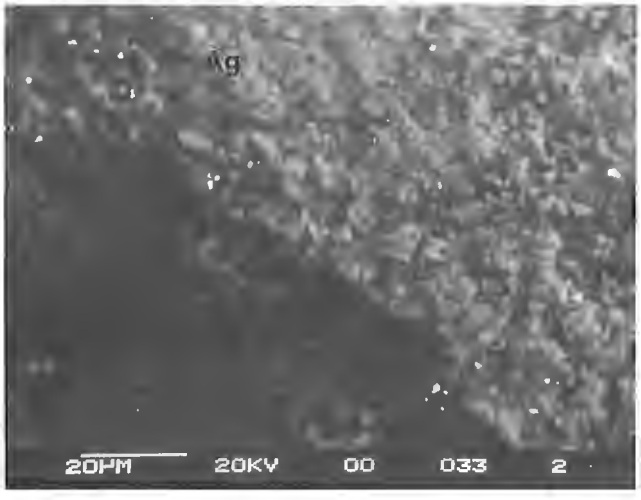
Ag
20µM 20KV 00 033 2

E

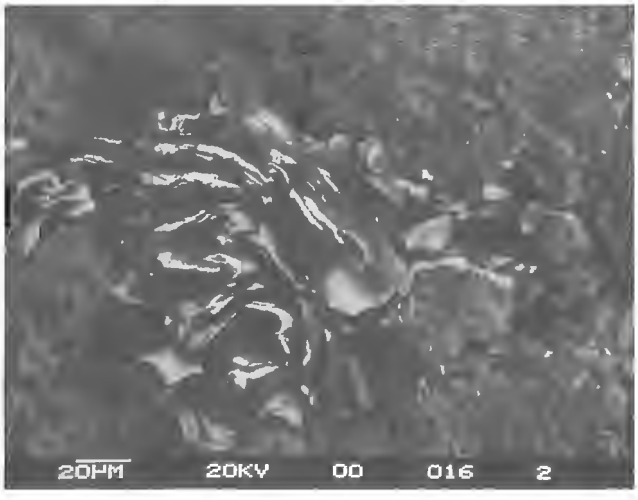
20µM 20KV 00 016 2

F

northeast Alberta Basin, formation waters contain abundant Cl, Br, and I, but relatively little or no H_2S (Hitchon et al., 1971; Hitchon, pers. comm., 1993). This makes Cl, Br, and I the most likely complexing agents to mobilize and transfer gold and other precious metals. However, these brines have relatively low Eh (Sverjensky, 1987; Hitchon, pers. comm., 1993), and Cl, Br, and I may not form soluble complexes with Au, Ag, and Cu (Maynard, 1983; Jaireth, 1992; Thornber, 1992). Sverjensky (1987) and Bloom et al. (1992) have calculated the chemical evolution of a saline brine during migration. If reducing formation waters react first with sulphate-rich evaporates and then with a typical redbed assemblage, oxygen fugacities well into the hematite (jarosite) field can be attained. Under these conditions, Au, Ag, Cu, and other metals are soluble as chloride complexes, and therefore may be leached from the redbed units or from basement rocks beneath (Jaireth, 1992; Thornber, 1992). This is supported by the fact that formation waters from the "Granite Wash" have higher Fe and Mn contents than those from other aquifers (Hitchon, pers. comm., 1993). The metals would precipitate from the solutions when encountering organic-rich layers, or mixing with brines with different Eh, pH, or salinities.

In the context of the regional hydrogeology of the formation waters in northeastern Alberta (Fig. 2), the generation of Au-Ag-Cu mineralization can be explained as follows. Formation waters or brines in aquifers beneath the Prairie Formation were oxidized during their updip migration through the redbeds and "Granite Wash" (Fig. 2). The resulting oxidized brine then leached gold and other metals from these rock units. The oxidized brines may also have circulated into the basement and leached gold there, subsequently circulating back to the basin through faults (Fig. 2). Owing to the impermeability of the Prairie Formation aquiclude, the ore-bearing brines could not flow vertically through the Prairie Formation salts, but rather flowed updip along the base of the Prairie Formation (Fig. 2). At the solution front of the Prairie Formation salts, vertical upward cross-formational flow became possible. Faults in the rocks further facilitated upward cross-formational flow (Fig. 2). When these ore-bearing, oxidized brines reached reducing environments in the overlying limestones and shales containing abundant organic matter, or when the brines mixed with other brines of different salinities and Eh-pH conditions, Au and other related metals precipitated and local mineralization took place.

In conclusion, the general geochemical environments and the possible genetic mechanism for the Au-Ag-Cu mineralization described here are very similar to those of so-called redbed Cu deposits and the unconformity-related Au-PGE-U mineralization in the South Alligator mineral field, Australia (Sverjensky, 1987; Eugster, 1989; Bloom et al., 1992). The discovery of Au-Ag-Cu mineralization signifies a great opportunity for extensive exploration of metallic minerals in the WCSB, which has been overlooked for almost one hundred years.

Figure 6.

A. Au+Cd micrograin, chlorite+illite, and calcite+clay aggregates occur within the same pore system in limestone, implying a genetic relationship (F02).

B. An Au+Ca grain occurs in the calcite veining network in limestone (F02).

C. An Au+minor Cl+K grain and a cluster of KCl cubes embedded in a NaCl+KCl+calcite mixture matrix (Au grains >10, AgCl grains >200; RR-43A).

D. Au+Ag alloys occur on top of matrix material with O+Na+S+Cl+Ca+C EDS peaks (gypsum+salt+organic matter). The gypsum+salt+organic matter aggregates have erupted out of a flat surface (WK-14, limestone).

E. AgCl micrograins in limestone (RR-43A).

F. Native Cu in limestone (sample A).

ACKNOWLEDGMENTS

This work was funded by the Alberta-Canada Mineral Development Agreement, and received funding and support in kind from the Alberta Geological Survey, Brougham GeoQuest Ltd., Focal Resources Ltd., NSR Resources, and Tintina Mines Ltd. Samples used in the study were provided by Focal Resources Inc., H.M.S. Properties Ltd., NSR Resources Inc., and Tintina Mines Ltd. The authors have benefitted from discussions with geologists from the above companies, especially S.F. Sabag of Tintina Mines Ltd. J. Wong and D. Walker are thanked for assistance in using SEM, and R. Davison, M. Fowler, and L. Snowdon for comments on the manuscript.

REFERENCES

Abercrombie, H.J. and Feng, R.
1994: Gold and PGE anomalies in Phanerozoic sedimentary rocks, northeastern Alberta - potential for new deposits (abstract); The Calgary Mining Forum, March 3-4, 1993, Program and Abstracts; Calgary Mineral Exploration Group Society, p. 51.

Anderson, G.M. and Macqueen, R.W.
1982: Mississippi Valley-type lead-zinc deposits; Geoscience Canada, v. 9, p. 108-117.

Bachu, S. and Underschultz, J.R.
1993: Hydrogeology of formation waters, northeastern Alberta Basin; American Association of Petroleum Geologists Bulletin, v. 70, p. 1745-1768.

Bloom, M.S., Gilbert, D.J., Gammons, C.H., and Wilde, A.R.
1992: Reaction path model for hydrothermal Au-PGE mineralization at Coronation Hill and similar deposits of the South Alligator Mineral Field, Australia; in Water-Rock Interaction, (ed.) Y.K. Kharaka and A.S. Maest; U.S. Geological Survey, p. 1569-1573.

Carrigy, M.A.
1959: Geology of the McMurray Formation, part III: General geology of the McMurray area; Research Council of Alberta, Geological Division, Memoir 1, 130 p.

Edwards, W.A.D.
1988: Metallic mineral occurrences and opportunities in Alberta; Geoscience Canada, v. 15, p. 109-112.

Eugster, H.P.
1989: Geochemical environment of sediment-hosted Cu-Pb-Zn deposits; Geological Association of Canada, Special Paper 36, p. 111-126.

Giusti, L.
1986: The morphology, mineralogy, and behaviour of "fine-grained" gold from placer deposits of Alberta: sampling and implications for mineral exploration; Canadian Journal of Earth Sciences, v. 23, p. 1662-1672.

Hackbarth, D.A. and Nastasa, N.
1979: The hydrogeology of the Athabasca oil sands area, Alberta; Alberta Research Council, Bulletin 38, 39 p.

Hamilton, W.N.
1971: Salt in East-Central Alberta; Research Council of Alberta, Bulletin 29, 53 p.

Hitchon, W.N., Billings, G.K., and Klovan, J.E.
1971: Geochemistry and origin of formation waters in the Western Canada Sedimentary Basin-III: factors controlling chemical composition; Geochimica et Cosmochimica Acta, v. 33, p. 1321-1349.

Jaireth, S.
1992: The calculated solubility of platinum and gold in oxygen-saturated fluids and the genesis of platinum and gold mineralization in the unconformity-related uranium deposits; Mineralium Deposita, v. 27, p. 42-54.

Martin, R. and Jamin, F.G.S.
1963: Paleogeomorphology of the buried Devonian landscape in Northeastern Alberta; in The K.A. Clark Volume, a collection of papers on the Athabasca Oil Sands, (ed.) M.A. Carrigy; Research Council of Alberta, Information Series No. 45, p. 31-42.

Maynard, J.B.
1983: Geochemistry of sedimentary ore deposits; Springer-Verlag, New York, 305 p.

Meijer Drees, N.C.
1986: Evaporitic deposits of Western Canada; Geological Survey of Canada, Paper 85-20, 118 p.

Ross, G.M., Parrish, R.R., Villeneuve, M.E., and Bowring, S.A.
1991: Geophysics and geochronology of the crystalline basement of the Alberta basin, Western Canada; Canadian Journal of Earth Sciences, v. 28, p. 512-522.

Sverjensky, D.A.
1987: The role of migrating oil-field brines in the formation of sediment-hosted Cu deposits; Economic Geology, v. 82, p. 1130-1141.

Thornber, M.R.
1992: The chemical mobility and transport of elements in the weathering environment; in Regolith Exploration Geochemistry in Tropical and Subtropical Terrains, (ed.) C.R.M. Butt and H. Zeegers; Commonwealth Scientific and Industrial Research Organization, p. 79-96.

Geological Survey of Canada Project 890053

Characterization of gold and PGE-bearing placer concentrates from the North Saskatchewan River, Edmonton, Alberta[1]

D.C. Harris and S.B. Ballantyne
Mineral Resources Division

Harris, D.C. and Ballantyne, S.B., 1994: Characterization of gold and PGE-bearing placer concentrates from the North Saskatchewan River, Edmonton, Alberta; in Current Research 1994-E; Geological Survey of Canada, p. 133-139.

Abstract: Electron microprobe and scanning electron microscope analyses show that the principal PGMs are Pt-Fe alloys, Os-Ir-Ru alloys, rare native platinum, hongshiite, and sperrylite. The Pt-Fe alloys occur mainly as platelets, rarely as spheres, and as rods. Their (Fe, Cu, Ni) content ranges from 10 to 32 at.%, with minor to trace amounts of Os, Ir, Rh, Pd, and Ru; inclusions consist of chalcopyrite, bornite, osmium, cooperite, irarsite, hollingworthite, laurite, and several unidentified sulphide, arsenide, telluride, and antimonide phases. The Os-Ir-Ru grains are of a size similar to those of the Pt-Fe alloys and plot in the osmium, iridium, ruthenium, and rutheniridosmine compositional fields.

Gold grains occur in a variety of shapes and sizes. Their chemical composition ranges in fineness from 550 to 950+ (electrum and native gold). Amalgamation with mercury was observed in many grains.

Résumé : Des analyses effectuées à l'aide de la microsonde électronique et du microscope électronique à balayage indiquent que les principales formes des métaux du groupe du platine sont les alliages Pt-Fe, les alliages Os-Ir-Ru, le platine natif (rare), l'hongshiite et la sperrylite. Les alliages Pt-Fe se présentent surtout sous forme de plaquettes, de sphères (rarement) et de bâtonnets. Leur contenu en Fe, Cu et Ni varie de 10 à 32 p. 100, avec de petites quantités ou des traces des éléments suivants : Os, Ir, Rh, Pd et Ru. Les inclusions qu'on y observe sont de chalcopyrite, de bornite, d'osmium, de coopérite, d'irarsite, d'hollingworthite, de laurite et de plusieurs phases non identifiées de sulfure, d'arséniure, de tellurure et d'antimoniure. Les grains des alliages Os-Ir-Ru ont des dimensions semblables à ceux des alliages Pt-Fe; ils se trouvent dans les champs de composition de l'osmium, de l'iridium, du ruthénium et de la ruthéniridosmine.

Les grains d'or se présentent sous diverses formes et dimensions. Du point de vue chimique, leur titre varie de 550 à 950+ (électrum et or natif). On a observé leur fusion avec le mercure dans de nombreux grains.

[1] Contribution to Canada-Alberta Agreement on Mineral Development (1992-1995), a subsidiary agreement under the Canada-Alberta Economic and Regional Development Agreement.

INTRODUCTION

The association of platinum with placer gold was first reported from the North Saskatchewan River near Edmonton, Alberta, by Hoffmann in 1893 and 1895. Morphological features of the gold (Guisti, 1986) and an electron microprobe study of some Alberta placer gold grains have been documented by Guisti and Smith (1984). These studies involved characterization of 435 placer gold grains from both the North Saskatchewan and Athabasca Rivers. Guisti (1983) reported the discovery of Pt-Fe and Os-Ir alloy nuggets, up to 400 µm in size, at the Groat Bridge in Edmonton. These nuggets gave a composition of 88-93.15 wt.% Pt, 3.93-8.69 wt.% Fe, and approximately 3 wt.% Rh. Bi (1993) and Bi and Morton (1993) investigated the platinum-group minerals (PGMs) associated with gold which were found within Pleistocene sediments in the Onoway area, approximately 50 km northwest of Edmonton. They report that in their samples, all the PGMs are the Pt-Fe alloy isoferroplatinum with some Os-Ir-Ru inclusions.

Morton et al. (1993) report that there are presently no major placer gold mining activities in the rivers of Alberta. This lack of mining activity is due to (1) too low a concentration of gold to support a commercial operation; (2) government regulations that now prevent large-scale mining operations in order to protect the province's drainage systems. However, individuals with tiny sluice boxes are permitted to recover gold from rivers. Other sources of recovered gold are from various land-based sand and gravel aggregate operations. In the Edmonton region, placer and paleoplacer deposits are commonly referred to as gold-platinum deposits because of the recovery of minor amounts of associated platinum-group element (PGE) alloys. Since so little has been done on the characterization of PGMs in the placers of Alberta, our current studies focus on the nature and distribution of these PGE alloys. Investigations are partly funded by the contribution to Canada-Alberta Agreement on Mineral Development (1992-1995).

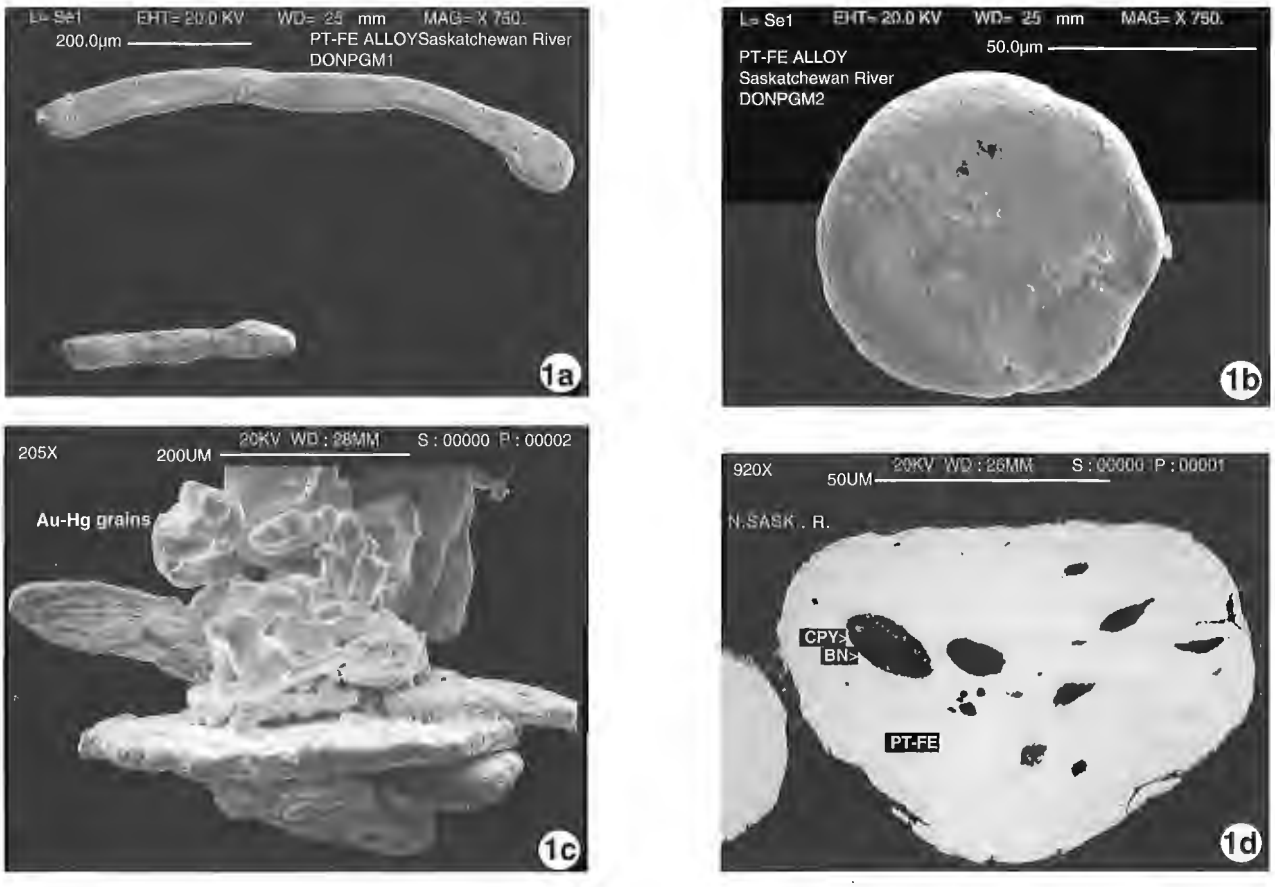

Figure 1.

a. *SEM photomicrograph of Pt-Fe alloy rods.*

b. *SEM photomicrograph of a Pt-Fe alloy sphere.*

c. *SEM photomicrograph of mercury-rich gold grains. The crystals within the cluster are Au-Hg alloys.*

d. *Backscattered electron image of a Pt-Fe alloy with inclusions of bornite and chalcopyrite.*

SOURCE OF MATERIAL

Materials used in this detailed study consist of: (1) panned heavy mineral concentrates of gold and PGMs, which were collected by Mr. Frank Scheibein from the North Saskatchewan River near the Capilona Bridge within the City of Edmonton and donated by Mr. Scheibein; (2) a gold concentrate (#12106) and a PGM (#5611) concentrate from the North Saskatchewan River, which were collected and donated in 1891 by Mr. M. Pearce and are curated in the National Mineral Collection Systematic Reference Series at the Geological Survey of Canada.

PRESENT STUDY

The gold-platinum concentrates were initially examined under a binocular microscope in order to characterize the various phases based on shape, size, and colour. A number of these particular grains were selected for detailed morphological SEM study. By far the largest number of grains were mounted in cold-setting araldite resin, polished with diamond paste on cloth laps, and examined under the reflecting microscope. These particular grains were then chemically analyzed quantitatively by electron microprobe and, where required, were further characterized by SEM energy dispersive (EDS) analyses. The electron microprobe utilized is a CAMECA SX-50 probe fitted with four wavelength dispersive spectrometers (WDS) and one EDS spectrometer. The EDS

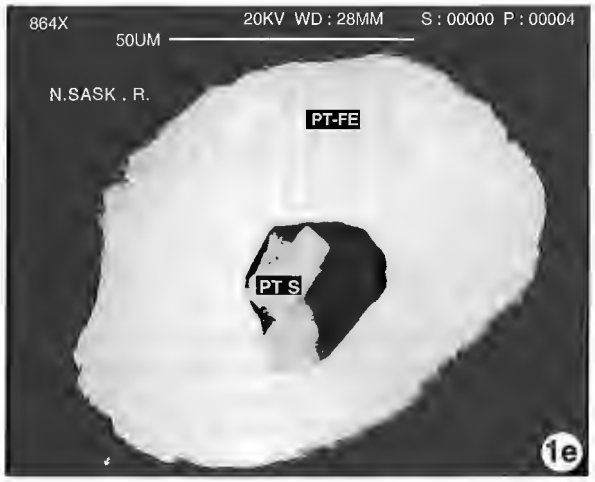

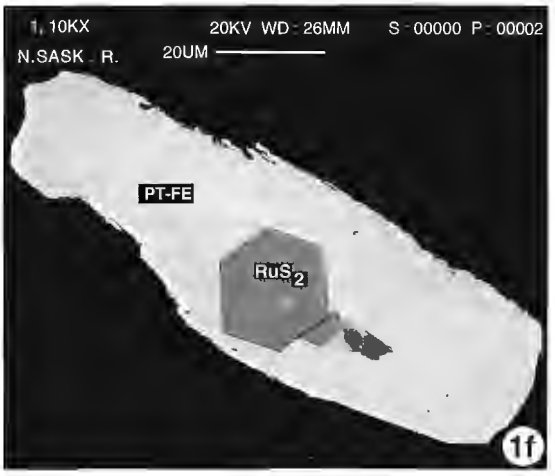

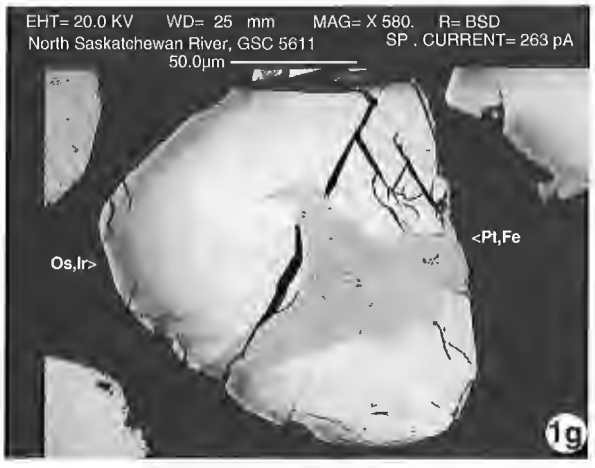

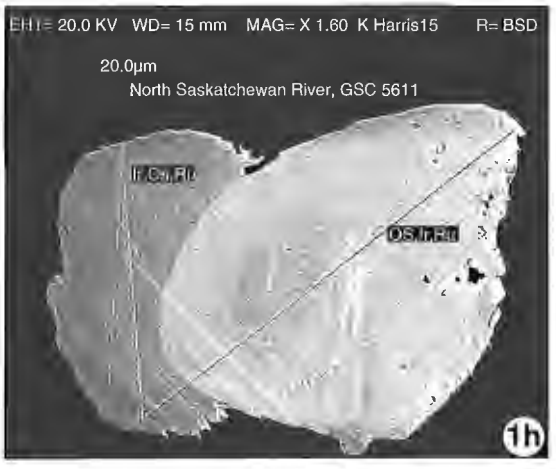

Figure 1. *(cont.)*

e. Backscattered electron image of a Pt-Fe alloy with an euhedral and fractured grain of Pt-S in a Cu-Fe-S + Fe-Ni-S matrix.

f. Backscattered electron image of a Pt-Fe alloy with an euhedral inclusion of laurite (RuS_2) and a rounded inclusion of Rh,Ir,Os,As,S. Attached to the laurite is a Pd-Te phase.

g. Backscattered electron image of an intergrowth of Pt-Fe and Os-Ir-Ru alloys.

h. Backscattered electron image of coexisting osmium and iridium.

spectrometer was used only for qualitative evaluation of the various phases. Two analytical routines with operating conditions of 20 kv and 20 na were used for the WDS quantitative analyses. For the gold grains and related phases, a 12-element routine consisting of Au Mα (metal), Ag Lα (metal), Hg Mβ (HgS), Sb Lα ($Cu_{11}FeSb_4S_{13}$), Cu Kα ($CuFeS_2$), Fe Kα ($FeAs_2$), Te Lα (metal), Sn Lα (metal), Pb Mα (PbS), Pd Lα (metal), Ni Kα (metal), and Mn Kα (metal) was used. For the PGE alloys, a 15-element routine consisting of Pt Lα (metal), Os Mα (metal), Ir Lα ($^{60}Ir^{40}Rh$), Ru Lα (metal), Rh Lα ($^{60}Ir^{40}Rh$), Pd Lα (metal), Au Mα (metal), Ag Lα (metal), Fe Kα ($FeAs_2$), Cu Kα ($CuFeS_2$), Ni Kα (NiSb), As Kα ($FeAs_2$), Sb Lα (NiSb), Te Lα (metal), and S Kα ($CuFeS_2$) was used. Where required, X-ray powder diffraction was used to identify the Pt-Fe alloys. Complex intergrowths of interior phases and inclusions were documented and characterized by SEM backscattered electron images and EDS analysis.

RESULTS

Platinum-group minerals

Of the platinum-group minerals (PGM), Pt-Fe and Os-Ir-Ru alloys are by far the most common discrete phases. However, rare native platinum, hongshiite (PtCu), sperrylite ($PtAs_2$), and composite grains of the Pt-Fe and Os-Ir-Ru alloys are also present.

Pt-Fe alloys

Pt-Fe alloys are the most abundant and occur as platelets up to 400 μm in diameter, as rods up to 600 μm in length (Fig. 1a), and as spheres less than 100 μm in size (Fig. 1b). Electron microprobe analyses determined that the (Fe,Cu,Ni) content of these alloys varies from 10 to 31 at.% in the Scheibein concentrate (Fig. 3) and from 10 to 32 at.% in the GSC concentrate (Fig. 2). Minor to trace amounts of Os, Ir, Rh, Pd, Ru and Cu were detected in most of the grains. The maximum concentrations are as follows: Os 10.2 wt.%, Ir 23.0 wt.%, Rh 7.3 wt.%, Pd 12.9 wt.%, Ru 4.4 wt.%, and Cu 4.8 wt.%. Ni is generally below the limit of detection (0.15 wt.%), but a few grains contain as much as 0.9 wt.%. Inclusions of variable size and shape were noted in several Pt-Fe alloys (Fig. 1d, e, f, g, h). They have been identified by ore microscopy and SEM-EDS as chalcopyrite, bornite, osmium, cooperite (PtS), irarsite (IrAsS), hollingworthite (RhAsS), laurite (RuS_2), and unidentified phases of Fe-Ni-S, Rh-Ir-As-S, Pd-Rh-Ni-S, Rh-Cu-S, Pd-As, Pd-Te, Pd-Sb, Pt-Rh-As-S, and Rh-S. In contrast to the North Saskatchewan River samples of this study, Bi (1993) reports that the Pt-Fe alloys (isoferroplatinum) from the Onoway locality contain only the five elements Pt, Rh, Fe, Cu, and Ni and only inclusions of Ir-Os-Ru as small exsolution laths. Following the nomenclature of Cabri and Feather (1975), isoferroplatinum (Pt_3Fe) is an ordered primitive cubic mineral, whereas ferroan platinum is a disordered face-centered cubic mineral. Unless one has X-ray confirmation of the cell type, the general name "Pt-Fe alloy" should be used, even if the electron microprobe composition corresponds to the ideal formula Pt_3Fe. As illustrated in Figures 2 and 3, the Pt-Fe alloys have a wide range of compositions, some of which correspond to Pt_3Fe (25 at.% Fe,Cu,Ni). X-ray powder pattern identification of two grains, corresponding in composition to Pt_3Fe, gave

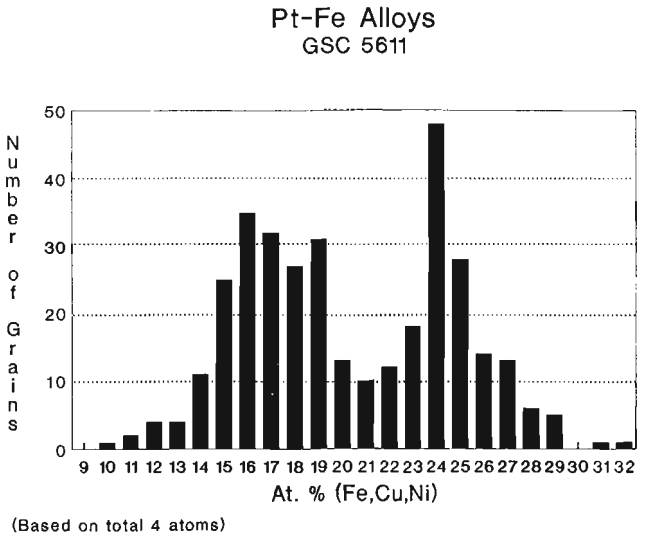

Figure 2. Electron microprobe analyses of Pt-Fe alloys from the North Saskatchewan River in a PGM concentrate housed in the National Mineral Collection Systematic Reference Series, Geological Survey of Canada. This concentrate was collected in 1891.

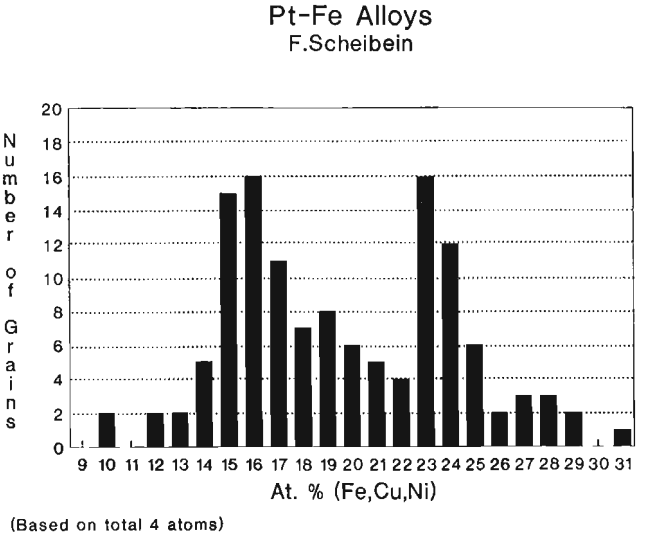

Figure 3. Electron microprobe analyses of Pt-Fe alloys from the North Saskatchewan River in a PGM concentrate collected and donated for this study by Mr. Frank Scheibein.

the disordered face-centered cubic cell of ferroan platinum. Based on the wide range of compositions and the X-ray powder diffraction results, the Pt-Fe alloys of the North Saskatchewan River appear to be ferroan platinum. A noteworthy feature discussed by Cabri and Feather (1975) is that cold working (e.g. mineral beneficiation or fluvial transport) may produce a transformation of the ordered primitive cubic structure to the disordered face-centered cubic structure. This may account for all the Pt_3Fe alloys X-rayed in this study being the disordered face-centered cubic ferroan platinum; we feel, however, that further careful studies of Pt-Fe alloys from other localities are warranted.

Native platinum

Two grains corresponding to native platinum were analyzed in the Scheibein concentrate. One grain gave a composition of pure platinum whereas the second grain contained 15.4 wt.% Ir. Two platinum grains were also analyzed from the GSC concentrate and contained 9.2, 11.0 wt.% Ir and 4.0, 5.6 wt.% Os, respectively.

Other platinum-group alloys

A Pt-Cu alloy, corresponding to the mineral hongshiite (PtCu), was analyzed in both the Scheibein and GSC concentrates and an Ir-rich alloy with Fe 10.5 wt.%, Ni 2.7 wt.%, and Pt 4.7 wt.% was analyzed in the Scheibein concentrate.

Os-Ir-Ru alloys

The Os-Ir-Ru alloys are the second most abundant PGMs in the samples. Bi (1993) made no mention of these alloys being present at the Onoway locality, except as inclusions in the Pt-Fe alloys. The size and shape of the Os-Ir-Ru alloys are very similiar to those of the Pt-Fe platelets. They are, however, more silvery in colour and a few grains actually exhibit good cleavage and hexagonal form. In polished section, these grains are whiter in colour than the Pt-Fe alloys and have moderate anisotropism. When the section is carbon coated for electron microprobe analysis, the contrast between the Os-Ir-Ru grains and the Pt-Fe grains is much more enhanced, allowing for easier recognition. Compositions of the grains, as determined by electron microprobe analyses in the Scheibein and GSC concentrates, are shown in Figures 4 and 5, respectively. Using the revised nomenclature of Harris and Cabri (1991), the analyses of these grains plot in the compositional fields of the minerals osmium, ruthenium, ruthenirridosmine, and iridium.

Gold alloys

Historically, gold has been the principal element of interest in placer and paleoplacer recovery operations within the province of Alberta. Gold-bearing grains are more abundant than PGMs in the concentrates that we examined. They occur in a wide variety of shapes and sizes ranging from flattened nuggets to small spheres. They vary in colour from yellow to a tarnished iridescent purple-blue to silver. Electron microprobe analyses reveal a wide range of compositions grading from electrum to native gold. Gold grains considered pristine have a core composition that ranges from 550 to 950+ fineness; most of it is above 800 fineness (Figure 6). Grains generally show zoning from an Ag-enriched core through to a high fineness gold rim.

Guisti and Smith (1984) and Guisti (1986) also characterized gold grains from the North Saskatchewan River and their studies gave similiar results. Besides Ag, the most common element found within the gold grains is Hg. The amalgamation of mercury with the gold nuggets varies from a thin surface rim to irregular replacement to almost total replacement. In the latter case, the "gold" grain is actually an Au-Hg alloy or occasionally an Ag-Hg alloy. It should be noted that these grains can easily be mistaken for PGM grains in the heavy mineral concentrates. They have a bright silver

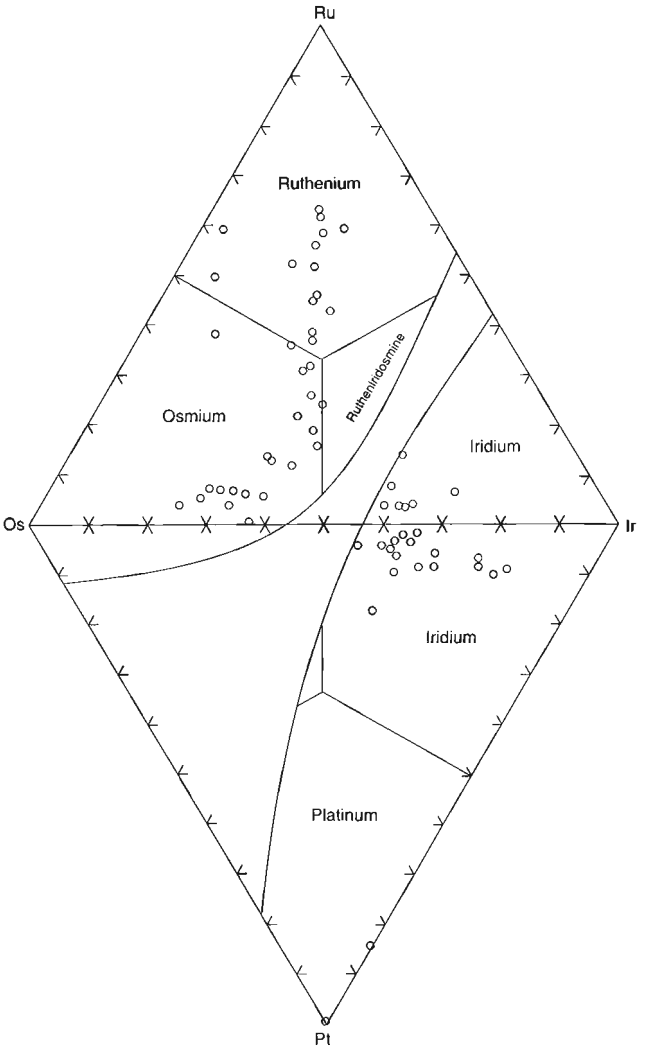

Figure 4. *Electron-microprobe analyses of Os-Ir-Ru alloys from the North Saskatchewan River in the PGM concentrate collected and donated by Mr. Frank Scheibein.*

colour, may occur as individual platelets, but occur more frequently as clusters of platelets and crystals (Figure 1c). In polished section, the grains have a porous surface and are extremely variable in composition. The highest mercury content alloyed with gold is 40.7 wt.%, which gives a composition close to Au_7Hg_5. The highest mercury content alloyed with silver is 51.9 wt.%, which gives a composition close to AgHg. An X-ray powder diffraction pattern of one such Au-Hg grain indicated a mixture of gold and Au_6Hg_5.

Other gold grain analyses reveal minor concentrations of Pt or Cu and Sn or Ni. Some homogeneous gold-PGE-bearing grains contain as much as 14.1 wt.% Pt, 8.0 wt.% Pd, and 4.0 wt.% Ag. The Cu-Sn-bearing grains are very inhomogeneous and it was difficult to obtain a representative analysis. Some grains present a discrete Ag-Hg-Sn-Cu phase. One gold grain was found to contain 17.2 wt.% Ni. The origin of these complex gold alloy grains is unknown. Mercury-enriched rims on some gold alloy grains may however be due to old placer operations or mill operations discharge as suggested by Guisti and Smith (1984).

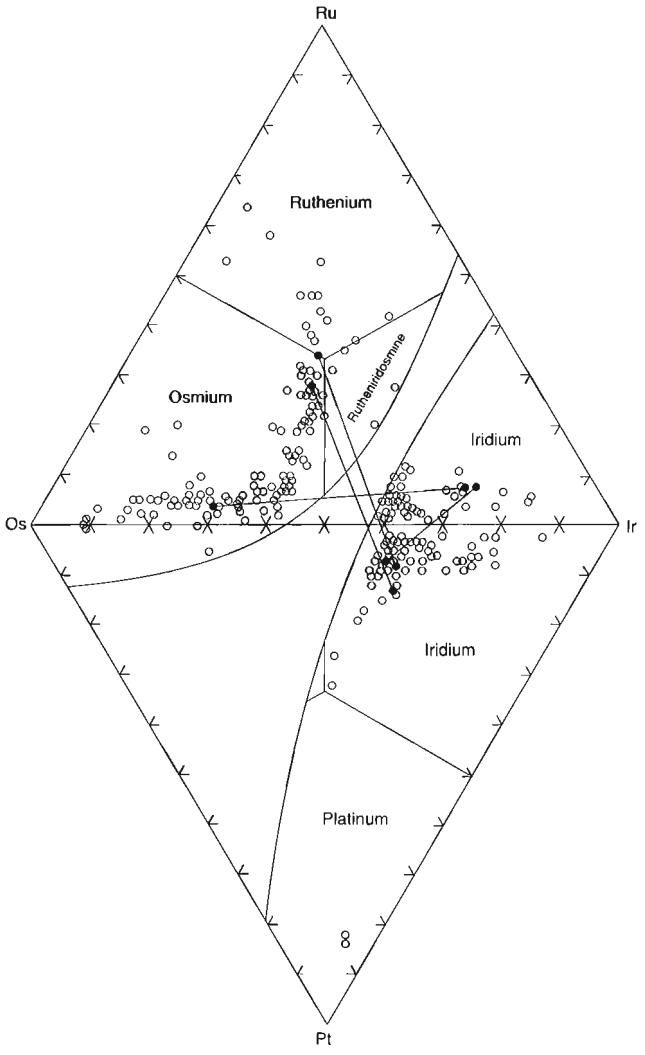

Figure 5. Electron microprobe analyses of Os-Ir-Ru alloys from the North Saskatchewan River in a PGM concentrate. These grains are housed in the National Mineral Collection Systematic Reference Series, Geological Survey of Canada. The compositions joined with a line represent coexisting optically distinct phases.

CONCLUSIONS

The principal platinum-group minerals found in placer concentrates from the North Saskatchewan River, Edmonton, Alberta are Pt-Fe alloys (ferroan platinum) and Os-Ir-Ru alloys. The compositions of the Os-Ir-Ru alloys are similar to those reported by Harris and Cabri (1973) from various British Columbia localities, e.g. Tulameen, Spruce Creek, Cariboo District, and Atlin. Because the compositions are so similar, it would appear that major element comparisons are not sufficient for geographic distinctions and trace element analyses by other micro-analytical techniques need to be explored.

However, the Pt-Fe alloys (ferroan platinum) are found to contain a wide variety of inclusions, which consist of PGE-bearing sulphides, base metal sulphides, PGE-bearing tellurides, antimonides, and arsenides, Os-Ir-Ru alloys and droplets of silicates.

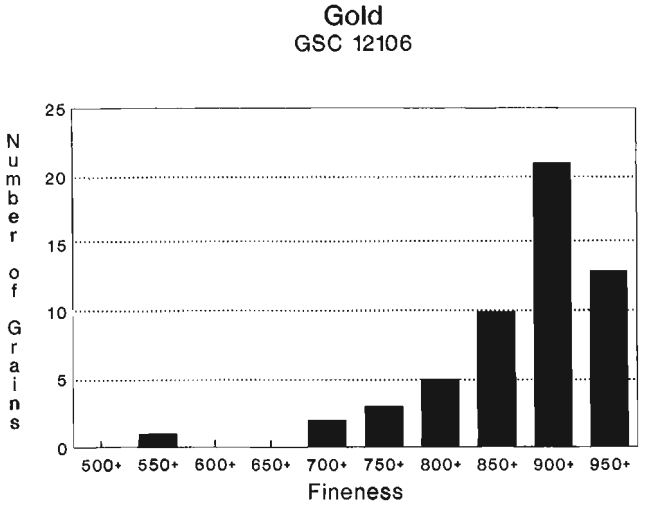

Figure 6. Electron microprobe analyses of gold grains from the North Saskatchewan River. These grains are housed in the National Mineral Collection Systematic Reference Series, Geological Survey of Canada and were originally collected in 1891. Fineness is Au / Au+Ag.

The associated gold grains show some contamination by mercury, which may be due to man-related activities. Some pristine gold grains contain Pt and Pd and these are considered to be natural; this suggests a common origin for the platinum-group minerals. Primary PGM enrichment is often clearly associated with mafic-ultrabasic intrusions (Alaskan type) or Alpine basic to ultrabasic rocks (ophiolite-complex type). Since these types of complexes are presently unknown in Alberta, derivation from a secondary source (i.e., paleoplacers) has been suggested as the source of the PGMs in the Pleistocene placers. Current studies are underway to explore the chemical composition of chromite and ilmenite associated with PGE-producing drainages in Alberta, in order to evaluate whether or not their source could be capable of preserving diamonds. If so, alluvial PGMs may be "indicator" minerals for kimberlite and lamproite fields within which some source rocks could be enriched in PGM-gold-diamonds.

Jedwab (1993) reported the occurrence of palladian gold, sperrylite, isoferroplatinum, palladoarsenide, cuproplatinum, and other PGE minerals in silicified dolostones of the Lower Roan of southwest Shaba (Zaire). Based on the mineralogy and textural relationships of these PGE minerals, Jedwab noted the prospects of a sedimentary PGE ore-type genetically connected with the evaporitic environment. Is it possible that the PGE minerals observed in this study within the province of Alberta have originated from a similiar type of environment?

ACKNOWLEDGMENTS

We wish to thank David Walker and Armand Tsai for assistance with the SEM studies, Andrew Roberts for X-ray powder-diffraction analysis, and the Cartography Section at the GSC for drafting and photography. The manuscript was critically read by Andrew Roberts.

REFERENCES

Bi, D.
1993: Platinum-group metals and extraterrestrial spherules in Pleistocene sediments in Alberta, Canada; Master of Science Thesis, Department of Geology, University of Alberta, 115 p.

Bi, D. and Morton, R.D.
1993: Platinum-iron alloys in Pleistocene placers from Alberta, Canada; Submitted to Mineralogy and Petrology.

Cabri, L.J. and Feather, C.E.
1975: Platinum-iron alloys: a nomenclature based on a study of natural and synthetic alloys; Canadian Mineralogist, v. 13, p. 117-126.

Guisti, L.
1983: The distribution, grades and mineralogical composition of gold-bearing placers in Alberta. Master of Science Thesis, University of Alberta.
1986: The morphology, mineralogy, and behaviour of "fine-grained" gold from placer deposits of Alberta: sampling and implications for mineral exploration; Canadian Journal of Earth Sciences, v. 23, p. 1662-1672.

Guisti, L. and Smith, D.G.W.
1984: An electron microprobe study of some Alberta placer gold; Tschermaks Mineralogische und Petrographische Mitteilungen, v. 33, p. 187-202.

Harris, D.C. and Cabri, L.J.
1973: The nomenclature of the natural alloys of osmium, iridium and ruthenium based on new compositional data of alloys from world-wide occurrences; Canadian Mineralogist, v. 12, p. 104-112.
1991: Nomenclature of platinum-group-element alloys: review and revision; Canadian Mineralogist, v. 29, p. 231-237.

Hoffmann, C.
1893: Geological Survey of Canada Annual Report, v. 5 , pt. 2, 1890-1891, 65R.
1895: Geological Survey of Canada Annual Report, v. 6, 1892-1893, 14R.

Jedwab, J.
1993: Palladium and platinum mineralogy of the evaporitic Lower Roan of SW Shaba, Zaire; TERRA NOVA abstract supplement no. 3, v. 5, p. 21-22. International Symposium on mineralization related to mafic and ultramafic rocks.

Morton, R.D., Bi, D., and Mussieux, R.
1993: Gold and platinum group element placer deposits of the North Saskatchewan River, Edmonton; Geological Association of Canada, Mineralogical Association of Canada, Joint Annual Meeting, 1993, Field Trip A-9, Guidebook, 11 p.

Geological Survey of Canada Project 680023

Borehole geophysics applied to mapping Paleozoic stratigraphy, Grand Rapids area, Manitoba

C.J. Mwenifumbo
Mineral Resources Division

Mwenifumbo, C.J., 1994: Borehole geophysics applied to mapping Paleozoic stratigraphy, Grand Rapids area, Manitoba; in Current Research 1994-E; Geological Survey of Canada, p. 141-149.

Abstract: Multiparameter geophysical measurements, including natural gamma-ray spectrometry, gamma-gamma density, resistivity, induced polarization (IP), magnetic susceptibility, temperature, and temperature gradient, were made in borehole M-6-91 in the Grand Rapids area of Manitoba. The stratigraphy intersected by M-6-91 consists of Silurian and Ordovician carbonate formations. The different Paleozoic carbonate formations are accurately mapped by their distinctive geophysical signatures. Argillaceous horizons that define some formation boundaries are characterized by relatively high radioactivity and can be easily detected on the total count gamma-ray log. The different formations, consisting mainly of dolomite, have distinctive densities and resistivities that proved useful in defining lithostratigraphic boundaries in zones without a prominent argillaceous marker horizon. There are slight variations in the natural gamma-ray count rate and IP response within the dolomites, and these variations are probably due to the presence of clay in the dolomites. Temperature logs show changes that indicate groundwater flow zones.

Résumé : Des mesures de plusieurs paramètres géophysiques, dont la spectrométrie à rayons gamma naturels, la densité gamma-gamma, la résistivité, la polarisation induite, la susceptibilité magnétique, la température et le gradient de température, ont été prises dans le trou de sondage M-6-91 foré dans la région de Grand Rapids au Manitoba. La stratigraphie traversée par le trou M-6-91 comporte des formations carbonatées d'âge ordovicien et silurien. Les différentes formations carbonatées paléozoïques sont cartographiées avec précision en utilisant leurs signatures géophysiques caractéristiques. Les horizons argileux qui définissent certaines limites de formation sont caractérisés par une radioactivité relativement élevée et ils peuvent être facilement détectées sur la diagraphie de rayons gamma à comptage total. Les différentes formations, composées surtout de dolomie, présentent des densités et résistivités distinctes qui se sont avérées utiles pour définir les limites lithostratigraphiques dans les zones sans horizon repère argileux marqué. Il existe de légères variations dans le taux de comptage des rayons gamma et la réponse de la polarisation induite au sein des dolomies, variations qui sont probablement dues à la présence d'argile dans les dolomies. Les diagraphies de la température indiquent des changements révélant des zones d'écoulement d'eau souterraine.

INTRODUCTION

The Manitoba Geological Services Branch drilled several holes in the Grand Rapids area (NTS 63F, 63K) to study the Paleozoic and Precambrian stratigraphy (Bezys, 1991, 1992, 1993). Some of these holes were kept open for hydrogeological and borehole geophysical measurements. Geological core logging in carbonate formations is sometimes difficult because the entire core appears to be quite similar. If the strata are without distinct horizons, such as structural or textural features, differences in the units can be difficult to see. In 1991, the Geological Survey of Canada (GSC) made multiparameter borehole geophysical measurements in stratigraphic hole M-6-91 at Cooks Cave Southeast, Grand Rapids, in order to define the Paleozoic stratigraphy. M-6-91 is a BQ-size hole (60 mm diameter), drilled to a total depth of 163.7 m and intersecting Precambrian granodiorite at 161.8 m.

STRATIGRAPHY AND LITHOLOGY

Hole M-6-91 intersected a Paleozoic carbonate sequence ranging in age from Ordovician to Silurian and comprised of dolomite, dolomitic mudstone, and argillaceous dolomitic mudstone. These dolomitic units overlies the Winnipeg Formation (shale and sandstone), which is underlain by Precambrian granodiorite. A description of the drill core geology (Bezys, 1993) is given in Figure 1, along with ages, formations, and members.

Silurian strata consist of the Interlake Group (East Arm, Atikameg, Moose Lake, Fisher Branch, and Upper Stonewall Formations). These various formations are defined by prominent argillaceous dolomitic mudstone units. The East Arm Formation is a crystalline brown to buff dolomite overlying the Atikameg Formation, which is a buff to yellow, vuggy dolomite. Porosity in the Atikameg Formation, estimated to be ~10%, may be due to fossil solutioning (Bezys, 1991). The Moose Lake Formation, an irregular laminated to mottled dolomite, is bounded above and below by argillaceous dolomitic mudstone beds. The lower argillaceous dolomitic mudstone, the U1-marker, forms the contact between the Moose Lake and Fisher Branch Formations. The Fisher Branch Formation is a fossiliferous, vuggy dolomite with porosity estimated to be 5-8%.

Ordovician carbonate beds include the Stonewall, Stony Mountain, and Red River Formations. The Stonewall Formation is subdivided into nine units (Figure 1), and is bounded by the Stonewall marker bed above and the Williams Member, an argillaceous dolomite unit, below. The argillaceous T-marker (unit 7) in the middle of the Stonewall Formation marks the Ordovician/Silurian boundary. The Stony Mountain Formation underlying the Williams Member consists of two major subdivisions: the Gunton Member, is a cherty, mottled, buff and grey nodular dolomite, and the Penitentiary Member, an argillaceous and slightly nodular dolomite. At the bottom of the Stony Mountain Formation is a transition bed consisting of mottled, crystalline dolomite with enhanced porosity due to fossil solutioning. The Red River Formation consists of the Upper Red River (Fort Garry Member), which is subdivided into five units, and the Lower Red River Formations. The Fort Garry Member is composed of interbedded argillaceous dolomite, calcitic dolomite, and massive dolomite. The Lower Red River Formation is a finely crystalline, massive, fossiliferous, slightly granular cherty dolomite.

Some of these formations are sources of industrial minerals. The Gunton Member of the Stony Mountain Formation and the Stonewall Formation are major sources of building stone (Bamburak, 1992). Geophysical measurements provide information on lithology and stratigraphy and may also yield information on the quality of the carbonate as a source of building stone.

GEOPHYSICAL MEASUREMENTS

Borehole geophysical measurements may detect changes in physical and chemical properties of rocks that are invisible to the geologist. These data complement observations made by examining cores. The GSC R&D logging system was used to acquire multiparameter borehole geophysical measurements in hole M-6-91. Measurements included self potential (SP), single point resistance (SPR), normal array resistivity, induced polarization, natural gamma-ray spectrometry, spectral gamma-gamma density, magnetic susceptibility, temperature, and temperature gradient. A brief description of the parameters measured follows.

Electrical resistivity of rocks depends on several factors. The most important factors affecting resistivity in carbonate rocks are fracturing, porosity, degree of saturation of pore spaces, and salinity of pore fluid. The presence of clay minerals may also have an affect. Argillaceous sediments containing conductive clay minerals may be detected on the resistivity and single point resistance log. Induced polarization measurements primarily respond to the presence of polarizable and conductive minerals such as base metal sulphides/oxides and graphite. There are no such minerals in the strata intersected by hole M-6-91. Variations in IP response in this hole are probably due to the presence of polarizable cation-rich clays such as illite and montmorillonite (Mwenifumbo, 1989).

Gamma-ray measurements detect variations in natural radioactivity originating from uranium (U), thorium (Th), and potassium (^{40}K) in rocks. Estimates of the equivalent concentrations of these three radioelements can be made from gamma-ray spectrometry measurements. Gamma-ray spectrometry measurements were taken in hole M-6-91. The low count rates recorded in the carbonates yield poor counting statistics that make it impossible to separate the different contributions from K, U, and Th in the spectra. Therefore, the gamma-ray log presented in this paper is the total count log (energy window, 0.3-3.0 MeV). In M-6-91, which intersects carbonates and argillaceous sediments, ^{40}K originating from clay minerals such as illite and montmorillonite is likely the principal source of natural gamma radiation. Variations in the concentrations of these minerals in carbonate rock make gamma-ray logs an important tool for lithological mapping and stratigraphic correlation.

Density response is primarily a function of rock bulk density, which depends on the mineralogical composition of the rock and on porosity and water saturation. In carbonate rocks, variations in porosity and possibly variations in magnesium content of dolomite are the primary causes of density variations.

Parameters affecting the temperature-depth profile in a borehole include drilling fluid circulation, variations in thermal conductivities of the rocks intersected, and ground water flow (Mwenifumbo, 1993). Dolomites and mudstones have distinctive thermal conductivities and can be distinguished on the temperature gradient profile, provided water is not moving in the borehole. Groundwater flow in the borehole from fractures and other porous zones produces easily detectable temperature anomalies that mask variations in the thermal conductivities of the formations.

Magnetic susceptibility measurements did not show any response.

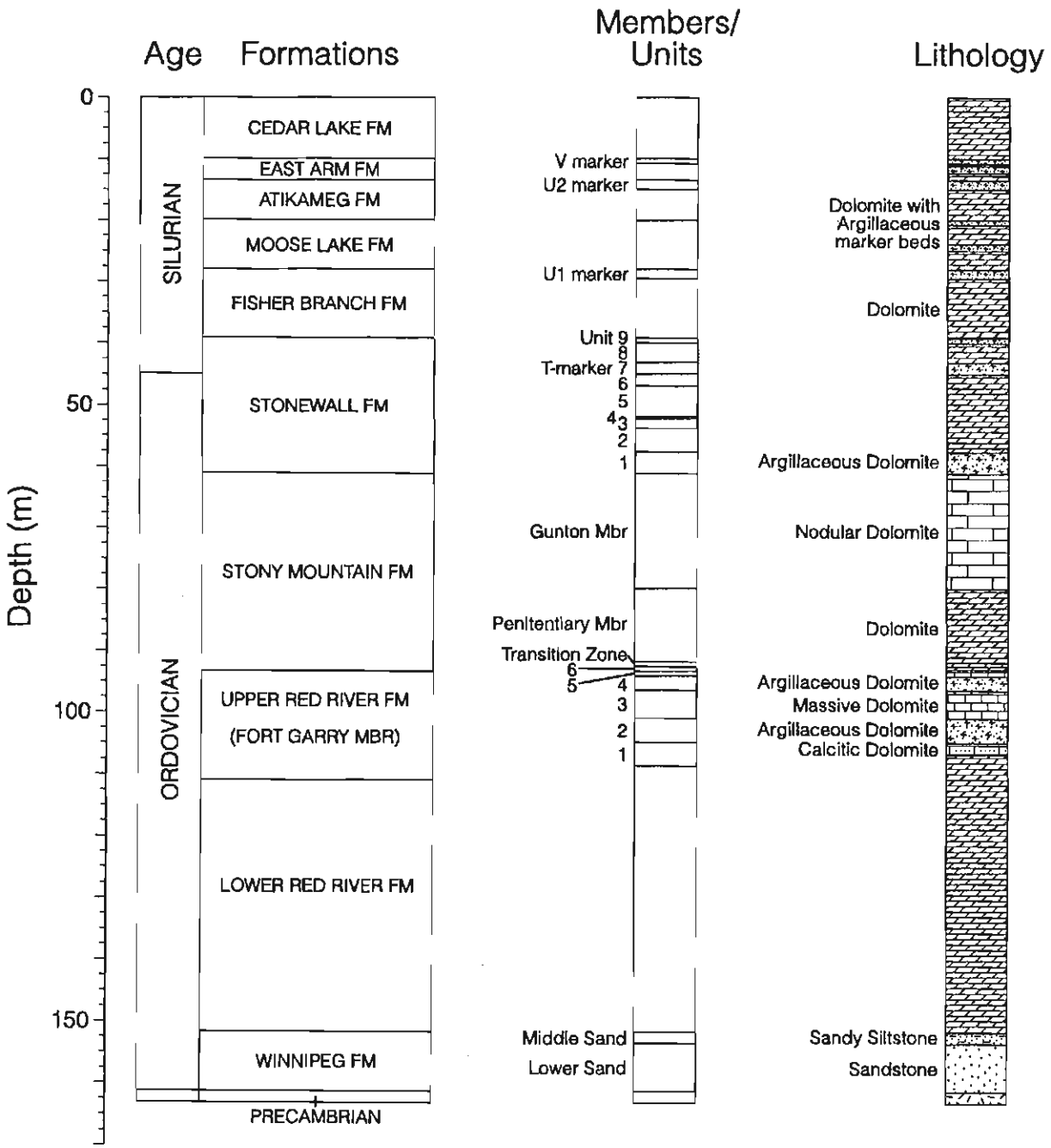

Figure 1. Summary of the stratigraphy and lithology intersected by hole M-6-91.

DISCUSSION OF RESULTS

Multiparameter borehole geophysical measurements acquired in hole M-6-91 are presented in Figures 2 and 3. Figure 2 shows lithology, gamma-ray, IP, resistivity, and density logs, and Figure 3, lithology, SPR, temperature gradient, and temperature logs (lithology is defined in Figure 1).

A distinctive, high gamma-ray response is associated with argillaceous dolomitic beds. These beds act as marker horizons and are used to determine the boundaries of the formation and/or member. They can be located on the gamma-ray log. A low gamma-ray response is observed from the carbonate formations. Three Silurian carbonate formations, the lower Moose Lake, Fisher Branch, and Stonewall Formations, are somewhat lower in gamma-ray activity than the underlying Ordovician carbonate formations. This suggests that these formations contain less clay minerals, and evidence of this is also seen in the lower IP response. The Stony Mountain and Lower Red River Formations have a slightly higher gamma-ray activity. Following this interpretation based on the gamma-ray log and other geophysical parameters, the drill core was re-examined and a more accurate stratigraphic sequence was constructed.

The IP log shows responses similar to gamma-ray activity in the dolomites, i.e. extremely low IP values in the Fisher Branch and Stonewall Formations correspond to extremely low gamma-ray activity. There is good positive correlation between IP and gamma-ray activity in the argillaceous dolomitic mudstones, with a notable exception, however, in unit 2 (101.2-105.1 m) of the Fort Garry Member where high gamma-ray activity is associated with a low IP effect. This suggests clay mineralogy different from that in the other argillaceous beds.

Resistivity and density logs show distinct responses in the various formations. Variations in these geophysical parameters in dolomites are mainly a function of variations in porosity. Resistivity and density show good positive correlation in the various formations except in the Penitentiary Member of the Stony Mountain Formation and the Fort Garry Member. Mean resistivities in these formations (Table 1) are lower than those of the overlying and underlying formations, and mean densities are higher.

Box-and-whiskers plots (Figures 4, 5, and 6) compare the distributions of density, resistivity, and IP parameters for the various formations intersected in hole M-6-91. They show how these geophysical parameters vary within the different formations. Both resistivity and density data indicate that the Moose Lake, Fisher Branch, and Stonewall Formations and the Gunton Member are significantly different. Resistivities and densities are quite variable within the Fort Garry Member as indicated by box spreads and whisker extensions. While box-and-whiskers plots are designed to compare median levels, they do not provide an accurate picture of the distribution of the parameters. The modality of the distributions is not apparent. Histograms provide a better graphical representation of how the parameters are distributed in the prescribed values. They provide information on whether the distributions consist of unimodal or multimodal populations. Figures 7 and 8 show histograms of the density and resistivity for six formations and members. The density distribution in the Fort Garry Member is bimodal while the resistivity is multimodal and shows a wide range of values.

From the geophysical measurements (refer to Figures 2 and 3), the Stonewall Formation can be subdivided into three major units, the upper unit consisting of geological units 6-9, the middle unit consisting of units 2-5, and the lower geophysical unit consisting of the Williams Member, an argillaceous dolomite. These units may correspond to the Upper Member, Middle Member, and Williams Member subdivisions (Bamburak, 1992). The Williams Member, an argillaceous and arenaceous dolomite, is characterized by higher density, higher resistivity, high IP effect, and higher gamma-ray activity. The Middle Member has the lowest gamma-ray activity and lowest resistivity of the three subdivisions. The Upper Member (39.5 to 46 m) consists of three argillaceous units that exhibit higher densities and lower resistivities than the Middle Member, except for the T-marker horizon.

The argillaceous T-marker bed that defines the Ordovician/Silurian contact is unique among the argillaceous marker beds; it has high natural gamma-ray activity, an anomalously low resistivity, and a corresponding high IP effect, but is higher in density. All other argillaceous marker beds show high radioactivity and high density, but the resistivity does not show a pronounced change relative to the dolomitic beds. In some areas of northern Manitoba the T-marker bed is rarely seen or absent (Bezys, 1991). Since the Silurian Stonewall beds have distinctly higher resistivities and densities than those observed within the Devonian Stonewall strata, it is possible to define the Ordovician/Silurian boundary using these geophysical parameters. The Silurian Stonewall geophysical response is similar to that of the Fisher Branch Formation.

The Gunton/Penitentiary Member contact within the Stony Mountain Formation was established from the drill core logs at 75.75 m. However, the geophysical logs indicate that this contact should be near 80 m, where there is a change

Table 1. Mean values of density, resistivity, and IP.

Formation/Member	Depth (m)	Density (g/cm³)	Resistivity (ohm-m)	IP (mV/m)
Moose Lake Fm	20-27	2.77	11148.00	4.33
Fisher Branch Fm	29-40	2.62	1246.00	2.42
Stonewall Fm	46-57	2.54	735.00	2.18
Stony Mountain Fm				
Gunton Mbr	62-80	2.74	3701.00	4.13
Penitentiary Mbr	80-92	2.78	1990.00	4.80
Red River Fm				
Forty Garry Mbr	92-108	2.74	1269.00	3.70
Lower Red River Fm	112-150	2.72	3213.00	5.06

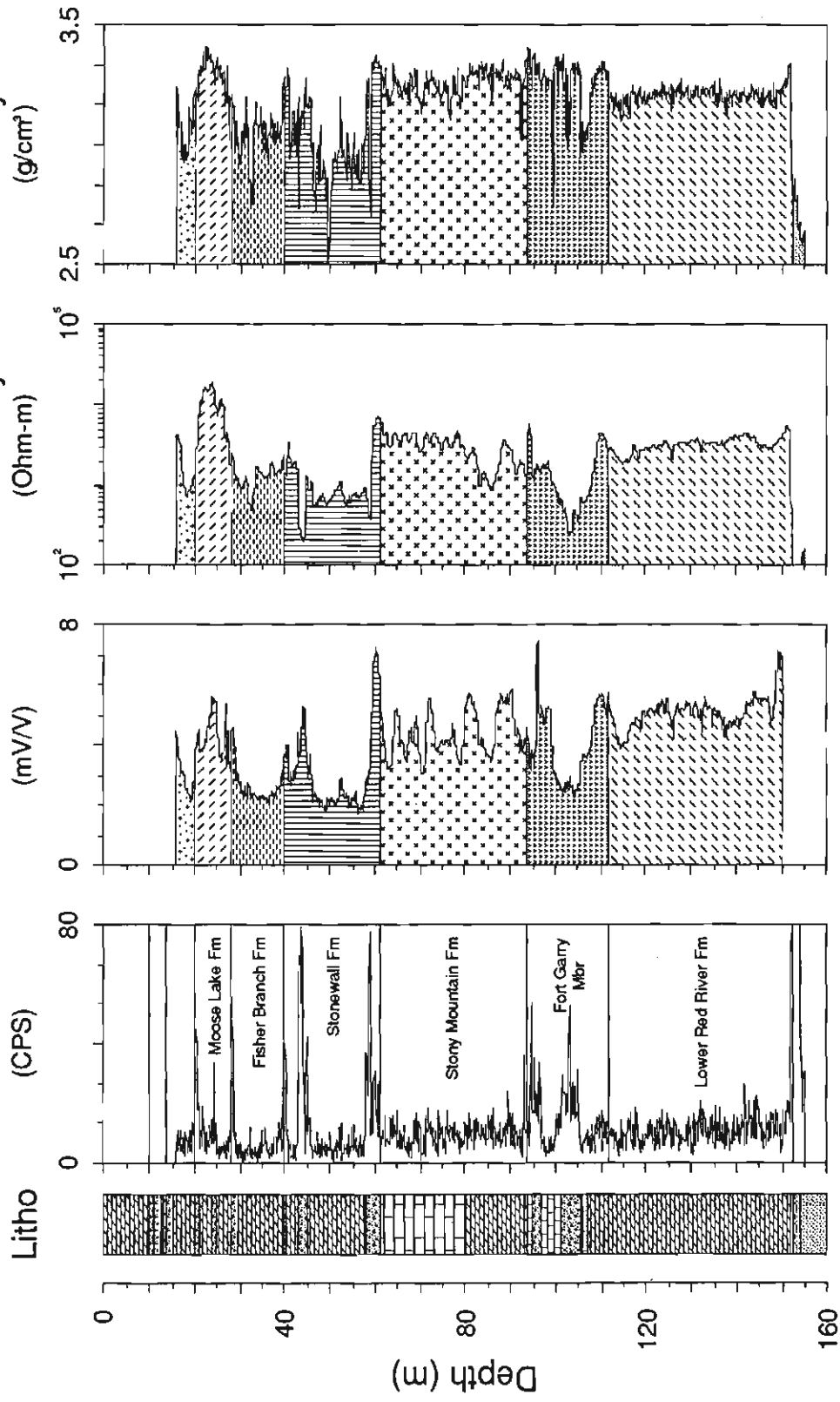

Figure 2. *Lithology, total count gamma-ray, IP, 40-cm normal array resistivity, and gamma-gamma density logs recorded in hole M-6-91. The shadings on each of the geophysical logs indicate the different formations. The lithology column is as indicated in Figure 1.*

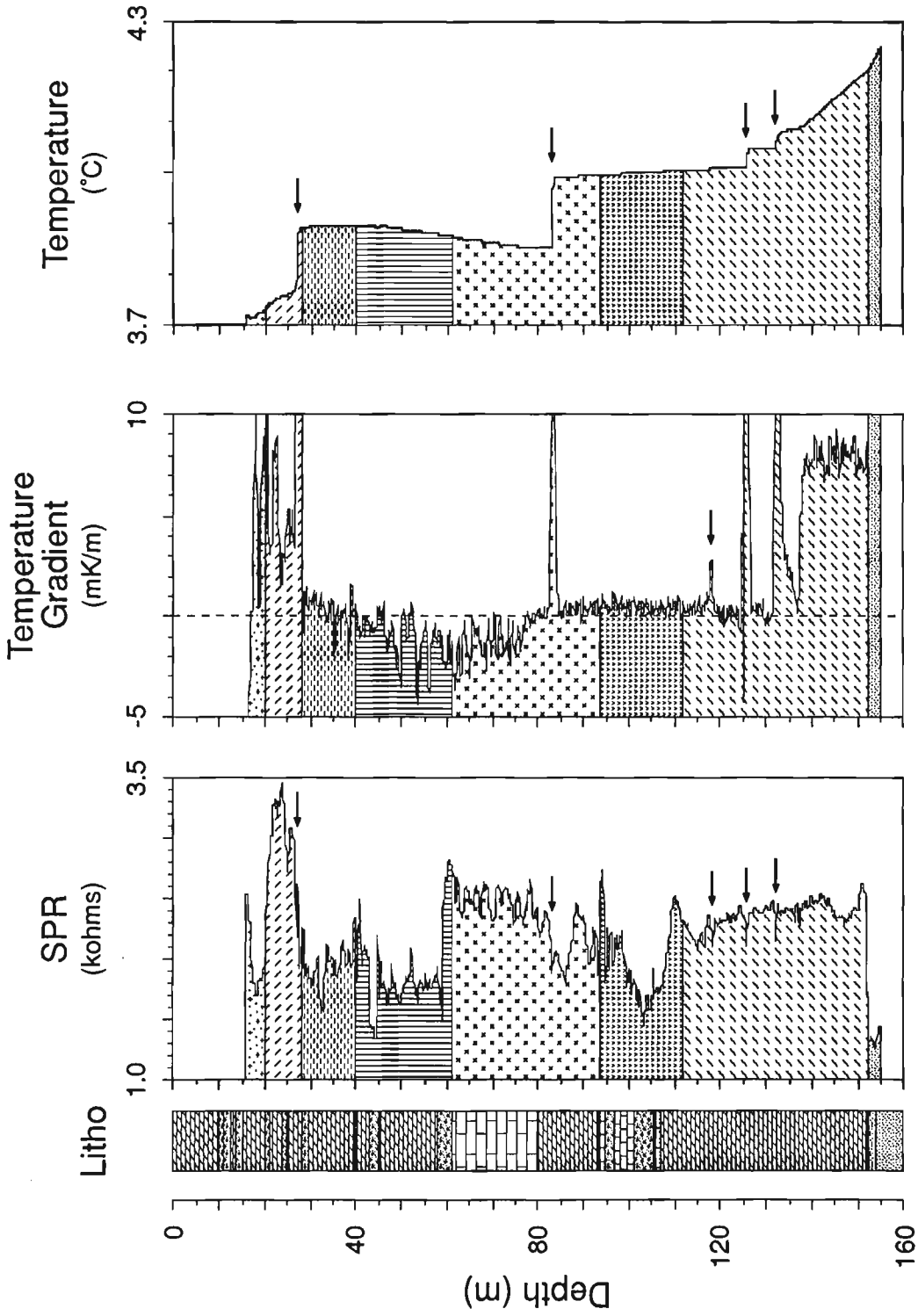

Figure 3. *Lithology, single point resistance (SPR), temperature, and temperature gradient logs recorded in M-6-91. Temperature gradient data are truncated at 10 mK/m (°C/km). The arrows on the temperature logs indicate the location of water entry/exit zones in the borehole. These correspond to low-resistance anomalies on the SPR log interpreted as fracture zones. The lithology column is as indicated in Figure 1.*

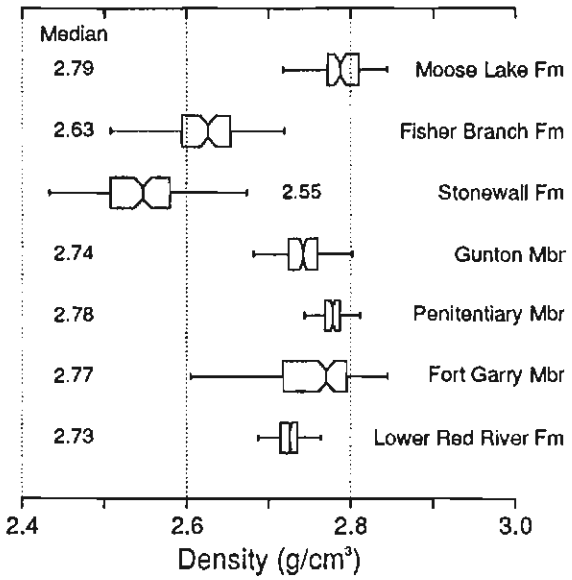

Figure 4. Box-and-whiskers plots showing density distribution for the different formations intersected in M-6-91. The boxes are bounded by the 25th and 75th percentiles while the whiskers represent the extension of data to the 10th and 90th percentiles. The notches represent the 95 percent confidence interval for the medians. The boxes for the Gunton and Penitentiary Members indicate that density distributions within these two Stony Mountain Formation Members are distinct.

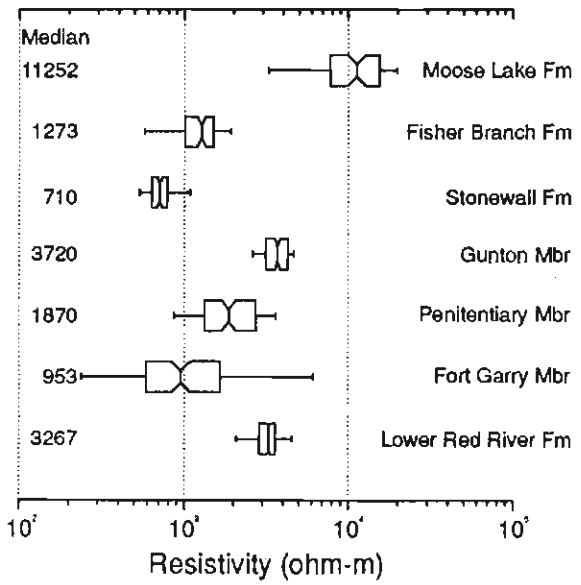

Figure 5. Box-and-whiskers plots showing resistivity distribution for the different formations intersected in M-6-91. Resistivities are lowest in the Stonewall Formation and highest in the Moose Lake Formation. The Fort Garry Member shows a wide range of resistivities because of the variability in lithology: dolomite, argillaceous dolomitic mudstone, and calcitic dolomite.

in resistivity and density. The overlying Gunton Member is noticeably lower in density and higher in resistivity than the Penitentiary Member. There is also a slight change in the character of the borehole gamma-ray signature at this location. The resistivity, IP, and density logs show periodicity in the Gunton Member, with high IP correlating with high density and high resistivity. This periodic signature reflects alternating lithological changes in the dolomite that may represent depositional cyclicity. The density and gamma-ray data show the Penitentiary Member to be homogeneous. The resistivity, however, is highly variable (Figures 5 and 8). There are subtle indications of fracture zones at approximately 83 and 86 m as seen on the resistivity, SPR, and density logs. Two zones portraying characteristic low density and low resistivity responses due to porosity changes occur within the Fisher Branch Formation (32-33 m, vuggy, very light yellow buff dolomite) and near the lower contact of the Fort Garry Member (105-107 m, vuggy, calcitic dolomite).

The temperature and temperature gradient logs (Figure 3) show distinct, abrupt temperature changes and high temperature gradients at several locations along the borehole. These temperature anomalies are characteristic of groundwater flow. Ground water enters or exits the borehole at these locations. The water flow zone at approximately 26.5 m occurs at the contact between the Moose Lake (a highly resistive and dense dolomite) and Fisher Branch Formations. This zone apparently rests directly upon a significant aquiclude, the U1-marker, a persistent dolomitic shale-mudstone horizon (Bezys, 1993). Temperature logging was carried out in another hole located 25 m away, where the temperature-depth profile was similar to that observed in M-6-91, suggesting laterally extensive groundwater flow zones. Another major water inflow/outflow zone is at approximately 83 m in the Stonewall Formation. Three other zones in the Lower Red

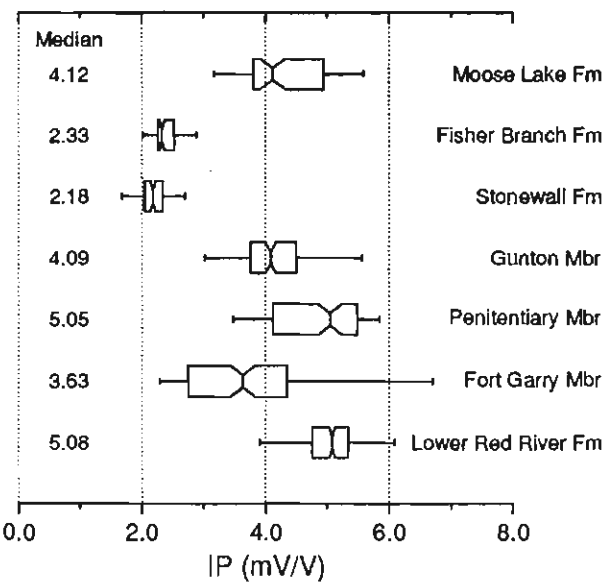

Figure 6. Box-and-whiskers plots showing induced polarization distribution (IP effect) for the different formations intersected in M-6-91.

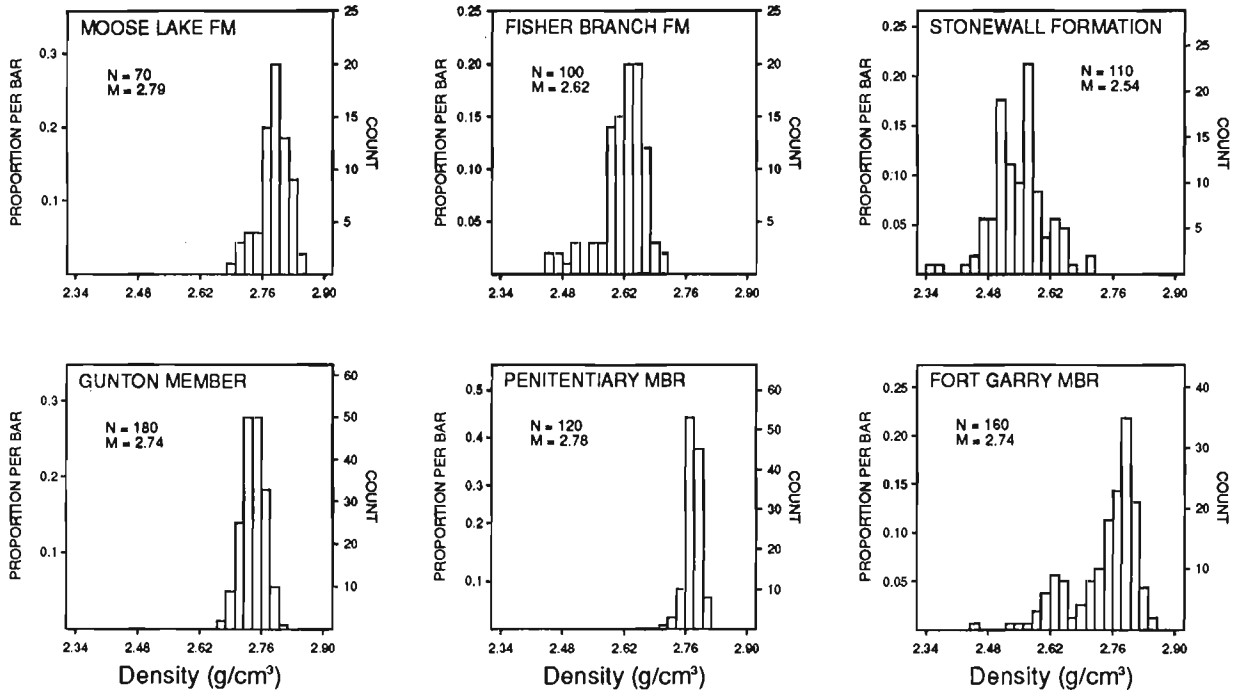

Figure 7. Histograms showing density distribution within six formations. Note that the Fort Garry Member shows a wide range of density values as portrayed on the box-and-whiskers plots. The histogram, however, shows that the distribution is bimodal. M – mean value.

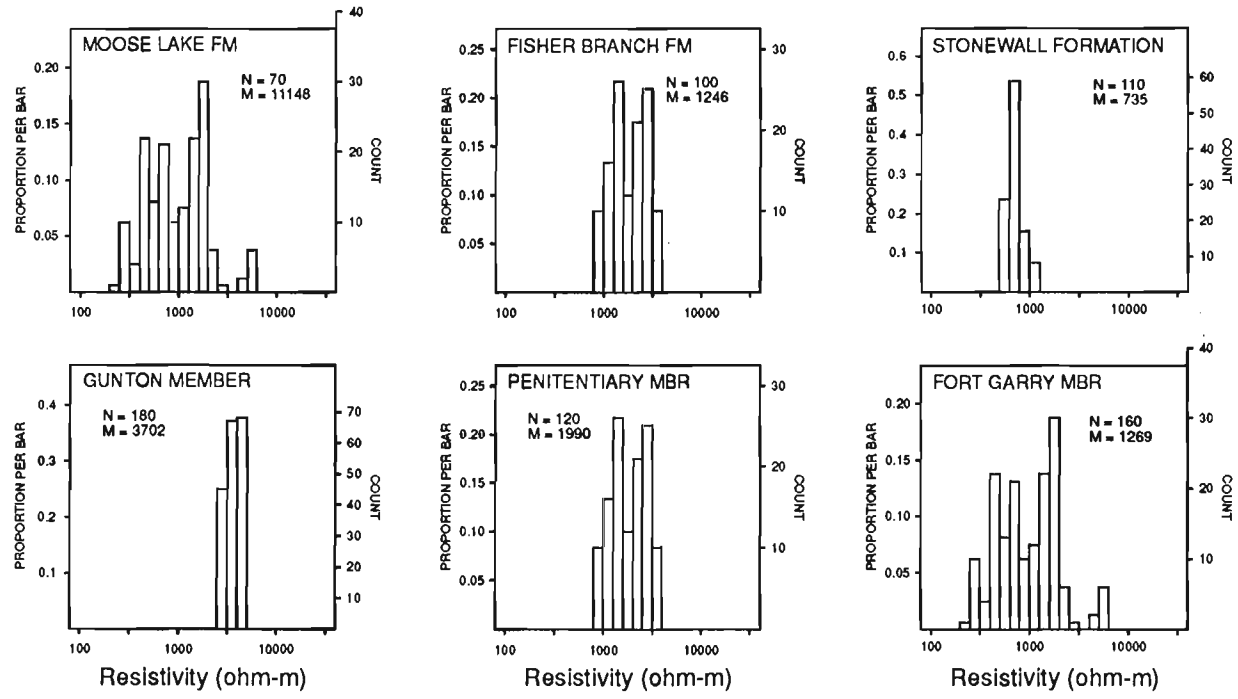

Figure 8. Histograms showing resistivity distribution (in logarithmic scale) within six formations. M – mean value.

River Formation are located at 125 m, 132 m, and 137.5 m. The electrical logs show distinct low-resistivity, v-type anomalies (possibly due to washouts) at these water inflow/outflow zones in the Red River Formation. Variations in the thermal conductivities of dolomite and argillaceous dolomitic mudstone could not be distinguished on the temperature gradient profile because of water movements in the borehole. For the same reason, the normal geothermal gradients could not be established. The bottom of the hole (140-150 m), however, shows temperature gradients that may be close to the normal geothermal gradients (mean=7.9 mK/m).

CONCLUSION

The geology and stratigraphy of Paleozoic carbonate formations intersected in hole M-6-91 were more clearly understood with the use of multiparameter geophysical logs. The gamma-ray log helped to identify and determine the positions of marker beds. Although some dolomitic beds in the various formations appear to be similar, they can be distinguished by their characteristic geophysical signatures. There are differences in electrical resistivity and density in different formations, and these differences are due to variations in porosity. Measurements from more than one hole are necessary to determine if these geophysical signatures (e.g., resistivity and density) are diagnostic of the different Paleozoic formations across a wider area. This information would help to correlate stratigraphy, especially where there are a few recognizable (marker) horizons. For this purpose, a proposal has been submitted to NATMAP to drill and log five stratigraphic coreholes in north-central Manitoba. Information from the geophysical logs will provide a more definitive stratigraphic signature for the Paleozoic formations and will enhance hole-to-hole correlations. Temperature logs may provide useful information on the hydrogeology of the area.

ACKNOWLEDGMENTS

Hole M-6-91 was funded and drilled by the Manitoba Department of Energy and Mines. Borehole logging was done with the GSC R&D system with A-base funding. Thanks are due to Bill Hyatt for the field data collection, and to Barbara Elliott for assistance in data processing.

REFERENCES

Bamburak, J.D.
1992: Industrial minerals investigations in the Selkirk Area (NTS 621); in Report of Activities, 1992, Manitoba Energy and Mines, Minerals Divisions, p. 145-148.

Bezys, R.K.
1991: Stratigraphic mapping (NTS 63F, 63K) and core hole program; in Report of Activities, 1991, Manitoba Energy and Mines, Minerals Division, p. 61-73.
1992: Stratigraphic mapping and core hole program; in Report of Activities, 1992, Manitoba Energy and Mines, Minerals Division, p. 123-131.
1993: Stratigraphic mapping and core hole program; in Report of Activities, 1993, Manitoba Energy and Mines, Minerals Division, p. 127-133.

Mwenifumbo, C.J.
1989: Optimization of logging parameters in continuous, time-domain induced polarization measurements; in Proceedings of the 2nd International Symposium on Borehole Geophysics for Mineral, Geotechnical, and Groundwater Applications, MGLS, Las Vegas, Nevada, v. I, paper N, p. 201-232.

Mwenifumbo, C.J.
1993: Temperature logging in mineral exploration; Journal of Applied Geophysics, v. 30, p. 297-313.

Geological Survey of Canada Project 880030

Diagenetic paragenesis of Swan Hills carbonates (Middle-Upper Devonian) in the Devonian Deep Basin of west-central Alberta

Hairuo Qing and Jack Wendte
Institute of Sedimentary and Petroleum Geology, Calgary

Qing, H. and Wendte, J., 1994: Diagenetic paragenesis of Swan Hills carbonates (Middle-Upper Devonian) in the Devonian Deep Basin of west-central Alberta; in Current Research 1994-E; Geological Survey of Canada, p. 151-156.

Abstract: Petrographic analyses of Swan Hills carbonates (Middle-Upper Devonian) from the deeply buried subsurface (2500-4000 m) of west-central Alberta indicate that these carbonates underwent diagenesis in submarine and subsurface environments, without significant modifications from shallow, meteoric waters. Submarine diagenetic products include syntaxial, micritic, microspar, and fibrous calcite cements that precipitated in interparticle pores of some carbonates and significantly reduced porosity. Meteoric waters associated with subaerial exposure had minimal effect due to the short intervals of exposure, the prevailing arid climate, and the original calcitic mineralogy. Subsurface diagenetic products include blocky calcite cement (400-500 μm), stylolites, matrix replacement dolomites and associated dissolution vugs, saddle dolomite, coarsely crystalline anhydrite cement, late stage macrocrystalline (centimetre size) calcite cement, elemental sulphur, and pyrobitumen. Dissolution associated with matrix dolomitization created sufficient porosity and permeability to sustain gas production. Limestones that did not undergo dolomitization lost porosity through stylolitization and cementation as they were more deeply buried and, as a consequence, lack reservoir quality.

Résumé : Des analyses pétrographiques des roches carbonatées de Swan Hills (Dévonien moyen et supérieur) provenant des grandes profondeurs (2,5 à 4 km) dans le centre ouest de l'Alberta indiquent que ces unités ont subi une diagenèse dans des milieux sous-marins et de subsurface, sans modifications importantes dues aux eaux peu profondes ou météoriques. Les produits diagénétiques sous-marins comprennent notamment des ciments de calcite formée en continuité optique, de micrite, de microspath et de calcite fibreuse, qui ont précipité dans des pores entre les particules de certains carbonates et en ont réduit la porosité de façon importante. Les eaux météoriques associées à une exposition subaérienne ont eu un effet minimal en raison des brefs intervalles d'exposition, du climat aride dominant et de la minéralogie originale riche en calcite. Les produits diagénétiques de subsurface comprennent notamment le ciment de calcite trapue (400 à 500 μm), les stylolites, les dolomites de remplacement de la matrice et les vacuoles de dissolution associées, la dolomite à faces composites incurvées, le ciment d'anhydrite cristalline grossière, le ciment tardif de calcite macrocristalline (de l'ordre du centimètre), le soufre élémentaire et le pyrobitume. La dissolution associée à la dolomitisation de la matrice a créé une porosité et une perméabilité suffisantes pour entraîner la production de gaz. Les calcaires qui n'ont pas subi de dolomitisation ont perdu leur porosité à la suite de la stylolitisation et de la cimentation, parce qu'ils étaient enfouis à une plus grande profondeur; aussi la qualité de réservoir fait-elle défaut.

INTRODUCTION

Understanding processes of dolomitization is important to hydrocarbon exploration in the Western Canada Sedimentary Basin because dolomites provide the reservoirs for many Devonian oil and gas fields: e.g., Keg River Formation in northwest Alberta (Hriskevich, 1970; Schmidt et al., 1980, 1985; Aulstead and Spencer, 1985; Qing and Mountjoy, 1989); Manetoe Facies in Northwest Territories (Morrow et al., 1986; Aulstead et al., 1988); Sulphur Point and Slave Point formations in northeastern British Columbia (Collins and Lake, 1989; Reimer and Teare, 1992; Qing and Mountjoy, 1992, 1994); Leduc Formation and Wabamun Group in the Peace River area (Stoakes, 1987; Mountjoy and Halim-Dihardja, 1991; Dix, 1993); and Leduc and Nisku formations in central Alberta (Machel and Anderson, 1989; Amthor et al., 1993).

Although dolomites with similar petrographic properties have been documented throughout the entire Devonian sequence of the Western Canada Sedimentary Basin, it is unclear whether or not these dolomites are genetically related. The intent of this project is to examine dolomites through the entire Devonian succession from the deeply buried part of the Western Canada Sedimentary Basin in west-central Alberta (Fig. 1, 2). This succession includes the Swan Hills, Leduc, and Nisku formations and the Wabamun Group. Our objectives are: 1) to identify the petrographic varieties of dolomites in these units; 2) to establish their paragenesis; 3) to map their spatial distribution; 4) to determine their geochemical characteristics (e.g., O, C, Sr isotopes, fluid inclusions); 5) to compare their petrographic and geochemical features; and 6) to determine their genesis and relate their occurrence and origin to hydrologic flow systems.

This report summarizes the preliminary results of the diagenetic paragenesis of the Swan Hills Formation, based on core and thin section examination. The diagenetic products are listed in a paragenetic sequence (Fig. 3). Overlapping phases are shown according to their first appearance. These diagenetic features are interpreted to have occurred in submarine, subaerial, and subsurface environments. A more detailed account of the diagenesis will be discussed after the results of geochemical analyses become available.

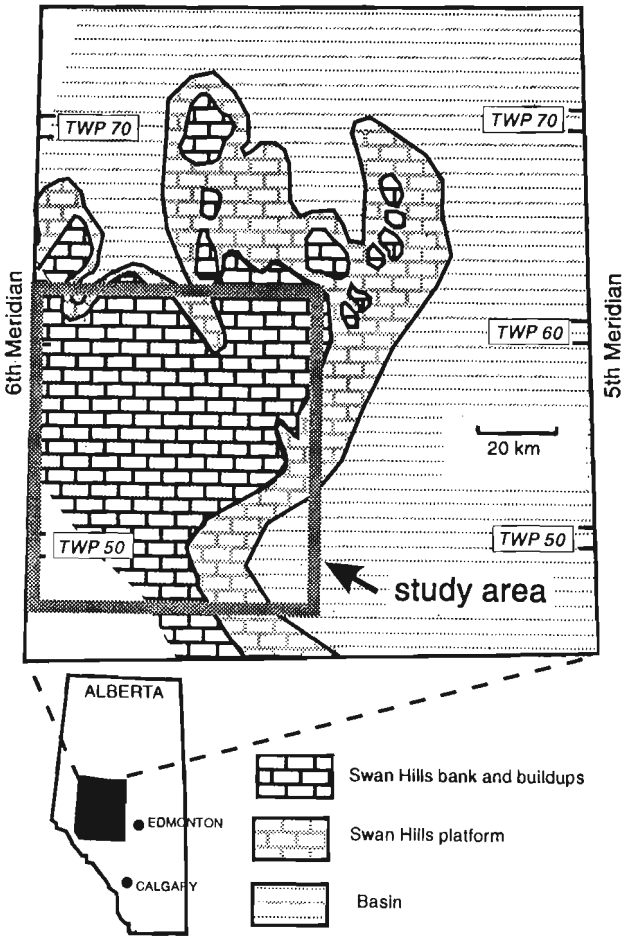

Figure 1. Paleogeographic and location map of the Swan Hills Formation in west-central Alberta. The present burial depth of the Swan Hills Formation ranges from 2800 to 4000 m. Detailed study area is shown in Figure 2.

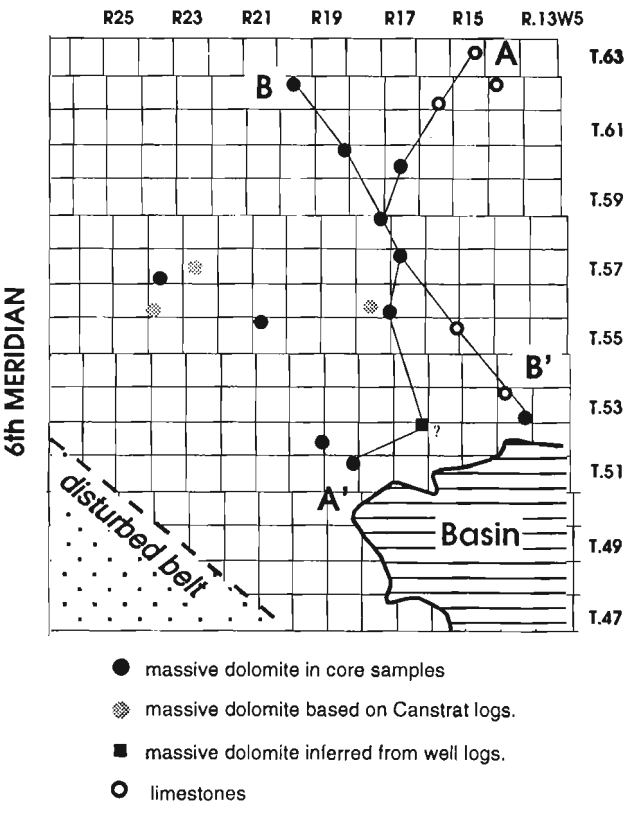

Figure 2. General map of study area showing location of core examined. Massive replacement dolomites are widespread in the region, except in the east and northeast where the Swan Hills Formation is mainly limestone. Cross-section A-A' is shown in Figure 4, and cross-section B-B' is shown in Figure 5.

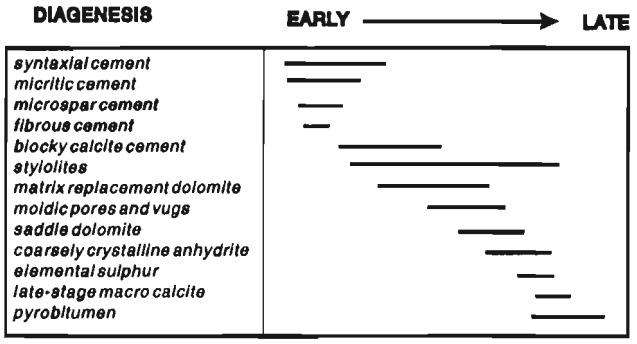

Figure 3. Diagenetic paragenesis of the Swan Hills carbonates.

SUBMARINE DIAGENESIS

The most important marine diagenetic products are calcite cements, including syntaxial, micritic, microspar, and fibrous cements. Micritic and microspar cements are most abundant in the interior of the Swan Hills bank, where they occur in peloidal packstones and wackestones and in *Amphipora* and stromatoporoid rudstones and floatstones. Fibrous calcite cements mainly occur in stromatoporiod rudstones deposited along the margin of the Swan Hills bank. Although the initial phases of syntaxial, micritic, and microspar cements precipitated in the marine environment, later phases of these cements probably formed during subsequent burial in the subaerial and subsurface environments.

Syntaxial cement

Syntaxial calcite cements occur as overgrowths on echinoderm particles, in optical continuity with these single crystal, host particles. These cements occur abundantly in crinoidal packstones and grainstones, and rarely in *Amphipora* and stromatoporoid rudstones and floatstones. The initial phase of syntaxial cement is interpreted to have precipitated from seawater prior to the formation of the micritic, microspar, and fibrous calcite cements.

Micritic cement

Micrite (crystals about 5 μm) occurs as cements in peloidal wackestone and packstone and is most abundant in the interior of the Swan Hills bank. These cements probably formed in all three diagenetic environments.

Microspar cement

Microspar cements occur as equant-anhedral crystals, which vary in diameter from 10 to 20 μm and are cloudy under plane light microscopy. These cements commonly occur in peloidal wackestones and packstones, and less often, in skeletal wackestones. In some peloidal packstones, precipitation of microspar preceded that of fibrous calcite cement and is therefore of marine origin.

Fibrous cement

Fibrous calcite cements usually form isopachous bands within shelter and interparticle pores in stromatoporoid rudstones. Microscopically, these elongated crystals occur with their long axes perpendicular to the host particles. In peloidal packstones, fibrous cements also occur around peloidal aggregates that were amalgamated by microspar cement. Fibrous cements greatly reduced the porosity and permeability of some limestones that occur along the margin of the Swan Hills bank.

SUBAERIAL DIAGENESIS

Subaerial exposure of Swan Hills carbonates occurred both as a consequence of repeated phases of depositional upbuilding to or above sea level and as a result of one relative lowering of sea level during the formation of the Swan Hills succession (Wendte, 1987, 1992; Kaufman and Meyers, 1988). Despite the occurrence of exposure surfaces, meteoric cements resulting from subaerial exposure have not been positively identified. Therefore, fresh water is interpreted to have had little impact on the diagenesis and reservoir quality of Swan Hills carbonates. We attribute this to the short intervals of exposure, the prevailing arid climate, and the original stable calcitic mineralogy of Devonian limestones (Wendte and Muir, 1993).

SUBSURFACE DIAGENESIS

Subsurface diagenetic products include blocky calcite cement, stylolites, matrix replacement dolomites and associated dissolution vugs, saddle dolomite, coarsely crystalline anhydrite cement, late stage macrocrystalline calcite cement, elemental sulphur, and pyrobitumen.

Blocky calcite cement

Blocky calcite cements occur as limpid to translucent, equant, and usually anhedral crystals of 100 to 1000 μm in diameter, with alternating ferroan and nonferroan zones. The precipitation of these cements postdated that of the micrite, microspar, and fibrous calcite cements and occluded the remaining pores in most limestones.

Stylolites

Stylolites with amplitudes from less than a millimetre to one centimetre occur throughout the Swan Hills succession. These features are marked by the concentration of dark, insoluble materials such as clays and organic carbon. The formation of stylolites is attributed to pressure solution during burial. Although some stylolites probably began to develop at burial depths of a few hundred metres, they only attained significant amplitudes after about a kilometre of burial (Choquette and James, 1990).

Matrix replacement dolomite

Replacive dolomite postdated the formation of low-amplitude stylolites. Macroscopically, dolomites are divided into two groups: 1) floating dolomite rhombs and patches in limestones and 2) massive, replacement dolomite.

Floating dolomite rhombs and patches occur in dolomitic limestones. Floating dolomite rhombs are usually subhedral to euhedral, range in diameter from 100 to 200 μm, and preferentially occur in the matrix of skeletal floatstones and rudstones. Local concentrations of dolomite rhombs form dolomite patches, which coalesce and grade into massive, replacement dolomite. Microscopically, some dolomite rhombs replace blocky calcite cement and crosscut wispy stylolites, indicating that dolomitization postdated blocky calcite cementation and the onset of stylolitization.

Massive replacement dolomites are brown or grey, and less fabric retentive, although fossils and sedimentary textures generally are recognizable. These dolomites vary from those that lack porosity to those that have abundant intercrystalline pores. Microscopically, massive replacement dolomite consists of anhedral to subhedral dolomite crystals (150-250 μm, average 200 μm), with well defined crystal boundaries. Some dolomite crystals have clear rims around cloudy centres.

Massive replacement dolomites have widespread distribution in the Swan Hills Formation. As illustrated in Figure 2, Swan Hills sections lacking massive dolomites occur only in the eastern and northeastern parts of the study area. As shown on the cross-sections in Figures 4 and 5, massive replacement dolomites occur at various stratigraphic levels within the Swan Hills Formation. Based on cores that we have examined, vertically continuous massive dolomites within the Swan Hills Formation occur only along bank-margin settings (e.g., 4-35-58-18W5 in Fig. 4, 5).

Dissolution vugs

Dissolution vugs and moulds up to a few centimetres in diameter occur selectively in the massive dolomites. Many of these voids have forms similar or identical to *Amphipora* and other stromatoporoids and are interpreted to be leached biotic constituents. Furthermore, the walls of some of the vugs contain the relict laminae and pillar structure of stromatoporoids. The selective occurrence of vugs and moulds in the massive replacement dolomites and their complete absence in limestones suggests that dissolution occurred as part of the dolomitization process. Vugs, moulds, and associated intercrystalline pores provide the reservoirs for major gas accumulations. Some vugs and moulds are partially filled with saddle dolomite, coarsely crystalline anhydrite, late stage macrocrystalline calcite, and pyrobitumen.

Saddle dolomite

Saddle dolomites in the Swan Hills Formation consist of coarse crystals up to 3 mm across, with shapes ranging from rhombohedral with slightly curved faces to symmetrical saddle forms

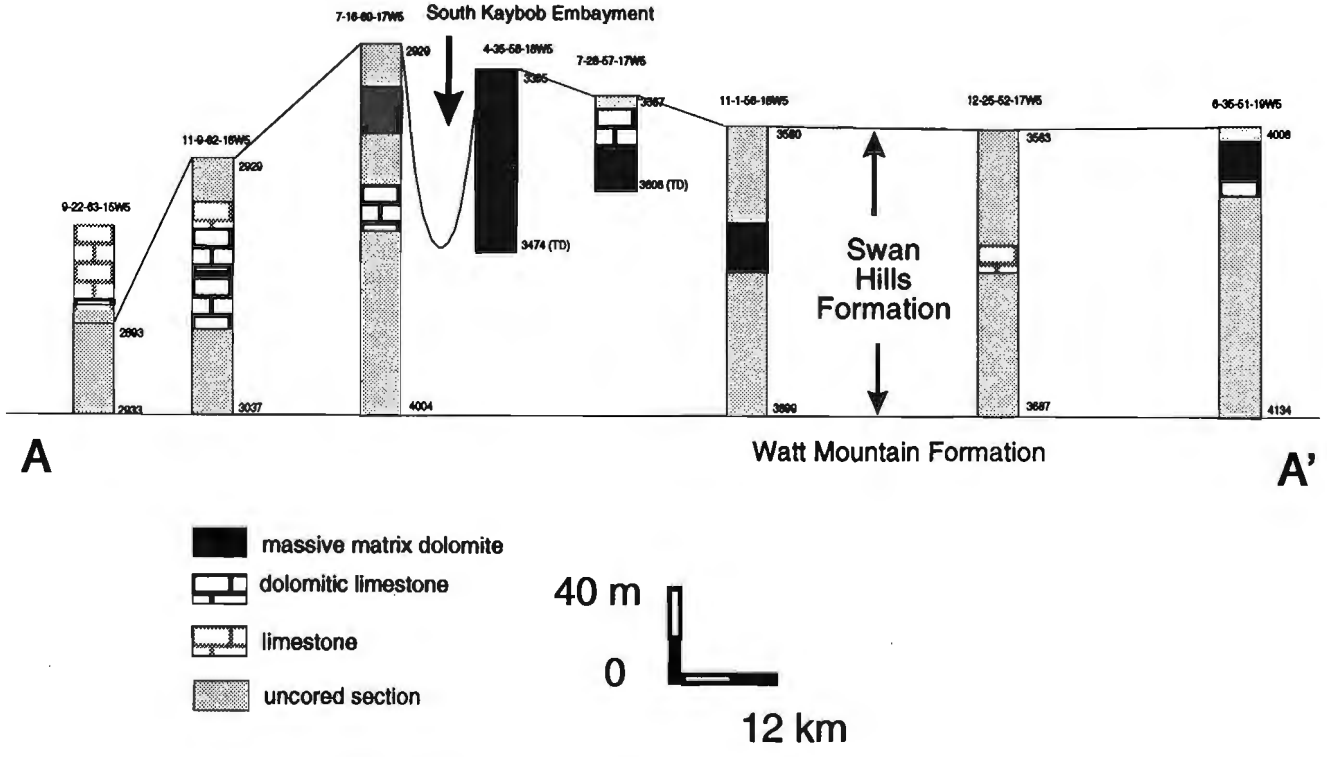

Figure 4. Cross-section A-A', showing stratigraphic distribution of massive dolomites in the Swan Hills Formation. See Figure 2 for the location of the cross-section.

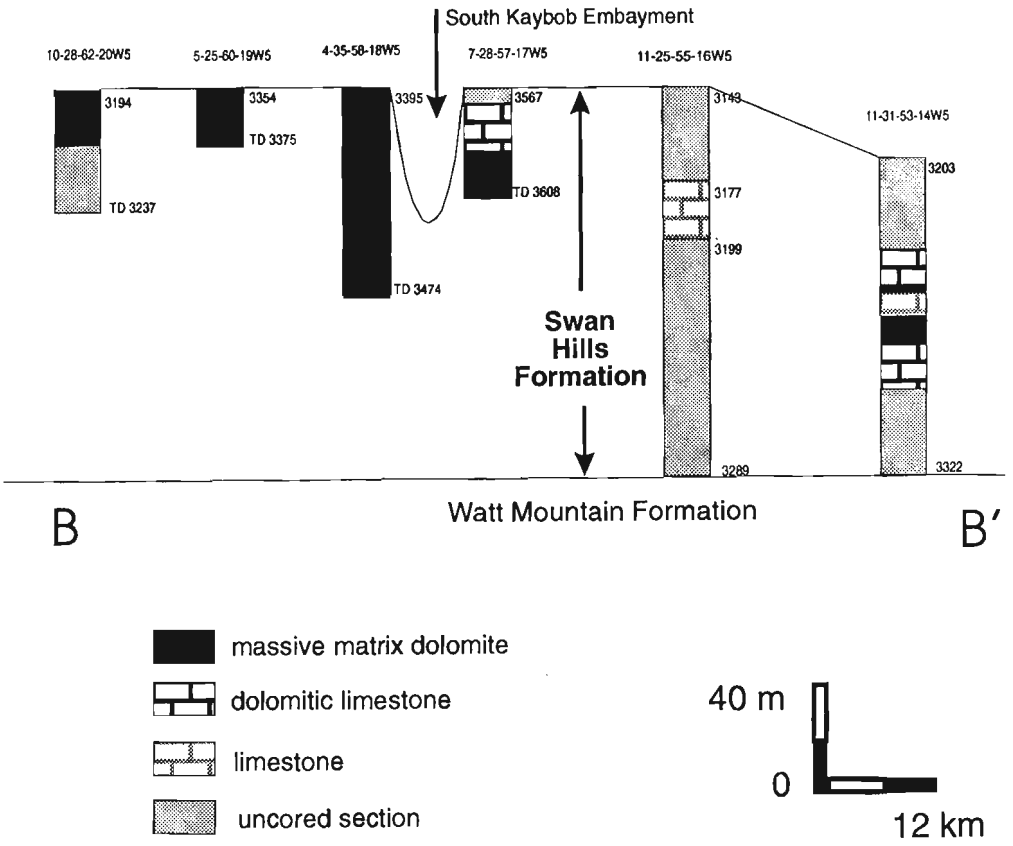

Figure 5. Cross-section B-B', showing stratigraphic distribution of massive dolomites in the Swan Hills Formation. See Figure 2 for the location of the cross-section.

with greater facial curvatures. These crystals occur mainly as cements in moulds and vugs in the matrix replacement dolomites. Locally, saddle dolomites also occur as cements in limestone interparticle pores, previously noted elsewhere by Wong and Oldershaw (1981) and Viau and Oldershaw (1984).

Coarsely crystalline anhydrite cement

Coarsely crystalline anhydrite cements consist of white, bladed euhedral crystals up to 4.25 mm long and 0.3 mm wide. These anhydrite cements fill moulds and vugs in dolomite and some late stage fractures in both limestones and dolomites. Precipitation of coarsely crystalline anhydrite cements postdates that of saddle dolomite.

Late stage, macrocrystalline calcite cement

Late stage, macrocrystalline calcite cements are semitranslucent to white with crystal diameters varying from a few millimetres to about 5 cm. The precipitation of late stage calcite cements postdates that of saddle dolomite and coarsely crystalline anhydrite. Macrocrystalline calcite occluded the porosity in some dolomites.

Elemental sulphur

Minor amounts of anhedral elemental sulphur occur as cements, filling moulds and vugs in dolomites. Precipitation of elemental sulphur postdates the formation of saddle dolomite.

Pyrobitumen

Pyrobitumen consists of a fine grained residue and/or a consolidated, shiny black solid hydrocarbon. It occurs as the latest diagenetic product in moulds, vugs, and fractures, coating the substrate of walls and/or earlier diagenetic products, such as saddle dolomite, coarsely crystalline anhydrite, and macrocrystalline calcite cements.

CONCLUSIONS

The results of this study indicate that Swan Hills carbonates from the deeply buried subsurface of west-central Alberta have undergone diagenesis in the submarine and especially the subsurface environments.

The most important marine diagenetic products are calcite cements, including syntaxial, micritic, microspar, and fibrous forms. Fibrous calcite cements precipitated in interparticle and shelter pores, significantly reducing the porosity in some bank-margin limestones.

Diagenetic products resulting from subaerial exposure of Swan Hills limestones are very minor, probably due to the short interval of exposures, the prevailing arid climate, and the original calcitic mineralogy. Thus, processes associated with subaerial exposure did not significantly alter the porosity and permeability of these limestones.

Diagenetic products that formed in the subsurface include blocky calcite cement, stylolites, matrix replacement dolomites and associated dissolution vugs, saddle dolomite, coarsely crystalline anhydrite cement, late stage macrocrystalline calcite cement, elemental sulphur, and pyrobitumen. Dissolution associated with matrix dolomitization created significant porosity, providing the reservoirs for major gas accumulations. Limestones that did not undergo dolomitization lost porosity through stylolitization and cementation during deeper burial and, as a result, lack porosity.

ACKNOWLEDGMENTS

We thank M. Bosman (Canadian Hunter Exploration Ltd.) for providing access to stratigraphic cross-sections and maps in the study area, and R.W. Macqueen (Geological Survey of Canada) for valuable advice, discussion, and review of this paper. Financial support for H. Qing came from an NSERC visiting fellowship and the Geological Survey of Canada.

REFERENCES

Amthor, J.E., Mountjoy, E.W., and Machel, H.G.
1993: Subsurface dolomites in Upper Devonian Leduc Formation buildups, central part of Rimbey-Meadowbrook reef trend, Alberta, Canada; Bulletin of Canadian Petroleum Geology, v. 41, p. 164-185.

Aulstead, K.L. and Spencer, R.J.
1985: Diagenesis of the Keg River Formation, northeastern Alberta: fluid inclusion evidence; Bulletin of Canadian Petroleum Geology, v. 33, p. 167-183.

Aulstead, K.L., Spencer, R.J., and Krouse, H.R.
1988: Fluid inclusion and isotopic evidence on dolomitization, Devonian of Western Canada; Geochimica et Cosmochimica Acta, v. 52, p. 1027-1035.

Choquette, P.W. and James, N.P.
1990: Limestones: the burial diagenetic environment; in Diagenesis, (ed.) I.A. McIlreath and D.W. Morrow; Geoscience Canada Reprint Series 4, p. 75-111.

Collins, J.F. and Lake, J.H.
1989: Sierra reef complex, Middle Devonian, northeastern British Columbia; in Reefs, Canada and Adjacent areas, (ed.) H.H.J. Geldsetzer, N.P. James, and G.E. Tebbutt; Canadian Society of Petroleum Geologists, Memoir 13, p. 414-421.

Dix, G.R.
1993: Patterns of burial- and tectonically controlled dolomitization in an Upper Devonian fringing-reef complex: Leduc Formation, Peace River Arch area, Alberta, Canada; Journal of Sedimentary Petrology, v. 63, p. 628-640.

Hriskevich, M.E.
1970: Middle Devonian reef production, Rainbow area, Alberta, Canada; American Association of Petroleum Geologists, Bulletin, v. 54, p. 2260-2281.

Kaufman, J. and Meyers, W.J.
1988: A backstepping platform reef, Swan Hills Formation, Rosevear Field, central Alberta; in Reefs, Canada and Adjacent areas, (ed.) H.H.J. Geldsetzer, N.P. James, and G.E. Tebbutt; Canadian Society of Petroleum Geologist, Memoir 13, p. 478-486.

Machel, H.G. and Anderson, J.H.
1989: Pervasive subsurface dolomitization of the Nisku Formation in central Alberta; Journal of Sedimentary Petrology, v. 59, p. 891-911.

Morrow, D.W., Cumming, G.L., and Koepnick, R.B.
1986: Manetoe Facies - a gas-bearing, megacrystalline, Devonian dolomite, Yukon and Northwest Territories, Canada; American Association of Petroleum Geologists, Bulletin, v. 70, p. 702-720.

Mountjoy, E.W. and Halim-Dihardja, M.K.
1991: Multiple phase fracture and fault-controlled burial dolomitization, Upper Devonian Wabamun Group, Alberta; Journal of Sedimentary Petrology, v. 61, p. 252-303.

Qing, H. and Mountjoy, E.
1989: Multistage dolomitization in Rainbow buildups, Middle Devonian Keg River Formation, Alberta, Canada; Journal of Sedimentary Petrology, v. 59, p. 114-126.
1992: Large-scale fluid flow in the Middle Devonian Presqu'ile barrier, Western Canada Sedimentary Basin; Geology, v. 20, p. 903-906.
1994: Formation of coarse-crystalline, hydrothermal dolomite reservoirs in the Presqu'ile barrier, Western Canada Sedimentary Basin; American Association of Petroleum Geologists, Bulletin, v. 78, p. 55-77.

Reimer, J.D. and Teare, M.R.
1992: Deep burial diagenesis and porosity modification in carbonate rocks by thermalorganic sulphate reduction and hydrothermal dolomitization: TSR-HTD; in Subsurface dissolution porosity in carbonates. Recognition, Causes and Implications; Canadian Society of Petroleum Geologists, Short Course Notes, 1992 CSPG-AAPG Convention, Calgary, 26 p.

Schmidt, V., McDonald, D.A., and McIlreath, I.A.
1980: Growth and diagenesis of Middle Devonian Keg River cementation reefs, Rainbow field, Alberta; in Carbonate reservoir rocks: notes for Society of Economic Paleontologists and Mineralogists Core Workshop No. 1, Denver, Colorado, June 1980, (ed.) R.B. Halley and R.G. Loucks; Society of Economic Paleontologists and Mineralogists, p. 43-63.

Schmidt, V., McIlreath, I.A., and Budwill, A.E.
1985: Middle Devonian cementation reefs encased in evaporites, Rainbow field, Alberta; in Carbonate petroleum reservoirs, (ed.) P.O. Roehl and P.W. Choquette; Springer-Verlag, p. 141-160.

Stoakes, F.A.
1987: Fault-controlled dolomitization of the Wabamun Group, Tangent Field, Peace River Arch, Alberta; in Devonian lithofacies and reservoir styles in Alberta, (ed.) F.F. Krause and B. Burrowes; 13th Canadian Society of Petroleum Geologists, Core Conference and Display and Second International Symposium on the Devonian System, p. 73-85.

Viau, C.A. and Oldershaw, A.E.
1984: Structure controls on sedimentation and dolomite cementation in the Swan Hill Formation, Swan Hill field, central Alberta; in Carbonates in subsurface and outcrop, (ed.) L.S. Eliuk; Canadian Society of Petroleum Geologists, Core Conference 1984, p. 103-131.

Wendte, J.C.
1987: Inception, growth and termination of the Judy Creek Reef Complex, Middle to Upper Devonian, central Alberta; in Reef Research Symposium, Banff, Alberta, January 27-30, 1987, (ed.) J.C. Packard; Canadian Society of Petroleum Geologists, p. 64.
1992: Evolution of the Judy Creek Reef Complex, a late Middle Devonian isolate platform-reef complex in west-central Alberta; in Devonian-Early Mississippian carbonates of the Western Canada Sedimentary Basin: a sequence stratigraphic framework, (ed.) J.C. Wendte, F.A. Stoakes, and C.V. Campbell; Society of Economic Paleontologists and Mineralogists, Short Course No. 28, p. 89-126.

Wendte, J.C. and Muir, I.D.
1993: Recognition and lack of effect of a sea-level fall on porosity generation in Devonian Swan Hills reef complexes, Alberta; in Abstract book of AAPG Hedberg Research Conference on "Unconformity and Porosity Development in Carbonate Strata: Recognition, Controls, and Predictive Strategies", organized by A. Saller, D. Budd, R. Mitchell, and P.M. Harris, July 13-16, 1993, Vail, Colorado.

Wong, P.K. and Oldershaw, A.E.
1981: Burial cementation in the Devonian Kaybob reef complex, Alberta, Canada; Journal of Sedimentary Petrology, v. 51, p. 507-520.

Geological Survey of Canada Project 890058

Major element composition of recent arctic marine sediments: some preliminary comparisons

D.N. Skibo and W.W. Nassichuk
Institute of Sedimentary and Petroleum Geology, Calgary

Skibo, D.N. and Nassichuk, W.W., 1994: Major element composition of recent arctic marine sediments: some preliminary comparisons; in Current Research 1994-E; Geological Survey of Canada, p. 157-164.

Abstract: In order to assess contaminant sources and mechanisms for transport and dispersal of contaminants in the Arctic Ocean, baseline data on organic and inorganic contaminant concentrations in seabed sediments are being assembled by scientists from Canada and other "polar" nations from the entire Arctic Ocean basin. In this report we present preliminary data on the major inorganic element composition of seabed sediments from selected areas of the Barents Sea, the Beaufort Sea, and the Polar Continental Shelf. These data complement organic data that we have previously released on polychlorinated biphenyls (PCBs), organochlorine pesticides, polycyclic aromatic hydrocarbons (PAHs), and total organic carbon (TOC) in the Arctic Ocean. Some anomalously high values for manganese are noted. Further, we discuss the dependency of concentrations of specific elements on the grain size composition (clay, silt, sand) of sediments on the seafloor.

Résumé : Pour évaluer les sources de contaminants et leurs mécanismes de transport et de dispersion dans l'océan Arctique, des scientifiques du Canada et d'autres nations «polaires» recueillent des données de base sur les concentrations de contaminants organiques et inorganiques dans les sédiments du fond marin. Le présent rapport présente les données préliminaires sur la teneur en principaux éléments inorganiques des sédiments du fond marin, en provenance de zones particulières de la mer de Barents, de la mer de Beaufort et du plateau continental polaire. Ces données complètent l'information sur les produits organiques publiée antérieurement : polychlorés biphényls (PCB), pesticides organochlorés, hydrocarbures aromatiques polycycliques (HAP) et carbone organique total (COT) dans l'océan Arctique. Des valeurs anormalement élevées ont été observées pour le manganèse. Le texte fait de plus état du lien qui existe entre les concentrations d'éléments particuliers et la grosseur des grains (argile, silt, sable) dans les sédiments du fond marin.

INTRODUCTION

Accumulation of metals in terrestrial and marine biota can ultimately result in reduced marine productivity or in trophic transfer of metals to man. Oceanic dumping of nuclear wastes and sunken and decommissioned nuclear submarines pose continuing concerns (Marshall, 1992; MacKenzie, 1994). Besides metals such as nickel, cadmium, mercury, and lead, additional human health concerns have been raised about radioactive metals and isotopes emanating from the nuclear fuel cycle and the legacies of weapons testing and the cold war including:

- actinide elements: thorium through plutonium and americium;
- fission products: ranging up the periodic table mainly from strontium-90 through radioactive isotopes of elements such as zirconium, molybdenum (e.g., $_{42}Mo^{93}$, half-life=35 000 years, decay mode: electron capture), technetium, ruthenium, cadmium, tin, iodine, up to cesium-137 (note: some fission products undergo up to three successive beta decays before becoming stable nuclides);
- activation products: materials exposed to a source of neutrons, for example, isotopes of cobalt and zinc and nuclear reactor by-products such as ^{241}Am, ^{155}Eu, ^{106}Ru, and ^{237}Np.

Marine organisms can accumulate metals from the dissolved phases, as well as from ingested nutrients. Phytoplankton cells are capable of concentrating some metals very appreciably from seawater. For several algal species, metal concentration factors range from nearly zero up to 2500 for elements such as neptunium and technetium, and up to nearly 1 000 000 for actinides such as thorium, plutonium, and americium. With the exception of mercury, metal concentrations in tissues does tend to decrease at higher trophic levels. However, this is not known to be the case for all metals, particulary radionuclides. Organic contaminants are also accumulated by marine animals from dissolved and particulate sources, and their geochemical cycling in marine systems may well be influenced by many of the same processes as those which govern metals.

The main purpose of this study is to provide data toward evaluation of the pathways and mechanisms of contaminant transport and dispersal in the Arctic Ocean. The mechanisms of contaminant transport, whether as solutes or particles, and the barriers to such transport differ in the Arctic, in some respects, from other parts of the world ocean. The study of the composition of marine sediments provides insight into the sources and pathways of contaminant input, biological interactions, and residence times in ocean waters.

Soils or sediments can be accurately analyzed for trace metal content more easily than water. As an additional advantage, sediment analyses provide an integrated input function over time, thus providing a chronological record of pollutant input. Such records can be used to determine background levels, which are particularly important in recognition of subtle or low-level contamination. Another possible background determination is from the analysis of sediments well away from any known point source of pollutant input. In either of these cases, care must be taken to compare similar sediment types. The most important factors controlling trace metal content are grain size and mineralogy. The major element chemistry of sediments provides valuable information about both of these parameters.

ARCTIC CONTAMINATION: OCEAN PROCESSES AND PHYSICAL FEATURES

The Arctic Ocean is a nearly land-locked deep ocean basin, subdivided by a series of undersea ridges. It has only one deep connection with the rest of the world ocean, through Fram Strait between Greenland and Spitsbergen. The Arctic Ocean is divided into two basins, the Canadian Basin and the Eurasian Basin, separated by the Lomonosov Ridge. Surrounding these basins are the worlds most extensive continental shelves, representing about 25% of the world's total. About 10% of the worlds rivers discharge into the Arctic Ocean although it contains only 1.5% of the world's ocean volume. Knowledge of the interactions between the shelves and the deep basins is basic to understanding the physical and biochemical properties of the Arctic Ocean. Waters from the Canadian and Eurasian shelf sources are not restricted to their respective adjacent basins, but are also found in the other basin. Both natural and anthropogenic contaminants introduced onto these various shelves will spread throughout the entire Arctic Ocean. Further, dissolved materials can also be transferred onto the shelves from the adjacent basins (compensating surface flow in years when shelf drainage is strong).

A documented example of contaminant import is that of low-level radionuclides from the nuclear fuel reprocessing plants in western Europe which entered the Polar Basin near Spitsbergen in about 1976 and were observed at mid-depth near the pole three years later, marked by a high $^{137}Cs/^{90}Sr$ ratio (Livingston et al., 1984). It was argued that this signal was initially transmitted into the Arctic Ocean by dense drainage from the Barents Sea. The water would subsequently have been carried counterclockwise around the Eurasian Basin to the Pole by the subsurface boundary current trapped over the basin margin (Livingston, 1988).

The Yablokov Commission Report (Yablokov et al., 1993) estimates that river runoff to the Barents Sea between 1961 and 1989 supplied about 6 kCi (kilo Curies) of radioactivity. Over the same period, atmospheric input from global fallout of nuclear testing was estimated to be 100 kCi (radioactivity is mainly from the isotopes ^{137}Cs and ^{90}Sr). However, the Commission Report also estimates that 200 kCi from nuclear reprocessing plants at Sellafield, England and La Hague, France, were transported from the Atlantic flow into the Barents Sea.

These radioactive releases are small on a global scale when compared to over 100 MCi released from Chernobyl, Ukraine, (official figures place the value at 47.3 MCi), or an estimated 122 MCi of contaminants in Lake Karchai in the southern Urals, Russia (total stored inventory at the Chelyabinsk complex is estimated at one billion Ci). Possibly a similar amount resides at Hanford, Washington. Clearly,

radionuclide as well as heavy metal and organic contaminants are a source of continuing and increasing concern, so that a study of their interaction with marine sediments is of extraordinary importance.

SAMPLES ACQUISITION AND ANALYSIS

During 1992, under the Canada-Russia Agreement on Cooperation in the Arctic and the North, drill core and grab seabed samples from the eastern Barents Sea were acquired from the Russian research vessel "Geolog Fersman" (Nassichuk et al., 1993). Samples from the Barents Sea were analyzed for major elements and some heavy metals, for total organic carbon (TOC) by Rock-Eval pyrolysis, for PAHs, PCBs, and other chlorinated hydrocarbons and pesticides. Locations, sediment intervals and water depths for these samples are given in Nassichuk et al. (1993) and Skibo and Nassichuk (1994).

Analyses are also presented here for five box core samples collected from Northwind Ridge, Canada Basin, and the continental slope of the Alaskan Beaufort Sea at water depths between 400 and 3808 m. All samples are from the top 2 cm of core (U.S. Geological Survey, Cruise P1-93-AR). In addition, five samples were analyzed from Ice Island samples collected in 1985 from the Polar Continental Shelf north of the Canadian Arctic Archipelago (Fig. 1). All major element analyses were carried out by the standard X-ray fluorescence (XRF) method. Results are given in Tables 1 and 2. Mineral determinations were carried out by standard X-ray automated powder diffraction.

BARENTS SEA SEDIMENTS

The Barents Sea covers approximately 1.2 million km^2 and is underlain by an extensive glaciated continental shelf that is cut by undersea valleys and troughs. Major riverine flow comes from the Northern (Severnaya) Dvina (110 km^3/a) and Pechora (130 km^3/a) rivers although flow from the Ob (530 km^3/a) and Yenisei (603 km^3/a) farther east in Siberia probably also provide significant input (mean annual runoff figures from Aagaard and Carmack, 1989). The circulation pattern of the Barents Sea (e.g., AMAP, 1993, Annex 1) is broadly cyclonic, activated by the inflow of a warm, saline Atlantic water mass (North Cape current) from the southwest between Norway and the Svalbard Bank (south end of Spitsbergen). At the northern end of Novaya Zemlya, a westward flow of arctic water (from the Kara Sea) converges with the northward flow of the Atlantic water mass along the west side of the island. This area of intensive vertical circulation, known as the "polar front", indicates possible areas of enhanced sedimentary input in the central Barents Sea and between the northern end of Novaya Zemlya and Franz Josef Land. Some of the cold northern water, along with local Barents Sea waters, leaves the sea along the southern edge of the Bear Island-Spitsbergen Bank (the Bear Island Current).

Recent sediments from the southern Barents Sea were studied by Price et al. (1970), Price and Wright (1971), and Wright (1974), all of whom suggested active redistribution of sediment. Coarse grained sands and muddy sands mantle wide areas of the southwestern sea. These shelf sediments are products of fairly rapid deposition of terrigenous material in an oxic environment. Hence, they differ in geochemical character from the deposits of confined basins and from deep sea

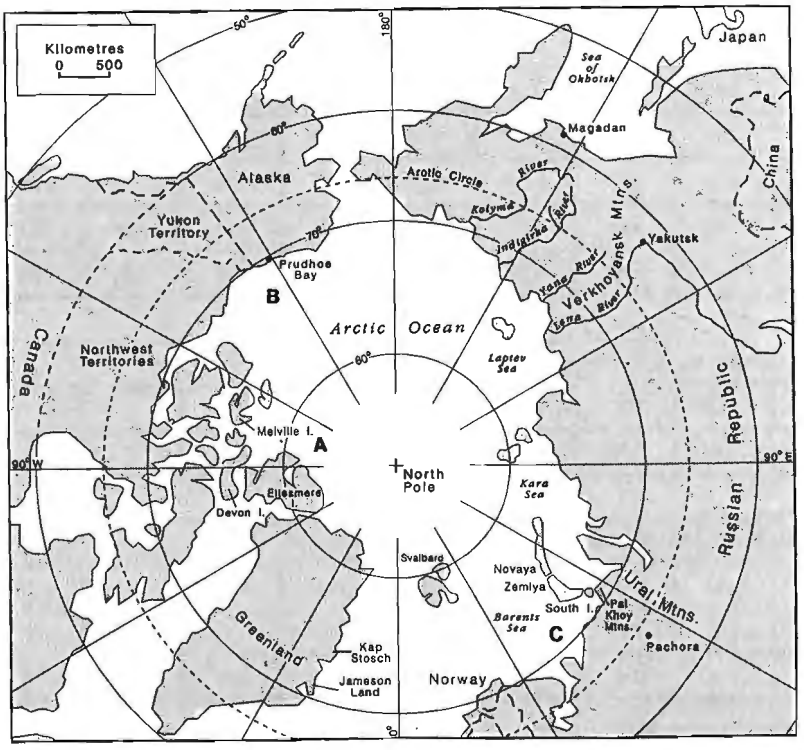

Figure 1.

Sample location areas: (A) Canadian Arctic, Polar Continental Shelf ICE ISLAND samples (from stations 86200-110, -120; 88200-001, -038, -011); (B) West part of Canada Basin, USCGC POLAR STAR box core samples (water depth: various, 400-3800 m); (C) Barents Sea samples from RRV GEOLOG FERSMAN (see Nassichuk et al., 1993).

or oceanic sediments. On the other hand, deposition of the fine sediments is generally restricted to water depths greater than 300 m. In these areas, clay sedimentation is represented by a post-Pleistocene succession over 3 m thick. This distribution of sedimentary types and conditions of deposition is also seen to be pertinent to our previous studies on organic carbon type and distribution (Nassichuk et al., 1993; Skibo and Nassichuk, 1994).

Sediments from locations nearest to shore have the highest fraction of extractable (immature, largely land-derived) hydrocarbons but tend to have lower TOC, possibly due to the more oxic conditions of deposition. This scenario is reversed for samples from deeper waters of the Central Depression. A positive correlation exists between weight per cent TOC and water depth. From the discussion presented here, and other evidence (see Mayer, 1994, for a recent discussion), it seems that the primary relationship controlling TOC content is clay mineral content/grain size as well as water depth (anoxic conditions).

Also, Wright (1974) observed that while a broad correlation appears to exist between organic carbon content and the concentration of many trace elements as determined within undifferentiated sediments, this may instead reflect the covariance of organic carbon with clay content and so does not imply a genetic relation between organic matter and the trace elements. In his experiments, the separated clay fractions of sediments from 7 sample stations were treated with 5% H_2O_2 solution to break down the organic component of the sediment, releasing the associated trace elements. Concentrations of Pb, As, Zn, Cu, Ni, Ce, Ba were diminished by 10% or less, indicating the lack of a direct association

Table 1. Major element chemistry of Barents Sea samples.

Barents sea floor sediments - Oxide composition (weight percent by XRF)													
I.D.	Fe_2O_3	MnO	Cr_2O_3	TiO_2	BaO	CaO	K_2O	P_2O_5	SiO_2	Al_2O_3	MgO	Na_2O	LOI
116	2.88	0.03	0.008	0.47	0.07	1.57	2.4	0.08	72	8.98	1.37	2.46	7.77
116-R	2.89	0.03	0.008	0.46	0.07	1.58	2.41	0.07	71.97	8.84	1.33	2.65	7.77
124-05	9.06	0.05	0.015	0.77	0.08	1.3	3.22	0.19	46.52	12.65	2.89	3.89	19.1
124-14	9.62	0.05	0.017	0.74	0.07	1.21	3.09	0.21	46.09	12.62	2.76	3.71	19.7
137-02	6.52	0.04	0.016	0.94	0.09	0.87	3.31	0.17	56.04	15.38	2.31	2.74	11.5
153-39	9.26	0.58	0.014	1.03	0.07	0.94	2.59	0.25	52.21	14.94	2.45	3.05	12.5
153-49	7.67	0.07	0.015	1	0.09	1.47	2.98	0.16	59.28	15.4	2.5	2.49	6.94
159-27	8.17	0.06	0.016	0.96	0.14	0.97	3.33	0.14	56.1	15.72	2.78	2.43	9.21
159-36	5.93	0.05	0.014	0.85	0.1	0.93	2.9	0.14	61.4	14.57	2.18	2.24	8.7
171-11	8.72	0.09	0.017	1	0.1	2.76	3.25	0.16	52.9	16.5	3.05	1.96	9.5
171-25	8.01	0.08	0.015	0.97	0.08	2.67	2.93	0.17	56.38	16.01	2.87	1.58	8.21
179-08	8.93	0.04	0.014	0.7	0.08	1.3	2.98	0.22	46.92	12.37	2.72	3.9	19.6
Average chemical composition (49 samples by A.A. spectrophotometer, AGC, Dartmouth)													
Mean	6.44	0.14	0.01	-	-	1.08	2.29	-	57.18	13.79	1.46	-	-
S.D.	2.86	0.16	0.01	-	-	0.8	0.72	-	15	4.53	1.18	-	-
South Barents Sea sediments - Grain-size fraction composition (Wright, 1974)													
SAND	1.63	0.04	-	0.16	-	0.84	2.01	0.07	84.65	7.72	0.54	-	2.5+
SILT	2.65	0.06	-	0.74	0.09	1.88	2.32	0.13	76.95	11.54	1.43	2.58	2.21
CLAY	10.8	0.1	-	1.12	0.07	1.02	3.97	0.42	55.67	21.84	3.62	-	0.8

R=repeat analysis; LOI=volatiles loss on ignition (SO_3, CO_2, H_2O, Cl); +=LOI mainly CO_2

between these trace elements and organic matter. Iodine, on the other hand, was completely removed. Phosphorus nearly doubled in concentration, indicating that soluble phosphorus was stabilized under the oxic conditions of the experiment.

In our project, we have found instances where from 15 to 45% of initial Pb is removed in the initial hydrogen peroxide or in some cases the final hot hydroxylamine hydrochloride leach. In addition, differences are seen in some instances in hydroxylamine hydrochloride in 25% (v/v) acetic acid extractions leaching behavior for major elements. These results will be presented in a separate publication.

The procedures are analagous to those used by Wright (1974) in his analysis of southern Barents Sea samples. Our sample coverage partly overlaps his area and will extend the results to the north and east of the sea. In future, we hope to extend the range of trace elements covered.

While our information on mineralogy is presently limited to the samples listed in Table 1, it is anticipated that additional analyses will provide further understanding of the relationship between major element composition and mineralogy. Noting that X-ray diffraction analyses are semi-quantitative and will not resolve fine changes in clay provenance, we agree with Wright (1974) that clay composition might be much more precisely evaluated through chemical analysis. In addition, further studies are intended, making use of information obtainable from SEM analyses.

According to his data (XRF element analysis and semi-quantitative XRD), Wright (1974) noted that the clay fraction at all his stations is dominated by illite (chemical formula: $K_{1.0\text{-}1.5}Al_4(Si,Al)_8O_{20}(OH)_4$; alkaline conditions favor high Al and K concentrations, e.g., seawater; $[SiO_2]/[Al_2O_3]$ ratio about 3; iron oxides about 5 wt.%). However, the author uses the term "illite" in the broad sense to include all clay-grade micas. Subordinate chlorite (sheet silicate with $[SiO_2]/[Al_2O_3]$ ratio=1-1.5; iron oxides about 15-45 wt.%) is noted, but nonetheless, chlorite was found to be abundant in the north and northeast of the author's area - the area of many of our sample sites. Along the north side of Novaya Zemlya we found chlorite to be the dominant clay mineral (Fig. 2, stations 153, 159, and 171). Montmorillonite (smectite group) was found to be detectable at most of our stations . Our X-ray diffraction measurements were done on total sediment sample rather than grain-size fraction separates and indicate sheet silicates and clay minerals: chlorites, micas, and kaolinites. Albites are present in mineral proportion from 2 to 16% and K-feldspars from trace to 16%; both tend to be in greater proportions from samples nearest land. Dolomite and calcite were found in the trace to 7% range. Up to 3 per cent anatase (TiO_2) and traces of pyrite and amphibole were found. Future work using SEM and mineral grain-size separations may help to further quantify these proportions (which are influenced by degree of crystallinity and nature of amorphous matter present).

Table 1 shows a wide range of oxide weight percentages for the eleven samples analyzed, with most elements showing nearly a two-fold variation between lowest and highest. This variation is explained in Wright's (1974) work on the chemistry and mineralogy of sediment grain-size fractions, summarized in the bottom three rows of Table 1. Wright (1974) separated sediment samples into grain-size fractions – >63 μm ("sand"), 8-63 μm ("silt"), <2 μm ("clay") – and measured the

Table 2. Major element chemistry Polar Continental and Beaufort shelves (areas A and B, Fig. 1).

Arctic - Ice Island														
I.D.	Fe_2O_3	MnO	Cr_2O_3	TiO_2	BaO	CaO	K_2O	P_2O_5	SiO_2	Al_2O_3	MgO	Na_2O	SO_3	LOI
SK01	7.41	0.15	0.013	1.01	0.06	3.66	3.05	0.24	52.76	16.09	2.31	1.86	0.01	11.38
SK02	5.71	0.13	0.009	0.79	0.05	5.29	2.29	0.19	61.01	12.23	1.92	1.66	0	8.73
SK03	6.34	0.15	0.011	0.9	0.07	2.74	2.64	0.21	57.64	15.03	2.01	1.61	0	10.72
SK04	4.30	0.13	0.007	0.67	0.05	2.58	1.8	0.14	71.97	9.41	1.33	1.25	0	6.43
SK05	6.37	0.17	0.012	0.86	0.07	3.98	2.75	0.22	55.52	15.43	2.33	1.68	0	10.67
Alaska-Canada Basin														
B0215	5.56	0.56	0.011	0.57	0.08	6.29	2.2	0.17	48.37	11.58	4.09	2.58	0	17.94
02-15	5.62	0.59	0.011	0.59	0.09	7.83	2.28	0.19	45.41	11.69	5.03	2.65	0.1	17.94
15-41	7.24	0.78	0.013	0.7	0.09	2.1	3.14	0.22	45.28	15.32	2.79	4.05	0.21	18.08
16-42	6.26	0.57	0.011	0.72	0.09	3.29	2.71	0.22	54.17	13.44	2.66	2.79	0.04	13.02
19-47	6.38	1.04	0.011	0.65	0.1	1.23	2.61	0.27	48.41	12.87	2.49	3.91	0.16	19.88
21-49	7.09	0.39	0.011	0.67	0.09	1.91	2.45	0.5	53.81	12.18	2.66	3.68	0	14.59

LOI=volatiles loss on ignition (CO_2 , SO_3 , H_2O, Cl)

partitioning of major (and trace) elements in these fractions. The average chemical composition of the 50 Barents Sea sediments (analysis by atomic absorption) reported in Table 1 may be compared to the analyses for these three mineral fractions. An oxide-by-oxide comparison shows that within statistical uncertainty, the 50-sample average composition can easily be placed between the silt and the clay "end member" grain-size fractions.

Possibly an even better statistical fit could be made by including a component of the "sand" fraction. Such methodology will be explored as more data becomes available. Additionally, the statistical methodologies such as correlation, factor, and correspondance analysis will be applied for both major and trace elements. For now, attention may be drawn to an additional observation: at the quartz-rich end of the compositional spectrum, the major oxide composition of sample 116, nearest to the Russian coastline in the southern Barents Sea, would compare favorably to a "sand"-"silt" mixture from the grain-size fraction compositions at the bottom of Table 1. Further, the total sediment composition from which these three size-fraction compositions were derived (Wright, 1974, Table 2) compares favorably with the average of the sample analyses of the first three locations in Table 1 from the same "mineralogical province" (116-R is a repeat analysis).

Marine chemistry of iron and manganese

Finally, measured manganese abundances warrant consideration. Fifty sample analyses of seafloor sediments show values that range from 20 to 4785 ppm Mn. Most analyses are from sediment intervals 0 to 1 cm below seafloor. There is no apparent correlation with water depth: the two lowest concentrations, 20 and 47 ppm, come from water depths of 280 and 91 m respectively; the two highest Mn samples, 4656 and 4785 ppm, come from 930 and 21 m respectively. The latter of these two samples is from very near shore, on the west side near the longitudinal center of Novaya Zemlya. The other high Mn sample is about 75 km southeast of Franz Josef Land.

On average, the ratio of total iron to total manganese in the world's rivers is about 50:1, approximately the ratio in average crustal rocks (Taylor and McLennan, 1985). From our Barents Sea sediments element analyses, the range in the ratio of iron to manganese is measured as: 13.4<Fe/Mn<1725. The lower limit is for samples most enriched in Mn (4785 ppm) and the upper limit for the least Mn enriched (20 ppm). Corresponding iron concentrations are nearly the same, 3.45 and 3.69 wt.% (highest and lowest Fe/Mn respectively). For all samples, Fe concentration varies from values less than 1 wt.% to values greater than 7 wt.%, but this range is small, compared to the range of 20 to 4785 ppm for Mn. In seawater, Fe/Mn=0.20 (and this low ratio is reflected in mean residence times of 0.7 and 32 years for Fe and Mn respectively); in an average shale, Fe/Mn=55 (Mn=850 ppm); and in a pelagic red clay Fe/Mn=10 (Mn=6700 ppm; Broecker, 1974, p. 97; Taylor and McLennan, 1985). Comparing shales to clays, Fe concentration has increased by only 40% while Mn concentration has increased by a factor of 8. In general, then, Mn abundance can change by a factor of ten or more while iron abundance does not change appreciably.

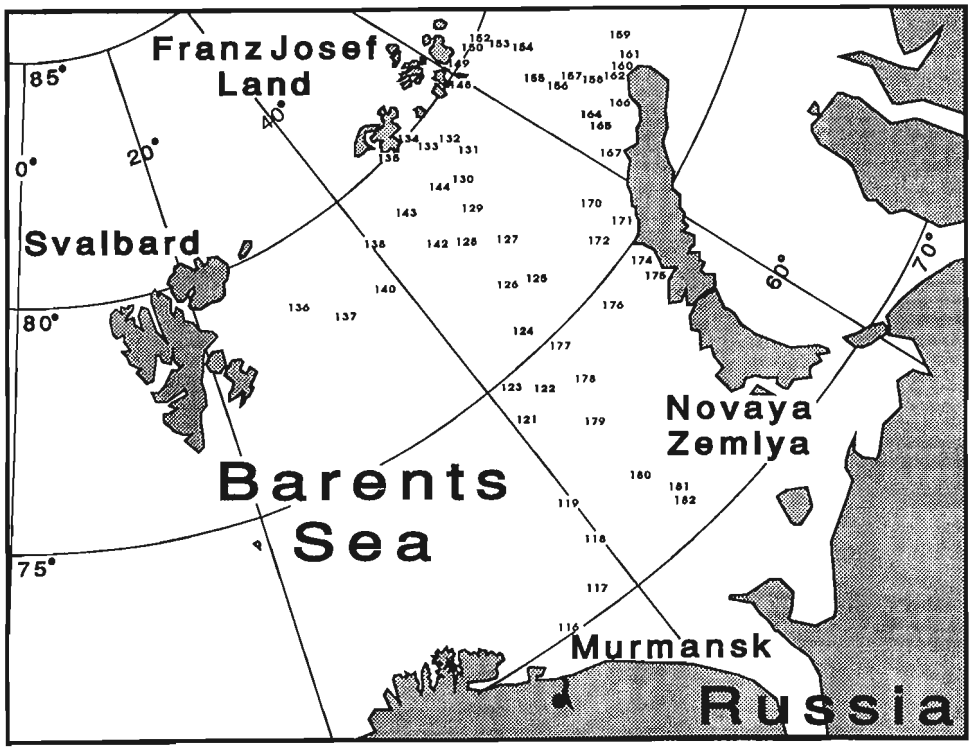

Figure 2. Map showing locations of sites in the Barents Sea where samples were collected from the research vessel "RRV Geolog Fersman" in 1992.

Furthermore, no mathematical (linear regression) correlation was found for the oxide concentration inter-sample variation between Mn and any other major element in our Barents Sea samples. The calculation of the correlation coefficient matrix was done using the program and methods of Jones and Facer (1982). Using our 11 sample analyses on Table 1 as input, a matrix of R-Mode Pearson product-moment coefficients was calculated. The program also calculates standard statistics for each variable, and creates a matrix of critical values for correlation coefficients at the 95 and 99% confidence levels. Further matricies are given, showing which correlation coefficients are significant for the analysed data, and for each pair of variables (or samples), the percentage of the variation in the values of one variable accounted for by a linear relationship with a second variable.

Full analysis of the correlation coefficient matrix for major element oxides in terms of mineral composition, and major and trace elements will be given in a separate paper. Here, it is noted that the trio of divalent cations Mn, Ca, and Ba show no significant correlation with any of the other 14 variables given for the 12 sample analyses in Table 1. MnO shows weak correlation with Fe_2O_3(0.3305), TiO_2(0.4144), and Al_2O_3(0.2500) - none of which attain the critical value at the 95% confidence level (0.5739). This may perhaps indicate that the three oxides (Mn, Ca, and Ba) are contained in an as yet unrecognized carbonate phase (no analysis was made for mineral CO_2 content, CO_2 is lost on ignition during XRF analysis). However, no correlation exists (r=0) between Mn, Ca, or Ba and LOI (loss on ignition). The weak association with the +3 and +4 valent cations may perhaps indicate some Mn in a +4 valence state. However, a weak negative correlation (-0.2834) with K_2 O argues against accommodation in some clay mineral phases.

Barents Sea: Manganese "Contaminant Plume"

Consequently, another alternative is considered. Concentration measurements for Mn in 50 samples from Barents seabed sediments show high concentrations at stations 130, 133, 138, 140, 144, 149, 150, 152, 153, 154, 155, 156, 157, 158, 164, 165, 171, and 174 (Fig. 2). All these locations and their associated higher Mn contents (>700 ppm) trace a pattern beginning at site 174 with the highest concentration (4785 ppm Mn, west side central Novaya Zemlya), proceeding northward to the tip of Novaya Zemlya Island (the "Polar Front") at site 165 (819 ppm Mn) and site 155 (3706 ppm) then veering west-southwest past Franz Josef Land (site 144, 4656 ppm) towards Svalbard (site 138, 1382 ppm). In approximate terms, what has been described here is a possible manganese "contaminant plume". If we remove the above 18 stations from consideration, then basin average ("background") Mn concentration drops from 1091 to 486 ppm, about 50% of average shale value, (850 ppm, Taylor and McLennan, 1985; Broecker, 1974), but perhaps in reasonable accord with grain-size fractions as measured by Wright (1974; see also Taylor and McLennan, 1985, Table 2.5, p. 21).

Current flow in the Barents Sea was discussed above. Flow directions and pattern are consistent with the distribution of anomalous Mn concentrations. Of the samples listed in Table 1, those from stations 153, 159, and 171 are within the putative "Mn plume". Sample 153-49 is from a sediment depth of 110 to 120 cm, 159-36 from 90 to 100 cm, 171-25 from 150 to 160 cm. All other samples are near the seafloor surface (0-10 cm). This might indicate that Mn input has occurred over a long period of time. The "point source" (near station 174) indicates a land-based origin for this Mn, such as manganese carbonates/ores (e.g., Platonov et al., 1992; Silayev et al., 1986). Further studies using SEM analyses and laboratory studies of Mn mineralization (e.g., Hem and Lind, 1994) will help in characterization of mineral speciation.

Toward the Asiatic side of the northern Russian coast, the Ob and Yennisey rivers introduce a considerable load of suspended matter into the surface waters of the Kara Sea (Nesterova, 1960; Kukal, 1971, Table 7; Aagaard and Carmack, 1989) and it is suggested that much of this fine suspensate passes into the north of the Barents Sea. Here, the influence of less saline Arctic water is also considered responsible for an increase in the concentration of dispersed iron and manganese (Gorshkova, 1966). Also, such an increase in concentration may contribute to local and regional anomalous manganese concentrations in bottom sediments as seen in results presented here.

ARCTIC CANADA (ICE ISLAND) AND OFFSHORE ALASKA SEDIMENTS

For some time, the dearth of geochemical analyses was noted with the recent increased emphasis on Arctic science and monitoring (e.g., AMAP, 1993), more data are becoming available. Here, we present major element analyses of 5 samples each: (1) from Ice Island (Hobson's Choice) sampling from the Arctic Polar Continental Shelf north of Axel Heiberg Island (Fig. 1, area A) and (2) from the Northwind Ridge and Beaufort Sea adjacent to the Canada basin (Fig. 2, area B; US Geological Survey, Cruise P1-93-AR, USCGC POLAR STAR, Aug.-Sept., 1993).

Detailed comparisons to available data on the two areas and a comparison to chemistry, composition, and mineralogy of the Barents Sea sediments will be given in a separate publication, together with further mathematical analyses of major and trace element content related to mineral composition and grain-size separates.

As well as major element composition and sample grain-size distribution, preliminary correlation analysis on these samples indicates the more benthic nature of these sediments compared to those from the Barents Sea. In addition, and as opposed to the Barents samples, there is a very high degree of positive correlation (0.8997 for both sample sets combined) between MnO and LOI (loss on ignition, presumed to be in part mineral CO_2), indicating manganese incorporation in carbonates.

CONCLUSIONS

Overall, our results on mineralogy and major element composition of the Barents Sea sediments corroborate and augment the work of Wright (1974) and his conclusions on the terrigenous character of the Barents Sea clay fraction. The conclusion that Atlantic water also introduces fine detritus into the southern part of the central depression is in accord with the known hydrography of the area. Similar arguments are used to demonstrate that arctic waters at the north end of Novaya Zemlya, flowing into the Barents from the Kara Sea, have their origin in the admixture of Siberian continental drainage with Arctic Ocean water – in accord with oceanographic observations (AMAP, 1993; Wright, 1974). Samples from this pivotal area and extending right into the Barents Sea are available to us. It will be pertinent to apply the methods discussed in this paper and extend the results to this area and thus add additional data for trace element and contaminant transport models in a key area of the Arctic Ocean system.

In accord with data on current flow in the Barents Sea, there may be seabed evidence for a manganese "contaminant plume" extending nearly 1000 km in an arc from central Novaya Zemlya, past the north of the island and then flowing southwest, toward the central Barents Sea. The "plume" may have been active since prehistoric time. If confirmed, valuable information will be provided on long-distance marine transport and dispersion mechanisms.

ACKNOWLEDGMENTS

We are indebted to A. Grantz (United States Geological Survey) and to P. Mudie (Atlantic Geoscience Centre) for providing samples from the Beaufort Sea and the Polar Continental Shelf respectively. Elemental compositions were determined by geochemists A.G. Heinrich and J.N.Y. Wong from the Institute of Sedimentary and Petroleum Geology. We also acknowledge the timely help of M. Labonté in supplying reference materials and software and for his review of this work.

REFERENCES

Aagaard, K. and Carmack, E.C.
1989: The role of sea ice and other fresh water in the Arctic Circulation; Journal of Geophysical Research, v. 94, p. 18163-18175.

AMAP (Arctic Monitoring and Assessment Program)
1993: The updated monitoring program for AMAP; Strømsveien 96, P.O. Box 8100 Oslo Norway.

Broecker, W.S.
1974: Chemical Oceanography; Harcourt Brace Jovanovich, Inc., New York. 214 p.

Gorshkova, T.I.
1966: Magranets v donnykh otlozhenniakh severnykh morei Sovetskogo Soiuza i ego biologicheskoe znachenie (Manganese in bottom sediments of the Northern Seas of the U.S.S.R. and its biological significance); Trudy, Vsesoiuznyi nauchno-issledovatelskii Institut Morskogo Rybnogo Khozianstva i Okeanografii (Proceedings, All Union Scientific Research Institute of the Fishing Economy and Oceanography), v. 60, p. 89-102.

Hem, J.D. and Lind, C.J.
1994: Chemistry of manganese precipitation in Pinal Creek, Arizona, USA: a laboratory study; Geochimica et Cosmochimica Acta, v. 58, p. 1601-1613.

Jones, B.G. and Facer, R.A.
1982: CORRMAT/PROB, a program to create and test a correlation coefficient matrix from data with missing values; Computers and Geosciences, v. 8, p. 191-198.

Kukal, Z.
1971: Geology of Recent Sediments; Academic Press, London, 490 p.

Livingston, H.D.
1988: The use of Cs and Sr isotopes as tracers in the Arctic and Mediterranean Sea; Philosophical Transactions of the Royal Society of London, Series A, v. 325, p. 161-176.

Livingston, H.D., Kupferman, S.L., Bowen, V.T., and Moore, R.M.
1984: Vertical profile of artificial radionuclide concentrations in the central Arctic Ocean; Geochimica et Cosmochimica Acta, v. 48, p. 2195-2203.

Marshall, E.
1992: A scramble for data on Arctic radioactive dumping; Science, v. 257, p. 608-609.

MacKenzie, D.
1994: Doubts lurk in graveyard for nuclear subs; New Scientist, v. 141, no. 1917, 19 March, p. 4.

Mayer, L.M.
1994: Surface area control of organic carbon accumulation in continental shelf sediments; Geochimica et Cosmochimica Acta, v. 58, p. 1271-1284.

Nassichuk, W.W., Skibo, D.N., Fowler, M.G., Stewart, K.R., and Snowdon, L.R.
1993: Update of Canada–Russia collaboration on Arctic Pollutants; in Current Research, Part E; Geological Survey of Canada, Paper 93-1E, p. 113-121.

Nesterova, I.L.
1960: Chemical composition of the suspended and dissolved loads of the Ob River; Geochemistry, v. 4, p. 424-431.

Platonov, Ye.G., Povysheva, L.G., and Ustritskii, V.I.
1992: Genesis of Mn-carbonate ores in the Pai-Khoi-Novaya Zemlya region; Lithology and Mineral Resources (USSR), v. 27, p. 332-341.

Price, N.B. and Wright, P.L.
1971: Variation in the mineralogy and chemistry of sediments from the southwestern Barents Sea; in The Geology of the East Atlantic Continental Margin, 2. Europe, (ed.) F.M. Delany; Great Britain Institute of Geological Sciences Report, no. 70/14, p. 17-31.

Price, N.B., Calvert, S.E., and Jones, P.G.W.
1970: The distribution of iodine and bromine in sediments of the southwestern Barents Sea; Journal of Marine Research, v. 28, p. 22-34.

Silayev, V.I., Tikhomirova, V.D., Yakovleva, O.A., and Gerasimov, A.Y.
1986: Tetrahedrite-group minerals in hydrothermal deposits of the Northern Ural-Novaya Zemlya province; International Geology Review, v. 28, p. 691-703.

Skibo, D.N. and Nassichuk, W.W.
1994: Persistent organic compounds in the Barents Sea: Canada-Russia collaboration on arctic pollutants; in Current Research 1994-B; Geological Survey of Canada, p. 1-9.

Taylor, S.R. and McLennan, S.M.
1985: The Continental Crust: its Composition and Evolution; Blackwell Scientific Publications, Oxford, 312 p.

Wright, P.L.
1974: The chemistry and mineralogy of the clay fraction of sediments from the southern Barents Sea; Chemical Geology, v. 13, p. 197-316.

Yablokov, A.V., Karasev, V.K., Rumyantsev, V.M., Kokeyev, M.Ye., Petrov, O.I., Lystsov, V.N., Yemelyenenkov, A.F., and Rubtsov, P.M.
1993: Facts and Problems Related to Radioactive Waste Disposal in Seas Adjacent to the Territory of the Russian Federation (Materials for a Report by the Government Commission on Matters Related to Radioactive Waste Disposal at Sea, Created by Decree No. 613 of the Russian Federation President, October 24, 1992); translated by Paul Gallager and Elena Bloomstein, Small World Publishers, Inc., 7813 Pickard Avenue, N.E., Albuquerque, NM 87110.

Geological Survey of Canada Project 840081

Preliminary stratigraphy of Lower and Middle Cambrian rocks, east-central Ellesmere Island, Canadian Arctic Islands

Carmen E. Thompson[1] and Brian R. Pratt[1]
Institute of Sedimentary and Petroleum Geology

Thompson, C.E. and Pratt, B.R., 1994: Preliminary stratigraphy of Lower and Middle Cambrian rocks, east-central Ellesmere Island, Canadian Arctic Islands; in Current Research 1994-E; Geological Survey of Canada, p. 165-168.

Abstract: The Lower and Middle Cambrian succession of east-central Ellesmere Island was examined between Bache Peninsula and Makinson Inlet. The basal unit consists of sandstone of the Dallas Bugt Formation. This is overlain by dolomitized ooidal grainstones and peritidal laminites of the Cape Leiper Formation. Succeeding Lower Cambrian units are shallow-subtidal dolostones of the Cape Ingersoll and Cape Kent formations, with a thin, intervening sandy limestone belonging to the Police Post Formation. The Middle Cambrian Cape Wood Formation is composed of limestone and dolostone that is also of shallow-subtidal aspect, and it is overlain by deeper subtidal, mixed siliciclastic-carbonate strata of the Upper Cambrian-Lower Ordovician Cass Fjord Formation. These units are readily mappable along strike for at least 250 km.

Résumé : La succession du Cambrien inférieur et du Cambrien moyen du centre est de l'île d'Ellesmere a été examinée entre la presqu'île Bache et l'inlet Makinson. L'unité basale est constituée de grès de la Formation de Dallas Bugt. Elle est recouverte de grainstones à oolites dolomitisés et de laminites péritidales de la Formation de Cape Leiper. Les unités successives du Cambrien inférieur sont des dolomies infratidales d'eau peu profonde des formations de Cape Ingersoll et de Cape Kent, avec de minces intercalations de calcaire sableux appartenant à la Formation de Police Post. La Formation de Cape Wood du Cambrien moyen est constituée de calcaire et de dolomie également de milieu infratidal d'eau peu profonde; elle est recouverte de strates infratidales d'eau plus profonde (carbonatées et silicoclastiques) de la Formation de Cass Fjord (Cambrien supérieur-Ordovicien inférieur). On peut facilement observer ces unités sur au moins 250 km dans la direction des couches.

[1] Department of Geological Sciences, University of Saskatoon, Saskatoon, Saskatchewan S7N 0W0

INTRODUCTION

Lower and Middle Cambrian strata are exposed on east-central and southern Ellesmere Island (Fig. 1). The sequence lies between the Precambrian basement and the Upper Cambrian-Lower Ordovician Cass Fjord Formation (Fig. 2). Christie (1967) erected the Cambrian stratigraphic framework based on rocks exposed on Bache Peninsula, and divided the succession into six formations. Crossbedded sandstones of the Dallas Bugt Formation unconformably overlie Precambrian gneiss, and are in turn overlain conformably by the dolostones of the Cape Leiper and Cape Ingersoll formations. The succeeding Police Post Formation is a thin bedded, arenaceous and glauconitic limestone. The overlying Cape Kent and Cape Wood formations are massive dolostone and dolomitic limestone, respectively. The Cass Fjord Formation is incompletely exposed on Bache Peninsula, and consists of recessive silty limestone.

Correlative Lower Cambrian strata are dominantly siliciclastic and reach a thickness of 3 km at the margin of the platform on Judge Daly Promontory. The Middle and Upper Cambrian carbonate portion increases to a thickness of 1.2 km and is made up of the Scoresby Bay and Parrish Glacier formations. These units thin to the northwest into resedimented carbonates of the Nesmith, Grant Land, and Hazen formations (Trettin et al., 1991).

STRATIGRAPHY

Dallas Bugt Formation

The Dallas Bugt Formation on Ellesmere Island is correlative with the type section in Greenland, and is assigned an Early Cambrian age, although no fossils have been collected from it (Troelsen, 1950).

At Bache Peninsula, the Dallas Bugt is 55 m thick, but only the upper 40 m are exposed, and a tripartite subdivision is apparent. The lower part of the unit consists of light grey, medium- to coarse-grained, commonly crosslaminated sandstone, whereas the middle part contains abundant *Skolithos*, and the upper 4 m is bioturbated, argillaceous, fine grained sandstone.

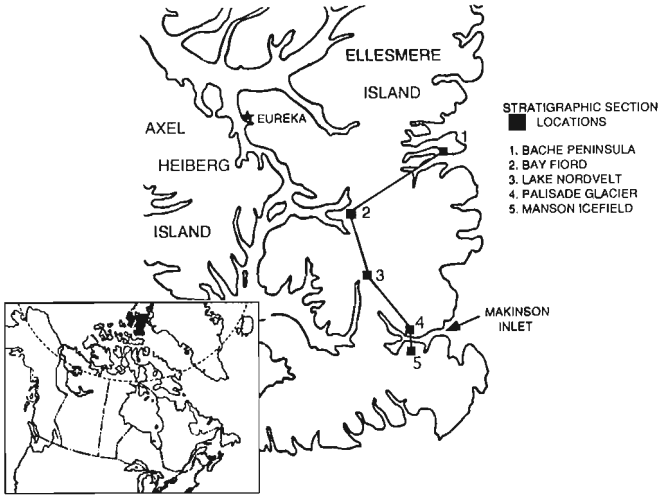

Figure 1. Location map of stratigraphic sections.

At Lake Nordvelt, the Dallas Bugt Formation is 200 m thick. The basal 15 m are grey-pink-weathering, coarse grained, crosslaminated, arkosic sandstones with abundant small scours and thin quartz pebble horizons. The overlying 70 m are very light grey, coarse grained, crosslaminated sandstones with abundant *Skolithos*. The upper 80 m are recessive, olive-green, fine grained, crosslaminated, bioturbated sandstones with thin shale interbeds.

Near Bay Fiord, the Dallas Bugt Formation is 120 m thick. The lower 80 m are similar to this interval on Bache Peninsula. The upper 40 m are argillaceous and highly bioturbated, and contain abundant arthropod trace fossils belonging to *Rusophycus*.

At Palisade Glacier, the lower 18 m of the Dallas Bugt Formation are composed of coarse grained, crosslaminated sandstones, and the upper 1 m is composed of olive-green, bioturbated, argillaceous sandstones. At Manson Icefield, the formation is 22 m thick but lacks the upper bioturbated interval.

Cape Leiper Formation

The type section of the Cape Leiper Formation is in Inglefield Land, North Greenland, and although no fossils have been recovered, an Early Cambrian age is assigned to it based on stratigraphic position (Troelsen, 1950). This dolostone unit was recognized on Bache Peninsula (Christie, 1967), and is lithologically consistent along strike to Makinson Inlet. The Cape Leiper Formation sharply, but conformably, overlies the Dallas Bugt Formation. It is 33.5 m thick on Bache Peninsula, 39 m near Bay Fiord, 54 m at Palisade Glacier, and 56 m at the Manson Icefield. The beds are resistant, light grey, and greyish orange- to light brown-weathering.

The lower part consists of thin and medium bedded, locally crosslaminated, well-sorted, medium grained ooidal grainstone that has been replaced by finely crystalline dolomite. The upper part is composed of dolomitized microbial laminites and thin bedded dolomitic mudstones, with scattered green-weathering clay seams. Fenestral fabric and intraclastic horizons are commonly visible in the laminites.

Cape Ingersoll Formation

The Cape Ingersoll Formation was also defined in Inglefield Land (Troelsen, 1950), and it was assigned an Early Cambrian age although it is unfossiliferous (Christie, 1967). The Cape Ingersoll Formation abruptly, but conformably, overlies the Cape Leiper Formation. It is 18 m thick at Bache Peninsula, 24 m at Palisade Glacier, and 50 m at the Manson Icefield. At the Bay Fiord section, the lower 10 m are covered. The unit is a resistant, greyish brown, pale reddish brown-weathering, bioturbated, locally vuggy, medium crystalline dolostone with coarsely crystalline patches. Original bedding and sedimentary structures have been obscured, either by bioturbation or subsequent dolomitization.

Police Post Formation

The type section of the Police Post Formation on Bache Peninsula is 4 m thick and contains trilobites of Early Cambrian age. It contains *Acrothele? pulchra* Poulsen 1946, *Hyolithes* sp., *Paedeumias? borealis* Poulsen 1946, *Bonniopsis nasuta*, and *B. rostrata*. Cowie (1968) identified the following trilobites: *Bonniopsis rostrata* Poulsen 1946, *Olenellus* sp., *Hyolithes* sp., *Circotheca* sp.

The brownish grey, recessive Police Post Formation has an abrupt but conformable contact with the underlying Cape Ingersoll Formation. On Bache Peninsula, the base and top of the Police Post Formation are marked by a thin bedded, bioturbated, glauconitic, pyritic, locally bioclastic, calcareous sandstone with minor detrital muscovite and feldspar. The unit is mainly a thin bedded, bioturbated, locally dolomitic, sandy limestone. An iron-stained hardground is found in the middle.

At Palisade Glacier the Police Post Formation consists of 2 m of thin bedded, bioturbated, finely crystalline, argillaceous dolostone that is pale green on fresh surfaces and weathers pale greyish orange. At Manson Icefield, the unit is 6 m thick and consists of finely crystalline, fossiliferous, bioturbated, argillaceous, lime mudstone. An abrupt lower contact with the Cape Ingersoll Formation is visible at both the Makinson Inlet and Manson Icefield localities. The Police Post Formation was not observed at Bay Fiord, where it is likely covered.

Cape Kent Formation

The type section of the Cape Kent Formation occurs in North Greenland and was identified on Bache Peninsula on the basis of its similar stratigraphic position and lithology (Troelsen, 1950). No fossils have been collected from the unit, but Poulsen (1927) assumed an Early Cambrian age. The Cape Kent Formation conformably overlies the Police Post Formation and is lithologically consistent along strike to Makinson Inlet. This resistant unit is greyish brown on fresh surfaces and moderate reddish brown on weathered surfaces. The Cape Kent Formation is a massive, bioturbated, locally vuggy, medium crystalline dolostone with coarsely crystalline patches. It is 14.5 m thick at Bache Peninsula, 25 m at Palisade Glacier, and 20 m at Manson Icefield. The lower contact is covered near Bay Fiord and only the upper 22 m are exposed.

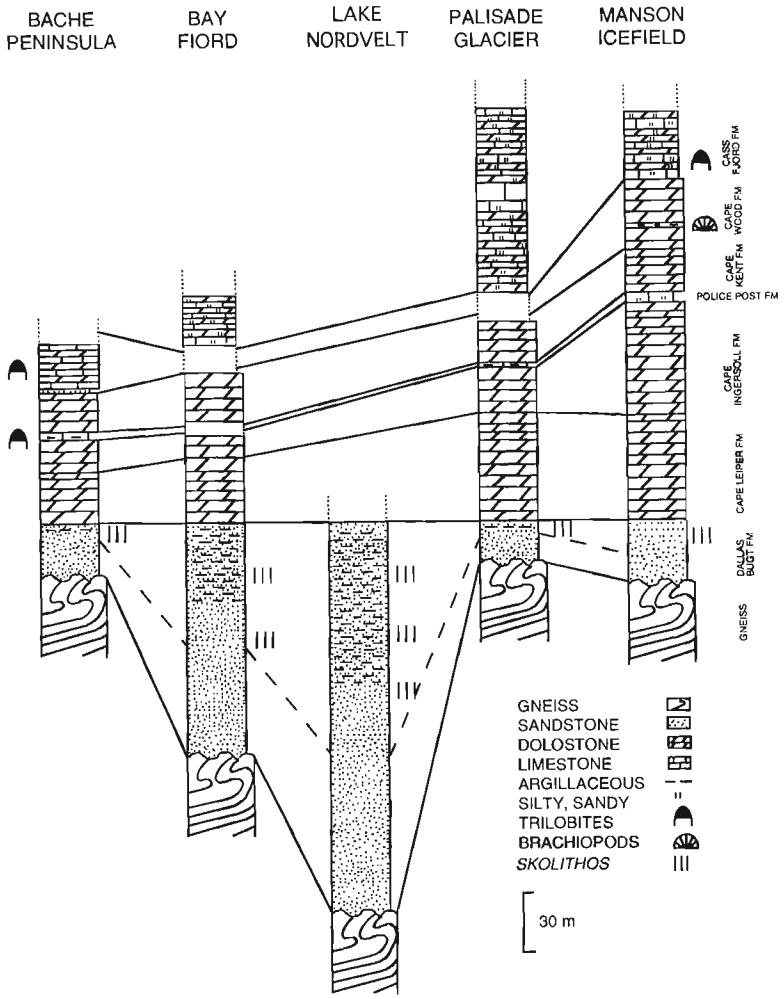

Figure 2.

Correlation of Lower and Middle Cambrian carbonate rocks of east-central Ellesmere Island. Thickness of Cape Wood at Bay Fiord and Palisade Glacier estimated.

Cape Wood Formation

The type section of the Cape Wood Formation is also in North Greenland. Troelsen (1950) assigned the former Cape Frederik II and Pemmican River formations on Bache Peninsula to the Cape Wood Formation and designated a lower Cape Russell Member and an upper Blomsterbaek Member. The Cape Wood Formation overlies the Cape Kent Formation, possibly with a disconformity (Kerr, 1967), although we found no evidence for this. The Cape Wood Formation contains a Middle Cambrian trilobite fauna, including *Clavaspidella*? sp., *Glossopleura* cf. *expansa* Poulsen 1946, *Glossopleura longifrons* Poulsen 1946, *Glossopleura walcotti* Poulsen 1946, *Blainiopsis benthami, Blainiopsis scheii, Blainiopsis*? sp., *Elrathia*? sp., *Kochina arctica*, and *Olenoides? fallax.*

On Bache Peninsula, the basal part of the Cape Wood Formation is marked by two thin, greenish grey, fine grained, glauconitic, bioturbated, calcareous sandstone beds, separated by 1.5 m of massive, bioturbated, vuggy, medium crystalline dolostone. The unit chiefly consists of alternating thin beds of finely crystalline, medium bedded, locally vuggy, burrow-mottled, light brown dolostone, and grey, finely crystalline lime mudstone with rare thin beds of cystoidal grainstone and trilobite packstone. Only the lower 31.5 m of the Cape Wood Formation is exposed at Bache Peninsula.

The basal 10 m of the Cape Wood Formation are not exposed at Manson Icefield. The lower part is composed of bioturbated, finely crystalline dolostone. The distribution of the burrow mottles gives the rock a distinctive moderate brown and pale orange colour-banded appearance. This dolostone passes abruptly into a thin bed of black, brachiopod-bearing, calcareous siltstone. The upper beds of the Cape Wood Formation are finely crystalline, burrow-mottled dolostone with two thin, crosslaminated, carbonate-cemented sandstone beds.

The Cape Wood Formation is unconformably overlain by the Upper Cambrian-Lower Ordovician Cass Fjord Formation. The abrupt contact is well exposed at Manson Icefield where the dolostone of the Cape Wood Formation is overlain by the reccessive, interbedded, thin bedded limestone, dolomitic mudstone, and intraclastic mudstone with thrombolite mounds in the middle of the formation.

DEPOSITIONAL ENVIRONMENTS

Skolithos indicates that the upper part of the Dallas Bugt Formation was deposited in shallow marine conditions. The lower part of the Cape Leiper Formation represents an offshore, high-energy, ooidal shoal, whereas the upper part is a low-energy, tidal flat complex. Late, fabric nonselective dolomitization of the Cape Ingersoll and Cape Kent formations makes it difficult to interpret the depositional setting of these units, but they, along with the Cape Wood Formation, appear to have been bioturbated, shallow-subtidal shelf, lime mud dominated sediments. The Police Post Formation similarly represents an open marine shelf, but with an influx of fine quartz sand and silt. Sporadic thin sandstones in the Cape Wood Formation indicate similar, but briefer pulses of siliciclastic influx.

ACKNOWLEDGMENTS

Support for this project was provided by the Institute of Sedimentary and Petroleum Geology, Polar Continental Shelf Project, Northern Scientific Training Program, and Natural Sciences and Engineering Research Council of Canada. We thank R. Thorsteinsson, T.A. de Freitas, J.C. Harrison, and D.G.F. Long for advice and help, and J. Montpetit, C. Lee, and R.G. Brown for field assistance.

REFERENCES

Christie, R.L.
1967: Bache Peninsula, Ellesmere Island, Arctic Archipelago; Geological Survey of Canada, Memoir 347, 63 p.

Cowie, J.W.
1968: Lower Cambrian faunas from Ellesmere Island, District of Franklin; Geological Survey of Canada, Bulletin 163, 38 p.

Kerr, J.W.
1967: Stratigraphy of central and eastern Ellesmere Island, Arctic Canada, Part I: Proterozoic and Cambrian; Geological Survey of Canada, Paper 67-27, part I, 63 p.

Poulsen, C.
1927: The Cambrian, Ozarkian, and Canadian faunas of Northwest Greenland; Meddelelser om Grnland, v. 70, p. 233-343.
1946: Notes on Cambro-Ordovician fossils collected by the Oxford University Ellesmere Land Expedition 1934-5; Quarterly Journal of the Geological Society of London, v. 102, p. 299-337.

Trettin, H.P., Mayr, U., Long, D.G.F., and Packard, J.J.
1991: Cambrian to early Devonian basin development, sedimentation, and volcanism, Arctic Islands; Chapter 8 in Geology of the Innutian Orogen and Arctic Platform of Canada and Greenland, (ed.) H.P. Trettin; Geological Survey of Canada, Geology of Canada, no. 3, (also Geological Society of America, The Geology of North America, v. E) p. 163-239.

Troelsen, J.C.
1950: Contributions to the geology of Northwest Greenland, Ellesmere Island, and Axel Heiberg Island; Meddelelser om Gronland, v. 149, no. 7, 86 p.

Geological Survey of Canada Project 860006

Canadian Shield

Bouclier canadien

Physical properties of Canadian kimberlites from Fort à la Corne, Saskatchewan[1]

N. Scromeda, T.J. Katsube, G. Bernius, and B.A. Kjarsgaard[2]
Mineral Resources Division

Scromeda, N., Katsube, T.J., Bernius, G., and Kjarsgaard, B.A., 1994: Physical properties of Canadian kimberlites from Fort à la Corne, Saskatchewan; in Current Research 1994-E; Geological Survey of Canada, p. 171-175.

Abstract: Physical properties (electrical resistivity, formation factor, magnetic susceptibility, density, and porosity) have been determined for five crater-facies kimberlite samples from Fort à la Corne (Saskatchewan), as part of a basic physical rock property study underway to provide information required for exploration activity in progress for kimberlite-hosted diamond deposits in Canada. Previous reports on physical properties had limited information on crater-facies kimberlites. The purpose of this study was to expand the data base.

Results indicate that physical properties of these crater-facies kimberlite samples somewhat differ from those previously reported. They include the largest magnetic susceptibility and smallest bulk electrical resistivity values. The bulk density is at the lower end and the effective porosity at the higher end within the previously reported values. Generally, crater-facies rocks appear to be relatively porous as compared to the hypabyssal facies, suggesting they are more susceptible to alteration. Therefore, the resistivity and porosity characteristics of these samples may be representative of typical crater-kimberlites.

Résumé : Les propriétés physiques (résistivité électrique, facteur de formation, susceptibilité magnétique, masse volumique et porosité) ont été déterminées dans le cas de cinq échantillons de kimberlite à faciès de cratère provenant de Fort à la Corne (Saskatchewan) dans le cadre d'une étude sur les propriétés physiques de base des roches entreprise pour recueillir des informations aux fins de la prospection en cours visant à découvrir des gisements de diamant dans des kimberlites au Canada. Les rapports précédents sur les propriétés physiques contenaient des informations limitées sur les kimberlites à faciès de cratère. La présente étude a pour objet d'accroître la base de données.

Les résultats indiquent que les propriétés physiques de ces échantillons de kimberlite à faciès de cratère diffèrent quelque peu de ceux présentés dans le passé. Ils donnent les valeurs les plus élevées sur la susceptibilité magnétique et les plus faibles sur la résistivité électrique de volume. La masse volumique apparente se situe à l'extrémité inférieure des valeurs indiquées antérieurement et la porosité réelle à leur extrémité supérieure. En général, les roches à faciès de cratère semblent être relativement poreuses comparativement aux roches à faciès hypabyssal, indiquant qu'elles sont plus susceptibles de s'altérer. Par conséquent, la résistivité et la porosité de ces échantillons peuvent être représentatives des kimberlites de cratère.

[1] Contribution to Canada-Saskatchewan Partnership Agreement on Mineral Development (1990-1995), a subsidiary agreement under the Canada-Saskatchewan Economic and Regional Development Agreement.
[2] Continental Geoscience Division

INTRODUCTION

Physical rock properties (electrical resistivity, formation factor, magnetic susceptibility, density, and porosity) have been determined for five crater-facies kimberlite samples from Fort à la Corne, Saskatchewan (Fig. 1). This is part of a basic physical rock property study (Katsube et al., 1992a; Katsube and Scromeda, 1994) being carried out to provide information required for exploration (planning and interpretation of geophysical data), a response to the Canadian mineral exploration activity in progress for kimberlite-hosted diamond deposits. Previous physical property studies had limited information on kimberlites of the crater-facies.

While rock property data on electrical resistivity, magnetic susceptibility, and density can be used directly for interpretation of surface and airborne geophysical methods, formation factor and porosity are used to analyze the physical structure of the rocks, and help link the geophysical parameters (electrical resistivity, magnetic susceptibility, and density) to the geological characteristics of the kimberlites. Examples of such analyses using these parameters can be found in the literature (Katsube and Hume 1987; Katsube et al., 1991; Katsube and Mareschal, 1993). This paper is primarily a documentation of physical properties of kimberlites with studies currently continuing (e.g., Katsube and Kjarsgaard, unpub. data, 1994) on quantitative relationships between mineralogy, petrographic textural type, and physical properties.

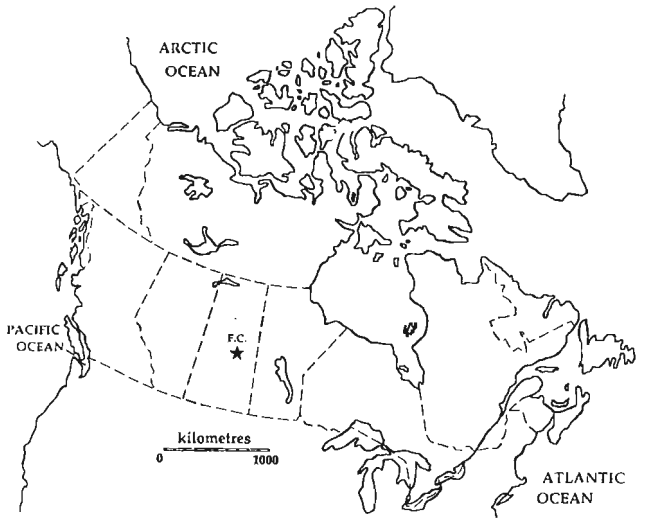

Figure 1. Location of the site from which the samples have been obtained; F.C. on the map represents the Fort à la Corne (Saskatchewan) site.

METHOD OF INVESTIGATION

Samples and sample preparation

Five drill core samples of kimberlite, representing crater-facies, were collected for this study. The sample numbers used in the laboratory, sampling locations, and field identification numbers used by the geologists who collected them are all listed in Table 1. First, magnetic susceptibility measurements were made on these samples. Then, rectangular specimens were cut from these core samples for electrical resistivity, formation factor, porosity and bulk density measurements. The geometric characteristics of the specimens used for the electrical (bulk electrical resistivity and formation factor) and bulk density measurements are listed in Table 2. The specimen dimensions are in the range of (1.2-2.9)x(1.8-2.7) cm for the cross-section, and 0.8-1.1 cm for thickness, dimensions similar to those previously reported (Katsube et al., 1992a; Katsube and Scromeda, 1994). Remaining chips, instead of the rectangular specimens, were used for effective porosity measurements. The geometric factor, K_G, used in the electrical measurements was determined for the rectangular specimens (Table 2) as part of the sample preparation procedure. Further details of the sample preparation procedures generally used for these kimberlites have been described previously (Katsube et al., 1992a).

Table 1. Kimberlite sample information (sample numbers used in the laboratory, sampling locations, Geological Survey of Canada I.D. numbers).

Sample number	Sampling location	Sample I.D.
CS-1	Fort à la Corne, Saskatchewan	KIA91-UK-120-4
CS-2	Fort à la Corne, Saskatchewan	KIA92-UK120-114.5
CS-3	Fort à la Corne, Saskatchewan	KIA92-UK120-221.7
CS-4	Fort à la Corne, Saskatchewan	KIA92-UK120-224.5
CS-5	Fort à la Corne, Saskatchewan	KIA91-UK-426-3

Table 2. Dimensions of specimens cut from the kimberlite samples for electrical measurements.

Sample	a_1 (cm)	a_2 (cm)	ℓ (cm)	W (g)	K_G (10^{-2}m)	δ (g/mL)
CS-1/1	1.248	1.978	0.883	5.7086	2.80	2.62
CS-2/1	1.741	1.828	1.100	7.6023	2.89	2.17
CS-3/1	1.491	2.170	1.009	7.8222	3.21	2.40
CS-4/1	1.927	2.692	0.786	9.5984	6.60	2.35
CS-5/1	1.384	1.838	0.908	5.6029	2.80	2.43

a_1, a_2 : Length of the two sides of the rectangular specimen
ℓ : Thickness of specimen
W : Weight of specimen under room dry conditions
K_G : Geometric factor
δ : Bulk density

Physical property measurements

The methods used to determine the physical properties of these samples (bulk electrical resistivity, ρ_r; formation factor, F; magnetic susceptibility, MS; bulk density, δ; and effective porosity, ϕ_E) have been described in detail in previous papers (Katsube et al., 1992a; Katsube and Scromeda, 1994), and shall not be repeated here. The calliper method (API, 1960) has been used to determine the bulk density (δ) of the samples, by measuring the dimensions and weight of the rectangular specimens. The effective porosity (ϕ_E) was determined from the difference in weight between the oven-dried and water-saturated rock specimen, generally following the API Recommended Practice for Core-Analysis Procedures (API, 1960). Details of the procedures routinely used in our measurements are described in the literature (Katsube et al., 1992b; Scromeda and Katsube, 1993). The methods used for the magnetic susceptibility (MS) measurements of these kimberlites are described in Katsube et al. (1992a).

The bulk electrical resistivity (ρ_r) is determined from the complex electrical resistivity measurements (Katsube, 1975b; Katsube and Walsh, 1987; Katsube et al., 1991) made over a frequency range of 1-10^6 Hz, and generally represents a value at frequencies of about 10^2-10^4 Hz. The formation factor (F) which, in principle, is the ratio of the bulk electrical resistivity (ρ_r) over the pore fluid resistivity, ρ_w (Archie, 1942), is actually determined by measuring the bulk electrical resistivity (ρ_m) for solutions of different salinities (NaCl: 0.02-0.50 N), and then inserting the results into the Patnode and Wyllie (1950) Equation. This is to eliminate the pore surface electrical conduction effect which reduces the accuracy of the formation factor (F) determinations. Details of the procedures used for these measurements can be found elsewhere (e.g., Katsube and Walsh, 1987; Katsube et al., 1991; Katsube and Scromeda, 1993).

EXPERIMENTAL RESULTS

The results of the bulk density (δ) determinations are listed in Table 2, and are in the range of 2.2-2.6. These values are at the lower end of those previously reported for these kimberlites (Katsube et al., 1992a; Katsube and Scromeda, 1994) and resemble those of sedimentary rocks (Daly et al., 1966). Results of the magnetic susceptibility (MS) measurements are listed in Table 6 (see below), displaying values in the range of (1.0-60)x10^{-3} SI units, which include some of the highest values reported for our kimberlite data set (Katsube et al., 1992a; Katsube and Scromeda, 1994). Results of the effective porosity (ϕ_E) measurements are listed in Table 3, displaying values of 9-19% which are well within the previously reported range of values for crater- and diatreme-facies kimberlites (Katsube et al., 1992a; Katsube and Scromeda, 1994). These values also resemble those for sedimentary rocks (Daly et al., 1966).

The results of the bulk electrical resistivity (ρ_r) measurements are listed in Table 4, displaying values in the range of 10-300 Ω-m. These include the smallest values in our kimberlite data set. Some are one order of magnitude lower than those previously reported for crater- and diatreme-facies kimberlites (Katsube and Scromeda, 1994), and resemble the bulk electrical resistivity (ρ_r) values of sedimentary and volcanic rocks (Keller, 1982). Measurements have been made at 24 and 48 hours after saturation, to ensure that they represent ρ_r values stable with time. However, since some of these values are close to the lower limit of this measuring system (approximately 1-5 Ω-m), difficulties have been experienced in determining the bulk electrical resistivity values (ρ_r) by the conventional method, which is from the arcs of the complex resistivity plots (e.g., Katsube and Walsh, 1987; Katsube and Scromeda, 1994). Therefore, the ρ_r values have had to be

Table 3. Results of the effective porosity measurements.

Sample	δ (g/mL)	W_w (g)	W_D (g)	S_{ir} (%)	ϕ_E (%)
CS-1	2.62	9.1450	8.8448	19.1	8.89
CS-2	2.17	28.1804	25.9966	4.9	18.23
CS-3	2.40	5.4030	5.0912	8.0	14.70
CS-4	2.35	5.5251	5.1716	7.5	16.06
CS-5	2.43	3.5284	3.3534	11.7	12.68

W_w = Wet weight
δ = Bulk density
W_D = Dry weight
ϕ_E = Effective porosity
S_{ir} = Static irreducible water saturation

Table 4. Results of electrical resistivity measurements.

Sample	ρ_r (Ω-m) Mes. #1	Mes. #2	Mean
CS-1/1	11	11	11 ± 0.5
CS-2/1	19	24	22 ± 3
CS-3/1	38	11	25 ± 14
CS-4/1	9	11	10 ± 1
CS-5/1	271	341	310 ± 40

ρ_r = Bulk electrical resistivity
Mes. (#1) = Measurement after 24 hours of saturation
Mes. (#2) = Measurement after 48 hours of saturation

Table 5. Formation-factor, surface resistivity, and bulk electrical resistivities for different NaCl solutions for sample CS-5/1.

NaCl (N)	ρ_w (Ω-m)	ρ_m (Ω-m)
0.02	5.21 ± 0.08	260
0.05	2.01 ± 0.08	310
0.1	1.08 ± 0.003	250
0.2	0.62 ± 0.04	180
0.5	0.27 ± 0.02	90
F ± %		400 ± 3
ρ_c ± %		450 ± 5

ρ_w = Pore fluid resistivity
ρ_m = Bulk electrical resistivity of the rock for solutions of different salinities
F = Formation factor
ρ_c = Surface resistivity

Table 6. Summary of petrophysical and physical properties.

Samples	δ (g/mL)	MS (10^{-3})	ϕ_E (%)	F	ρ_r (Ω-m)	ρ_c (Ω-m)
CS-1	2.62	25.	8.9	-	11 ± 0.5	-
CS-2	2.17	60.	18.2	-	22 ± 3	-
CS-3	2.40	36.	14.7	-	25 ±14	-
CS-4	2.35	44.	16.1	-	10 ± 1	-
CS-5	2.43	1.0	12.7	400 ± 20	310 ±40	450 ± 30

δ = Bulk density
MS = Mean MS in SI units
ϕ_E = Effective porosity
F = Formation factor
ρ_r = Bulk electrical resistivity
ρ_c = Surface resistivity

determined from the complex resistivity versus frequency plots (e.g., Katsube and Collett, 1975; Katsube 1975a, 1977), which essentially produce error ranges larger than those listed in Table 4: 5-50%. Results of the resistivity measurements (ρ_m) used for formation factor (F) determination are listed in Table 5. Only one determination (sample CS-5) was possible for these samples, since most of them had ρ_m values too small to be measured accurately. The results of 400 for F and 450 Ω-m for surface resistivity (ρ_c) are similar to values previously reported for these crater- and diatreme-facies kimberlites (Katsube and Scromeda, 1994). The percentage errors listed in Table 5 are determined by taking the differences in the F and ρ_c values obtained using the different regression lines: the reduced major axis (RMA) and the normal regression lines (NRL). The principles of the RMA are described in Davis (1986), and examples of related applications are found in the literature (Katsube and Agterberg, 1990).

DISCUSSION AND CONCLUSIONS

Results for all six parameters: bulk density (δ), magnetic susceptibility (MS), effective porosity (ϕ_E), formation factor (F), bulk resistivity (ρ_r) and surface resistivity (ρ_c), are compiled in Table 6 for all five kimberlite samples. These crater-facies kimberlite samples are somewhat different from those previously measured (Katsube et al., 1992a; Katsube and Scromeda, 1994). They include the largest magnetic susceptibility (MS) and smallest bulk electrical resistivity (ρ_r) values. The low bulk density (δ) and high effective porosity (ϕ_E) values of these samples are similar to the previously reported data for the crater- and diatreme-facies kimberlites. The results of formation factor (F) and surface resistivity (ρ_c) measurements, for one sample out of these five samples (Table 5), produced values also within the known range of values for kimberlites. However, because the bulk electrical resistivities (ρ_m) of the other four samples were too small for determining accurate formation factor (F) and surface resistivity (ρ_c) values, it might be assumed that these remaining samples also have very low F and ρ_c values.

Generally, crater- and diatreme-facies rocks are relatively porous as compared to the hypabyssal-facies. As a result, they are more susceptible to alteration (secondary clay minerals and carbonates). Therefore, the resistivity and porosity characteristics of these Fort à la Corne samples may represent typical crater-facies kimberlites. Further studies are underway (e.g., Katsube and Kjarsgaard, unpub. data, 1994) to determine the relationship between these samples and those previously reported, and to investigate the quantitative relationship between the mineralogy and the physical properties.

ACKNOWLEDGMENTS

The authors acknowledge support for this kimberlite study from the Canada-Saskatchewan Mineral Development Agreement (1990-1995). The samples were obtained from the Fort à la Corne Joint Venture Project, consisting of Uranerz Exploration and Mining Limited, Cameco Corporation, and Monopros Limited; the project is operated by Uranerz.

REFERENCES

API (American Petroleum Institute)
1960: Recommended practices for core-analysis procedure; API Recommended Practice 40 (RP 40) First Edition, American Petroleum Institute, Washington, D.C., p. 55.

Archie, G.E.
1942: The electrical resistivity log as an aid in determining some reservoir characteristics; Transactions of the American Institute of Mining, Metallurgical and Petroleum Engineers, v. 146, p. 54-67.

Daly, R.A., Manger, E.G., and Clark, S.P., Jr.
1966: Density of rocks; Sec.4 (p. 23) in Handbook of Physical Constants, The Geological Society of America, Inc., Memoir 97, p. 19-26.

Davis, J.C.
1986: Statistics and Data Analysis in Geology; John Wiley & Sons, p. 200-204.

Katsube, T.J.
1975a: The critical frequency and its effect on EM propagation; Geological Survey of Canada, Paper 75-1A, p. 101-105.
1975b: The electrical polarization mechanism model for moist rocks; Geological Survey of Canada, Paper 75-1C, p. 353-360.
1977: Electrical properties of rocks; in Induced Polarization for Exploration Geologists and Geophysicists, Short Course Presented by the University of Arizona, Tucson, March 14-16, p. 15-44.

Katsube, T.J. and Agterberg, F.P.
1990: Use of statistical methods to extract significant information from scattered data in petrophysics; in Statistical Applications in the Earth Sciences, (ed.) F.P. Agterberg and G.F. Bonham-Carter; Geological Survey of Canada, Paper 89-9, p. 263-270.

Katsube, T.J. and Collett, L.S.
1975: Electromagnetic propagation characteristics of rocks; in The Physics and Chemistry of Rocks and Minerals, (ed.) R.G.J. Strens; John Wiley & Sons Ltd., p. 279-295.

Katsube, T.J. and Hume, J.P.
1987: Permeability determination in crystalline rocks by standard geophysical logs; Geophysics, v. 52, p. 343-352.

Katsube, T.J. and Mareschal, M.
1993: Petrophysical model of deep electrical conductors; Graphite lining as a source and its disconnection due to uplift; Journal of Geophysical Research, v. 98, B5, p. 8019-8030.

Katsube, T.J. and Scromeda, N.
1993: Formation factor determination procedure for shale sample V-3; in Current Research, Part E; Geological Survey of Canada, Paper 93-1E, p. 321-330.
1994: Physical properties of Canadian kimberlites; Somerset Island and Saskatchewan; in Current Research, Part B; Geological Survey of Canada, Paper 94-1B, p. 35-42.

Katsube, T.J. and Walsh, J.B.
1987: Effective aperture for fluid flow in microcracks; International Journal of Rock Mechanics and Mining Sciences and Geomechanics Abstracts, v. 24, p. 175-183.

Katsube, T.J., Best, M.E., and Mudford, B.S.
1991: Petrophysical characteristics of shales from the Scotian shelf; Geophysics, v. 56, p. 1681-1689.

Katsube, T.J., Scromeda, N., Bernius, G., and Kjarsgaard, B.A.
1992a: Laboratory physical property measurements of kimberlites; in Current Research, Part E; Geological Survey of Canada, Paper 92-1E, p. 357-364.

Katsube, T.J., Scromeda, N., and Williamson, M.
1992b: Effective porosity of tight shales from the Venture Gas Field, offshore Nova Scotia; in Current Research, Part D; Geological Survey of Canada, Paper 92-1D, p. 111-119.

Keller, G.V.
1982: Electrical properties of rocks and minerals; in Handbook of Physical Properties of Rocks, Vol.I (ed.) R.S. Carmichael; CRC Press, Inc., Florida, p. 217-293.

Patnode, H.W. and Wyllie, M.R.J.
1950: The presence of conductive solids in reservoir rocks as a factor in electric log interpretation; Transactions of the American Institute of Mining, Metallurgical and Petroleum Engineers, v. 189, p. 47-52.

Scromeda, N. and Katsube, T.J.
1993: Effect of vacuum-drying and temperature on effective porosity determination for tight rocks; in Current Research, Part E; Geological Survey of Canada, Paper 93-1E, p. 313-319.

Geological Survey of Canada Project 880029HL

Apparent tortuosity of granitic rock samples from the Lac du Bonnet batholith, Manitoba

T.J. Katsube, N. Scromeda, and T.T. Vandergraaf[1]
Mineral Resources Division

Katsube, T.J., Scromeda, N., and Vandergraaf, T.T., 1994: Apparent tortuosity of granitic rock samples from the Lac du Bonnet batholith, Manitoba; in Current Research 1994-E; Geological Survey of Canada, p. 177-182.

Abstract: Effective porosity(ϕ_E) and formation factor(F) have been determined for twelve specimens cut from three granite samples taken at the surface of Lac du Bonnet batholith (Manitoba), to determine their apparent tortuosities(τ_a). This parameter influences radionuclide or ionic transport by diffusion in rocks, and is defined by

$$\tau_a = \sqrt{(F\phi_E)}.$$

The results indicate that the formation factor(F) and effective porosity(ϕ_E) values are in the ranges of 4800-8300 and 0.42-0.56%, respectively. These ranges are within, but at the higher end of those reported previously. The apparent tortuosity(τ_a) values are 5.0-6.4. There is a similar parameter represented by diffusion tortuosity(τ_D) which is directly determined from the diffusion measurements. The apparent tortuosity (τ_a) values obtained by this study are slightly higher than those previously reported for this type of rock, but resemble previously reported diffusion tortuosity (τ_D) values.

Résumé : La porosité réelle (ϕ_E) et le facteur de formation (F) ont été déterminés dans douze échantillons provenant de trois morceaux de granite prélevés à la surface du batholite du Lac du Bonnet (Manitoba) pour établir leur tortuosité apparente (τ_a). Ce paramètre influe sur le transport des ions ou des radionuclides par diffusion dans les roches et est défini par

$$\tau_a = \sqrt{(F\phi_E)}.$$

Les résultats indiquent que le facteur de formation (F) et la porosité réell (ϕ_E) varient respectivement entre 4800 et 8300 et entre 0,42 et 0,56 %. Ces intervalles se situent à l'extrémité supérieure des intervalles indiqués antérieurement. La tortuosité apparente (τ_a) varie entre 5,0 et 6,4. Il existe un paramètre semblable représenté par la tortuosité de la diffusion (τ_D) qui est directement déterminé à partir des mesures de la diffusion. Les valeurs de la tortuosité apparente (τ_a) obtenues dans la présente étude sont légèrement plus élevées que celles indiquées dans les études antérieures portant sur ce type de roche, mais elles sont semblables aux valeurs de la tortuosité (τ_D) déjà indiquées.

[1] Atlantic Energy of Canada Limited Research, Whiteshell Laboratories, Pinawa, Manitoba R0E 1L0

INTRODUCTION

Effective porosity, ϕ_E, and formation factor, F, have been determined for twelve specimens cut from three granite samples taken at the surface of Lac du Bonnet batholith (located approximately 100 km east of Winnipeg, Manitoba), in order to determine their apparent tortuosity, τ_a, a parameter that influences radionuclide or ionic transport by diffusion (Katsube et al., 1986). Apparent tortuosity (τ_a) is defined by (Ward and Fraser, 1967)

$$\tau_a = \sqrt{(F\phi_E)}, \quad (1)$$

It is a parameter originally considered to represent the true tortuosity, τ, defined by

$$\tau = \ell_p / \ell, \quad (2)$$

where ℓ_p and ℓ are the actual distance between two points along a connecting pore, and the shortest distance between these two points, respectively. However, since effective porosity (ϕ_E) consists of pore space not only of the connecting pores (connecting porosity, ϕ_c), but also of the pocket pores (Katsube et al., 1985; 1991; Agterberg et al., 1985):

$$\phi_E = \phi_p + \phi_c \quad (3)$$

$$\phi_c = bt^2/F, \quad (4)$$

where ϕ_p is the pocket porosity and b is a coefficient equal to 1.5 for an isotropic rock (Katsube et al., 1991), $\tau_a = \tau$ only when $\phi_p = 0$. That is, true tortuosity (τ) represents the actual tortuosity of the fluid flow paths in the rock, and apparent tortuosity (τ_a) also includes the effect of pocket porosity. Pocket porosity (ϕ_p) represents the porosity of all space in blind pores and enlargements along the flow paths. The apparent tortuosity (τ_a), however, appears to be the petrophysical parameter that influences ionic diffusion (Katsube et al., 1986).

The purpose of this paper is to report the results of the apparent tortuosity(τ_a) determinations for the three granite samples.

Table 1. Dimensions of specimens cut out from the granite samples for electrical measurements.

Sample No.	a_1	a_2	ℓ	W	K_G	δ
1-1-1	1.548	2.211	1.407	12.8514	2.433	2.67
1-1-2	1.920	2.527	1.424	18.3127	3.407	2.65
1-2-1	1.785	2.565	1.421	17.2144	3.222	2.65
1-2-2	2.192	2.230	1.379	17.7850	3.545	2.64
2-1-1	1.951	2.591	1.561	20.9359	3.238	2.65
2-1-2	2.057	2.843	1.585	24.5020	3.690	2.64
2-2-1	1.979	2.514	1.415	18.6652	3.516	2.65
2-2-2	1.919	2.579	1.414	18.6896	3.500	2.67
3-1-1	2.079	2.868	1.349	21.3629	4.420	2.66
3-1-2	1.988	2.653	1.368	19.2368	3.855	2.67
3-2-1	1.952	2.608	1.232	16.7722	4.132	2.67
3-2-2	2.010	2.875	1.244	19.2633	4.645	2.68
Units	(cm)	(cm)	(cm)	(gm)	(10^{-2} m)	(g/mL)

a_1, a_2: Lengths of the two sides of the rectangular specimen.
ℓ: Thickness of specimen.
W: Weight of specimen.
K_G: Geometric factor.
δ: Bulk density.

METHOD OF INVESTIGATION

Samples and sample preparation

Twelve rectangular specimens cut from three surface granite samples, were obtained from the Lac du Bonnet batholith (Pinawa, Manitoba) by Atomic Energy of Canada Limited. The samples were cut with a high speed diamond impregnated wheel saw using tap water, and then rinsed with distilled water. The dimensions of the specimens were in the range of (2.5-3)x(2.5-3) cm for the cross-section, and 1.2-1.6 cm for thickness. Each of these specimens were cut into two sub-specimens, one used for electrical resistivity(ρ_r), formation factor (F), and bulk density (δ) measurements, their dimensions in the range of (1.5-2.2)x(2.2-2.9) cm for the cross-section with no change in thickness. The geometric characteristics of these specimens are listed in Table 1. The other sub-specimens were used for effective porosity (ϕ_E) and static irreducible water saturation (S_{ir}) measurements, their approximate dimensions in the range of 1x3 cm for the cross-section, again with no change in thickness. As part of the sample preparation procedure, bulk density (δ) used for the porosity measurements and geometric factor (K_G) used for electrical measurements were determined for all specimens by the following equations:

$$\delta = W/(A\ell) \quad (5)$$

$$K_G = A/\ell \quad (6)$$

$$A = a_1 a_2, \quad (7)$$

where W, A and ℓ are the weight, cross-section area and thickness of the sub-specimens, and a_1 and a_2 are the lengths of the two sides of the rectangular sub-specimens. The calliper method (API, 1960) was used to determine bulk density (δ), by measuring the dimensions (a_1, a_2 and ℓ) and weight (W) of the sub-specimens. The bulk density (δ) and geometric factor (K_G) data are listed in Table 1.

Effective porosity measurements

The effective porosity (ϕ_E) is determined from the difference in weight between the oven-dried and water-saturated rock specimen:

$$\phi_E = (W_W - W_D)\delta/(W_D\delta_W), \quad (8)$$

where W_W is the weight of the fluid saturated rock specimen, W_D is that of the dry rock specimen at 116°C, and δ_W is the bulk density of the pore water (at 25°C, usually considered to be unity). The API Recommended Practices for Core-Analysis Procedures (API, 1960) have generally been followed in these measurements, with details of the procedures routinely used in our measurements described in the literature (e.g., Katsube et al., 1992a, b; Scromeda and Katsube, 1993). The static irreducible water saturation (S_{ir}):

$$S_{ir}=(W_r-W_D)/(W_W-W_D), \quad (9)$$

where W_r is the weight of the specimen which includes the free and bound (or adsorbed) water on the pore surfaces, was determined by drying the vacuum saturated specimens at room temperature (25°C) for a time period of over 300 minutes until the variation of its value decreased below 0.1%/hour. The effective porosity (ϕ_{ES}) which excludes the space occupied by the surface water layers is derived using the following equation:

$$\phi_{ES} = \phi_E(1 - S_{ir}) = (W_W-W_r)\delta/(W_D\delta_W). \quad (10)$$

Formation factor determination

Formation factor(F) represents the characteristics of the pore structure specifically related to the flow of fluids and ions through the rock (Katsube et al, 1991; Katsube and Mareschal, 1993). In principle, it is determined by taking the ratio of the bulk electrical resistivity (ρ_r) over the pore fluid resistivity, ρ_w (Archie, 1942). Actually, in order to eliminate the pore surface electrical conductivity or surface resistivity, ρ_c, effect (Patnode and Wyllie, 1950), the formation factor (F) is determined by measuring the bulk electrical resistivity (ρ_m) of the rock for solutions of different salinities (NaCl: 0.02-0.50 N), and then inserting the results into the Patnode and Wyllie (1950) equation:

$$1/\rho_m = 1/F\rho_w + 1 / \rho_c. \quad (11)$$

Linear regression is used to determine the slope (1/F) and intercept ($1/\rho_c$), of the $1/\rho_m$-$1/\rho_w$ curve (equation 11), from which F and ρ_c are derived. The conventional method used to determine the formation factor (F), first determines the apparent formation factor, F_a, for each NaCl solution:

$$F_a = \rho_m/\rho_w, \quad (12)$$

Table 2. Results of the effective porosity and static irreducible water saturation measurements.

Sample	δ (g/mL)	W_W (g)	W_D (g)	S_{ir} (%)	ϕ_E (%)
1-1-1	2.67	6.4184	6.4083	35.64	0.42 ± 0.04
1-1-2	2.65	3.8217	3.8137	22.50	0.56 ± 0.06
1-2-1	2.65	4.9249	4.9167	24.39	0.44 ± 0.04
1-2-2	2.64	3.4915	3.4850	20.00	0.49 ± 0.05
2-1-1	2.65	4.9884	4.9803	19.75	0.43 ± 0.04
2-1-2	2.64	5.0344	5.0257	19.54	0.46 ± 0.05
2-2-1	2.65	3.6637	3.6563	28.38	0.54 ± 0.05
2-2-2	2.67	4.3776	4.3694	32.93	0.50 ± 0.05
3-1-1	2.66	5.6965	5.6870	27.37	0.44 ± 0.04
3-1-2	2.67	3.4213	3.4149	18.75	0.50 ± 0.05
3-2-1	2.67	5.5632	5.5536	32.29	0.46 ± 0.05
3-2-2	2.68	5.8481	5.8374	31.78	0.49 ± 0.05

W_w = wet weight δ = bulk density
W_D = dry weight ϕ_E = effective porosity
S_{ir}= static irreducible water saturation

Table 3. Formation-factor, surface resistivity and bulk resistivities for different NaCl solutions for the granite samples.

Sample	ρ_m (x10³ Ω-m)					F ±%	ρ_c ±%
ρ_w (Ω-m)	0.32 ±0.01	0.68 ±0.02	1.28 ±0.11	2.13 ±0.05	4.96 ±0.31	(x10³)	(x10⁴) (Ω-m)
NaCl (N)	0.5	0.2	0.1	0.05	0.02		
1-1-1 c	1.3	3.4	6.5	11.	17.	7.0 ± 1.5	-
n			X	X	X	6.0 ± 1.0	4.9 ± 4.1
1-1-2 c	1.2	2.9	5.5	9.5	16.	5.5 ± 0.9	-
n			X	X	X	4.8 ± 0.7	6.4 ± 4.8
1-2-1 c	1.1	3.1	7.1	11.	19.	6.9 ± 1.4	-
n			X	X	X	6.6 ± 0.1	4.8 ± 0.2
1-2-2 c	1.0	3.1	5.8	9.3	15.	6.0 ± 1.1	-
n			X	X	X	5.4 ± 0.4	3.8 ± 1.3
2-1-1 c	1.3	3.3	8.2	14.	19.	10.6 ± 3.9	-
n			X	X	X	8.1 ± 2.3	4.5 ± 6.8
2-1-2 c	1.3	3.7	8.3	14.	19.	10.8 ± 3.9	-
n			X	X	X	8.3 ± 2.2	4.3 ± 5.9
2-2-1 c	1.3	3.9	8.1	14.	21.	9.3 ± 2.6	-
n			X	X	X	7.5 ± 1.4	6.2 ± 6.1
2-2-2 c	1.1	3.7	7.6	12.	18.	8.8 ± 2.4	-
n			X	X	X	7.5 ± 0.6	3.9 ± 1.5
3-1-1 c	1.5	4.2	7.9	14.	19.	7.7 ± 1.0	-
n			X	X	X	7.6 ± 2.8	5.2 ± 10.
3-1-2 c	1.3	3.5	6.6	12.	16.	6.5 ± 0.9	-
n			X	X	X	6.3 ± 3.3	4.7 ± 14.
3-2-1 c	1.1	3.3	6.5	10.	15.	5.8 ± 0.7	-
n			X	X	X	6.6 ± 0.4	6.6 ± 1.0
3-2-2 c	1.4	3.8	6.9	12	18.	6.4 ± 0.6	-
n			X	X	X	6.3 ± 1.5	5.5 ± 6.6

ρ_w = Pore fluid resistivity.
ρ_m= Bulk resistivity of the rock for solutions of different salinities.
F = Formation factor.
ρ_c = Surface resistivity.
c = Analyzed by conventional method (Equation 13; Katsube and Scromeda, 1993).
n = Analyzed by new method (Equation 11; Katsube and Scromeda, 1993).
X = Data points used for F determination.
- = Data not available due to reduced accuracy.

and then inserts the results into the following equation to determine F:

$$1/F_a = 1/F + \rho_w/\rho_c. \quad (13)$$

The same statistical method, as that used for equation (11), is used to determine F and ρ_c from the $1/F_a$-ρ_w curve (equation 13). However, there has been a case where it was shown (Katsube and Scromeda, 1993) that the conventional method is less accurate, compared to determining F directly from equation (11). This is probably due to the fact that the calculation of F_a (equation 12), before entering the data into equation (13), adds an error not experienced when using equation (11).

The bulk electrical resistivity (ρ_r) is determined from the complex electrical resistivity, ρ^*, measurements made over a frequency range of 1-10^6 Hz (e.g., Katsube, et al., 1991; Katsube and Salisbury, 1991), with ρ_r representing an electrical resistivity at a frequency of about 10^2-10^3 Hz. It is a function of the pore structure and pore fluid resistivity, and is understood to exclude any other effects, such as pore surface, dielectric or any other polarizations (Katsube, 1975, 1977; Katsube and Walsh, 1987). The complex resistivity (ρ^*) is expressed by

$$\rho^* = \rho_R + i\rho_I, \quad (14)$$

where ρ_R and ρ_I are the real and imaginary resistivities. The complex resistivity (ρ^*) is derived from the impedance, Z:

$$\rho^* = K_G Z. \quad (15)$$

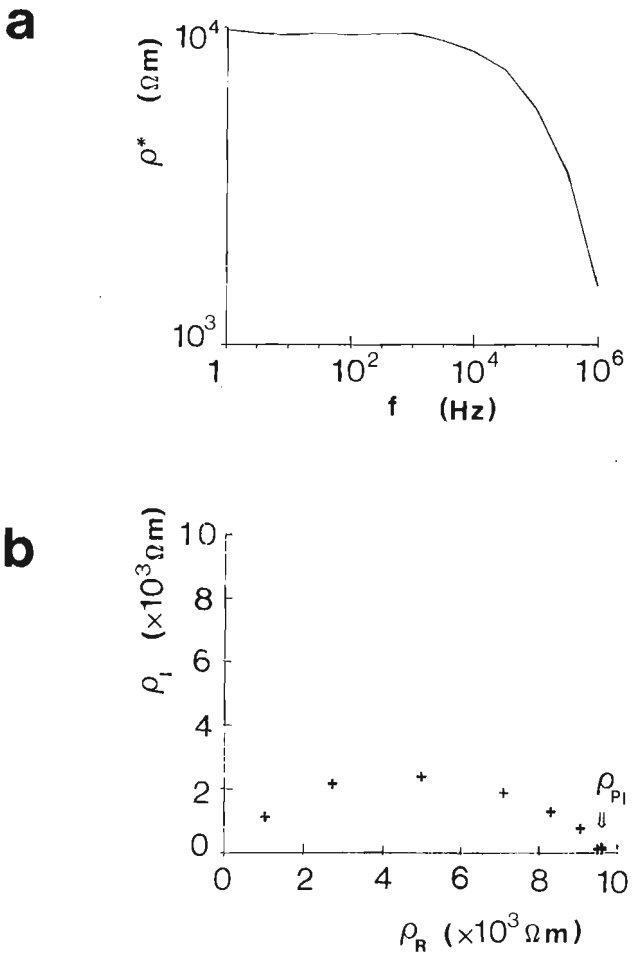

Figure 1. Description of the method (Katsube, 1975; Katsube and Walsh, 1987) used to determine bulk electrical resistivity, ρ_{rn} (ρ_{pl} in this figure), using a typical example of [a] a plot for complex resistivity (ρ^*) as a function of frequency (f), and [b] a Cole-Cole complex resistivity plot both, for sample 1-1-2 (NaCl 0.05N).

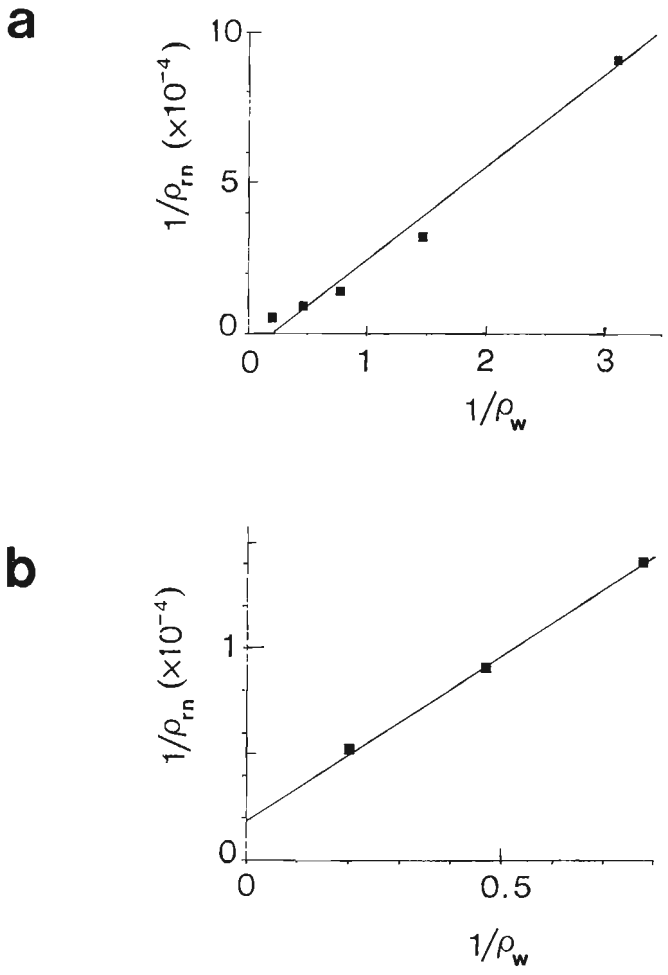

Figure 2. Description of the method (Katsube and Scromeda, 1993) used to determine formation factor (F), using typical examples of the reciprocal of bulk electrical esistivity ($1/\rho_{rn}$) plotted as a function of the reciprocal of fluid resistivity ($1/\rho_w$), for sample 1-2-1. The solid line is the reduced major axis (RMA).
[a] The result for all 5 points (slope = 0.0003).
[b] Result for 3 points representing smaller $1/\rho w$ values (slope = 0.00015).

Table 4. Results of the apparent tortuosity measurements.

Sample	δ (g/mL)	ϕ_E (%)	ϕ_{ES} (%)	F ($x10^3$)	τ_a
1-1-1	2.67	0.42 ± 0.04	0.27 ± 0.03	6.0 ± 1.0	5.0 ± 0.4
1-1-2	2.65	0.56 ± 0.06	0.43 ± 0.04	4.8 ± 0.7	5.2 ± 0.3
1-2-1	2.65	0.44 ± 0.04	0.33 ± 0.03	6.6 ± 0.3	5.4 ± 0.1
1-2-2	2.64	0.49 ± 0.05	0.39 ± 0.04	5.4 ± 0.6	5.1 ± 0.3
2-1-1	2.65	0.43 ± 0.04	0.34 ± 0.03	8.1 ± 2.5	5.9 ± 0.9
2-1-2	2.64	0.46 ± 0.05	0.37 ± 0.04	8.3 ± 2.5	6.2 ± 0.9
2-2-1	2.65	0.54 ± 0.05	0.39 ± 0.04	7.5 ± 1.8	6.4 ± 0.7
2-2-2	2.67	0.50 ± 0.05	0.33 ± 0.03	7.5 ± 1.3	6.1 ± 0.5
3-1-1	2.66	0.44 ± 0.04	0.32 ± 0.03	7.6 ± 0.1	5.8 ± 0.1
3-1-2	2.67	0.50 ± 0.05	0.41 ± 0.04	6.3 ± 0.2	5.6 ± 0.1
3-2-1	2.67	0.46 ± 0.05	0.31 ± 0.03	6.6 ± 0.8	5.5 ± 0.3
3-2-2	2.68	0.49 ± 0.05	0.33 ± 0.03	6.3 ± 0.1	5.6 ± 0.1

δ =Bulk Density
ϕ_E =Effective Porosity (Equation 8)
ϕ_{ES}=Effective porosity excluding the space occupied by surface water layers (Equation 10)
F =Formation Factor
τ_a =Apparent Tortuosity
S_{ir}=Static irreducible water saturation

These measurements were made at room temperature conditions. The errors for ρ_m and F are estimated to be in the ranges of 10-20 percent (%) and 20-40 percent (%), respectively (Katsube, 1981; Wadden and Katsube, 1982; Katsube and Scromeda, 1993). Further details of the procedures used for these measurements can be found elsewhere (Katsube, 1981; Katsube and Walsh, 1987; Katsube, et al., 1991; Katsube and Scromeda, 1993).

EXPERIMENTAL RESULTS

The results of effective porosity (ϕ_E) and static irreducible water saturation (S_{ir}) measurements for the 12 specimens are listed in Table 2. Results of the bulk electrical resistivity (ρ_m) measurements used for formation factor (F) determination are listed in Table 3. A typical example of the complex resistivity measurements used to determine ρ_m is illustrated in Figure 1, showing complex resistivity plots with characteristics common for high resistivity rocks (Katsube et al., 1992b). The results of the formation factor (F) determination using both the conventional method (equation 13) and the new method (equation 11) are listed in the table. The surface resistivity (ρ_c) values determined by the new method (Katsube and Scromeda, 1993) are also listed in the table. Those determined by the conventional method are excluded due to the possibility of reduced accuracy. Typical examples of the $1/\rho_m$ versus $1/\rho_w$ relationships observed when determining F and ρ_c are shown in Figure 2.

Unlike the case reported in Katsube and Scromeda (1993), all $1/\rho_m$ values for the higher NaCl concentrations (0.2 and 0.5 N) in this study caused negative $1/\rho_c$ (Fig. 2a) values in equation (11), results that disagree with theory. Therefore, those data were not used in the determination of F and ρ_c (Fig. 2b). The data points used to determine the two parameters are identified by the symbol "X" in Table 3. The percentage errors, listed in the table are determined by taking the differences in the F and ρ_c values obtained by using the different regression lines: the reduced major axis (RMA) and the normal regression lines (NRL). The principles of the reduced major axis are described in Davis (1986), and examples of related applications are found in Katsube and Agterberg (1990).

The results for both effective porosities (ϕ_E and ϕ_{ES}), formation factor (F) and apparent tortuosity (τ_a) are summarized in Table 4. The F and τ_a values in this table are those determined by the new method, using equation (11). Their error ranges have been determined by taking the difference between the values determined using the new method (equation 11) and those determined by the conventional method (equation 13).

DISCUSSIONS AND CONCLUSIONS

The values for formation factor (F) and effective porosity (ϕ_E), which are 4800-8300 and 0.42-0.56% respectively, are within but on the higher end of the previously reported range of values for these types of rocks (Katsube, et al., 1985; Katsube and Hume, 1987). The apparent tortuosity (τ_a) values

of 5.0-6.4 are slightly higher than the previously reported values (Wadden and Katsube, 1982; Katsube and Kamineni, 1983) for these types of rocks. There is a similar parameter represented by diffusion tortuosity, τ_D, which is directly determined from the diffusion measurements (Wadden and Katsube, 1982; Katsube et al., 1986). The apparent tortuosity (τ_a) values obtained by this study resemble the diffusion tortuosity (τ_D) values reported by Katsube et al. (1986). The effective porosity (ϕ_{ES}) values which exclude the space taken up by pore surface water layers was not used for the apparent tortuosity (τ_a) calculations, but would result in slightly smaller τ_a values if used.

ACKNOWLEDGMENTS

The authors thank D.J. Drew (AECL Research, Whiteshell Laboratories) for supplying the samples used in this study. The authors also thank Q. Bristow (Geological Survey of Canada) for critically reviewing this paper and for his constructive comments.

REFERENCES

Agterberg, F.P., Katsube, T.J., and Lew, S.N.
1985: Use of multiple regression for petrophysical characterization of granites as a function of alteration; in Current Research, Part B; Geological Survey of Canada, Paper 85-1B, p. 451-458.

API (American Petroleum Institute)
1960: Recommended practices for core-analysis procedure; API Recommended Practice 40 (RP 40) First Edition, American Petroleum Institute, Washington, D.C., p. 55.

Archie, G.E.
1942: The electrical resistivity log as an aid in determining some reservoir characteristics: Transactions of the American Institute of Mining, metallurgical and Petroleum Engineers, v. 146, p. 54-67.

Davis, J.C.
1986: Statistics and Data Analysis in Geology; John Wiley & Sons, p. 200-204.

Katsube, T.J.
1975: The electrical polarization mechanism model for moist rocks; in Report of Activities, Part C; Geological Survey of Canada, Paper 75-1C, p. 353-360.
1977: Electrical properties of rocks; in Induced Polarization for Exploration Geologists and Geophysicists, Short Course Presented by the University of Arizona, Tucson, March 14-16, p. 15-44.
1981: Pore structure and pore parameters that control the radionuclide transport in crystalline rocks; Proceedings of the Technical Program, International Powder and Bulk Solids Handling and Processing, Rosemont, Illinois, p. 394-409. (Available from: CAHNERS Exposition Group, 222 West Adams Street, Chicago, Illinois 60606 U.S.A.).

Katsube, T.J. and Agterberg, F.P.
1990: Use of statistical methods to extract significant information from scattered data in petrophysics; in Stastistical Applications in the Earth Sciences, F.P. Agterberg and G.F. Bonham-Carter (ed.) ; Geological Survey of Canada, Paper 89-9, p. 263-270.

Katsube, T.J. and Hume, J.P.
1987: Pore structure characteristics of granitic rock samples from Whiteshell Research Area; in Geotechnical Studies at Whiteshell Research Area (RA-3); CANMET, Report MRL 87-52, p. 111-158.

Katsube, T.J., and Kamineni, D.C.
1983: Effect of alteration on pore structure of crystalline rocks; Core samples from Atikokan, Ontario; Canadian Mineralogist, v. 21, p. 637-646.

Katsube, T.J. and Mareschal, M.
1993: Petrophysical model of deep electrical conductors; Graphite lining as a source and its disconnection due to uplift; Journal of Geophysical Research, v. 98, B5, p. 8019-8030.

Katsube, T.J. and Salisbury, M.
1991: Petrophysical characteristics of surface core samples from the Sudbury structure; in Current Research, Part E, Geological Survey of Canada, Paper 91-1E, p. 265-271.

Katsube, T.J. and Scromeda, N.
1993: Formation factor determination procedure for shale sample V-3; in Current Research, Part E; Geological Survey of Canada, Paper 93-1E, p. 321-330.

Katsube, T.J. and Walsh, J.B.
1987: Effective aperture for fluid flow in microcracks: International Journal of Rock Mechanics and Mining Sciences and Geomechanics Abstracts, v. 24, p. 175-183.

Katsube, T.J., Best, M.E., and Mudford, B.S.
1991: Petrophysical characteristics of shales from the Scotian shelf; Geophysics, v. 56, p. 1681-1689.

Katsube, T.J., Melnyk, T.W., and Hume, J.P.
1986: Pore structure from diffusion in granitic rocks; Atomic Energy of Canada Limited , Technical Record, TR-381, 28 p.

Katsube, T.J., Percival, J.B., and Hume, J.P.
1985: Characterization of the rock mass by pore structure parameters; Atomic Energy of Canada Limited, Technical Record, TP-299, p. 375-413.

Katsube, T.J., Scromeda, N., Mareschal, M., and Bailey, R.C.
1992b: Electrical resistivity and porosity of crystalline rock samples from the Kapuskasing Structural Zone, Ontario; in Current Research, Part E; Geological Survey of Canada, Paper 92-1E, p. 225-236.

Katsube, T.J., Scromeda, N., and Williamson, M.
1992a: Effective porosity of tight shales from the Venture Gas Field, offshore Nova Scotia; in Current Research, Part D; Geological Survey of Canada, Paper 92-1D, p. 111-119.

Patnode, H.W. and Wyllie, M.R.J.
1950: The presence of conductive solids in reservoir rocks as a factor in electric log interpretation;Transactions of the American Institute of Mining, Metallurgical and Petroleum Engineers, v. 189, p. 47-52.

Scromeda, N. and Katsube, T.J.
1993: Effect of vacuum-drying and temperature on effective porosity determination for tight rocks; in Current Research, Part E; Geological Survey of Canada, Paper 93-1E, p. 313-319.

Wadden, M.M. and Katsube, T.J.
1982: Radionuclide diffusion rates in crystalline rocks; Chemical Geology, v. 36, p. 191-214.

Ward, S.H. and Fraser, D.C.
1967: Conduction of electricity in rocks; in Mining Geophysics, Volume II; Society of Exploration Geophysics, and Mining Geophysics Volume Editing Committee, Society of Exploration Geophysics, Tulsa, Oklahoma, p. 197-223.

Geological Survey of Canada Project 870057

Mapping the magma flow pattern in the Sudbury dyke swarm in Ontario using magnetic fabric analysis

Richard E. Ernst[1]
Continental Geoscience Division

Ernst, R.E., 1994: Mapping the magma flow pattern in the Sudbury dyke swarm in Ontario using magnetic fabric analysis; in Current Research 1994-E; Geological Survey of Canada, p. 183-192.

Abstract: Based on a detailed magnetic fabric study, it is concluded that dykes of the 1235 Ma Sudbury swarm were emplaced laterally and that the source direction for most dykes was from the southeast probably from a mantle plume located under what is now the Grenville Province.

Résumé : En se basant sur une étude détaillée de la fabrique magnétique, l'auteur conclut que les dykes de l'essaim de Sudbury, qui remonte à 1 235 Ma, ont été mis en place latéralement et que la source de la plupart des dykes était vraisemblablement un panache mantellique venu du sud-est, qui se trouvait sous ce qui est actuellement la Province de Grenville.

[1] Ottawa-Carleton Geoscience Centre and Department of Geology, University of Ottawa, Ottawa, Ontario K1N 6N5

INTRODUCTION

Diabase dykes of the 1235 Ma (Krogh et al., 1987) Sudbury swarm trend northwest in the Superior and Southern provinces (Fig. 1; Table 1). Some dykes can be traced as linear aeromagnetic anomalies for distances greater than 200 km. The Sudbury swarm can also be traced into the adjacent part of the Grenville Province for at least 50 km (Davidson and Bethune, 1988) and perhaps for as much as 100 km (A. Davidson, pers. comm., 1993). Dykes northwest of the Grenville Front are straight and composed of fresh diabase, but in the vicinity of the front may show abrupt changes in primary trend and southeast of the front are deformed and metamorphosed (Palmer et al., 1977; Bethune, 1989, 1993; Davidson and Ketchum, 1993). In an attempt to understand the emplacement of the Sudbury swarm and to locate its source mantle plume in relation to the Grenville Province, the primary flow pattern in the undeformed part of the swarm was mapped through measurements of anisotropy of magnetic susceptibility (AMS).

The AMS fabric is represented by a symmetrical second rank tensor which has graphical representation as a triaxial ellipsoid. Data are typically presented in terms of the orientation (declination and inclination) and the magnitude of the three principal axes of this ellipsoid (Rochette et al., 1992; Tarling and Hrouda, 1993).

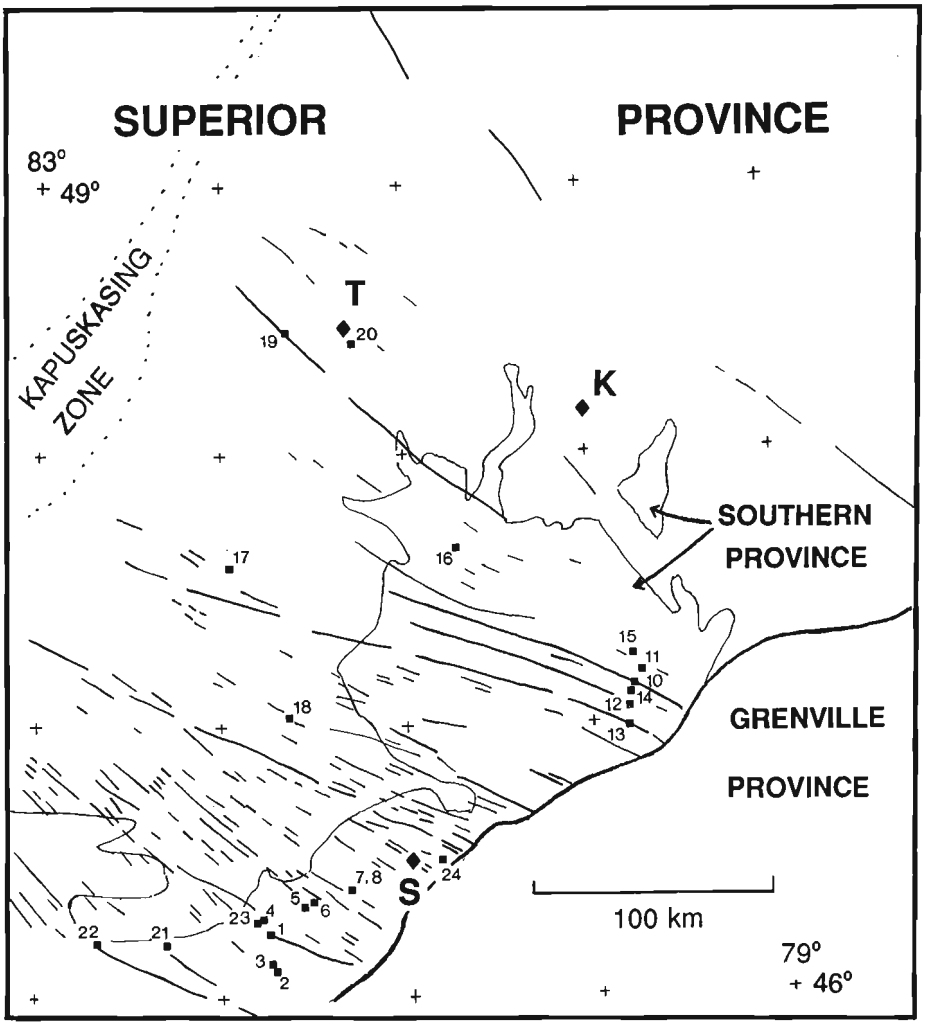

Figure 1. *Distribution of dykes of the Sudbury Swarm. Diamond-symbols mark towns, labelled, T, K and S for Timmins, Kirkland Lake and Sudbury, respectively. Numbered squares mark sample sites of this study. Distribution of Sudbury dykes (after Fahrig and West, 1986) with modifications based on the shaded aeromagnetic map of Ontario (Gupta, 1991a,b). Site 9, located 100 m south of site 10, is not shown; the northwest-trending dyke sampled at this locality was subsequently determined not to be a Sudbury dyke based on its field appearance (fine grain size throughout and apparent low grade metamorphism). Major geological boundaries were traced from maps by the Ontario Geological Survey (1992a,b).*

In diabase dykes, the AMS technique records the anisotropic distribution of magnetite grains. The rock fabric is dominated by lath- and tabular-shaped plagioclase and the magnetite distribution mimics this fabric regardless of the timing of magnetite growth. Early-crystallizing magnetite grains will be redistributed during plagioclase growth and late-crystallizing magnetite will infill between plagioclase grains (e.g. Hargraves et al., 1991). The result in both cases is that the magnetite fabric will mimic that of plagioclase and hence that of the overall rock. The AMS technique is sensitive to a few per cent anisotropy, making it useful for revealing very subtle fabrics in diabase dykes. When the fabric is due to flow, then

Table 1. Site location and simple dyke-geometry information

	Location					
Site[1]	UTM coordinates (Zone 17)		Trend[2]	Width	Dip (field)	Dip (AMS)[3]
	Northing	Easting	(°)	(m)	(°)	(°)
1	5121010	442130	325	–	–	85 NE
2	5105650	444770	312	27	80 SW	60 SW
3	5107440	443360	330	–	85 SW	~65 NE
4	5126080	439090	324	~110	–	70 SW
5	5131060	456000	307	30	–	50 NE
6	5133340	466360	299	>14	~70 SW	65 SW
7	5138260	475620	323	6	85 NE	85 NE
8	5138270	475650	333	22	85 SW	65 NE
10	5220180	592880	272	13	90	~30 NE
11	5226260	595810	302	40	90	~50 NE
12	5211510	591470	281	8	80 SW	~65 SW
13	5203990	590770	290	>33	–	25 SW
14	5217200	591540	276	2	–	80 SW
15	5233710	593350	320	45	–	90
16	5277280	521080	300-340	20	80 NE	9 SW
17	5269480	428420	301	20-30	–	70 SW
18	5208430	451620	298	>45	75 NE	55 NE
19	5366460	453450	317	>10	–	85 NE
20	5362620	480000	285	>35	–	85 SW
21	5115990	399120	~315	20	–	50 SW
22	5117820	371170	285	>10	–	60 SW
23	5125680	437530	300	>26	–	60 NE
24	5149720	512770	299	>10 <30	~70 NE	55 NE

[1] Site 2 = U-Pb geochronological site DUD05, dated by F. Dudas (A. Davidson, pers. comm., 1993); Site 3= 3 old paleomagnetic drill holes found; Site 4 = site dated by Krogh et al., 1987; Site 6 = geochemical site DM140 (A. Davidson, pers. comm., 1993); Site 10 = paleomagnetic site CP93 (Palmer et al., 1977); Site 11 = paleomagnetic site BXA8461 (K. Buchan, pers. comm., 1993); Site 13 = paleomagnetic site CP84 (Palmer et al., 1977); Site 14 = paleomagnetic site CP92 (Palmer et al., 1977); Site 22 = 4 old paleomagnetic drill holes found.

[2] Trend at site 23 determined from dyke-parallel banding in groundmass plagioclase.

[3] Dip (AMS) values equal 90 minus the inclination of the minimum AMS axes (Table 2).

the AMS fabric will typically be aligned such that the minimum axis is perpendicular to the dyke-wall and the maximum axis is in the direction of flow (e.g. Knight and Walker, 1988). Flow-mapping using the AMS technique has been successfully applied to several swarms such as the Koolau swarm in Hawaii (Knight and Walker, 1988) and to the Mackenzie swarm of the Canadian Shield (Ernst and Baragar, 1992).

METHODOLOGY

A total of 299 samples were collected from 23 sites distributed throughout the undeformed part of the Sudbury swarm (Fig. 1). All samples were field oriented using both magnetic and sun compasses, except for those from site 22, where topographic sightings replaced the sun compass readings. Most samples were collected from within a metre of dyke margins where the flow velocity gradient would have been largest and the chances of obtaining a preserved flow fabric the greatest. The low-field AMS fabric from at least 2 standard cylindrical specimens (2.54 cm diameter ~2.2 cm long) per sample were measured using an instrument, the SI-1 (from Sapphire Instruments), designed to measure magnetic susceptibility in different sample orientations.

Sites 2, 4, 10, 11, 13, and 14 are known to belong to the Sudbury swarm on the basis of dating, chemical composition, and paleomagnetism (see footnotes to Table 1). The remaining sites are interpreted to be Sudbury dykes on the basis of trend and field appearance (fresh, unmetamorphosed, oliving-bearing and locally containing abundant fresh plagioclase phenocrysts in the near margin regions).

Mean results from each site were determined according to the tensor averaging procedure proposed by Jelinek (1978) based on the work of Hext (1963) and discussed by Ernst and Pearce (1989) and Lienert (1991). Calculations and plots were generated using the computer program discussed in Lienert (1991).

RESULTS

Shape and degree of anisotropy

The degree of anisotropy and the shape of the AMS ellipsoid are represented by P_J and T, respectively (Jelinek, 1981) and are presented in Table 2 and displayed in Figures 2 and 3. The percentage of anisotropy from all samples is typically between 2 to 8% (P_J=1.02-1.08). The observation of both negative and positive values of T reflects the presence of both prolate and oblate ellipsoid fabrics, respectively. Sites 2, 3, 8, 15, 16 and perhaps 10 have prolate fabrics while sites 18, 19, 21, 23 and 24 have distinctive oblate fabrics. Sites 20 and 22 have distinctively low degrees of anisotropy (low values of P_J). The origin of the inter-site variations in T and P_J is not clear. Figure 3 shows that there is no obvious trend in either T or P_J with respect to distance from the margin. Since grain size decreases toward the margin, then the absence of a trend in Figure 3 indicates that grain size differences are not responsible for the inter-site variations. Variation in flow-regime (e.g. rate of flow or position within magma pulses) is an intriguing possible explanation, and is currently being investigated.

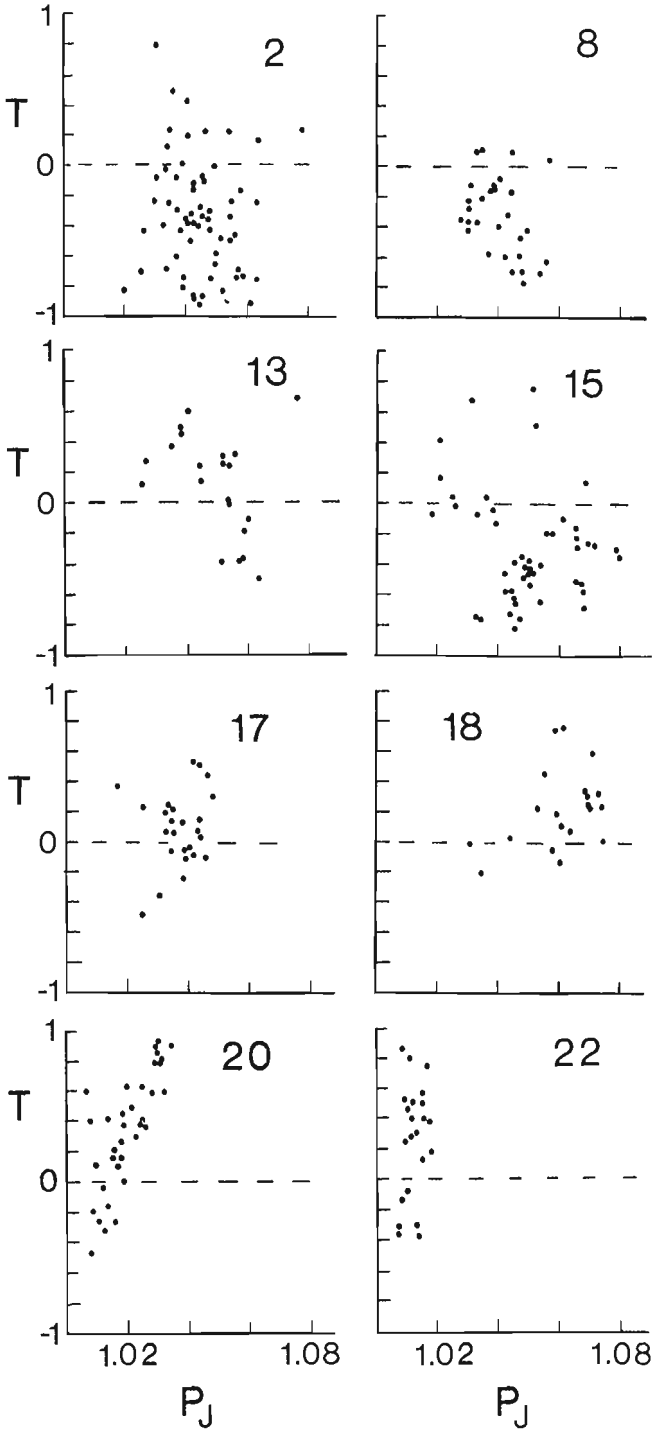

Figure 2. Ellipsoid shape (T) vs. Degree of Anisotropy (P_J) for representative sites. Values of T>0 indicate an oblate shape and T<0 indicates a prolate shape. T and P_J are defined in Jelinek (1981). $T = (2n_2-n_1-n_3)/(n_1-n_3)$ and $P_J = exp\{sqrt[2((n_1-n_m)^2+(n_2-n_m)^2+(n_3-n_m)^2)]\}$ where $n_1=ln(K_{max})$, $n_2=ln(K_{int})$, $n_3=ln(K_{min})$ and $n_m=(n_1+n_2+n_3)/3$.

Table 2. Summary of AMS data for the Sudbury dyke swarm

Site	N,n	D_{max}	I_{max}	A_{max}	D_{int}	I_{int}	A_{int}	D_{min}	I_{min}	A_{min}	K_{mean}	$K_{n,max}$	$K_{n,int}$	$K_{n,min}$	T	P_J
1	13,28	105.5	29.1	27:5	296.4	60.5	27:4	198.1	4.7	6:4	2.95	1.013	1.005	0.982	0.490	1.032
2	29,63	298.8	2.0	5:3	205.5	58.0	13:5	30.0	31.9	13:3	3.60	1.020	0.994	0.986	-0.523	1.036
3	8,18	297.1	4.0	14:7	34.9	63.0	51:9	205.1	26.0	51:8	3.41	1.012	0.996	0.993	-0.682	1.020
4	15,37	132.4	40.2	48:11	274.9	43.2	48:15	24.7	19.8	15:11	2.26	1.005	1.003	0.991	0.716	1.015
5	8,17	129.7	3.3	7:3	36.0	47.8	16:5	222.6	42.0	16:5	3.99	1.023	0.996	0.981	-0.293	1.044
6	14,28	131.8	2.2	7:4	226.6	65.0	14:4	40.8	24.9	14:6	3.68	1.026	0.995	0.978	-0.295	1.050
7	14,28	135.1	6.5	9:4	356.3	81.4	9:7	225.7	5.6	9:5	5.14	1.013	1.001	0.986	0.078	1.028
8	15,30	322.6	2.2	7:3	57.2	64.1	7:5	231.5	25.8	7:6	4.53	1.019	0.995	0.986	-0.448	1.034
10	11,35	329.9	3.9	8:5	62.1	29.8	24:6	233.2	59.9	24:6	3.61	1.021	0.992	0.987	-0.652	1.037
11	22,44	300.4	6.2	12:7	38.4	51.6	25:7	205.6	37.7	26:8	3.42	1.012	0.998	0.991	-0.329	1.021
12	8,17	284.6	20.4	11:9	160.2	56.7	23:10	24.7	25.1	23:8	6.04	1.022	1.000	0.978	-0.011	1.045
13	11,22	294.0	9.1	7:2	200.5	21.2	10:7	45.8	66.8	10:3	5.02	1.022	0.998	0.980	-0.106	1.043
14	5,10	314.0	6.1	20:4	196.4	77.0	25:9	45.2	11.5	19:4	5.51	1.017	0.999	0.984	-0.050	1.034
15	24,49	314.8	14.7	4:3	139.2	75.3	11:3	45.1	1.1	11:4	4.14	1.022	0.993	0.985	-0.573	1.040
16	19,41	350.2	2.4	26:5	259.9	8.4	26:4	95.8	81.2	8:4	3.77	1.012	1.003	0.985	0.292	1.028
17	13,25	105.2	0.3	6:3	196.1	68.9	6:5	15.1	21.1	5:4	2.25	1.016	1.001	0.983	0.067	1.034
18	10,20	327.7	18.5	7:3	82.4	51.3	7:4	225.3	32.6	4:3	3.08	1.025	1.005	0.970	0.276	1.058
19	12,25	315.7	8.3	4:3	98.1	79.6	6:4	224.8	6.3	6:3	4.10	1.021	1.001	0.978	0.080	1.043
20	18,35	287.7	9.2	10:3	135.8	79.6	10:5	18.4	4.8	5:3	4.44	1.007	1.003	0.990	0.532	1.018
21	7,14	150.4	24.3	23:4	263.5	40.9	24:16	38.8	39.3	17:4	4.21	1.014	1.005	0.981	0.419	1.035
22	7,22	305.8	13.6	38:12	195.1	55.5	38:14	44.1	31.0	15:12	4.47	1.003	1.001	0.995	0.501	1.008
23	8,18	100.6	22.0	9:6	340.1	51.6	22:9	204.0	29.8	22:5	2.86	1.015	0.999	0.986	-0.126	1.030
24	8,15	111.0	4.1	10:4	15.5	53.3	17:6	204.0	36.4	15:3	3.53	1.022	1.004	0.974	0.276	1.050
Site Mean	23 sites	306.3	2.3	9:5	2.3	85.9	34:5	216.2	3.4	34:8	–	1.015	0.996	0.990	-0.515	1.026

N, n are the number of samples and specimens respectively used for computation. Subscripted 'max', 'int' and 'min' denote the maximum, intermediate and minimum principal AMS axes. D and I are the declination and inclination of the axes. A consists of two numbers equalling the long and short radii of the 95% uncertainty ellipse, K is the magnetic susceptibility in 10^{-6} SI units. $K_{n,max}$, $K_{n,int}$, $K_{n,min}$ are the susceptibility axes of the principal axes normalized such that their sum equals 3. T and P_J are the ellipsoid shape and degree of anisotropy (Jelinek, 1981). Site mean calculation based on site-data which were not corrected to a common dyke trend (Fig. 5).

Fabric orientation

At 20 of the sites (1-8, 11-12, 14-15, 17-24), the minimum axes cluster in a direction approximately perpendicular to the dyke trend (Fig. 4, and 5; Table 2). There is also rough correspondence at many sites between the inclination of these minimum AMS axes and the field-measured dyke dips (Table 1). In detail, however, the AMS determined dips are typically 10-20° shallower than the true dips. Dyke-perpendicular minimum axes are indicative of a flow fabric; in such cases the maximum axes will be aligned in the flow direction.

In all of these sites the maximum axes are shallow indicating a sub-horizontal flow trajectory, which varies only slightly in inclination. Sites 2, 5, 6, 8, 11, 12, 14, 17, 20, 24 and perhaps 3 have horizontal axes within statistical uncertainties whereas sites 15, 18, and 19 have shallow northwest inclinations and sites 7, 21, 23 and perhaps 1 indicate a shallow southeast inclination.

The three remaining sites (10, 13 and 16) have a fabric characterized by steep minimum axes (Fig. 4). This fabric is also observed in scattered samples from other sites. Similar

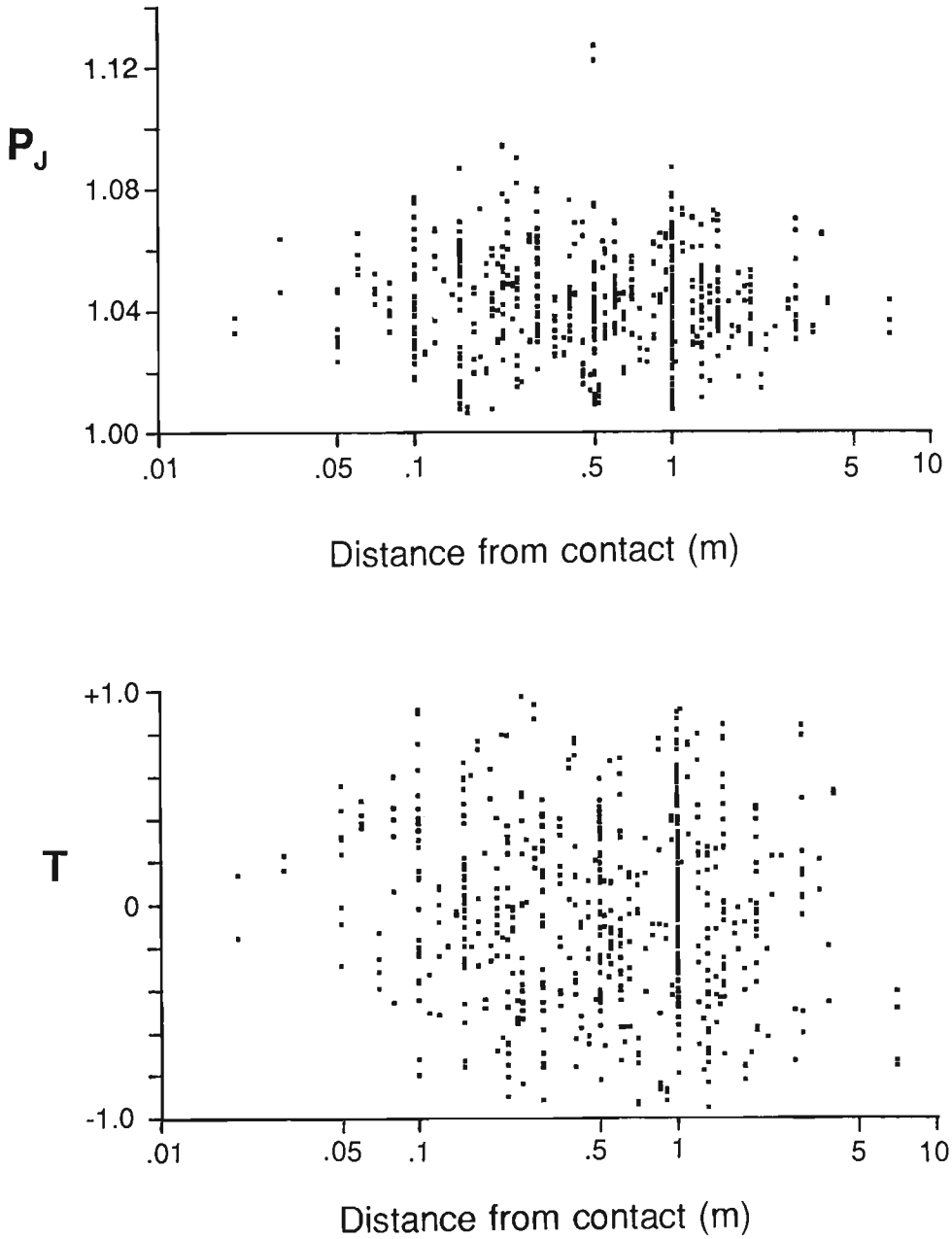

Figure 3. T and P_J plotted against distance from the contact. Each plot consists of 560 specimens. An additional 81 specimens were not plotted because their contact distance could not be accurately measured.

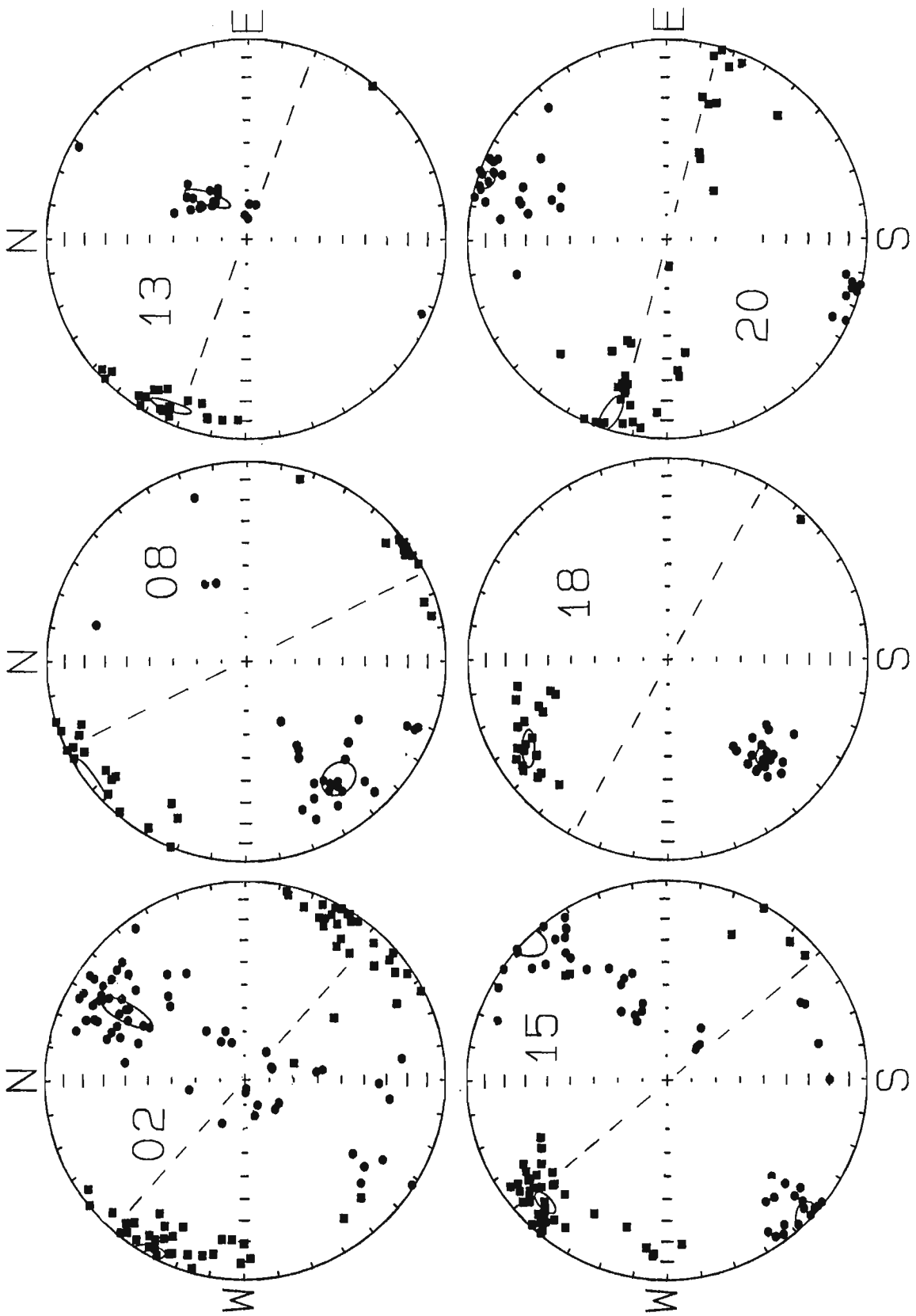

Figure 4. Stereonet plots of AMS data from selected sites. The AMS maximum (squares) and minimum (circles) axes are plotted on the lower hemisphere of equal area stereonets. For each site 95% confidence ellipses were calculated based on the Hext (1963) - Jelinek (1978) method using the computer program of Lienert (1991). The dashed line on each plot gives the dyke trend (Table 1). Corresponding data from all sites is available in Table 2.

fabrics in other studies have been interpreted as due to vertical compaction at a late stage of crystallization (Ernst and Baragar, 1992; Park et al., 1988). Rock magnetic explanations may also be possible (e.g. Rochette et al., 1992).

Imbrication

In their study of Koolau dykes in Hawaii, Knight and Walker (1988) found that most dykes exhibit a symmetrical imbrication which can be used to give the flow polarity (Fig. 6). This effect is thought to be most prominent near a

Table 3. Evaluation of AMS imbrication using samples from ≤0.5 metres distance from margin

Site	NE margin		SW margin		Interpreted Source Direction
	Imbrication Angle[1]	N1,N2,n3,n4[2]	Imbrication Angle[1]	N1,N2,n3,n4[2]	
1	–	–	−16.3 ± 1.7	2,4,0,0	NW?
1 (dykelet)	46.5 ± 22.7	2,4,0,0	− 6.1 ± 5.0	1,2,0,0	NW
2	−18.0 ± 10.5	7,14,1,2	10.5 ± 15.5	6,14,1,2	SE
3	–	–	−18.7 ± 31.0	5,12,1,2	NW?
4	11.7 ± 44.7	3,7,0,0	–	–	NW?
5	–	–	12.8 ± 6.1 17.3 ± 8.1	3,6,2,4 5,10,0,0	SE?
6	–	–	25.8 ± 14.5	5,10,0,0	SE?
6 (dykelet)	15.4 ± 9.3	3,6,0,0	3.6 ± 4.8	3,6,0,0	NW
7	−20.8 ± 10.3	1,2,0,0	22.2 ± 1.1	1,2,0,0	SE
8	1.8 ± 4.7	2,4,0,0	23.1 ± 8.0	3,6,0,0	SE
10	34.9 ± 6.1	1,2,1,3	–	–	(overprint fabric)
11	−14.0 ± 14.9	3,7,1,2	2.0 ± 22.1 10.6 ± 12.1	6,12,0,0 5,10,1,2	SE
12	−8.8 ± 3.1	3,6,0,0	26.9 ± 15.9	2,5,0,0	SE
13	–	–	−1.6 ± 2.1 − 3.0 ± 11.8	1,2,8,16 9,18,0,0	(overprint fabric)
15[3]	−17.5 ± 13.1	6,12,1,2	3.0 ± 8.5	6,12,0,0	SE
17	−12.4 ± 14.8 −17.8 ± 6.8	7,14,0,0 6,12,1,2	–	–	SE?
18	–	–	34.4 ± 9.7	4,8,0,0	SE?
19	–	–	18.2 ± 8.6	7,14,0,0	SE?
20	–	–	5.1 ± 7.3	11,22,0,0	SE?
23	–	–	26.4 ± 36.9	2,6,0,0	SE?

[1] Imbrication Angle equals the difference between the trends of the AMS maximum axes and the local dyke margin. Positive values mean that the AMS maximum axes are clockwise rotated from the dyke trend. The opposite interpretation applies to negative values. Uncertainties are one standard deviation values.

[2] N1 and N2 are the number of sample and specimens, respectively, used for averaging. n3 and n4 are numbers of samples and specimens, respectively, rejected for averaging. Reasons for rejection include: the inclination for the AMS minimum axes exceeds 60 degrees, the "Imbrication Angle" is greater than 70 or the samples which are nearly equidistant from both margins.

[3] For site 15, most of the data used for averaging was from internal contacts. However, the averages based on the main dyke margins gives a similar result.

dyke's margin (Walker, pers. comm., 1993). To test for imbrication in the Sudbury data, a subset of data was extracted consisting of data from within 0.5 m of the contact. These data were also corrected for variation in local contact trend. Since these local trends were measured using a magnetic compass (held about 1 m above ground), the possibility of orientation errors due to dyke magnetization must be considered. A comparison of differences between the sun and magnetic compass field orientations of near margin samples indicates that any bias in the measured local contact trends is no larger than about 5°.

An imbrication effect is clearly evident in the data of Table 3 and the magma source direction could in may cases be clearly evaluated (with reference to Fig. 6). The overall statistics indicate 13 dykes with a southeast source area and 5 dykes with a northwest source area. Two of the latter are from satellite dykelets which are splays from an adjacent main dyke and whose flow direction may, therefore, have no regional significance. The most reliable determinations are from sites having data from both dyke margins. These exhibit a symmetrical imbrication pattern which have the following interpretation: 6 dykes show a southeast source area, and 2 (both satellite dykelets) indicate a northwest source area.

DISCUSSION

The AMS data from this study clearly demonstrate that lateral magma emplacement occurred throughout the Sudbury dyke swarm. Furthermore, the imbrication pattern for most sites

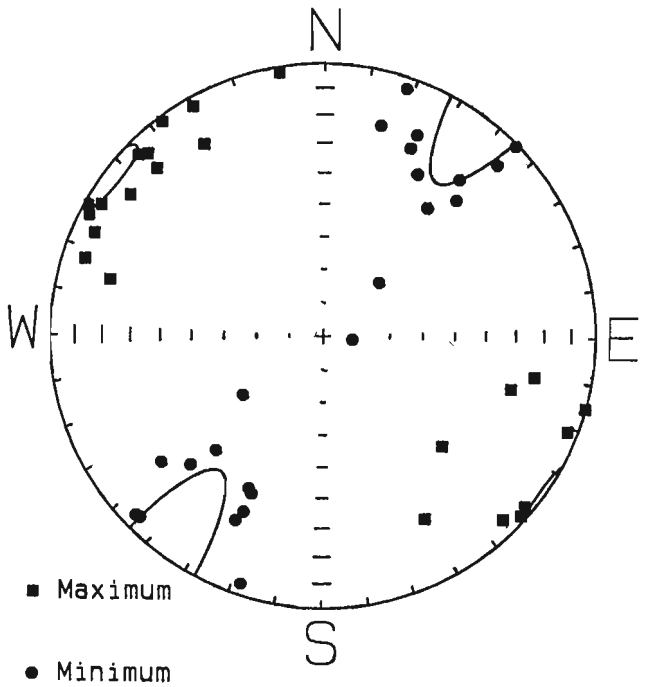

Figure 5. Summary of AMS site mean data. No correction was made for differences in dyke trend.

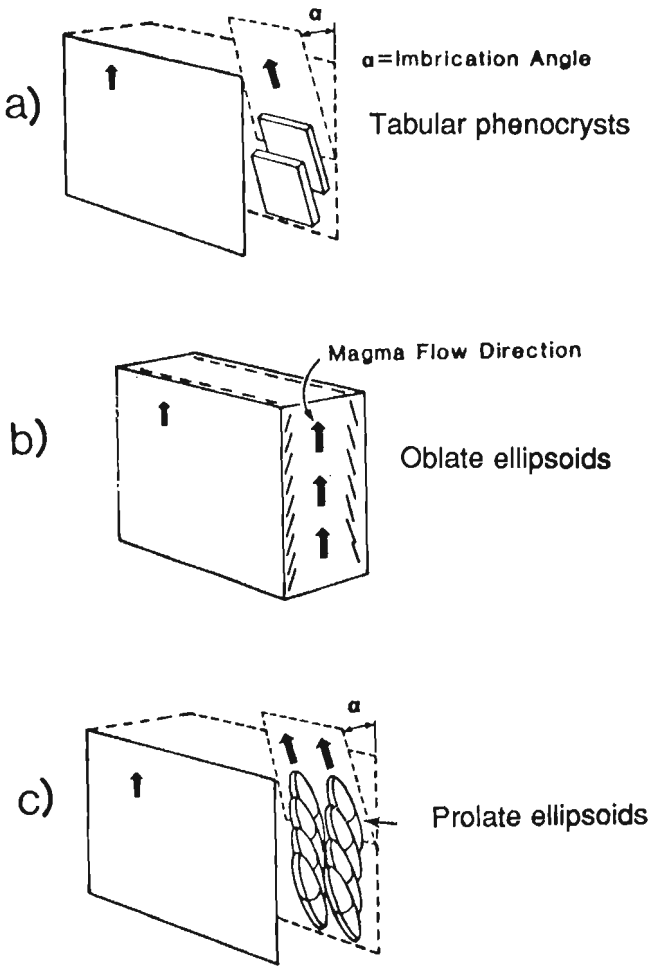

Figure 6. Illustration of imbrication effect (after Knight and Walker, 1988).

suggests a source area to the southeast. However, some of the sites in the southern part of the swarm indicate a northwest source area.

Many large fanning swarms are thought to be plume-related (Ernst et al., in prep.) with the magma being injected laterally in dykes away from the plume centre (Ernst and Baragar, 1992). According to such a model, the AMS data from the Sudbury swarm are most consistent with a plume centre to the southeast, under the present-day Grenville Province.

ACKNOWLEDGMENTS

This work was supported by a GSC conract from A. Davidson under project 760061. Field work was done with the assistance of Eric Grosfils whose observations on plagioclase phenocryst distributions in the Sudbury dykes will contribute to a subsequent publication. AMS measurements were made in the GSC paleomagnetic laboratory of Ken Buchan. Discussions with A. Davidson and K. Bethune on the Sudbury swarm were invaluable.

REFERENCES

Bethune, K.M.
1989: Deformation, metamorphism, diabase dykes and the Grenville Front southwest of Sudbury, Onario; in Current Researc, Part C; Geological Survey of Canada, Paper 89-1C, p. 19-28.
1993: Evolution of the Grenville Front in the Tyson Lake area, southwest of Sudbury, Ontario, with emphasis on the tectonic significance of the Sudbury diabase dykes; Ph.D. Thesis, Queen's University, Kingston, Ontario, 263 p.

Davidson, A. and Bethune, K.M.
1988: Geology of the north shore of Georgian Bay, Grenville Province of Ontario; in Current Research, Part C; Geological Survey of Canada, Paper 88-1C, p. 135-144.

Davidson, A. and Ketchum, J.W.F.
1993: Grenville Front studies in the Sudbury region, Ontario; in Current Research, Part C; Geological Survey of Canada, Paper 93-1C, p. 271-278.

Ernst, R.E. and Baragar, W.R.A.
1992: Evidence from magnetic fabric for the flow pattern of magma in the Mackenzie giant radiating swarm; Nature, v. 356, p. 511-513.

Ernst, R.E. and Pearce, G.W.
1989: Averaging of anisotropy of magnetic susceptibility data; in Statistical Applications in the Earth Sciences, F.P. Agterberg and G.F. Bonham-Carter (ed.); Geological Survey of Canada, Paper 89-9, p. 297-305.

Fahrig, W.F. and West, T.D.
1986: Diabase dyke swarms of the Canadian Shield; Geological Survey of Canada, Map 1627A.

Gupta, V.K.
1991a: Shaded image of total magnetic field of Ontario, east-central sheet; Ontario Geological Survey, Map 2586, scale 1:1 000 000.
1991b: Shaded image of total magnetic field of Ontario, southern sheet; Ontario Geological Survey, Map 2587, scale 1:1 000 000.

Hargraves, R.B., Johnson, D., and Chan, C.Y.
1991: Distribution anisotropy: the cause of AMS in igneous rocks; Geophysical Research Letters, v. 18, p. 2193-2196.

Hext, G.R.
1963: The estimation of second-order tensors, with related tests and designs; Biometrika, v. 50, p. 353-373.

Jelinek, V.
1978: Statistical processing of anisotropy of magnetic susceptibility measured on groups of sediments; Studia Geophysica et Geodaetika, Praha, v. 22, p. 50-62.
1981: Characterization of the magnetic fabric of rocks; Tectonophysics, v. 79, p. T63-T67.

Knight, M.D. and Walker, G.P.L.
1988: Magma flow directions in dikes of the Koolau Complex, Oahu, determined from magnetic fabric studies; Journal of Geophysical Research, v. 93, p. 4301-4319.

Krogh, T.E., Corfu, F., Davis, D.W., Dunning, G.R., Heaman, L.M., Kamo, S.L., Machado, N., Greenough, J.D., and Nakamura, E.
1987: Precise U-Pb isotopic ages of diabase dykes and mafic to ultramafic rocks using trace amounts of baddeleyite and zircon; in Mafic Dyke Swarms, H.C. Halls and W.F. Fahrig (ed.); Geological Association of Canada, Special Paper 34, p. 147-152.

Lienert, B.R.
1991: Monte Carlo simulation of errors in the anisotropy of magnetic susceptibility: a second-rank symmetric tensor; Journal of Geophysical Research, v. 96, p. 19539-19544.

Ontario Geological Survey (OGS)
1992a: Tectonic Assemblages of Ontario, east-central sheet; Ontario Geological Survey, Map 2577, scale 1:1 000 000.
1992b: Tectonic Assemblages of Ontario, southern sheet; Ontario Geological Survey, Map 2578, scale 1:1 000 000.

Palmer, H.C., Merz, B.A., and Hayatsu, A.
1977: The Sudbury dikes of the Grenville Front region: paleomagnetism, petrochemistry, and K-Ar age studies; Canadian Journal of Earth Sciences, v. 14, p. 1867-1887.

Park, J.K., Tanczyk, E.I., and Desbarats, A.J.
1988: Magnetic fabric and its significance in the 1400 Ma Mealy diabase dykes of Labrador, Canada; Journal of Geophysical Research, v. 93, p. 13689-13704.

Rochette, P., Jackson, M., and Aubourg, C.
1992: Rock magnetism and the interpretation of anisotropy of magnetic susceptibility; Reviews of Geophysics, v. 30, p. 209-226.

Tarling, D.H. and Hrouda, F.
1993: The Magnetic Anisotropy of Rocks; Chapman and Hall, 217 p.

Geological Survey of Canada Project 760061

Origin of a carbonate-rich breccia at Lake Minogami, Shawinigan area, Grenville Province, Quebec

L. Nadeau, S. Nadeau, and P. Brouillette
Quebec Geoscience Centre, Sainte-Foy

Nadeau, L., Nadeau, S., and Brouillette, P., 1994: Origin of a carbonate-rich breccia at Lake Minogami, Shawinigan area, Grenville Province, Quebec; in Current Research 1994-E; Geological Survey of Canada, p. 193-202.

Abstract: The Lake Minogami carbonate breccia (LMCB) exhibits field characteristics similar to those of a carbonatite diatreme, but a geochemical signature reflecting derivation from nearby marbles. The rocks display a very fine grained calcite matrix containing mechanically abraded rounded rock fragments. The breccia shows mineralogy and geochemistry distinct from carbonatites, namely a high SiO_2 content (≈30%), low abundances of compatible and incompatible trace elements and limited REE fractionation. In addition, breccia samples show REE normalized patterns parallel to those of nearby tectonic marble and comparable $\delta^{13}C$ and $\delta^{18}O$ values.

These features provide strong evidence for the derivation of the Lake Minogami carbonate breccia matrix by remobilization of a marble protolith. The presence of microfractures filled by calcite in both rock fragments and xenocrysts, rare subgrains and neoblasts around xenocrysts, as well as bent twins and kinks in matrix calcite provide additional support for a tectonic origin.

Résumé : La brèche carbonatée du lac Minogami, bien qu'elle montre des caractéristiques sur le terrain évoquant celles d'un diatrème carbonatitique, présente une signature géochimique comparable à celle des marbres avoisinants. La brèche comporte une matrice calcitique à grain très fin et de nombreux fragments rocheux arrondis mécaniquement. La minéralogie et la géochimie de la brèche sont différentes de celles des carbonatites; en effet, la brèche présente une haute teneur en SiO_2 (≈30%), de faibles abondances en éléments traces compatibles et incompatibles et un faible fractionnement entre les terres rares. De plus, les échantillons de brèche montrent un spectre normalisé des terres rares qui se campare à celui des marbres, ainsi que des valeurs de $\delta^{13}C$ et $\delta^{18}O$ qui sont également comparables à celles des marbres

Ces caractéristiques suggèrent que la matrice de la brèche s'est formée à partir d'un marbre. De plus, la présence de microfractures remplies de calcite dans les xénocristaux et les fragments de roches, de rares sous-grains et de néoblastes en bordure des xénocristaux, de même que de mâcles tordues et de kinks dans la calcite formant la matrice suggèrent également une origine tectonique.

INTRODUCTION

Carbonate-rich intrusive rocks may be of various origins: 1) igneous carbonatites e.g., Oka, Alnö (Wolley, 1989), 2) replacement carbonatites of magmatic origin, e.g., Wet Mountains area (Armbrustmacher, 1979), 3) small carbonate dykes of carbonatite affinities eg. Grenville Province and along the Great Glen Fault (Hogarth et al., 1985; Garson et al., 1984), 4) carbonate veins associated with skarn deposits (Lentz, 1991), and 5) tectonic and hydraulic breccia pipes (Laznicka, 1988).

Igneous carbonatites are characterized by some specific chemical signatures: 1) low SiO_2 (<10%) with high contents in CaO, P_2O_5, Sr and CO_2, 2) high rare earth element (REE) contents reflected the occurrence of accessory minerals such as apatite, britholite, and zircon and marked fractionation between light (LREE) and heavy rare earth elements (HREE), and 3) low initial Sr isotopic ratios typical of mantle-derived magmas (Wolley and Kempe, 1989). Carbonatite intrusions occur mainly in association with continental rifting and aulacogen formation (Kumarapeli, 1978; Barker, 1989; Wooley 1989).

In metamorphic terranes and in fault zones the identification of true carbonatite may be obscured where primary textures, mineralogy and chemical composition have been significantly modified. However, rock association, intrusive contacts, fenitisation and rock chemistry help to distinguish true carbonatites from skarns (Lentz, 1991), tectonic marbles and fault breccia pipes (Laznicka, 1988).

In this study we describe the occurrence and discuss the origin of an unmetamorphosed carbonate-rich breccia, the Lake Minogami carbonate breccia (LMCB) from the Shawinigan area in Grenville Province (Fig. 1, 2). This body was first interpreted in the field as a carbonatite diatreme because of the fine grained nature of the carbonate matrix, the presence of abundant fragments and xenocrysts and the lack of mesoscopic primary deformation textures and tectonic flow structure. A petrological and geochemical study was undertaken to test this hypothesis and here we contrast the chemistry of the Lake Minogami carbonate breccia with nearby marbles and carbonatite rocks from elsewhere.

REGIONAL SETTING

The St. Maurice region in south-central Grenville Province, includes the eastern boundary between the Allochthonous Monocyclic Belt and polycyclic domains farther east (Fig. 1). Two lithotectonic domains are recognized in the Shawinigan area (Fig. 2). The northern Mékinac domain is dominated by granulite facies, monotonous, highly deformed granoblastic charnockitic orthogneisses with widespread centimetre to decametre thick mafic layers and lenses and rare screens of paragneisses, quartzite and marble (Nadeau and Corrigan, 1991). The southern Shawinigan domain, which is a northeast extension of the Morin terrane, is underlain by mixed amphibolite and granulite facies rocks and characterized by abundant pelitic gneisses, marble and quartzite and the associated noritic and granitic rocks of the Shawinigan-St. Didace complex.

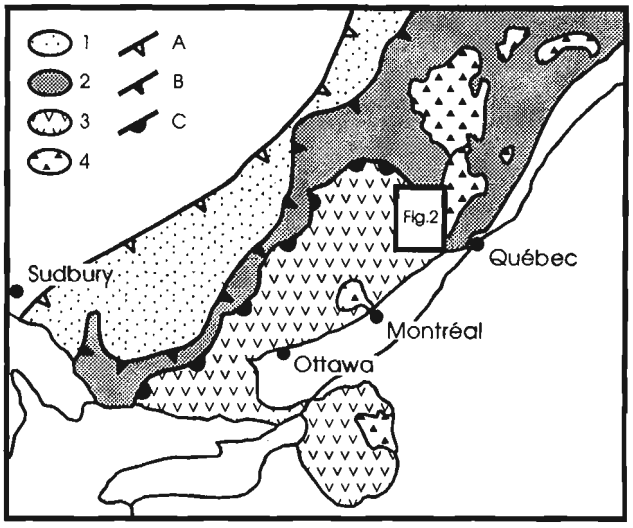

Figure 1. Location sketch map and tectonic subdivisions of the Grenville Orogen (Rivers et al., 1989). (1) Parautochthonous Belt; (2) Allochthonous Polycyclic Belt; (3) Allochthonous Monocyclic Belt; (4) Anorthosite-mangerite-charnockite-granite suite; (A) Grenville Front; (B) Allochthon boundary thrust; (C) Monocyclic belt boundary thrust.

These lithotectonic domains are structurally juxtaposed via a shallow southerly dipping Grenvillian ductile shear zone (Fig. 2). Northwest of Shawinigan, this ductile shear zone is cut by the St. Maurice fault, a major post-Grenvillian and long-lived brittle normal fault part of the fault system which marks the margin of the shield north of the St. Lawrence River. Brittle fracturing and pseudotachylyte injections are ubiquitous in the St. Maurice fault zone (Fig. 3A); pseudotachylyte in the area yielded a K-Ar minimum age of 925 Ma (Philpotts and Miller, 1963). The Lake Minogami carbonate breccia occurs near the intersection of the St. Maurice Fault with the Mékinac-Shawinigan boundary ductile shear zone (Fig. 2); brittle fracturing related to the St. Maurice Fault overpaints the carbonate breccia.

FIELD RELATIONSHIPS

The Lake Minogami carbonate breccia outcrops discontinuously over an area of 1000 m^2. The extension of the body in the subsurface is unknown. No magnetic anomaly is associated with this area, implying that this body is of a small size. The breccia intrudes and displays sharp contacts with the host rock gneisses (Fig. 3B). It shows marked relief and colour contrasts with the enclosing gneisses; subrounded breccia fragments show a positive relief within a recessive, earthy orange calcite matrix (Fig. 3C). The absence of Grenvillian deformation features and metamorphic recrystallization provides clear evidence of a post-grenvillian emplacement. Late fractures are indicative of minor post-emplacement brittle deformation.

PETROGRAPHY AND MINERALOGY

Lake Minogami carbonate breccia matrix

The Lake Minogami carbonate breccia shows an orange to brown earthy crust on surface (Fig. 3C). The interior of these rocks shows a more greyish matrix due to iron oxide staining. The matrix is composed of very fine grained (10-50 μm) pure sparric calcite crystals (Table 1) in a massive interlocking texture. The calcite crystals show no preferred orientation or evidence of tectonic flow. They show either clear subpolygonal boundary and rare cleavage planes, or ubiquitous bent cleavage planes and mechanical twins, and rare kink-bands. Calcite neoblasts are scarce and occur along larger deformed grains. These textural features contrast with those exhibited in the tectonic marbles described below.

Lake Minogami carbonate breccia enclaves and xenocrysts

Subrounded to subangular enclaves, up to 15 cm in maximum dimension, show as positive relief on a weathered surface (Fig. 3C). Some sample fragments and wallrock gneisses have a strong reddish colour attributed in the field to fenitization. Breccia clasts include intermediate granulite, quartzite, amphibolitized gabbro and calc-silicates. The clasts contain the minerals clinopyroxene, scapolite, quartz, K-feldspar, titanite, and calcite. The xenocrysts derived from fragmented enclaves are characterized by the same mineral assemblage plus metamict zircons, but without calcite. They show subidiomorphic to subrounded shapes (Fig. 3D). Many xenocrysts are in sharp contact with very fine grained polycrystalline and polymineralic discontinuous rims which preferentially fill crystal embayments (Fig. 3E). Some display undulose extinction and a granoblastic mortar structure (Fig. 3F); a few xenocrysts are entirely recrystallized.

Clinopyroxene commonly displays xenomorphic to subidiomorphic shapes. Xenocrystic clinopyroxene is partly rimmed by tiny crystals of quartz±scapolite and±calcite (Fig. 3E). The rim is composed of small serrated grains possibly derived from larger crystals that have undergone recrystallization. In addition, some clinopyroxene show embayments filled by coarse grained scapolite, quartz or calcite (Fig. 3E). Clinopyroxene crystals are cut by micro-fractures filled with the alteration assemblage, calcite±actinolite± opaque oxide grains.

Clinopyroxene cores and rims are salite (Table 1). Slight chemical variations in CaO, FeO_T and MgO contents are observed at crystal rims and near crystal face embayments. There are no chemical variations that could be attributed to reaction with the calcite matrix. Thus the lack of systematic chemical variation in clinopyroxene rims, together with regular crystal faces in contact with the rock matrix, suggest that

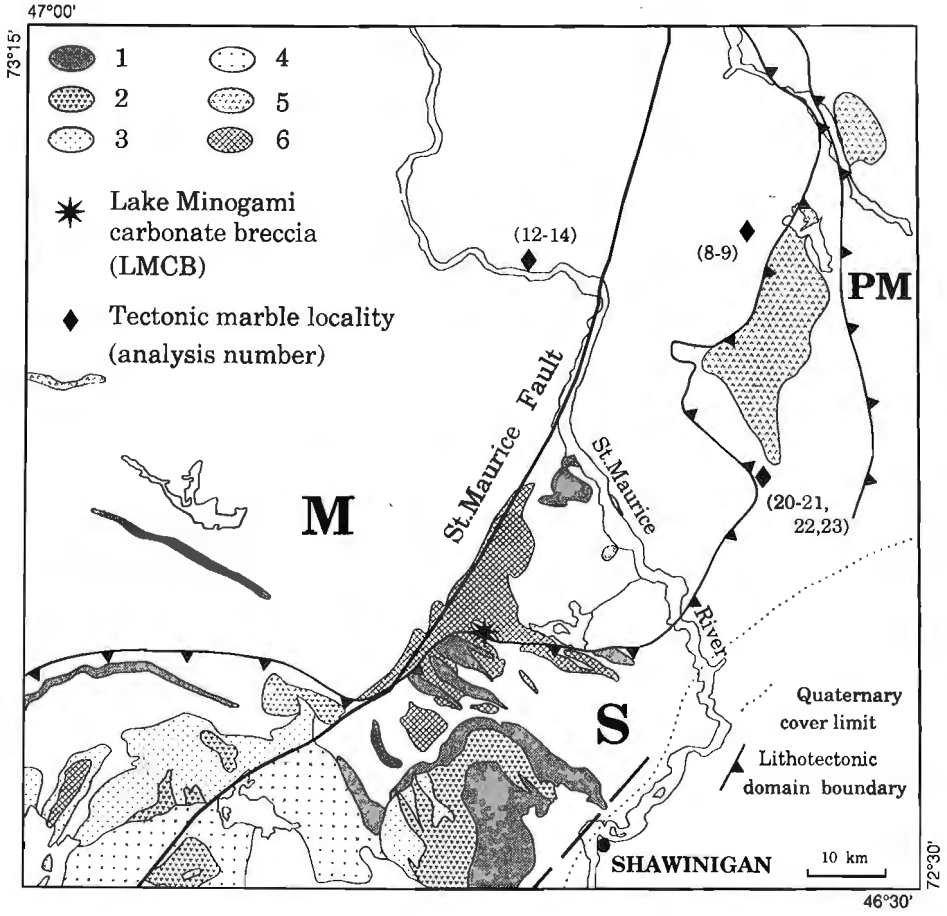

Figure 2.

Geological sketch map of the Shawinigan area. Lithotectonic domains include: (M) Mékinac; (S) Shawinigan; and (PM) Portneuf-St. Maurice. Major map units comprise: (1) paragneiss; (2) anorthosite and gabbronorite; (3) hyper- sthene monzonite; (4) St. Didace porphyritic granite; (5) monzodiorite; and (6) leucocratic granite, UTM coordinate of the Lake Minogami carbonate breccia: E663658, N516836:; NTS(31I10).

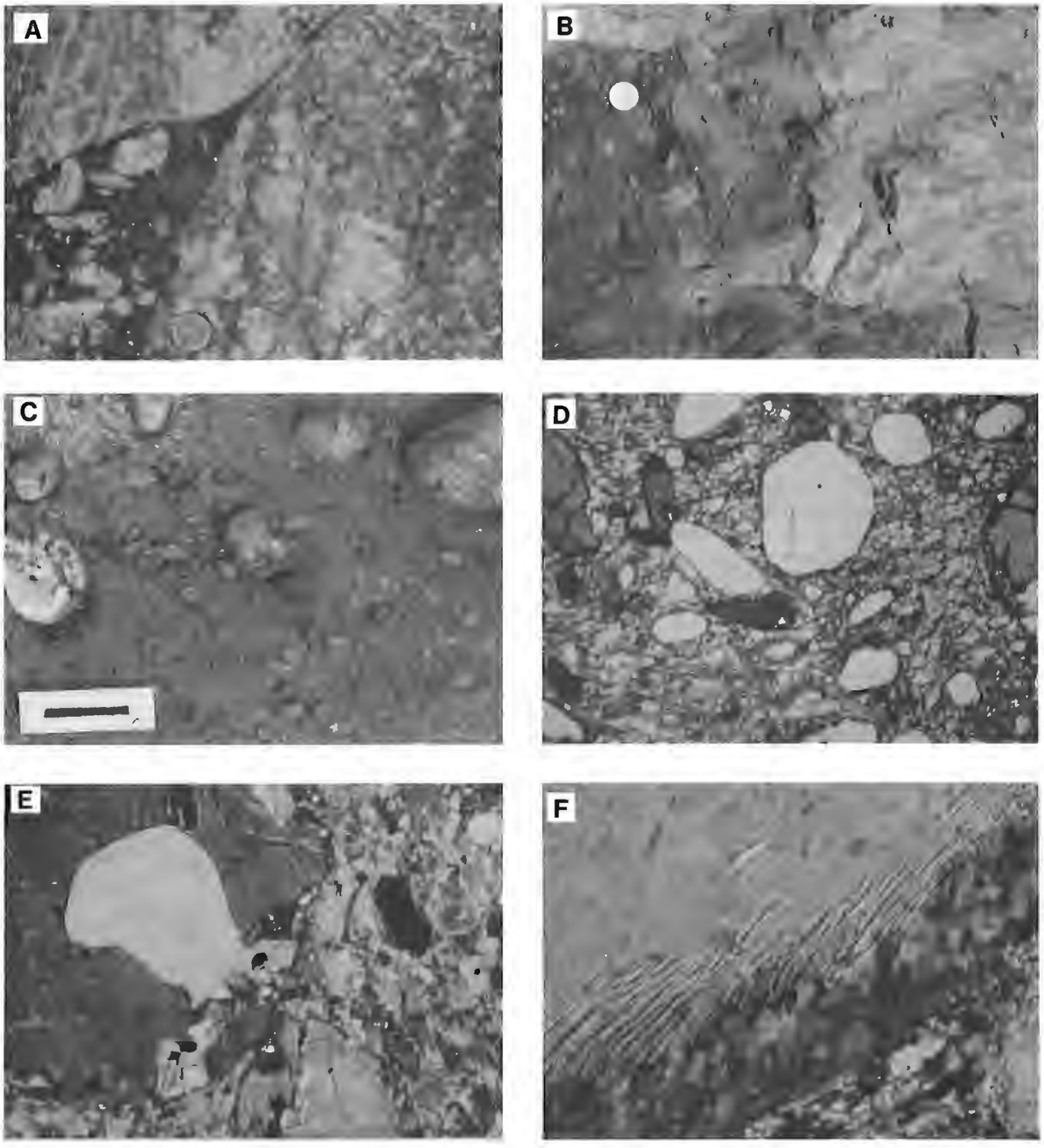

A. Pseudotachylyte injection carrying angular wallrock fragments, St.Maurice fault zone; coin is 2.5 cm.

B. Cross-cutting contact of Lake Minogami carbonate breccia with high grade gneiss; coin is 2.5 cm.

C. Typical weathered surface showing the recessive calcite matrix with subrounded rock fragments; scale is 2 cm.

D. Typical texture of Lake Minogami carbonate breccia matrix, xenocrysts and rock fragments; note the shape of the xenocrysts; field of view = 3.2 mm wide.

E. Clinopyroxene xenocryst with an embayment fill with calcite and a finer grained sharply bounded polycrystalline and polymineralic discontinuous rims; field of view = 3.2 mm wide.

F. Bent and recrystallized margin of a perthitic microcline xenocryst; field of view = 1 mm wide.

Figure 3. *Pseudotachylyte and characteristic features of the Lake Minogami carbonate breccia.*

Table 1. Range in mineral chemistry of Lake Minogami carbonate breccia sample 7. Microanalyses were obtained by wavelength dispersive spectrometry at the Geological Survey of Canada.

	Clinopyroxene (N=34)	Scapolite (N=27)	Amphibole (N=3)	K-Feldspar (N=29)	Calcite (N=1)
SiO_2	49.45-53.24	50.19-52.62	40.66-41.43	62.75-64.73	0.00
TiO_2	0.07-0.23	n.d	0.58-0.66	n.d	n.d
Al_2O_3	0.88-2.00	24.19-25.32	10.26-10.97	18.31-18.98	0.00
FeO_T	7.05-13.95	0.00-0.45	18.81-18.92	0.00-0.10	0.88
MnO	0.07-0.41	n.d	0.07-0.09	n.d	n.d
MgO	9.63-14.01	n.d	9.68-10.10	n.d	n.d
CaO	22.42-24.68	12.21-14.13	11.83-11.99	0.00-0.05	54.50
Na_2O	0.40-0.93	5.45-6.58	1.39-1.45	0.61-1.35	0.00
K_2O	0.00-0.03	0.40-0.64	1.80-1.95	14.88-16.47	0.00
P_2O_5	n.d	n.d	0.01-0.02	n.d	n.d
Cr_2O_3	0.00-0.08	n.d	0.05-0.13	n.d	n.d
NiO	0.00-0.12	n.d	0.00-0.04	n.d	n.d
ZnO	n.d	n.d	0.07-0.20	n.d	n.d
SrO	n.d	n.d	0.00-0.12	n.d	n.d
V_2O_3	n.d	n.d	0.09-0.12	n.d	n.d
SO_3	n.d	n.d	0.10-0.19	n.d	n.d
F	n.d	n.d	0.33-0.49	n.d	n.d
Cl	n.d	n.d	0.38-0.55	n.d	n.d

the polymineralic rims were not formed by a chemical reaction between clinopyroxene and calcite. Rather the matrix evolution from scapolite-quartz-calcite to pure calcite is interpreted to reflect a paragenetic evolution from early to late remobilization. Moreover, the presence of similar rim textures around diopside crystals in a mylonitized marble (A-8 from Lake Jésuite) suggests a tectonic origin.

Orthoclase xenocrysts are locally transformed to perthitic microcline (Table 1). Scapolite composition is close to mizzonite (Table 1). It is noteworthy that there is no partial replacement of plagioclase crystals within rock fragments and in xenocrysts by scapolite. Small green xenomorphic amphibole crystals occur in the calcite matrix. Larger hornblende crystals replace clinopyroxene in gabbroic fragments (Table 1). Well-crystallized titanite is distributed throughout the rock matrix. It is similar to that observed in some calc-silicate enclaves. Several titanite crystals show partial alteration marked by the formation of opaque rims. Sub-euhedral zircon, restricted to the rock matrix, is less common than titanite and commonly displays a wide metamict rim with a small anhedral core. Rare apatite included in clinopyroxene and titanite is observed.

Tectonic marbles

Tectonic marbles are riddled with boudins and wall rock fragments and show mesoscopic structures including complex fold patterns indicative of ductile flow. They range from medium grained granoblastic at St. Tite (A-20 to 23A) and St. Joseph (A-12, 14) localities, to fine grained and mylonitic at Lake Jésuite (A-8, 9; Fig. 2). Calcite in the marble is either white or salmon pink.

Marbles from St. Roch contain angular fragments only of charnokite, whereas those from St. Tite include both charnokite and pegmatite chunks. The Lake Jésuite marbles enclose a variety of fragments including metapelite, marble and pyroxenite. Marbles in contact with charnokite and charnokitic fragments within breccias commonly show a thin metasomatic reaction rims enriched in diopside. In the field, the Lake Jésuite tectonic marbles show severe grain comminution, strong foliation and flow structure.

Marble mineralogy is characterized by large calcite rhombohedra commonly containing solid and fluid inclusions. Locally a second generation of clear calcite occurs interstitially between the larger crystals. Diopside, scapolite, phlogopite, K-feldspar, serpentine after olivine, and titanite are present in variable amounts. Within the Lake Jésuite mylonites, subrounded diopside crystals are rimmed by fine grained quartz + calcite, and some mineral embayments are filled by calcite. The mylonitic rocks display ribbons of large calcite crystals and highly fractured larger xenocaysts and rock fragments within a very fine grained calcite matrix.

GEOCHEMISTRY

Analytical methods

Major and trace elements were determined in three Lake Minogami carbonate breccia and nine tectonic marble samples by X-ray flouresence spectroscopy (XRP) at the Quebec Geoscience Centre (Table 2). REEs were determined at the Quebec Geoscience Centre by neutron activation with an analytical precision of 10% for La, Ce, Nd and Sm but ~20% for Eu, Tb, Yb and Lu (Table 2). Several samples were also investigated by cathodoluminescence to characterize the different carbonate generations that may occur in the rocks. Calcite was extracted from marble slabs for stable isotope analysis by drilling large calcite crystals. Calcite in breccia matrix was drilled from zones enriched in fine grained calcite crystals. These calcite powders were further ground in an agate mortar and were subsequently analyzed for their C and O stable isotopes by reaction with 100% H_3PO_4 following McCrea (1950). C and O isotopic ratios are given in the delta notation, δ, (‰) relative to PDB and SMOW international standards and were measured using a VG SIRA 12 mass spectrometer at the Quebec Geoscience Centre. Analytical precision of the $\delta^{13}C$ and $\delta^{18}O$ values are 0.01 and 0.1‰, respectively.

It is possible that we may have inadvertently incorporated some scapolite crystals during drilling. This, however, would have a limited effect on calcite isotopic results. Scapolite reacting with H_3PO_4 at 25°C, typical for calcite decomposition, yielded only 10% of its CO_2 after 60 hours (Moecher et al., 1994). In addition, the C isotopic fractionation between scapolite and calcite is in the order of 0.1 ± 1.0‰, at the high grade P-T conditions of the Lake Minogami carbonate breccia protoliths.

Table 2. Rock chemistry, (L. Min.: Lake Minogami; L. Jes.: Lake Jésuite; St. Jos.: St. Joseph de Mékinac).

Sample	A-6*	A-6A	A-7	A-8*	A-8	A-9A	A-12	A-14	A-20	A-21	A-22	A-23A
Rock	breccia	breccia	breccia	Marble White	Marble Pink	Marble White	Marble White	Marble White	Marble Pink	Marble White	Marble White	Marble White
Local	L. Min.	L. Min.	L. Min.	L. Jes.	L. Jes.	L. Jes.	St Jos.	St Jos.	St Tite	St Tite	St Tite	St Tite
SiO_2	29.02	27.49	29.51	10.90	11.02	6.02	8.27	1.56	4.37	23.09	14.77	1.59
TiO_2	0.29	0.35	0.29	0.13	0.12	0.06	0.10	0.04	0.07	0.18	0.07	--
Al_2O_3	5.95	5.91	6.08	1.78	2.20	1.39	2.07	--	0.51	3.70	1.42	0.06
Fe_2O_3	0.17	0.14	0.15	--	--	--	--	--	--	0.02	0.02	--
FeO	1.37	1.16	1.25	--	--	--	--	--	--	0.16	0.12	--
MnO	0.06	0.06	0.07	0.04	0.04	0.04	0.03	0.02	0.04	0.04	0.08	0.04
MgO	1.54	2.10	1.76	1.25	1.54	2.93	4.69	2.59	2.09	2.25	11.38	2.74
CaO	33.28	35.33	33.23	50.15	49.68	50.45	46.66	55.63	54.27	40.79	38.34	55.60
Na_2O	0.93	0.93	1.18	0.21	0.21	--	--	--	--	0.21	--	--
K_2O	1.49	1.41	1.51	0.45	0.53	0.30	0.61	--	0.30	1.39	0.96	0.01
P_2O_5	0.07	0.09	0.08	0.06	0.07	0.04	0.05	0.04	0.04	0.06	0.03	0.05
LOI	23.84	29.09	22.95	36.71	36.13	39.49	37.00	41.41	39.24	27.68	32.41	41.32
TOTAL	98.01	104.06	98.06	101.68	101.54	100.72	99.48	101.29	100.93	99.57	99.60	101.41
$\delta^{13}C$	-1.37	-0.81	-1.06	-0.09	-0.89	--	-0.74	--	-1.04	--	--	-0.60
(‰)	-1.40	-0.92	-1.29									-0.64
$\delta^{18}O$	11.60	14.48	13.90	17.70	17.39	--	21.92	--	15.65	--	--	14.81
(‰)	11.68	14.47	13.95									14.81
Rb	57	47	61	12	15	18	23	5	18	32	49	3
Ba	908	865	1023	238	318	657	210	50	153	432	401	50
Sr	752	612	789	1525	1234	431	372	447	327	2366	209	942
Nb	10.0	7.0	9.0	2.0	2.0	7.0	8.0	8.0	8.0	2.0	5.0	2.0
Hf	2.19	2.22	2.49	0.77	0.94	0.35	0.77	0.20	0.34	3.26	0.87	0.20
Zr	26	32	24	3	3	3	20	3	3	3	34	3
Y	25	22	23	10	8	10	12	7	12	7	14	7
Th	10.20	8.79	10.7	1.57	2.32	1.24	1.35	0.46	0.92	2.40	0.80	1.34
U	2.52	2.80	2.83	1.93	1.52	0.50	0.50	0.50	0.50	2.78	0.50	0.50
La	55.70	48.80	68.20	11.00	14.20	7.21	5.75	1.15	9.37	13.30	15.50	19.40
Ce	105.00	92.50	132.00	22.90	28.50	14.70	12.10	< 2	15.50	28.10	27.40	32.60
Nd	32.50	29.60	40.10	12.20	11.00	5.88	6.39	< 5	5.00	11.10	7.25	9.29
Sm	5.00	4.47	5.97	1.89	2.02	1.19	1.17	0.13	0.94	2.51	1.69	1.13
Eu	0.81	0.77	0.94	0.37	0.45	0.32	0.30	< 0.1	0.28	0.58	0.35	0.24
Tb	0.54	0.49	0.60	0.20	0.19	0.11	0.14	< 0.1	0.12	0.28	0.20	0.11
Yb	2.07	1.92	2.26	0.76	0.69	0.29	0.60	< 0.2	0.47	1.25	1.09	0.55
Lu	0.33	0.30	0.37	0.12	0.11	0.06	0.09	< 0.05	0.07	0.19	0.14	0.09
ΣREE	202.78	179.69	250.44	50.14	57.86	30.46	27.24	9.43	32.45	58.01	54.32	64.11
(La/Sm)n	6.87	6.74	7.05	3.59	4.34	3.74	6.38	5.46	6.15	3.27	5.66	10.59
(Ce/Yb)n	12.90	12.25	14.85	7.66	10.51	12.89	5.13	2.54	8.39	5.72	6.39	15.08

Results

The Lake Minogami carbonate breccia rocks have low SiO_2, high CaO and loss-on-ignition (LOI) contents typical of calcite-rich rocks (Table 2). The major and trace element chemistry of the Lake Minogami carbonate breccia is significantly distinct, however, from the nearby tectonic marbles analyzed in this study (Table 2) and the values estimated for the composite Grenville marble of Shaw et al. (1976) (Fig. 4A). The breccia is enriched in SiO_2, TiO_2, Al_2O_3, FeO, Na_2O, K_2O, P_2O_5 and most trace elements but poorer in MgO, CaO and LOI than tectonic marbles (Table 2).

The various Lake Minogami carbonate breccia rocks show parallel normalized REE patterns (Fig. 4B). They display an enrichment in LREE relative to HREE but no fractionation within the HREE. Their REE contents are higher by a factor of two to ten compared to tectonic marbles (Fig. 4B). The latter have more variable LREE/HREE ratios than the breccia rocks, although they present a similar lack of fractionation among the HREE.

The $\delta^{13}C$ and $\delta^{18}O$ values of calcite in Lake Minogami carbonate breccia rocks show a limited range from -0.82 to -1.40‰ and +11.60 to +14.48‰, respectively. The C isotopic values of calcite in the breccia partly overlap the range of values in marbles (-0.60 to -1.04δ, Table 2).

DISCUSSION

The fine grained and massive nature of the calcite matrix and cross-cutting relationships observed in the field provide good evidence for the intrusive nature of the Lake Minogami carbonate breccia rocks. In addition, the presence of an alteration zone in the gneisses in contact with the breccias was inferred to result from fenitization and was also considered as an additional field characteristic of a magmatic origin. Lastly, the occurrence of subangular to subrounded country rocks and mafic fragments within a brownish to orange coloured carbonate matrix was interpreted to be characteristic of a diatreme breccia associated to carbonatite intrusions.

These field observations are not sufficient and can be misleading in the interpretation of the Lake Minogami carbonate breccia rocks. These characteristics may be attributed to the operation of several distinct processes that are discussed below: a) carbonatite diatreme, b) marble melt produced by frictional melting, and c) tectonic breccia.

Carbonatite diatreme

Although on a CaO-MgO-FeO+Fe_2O_3+MnO ternary diagram (not shown) the Lake Minogami carbonate breccia samples will plot in the field of calciocarbonatite composition, they have higher and atypical SiO_2 contents for given CaO and LOI values than reported in general in carbonatite rocks (Wolley and Kempe, 1989; Table 2). The Lake Minogami carbonate breccia samples are closer to the composition of some carbonatite type breccias of the Oka complex (Table 1 in Gold, 1972) and isolated veins within the Great Glen Fault (Garson et al., 1984) that have similar SiO_2, CaO and LOI values.

The compatible elements Sr, Ba and P_2O_5 and the incompatible elements Zr, Y, Nb, Th, U and Hf are low in the Lake Minogami carbonate breccia (Fig. 4A), although they fall within the range of the lowest values reported in primary and replacement carbonatites (Wolley and Kempe, 1989; Armbrustmacher, 1979). However, the low REE contents, the shape of the REE normalised patterns with the low LREE/HREE ratios and absence of fractionation between the HREE in Lake Minogami carbonate breccia are not typical signatures of REE reported in carbonatite rocks (Fig. 4B). These observations cannot be explained by dilution with country-rock fragments and xenocrysts, and by the lack of minerals such as apatite and REE-rich minerals, as carbonatite calcite is also relatively rich in REE with strongly fractionated HREE patterns (Wolley and Kempe, 1989; Armbrustmacher, 1986).

The $\delta^{13}C$ and $\delta^{18}O$ values in the Lake Minogami carbonate breccia rocks are much higher than most values measured in carbonatite rocks (-4 to -8‰ and +6 to +10‰, respectively, in primary carbonatites: Taylor et al., 1967; Deines, 1989 and references therein). Although several carbonatite complexes contain some calcite-rich rocks with similarly high $\delta^{13}C$ and $\delta^{18}O$ values as Lake Minogami carbonate breccia e.g. Tororo, Sukulu, Rangwa, St-André, Dicker Willem carbonatite complexes (Deines, 1989; Cooper and Reid, 1991) and calcite-rich lavas from Nyiragongo (Louaradi et al., 1992), they are associated with a suite of other carbonatitic rocks. Their atypical values have been attributed either to low temperature alteration by hydrothermal fluids (Knudsen and Buchardt, 1991; Cooper and Reid, 1991) or to extreme isotopic fractionation during degassing (Pineau et al., 1973; Knudsen and Buchardt, 1991).

All carbonatite complexes present a spectrum of rocks that show an evolution trend in C and O isotopes from the primary carbonatite values to those observed in the Lake Minogami carbonate breccia. In addition, carbonatite intrusions are commonly surrounded by small breccia plugs and veins, e.g. Castignon Lake intrusion in Labrador Trough (Chevé, 1986) and the Oka complex (Gold, 1972). In our case, we cannot confirm such an isotopic trend as our sampling is limited to an isolated small body and there is no field evidence for the presence of a larger carbonatite body.

Lastly, diatreme breccias, carbonate-rich veins, and replacement carbonatites are commonly accompanied by fenitization zones indicative of alkaline-rich fluid reactions with the enclosing rocks. Indeed, Garson et al. (1984) concluded that veins of alkaline-rich amphibole and/or pyroxene are a strong and sufficient indicator of a carbonatitic origin for carbonate-rich rocks. Such features are lacking in the Lake Minogami carbonate breccia rocks.

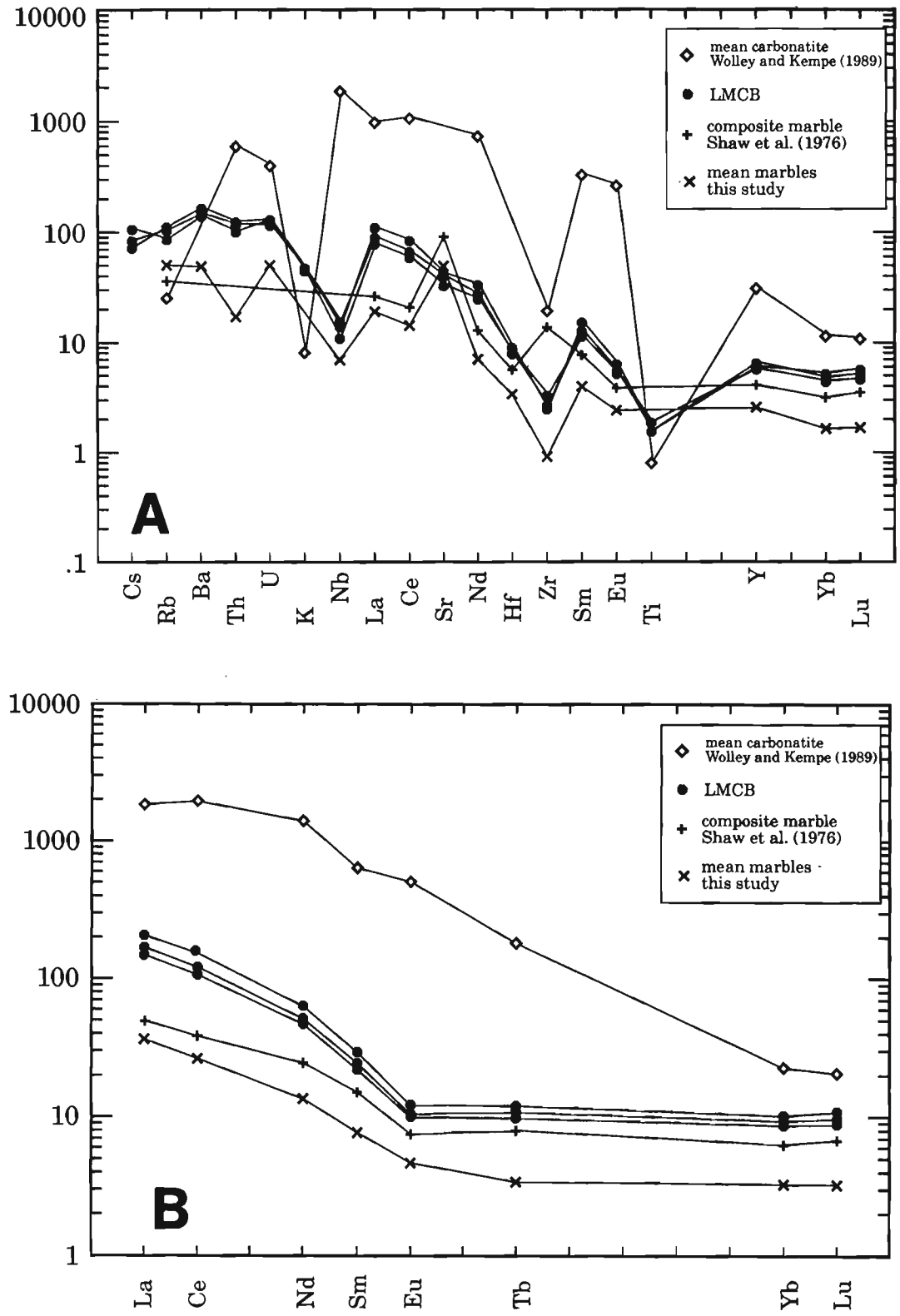

Figure 4. Comparison of (A) trace element abundances normalized to the primitive mantle values of Taylor and McLennan (1985), and (B) chondrite normalized REE distribution between (Lake Minogami carbonate breccia) samples and mean nearby tectonic marbles, mean carbonatite values (Wolley and Kempe, 1989), and composite Grenville marble from southwestern Quebec (Shaw et al., 1976).

Marble melt by frictional melting

An alternative that could account for the breccia and the intrusive relationship with the country rocks would be that the Lake Minogami carbonate breccia was a carbonate-rich melt derived by frictional melting of a marble protolith and subsequent incorporation of country-rock fragments. It should be remembered that the breccia is located within a major fault zone, the St. Maurice fault, which has a protracted deformation history (Fig. 2). Pseudotachylyte veins, generally attributed to coseismic frictional melting (Sibson, 1977), are ubiquitous in this fault zone (Fig. 3A) and that brittle fracturing is common in Lake Minogami carbonate breccia wallrocks.

However, if the Lake Minogami carbonate breccia represents a pseudotachylitic marble intrusion it would be a rather unusual and larger equivalent to silicate-derived pseudotachylyte veins, that generally range from a few centimetres up to one metre thick. To our knowledge, there is only one reported occurrence, described from China, of carbonate sediments transformed into pseudotachylyte (Shangguan-Zhi-Guan, 1990). The lack of such marble-derived pseudotachylyte veins is rather surprising since it has long been experimentally demonstrated that calcite, in the carbonate-water system, melts under relatively low temperature and pressure conditions, ~650°C and 1 kb (Wyllie, 1989).

Interestingly, the carbonate melting process would result in loss of CO_2, a process that would have produced a decrease in both heavy C and O isotopes within residual carbonate minerals. Such a process would explain the slight differences in $\delta^{13}C$ and $\delta^{18}O$ values in calcite from the Lake Minogami carbonate breccia when compared to marbles. There is no petrographic evidence other than the fine grain size of calcite in the matrix to suggest a melt derivation. In addition, a calcite-rich melt would have produced significant dissolution and/or chemical reactions of the fragments and xenocrysts.

Tectonic breccia

Tectonic breccias are often reported to occur in large shear zones (e.g. Laznicka, 1988). Brecciation may result from contrasting rheologies of units; the more ductile rocks recrystallize readily whereas the more brittle rocks are fragmented into clasts of various sizes and shapes. This is exactly what we observe in the Lake Minogami carbonate breccia where the more ductile marble protolith is transformed into a homogeneous and fine grained calcite matrix. The various gneissic host rocks were broken into fragments down to individual mineral grains that compose the xenocryst populations. The fact that some of the fragments and xenocrysts show subrounded to rounded shapes indicates that significant mechanical abrasion occurred between the fragments.

The mechanical mixing of the country-rock fragments and xenocrysts with a carbonate-rich matrix, derived from marbles, would explained the high SiO_2 contents of the Lake Minogami carbonate breccia rocks. As noted previously, the similar REE patterns in marbles and the breccia and the 3 to 10 times enrichment factor of the breccia is puzzling and would require also the effect of a mechanical mixing process. The distinct Rb-Sr-Ba-P-REE characteristics of the breccia rocks probably result from the local concentration, by mechanical mixing, of trace element enriched minerals such as titanite and zircon from the country-rock marbles and gneisses. The similarity in C and O isotopic ratios in calcite from the Lake Minogami carbonate breccia and the nearby marbles is also suggestive of the derivation of calcite from similar marble protoliths by mechanical crushing and mixing. In fact, all breccia samples contain fragments of the enclosing rocks, but marble fragments were never observed.

Hydraulic fracturing may also be a process that could yield a breccia-pipe by the accumulation and dynamic release of hydrothermal fluids along a fault zone (Laznicka, 1988). However, the Lake Minogami carbonate breccia does not correspond to breccias formed by hydraulic fracturing process as such a process induces extensive alteration haloes represented by hydrous minerals, e.g. chlorite, serpentine etc., of the fragments present in the breccia and of the enclosing rocks (Lachapelle, 1993). Significant hydrothermal alteration was not observed and quartz which typically occurs in abundance with hydro- thermal calcite is only a minor component of the breccia.

CONCLUSIONS

The intrusive Lake Minogami carbonate breccia exhibits limited wallrock alteration, a fine grained matrix and a fragmented structure, with rounded rock fragments and xenocrysts, which resemble those of typical carbonatite diatremes. However, mineralogical and geochemical characteristics do not confirm a carbonatitic origin.

The matrix is composed of calcite and the xenocryst population includes anorthoclase, scapolite, salite, titanite and zircon. Lake Minogami carbonate breccia lacks characteristic carbonatite minerals.

The chemical characteristics are: i) high silica contents (~30% SiO_2), ii) low abundances of compatible and incompatible trace elements (e.g. total REE = 180-250 ppm), iii) limited fractionation between LREE and HREE, as well as, lack of fractionation within the HREE, iv) similar REE normalized patterns (although 3 to 10 times more enriched) than marbles, and v) similar $\delta^{13}C$ and $\delta^{18}O$ values of Lake Minogami carbonate breccia matrix and tectonic marble.

The similarities in $\delta^{13}C$ and $\delta^{18}O$ values and REE pattern provide strong evidence for the derivation of the Lake Minogami carbonate breccia matrix by the mylonitisation of a tectonic marble. The 3 to 10 times REE enrichment of the breccia relative to marble protolith is probably the result of mechanical concentration of zircon and titanite in the calcite matrix after mechanical crushing and separation from wallrock gneisses. The presence of microfractures filled with calcite in both rock fragments and xenocrysts, rare subgrains and neoblasts around and within xenocrysts and bent mechanical twins and kinks in matrix calcite provide additional support for a mylonitic origin.

Accordingly, the Lake Minogami carbonate breccia is best interpreted as the result of tectonic brecciation and mechanical flow producing rounded wallrock fragments and xenocrysts. The process has lead to the complete disruption of the marble protolith and to the mobilization of fine grained calcite sparic matrix which invaded micro-fractures subsequent to tectonic activity in the adjacent St. Maurice Fault.

ACKNOWLEDGMENTS

We thank J. Stirling, G. Pringle, M. Luzincourt, J.P. Ricbourg for assistance with the microprobe and geochemical analyses and G. Lynch and T. Birkett for constructive reviews.

REFERENCES

Armbrustmacher, T.J.
1979: Replacement and primary magmatic carbonatites from the Wet Mountains area, Fremon and Custer counties, Colorado; Economic Geology, v. 74, p. 888-901.

Barker, D.S.
1989: Field relations of carbonatites; in Carbonatites: Genesis and Evolution; (ed.) K. Bell; Unwin Hyman, p. 38-69.

Chevé, S.
1986: Le complexe carbonatitique du Lac Castignon (Nouveau-Québec), deuxième partie; Rapport préliminaire, Ministère de l'Énergie et des ressources du Québec, p. 32.

Cooper, A. and Reid, D.L.
1991: Oxygen and carbon isotope patterns in the Dicker Willem carbonatite complex, southern Namibia; Chemical Geology, v. 94, p. 293-305.

Deines, P.
1989: Stable isotope variations in carbonatites; in Carbonatites: Genesis and Evolution; (ed.) K. Bell; Unwin Hyman, p. 301-359.

Garson, M.S., Coats, J.S., Rock, N.M.S., and Deans, T.
1984: Fenites, breccia dykes, albitites, and carbonatitic veins near the Great Glen Fault, Inverness, Scotland; Journal of Geological Society of London, v. 141, p. 711-732.

Gold, D.P.
1972: Monteregian Hills: diatremes, kimberlites, lamprophyres and intrusive breccias west of Montreal; in Twenty Fourth International Geological Congress, Montreal, Guidebook B-10.

Hogarth, D.D., Hartree, R., Loop, J., and Solberg, T.N.
1985: Rare-earth element minerals in four carbonatites near Gatineau, Quebec; American Mineralogist, v. 40, p. 1135-1142.

Knudsen, C. and Buchardt, B.
1991: Carbon and oxygen isotope composition of carbonates from the Qaqarssuk carbonatite complex, southern West Greenland; Chemical Geology, v. 86, p. 263-274.

Kumarapeli, P.S.
1978: The St-Lawrence rift system: a comparative study; in Tectonics and geophysics of continental rifts; (ed.) I.B. Ramberg and E.R. Neumann; D. Reidel Publishing company, Dorrecht, Holland, p. 367-384.

Lachapelle, R.
1993: The edge of the Canadian Shield in the Quebec City area: a continental beakup feature related to the opening of Iapetus; Mémoire de maîtrise, Université du Québec à Montréal, 81 p.

Laznicka, P.
1988: Breccias and coarse fragmentites; petrology, environments, associations, ores; Developments-in-Economic-Geology, v. 25, 832 p.

Lentz, D.R.
1991: U-, Mo-, and REE-bearing pegmatites, skarns and veins in the Central Metasedimentary Belt, Grenville Province, Ontario; Geological Association of Canada, Field Trip A9, 61 p.

Louaradi, D., Pineau, F., Nadeau, S., Javoy, M., and Demant, A.
1992: Origin of carbonates in the Nyiragongo magma: evidence from carbon and oxygen isotopes (abstract); in Transactions, American Geophysical Union, v. 73, p. 376.

McCrea, J.M.
1950: On the isotopic chemistry of carbonates and a paleotemperature scale; Journal of Chemical Physics, v. 18, p. 849-857.

Moecher, D.P., Valley, J.W., and Essene, E.J.
1994: Extraction and carbon isotope analysis of CO_2 from scapolite in deep crustal granulites and xenoliths; Geochimica et Cosmochimica Acta, v. 58, p. 959-967.

Nadeau, L. and Corrigan, D.
1991: Preliminary notes on the geology of the St. Maurice tectonic zone, Grenville orogen, Quebec; in Current Research, Part E; Geological Survey of Canada, Paper 91-1E, p. 245-255.

Philpotts, A.R. and Miller, J.A.
1963: A Precambrian glass from St.Alexis-des-Monts, Québec; Geological Magazine, v. 100, p. 337-345.

Pineau, F., Javoy, M., and Allègre, C.J.
1973: Étude systématique des isotopes de l'oxygène, du carbone et du strontium dans les carbonatites; Geochimica et Cosmochimica Acta, v. 29, p. 2363-2377.

Rivers, T., Martignole, J., Gower, C.F., and Davidson, A.
1989: New tectonic divisions of the Grenville Province, southeast Canadian Shield; Tectonics, v. 8, p. 63-84.

Shangguan-Zhi-Guan
1990: Preliminary study on carbon and oxygen isotopic compositions in carbonate-mylonite and carbonate-pseudotachylyte, Beijing area; Dizhen-Dizhi (Sessmology and Geology), v. 12, p. 215-220.

Shaw, D.M., Dostal, J., and Keays, R.R.
1976: Additional estimates of continental surface Precambrian Shield composition in Canada; Geochimica et Cosmochimica Acta, v. 40, p. 73-83.

Sibson, R.H.
1977: Fault rocks and fault mechanisms; Journal Geological Society of London, v. 133, p. 191-213.

Taylor, H.P., Frechen, J., and Degens, E.T.
1967: Oxygen and carbon isotope studies of carbonatites from the Laacher See district, West Germany and Alnö district, Sweden; Geochimica et Cosmochima Acta, v. 31, p. 407-430.

Taylor, S.R., and McLennan, S.M.
1985: The continental crust: its composition and evolution; Blackwell Scientific Publications, Oxford, 311 p.

Wyllie, P.J.
1989: Origin of carbonatites: evidence from phase equilibrium studies; in Carbonatites: Genesis and Evolution; (ed.) K. Bell, Unwin Hyman, p. 500-545.

Wolley, A.R.
1989: The spatial and temporal distribution of carbonatites; in Carbonatites: Genesis and Evolution; (ed.) K. Bell, Unwin Hyman, p. 15-37.

Wolley, A.R., and Kempe, D.R.C.
1989: Carbonatites: Nomenclature, average chemical compositions, and element distribution; in Carbonatites: Genesis and Evolution; (ed.) K. Bell, Unwin Hyman, p. 1-14.

Geological Survey of Canada Project 920002

Eastern Canada and National and General Programs

Est du Canada et programmes nationaux et généraux

The stratigraphic and tectonic significance of the Rocky Brook conglomerate in the western Cape Breton Highlands, Nova Scotia: a re-evaluation[1]

Shoufa Lin, Cees R. van Staal, and Sandra M. Barr[2]
Continental Geoscience Division

Lin, S., van Staal, C.R., and Barr, S.M., 1994: The stratigraphic and tectonic significance of the Rocky Brook conglomerate in the western Cape Breton Highlands, Nova Scotia: a re-evaluation; in Current Research 1994-E; Geological Survey of Canada, p. 205-210.

Abstract: The Jumping Brook Metamorphic Suite of the Aspy terrane mainly consists of a metasedimentary sequence and meta-pillow basalt. The Rocky Brook conglomerate was previously interpreted to be basal to the former and to stratigraphically overlie the latter. New observations indicate that the conglomerate is not an integral part of the suite. Therefore, the previous interpretation of the internal stratigraphic sequence of the Jumping Brook Metamorphic Suite should be re-evaluated, and the presence of clasts of the Cheticamp Pluton (a possible piece of Bras d'Or terrane rocks in the Aspy terrane) in the conglomerate has no direct bearing on the relationship between the pluton and the suite or between the Aspy and Bras d'Or terranes. The conglomerate is interpreted to be associated with, and possibly basal to, greywacke that was previously mapped incorrectly as correlative with the pillow basalt. A likely Late Silurian-Early Devonian age is inferred for the conglomerate and greywacke.

Résumé : La suite métamorphique de Jumping Brook du terrane d'Aspy est surtout constituée d'une séquence métasédimentaire et de métabasalte en coussins. On considérait auparavant que le conglomérat de Rocky Brook formait la base de la séquence et qu'il surmontait le basalte dans la stratigraphie. De nouvelles observations permettent d'indiquer que le conglomérat ne fait pas partie intégrante de la suite métamorphique de Jumping Brook; aussi devrait-on réévaluer l'interprétation antérieure de la séquence stratigraphique interne de la suite, et admettre que la présence de clastes du pluton de Cheticamp (élément possible des roches du terrane de Bras d'Or dans le terrane d'Aspy) dans le conglomérat n'a aucune incidence sur les relations entre le pluton et la suite, ou entre le terrane d'Aspy et celui de Bras d'Or. On suppose que le conglomérat est associé au grauwacke (et est peut-être basal par rapport à ce dernier) que l'on avait auparavant incorrectement mis en corrélation avec le basalte en coussins. On conclut que le conglomérat et le grauwacke sont probablement du Silurien tardif-Dévonien précoce.

[1] Contribution to Canada-Nova Scotia Cooperation Agreement on Mineral Development (1992-1995), a subsidiary agreement under the Canada-Nova Scotia Economic and Regional Development Agreement.
[2] Department of Geology, Acadia University, Wolfville, Nova Scotia B0P 1X0

INTRODUCTION

Pre-Carboniferous rocks of Cape Breton Island have been divided into four zones: Blair River Complex, Aspy terrane, Bras d'Or terrane and Mira terrane (Fig. 1; Barr and Raeside 1989). Geological evolution of individual terranes and relationships between the terranes have been a topic of much debate in recent years (e.g., Jamieson et al., 1987, 1990; Keppie, 1990; Raeside and Barr, 1990; Barr and Jamieson, 1991; Lynch and Tremblay, 1992b; Lin, 1993). During this debate, the Rocky Brook conglomerate in the western Cape Breton Highlands, which was previously mapped as part of the Jumping Brook Metamorphic Suite (JBMS) of the Aspy terrane (Fig. 1, 2; Jamieson et al., 1987), has drawn our attention, mainly for two reasons: (1) the previous interpretation of the internal stratigraphic sequence of the suite relied heavily on the interpretation of the conglomerate, which was suggested to mark a possible unconformity in the Jumping Brook Metamorphic Suite (Jamieson et al., 1987, 1990; Barr and Jamieson 1991), and thus in the Aspy terrane; (2) the conglomerate contains clasts that closely resemble the nearby Cheticamp Pluton (a possible piece of Bras d'Or terrane rocks exposed in the Aspy terrane; Dunning et al., 1990; Raeside and Barr, 1990) (Jamieson et al., 1987), and thus has significant implications for the relationship between the Jumping Brook Metamorphic Suite and the Cheticamp Pluton or between the Aspy and Bras d'Or terranes if the conglomerate is part of the Jumping Brook Metamorphic Suite. The conglomerate was re-examined during the 1993 field season to assess its tectonic significance. New observations reported here suggest that the conglomerate is not an integral part of the Jumping Brook Metamorphic Suite. Therefore, it has no bearing on the internal stratigraphy of the suite or on the relationship between the Cheticamp Pluton and the Jumping Brook Metamorphic Suite.

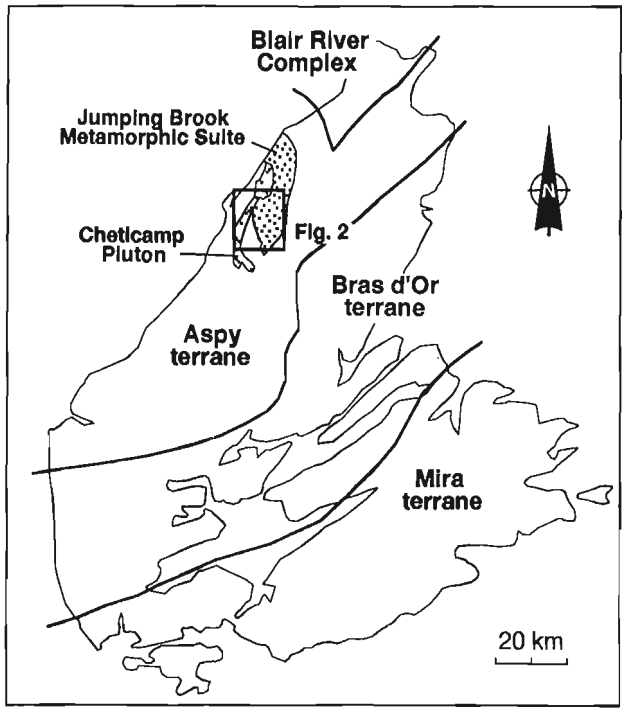

Figure. 1. Four zones on Cape Breton Island as suggested by Barr and Raeside (1989). Area of Figure 2 is shown.

JUMPING BROOK METAMORPHIC SUITE

The Jumping Brook Metamorphic Suite was defined by Jamieson et al. (1987) to include low- (chlorite- to garnet-), medium- (staurolite-), and high- (kyanite-) grade metasedimentary, metavolcanic, and metaplutonic(?) rocks in the western Cape Breton Highlands, including those of the Jumping Brook Complex of Currie (1983, 1987a). In the following description of the Jumping Brook Metamorphic Suite, we are only concerned with the low- to medium-grade rocks. In the high-grade rocks, primary structures were obliterated during deformation and metamorphism, which makes correlation difficult. The description is based on the authors' observations along Faribault Brook, on the Cabot Trail north of Cheticamp, and on Park Spur (Road) Extension, as well as on data in Connors (1986), Jamieson et al. (1987) and Lynch and Tremblay (1992b).

The low- to medium-grade rocks of the Jumping Brook Metamorphic Suite can be divided into two main parts: structurally lower mafic metavolcanic rocks (the Faribault Brook metavolcanics of Jamieson et al., 1987) and structurally higher metasedimentary rocks (the Barren Brook schist and the Dauphine Brook schist of Jamieson et al., 1987; hereafter termed the Jumping Brook Metamorphic Suite metasedimentary rocks). The Faribault Brook metavolcanics are tholeiitic pillow basalts (Connors, 1986) and are hereafter termed the Faribault Brook basalt. In spite of strong deformation, pillow structures are still recognizable locally (Fig. 3). The basalts have been interpreted as volcanic flows that erupted in an island-arc setting (Connors, 1986; Jamieson et al., 1987; Barr and Jamieson 1991).

The Jumping Brook Metamorphic Suite metasedimentary rocks are moderately to thinly bedded psammites, semipelites and pelites (Fig. 4), interpreted as turbidites (Lynch and Tremblay, 1992b). At low grade, primary structures are locally well preserved and graded bedding is clearly recognizable. The psammites are siliceous and mainly grey to dark grey. They are characterized by up to 10% (locally up to 40%, modal proportion; Tallman et al., 1988) 2- to 5-mm white and bluish quartz-eyes. The pelites are dark grey to black slate (or schist at higher grade). In the Faribault Brook area, several felsic layers occur in the metasedimentary rocks. Sulphide deposits are associated with the felsic layers (Tallman et al., 1988; Jamieson et al., 1990).

Both the Faribault Brook basalt and the Jumping Brook Metamorphic Suite metasedimentary rocks are strongly deformed. Foliation and lineations are well developed, and up to three generations of tight to isoclinal folding have been recognized in the metasedimentary rocks (Plint and Jamieson, 1989; Jamieson et al., 1990). The relationship between the two packages is not well defined. Jamieson et al. (1987) and Barr and Jamieson (1991) interpreted the Jumping Brook Metamorphic Suite metasedimentary rocks to stratigraphically overlie the Faribault Brook basalt. However, this is mainly based on their interpretation of the Rocky Brook conglomerate, with which we disagree (see later).

The Jumping Brook Metamorphic Suite has been interpreted to be of Ordovician-Silurian age (Currie, 1982, 1987b), although a precise age is not known. Currie et al. (1982) suggested that 439 ± 7 Ma (U-Pb zircon age) rhyolite dykes in the Cheticamp Pluton are feeders to the Jumping Brook Metamorphic Suite, but no conclusive evidence was presented. Lin et al. (in press) suggested that the Jumping Brook Metamorphic Suite could be an Ordovician member of the Appalachian Central Mobile Belt in Cape Breton Island, based on observations that the Jumping Brook Metamorphic Suite is lithologically and geochemically distinct from dated Early Silurian units in Cape Breton Island but closely resembles the Middle Ordovician Tetagouche and Fournier groups in northern New Brunswick and the Bay du Nord and Harbour le Cou groups in southwestern Newfoundland. Work on regional correlation of the Jumping Brook Metamorphic Suite, including U-Pb geochronology, is presently under way.

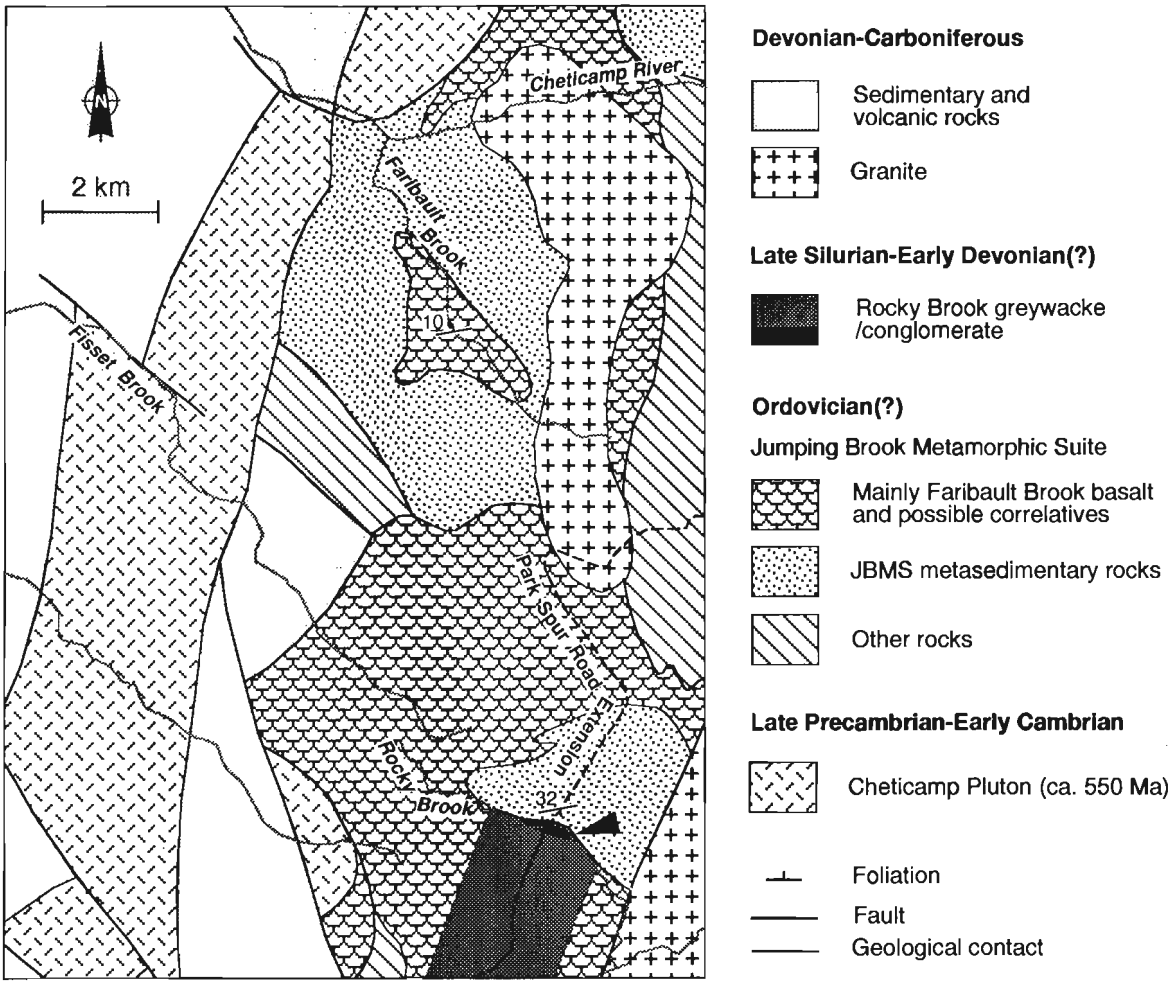

Figure 2. A simplified geological map of the Faribault Brook-Rocky Brook area, western Cape Breton Highlands (simplified and modified from Lynch and Tremblay, 1992a and Jamieson et al., 1987). The Rocky Brook conglomerate (shown as black) is indicated by an arrow at the lower right. Note that both the extent of the Rocky Brook greywacke away from the Park Spur (Road) Extension and the nature of the contact between the Rocky Brook greywacke-conglomerate and the Jumping Brook Metamorphic Suite (depositional or tectonic) are unknown.

ROCKY BROOK GREYWACKE AND CONGLOMERATE

Jamieson et al. (1987) mapped a conglomerate in Rocky Brook near the Park Spur (Road) Extension, here referred to as the Rocky Brook conglomerate (Fig. 2). The conglomerate is exposed between typical Jumping Brook Metamorphic Suite metasedimentary rocks to the north and a sequence of mainly dark-coloured rocks to the south. Jamieson et al. (1987) correlated the dark-coloured rocks with the Faribault Brook basalt (see also Lynch and Tremblay, 1992b). The conglomerate was interpreted as the base of the Jumping Brook Metamorphic Suite metasedimentary package and, because it contains mafic clasts, it was also interpreted to lie, possibly unconformably, over the "basalt". However, during this study, the "basalt" was found to be clastic sedimentary rocks, here termed the Rocky Brook greywacke, and the conglomerate was found to be associated with the greywacke, instead of being unconformable on it.

Figure 3. *Pillow structures in the Faribault Brook basalt of the Jumping Brook Metamorphic Suite, (from Faribault Brook). GSC 1993-245*

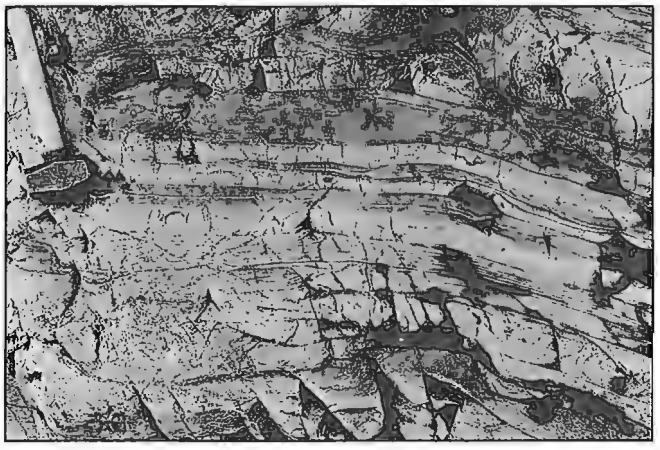

Figure 4. *Turbiditic sandstone and black slate in the metasedimentary rocks of the Jumping Brook Metamorphic Suite (from Faribault Brook).*

The Rocky Brook greywacke is massive and lacks clear bedding. It contains variable, but considerable amounts of quartz (Fig. 5). Its dark colour is due to the dark matrix, which is composed of biotite+tourmaline+clinozoizite+Ca-amphibole+chlorite. Although weak penetrative deformation is present, as indicated by dynamic recrystallization of quartz, the rock lacks an easily recognizable penetrative foliation or lineation, or evidence for multi-generations of folding, in contrast to rocks of the Jumping Brook Metamorphic Suite described above.

The Rocky Brook conglomerate is mainly matrix-supported and poorly sorted. The clasts include granite and volcanic rocks (ranging from mafic to felsic). Many of the granite clasts closely resemble the nearby Cheticamp Pluton (Jamieson et al., 1987). The size of the clasts ranges from several millimetres up to 50 cm. The granite clasts are generally well rounded, whereas the volcanic clasts vary from rounded to angular (Fig. 6). Some clasts contain a pre-depositional tectonic foliation (Fig. 6). The matrix of the conglomerate is similar to the greywacke described above. Deformation in the conglomerate is generally weak, as in the greywacke. These similarities suggest that the conglomerate and the greywacke form part of the same sequence. The contrast between the Rocky Brook sequence and the Jumping Brook Metamorphic Suite metasedimentary rocks in composition, primary structure (massive vs. well-bedded), and deformation history indicates that the former is not an integral part of the Jumping Brook Metamorphic Suite.

The contact between the Rocky Brook conglomerate and the Jumping Brook Metamorphic Suite is not exposed. However, near the contact, a foliation is locally well developed in the matrix of the conglomerate and brittle slickensides are a common feature, suggesting that the present contact is probably faulted.

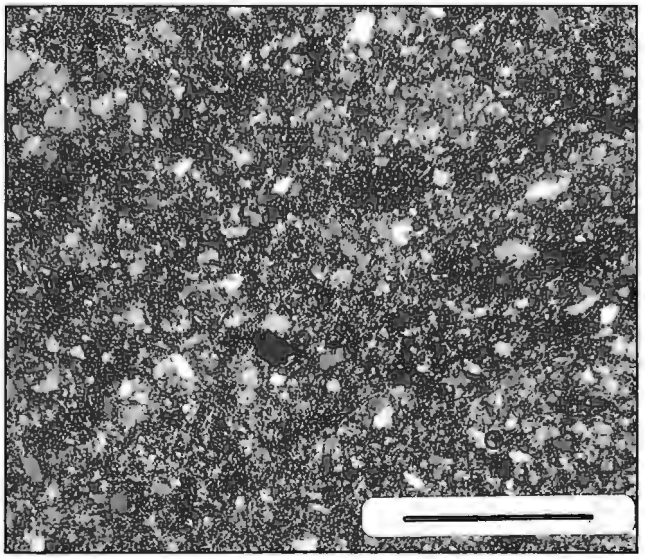

Figure 5. *Photomicrograph of the Rocky Brook greywacke (from Park Spur (Road) Extension). The white-colour clasts are quartz. Scale bar = 0.5 mm.*

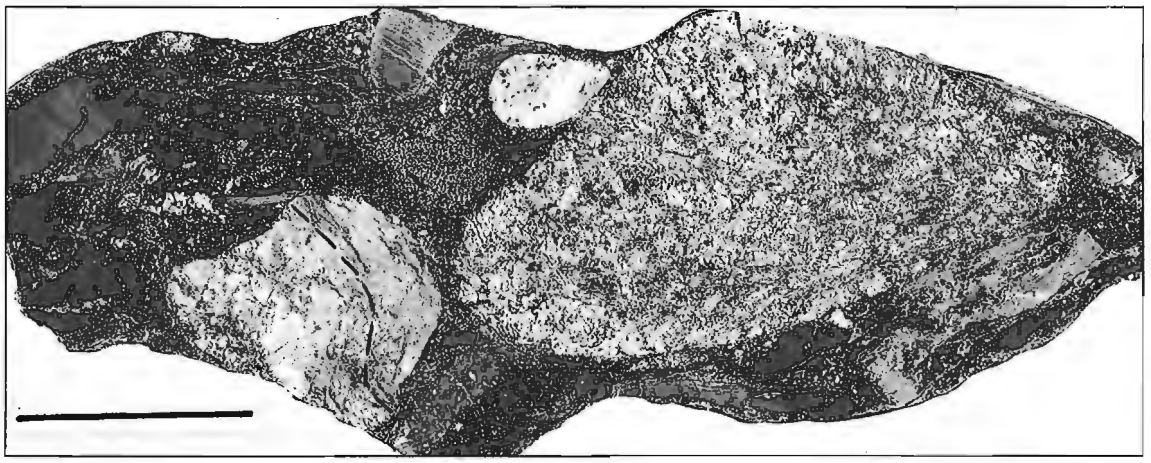

Figure 6. A sample of the Rocky Brook conglomerate (from Rocky Brook). The black dashed line indicates the pre-depositional foliation in a granitic clast. Scale bar = 5 cm. GSC 1993-244B

DISCUSSION

New observations indicate that (1) the rocks exposed along Park Spur (Road) Extension immediately to the south of Rocky Brook are not correlatives of the Fabribault Brook pillow basalt, but are greywackes (the Rocky Brook greywacke); (2) the Rocky Brook conglomerate is not basal to the Jumping Brook Metamorphic Suite metasedimentary rocks, but is associated with, and possibly basal to, the Rocky Brook greywacke; and (3) the Rocky Brook greywacke and conglomerate are not an integral part of the Jumping Brook Metamorphic Suite.

As described above, the previous interpretation that the Jumping Brook Metamorphic Suite metasedimentary rocks lie stratigraphically, possibly unconformably, on the Faribault Brook basalt (Jamieson et al., 1987; Barr and Jamieson, 1991) relies heavily on the interpretation that the conglomerate is basal to the Jumping Brook Metamorphic Suite metasedimentary rocks. If the conglomerate is not an integral part of the Jumping Brook Metamorphic Suite, such an interpretation should be re-evaluated. If the contact between the two parts of the Jumping Brook Metamorphic Suite is depositional, this interpretation could be correct, considering that no mafic dykes related to the Faribault Brook basalt have been reported in the Jumping Brook Metamorphic Suite metasedimentary rocks. The contact as now observed along the Faribault Brook is tectonic (Lynch and Tremblay 1992a). Similarly, because the Rocky Brook conglomerate is not an integral part of the Jumping Brook Metamorphic Suite, the presence of clasts of the Cheticamp Pluton (a possible piece of Bras d'Or terrane rocks exposed in the Aspy terrane; Dunning et al., 1990; Raeside and Barr, 1990) in the conglomerate has no bearing on the relationship between the pluton and the Jumping Brook Metamorphic Suite, nor does it have any direct implications for the relationship between the Aspy and Bras d'Or terranes, unless the conglomerate can be demonstrated to be an integral part of the Aspy terrane. The relationship between the two terranes has been suggested to be depositional based on field and geochronological work in the northeastern Cape Breton Highlands (Lin et al., 1991; Lin, 1993; Chen et al., in press; see also Lynch and Tremblay, 1992b).

Unlike the nearby Late Devonian-Early Carboniferous Fisset Brook Formation (Blanchard et al., 1984) and Carboniferous sedimentary rocks, the Rocky Brook greywacke and conglomerate are well cemented, not associated with red beds, and penetratively, though weakly, deformed and metamorphosed. Therefore, it is probably older than the Late Devonian. It is probably younger than the ca. 550 Ma Cheticamp Pluton, because it contains clasts closely resembling the pluton. Considering that the most likely sources of the mafic and felsic volcanic clasts in the conglomerate are the Faribault Brook basalt of the Jumping Brook Metamorphic Suite and Early Silurian volcanic rocks, and in light of the difference in deformation and metamorphism between the Rocky Brook sequence and the Jumping Brook Metamorphic Suite and Early Silurian rocks, a Late Silurian-Early Devonian age for the Rocky Brook sequence is most likely. However, uncertainty in the nature of its contacts with the Jumping Brook Metamorphic Suite and the Early Silurian units makes this interpretation difficult to prove.

ACKNOWLEDGMENTS

We are grateful to Karen Connors, Ken Currie, and Janet King for comments on the manuscript, and to Fred Chandler, Becky Jamieson, and Chris White for discussions.

REFERENCES

Barr, S.M. and Jamieson, R.A.
1991: Tectonic setting and regional correlation of Ordovician-Silurian rocks of the Aspy terrane, Cape Breton Island, Nova Scotia; Canadian Journal of Earth Sciences, v. 28, p. 1769-1779.

Barr, S.M. and Raeside, R.P.
1989: Tectonostratigraphic divisions in Cape Breton Island, Nova Scotia: implications for the configuration of terranes in the northern Appalachian orogen; Geology, v. 17, p. 822-825.

Blanchard, M.-C., Jamieson, R.A., and More, E.B.
1984: Late Devonian-Early Carboniferous volcanism in western Cape Breton Island, Nova Scotia; Canadian Journal of Earth Sciences, v. 21, p. 762-774.

Chen, Y., Lin, S., and van Staal, C.R.
in press: A reassessment of the relationship between the Aspy, Bras d'Or and Mira terranes in Cape Breton Island, the Canadian Appalachians, based on detrital zircon geochronology; Geological Association of Canada/Mineralogical Association of Canada, Program With Abstracts, v. 19.

Connors, K.A.
1986: Relationship between the sulphide minerals, metamorphism, and deformation in the Faribault Brook area of the Cape Breton Highlands, Nova Scotia; B.Sc thesis, Dalhousie University, Halifax, Nova Scotia.

Currie, K.L.
1982: Paleozoic supracrustal rocks near Cheticamp, Nova Scotia; Maritime Sediments and Atlantic Geology, v. 18, p. 94-103.
1983: Repeated basement reactivation in the northeast Appalachians; Geological Journal, v. 18, p. 223-239.
1987a: Relations between metamorphism and magmatism near Cheticamp, Cape Breton Island, Nova Scotia; Geological Survey of Canada, Paper 85-23.
1987b: Contrasting metamorphic terranes near Cheticamp, Cape Breton Highlands, Nova Scotia; Canadian Journal of Earth Sciences, v. 24, p. 2422-2435

Currie, K.L., Loveridge, W.D., and Sullivan, R.W.
1982: A U-Pb age on zircon from dykes feeding basal rhyolitic flows of the Jumping Brook complex, northwestern Cape Breton Island, Nova Scotia; in Rb-Sr and U-Pb Isotopic Age Studies, Report 5; Geological Survey of Canada, Paper 82-1C, p. 125-128.

Dunning, G.R., Barr, S.M., Raeside, R.P., and Jamieson, R.A.
1990: U-Pb zircon, titanite, and monazite ages in the Bras d'Or and Aspy terranes of Cape Breton Island, Nova Scotia: implications for magmatic and metamorphic history; Geological Society of America Bulletin, v. 102, p. 322-330.

Jamieson, R.A., van Breemen, O., Sullivan, R.W., and Currie, K.L.
1986: The age of igneous and metamorphic events in the western Cape Breton Highlands, Nova Scotia; Canadian Journal of Earth Sciences, v. 23, p. 1891-1901.

Jamieson, R.A., Tallman, P.C., Marcotte, J.A., Plint, H.E., and Connors, K.A.
1987: Geology of the west-central Cape Breton Highlands, Nova Scotia; Geological Survey of Canada, Paper 87-13.

Jamieson, R.A., Tallman, P.C., Plint, H.E., and Connors, K.A.
1990: Regional geological setting of pre-Carboniferous mineral deposits in the western Cape Breton Highlands; in Mineral deposit studies in Nova Scotia. A. Sangster, (ed.); Geological Survey of Canada, Paper 90-8, p. 77-99.

Keppie, J.D.
1990: Comment on "Tectonostratigraphic divisions in Cape Breton Island, Nova Scotia: implications for the configuration of terranes in the northern Appalachian orogen"; Geology, v. 18, p. 669-670.

Lin, S.
1993: Relationship between the Aspy and Bras d'Or "terranes" in the northeastern Cape Breton Highlands, Nova Scotia; Canadian Journal of Earth Sciences, v. 30, p. 1773-1781.

Lin, S., Williams, P.F., and Raeside, R.P.
1991: The discovery of a conglomerate at the base of the Cheticamp Lake Metamorphic Suite and its implication for the geological interpretation of Cape Breton Island, Nova Scotia (abstract); in Program and Summaries, Fifteenth Annual Open House and Review of Activities, Nova Scotia Department of Natural Resources, Report 91-5, p. 50.

Lin, S., van Staal, C.R., Barr, S.M., and Chen, Y.
in press: Candidates for rocks of the Appalachian Central Mobile Belt in the Aspy terrane of Cape Breton Island, Nova Scotia (abstract); Atlantic Geology, v. 30.

Lynch, J.V.G. and Tremblay, C.
1992a: Geology of the Cheticamp River map (11K/10), central Cape Breton Highlands, Nova Scotia; Geological Survey of Canada, Open File 2448.

Lynch, J.V.G. and Tremblay, C.
1992b: Imbricate thrusting, reverse-oblique shear, and ductile extensional shear in the Acadian Orogen, Central Cape Breton Highlands, Nova Scotia; in Current Research, Part D; Geological Survey of Canada, Paper 92-1D, p. 91-100.

Raeside, R.P. and Barr, S.M.
1990: Geology and tectonic development of the Bras d'Or suspect terrane, Cape Breton Island, Nova Scotia; Canadian Journal of Earth Sciences, v. 27, p. 1371-1381.

Tallman, P., Sangster, A.L., and Jamieson, R.A.
1988: Geology and mineralization of the Jumping Brook metamorphic suite, Faribault Brook area, western Cape Breton Island, Nova Scotia; in Current Research, Part B; Geological Survey of Canada, Paper 88-1B, p. 109-117.

Geological Survey of Canada Project 890020

A preliminary report on the stratigraphy and petrography of coarse clastic facies, Horton Group (Upper Devonian-Lower Carboniferous), Lake Ainslie map area, Cape Breton Island, Nova Scotia[1,2]

Frances J. Hein[3]
Atlantic Geoscience Centre

Hein, F.J., 1994: A preliminary report on the stratigraphy and petrography of coarse clastic facies, Horton Group (Upper Devonian-Lower Carboniferous), Lake Ainslie map area, Cape Breton Island, Nova Scotia; in Current Research 1994-E; Geological Survey of Canada, p. 211-218.

Abstract: In west-central Cape Breton Island, clastic rocks of the Horton Group and underlying Fisset Brook Formation are distinguished on lithological criteria. The proposed stratigraphic framework is preliminary and is developed mainly for the eastern and southeastern margin of the subbasin. Here, two unconformity-bounded successions occur. The lower coarse green conglomerate facies flanks pre-Carboniferous basement. The upper red fanglomerate facies unconformably overlies both pre-Carboniferous rocks and the older green conglomerate. Associated with the basal green conglomerate facies, are grey quartz sandstone and grey/white quartz-pebble conglomerate as interfingering tongues or as infill along the basal unconformity. Thus, the traditional three-part subdivision of the Horton Group is valid, but must be modified to accommodate complex facies changes in proximal areas to pre-Carboniferous highlands.

Résumé : Dans le centre ouest de l'île du Cap-Breton, les roches clastiques du Groupe de Horton et celles de la Formation de Fisset Brook sous-jacente se laissent différencier par leurs caractères lithologiques. Le cadre stratigraphique proposé est préliminaire et a principalement été établi pour les marges est et sud-est du sous-bassin. À cet endroit, on observe deux successions limitées par des discordances. Le faciès conglomératique inférieur à grain grossier, de couleur verte, se trouve en bordure du substratum pré-carbonifère. Le faciès supérieur rouge de fanglomérat recouvre en discordance à la fois les roches pré-carbonifères et le conglomérat vert plus ancien. On trouve, associés au faciès du conglomérat basal vert, un grès quartzeux gris et un conglomérat gris/blanc à cailloux quartzeux qui forment des interdigitations ou un colmatage le long de la discordance basale. Ainsi, la division tripartite traditionnelle du Groupe de Horton reste valide, mais doit être modifiée pour tenir compte des variations complexes de faciès dans les secteurs proximaux des hautes terres pré-carbonifères.

[1] Contribution to Canada-Nova Scotia Cooperation Agreement on Mineral Development (1992-1995), a subsidiary agreement under the Canada-Nova Scotia Economic and Regional Development Agreement.
[2] Contribution to the NATMAP Magdalen Basin project.
[3] Department of Geology and Geophysics, University of Calgary, Calgary, Alberta T2N 1N4

INTRODUCTION

This report summarizes the results of the first field season investigating the stratigraphy and sedimentology of coarse clastic facies within the Upper Devonian-Lower Carboniferous Horton Group, Lake Ainslie area, Cape Breton Island, Nova Scotia.

In central and western Cape Breton Island the Horton Group comprises the initial post-Acadian nonmarine deposits that overlie the volcanic Fisset Brook Formation and underlie the marine deposits of the Windsor Group. Previous work has established a three-fold subdivision of finer grained Horton facies (Murray, 1960; Hamblin, 1989; Hamblin and Rust, 1989) that characterize the centre of the Lake Ainslie map area (NTS 11K/3) (Fig. 1, 2, 3). At present, it is not known how this subdivision applies to coarser grained facies within the Horton Group that flank the pre-Carboniferous highlands. Additionally, detailed work must be done to assess how the Fisset Brook volcaniclastic deposits relate to the overlying coarse clastic facies, more typical of the Horton Group.

OBJECTIVES

This project is a subset of the Lake Ainslie Project that commenced in the spring of 1993, with the following aims:

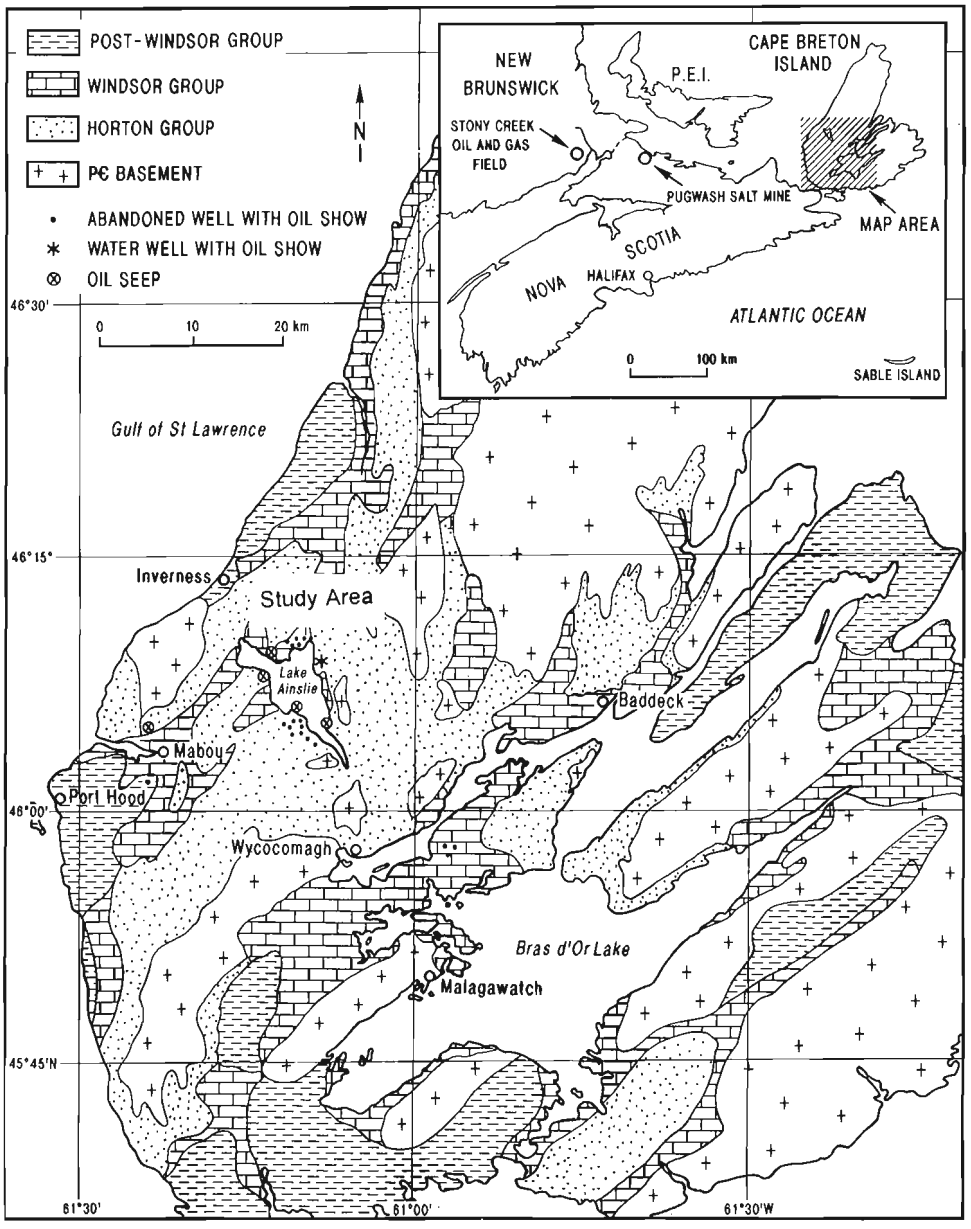

Figure 1. Simplified geological map of western Cape Breton Island, showing the distribution of Devonian and older basement, Horton, Windsor and post-Windsor groups, with oil shows from Horton Group rocks (from Fowler et al., 1993).

- to map the Carboniferous strata exposed in the map area, combining these new data with the 1992 work of G. Lynch and colleagues (Lynch et al., 1993) which emphasized pre-Carboniferous rocks.
- to determine the regional stratigraphy for Upper Devonian and Carboniferous successions in the Lake Ainslie map area, with emphasis on the coarse clastic facies in the marginal areas of the subbasin, and to compare stratigraphic units within the coarse clastic succession with the finer grained facies in the centre of the basin.
- to compile new stratigraphic and structural data in a digital database, and to apply digital technology in map-making.

STRATIGRAPHIC NOMENCLATURE AND PREVIOUS WORK

Bell (1929) originally defined the type Horton Group at Horton Bluff, mainland Nova Scotia. Since that time, several workers have tried to extrapolate the Horton Group stratigraphic nomenclature to equivalent strata in Cape Breton Island (Norman, 1935; Weeks, 1954; Bell, 1958; Kelley, 1958; Neale and Kelley, 1960; Murray, 1960; Kelley, 1967; Hamblin, 1989; Hamblin and Rust, 1989). In the Lake Ainslie map area much of the sedimentary cover has not been mapped since Norman's (1935) work, and on his original map a large proportion of the Lake Ainslie area is designated as undivided Horton Group.

Devonian-Carboniferous rocks in the Lake Ainslie map area unconformably overlie Devonian and older metamorphosed basement (Fig. 1, 2, 3). The initial Devonian-Carboniferous deposits in the Lake Ainslie map area belong to the Fisset Brook Formation. Within the Fisset Brook, a basal polymictic conglomerate is conformably overlain by massive to amygdaloidal basaltic flows, including partially baked red siltstone interbeds, and a thick ash rhyolitic-flow tuff near the top of the formation. Regional variations include red or green, arkosic sandstone and conglomerate, minor volcanilithic or tuffaceous volcaniclastic interbeds. Late Devonian plant fragments are abundant in some locations (Mackasey, 1963; Blanchard et al., 1984); radiometric K-Ar age dates range from 384 to 328 Ma, clustering between 370-375 Ma (Blanchard et al., 1984); and radiometric Rb-Sr dates east of Lake Ainslie and to the north, at the type section near Cheticamp, indicate a Viséan age (Huard, 1984).

Murray (1960) originally subdivided the Horton Group in Cape Breton Island into the following three formations (in ascending order): Craignish, Strathlorne, and Ainslie (Fig. 1, 2, 3). The Craignish consists of a 2000 m-thick (maximum) succession of red and grey conglomerate, sandstone and siltstone that unconformably overlies basement (Hamblin, 1989), and in local areas conformably (or unconformably on a more regional basis) overlies the Upper Devonian Fisset Brook Formation (Fig. 2, 3). The Strathlorne Formation abruptly overlies the Craignish and comprises 300 m (maximum) of grey siltstone/mudstone, with thin sandstone and limestone interbeds. The Ainslie conformably overlies and intertongues with the Strathlorne deposits, and consists of a 700 m-thick (maximum) succession of grey and red sandstone, siltstone and conglomerate.

Cote (1959) reported on geological and subsurface oil exploration in the Lake Ainslie area, and, most recently, Fowler et al. (1993) have re-examined oil showings hosted within the Horton Group rocks of this area. Huard (1984) assessed barite mineralization in the Lake Ainslie area. Detailed work by Hamblin (1989) and Hamblin and Rust (1989) defined regional facies variation within the Craignish-Strathlorne-Ainslie formations in the centre of the Lake Ainslie map area, and developed a tectono-stratigraphic model for the finer Horton facies that incorporated resource potential of the area (Fig. 2, 3). Palynological dating by Utting and Hamblin (1991) suggests that the Craignish sediments are Tournaisian Tn2 in age, and the Strathlorne and Ainslie deposits are late Tn2 to mid-Tn3 in age, using the European age designations for the Tournaisian (Utting et al., 1989; Utting and Hamblin, 1991). Prior to the present study, the coarse clastics flanking

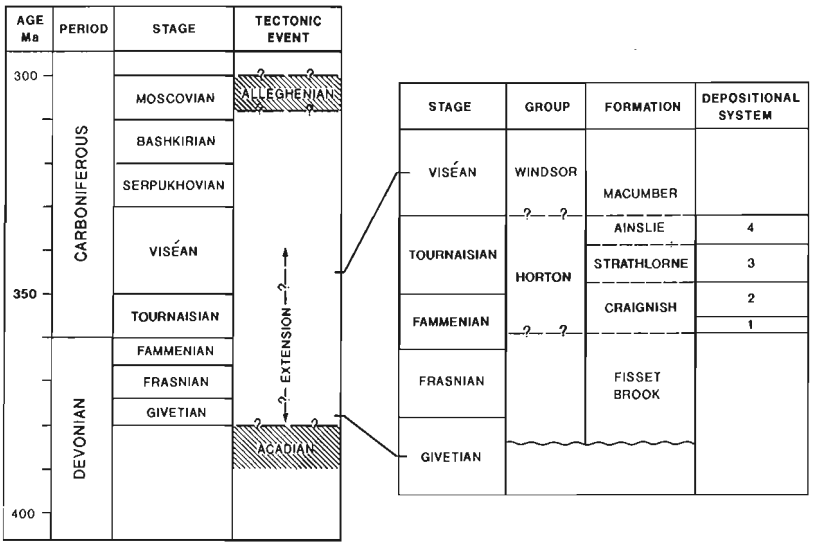

Figure 2.

Stratigraphy of the Horton Group on Cape Breton Island (from Hamblin, 1989 and Hamblin and Rust, 1989).

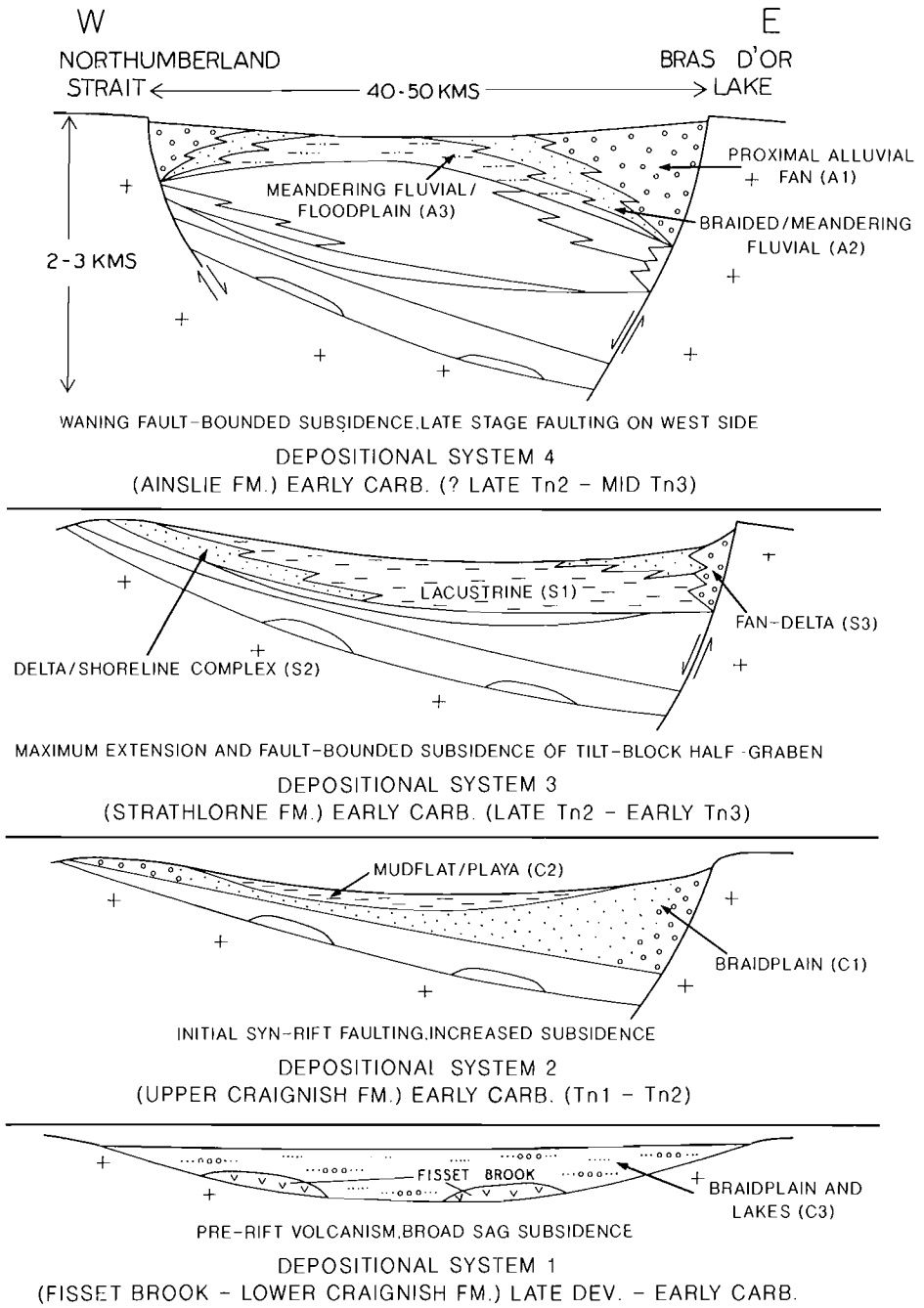

Figure 3. *Stratigraphy and four-phase tectonic evolution of fine grained Horton depositional systems along the axis of the Western Cape Breton Basin in the Lake Ainslie area. Fisset Brook Formation (FB) – extrusive volcanics and alluvial sediments; lower Craignish Formation (C3) – lacustrine in the centre and unoxidized braidplain fluvial deposits along the flanks of the basin; upper Craignish Formation – reddened braidplain fluvial deposits near fault-margins of the subbasin (C1) and mudflat/playa sediments (C2) in the centre of the basin; Strathlorne Formation – prograding delta/shoreline deposits (S2) near margins of basin and open lacustrine sediments (S1) in the centre of the basin; Ainslie Formation – with proximal to distal trends from alluvial fan (A1) to low sinuosity (A2) to high sinuosity (A3) fluvial deposits (from Hamblin, 1989 and Hamblin and Rust, 1989).*

the basement highlands, were mapped as undivided Horton Group (Norman, 1935), and it was not known if there were mappable facies that correlate with the formations and facies belts defined in the centre of the subbasin.

HORTON COARSE CLASTICS: PRELIMINARY STRATIGRAPHIC FRAMEWORK

Mapping of the Lake Ainslie map sheet is not complete, especially in the central and north-central parts of the sheet. Thus, the stratigraphic framework is preliminary (Fig. 4) and is developed mainly for the eastern and southeastern margin of the subbasin. These relationships may not hold elsewhere, and at present the relationships with the basin-centre and northern margins are unclear. Thus, the preliminary stratigraphic framework presented as follows, only strictly applies to the eastern part of the map sheet.

Pre Late Devonian rocks are unconformably overlain by the Upper Devonian-Lower Carboniferous Fisset Brook Formation (DCFB, Fig. 4), that, in turn, is overlain by the Early Carboniferous Horton Group (ECH, Fig. 4). Initial coarse grained deposits of the Horton Group consist of a white, well-rounded, quartz-pebble conglomerate (ECHq, Fig. 4) near the subbasin margin, and an angular polymictic conglomerate with green- and white-altered matrix (ECHgn, Fig. 4). These coarse facies infill lows along the basal unconformity with basement on the southeastern and eastern margins of the subbasin, and occur as an offlap wedge, that becomes finer grained towards the basin centre and interfingers with grey coarse sandstone and quartz pebble conglomerate (ECHgs, Fig. 4) and fine grained clastics more typical of the Craignish Formation (ECHC, Fig. 4). The grey coarse sandstone and quartz pebble conglomerate facies (ECHgs, Fig. 4) is equivalent to Hamblin's (1989) facies association 3, typical of the lower Craignish Formation; and the white, well-rounded, quartz-pebble conglomerate (ECHq, Fig. 4) near the subbasin margin was not seen by Hamblin (1989).

Overlying the Craignish Formation (ECHC, Fig. 4) and the angular polymictic green conglomerate (ECHgn, Fig. 4) are the fine grained deposits of the Strathlorne Formation (ECHS), which towards the basin margins interfinger with a coarse pebble to boulder red fanglomerate (ECHfgl, Fig. 4). Near the subbasin margins in the southeastern and eastern parts of the map sheet, this relationship is an unconformity; elsewhere, towards the centre of the map sheet this relationship has been mapped as conformable (Hamblin, 1989). Preliminary mapping in this area (P. Giles, pers. comm., 1993) shows that there are biohermal limestone within what have been previously mapped as the upper part of the Strathlorne Formation, with age dates (G. Dolby, pers. comm., 1994) equivalent to the younger Wilkie Brook Formation (younger than Horton Group, but older than Windsor Group) of mainland Nova Scotia (Murray, 1960; Keppie et al., 1978; Utting et al., 1989). If this age- and stratigraphic-relationship is correct, then no other sample of Strathlorne Formation has ever come out as young as Wilkie Brook. These relationships are equivocal, at present, and will be confirmed by further mapping and sampling in the study area. The Strathlorne Formation is conformably overlain by the Ainslie Formation (ECHA, Fig. 4). Towards the subbasin margins, flanking the highlands, the fine grained Ainslie fluvial and lacustrine deposits interfinger with coarse pebble to boulder red fanglomerate (ECHfgl, Fig. 4), that has been previously included by Hamblin (1989) as part of the Ainslie Formation. Mapping and section-measuring during the present study, indicate that near the subbasin margins flanking the highlands this red fanglomerate facies is virtually indistinguishable from red fanglomerates associated with the older Strathlorne Formation. The topmost Horton Group sediments are abruptly and unconformably overlain by marine limestones and a locally tectonized breccia and calc-mylonite (along the Ainslie Detachment) of the basal Windsor Macumber Formation (ECWM, Fig. 4).

HORTON COARSE CLASTICS: PRELIMINARY PETROGRAPHIC RESULTS

Petrographic summary

Twenty-nine samples from the Lake Ainslie map area were analyzed, with another six samples from equivalent strata in mainland Nova Scotia for comparison. More detailed petrographic analysis is ongoing, but to date, the following generalizations can be made.

Horton group coarse grained clastics

White quartz-pebble conglomerate

The white quartz-pebble conglomerate (ECHq, Fig. 4) typically consists of vein quartz (rarely chert) pebbles. The matrix between the pebbles is a quartzose sandstone that contains clasts of rounded vein- and polycrystalline quartz. Less commonly, quartz-pebble sandstone has an arkosic and micaceous (biotite) matrix.

Green polymictic conglomerate

The polymictic conglomerate (ECHgn, Fig. 4) with the green- and white-altered matrix is a very poorly sorted lithic subarkose to feldspathic litharenite, less commonly a lithic arenite or feldspathic arenite. Rock fragments are very diverse, including plutonic, volcanic and sedimentary types. Many are altered, less commonly fresh. Feldspars are both angular and fresh, as well as very degraded; degraded biotite rarely occurs. In some samples, the matrix is micaceous (muscovite), but this appears to be very fresh and crystalline, and is interpreted as diagenetic in origin. Three varieties of quartz clasts occur within the matrix of the conglomerate: strained polycrystalline quartz, unstrained polycrystalline quartz, and monocrystalline quartz. The quartz grains are either angular and fresh,

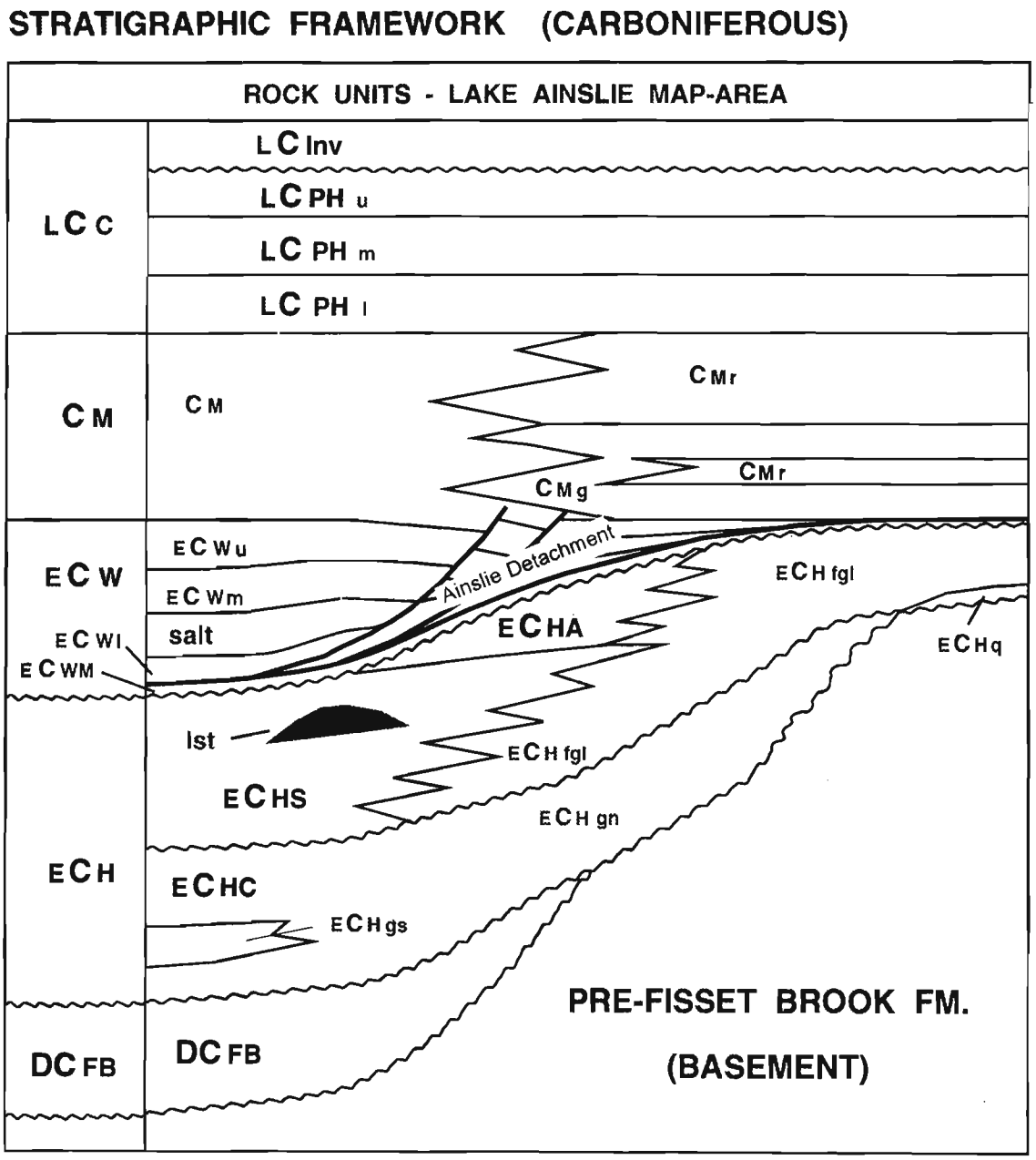

Figure 4. *Preliminary stratigraphic framework for Carboniferous rock units in the eastern and southeastern parts of the Lake Ainslie map area of western Cape Breton Island. Age designations: DC – Devono-Carboniferous; EC – Early Carboniferous; C – Carboniferous; LC – Lower Carboniferous. Group and formation designations: FB – Fisset Brook Formation; H – Horton Group; W – Windsor Group; M – Macumber Formation; Wl – lower Windsor Group; Wm – middle Windsor Group; Wu – upper Windsor Group; M- Mabou Group; Mg – grey Mabou; Mr – red Mabou; C -- Cumberland Group; PHl – lower Port Hood Formation; PHm – middle Port Hood Formation; PHu – upper Port Hood Formation; Inv – Inverness Formation. Unconformities shown by wavy lines; interfingered relationships shown by jagged lines; major fault splays along the Ainslie Detachment (shown by smooth arching lines) climb upsection from the top of the Macumber Formation at the base of the Windsor Group. It is along the Ainslie Detachment where the tectonized carbonate breccia and calc-mylonite occurs within the Macumber Formation.*

or rounded and corroded. Rarely, at the contact with basement, this facies consists of a litharenite breccia, with degraded plagioclase feldspar and igneous and metamorphic rock fragments.

Grey quartz-pebble conglomerate and coarse sandstone

The grey quartz-pebble conglomerate and coarse sandstone (ECHgs, Fig. 4) is a matrix-rich, very poorly sorted, lithic or arkosic quartz wacke. The matrix is commonly very degraded, and possibly tuffaceous. In samples where the matrix is less degraded, the matrix consists of angular biotite and muscovite grains. Coarser clasts within the conglomerate and sandstone are a variety of lithologies, including rock fragments (metamorphic, volcanic, and plutonic), strained monocrystalline quartz, polycrystalline quartz and altered feldspar. The feldspars and rock fragments are commonly very altered, rarely fresh.

Red coarse fanglomerate

The red coarse fanglomerate and pebbly sandstone (ECHfgl, Fig. 4) is a very poorly sorted, clayey, matrix-supported to clast-supported, litharkose and feldspathic litharenite. Coarser clasts include igneous and metamorphic rock fragments, feldspar, quartz and rare sedimentary rock fragments. The quartz is dominantly monocrystalline and very angular. The feldspars are most commonly degraded plagioclase. Both muscovite and biotite are common in the clayey matrix. Rare calcite cement occurs.

Comparison with other Lower Carboniferous coarse clastic units

In the Lake Ainslie map area, the Fisset Brook clastics are volcanic arenites and volcanic litharenites, characterized by a very high percentage of volcanic clasts, with altered igneous and metamorphic rock fragments, altered feldspar, biotite and rare sedimentary rock fragments. Clasts are very angular and, in some cases, appear to have a fragmental texture.

For comparison, six samples were examined from the Devono-Carboniferous, pre-Horton and Horton-equivalent coarse clastics of mainland Nova Scotia. These include: 1) pre-Horton Fountain Lake conglomerate at Whirley Brook in the Cobequid Highlands; 2) pre-Horton Murphy Brook siltstone north of Economy; 3) Horton-equivalent Rapid Brook fine conglomerates in the Cape Chignecto area; 4) Horton-equivalent Nuttby conglomerate in the North River area; and 5) an unnamed Horton-equivalent unit, north of the Pleasant Hills pluton, near West Economy River.

The Fountain Lake conglomerate consists mainly of very well-rounded igneous clasts, with less common altered and fresh, rounded and subrounded feldspar, altered igneous rock fragments, and an altered clayey matrix. The Murphy Brook siltstone is very fine grained with very angular laths of fresh biotite, angular fresh quartz and feldspar, and an altered clay matrix. The Horton-equivalent facies examined in the present study are the unmetamorphosed Nuttby conglomerate, and the strained and metamorphosed Rapid Brook conglomerate and unnamed unit north of the Pleasant Hills pluton. The Rapid Brook fine conglomerate is very altered, with a degraded matrix containing laths (?) of unknown composition, altered and degraded volcanic and plutonic rock fragments, and angular/fresh clasts of feldspar, biotite, polycrystalline and strained monocrystalline quartz. The unnamed Horton unit north of the Pleasant Hills pluton has a very altered, strained matrix, with predominantly metamorphic clasts. By comparison, the Nuttby conglomerate is a lithic arkose, with altered to very altered plutonic and volcanic rock fragments; very angular, fresh and very altered feldspar clasts; angular polycrystalline quartz and micaceous matrix.

These predominantly coarse clastic facies lie unconformably upon basement, within what appear to be small, fault-offset subbasins. How these relate to the Horton-equivalent coarse grained facies that unconformably overlie basement in the Lake Ainslie map area is, at present, unknown. Petrographically there are some similarities between these coarse clastic units and the green polymictic conglomerate (ECHgn, Fig. 4) as well as with the grey quartz-pebble conglomerate/sandstone (ECHgs, Fig. 4) facies mapped in the present study. Ongoing work in both mainland Nova Scotia (by D.J.W. Piper, B. Murphy and R. Rice) and in Cape Breton Island (by F.J. Hein and P. Giles) will hopefully resolve these stratigraphic questions.

HORTON CLASTICS: PRELIMINARY PALYNOLOGICAL RESULTS

These results are preliminary and further work concerning the palynological distinctions between the various rock units in the map area is being done (by G. Dolby). To date, the following generalizations can be made. The grey shales that occur along the Lower Miramichi River are the oldest Horton Group rocks in the area, and can be assigned to the lower Craignish Formation. The rest of the rocks sampled in the study area belong to the Strathlorne and Ainslie formations, with the exception of the biohermal limestones within what has been mapped as the Strathlorne Formation (ECHs, Fig. 4). These limestones may be time-equivalent to the Wilkie Brook Formation (Murray, 1960; revised by Keppie et al., 1978) of mainland Nova Scotia (G. Dolby, pers. comm., 1994).

CONCLUSIONS

1. Rock units assigned to the Horton Group appear to be unconformable on the Fisset Brook Formation, and can be separated from that formation on lithostratigraphic criteria.
2. Within the Horton Group in this map area, two unconformity bounded successions occur. The lower coarse green conglomerate facies (ECHgn) flanks pre-Carboniferous basement in the eastern and southern parts of the map area.

The upper red fanglomerate facies (ECHfgl) unconformably overlies both pre-Carboniferous rocks and the older green conglomerate (ECHgn).

3. Grey quartz sandstone (ECHgs) and grey and white quartz-pebble conglomerate (ECHq) are associated with the basal green conglomerate facies (ECHgn), occurring as interfingering tongues within the centre of the subbasin (ECHgs) or infilling lows along the basal unconformity (ECHq).

4. The traditional three-part subdivision of the Horton Group is valid, but must be modified to accommodate complex facies changes in proximal areas to pre-Carboniferous highlands.

5. Preliminary palynological analyses indicate that limestone bioherms within the Strathlorne Formation (ECHs) occur within the highest zone of the Horton Group, and are probably time-equivalent to the Wilkie Brooke Formation of mainland Nova Scotia.

ACKNOWLEDGMENTS

T. Allen (Dalhousie University) and R. Brown (University of Calgary) provided capable field assistance, and T. Allen is particularly thanked for her help with the computer database. Principal funding and logistical support for the project was provided under Canada-Nova Scotia Cooperation Agreement on Mineral Development (1992-1995), a subsidiary agreement under the Canada-Nova Scotia Economic and Regional Development Agreement. G. Dolby conducted the palynological analyses with funding provided by NATMAP to the Magdalen Basin project. Partial support for field, laboratory and computer costs was provided by an NSERC Operating Grant to Hein. P. Giles and G. Lynch are thanked for their enthusiastic input and support in the field. David J.W. Piper provided additional rock samples for petrographic analysis. A. P. Hamblin, J. Utting and P.S. Giles are thanked for their critical reviews of an earlier version of the manuscript.

REFERENCES

Bell, W.A.
1929: Horton-Windsor district, Nova Scotia; Geological Survey of Canada, Memoir 155, 268 p.
1958: Possibilities for occurrence of petroleum reservoirs in Nova Scotia; Province of Nova Scotia, Department of Mines, Report, 177 p.

Blanchard, M-C., Jamieson, R.A., and Moore, E.B.
1984: Late Devonian-Early Carboniferous volcanism in western Cape Breton Island, Nova Scotia; Canadian Journal of Earth Sciences, v. 21, p. 762-774.

Cote, P.R.
1959: Report of geological exploration in the Ainslie Basin, Cape Breton Island, for the year 1958; Imperial Oil, Toronto, Open File Report, Nova Scotia Department of Natural Resources.

Fowler, M.G., Hamblin, A.P., MacDonald, D.J., and McMahon, P.G.
1993: Geological occurrence and geochemistry of some oil shows in Nova Scotia; Bulletin of Canadian Petroleum Geology, v. 41, p. 422-436.

Hamblin, A. P.
1989: Sedimentology, tectonic control and resource potential of the Upper Devonian-Lower Carboniferous Horton Group, Cape Breton Island, Nova Scotia; Ph.D. thesis, Ottawa-Carleton University, Ottawa, On, 300 p.

Hamblin, A.P. and Rust, B.R.
1989: Tectono-sedimentary analysis of alternate-polarity half-graben basin-fill successions: Late Devonian-Early Carboniferous Horton Group, Cape Breton Island, Nova Scotia; Basin Research, v. 2, p. 239-255.

Huard, A.A.
1984: The Carboniferous volcanic rocks at Lake Ainslie, Nova Scotia; implications for tectonic regime and barite mineralization; B.Sc. Honors thesis, St. Francis Xavier University, Antigonish, Nova Scotia, 72 p.

Kelley, D.G.
1958: Mississippian stratigraphy and petroleum possibilities of central Cape Breton Island, Nova Scotia; Transactions of the Canadian Institute of Mining and Metallurgy, v. 61, p. 175-185.
1967: Baddeck and Whycocomagh map-areas; Geological Survey of Canada, Memoir 351, 65 p.

Keppie, J.D.
1979: Geological map of Nova Scotia; Nova Scotia Department of Mines and Energy, scale 1:5 000 000.

Keppie, J.D., Giles, P.S., and Boehner, R.C.
1978: Some Middle Devonian to Lower Carboniferous rocks of Cape George, Nova Scotia: Nova Scotia Department of Mines and Energy, Paper 78-4, 37 p.

Lynch, J.V.G., Tremblay, C., and Rose, H.
1993: Geological map (1: 50 000) of Lake Ainslie area, Cape Breton Island, Nova Scotia (11K3 and 11K2); Geological Survey of Canada, Open File 2613, map sheet 1/1.

Mackasey, W.O.
1963: Petrography and stratigraphy of a Lower Mississippian, pre-Horton volcanic succession in northwest Cape Breton Island; M.Sc. thesis, Carleton University, Ottawa, On, 121 p.

Murray, B.C.
1960: Stratigraphy of the Horton Group in parts of Nova Scotia; Nova Scotia Research Foundation, Halifax, 160 p.

Neale, E.R.W. and Kelley, D.G.
1960: Stratigraphy and structure of Mississippian rocks of northern Cape Breton Island; Proceedings of the Geological Association of Canada, v. 12, p. 79-96.

Norman, G.W.R.
1935: Lake Ainslie map-area, Nova Scotia; Geological Survey of Canada, Memoir 177; scale 1:63,360 map.

Utting, J. and Hamblin, A.P.
1991: Thermal maturity of the Lower Carboniferous Horton Group, Nova Scotia; International Journal of Coal Geology, v. 19, p. 439-456.

Utting, J., Keppie, J.D., and Giles, P.S.
1989: Palynology and stratigraphy of the Lower Carboniferous Horton Group, Nova Scotia; in Contributions to Canadian Paleontology; Geological Survey of Canada, Bulletin 396, p. 117-143.

Weeks, L. J.
1954: Southeast Cape Breton Island, Nova Scotia; Geological Survey of Canada, Memoir 227, 112 p.

Geological Survey of Canada Project 920062

Ground electromagnetic surveys for environmental investigations at the Heath Steele mines area, New Brunswick

Ajit K. Sinha
Mineral Resources Division

Sinha, A. K., 1994: Ground electromagnetic surveys for environmental investigations at the Heath Steele mines area, New Brunswick; in Current Research 1994-E; Geological Survey of Canada, p. 219-225.

Abstract: As part of the Geological Survey of Canada's on-going research on the application of geophysical, mainly electromagnetic, methods in environmental investigations, a ground electromagnetic survey was conducted at two locations near the Heath Steele mine in New Brunswick. The purpose of the survey was to determine if such surveys are useful for mapping the movement of acid mine drainage from a tailing pond and a stockpile of waste rock containing sulphide ores from an open-pit operation. Since acid mine drainage is normally more conductive than the surrounding material, its movement in the direction of the hydraulic gradient can form a distinctive plume, which may be detected by a systematic mapping of ground conductivity in its neighbourhood. The conductive plume was successfully located at one location, but was not detected at the other location. It is suspected that the contaminated fluids moved through fractures in the bedrock.

Résumé : Dans le cadre des recherches permanentes de la Commission géologique du Canada sur l'application des méthodes géophysiques – surtout électromagnétiques – aux études en environnement, on a effectué un levé électromagnétique au sol à deux sites proches de la mine Heath Steele au Nouveau-Brunswick. Ce levé avait pour but de déterminer si ces méthodes étaient utiles à la représentation du mouvement du drainage minier acide qui sort d'un bassin de décantation des stériles et d'une réserve de roche stérile contenant des minerais sulfurés dans une exploitation à ciel ouvert. Comme le drainage minier acide est normalement plus conducteur que les matériaux qui l'entourent, son mouvement dans le sens du gradient hydraulique peut former un panache distinctif que l'on peut détecter au moyen d'un levé systématique de la conductivité du sol, dans son voisinage. On a réussi à repérer le panache conducteur à un site, mais pas au second. On soupçonne que les fluides contaminés ont emprunté les fractures du substratum rocheux.

INTRODUCTION

The Heath Steele mine complex is located about 50 km northwest of the town of Newcastle in northeastern New Brunswick. The sulphide deposits were the first to be discovered by airborne electromagnetic (EM) techniques in Canada in early 1950s. The mine development began in 1955 and production continued till 1993 from several ore bodies except for brief periods when the mines were closed down due to depressed base metal prices. The location of the mine complex is shown in Figure 1.

Tailings from the mining operations at Heath Steele are contained in two impoundments: the 6.1 ha old pond at the eastern edge of the tailing area and the 200 ha new pond, about 1.5 km south of the mill. The old and new ponds are separated by a retaining dam on a rock ridge and contain 1.3 and 14.6 million tonnes of tailings (Yanful and Aiken, 1990). Hydrogeochemical investigations of sulphide mine tailing impoundments started in late 1960s in response to growing awareness of their potential environmental impacts on human health. In New Brunswick, the principal concern was the potential effect of the tailings on the water quality of rivers, such as the Northwest Miramichi River, used as spawning grounds by Atlantic Salmon. Bell and Nancarrow (1974) and Busse (1974) described the steps taken by the mining industry in New Brunswick to preserve the water quality of rivers, and to treat acid mine drainage from the Heath Steele area. Blowes (1990) has described the results of extensive tests on the tailings pore water chemistry.

The Stratmat deposit is located about 5 km northwest of the tailing ponds as shown in Figure 1, and mining started in 1989. Substantial volumes of waste rock and marginal ores were produced from underground development as well as open-pit mine development. Much of the waste rock was stockpiled near the open-pit mine. Waste rock may cause environmental pollution as a result of biological oxidation of sulphide minerals, which generates sulphuric acid and releases heavy metals. The mine authorities have conducted extensive hydrogeological tests at this site to learn about the movement of the acid mine drainage from the waste pile.

A ground electromagnetic survey was carried out at two sites near the tailing pond and the Stratmat rock pile in 1993 as part of Geological Survey of Canada's on-going research on the application of geophysical, mainly electromagnetic, methods in environmental investigations (Sinha, 1993). The two sites, shown in Figure 1, were chosen in consultation with the chief mine geologist. The presence of the dissolved metallic and sulphate ions in the acid mine drainage greatly increases its electrical conductivity which may move as a conductive plume in the direction of the hydraulic gradient. The purpose of the survey was to detect and, if possible, to delineate the presence of acid mine drainage at the two sites, and to help in the environmental monitoring of the movement of the acid mine drainage plume. This was achieved by measurement of the ground conductivity at various positions of two grids established near the survey areas.

QUATERNARY GEOLOGY AND TOPOGRAPHY OF THE AREA

The stratigraphic sequence in northern New Brunswick seems to record a unique depositional event of one till sheet. Most of northern New Brunswick, including the Heath Steele area,

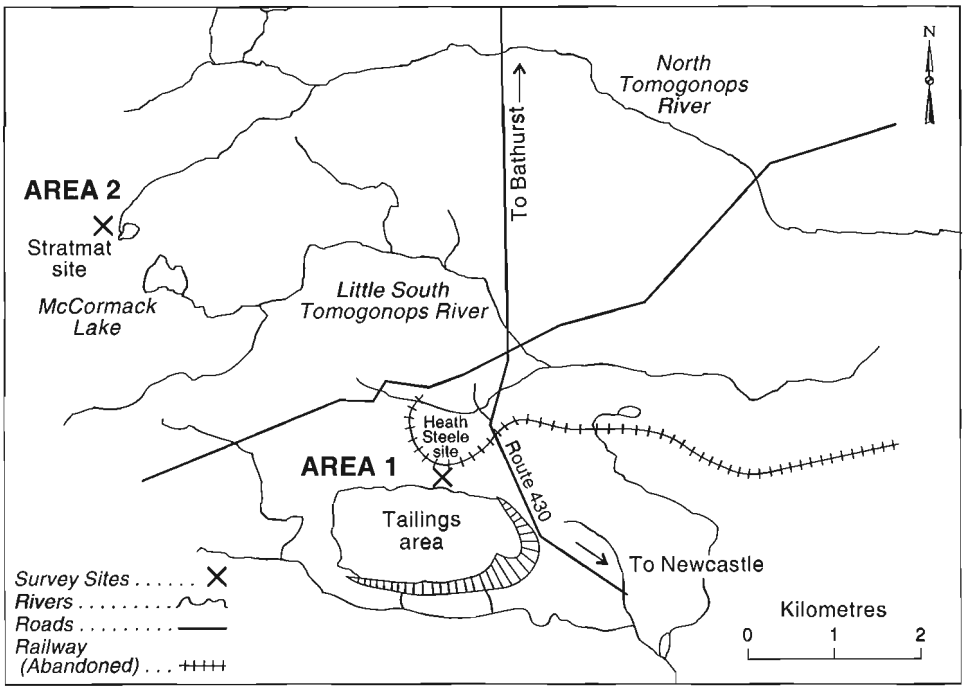

Figure 1. *Location map of the Heath Steele mines area. The two survey locations are shown by X.*

is covered by a till, generally less than 2 m thick, increasing to depths greater than 10 m in valleys. From lithological studies, it was concluded that the till is mostly locally derived from the underlying bedrock consisting of mafic volcanic, felsic volcanic and metasedimentary rocks. Bedrock structural features such as bedding and foliation are oriented in an east-west direction with some local variations. Foliations generally dip between 60 and 80 degrees, but in some areas a subhorizontal foliation is strongly developed. Rampton et al. (1984) and Pronk and Lamothe (1988) have summarized the Quaternary geology of New Brunswick adequately.

The topography is flat to gently undulating at both survey sites. North of the tailing pond, the ground is mostly flat, with the terrain gently sloping towards the north, where the ground becomes waterlogged. An abandoned railway track forms the approximate northern limit of the survey area. The survey area near the Stratmat mine lies between the waste rock pile to the west and McCormack and Mosquito lakes to the east. The topography is flat in the south and the central area of the grid, whereas it is rolling at the northern end. The overburden is shallow in the northern end, where bedrock exposures are common.

ELECTROMAGNETIC SYSTEMS

The two electromagnetic instruments used during the survey operate on the principle of the magnetic induction at low induction values. Under such a condition (when the separation between the transmitter and the receiver is much less than the skin depth in the top layer), the quadrature component of the secondary field is linearly proportional to conductivity or, more accurately, apparent conductivity of the ground. Therefore, in areas of low to moderate ground conductivity, where the requirement of low induction value is satisfied, this type of survey is useful for shallow environmental investigations, since the method is fast, has good lateral resolution, and directly provides values of apparent ground conductivity at several depth ranges at low cost.

Two instruments, a Geonics EM-31 and a Geonics EM-34 were used for the surveys. Geonics EM-31 is a one-operator instrument, which provides apparent ground conductivity values in mS/m at each station directly from the instrument panel. The instrument was used in three modes at waist level, about 0.8 m above the ground: the horizontal coplanar and vertical coplanar modes along the survey line and horizontal coplanar mode normal to the survey line. The maximum depth penetration achievable with this system is about 6 m in the horizontal coplanar mode. The depth penetration in the vertical coplanar mode is approximately half of that in the horizontal coplanar mode. Hence the variation of the conductivity of the ground in the two modes gives an idea of the nature of the variation of ground conductivity with depth. A comparison of the conductivity variations along and normal to the line provides an idea about the conductivity anisotropy in the area.

Geonics EM-34 is a two-operator instrument, which can be used in both horizontal and vertical coplanar modes at three coil separations, 10, 20, and 40 m. Due to the limited survey time available, it was decided to use the instrument in the vertical coplanar mode only. No attempt was made to take any reading using the 40 m coil spacings (for maximum depth penetration with this instrument) since that would have required clean cut lines, something that was not available.

SURVEY STATISTICS

The exact lines to be surveyed at the two areas were decided in consultation with the chief Geologist at the mine. Since the area north of the tailing pond (area 1) was surveyed earlier using an imperial grid, it was decided to use those lines for our survey. Five lines, 400 feet (122 m) apart (60+00 W, 64+00 W, 68+00 W, 72+00 W and 76+00W) were cleared for the survey. The lines were picketed every 50 feet (15.25 m) and the survey lengths of the lines were:

Line 60+00 W : 34+00 S to 41+00 S

Line 64+00 W : 34+00 S to 42+00 S

Line 68+00 W : 35+00 S to 41+90 S

Line 72+00 W : 38+00 S to 42+90 S

Line 76+00 W : 38+00 S to 43+00 S

It should be mentioned here that the northern extent of all the lines were limited by the presence of swamps or pools of water, which limited the total extent of the survey area.

In the Stratmat area (area 2), it was suggested that surveys be conducted on five lines, 100 m apart. Although there was a fair amount of overgrowth on the lines, it was possible to clear them sufficiently for carrying out surveys using both EM-31 and EM-34 instruments with station spacings of 25 m. The line numbers, and the lengths of the survey lines are:

Line 11+175 E : 9+900 N to 10+300 N

Line 11+075 E : 9+900 N to 10+300 N

Line 10+975 E : 9+900 N to 10+300 N

Line 10+875 E : 9+900 N to 10+300 N

Line 10+775 E : 9+900 N to 10+275 N.

Steel pipes and drill hole collars were encountered at several locations in this grid. Survey station locations were moved 5 to 10 m from such features to avoid undue influences by them when they were close to the station locations and a note was made of their presence.

FIELD RESULTS

Area 1: Tailing Pond Grid

As stated earlier, five lines, 400 ft (122 m)apart were surveyed in this area. The orientation of the generally north-south lines was 13 degrees west of north. Lines 72+00 W and 76+00 W were shorter than the rest since the area north of 38+00 S was waterlogged and thus could not be surveyed.

Both instruments, EM-31 and EM-34, were used in this grid. Apparent conductivity values were measured with the EM-31 in three modes: horizontal coplanar and vertical coplanar along the survey line, and horizontal coplanar normal to the survey line. The EM-34 was used in the vertical coplanar mode only with two coil separations of 10 and 20 m to determine the nature of the conductivity variations at greater depths.

Figure 2 shows the contours of apparent conductivity in mS/m from the EM-31 results in the horizontal coplanar mode. The anisotropy effect was found to be negligible in this grid. Hence the conductivity values in the horizontal coplanar mode normal to survey line direction are not shown. A similar response was obtained in the vertical coplanar mode, and is not shown here. The figure shows that the ground is much more conductive at the southern end of the four western lines (64 W to 76 W), where the lines end close to the tailing pond. There is little variation in apparent conductivity in the central area of the grid. On all lines except 60 W, the northernmost points are close to waterlogged areas, which explains the increased conductivities at the northern end of the lines. Although the measured conductivity values in the two modes are close, the conductivities in the horizontal coplanar mode are somewhat higher, implying that the conductivity in the ground is increasing with depth within the depth range of investigation of this instrument.

Figures 3 and 4 show the variations of the apparent conductivity values in mS/m at the grid using the instrument EM-34 in vertical coplanar mode with coil separations of 10 and 20 m, respectively. The most interesting feature in these two diagrams is the fact that the apparent conductivities are much smaller in EM-34 measurements with greater depth penetration than in EM-31 results. It may be noted here that the calibrations of both instruments were checked before the survey by the instrument manufacturer in Toronto. Also, a test survey in Ottawa with both instruments over a homogeneous ground after the Heath Steele survey produced almost identical conductivity readings. Obviously, the shallow overburden, which contributes most to EM-31 response is more conductive than the material at greater depth (presumably the bedrock). In general, the apparent conductivities are slightly higher at 20 m coil spacing in the central area, implying that the material at depth is more conductive, although exceptions to this trend occur elsewhere. As in EM-31 results, the conductivities are higher at the southern end of the lines, which are close to the tailing pond. The conductivities are also higher at the northern ends of the lines, which are close to wet, waterlogged ground. In fact, on lines 72 W and 76 W, the northernmost stations were on wet yellow-orange ground, which could have been caused by seepage of acidic water from the tailing ponds. The central area, however, does not show any significant conductivity anomaly. Station 40+50 S on line 60 W exhibited an unusually high conductivity. However, this station was very close to a power line, and the results might have been affected by that. Line 64 W ran parallel to a pipeline and a hydro line, and it is possible that some results on that line may be somewhat inaccurate.

The ground EM results do not show the presence of any conductive plume in the survey area. It is possible, however, that a plume or conductive zone may have been missed because of the large separation between the lines. The fact that the northern ends of the area are so conductive may lead one to speculate that conductive fluids may have moved northward through cracks and fissures in the bedrock, something that the two instruments were ill-equipped to detect.

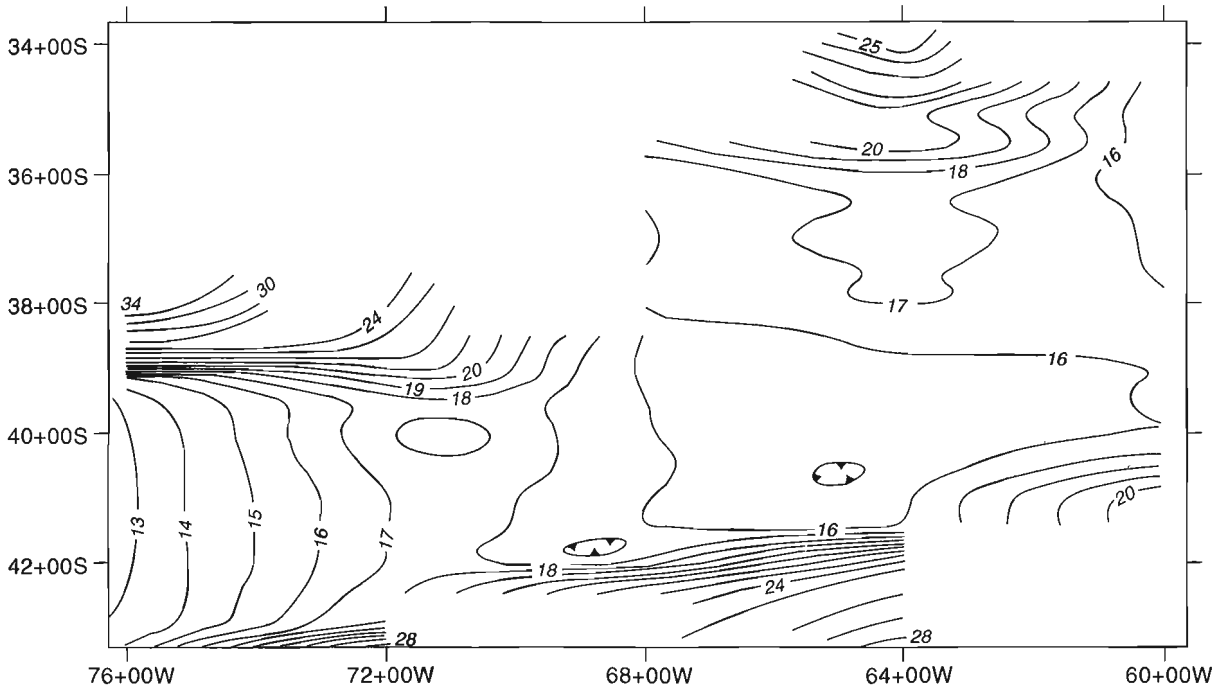

Figure 2. *Contours of apparent conductivity in mS/m in area 1 obtained with Geonics EM-31 instrument; horizontal coplanar coils.*

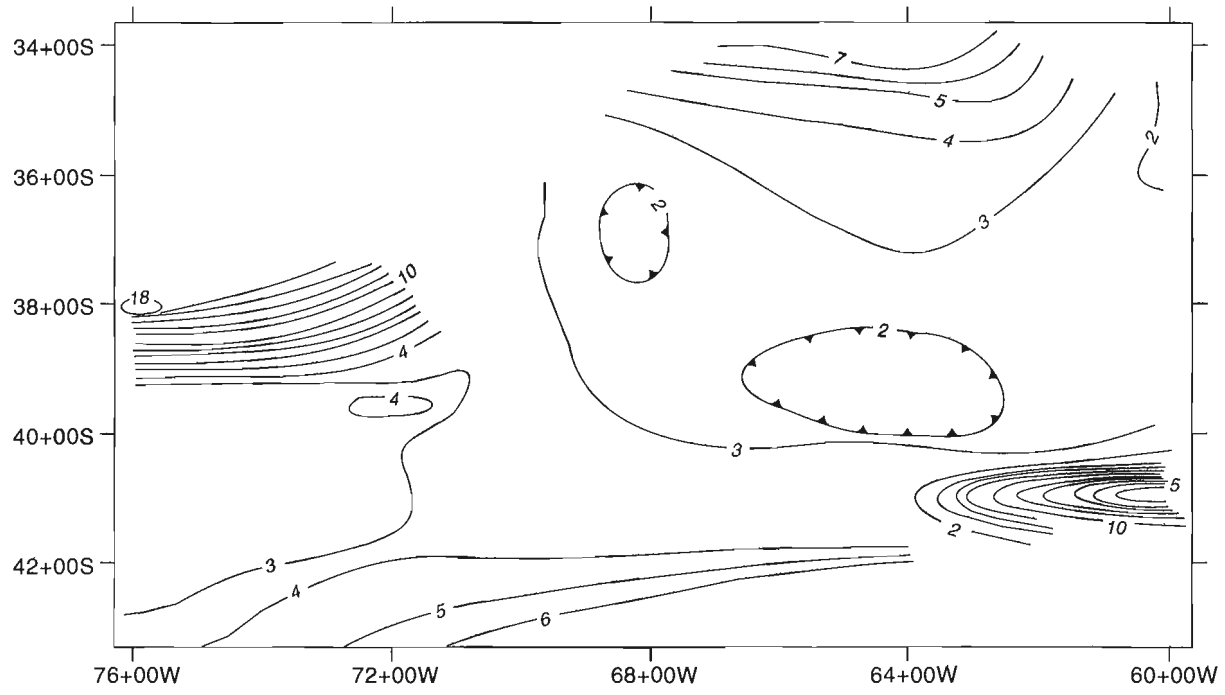

Figure 3. *Contours of apparent conductivity in mS/m in area 1 obtained with Geonics EM-34 instrument; vertical coplanar mode with 10 m coil separation.*

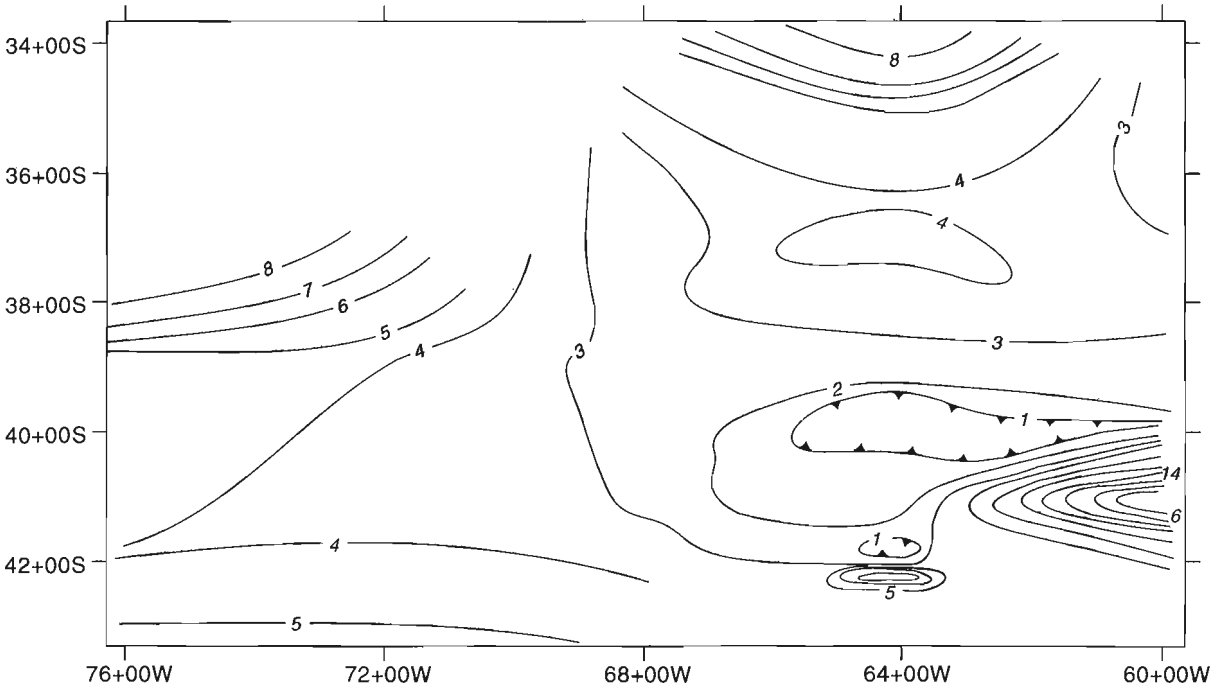

Figure 4. *Contours of apparent conductivity in mS/m in area 1 obtained with Geonics EM-34 instrument; vertical coplanar mode with 20 m coil separation.*

Area 2: Stratmat Waste Pile Grid

As in area 1, the EM-31 was used in three modes, and EM-34 was used in the vertical coplanar mode with two coil separations of 10 and 20 m. Examination of the apparent conductivity variations measured by EM-31 in the horizontal coplanar mode in two orthogonal directions (along and normal to the survey line direction) showed little anisotropy effect. Also, the EM-31 responses in horizontal and vertical coplanar modes were so similar that only the response in the horizontal coplanar mode will be presented here. The orientation of the generally north-south trending lines was 20 degrees west of north.

Figure 5 shows the apparent conductivity variations in mS/m in the horizontal coplanar mode. The northern end of the grid is featureless, while the central area shows a distinct east-west trend, with higher conductivity values in the west (up to 20 mS/m on line 10 875 E) and somewhat lower values of about 16 mS/m in the east. In the southern end of the grid, higher conductivities are encountered at around 9950 N between lines 10 975 E and 11 075 E. The ground was wet and mossy in this area, and a settlement tank was located close to station 9950 N on line 10 975 E, which could have leaked water into the ground. Comparing the responses in the horizontal and vertical coplanar modes, the values in the latter case were slightly higher, implying that the more conductive material is closer to the ground surface.

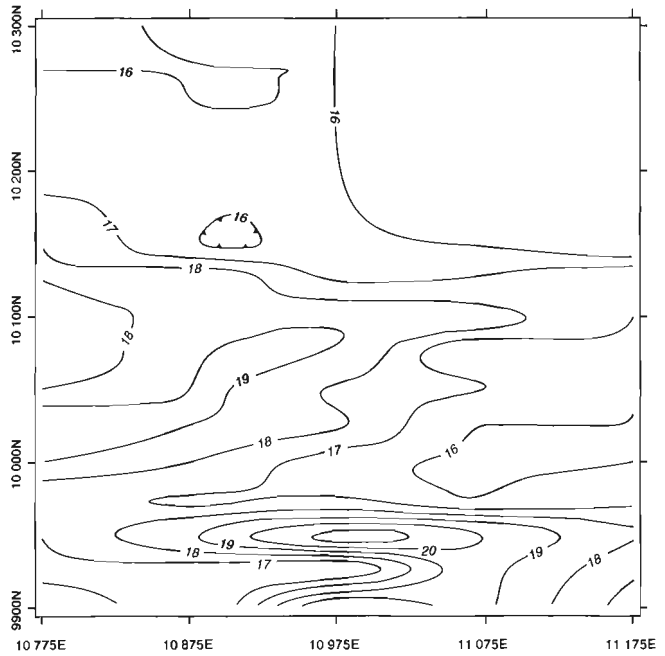

Figure 5. *Contours of apparent conductivity in mS/m in area 2 obtained with Geonics EM-31 instrument; horizontal coplanar coils.*

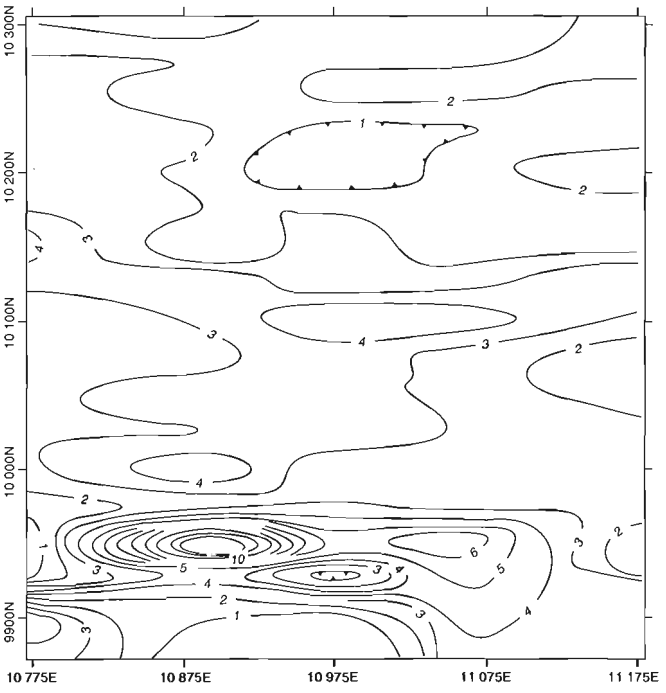

Figure 6. *Contours of apparent conductivity in mS/m in area 2 obtained with Geonics EM-34 instrument; vertical coplanar mode with 10 m coil spacing.*

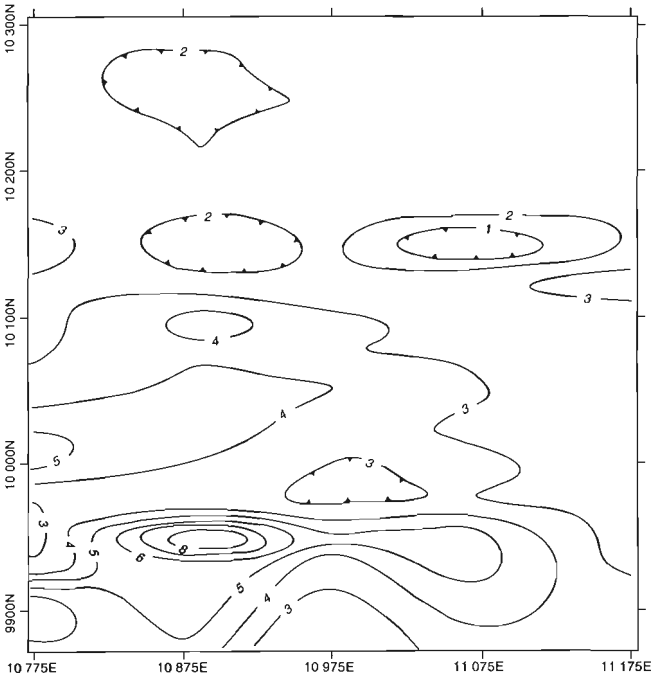

Figure 7. *Contours of apparent conductivity in mS/m in area 2 obtained with Geonics EM-34 instrument; vertical coplanar mode with 20 m coil spacing.*

Figures 6 and 7 illustrate the variation of the apparent conductivity in mS/m measured by EM-34 with coil separations of 10 and 20 m respectively. One should note that the conductivity values measured by EM-34 are again much less than those measured by EM-31. Thus, it is obvious that the deeper layers of the ground are more resistive than the overburden, which influence the conductivity values in EM-31. Figure 6 shows that the northern end is fairly resistive (1-2 mS/m) , whereas the central area is more conductive (up to 4 mS/m), and shows a generally east-west trend. In the southern end, the area around the wet, mossy ground (around 9950 N between 10 875 E and 11 075 E) has much higher conductivity. An interesting feature is the presence of a very high conductivity zone at 9950 N on line 10 875 E (>12 mS/m), where only a moderate conductivity high was detected by EM-31.

Figure 7 looks similar to Figure 6. However, the zone of higher conductivity is further to the west compared to that in Figure 6. If the conductive zone was caused by a plume formed by the leaching of sulphide and other waste materials piled up to the west of the grid by ground water and surface run off, then the survey results indicate maximum movement of the conductive zone in Figure 6. This also suggests that the plume, if present, has not gone very deep, since Figure 7 shows less movement to the east than Figure 6. It may be noted that the zone of high conductivity seen in Figure 6 at 9950 N on line 10 875 E is also present here, but the magnitude of the anomaly is less, which would corroborate the conclusion stated above.

CONCLUSIONS

As part of an on-going research at GSC on the application of ground and airborne EM methods in environmental investigations, a ground EM survey was conducted at two sites near the Heath Steele mines, New Brunswick. The survey, to detect and map the acid mine drainage plumes at the sites produced somewhat ambiguous results. The absence of a plume near the tailing pond (area 1) is intriguing and merits further study with a closer line and station spacings. A possible explanation for the finding may be the presence of very shallow overburden in the area. The conductive material could have moved northward through fractures in the bedrock, as evidenced by the presence of highly conductive yellow soil at the northern end of the grid.

In the second area, near Stratmat, the EM methods successfully detected and mapped a conductive plume east of a waste rock pile containing sulphide ores, but this result has not yet been confirmed by follow-up hydrological or geological investigations. To better define the plume, this area should also be resurveyed with closer line and station spacings.

ACKNOWLEDGMENTS

I wish to acknowledge the help of Chris Neal, a Co-Op student for assisting me in the field operations and plotting of the data. I also thank Luc St-Arnaud of the Noranda Technology Centre, Pointe Claire, Quebec, and A. Hamilton, Chief Geologist, Heath Steele Mines, New Brunswick for providing background information and maps about the two sites.

REFERENCES

Bell, A.V. and Nancarrow, D.R.
1974: Salmon and mining in northeastern New Brunswick; Canadian Institute of Mining and Metallurgy Bulletin, Nov., p. 44-53.

Blowes, D.W.
1990: The geochemistry, hydrogeology and mineralogy of decommissioned sulphide tailings; Ph.D. Thesis, University of Waterloo, Waterloo, Ontario.

Busse, E.
1974: Acid drainage control and water treatment at Heath Steele; Canadian Institute of Mining and Metallurgy Bulletin, v. 67, p. 54-61.

Pronk, A.G. and Lamothe, M.
1988: Quaternary geology, till geochemistry and gold exploration in northern New Brunswick; 8th Int. Symp., Prospecting in areas of glaciated terrain, Institute of Mining and Metallurgy, London, 27p.

Rampton, V.N., Gauthier, R.C., Thibault, J. and Seaman, A.A.
1984: Quaternary geology of New Brunswick; Geological Survey of Canada, Memoir 416, 77p.

Sinha, A.K.
1993: Application of two ground electromagnetic systems in environmental investigations; Proceedings, Symposium on the Application of Geophysics in Engineering and Environmental Problems, San Diego, p.163-166.

Yanful, E.K. and Aiken, S.R.
1990: A hydrogeological evaluation of the Heath Steele old tailings area; Research Report EN2-9306-007:RR 90-1, Noranda Technology Centre, Pointe Claire, Quebec.

Geological Survey of Canada Project 850058

Preliminary interpretation of sub-North Mountain Basalt strata, Dark Harbour, Grand Manan Island, New Brunswick

John A. Wade and Lubomir F. Jansa
Atlantic Geoscience Centre, Dartmouth

Wade, J.A., and Jansa, L.F., 1994: Preliminary interpretation of sub-North Mountain Basalt strata, Dark Harbour, Grand Manan Island, New Brunswick; in Current Research 1994-E; Geological Survey of Canada, p. 227-231.

Abstract: A sequence of argillaceous siltstones on Grand Manan Island, which underlies thick flows of North Mountain Basalt, is preliminarily interpreted as being equivalent to the Triassic/Early Jurassic Blomidon Formation of Nova Scotia. Deposition occurred in a playa environment.

Résumé : Une séquence de siltstones argileux de l'île Grand Manan, qui est sous-jacente aux épaisses coulées du basalte de North Mountain, est provisoirement interprétée comme l'équivalent de la Formation de Blomidon en Nouvelle-Écosse (Trias-Jurassique précoce). La sédimentation a eu lieu dans un milieu de playa.

INTRODUCTION

In his comprehensive description of the Acadian Triassic rocks, Powers (1916) reported, "The Triassic rocks of the island [Grand Manan] consist of basalt flows underlain by purple shale. The shale is exposed to a thickness of only 50 feet, and this exposure is at Dark Harbour, on the western side of the island." No other description of these rocks has been found in the literature. As part of a study of the extent and facies of Triassic-Jurassic rocks in the Fundy Basin (Wade et al., pers. comm.), the Dark Harbour section was visited and sampled in 1993.

Grand Manan Island lies at the mouth of the Bay of Fundy about 10 km southwest of Campobello Island, New Brunswick. It is roughly 25 km long by 10 km wide and consists of two geologic provinces. The western two-thirds of the Island is comprised of slightly westward dipping flows of Early Jurassic North Mountain Basalt down-faulted against highly deformed metasedimentary and volcanic sequences of probable early Paleozoic age (Stringer and Pajari, 1981). The faulted contact between the two provinces is well exposed in low cliffs just west of Red Point on the southeast side of the Island (Fig. 1).

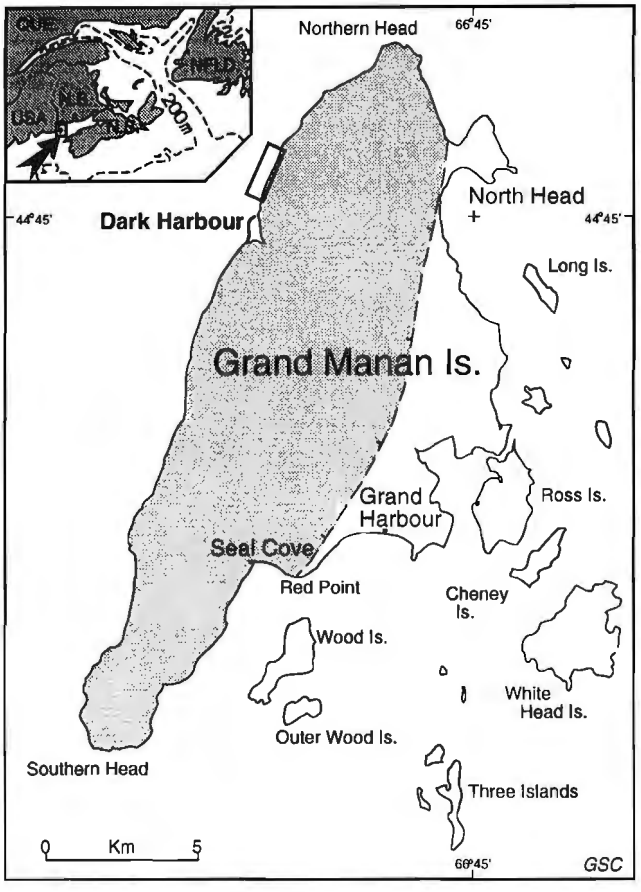

Figure 1. *Generalized geological map – Grand Manan Island. Shaded area is North Mountain Basalt; unshaded area is lower Paleozoic metasediments and metavolcanics. The box, north of Dark Harbour, encloses the study area.*

Dark Harbour is the name given a small lagoon on the northwest coast of Grand Manan, formed by a notch in the basalt cliffs and protected by a bay mouth bar. The narrow, steep, rocky beach to the north of Dark Harbour is bordered by talus slopes of loose basaltic debris and near vertical cliffs of tholeiitic basalt, which reach a height of about 100 m. A few hundred metres north of the inlet to Dark Harbour, and then for a distance of approximately 1000 m, the area normally covered by basalt talus was found to consist of a series of thin and flat-lying dusky red to light grey beds of argillaceous siltstone. The full extent of these beds, northward along the shore, was not investigated; however, aerial video surveys of the coastline (Thibault and Frobel, unpub video, Grand Manan Island) suggest they may extend for more than 1500 m.

STRATIGRAPHY

The contact of the Dark Harbour siltstones with the overlying North Mountain Basalt, although poorly exposed, appears to be essentially conformable (Fig. 2). Where seen, the contact is sharp with a narrow (<1 m) zone of weathered and leached basalt overlying the bedded sequence. Field interpretation of the subbasalt lithology was baked, argillaceous siltstone. Slight variations in lithology, usually due to greater or lesser amounts of clay or cementing material, give the impression of bedding. However, distinct bedding contacts are difficult to see in outcrop. This is in part due to the lithological homogeneity of the strata and in part to the rubbly nature of the outcrop (Fig. 2). In spite of their initial appearance, these rocks are well indurated and resistant, standing in relief to the basalt.

The strata at Dark Harbour are unlike any other found beneath the North Mountain Basalt in the Fundy Basin (Wade et al., pers. comm.). The section was selectively sampled for petrographic study using the base of the basalt as a datum.

DESCRIPTION

The Dark Harbour samples, viewed under binocular microscope, are light dusky red to light grey, fine- to very fine-grained, well sorted argillaceous siltstone to silty mudstone. Many samples have a fine to coarse vuggy porosity caused by leaching. Vugs may be lined with two or three types of crystals, eg. calcite, ?gypsum, ?zeolite. In outcrop, water was seeping from several of these leached beds.

Petrographic study confirms that the sedimentary rocks are argillaceous siltstones, with occasional laminae of argillaceous sandstone and sandy mudstone.

The dominant textural characteristic of all of these rocks is lack of sorting, and frequent wispy, irregular texture. The wispy character is caused by the presence of thin clayey laminae, which have dense tops, commonly with signs of erosion. The base of these clayey laminae have a gradational contact with the underlying siltstone. Another type of texture, which can best be described as "sand-patch", results from the

Figure 2a, b. *Outcrops of argillaceous siltstone, Dark Harbour area. The more massive beds in 2a are due to increased amounts of secondary silica. The white line indicats approximate contact with the North Mountain Basalt. Photos by W.C. MacMillan.*

occurrence of irregular patches of fine-grained sandstone. These patches are ~1 mm in length, have no sharp boundaries, and, in general, are of elongated shape. The sandy patches frequently are cemented by ferroan sparry calcite.

Vugs, which occasionally occur in the argillaceous siltstone beds, are mm to cm size, and pod shaped, with the long axis usually parallel to the bedding plane. Most vugs are empty, but some have walls coated by a mesh of needle-shaped crystals, up to 45 microns in length, most of which probably are chlorite as indicated by light pleochroism and greenish tint. In some of the vugs, the crystals are iron stained. Another type of needle-shaped crystal, which sometimes occurs in association with the chlorite, are clear, nonpleochroic crystals. In some of the vugs, kaolinite occasionally is mixed with the chlorite needles or coats the walls of the vugs. Another mineral phase occasionally found lining the walls of some vugs is ferroan sparry calcite. The calcite forms rhombic crystals, which are commonly zoned. The origin of the vugs is unknown. They most probably represent a leached out pod-shaped mineral phase. Similar pods occur in the Blomidon Formation, where they are formed by anhydrite.

Another textural feature of some of the argillaceous claystones is the occurrence of swirl fabric and ~0.5 mm tubes with clay condensed on the walls of the tubes. Such tubes are bioturbation features and may represent traces of fine roots.

The sand size fraction of the deposits is dominated by poorly-sorted quartz grains, which are subangular to subrounded in shape. Feldspars (4-6%) are dominated by plagioclase>orthoclase>microcline. Trace amounts of myrmekite and granophyric intergrowths of quartz and feldspar are present. Grains of metaquartzite, chert, biotite, and chlorite are rare. Zircon, rutile, and tourmaline occur in trace amounts.

The argillaceous matrix of the siltstone and sandstone is a mixture of clay, fine quartz silt, iron oxide, and, possibly, poorly recrystallized chalcedony. Iron oxide (6%) occurs as blackish micron-sized particles and occasionally as hematite crystals, all dispersed through the matrix. The chalcedony, which fills voids between clay particles, is < 4 microns in size. The presence of void-filling silica is most probably the main cause of the observed hardness of the siltstones. X-ray diffractometer analyses indicate that the clay fraction of the siltstones is formed by a mixed layered chlorite-vermiculite. These minerals are typical constituents of soils formed by the alteration of mica and illite (Bailey, 1980).

In one of the slides of argillaceous, fine-grained sandstone there were several pseudo-olites, formed by finely crystalline kaolinite, with several layers concentrically stained by iron. The pseudo-olites are 0.18 mm in diameter.

The petrographic study suggests that the source of clastics was predominantly a metamorphic terrane, with subordinate input from either granitic rock or acidic dykes. The unsorted character and generally very fine grain size of the clastic strata indicate low relief, flash-flood type of sediment transport (or even only heavy rain), when beds of from ~1 cm to only laminae thickness were deposited. As the flow waned, the clay lamina was deposited and its surface dried in a subaerial environment. During the next depositional event, the surface of the clay lamina was eroded.

Neither microfossils nor plant debris were found in the sediments. The high occurrence of Fe oxide indicates an intensive oxidizing environment; thus, even if plant debris were present, it would be oxidized. That plants may have colonized the surface of the sediments is indicated by occasional root texture and the presence of possible soil horizons. The occurrence of pod-shaped voids, several millimetres to several centimetres in size, can be best explained, by analogy with the Blomidon Formation, as voids resulting from leaching out of anhydrite nodules.

The depositional setting of the rocks is interpreted as continental, arid, with periodic heavy rains, probably playa type.

DISCUSSION

The age of the sub-North Mountain Basalt sedimentary sequence is unknown but it can be considered in three ranges – early Paleozoic, late Paleozoic or early Mesozoic.

The quartzites, slates, and volcaniclastics that are juxtaposed against the basalt on the east side of Grand Manan are considered by most workers to be Cambro-Ordovician and Silurian in age and correlative to the Cookson Formation of southwestern New Brunswick and southeastern Maine (Stringer and Pajari, 1981). These rocks are intensely deformed whereas the Dark Harbour sequence shows only low grade metamorphism. Also the Dark Harbour rocks show evidence of bioturbation and/or root casts, which do not exist in the early Paleozoic and hence an Ordovician or Silurian age can be eliminated.

Upper Devonian and Carboniferous strata are widespread in the Maritimes Basin. In southwestern New Brunswick, the Visean to Westphalian Balls Lake Formation is a deformed, alluvial fan sequence of red conglomerates, arkoses, and shales, approximately 200 m thick, which unconformably overlies Proterozoic-Cambro-Ordovician volcanics and metasediments. In places, it is gradationally overlain by 100-200 m of grey-green fluvial sandstone and shale of the Lancaster Formation (Currie and Nance, 1983). Although located 50-75 km to the southwest, the Grand Manan sequence could be a stratigraphic equivalent of either of these formations.

Upper Triassic-Lower Jurassic Blomidon Formation sediments are widespread beneath the North Mountain Basalt in Nova Scotia. The formation consists of repetitive cycles of red to dark reddish brown, sheet flood/sand flat, playa mud flat and playa lake deposits with some high salinity episodes (Hubert and Hyde, 1982, Jong, 1985; Mertz and Hubert, 1990). The upper contact with the North Mountain Basalt is sharp and apparently conformable. There is a very thin baked contact apparent in some locations but often there is no indication of alteration 30 cm below the basalt.

The degree of diagenesis observed in the Dark Harbour sediments can best be explained as resulting from the percolation of ground waters enriched in dissolved silica. No convincing petrographic evidence was found to indicate that the increased hardness of these rocks was due to thermal alteration.

Based on the relatively conformable structural relationship between the basalt and underlying strata, the homogeneity of the facies, and the indication of evaporitic minerals, we consider these beds to be a distal playa facies of the Late Triassic/Early Jurassic Blomidon Formation.

REFERENCES

Bailey, S.W.
1980: Structures of layer silicates; in Crystal structures of clay minerals and their X-Ray identification, (ed.) G.W. Brindley and G. Brown; Mineralogical Society Monograph no. 5, London, p. 1-124.

Currie, K.L. and Nance, R.D.
1983: A reconsideration of the Carboniferous rocks of Saint John, New Brunswick; in Current Research, Part A; Geological Survey of Canada, Paper 83-1A, p. 29-36.

Hubert, J.F. and Hyde, M.G.
1982: Sheet-flow deposits of graded beds and mudstones on an alluvial sandflat-playa system: Upper Triassic Blomidon redbeds, St. Mary's Bay, Nova Scotia; Sedimentology, v. 29, p. 457-474.

Jong, W.
1985: The subsurface lithostratigraphy of the Triassic Blomidon and Upper Wolfville formations (Fundy Basin) of the central Annapolis Valley, Nova Scotia; thesis, Acadia University, 142 p.

Mertz, K.A. and Hubert, J.F.
1990: Cycles of sand-flat sandstone and playa-mudstone in the Triassic-Jurassic Blomidon redbeds, Fundy rift basin, Nova Scotia: Implications for tectonic and climatic controls; Canadian Journal of Earth Sciences, v. 27, p. 442-451.

Powers, S.
1916: The Acadian Triassic; Journal of Geology, p. 1-26, 105-122, 254-268.

Stringer, P. and Pajari, G.E.
1981: Deformation of pre-Triassic rocks of Grand Manan, New Brunswick; in Current Research, Part C; Geological Survey of Canada, Paper 81-1C, p. 9-15.

Geological Survey of Canada Projects 720104, 710059

Dispersion des métaux lourds dans l'eau et les sédiments d'un ruisseau s'écoulant du parc à résidus de la mine de Montauban (comté de Portneuf, Québec)

M.R. La Flèche[1], A. Bolduc, G. Camiré[2], L. Talbot[3] et J. Bélanger[1]
Centre géoscientifique de Québec, Sainte-Foy

La Flèche, M.R., Bolduc, A., Camiré, G., Talbot, L. et Bélanger, J., 1994 : Dispersion des métaux lourds dans l'eau et les sédiments d'un ruisseau s'écoulant du parc à résidus de la mine de Montauban (comté de Portneuf, Québec); dans Recherches en cours 1994-E; Commission géologique du Canada, p. 233-241.

Résumé : L'eau et les sédiments d'un petit affluent de la Rivière Batiscan, provenant du parc à résidus miniers de Montauban (comté de Portneuf, Québec), contiennent des concentrations variables de plusieurs métaux dont certains peuvent être toxiques. La forte alcalinité de l'eau du ruisseau et la présence de carbonates dans les résidus régularisent en partie le cycle des métaux traces. Cependant, l'analyse géochimique de l'eau et des sédiments du ruisseau montre qu'il y a relargage de Cd et de Zn dans l'eau du ruisseau, phénomène qui s'accentue en s'éloignant du parc vers la rivière Batiscan, alors que le pH de l'eau diminue et que d'importantes concentrations en Cd, en Zn, en Pb et en As sont présentes dans la fraction extractible des sédiments du ruisseau. Le relargage est expliqué par la diminution du pH de l'eau qui semble entraîner la déstabilisation des hydroxydes de fer sur lesquels sont adsorbés les cations métalliques.

Abstract: A small stream drains mine tailings at Montauban (Portneuf County, Québec) toward the Batiscan River. The stream water and sediments contain variable concentrations of metals, some of which are potentially toxic. The high alkalinity of the stream water and the presence of carbonates in the tailings control in part the trace metal cycle. Stream water and sediment geochemistry, however, shows that large concentrations of Cd, Zn, Pb, and As are present in the extractable fraction of the stream sediment and that Cd and Zn are released in the stream water. This process becomes more important downstream, i.e., away from the tailings and toward the river as the pH of water decreases. The lowering of the pH in the stream explains this phenomenon, which seems to destabilize the iron hydroxides on which the metallic cations are adsorbed.

[1] INRS-Géoressources, 2700, rue Einstein, C.P. 7500, Sainte-Foy (Québec) G1V 4C7
[2] Consultante en géosciences, 16, rue Hébert, Québec (Québec) G1R 3T7
[3] Département de géologie, Université Laval, Cité universitaire, Sainte-Foy (Québec) G1K 7P4

INTRODUCTION

À Montauban, dans le comté de Portneuf (Québec; fig.1), des lentilles métamorphisées de sulfures massifs polymétalliques ont été exploitées par intermittence depuis le début du siècle. Du premier gîte découvert en 1910, plus de 2,7 millions de tonnes de minerai (4,5 % Zn; 1,5 % Pb; 0,70 g Au/tonne et 85 g Ag/ tonne) ont été extraites avant les années soixante (Bernier et al., 1987). À la fin des années soixante-dix, un second gisement plus riche en or (4,02 à 5,77 g Au/tonne) a été découvert et a été exploité au cours des années quatre-vingts. Aujourd'hui l'ensemble des résidus issus de cette exploitation repose dans un parc unique, situé au coeur du bassin versant de la rivière Batiscan, l'un des principaux affluents du Saint-Laurent entre Trois-Rivières et Québec. Le site est contaminé par de nombreux polluants inorganiques qui sont partiellement drainés vers la rivière Batiscan. Même si les résidus miniers sont retenus dans un parc fermé par un barrage de béton, les eaux de ruissellement provenant du parc contribuent à la dispersion de plusieurs métaux toxiques dans l'environnement et à une éventuelle contamination de l'écosystème aquatique environnant.

Ce court texte présente les résultats préliminaires d'une étude portant sur la caractérisation géochimique et hydrogéochimique du parc à résidus miniers de Montauban, d'un ruisseau effluent contaminé par celui-ci et de la section de la rivière Batiscan située à l'embouchure de ce ruisseau. Elle présente également les méthodes d'analyse utilisées, en plus de décrire les propriétés physico-chimiques et les mécanismes de transport des métaux toxiques dans l'eau et dans les sédiments du ruisseau. Les résultats préliminaires ont révélé des concentrations non soupçonnées en Cd, Zn et Pb, excédant les normes gouvernementales.

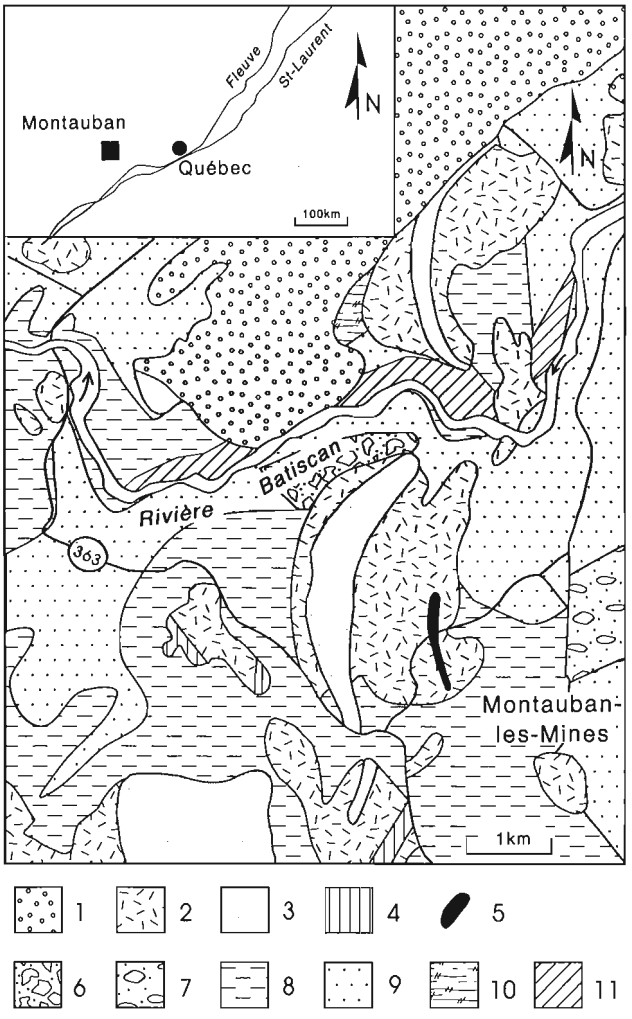

Figure 1. *Carte géologique simplifiée de la région de Montauban (modifiée de MacLean et al., 1982). 1 = diorite quartzifère, 2 = gneiss quartzo-feldspathique, 3 = amphibolite et gneiss mafiques, 4 = quartzite, 5 = zone minéralisée, 6 = till, 7 = sédiments fluvioglaciaires, 8 = sédiments marins d'eau profonde, 9 = sédiments marins sublittoraux, 10 = sédiments glaciolacustres, 11 = Alluvions.*

CONTEXTE GÉOLOGIQUE ET SITUATION GÉOGRAPHIQUE

La géologie de la région de Montauban est caractérisée par la présence de dépôts quaternaires reposant sur un socle grenvillien métamorphisé qui affleure localement (fig. 1). Ces dépôts sont essentiellement constitués de till (épaisseur moyenne < 2 m), de sédiments fluvioglaciaires (localement jusqu'à 30 mètres d'épaisseur), ainsi que de sédiments sublittoraux (épaisseur moyenne < 5 m) et argilo-marins (épaisseur moyenne < 15 m). Le socle rocheux est constitué de paragneiss et d'orthogneiss du Groupe de Montauban, mais aussi d'amphibolites mafiques datées à 1 450 Ma et recoupées par les roches calco-alcalines intrusives du Complexe de la Bostonnais (daté à 1 400 Ma; Nadeau et van Breemen, 1993).

Les zones minéralisées sont comprises à l'intérieur d'une bande d'une centaine de mètres d'épaisseur incluant un gneiss à cordiérite et à anthophyllite, un gneiss à sillimanite et des roches calco-silicatées. Ces dernières sont responsables du caractère basique et alcalin d'une partie des résidus miniers de Montauban et sont constituées d'un assemblage de trémolite, de diopside, d'anorthite, de calcite et de dolomie. De la sphalérite, de la galène, de la pyrrhotine, de la pyrite et des quantités moindres de chalcopyrite, d'arsénopyrite, de molybdénite et de tétraédrite comptent parmi les sulfures du gisement. Tous ces sulfures ont été recristallisés au cours du métamorphisme régional grenvillien (Stamatelopoulou-Seymour et MacLean, 1984).

D'une superficie de plus de 48 640 m^2, le parc à résidus miniers de Montauban est situé dans une dépression naturelle au sommet d'une petite colline. Les eaux de ruissellement du parc à résidus s'écoulent vers la rivière Batiscan située à environ 2 kilomètres au nord, en formant un petit ruisseau à débit très variable. Le ruisseau naît à la base d'un mur de béton d'une hauteur d'environ 3,5 mètres barrant la limite nord du parc à résidus. Il recueille (1) les eaux de ruissellement s'écoulant à la surface du parc à résidus et canalisées vers un puisard qui les acheminent jusqu'au pied du mur de

béton et (2) les eaux d'infiltration percolant à travers la colonne de résidus miniers jusqu'à la nappe phréatique (nommées ci-après «eau souterraine»). Cette eau souterraine se mélange à l'eau du puisard à 200 mètres en aval du barrage, de telle sorte qu'à cet endroit le débit du ruisseau augmente considérablement. La dénivellation verticale entre la tête du ruisseau et la rivière Batiscan est d'environ 65 mètres. En aval du parc à résidus, le ruisseau recoupe sur une distance de 400 mètres une zone constituée d'anciens résidus miniers partiellement recouverts de végétation.

Pétrographie des résidus miniers

Les résidus à la surface du parc (entre 0 et 100 cm de profondeur) sont principalement composés de minéraux micacés (biotite et muscovite), de quartz, de feldspaths, d'amphiboles et de 10 à 15 % de minéraux opaques, principalement de la pyrrhotine, de la pyrite et des oxydes de Fe-Ti. La pyrrhotine est plus corrodée que la pyrite, mais les deux phases sont partiellement remplacées par de la goethite. Une matrice, composée de sulfates (gypse) et représentant 10 à 15 % du volume total des résidus, cimente faiblement les grains de sulfures. L'absence de carbonates et la corrosion prononcée des sulfures contribuent à l'acidification des eaux de ruissellement s'écoulant dans le puisard du parc à résidus. Cependant, il semble qu'une quantité importante de carbonates se concentre dans la partie inférieure du parc à résidus, car l'eau acide de ruissellement est rapidement tamponnée avant d'atteindre la nappe phréatique. Ce processus de neutralisation de l'acidité est reflété indirectement par la très forte alcalinité de l'eau dans la partie amont du ruisseau.

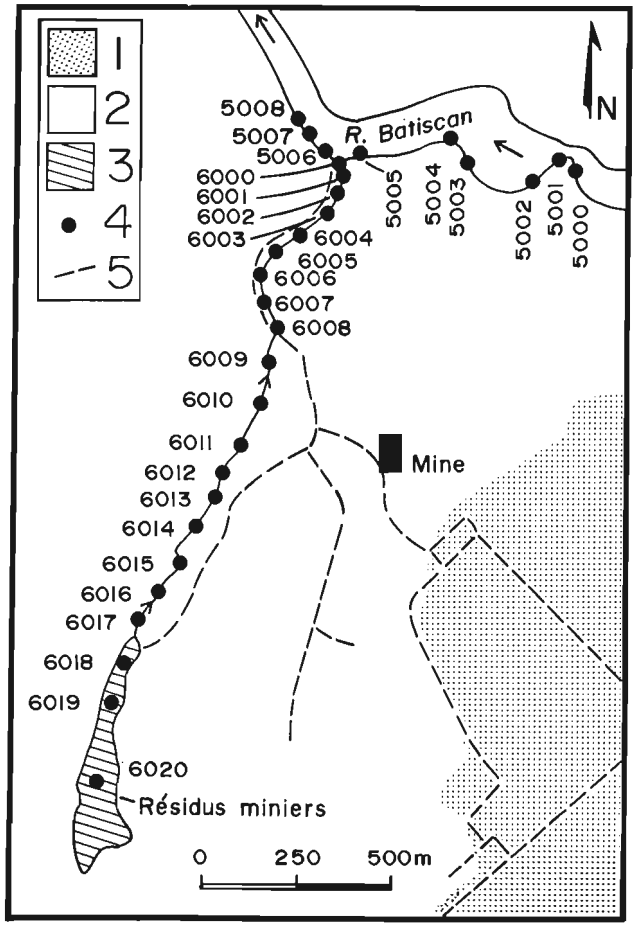

Figure 2. *Localisation des échantillons. 1 = terres agricoles, 2 = zones boisées, 3 = résidus miniers, 4 = site d'échantillonnage, 5 = route.*

MÉTHODOLOGIE

L'eau et les sédiments du ruisseau effluent du parc à résidus de Montauban ont été échantillonnés à intervalles réguliers de 100 mètres jusqu'à la rivière Batiscan (fig. 2). Deux séries d'échantillons ont été prélevées, la première en période d'étiage (juin 1993) et la seconde en période de crue automnale (octobre 1993). Des échantillons provenant du parc à résidus et de la rivière Batiscan (intervalles variant de 50 à 300 m) ont aussi été prélevés. Les sédiments en suspension (le seston) ont été extraits des échantillons d'eau par filtration et analysés. Seuls les résultats préliminaires obtenus à partir des échantillons d'eau recueillis en octobre dans le ruisseau font l'objet de ce texte.

Les échantillons d'eau de 1 litre chacun ont été embouteillés sur place dans des contenants de polyéthylène à haute densité préalablement décontaminés. La décontamination des bouteilles, par immersion dans des bacs remplis d'une solution acide composée à 20 % de HCl et 10 % de HNO_3, a duré deux semaines. De l'eau ultrapure ayant une résistivité inférieure à 18,2 mohm (système Milli-Q + de Millipore) a été utilisée pour l'ensemble des manipulations au laboratoire (incluant le nettoyage et le rinçage des instruments d'analyse).

Les échantillons d'eau ont été rapidement réfrigérés (à 4°C) et préservés à l'obscurité durant le transport du site d'échantillonnage au laboratoire. À l'arrivée, ils ont été filtrés sous une hotte à flux laminaire et à confinement biologique de classe 100 pendant une période n'excédant pas 48 heures. La filtration du seston a été effectuée à l'aide de filtres de 0,45 µm (Millipore), préalablement décontaminés dans une solution titrant à 5 % HCl (Aristar) et conservés par la suite dans un dessiccateur jusqu'à la pesée du seston. Immédiatement après la filtration, le pH de tous les échantillons d'eau a été diminué à une valeur de 2 à l'aide d'une solution de HNO_3 (Aristar) coupée d'eau ultrapure. Les bouteilles d'eau filtrée et ainsi acidifiée ont été conservées en chambre froide (à 4°C) jusqu'à l'analyse.

La plupart des paramètres physico-chimiques (pH, Eh, température, conductivité, etc.) ont été mesurés directement dans le ruisseau et vérifiés par la suite en laboratoire. Les valeurs de pH ainsi obtenues sont précises à ± 0,01, celles de Eh à ± 1 mV et la conductivité à ± 0,1 msv.

Les cations de Si, Al, Fe, Mn, Ca, Na et K présents dans l'eau ont été analysés par technique d'absorption atomique et par spectroscopie d'émission avec plasma induit par haute fréquence (SE/PIHF). Le Cd et le Pb ont été déterminés par technique d'absorption atomique couplée à l'utilisation d'un

four au graphite. Un modificateur de matrice (soit 2,5 % de $NH_4H_2PO_4$) a été utilisé pour l'analyse du Cd et les températures de carbonisation et d'atomisation ont été respectivement maintenues à 500°C et 2 100°C; la température de carbonisation pour la détermination du Pb était de 400°C. Le Zn, très abondant dans l'eau s'écoulant du parc à résidus, a été analysé directement à la flamme. L'arsenic a été déterminé par technique d'absorption atomique couplée à l'utilisation d'un appareil de génération d'hydrure (Varian) avec du $NaBH_4$ comme composé réducteur. Les anions SO_32-, NO_3-, PO_43- et Cl^- de l'eau ont été mesurés par chromatographie ionique (Dionex) et l'alcalinité, par technique électrochimique (précision ± 0,5 ppm de $CaCO_3$; Orion Research Inc.).

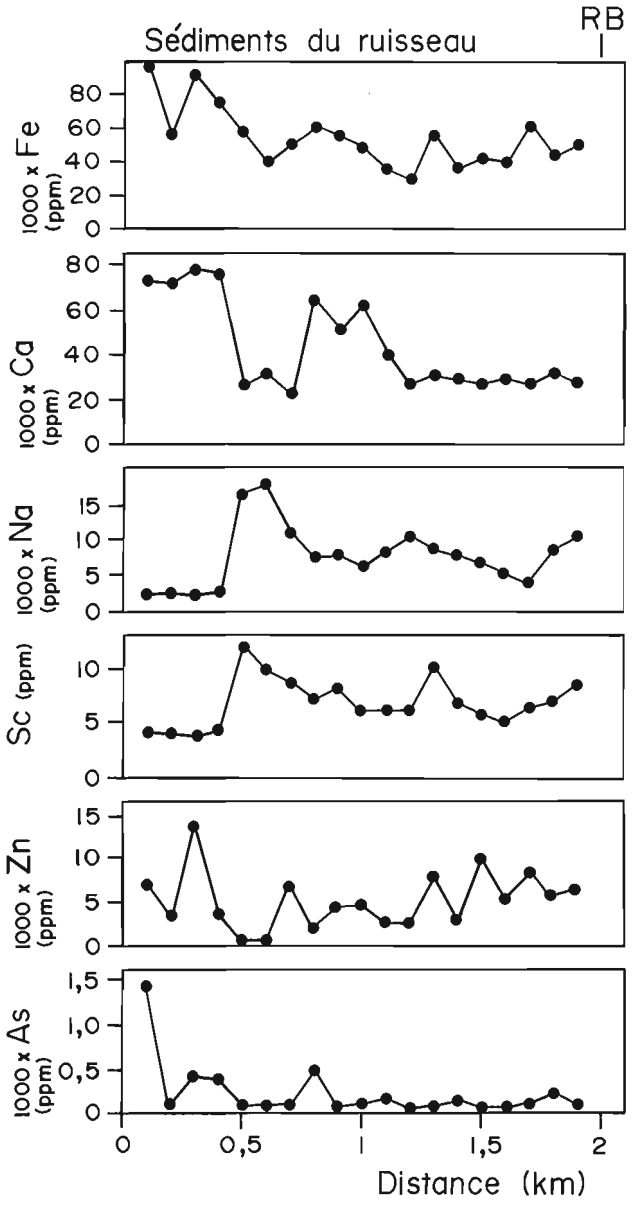

Figure 3. Composition des sédiments du ruisseau effluent du parc à résidus miniers de Montauban en fonction de la distance. La rivière Batiscan (RB) est située à 2 km en aval du mur du barrage limitant le parc à résidus.

Les échantillons de sédiments ont été embouteillés dans des contenants de 250 mL de polyéthylène à haute densité (Nalgene), préalablement décontaminés. Des outils de PVC et d'acrylique ont été utilisés pour le prélèvement des sédiments afin de minimiser les contaminations métalliques. Le seston et les sédiments du lit du ruisseau ont été analysés par activation neutronique instrumentale pour les éléments suivants : Cr, Co, Sc, Zn, Se, As, Sb, Au, Ag, Ca, Na, Fe, Cs, Ba, Rb, Sr, La, Ce, Nd, Sm, Eu, Tb, Yb, Lu, Th, U et Hf. Le seston a été irradié pendant 2 heures et les sédiments des lits du ruisseau et de la rivière Batiscan, pendant 30 minutes. Les fractions non silicatées et extractibles des sédiments de ruisseau (cations échangeables, carbonates, oxydes et hydroxydes de Fe et de Mn, etc.) ont aussi été analysées après attaque partielle à l'acide chlorhydrique (0,4 M HCl) et agitation pendant 6 heures dans de l'eau ultrapure. Les éléments traces et les ultratraces ainsi libérés ont ensuite été analysés par technique d'absorption atomique couplée à l'utilisation d'un four au graphite ou à celle d'un système de génération d'hydrures. Le pH des sédiments a été déterminé en mélangeant et en agitant, pendant 30 minutes, 5 g de sédiments coupés d'une solution de 50 mL de $CaCl_2$ (0,01 M).

GÉOCHIMIE

Sédiments

À la sortie du parc à résidus, le ruisseau s'écoule sur d'anciens résidus miniers sur une distance d'environ 400 m puis sur des silts marins jusqu'à la rivière Batiscan. Les résidus miniers sont caractérisés par de faibles teneurs en Na et en Sc et de fortes teneurs en Fe et en Ca (fig. 3). Les faibles teneurs en Na témoignent de la nature de la roche hôte lessivée en Na par hydrothermalisme au cours de la période de minéralisation (Bernier et al., 1987). Les fortes teneurs en As

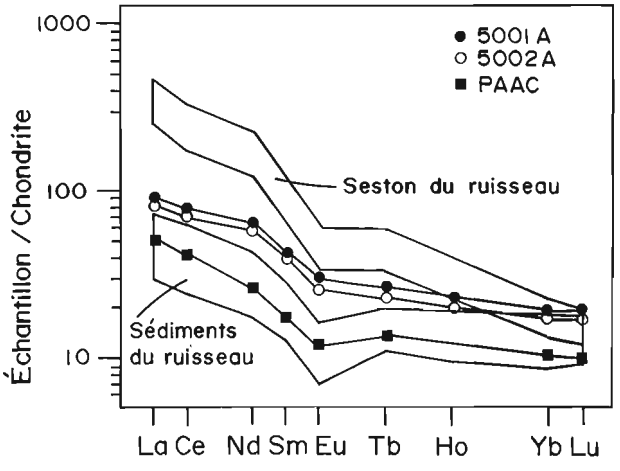

Figure 4. Spectres normalisés aux chondrites des sédiments (champ inférieur) et du seston du ruisseau (champ supérieur). Deux échantillons de sédiment provenant de la rivière Batiscan (échantillons 5001A et 5002A) sont représentés à titre de comparaison. PAAC = Post Archean Average Continental Crust de Taylor et McLennan, 1985.

(599 ± 506 ppm) et en Zn (7 093 ± 4 304 ppm) des sédiments du ruisseau proviennent de la présence de sulfures (ex. arsénopyrite, sphalérite) et ne réflètent pas les valeurs du till régional (As : 5 ± 8 ppm; Zn : 206 ± 50 ppm). Les teneurs dans les sédiments du ruisseau dépassent les normes américaines établis par l'*EPA* (*Environmental Protection Agency*), qui sont respectivement de 8 ppm et de 200 ppm (Baudo et al., 1990).

Les sédiments du ruisseau échantillonnés entre 500 m et 1 000 m du parc à résidus ont une composition chimique intermédiaire entre celle des résidus miniers et celle des silts marins quaternaires (fig. 4). Les sédiments situés à plus de 1 km du barrage sont essentiellement dérivés de silts marins de la Mer de Champlain, c'est-à-dire de particules minérales détritiques (quartz, feldspaths, micas, amphiboles et oxydes), et d'une faible quantité de matière organique (débris provenant du couvert forestier). Ces sédiments ont une signature géochimique semblable à celle de la croûte continentale précambrienne (ex. PACC; fig. 4), ce qui suggère que des gneiss felsiques et des granites anatexiques abondent dans la région source. Sur un diagramme mettant en relation Sc et Na (fig. 5), les sédiments du ruisseau se projettent sur une droite de mélange calculée entre un pôle «résidus miniers» (1; fig. 5) et la composition moyenne de la croûte précambrienne (PAAC; fig. 5). Sur cette figure, les sédiments échantillonnés à proximité du parc à résidus sont plus pauvres en Na. En s'éloignant du parc à résidus, les sédiments du ruisseau s'enrichissent progressivement en Na et en Sc parce qu'ils contiennent une plus grande proportion de silts marins, lesquels sont dérivés de roches felsiques.

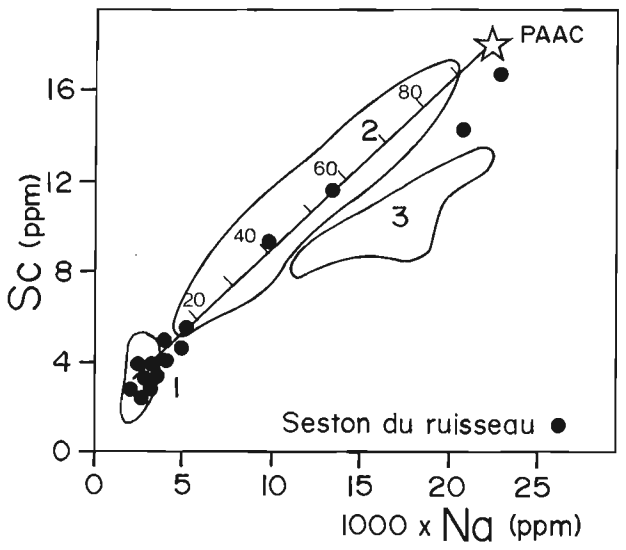

Figure 5. *Diagramme avec en abscisse 1 000 X Na et en ordonnée Sc (ppm), soulignant la composition chimique des résidus miniers (champ 1), des sédiments de ruisseau (champ 2) et des sédiments de la rivière Batiscan (champ 3). PAAC = Post Archean Average Continental Crust de Taylor et McLennan, 1985. La droite calculée entre le pôle «PAAC» et la composition moyenne des résidus miniers correspond à une droite de mélange binaire. La composition du seston recueilli par filtration est reportée sur cette figure. À l'exception de 4 échantillons provenant de la partie aval, la majorité du seston provient de l'érosion directe des résidus miniers.*

Une fois déposés sur le lit du ruisseau avec les autres sédiments, les métaux toxiques tels que le Zn, l'As, le Cd et le Pb ne sont pas nécessairement mis en solution ou relargués dans l'eau du ruisseau dans les mêmes proportions. En réalité chaque élément possède une courbe d'adsorption-désorption (en fonction du pH) qui lui est propre. Dans le milieu aquatique, l'adsorption du Pb sur les hydroxydes de fer est maximale en milieu légèrement acide (75 % d'adsorption à un pH de 6,0), tandis que pour des métaux comme le Cd, ce processus est particulièrement efficace en milieu légèrement alcalin (75 % d'adsorption à un pH de 7,7).

Selon Salomons et Förstner (1984) ainsi que Baudo et al. (1990), sont principalement extractibles les hydroxydes de Fe et de Mn, les carbonates et les cations échangeables. La fraction extractible des sédiments du ruisseau a été obtenue à l'aide d'une attaque partielle à l'acide chlorhydrique (0,4 M HCl); les résultats sont reportés sur la figure 6. Même si la fraction extractible d'As est maximale dans les premiers

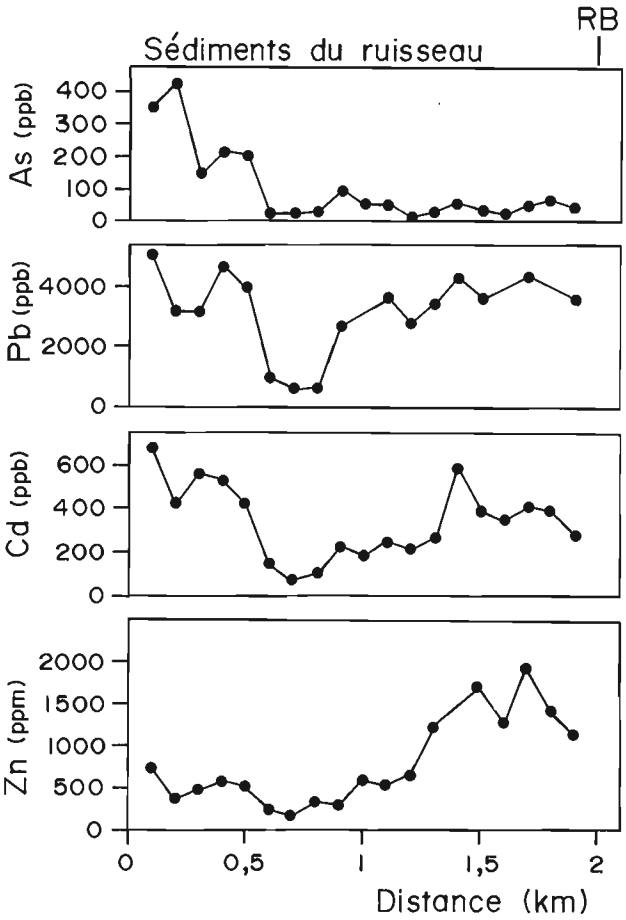

Figure 6. *Composition de la fraction extractible des sédiments du ruisseau en fonction de la distance, laquelle est obtenue après une attaque partielle des sédiments par une solution d'acide chlorhydrique titrant à 0,4 M HCl (RB = rivière Batiscan).*

500 mètres du ruisseau et qu'elle décroît brusquement ensuite, le pourcentage d'As extrait sur la quantité totale d'As présent dans les sédiments du ruisseau augmente en s'éloignant du parc à résidus (0,03 % à 100 m contre 0,15 % à 1 600 m). À l'opposé, la fraction extractible de Zn est maximale dans les derniers 500 mètres et augmente avec le pourcentage de Zn extrait (soit 5 % à 100 m et 25 % à 1 600 m). Le Cd et le Pb extractibles montrent des comportements intermédiaires entre ceux de l'As et du Zn (fig. 6).

Seston

La quantité de seston recueillie par filtration dans les échantillons d'eau varie de 1 à 17 mg/500 mL et augmente de façon générale vers l'aval (fig. 7), en fonction du débit du ruisseau. Les concentrations en métaux traces du seston sont dans la majorité des cas semblables à celles observées dans les sédiments du ruisseau (figs. 3 et 7). Les fortes concentrations en métaux s'expliquent par la présence de particules fines provenant de l'érosion des résidus miniers (une contribution de 85 à 100 %; fig. 5).

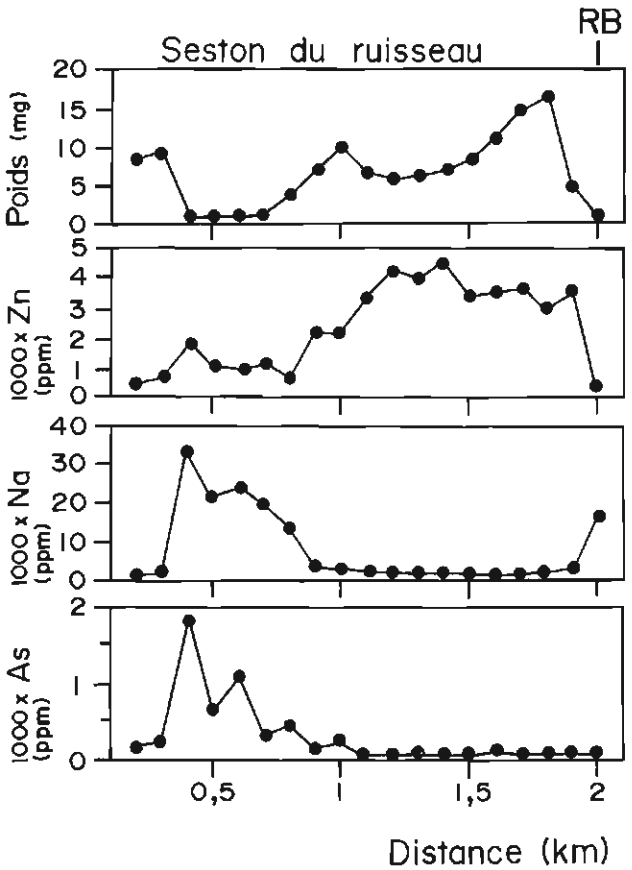

Figure 7. Composition en éléments traces (As, Na, Zn) et poids du seston (recueilli après filtration des échantillons d'eau du ruisseau) en fonction de la distance (RB = rivière Batiscan).

Les teneurs en As et en Sb du seston sont plus élevées en amont qu'en aval (tableau 1), tandis que celles en Zn sont plus élevées en aval, même si la nature et les proportions des particules minérales (c.-à.-d. micas, amphiboles, quartz, etc.) changent peu.

Eau

L'eau du ruisseau est composée des eaux de ruissellement provenant du puisard et des eaux souterraines qui se mêlent aux premières à quelque 200 mètres du barrage. Les deux premiers échantillons d'eau prélevés à 0 et à 100 m du barrage ont donc la composition des eaux de ruissellement avant leur mélange avec l'eau souterraine, laquelle provient essentiellement de la zone saturée du parc à résidus.

Les eaux de ruissellement du parc et l'eau du ruisseau échantillonnée sur ses premiers 200 mètres présentent une insaturation en carbonates et une sursaturation en alunite ($KAl_3(SO_4)_2(OH)_6$ (paramètres calculés à l'aide d'une version modifiée en 1993 du programme PHREEQM de Parkhurst et al., 1980). Là où l'eau souterraine se mélange aux eaux de ruissellement (après 200 m), l'eau du ruisseau est caractérisée par une sursaturation en carbonates (calcite, aragonite et dolomie), en sulfates (ex. barite), en kaolinite et en gibbsite ($Al(OH)_3$), et ce jusqu'à environ 900 mètres du barrage. Entre cette distance et la jonction avec la rivière Batiscan, l'eau du ruisseau redevient sous-saturée en carbonates, mais une forte sursaturation en oxydes et en hydroxydes de fer (goethite, hématite et $Fe(OH)_3$ amorphe) est maintenue. L'eau de la rivière Batiscan est fortement sous-saturée en

Tableau 1. Composition moyenne des sédiments en suspension du ruisseau selon la distance séparant les sites d'échantillonnage du parc à résidus.

Distance	200-400 m	500-1 200 m	1 300-1 900 m	Batiscan
Nombre d'échantillons	3	8	7	6
Fe (ppm)	506 237	260 520	186 368	198 091
Na	12 869	11 767	3 238	17 610
Ba		1 534	596	
Cr	73	81	44	248
Co	507	314	87	665
Ag	43	40	7	
Sc	7	9	3	10
La	62,9	103,9	124,3	133,6
Ce	29,6	158,6	235,2	150,4
Nd	101,6	126,4		
Sm	6,7	16,7	21,7	19,3
Eu	4,74	4,3	3,77	9,55
Tb	1,78	2,53	7,73	
Yb	1,32	3,66	5,17	22,84
Lu	0,58	0,71	2,54	
Hf	4,58	1,07	10,45	
Th	3,6	4,9	2,4	11,6
Cs	10,9	4,4	3,0	36,4
U	7,3	10,9	12,4	
Au	0,5	0,3	0,1	1,2
Sb	118	95	13	141
As	797	340	67	39
Zn	11 560	21 109	37 408	3 079

carbonates et en sulfates, ce qui s'explique par l'absence de formations géologiques calcaires ou évaporitiques dans cette partie de la Province de Grenville.

Les caractéristiques chimiques de l'eau du ruisseau sont reportées sur la figure 8. L'alcalinité, le pH et la conductivité de l'eau du ruisseau contrastent nettement avec les valeurs mesurées dans la rivière Batiscan (pH = 6,38 ± 0,14; alcalinité = 3,2 ± 0,5 ppm de $CaCO_3$; conductivité = 22 ± 3 msv).

DISCUSSION

Processus hydrogéochimiques

La forte alcalinité de l'eau et les teneurs élevées en sulfates (fig. 8) indiquent que les résidus miniers de Montauban, dans leur ensemble, sont riches en carbonates et que les processus d'oxydation des sulfures y sont particulièrement efficaces. L'enrichissement simultané en carbonates et en sulfates s'explique par des réactions de type eau-minéral ayant lieu en profondeur dans la zone non saturée en eau du parc à résidus miniers, telles que :

(pyrite) $FeS_2 + 14Fe^{3+} + 8\ H_2O \rightarrow 15\ Fe^{2+} + 2\ SO_4^{2-} + 16\ H^+$ (1)

$FeS_2 + 7/2\ O_2\ (aq) + H_2O \rightarrow Fe^{2+} + 2\ SO_4^{2-} + 2\ H^+$ (2)

$Fe^{2+} + 1/4\ O_2\ (aq) + H^+ \rightarrow Fe^{3+} + 1/2\ H_2O$ (3)

$Fe^{3+} + 3\ H_2O \rightarrow Fe(OH)_3 + 3\ H^+$ (4)

$CaCO_3 + 2H^+ \rightarrow Ca^{2+} + H_2CO_3$ (5)

$H_2CO_3 \rightarrow H_2O + CO_2$ (6)

Bien qu'elles puissent avoir été catalysées en partie par l'activité de bactéries du type *Thiobacillus*, les réactions 1 et 2 expliquent la transformation des sulfures de fer (pyrite dans les réactions 1 et 2) en sulfates et la réaction 3, l'oxydation du Fe^{2+} en Fe^{3+} (Brown et Jurinak, 1989). La déstabilisation des sulfures de fer est à l'origine de la formation de complexes de surface qui permettent le transfert d'électrons. Les travaux de Luther (1988) ont montré que l'oxydation des sulfures dépend davantage de la quantité disponible de cations de fer trivalents (réaction 1) que de la quantité d'oxygène (réaction 2). La déstabilisation des sulfures de fer augmente avec l'abondance des cations Fe^{3+} dans les eaux souterraines. La réaction 4, soit l'hydratation des cations Fe^{3+}, explique la formation de goethite, omniprésente dans les résidus miniers de surface et dans l'eau du ruisseau. Cette réaction est favorisée en milieu alcalin et susceptible d'être inversée lors d'un changement des conditions physico-chimiques de l'eau (Jambor et Blowes, 1991). Une faible diminution du pH de l'eau peut facilement entraîner l'inversion de cette réaction et le relargage de certains métaux toxiques, facilement adsorbés sur les hydroxydes de fer (ex. Salomons et Förstner, 1984). L'oxydation de la pyrite (réactions 1 à 4) donne lieu à une augmentation importante de l'acidité de l'eau. Pourtant l'eau du ruisseau échantillonnée à plus de 200 mètres du barrage est plutôt alcaline et il semble que l'acide sulfurique produit par ces réactions soit neutralisé en profondeur, dans la zone sous-saturée du parc à résidus, par des réactions telles que les numéros 5 et 6 ci-haut. Ces réactions provoquent la mise en solution des carbonates (calcite et dolomie) et pourraient expliquer les teneurs relativement élevées en Ca et en Mg de l'eau du ruisseau (moyenne pour le secteur amont : Ca = 233 ± 89 ppm et Mg = 71 ± 23 ppm).

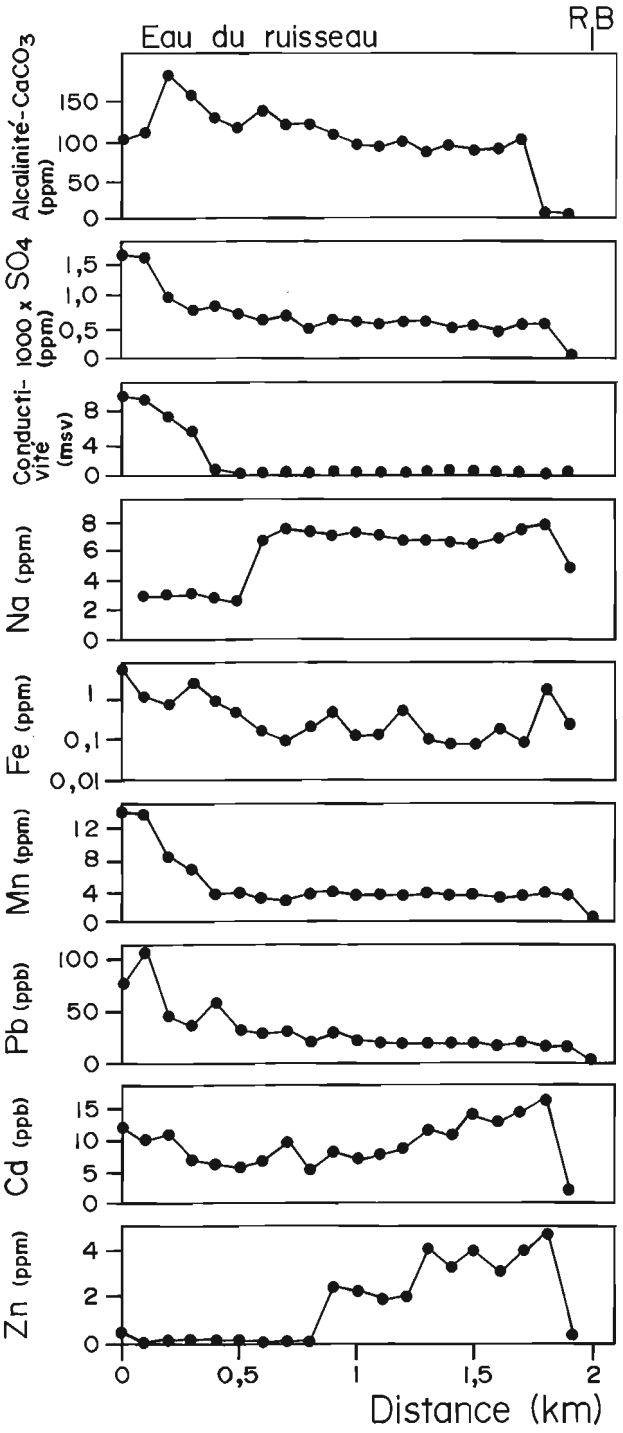

Figure 8. Alcalinité, conductivité et composition en éléments traces de l'eau du ruisseau en fonction de la distance (RB = rivière Batiscan).

Transport et relargage des métaux toxiques dans l'eau

La forte alcalinité de l'eau du ruisseau de Montauban et la présence de carbonates dans les résidus régularisent en partie le cycle des métaux traces et justifient l'absence de système de neutralisation à la chaux à la sortie du parc. Le pH relativement élevé de l'eau du ruisseau devrait en principe maintenir en faibles concentrations les ions métalliques dissous dans l'eau (ex. Leckie et al., 1984; Davis et Kent, 1990). Cependant tel n'est pas le cas et des bassins de floculation et de sédimentation devraient être ajoutés afin d'empêcher le transport des composés ferriques et des cations métalliques associés.

À Montauban, les hydroxydes de fer et les métaux adsorbés sur ces composés sont partiellement transportés vers le ruisseau et ce même si le pH de l'eau est neutralisé par la présence de carbonates dans les résidus miniers. À la sortie des eaux souterraines, à environ 200 mètres du barrage, il y a précipitation d'oxydes et d'hydroxydes de fer et augmentation rapide du Eh. Ce processus pourrait expliquer les fortes teneurs en As, en Cd et en Pb extractibles des sédiments situés dans la partie amont du ruisseau (fig. 6), puisqu'il semble que les polluants métalliques soient adsorbés sur les revêtements d'hydroxydes de fer entourant les particules en suspension dans l'eau. Ce revêtement est chimiquement instable et peut être dissous ou perdre ses capacités d'adsorption des métaux si le pH de l'eau diminue. Ainsi la diminution graduelle du pH de l'eau du ruisseau de l'amont vers l'aval (mis à part les 200 premiers mètres) a pu provoquer, en partie, le relargage de certains métaux traces comme le Zn et le Cd qui sont reconnus pour être facilement désorbés dans des conditions de pH neutre à légèrement basique (pH = 7,5).

D'un autre côté, des mécanismes de précipitation-dissolution pourraient aussi être invoqués pour expliquer le relargage du Cd dans l'eau, puisque l'eau du ruisseau est alcaline. Certains travaux, tels que ceux de Madrid et Diaz-Barrientos (1992), ont montré que le Cd, en plus de pouvoir s'adsorber facilement, peut également former des complexes de surface avec le $CaCO_3$ (ex. $CdCO_3$). Si les carbonates sont ensuite dissous, il s'ensuivra une augmentation des teneurs en Cd dans l'eau. Notons toutefois que Zn et Cd ont un comportement similaire dans l'eau du ruisseau et que la spéciation du Zn, contrairement à celle du Cd, est presque entièrement contrôlée par les processus d'adsorption (Papadopoulos et Rowell, 1988). Pour cette raison, nous croyons que l'adsorption sur les particules en suspension demeure le mécanisme principal de transport du Zn et du Cd dans le ruisseau de Montauban et que des mécanismes de précipitation-dissolution ne peuvent pas expliquer adéquatement l'augmentation simultanée des concentrations en Zn et en Cd dans l'eau du ruisseau (fig. 8).

CONCLUSIONS

Contrairement à plusieurs parcs à résidus de l'Abitibi, celui de Montauban est situé dans une zone peuplée à vocation agricole et récréo-touristique. C'est un parc semi-abandonné (ou semi-orphelin) dont les eaux de ruissellement se déchargent dans un petit ruisseau qui se jette dans la rivière Batiscan, où l'on pratique la pêche sportive et nombre d'activités récréatives. On serait porté à croire que le caractère alcalin de l'eau de sa décharge ne représente pas une grande menace pour l'environnement aquatique. Cependant, les résultats préliminaires présentés dans le cadre de cette étude montrent qu'il y a relargage du Cd et du Zn dans l'eau du ruisseau, que ce phénomène s'accentue en s'éloignant du parc vers la rivière Batiscan et que d'importantes concentrations en Cd, en Zn, en Pb et en As sont présentes dans la fraction extractible des sédiments du ruisseau. L'étendue et la répartition de ces métaux toxiques demeurent inconnues présentement. Notons toutefois que des travaux récents ont révélé la présence de concentrations anormales en Cd dans l'estuaire de la rivière Batiscan (Roy et al., 1993). La source de cette contamination inexpliquée en Cd des eaux de l'estuaire pourrait être le site minier de Montauban, même s'il est situé à plus de 60 kilomètres en amont.

Les travaux qui suivront au cours de l'année 1994 porteront sur les effets des crues printanières de même que sur le calcul de la charge totale particulaire et de la charge dissoute transportées vers la Batiscan. De plus, des carottes de résidus devront être prélevées afin d'en établir la composition et la minéralogie en profondeur. L'installation de piézomètres dans le parc permettrait d'étudier la composition des eaux souterraines et de suivre le comportement de la nappe phréatique en fonction des saisons. Un échantillonnage des poissons juvéniles de la rivière Batiscan ainsi que des sédiments et des macrophytes de ses rives permettrait d'évaluer les effets et la répartition de la contamination.

REMERCIEMENTS

Les commentaires de Diane Germain (INRS-Géoressources) en matière de modélisation hydrogéochimique et le support de Réal Gosselin pour l'activation neutronique ont été grandement appréciés. Ce projet conjoint INRS-Géoressources–Centre géoscientifique de Québec a bénéficié d'une subvention du CRSNG (OGP 0138413) accordé à «M.R.L Projet 920005 de la Commission géologique du Canada».

RÉFÉRENCES

Baudo, R., Giesy, J. et Muntau, H.
1990: Sediments: Chemistry and toxicity of in-place pollutants; Lewis Publishers Inc., Michigan, 405 p.

Bernier, L., Pouliot, G. et MacLean, W.H.
1987: Geology and metamorphism of the Montauban North Gold Zone: a metamorphosed polymetallic exhalative deposit, Grenville Province, Québec; Economic Geology, v. 82, p. 2076-2090.

Brown, A.D. et Jurinak, J.J.
1989: Mechanism of pyrite oxidation in aqueous mixtures; Journal of Environmental Quality, v. 18, p. 545-550.

Davis , J.A. et Kent, D.B.
1990: Surface complexation modeling in aqueous geochemistry; in Mineral-water Interface Geochemistry, Reviews in Mineralogy, Mineralogical Society of America, v. 23, p. 177-260.

Jambor, J.L. et Blowes, D.W.
1991: Mineralogical study of low-sulfide, high carbonate, arsenic bearing tailings from the Delnite Minesite, Timmins Area, Ontario; NEDEM-1991-MEND Proceedings, tome 3, Second international conference on the abatement of acidic drainage, p. 173-197.

Leckie, J.O, Benjamin, M.M., Hayes, K.F. et Honeyman, B.D.
1984: Adsorptive removal of trace elements from fly-ash pond effluents onto iron oxyhyroxide; EPRI Report RP-910-1, Electric Power Research Institute, Palo Alto, CA.

Luther, G.W.
1988: Pyrite oxidation and reduction: molecular orbital theory considerations; Geochimica and Cosmochimica Acta, 51, p. 3193-3199.

MacLean, W.H., St. Seymour, K. et Prabhu, M.K.
1982: Sr, Y, Zr, Nb, Ti, and REE in Grenville amphibolites at Montauban-les-Mines, Québec; Revue canadienne des sciences de la Terre, v. 19, p. 633-644.

Madrid, L. et Diaz-Barrientos, E.
1992: Influence of carbonate on the reaction of heavy metals in soils; Journal of Soil Science, v. 43, p. 709-721.

Nadeau, L. et van Breemen, O.
1993: The Montauban group and La Bostonnais complex: arc magmatism ca 1.4 Ga in the Grenville Province, Quebec; Geological Survey of Canada Annual Forum 1993, Program with Abstracts, p. 5.

Papadopoulos, P. et Rowell, D.L.
1988: The reactions of cadmium with calcium carbonate surfaces; Journal of Soil Science, v. 39, p. 23-36.

Parkhurst, D.L., Thorstenson, D.C. et Plummer, L.N.
1980: PHREEQE- A computer program for geochemical calculations; U.S. Geological Survey, Water-Resources Investigations 80-96, 193 p.

Roy, A.G., Courchesne, F., Giguère, N., Gaudet, J. et Chaumont, D.
1993: Dynamics of the confluence between the Batiscan and St. Lawrence Rivers; in Conférences conjointes de la SCGC-ASCE sur le génie environnemental, Montréal.

Salomons, W. et Förstner, U.
1984: Metals in the hydrocycle; Springer-Verlag, Berlin-Heidelberg-New York-Tokyo, 349 p.

Stamatelopoulou-Seymour, K. et MacLean, W.
1984: Metamorphosed volcanogenic ores at Montauban, Grenville Province, Québec; Canadian Mineralogist, v. 22, p. 595-604.

Taylor, S.R. et McLennan, S.M.
1985: The continental Crust: Its Composition and Evolution. An Examination of the Geological Record Preserved in Sedimentary Rocks; Blackwell, Oxford, 307 p.

Projet 920005 de la Commission géologique du Canada

Application of computer neural network and fuzzy set logic to petroleum geology, offshore eastern Canada

Zehui Huang, John Shimeld[1], and Mark Williamson
Atlantic Geoscience Centre, Dartmouth

Huang, Z., Shimeld, J., and Williamson, M., 1994: Application of computer neural network and fuzzy set logic to petroleum geology, offshore eastern Canada; in Current Research 1994-E; Geological Survey of Canada, p. 243-250.

Abstract: Computer neural networks and fuzzy set logic are new advances in artificial intelligence that hold promise for geological applications. A neural network can model complicated geological problems better than most conventional approaches. Fuzzy set logic can more efficiently process incomplete and imprecise information typically found in geosciences. In this paper, we outline both neural networks and fuzzy set logic and illustrate their utility in geoscientific research. One example models the relationship between well logs and rock permeability through application of neural networks for the Venture Gas Field, Sable Basin. The trained neural network performs well in permeability prediction from well logs. Another example demonstrates how open fracture are detected with conventional well logs using a fuzzy set logic algorithm in the Jeanne d'Arc Basin. The fractures index curves produced by fuzzy inference algorithms correlate with known fractured zones, and reveal the extent of fracturing in zones where direct fracture information is not available.

Résumé : Les réseaux neuronaux informatiques (RNI) et la logique des ensembles flous sont les derniers progrès enregistrés dans le domaine de l'intelligence artificielle susceptibles de trouver des applications géologiques. Un RNI permet de modéliser des problèmes géologiques compliqués mieux que la plupart des approches traditionnelles. La logique des ensembles flous permet de traiter de façon plus efficace l'information incomplète et imprécise qui caractérise en général les sciences de la Terre. Dans le présent document, les auteurs donnent un aperçu des RNI et de la logique des ensembles flous et illustrent leur utilité dans le domaine de la recherche relative aux sciences de la Terre. L'un des exemples donnés consiste en un modèle des relations qui existent entre les diagraphies de forage et la perméabilité des roches, grâce à l'utilisation d'un RNI dans le cas du champ de gaz Venture (bassin de Sable). Le RNI en question conduit à de bons résultats en matière de prévision de la perméabilité à partir des diagraphies de forage. Un autre exemple permet de démontrer la façon dont on détecte les fractures ouvertes à l'aide d'un algorithme flou appliqué à des diagraphies de forage traditionnelles effectuées dans le bassin de Jeanne d'Arc. Les courbes de l'indice de fracturation produites par des algorithmes d'inférence floue établissent des corrélations avec des zones fracturées connues, et révèlent l'ampleur des fractures dans les régions où il n'y a aucune information directe.

[1] Department of Earth Sciences, Dalhousie University, Halifax, Nova Scotia B3H 3J5

INTRODUCTION

The past two decades have seen the development and application of numerous quantitative approaches in the geosciences (Agterberg and Bonhan-Carter, 1990). Most of them have been statistical in nature. The usefulness of any these methods depends in large part on the nature of the problem to be solved as they often try to simplify processes that are acting in an extremely complicated, dynamic way. As a result of this, geoscientists are constantly searching for and embracing new quantitative techniques to provide solutions for new and old problems. Among the new techniques introduced during the last five years, the geological application of expert systems, computer neural networks and fuzzy set logic, which all belong to the field broadly defined as artificial intelligence, has seen rapid development (Simaan and Aminzadeh, 1989; Baldwin et al., 1990; Pulli and Dysart, 1990; Rogers et al., 1992; Wang, 1992; Osborne, 1992; Chen and Fang, 1990). This growth is because of their distinct advantages over traditional statistical and deterministic approaches.

Over the last year, we have applied the neural network and fuzzy set logic approaches to problems in the Hydrocarbon Charge Modelling Project carried out at the Atlantic Geoscience Centre (Williamson et al., 1993). In this paper, we first outline the background of these new techniques and then present examples of their application to petroleum geology.

BACKGROUND

Computer neural networks

Computer neural networks are an information processing technique inspired by studies of the brain's nervous systems (Stephen, 1990; Hertz et al., 1991). Following "training" with a series of input values (patterns) and corresponding output values (definition of the patterns) a computer neural network is able to recognize patterns through the generation of specific rules. A neural network stores information acquired during training in numerous associative memory units. The nature of neural network memory leads to efficient network responses (i.e., giving answers) when presented with incomplete, noisy, or previously unseen inputs. Advantages of a neural network approach over conventional statistical and deterministic approaches include less need for a priori information, the fact that a problem is modelled directly and in a more sophisticated way, and increased tolerance to noisy data because of the abundance of input factors.

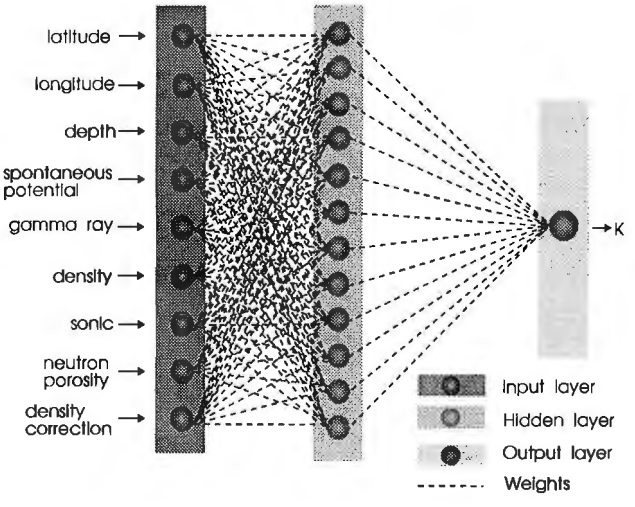

Figure 1. *The structure of the back propogation neural network used for modelling.*

One of the most popular types of networks is known as a back-propagation neural network (Rumelhart et al., 1986). A variation of this, known as Quickprop (Fahlman, 1988), was used in our study. A back propogation neural network always has an input layer containing several input elements, an output layer containing one or more output elements and at least one hidden layer which contains several processing elements (neurons) (Fig. 1). The elements of different layers are interconnected by weights, but there is no interconnection among elements in the same layer for this particular type of neural network. Upon exposure to training examples, the network automatically adjusts the weights until a best generalization has been achieved. Information about relationships between all variables is represented by the final values of the connection weights. Once trained and tested, a back propo- gation neural network can be used for solving problems that are similar in nature to those presented in the training stage.

Fuzzy set logic

Fuzzy set logic (often abbreviated as fuzzy logic) is a mathematical tool developed by a number of workers (e.g., Zadeh, 1965). It is an extension of the traditional Boolean logic (based on "crisp" sets) which classifies or describes things on a "yes-or-no" basis. With fuzzy set logic, one can more flexibly describe things by a "degree-of-truth", which is very useful in handling many real world problems.

In geology, there are many cases one would find hard to handle with crisp sets. For example, with traditional logic, one has to use a cutoff value to differentiate shale from sandstone in well log analysis (e.g., 20 API on a gamma ray log) (Fig. 2a). However, it is not realistic to define one layer as shale when the gamma ray reading is 21 API and another layer as sandstone when the reading is 19 API. Fuzzy sets can overcome this difficulty. By using "degree-of-truth" (or, more mathematically, by defining membership functions), one can describe the layer with a 19 API gamma ray reading in a more realistic but still quantitative way (Fig. 2b). Therefore, it is possible to describe and handle problems involving large, imprecise data sets that, commonly, only experts are able to express using subjective, linguistic variables.

Fuzzy set logic involves the following principal steps: (1) fuzzification of inputs using membership functions built from expert knowledge, analysis of data structure, or some combination of the two, (2) rule evaluation, and (3) defuzzification of outputs.More detail on the method may be found

in textbooks on the subject (e.g., Kaufmann, 1975; Kosko, 1992). Recent applications demonstrate that these techniques are well suited to problems of a geological nature (e.g., Chen and Fang, 1990).

GEOLOGICAL APPLICATIONS

Example 1: permeability prediction using a back propogation neural network in the Venture Gas Field, Sable Basin

Permeability is an important parameter in seal/reservoir characterization, resource assessment and basin modelling. However, the estimation of permeability in uncored wells or intervals is a difficult petrophysical problem as there is no simple way to estimate permeability from well logs. Simple porosity-permeability relationships do not offer reliable permeability estimations in most cases since they are only directly applicable in unconsolidated sand and homogeneous rocks. However, most reservoir intervals are heterogeneous (Beard and Weyl, 1973; Bos, 1982).

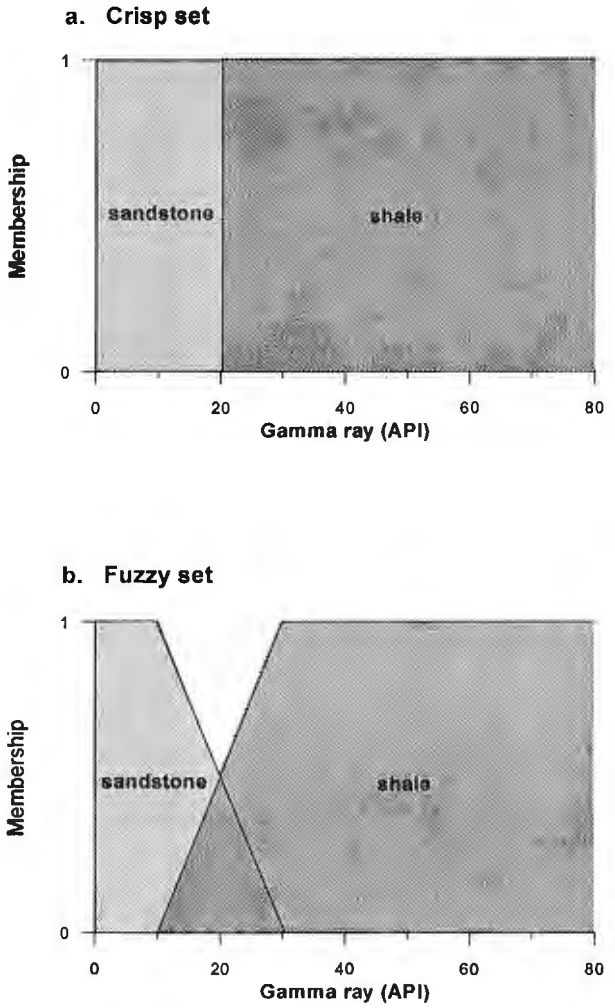

Figure 2. Crisp and fuzzy sets for sandstone and shale. With crisp set (a), if the rock has a gamma ray reading of 25 API, its membership to the set "sandstone" is 0 and to "shale" is 1. With fuzzy set (b), however, the rock's membership to "sandstone" is 0.25 and to "shale" is 0.75.

Relationships between permeability, porosity, and other rock properties such as grain size, type and amount of cement etc., are very complex and area-specific. In general though, well log responses are functions of lithology, pore-fluid composition, and porosity. Similarly, permeability is also a function of lithology and porosity. Therefore, with an adequate data set, correlations between permeability and several well log responses can be used to estimate permeability. For example, a predictive equation can be built from well logs and core measurements using multiple linear regression (MLR) for estimating permeability in uncored intervals (Wendt et al., 1986). However, the fundamental assumption of linear relationships among well logs and rock permeability may not be valid, and this limits the usefulness of such prediction equations.

As an alternative to conventional methods, we use computer neural network (CNN) techniques to model permeability in overpressured reservoirs of the Venture Gas Field of Sable Basin, offshore eastern Canada (Grant et al., 1986; Mudford and Best, 1989). Our data are from five wells in this field (Venture B-13, Venture B-43, Venture B-52, Venture H-22 and Venture C-62). The permeability measurements were made by Core Laboratories-Canada Ltd. under conditions which approximate the in situ overburden stresses present at Venture. The data set also includes a few measurements on low permeability shale published by Katsube et al. (1991).

We first pre-processed the well logs and measured permeability data to address such problems as shifts between recorded well log depths and sample depths, the difference in spatial resolution between well logs and core samples, uneven distribution of core measurements, and so on.

Data from the first four wells were grouped into neural network training and testing data sets. Each data set consists of permeability measurements with the corresponding spontaneous potential, gamma ray, density, sonic, neutron porosity and density correction logs digitized at 0.2 m, and spatial information (depth and well location). The training data set contains 223 examples and the testing data set has 73. Data from Venture C-62 were retained as a totally independent data set to test the performance of the trained back propogation neural network.

The network is given the nine input values, from which it calculates one value (permeability) as the output. The number of nodes in the hidden layer was chosen after a series of trials with networks of different architectures. The network found to have the best generalization ability has 12 nodes in the hidden layer (Fig. 1).

Figure 3a compares the measured permeability and the back propogation neural network predicted permeability of the testing data set. The slope of the best-fit line, determined using the reduced matrix axis (RMA) method (Davis, 1986), is 45.3° and the correlation coefficient is 0.8. This indicates that the best trained neural network can make an almost one-to-one prediction. Scatter around the best-fit line may be caused by problems related to resolution, local borehole conditions, and, to a lesser extent, errors in the permeability measurements themselves.

For comparison, we built a predictive equation with the same training data set using the MLR approach (Davis, 1986). The calculated permeability from the nine input values in the testing data set is plotted against measured permeability (Fig. 3b). The slope of the reduced matrix axis is 28° while the correlation coefficient is 0.65. These results indicate that the predictive equation from MLR analysis is less successful than the trained back propogation neural network (Fig. 3a). This is especially true at the data extremes.

Figure 4 shows the continuous permeability profile calculated from the trained back propogation neural network and measured values in the reservoir interval (4788-5230 m) of the Venture C-62 well. The general and specific comparisons in Figure 4 between measured and predicted values are impressive, particularly as the neural network was trained and tested with data sets that do not include any information from the C-62 well. Given the good performance of the trained back propogation neural network, we calculated continuous

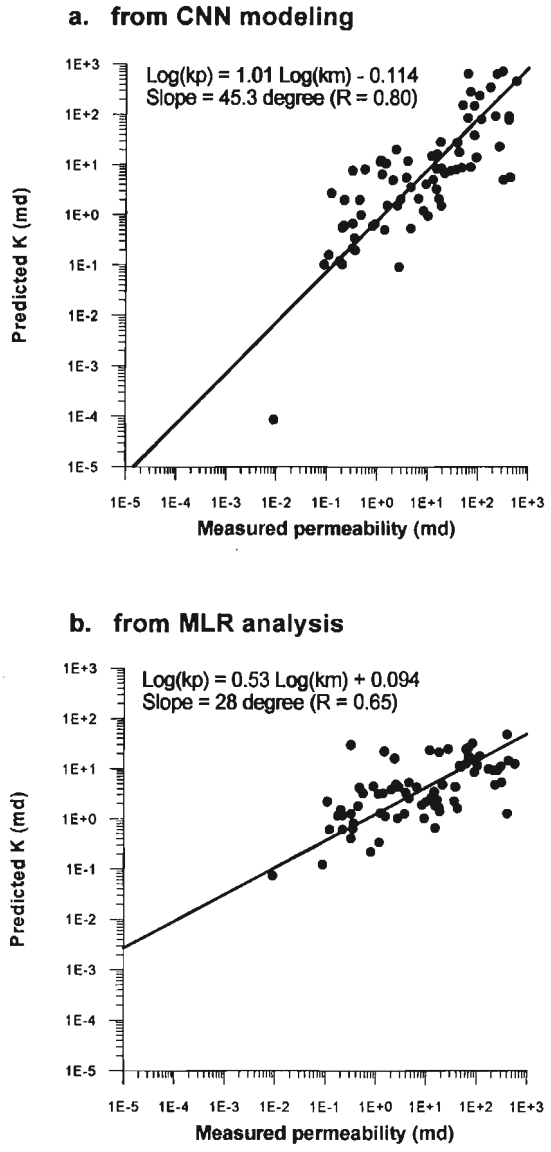

Figure 3. Crossplot of measured permeability against predicted permeability from Computer neural network (CNN) modelling (a), and from MLR analysis (b).

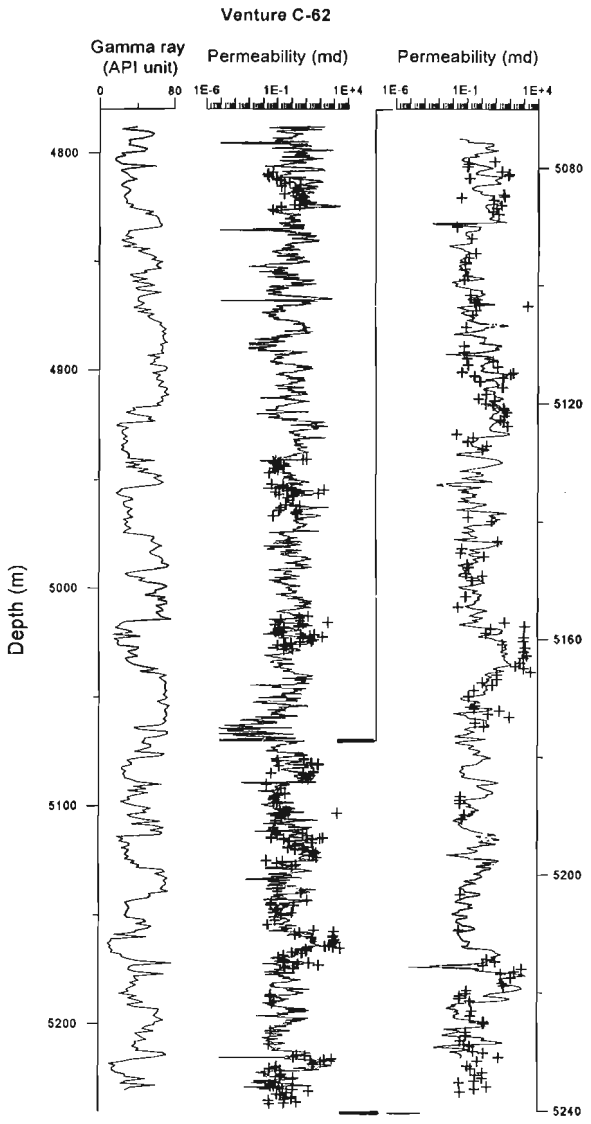

Figure 4. Continuous predicted permeability (curve) and measured permeability values (crosses) at Venture C-62.

permeability curves at the four Venture wells over the interval from 4400 m to 5800 m (Fig. 5). With the aid of gamma ray logs (not shown), we successfully correlated high permeability zones (sandstone and siltstone intervals) and low permeability zones (shale and limestone intervals) between the Venture wells. Correlation of the neural network-derived permeability curves reveals the relative importance of various seals in terms of their thickness, thickness variation, lateral continuity, and the predicted permeability. This detailed information on distribution of low and high permeability zones within the reservoir intervals can serve as a useful platform, in conjunction with pressure and flow test data, for analysis of producing zone potential and connectivity. The level of detail shown in Figure 5 would not be possible if we had only used unevenly distributed permeability measurements (preferentially sampled from sandy intervals), or if we only had used one or two well logs indirectly related to permeability (e.g., the gamma ray and sonic logs). Examination of Figure 5 indicates that, over this reservoir interval, the important seals appear at the top of No. 2, No. 2A, No. 3, No. 4, No. 6, No. 10, No. 13 and No. 16 sandstones. These shale and limestone seals may have significantly influenced the development of overpressure in the reservoir.

Example 2: open fracture detection with conventional well logs using fuzzy set logic in the Jeanne d'Arc Basin

Since open fractures greatly increase porosity and permeability, it is important to know their distribution down the length of a vertical or horizontal borehole. Modern well logs, such

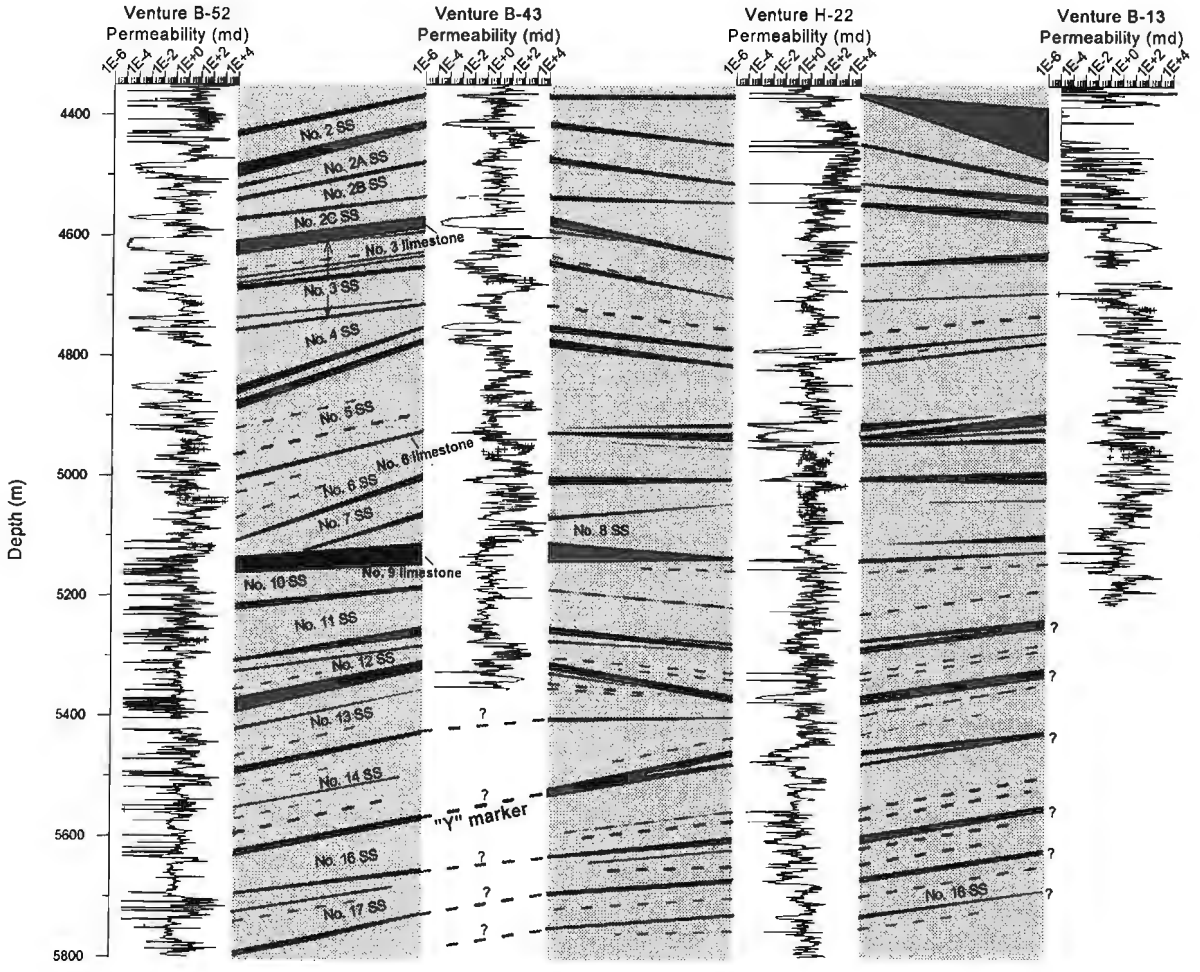

Figure 5. *Predicted permeability curve and measured permeability values at Venture B-52, Venture B-43, Venture H-22, and Venture B-13 and the inter-well correlation. The labels for the lithological units (e.g., No. 2 SS, No. 6 limestone) are the same as is used by Mudford and Best (1989). Dark grey zones stand for low permeability shale, claystone and limestone, and light grey zones for high permeability silt/sandstone.*

as the Formation Microscanner (FMS), provide detailed information and clear images of open fractures. However, these logs are generally very expensive to collect and process. Furthermore, the large data sets available from wells drilled before modern fracture detection tools were widely applied still provide useful information about fracturing on a regional or individual pool scale (the Formation Microscanner Service was introduced by Schlumberger in 1985).

Conventional well logs, such as resistivity, porosity, density correction, and caliper logs, often exhibit abnormal values in response to open fracture zones. No single log response is completely diagnostic of fracturing though, since each log responds to a number of formation properties and borehole conditions. Indeed, for a specific log, it is difficult to quantitatively define what response might be expected in the presence of a fracture. A fracture occurring in sandstone typically generates a much different caliper log response than a fracture occurring in shale.

To overcome these difficulties, fuzzy set logic was applied using conventional, digital well log data to detect open fractures. The algorithm was tested offshore eastern Canada with well information from Hibernia I-46 and Terra Nova H-99. These locations were chosen since the well log data are publicly available, and a number of faults are known to intersect both boreholes.

Log data from the wells are pre-processed to statistically evaluate the deviation of a given log response from a local averaged response. This approach allows any available log, which responds to fracturing in a reasonably predictable manner to be incorporated into the algorithm. Using a full suite of logs allows the final prediction of fracture occurrence not to be dependent on the subjective examination of a small number of arbitrarily chosen well log responses.

The pre-processing results are then used to construct membership functions for a number of fuzzy sets that express various degrees of "fracture relatedness". For instance, "fracture relatedness" might be described by three fuzzy sets: high, medium, and low. These membership functions are then used to describe quantitatively each well log response at some depth in terms of its "fracture relatedness".

To translate the grades for the given depth into a relative measure of the likelihood of fracture occurrence, called the fracture index, a database of rules is then used. These rules are created to reflect the "rule of thumb" in petrophysical knowledge (e.g., Schlumberger, 1989). For example, one rule or expression could be: if the pre-processed caliper log is high, and the pre-processed sonic log is high, and the pre-processed density correction log is high, then the fracture index is high. In a manner analogous to Boolean logic, fuzzy set logic provides a method of evaluating the truth of this expression (defuzzification). Instead of requiring a discrete truth value of either 0 or 1 (no or yes), fuzzy set logic allows for a continuous range of values between 0 and 1. Actually, the fuzzy set approach can be considered a superset of traditional Boolean logic (Schmucker, 1984).

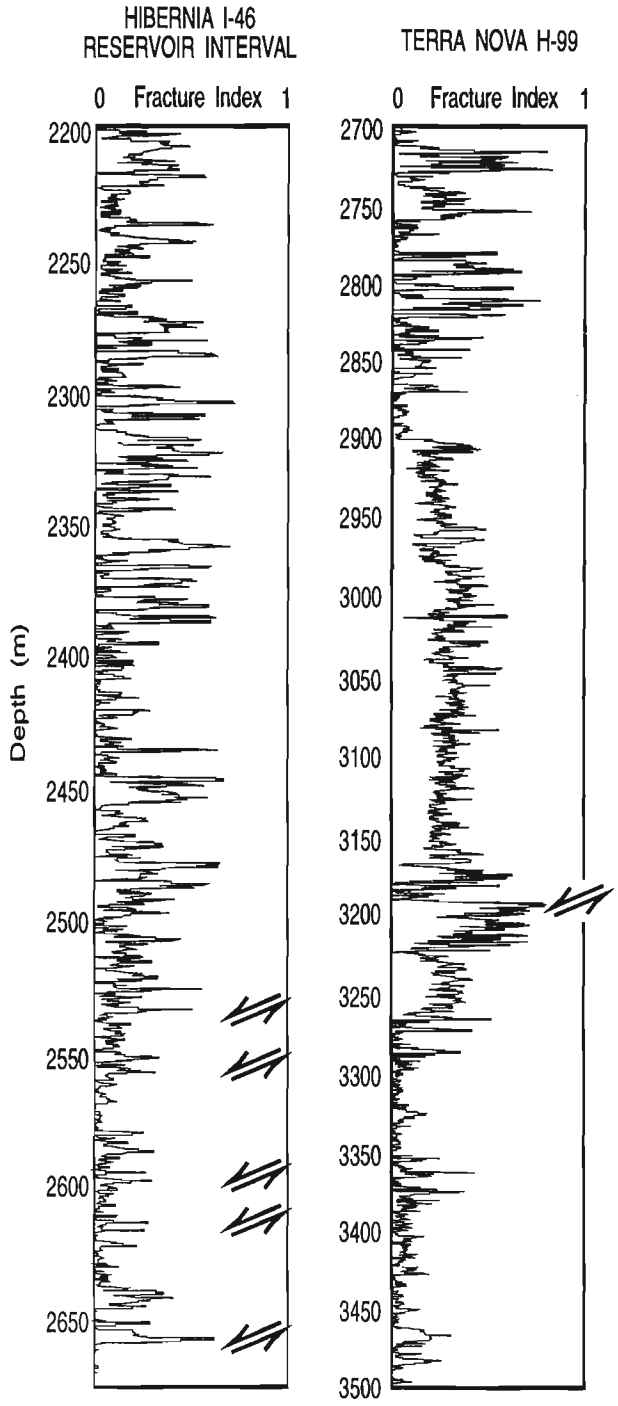

Figure 6. *Fracture index curves at Hibernia I-46 and Terra Nova H-99.*

After calculating fracture index at each depth, a continuous fracture index profile is generated (Fig. 6). The results shown in Figure 6 were calculated over the entire length of the borehole using the following logs: caliper, sonic, density correction, density, and resistivity. Relative peaks in the fracture index curve in Figure 6 correspond to slickensides (marked with fault symbol) described in the well history report over the Hibernia I-46 reservoir interval (Mobil Oil Canada, 1983). Although the report on the core describes a number of fractures, the descriptions are not detailed enough to allow distinction between drilling induced and natural fractures. For this reason, slickensides mentioned in the report are considered the only independent evidence of fracturing. However, personal communication with John Hogg of Petro-Canada Incorporated supports the fracture index results which show the reservoir interval is highly fractured.

At Terra Nova H-99, a 25 metre interval of elevated fracture indices values corresponds with a fault, mapped using 3D seismic data, that intersects the borehole at approximately 3180 m. In this instance, the fracture index log provides a method of determining the downhole depth to a fault zone, and indicates that a number of open fractures are associated with the fault. Such information is important for reservoir production plans.

SUMMARY AND FUTURE WORK

Our work with a back propogation netural network and fuzzy set logic illustrates the usefulness of these computer learning techniques in geological applications. These examples show how further quantitative information can be extracted from existing data sets.

Planned further neural network studies include: (1) Experimention with other neural network algorithms using our permeability and well log data sets, (2) Use and calibration of the method with well data sets from the Western Canada Sedimentary Basin where permeability and core data are more readily available, (3) Construction of a more comprehensive database to include as much information as possible for the Sable and other eastern Canada offshore basins. This will allow the development of neural network models which are applicable for large areas, instead of just a field. (4) Calculation of continuous permeability profiles for as many wells as possible to provide more information for reservoir evaluation, seal development, and basin history modelling.

Further fuzzy set research will include: (1) Refinement of the algorithm through more case studies with better calibrating data sets in a variety of geological settings, (2) Incorporation of other methods to build the database of rules (e.g., Computer neural network techniques), (3) Mapping fracture distribution in areas of major oil occurrence in the Jeanne d'Arc Basin (e.g., the Hibernia Oil Field and Terra Nova area).

ACKNOWLEDGMENTS

The authors wish to thank the staff of the Canada-Nova Scotia Offshore Petroleum Board for their assistance during permeability data collection. Z.H. was partially supported by a Canadian Government Laboratory Visiting Fellowship. In this study, we used a publicly available neural network software package, called Nevprop, developed by the Centre for Biomedical Modelling Research at the University of Nevada. The manuscript was reviewed by K. Coflin and A. Agrawal of the Atlantic Geoscience Centre.

REFERENCES

Agterberg, F.R. and Bonhan-Carter, G.F. (ed.)
1990: Statistical applications in the earth sciences; Geological Survey of Canada, Paper 89-9, 588 p.

Baldwin, J.L., Otte, D.N., and Wheatley, C.L.
1990: Application of neural network to problem of mineral identification from well logs; The Log Analyst, v. 3, p. 279-293.

Beard, D.C. and Weyl, P.K.
1973: Influence of texture on porosity and permeability of unconsolidated sand; American Association of Petroleum Geologists Bulletin, v. 57, p. 349-369.

Bos, M.R.E.
1982: Prolific dry oil production from sands with water saturation in excess of 50%, a study of a dual porosity system; Society of Professional Well Log Analysts, Transactions, Paper BB.

Chen, H.C. and Fang, J.H.
1990: Uncertainties are better handled by fuzzy arithmetic; American Association of Petroleum Geologists Bulletin, v. 74, p. 1228-1233.

Davis, J.C.
1986: Statistics and data analysis in geology; 2nd edition, John Wiley, New York, 646 p.

Fahlman, S.E.
1988: Fast learning variations on back-propagation: an empirical study; in Proceedings, 1988 Connectionist Models Summer school, D.S. Touretzky, G. Hinton, and T. Sejnowski, (ed.); Morgan Kaufmann Publishers, San Mateo, California, p. 38-51.

Grant, A., McAlpine, D., and Wade, J.
1986: The continental margin of eastern Canada--geological framework and petroleum potential; in Future Petroleum Povinces of the World, M.T. Halbouty, (ed.); American Association of Petroleum Geologists Memoir 40, p. 177-205.

Hertz, J., Krogh, A., and Palmer, R.G.
1991: Introduction to the theory of neural computation; Addison-Wesley Publ. Co., Redwood City, California, 327 p.

Katsube, T.J., Mudford, B.S., and Best, M.E.
1991: Petrophysical characteristics of shales from the Scotian shelf; Geophysics, v. 56, p. 1681-1689.

Kaufmann, A.
1975: Introduction to the Theory of Fuzzy Sets; Volume 1; Academic Press, New York, 415 p.

Kosko, B.
1992: Neural networks and fuzzy systems: a dynamical systems approach to machine intelligence; Prentice Hall, Engelwood Cliffs, New Jersey, 449 p.

Mobil Oil Canada Ltd.
1983: Well history report Mobil et al. Hibernia I-46; Canada-Newfoundland Offshore Petroleum Board.

Mudford, M. and Best, M.
1989: Venture Gas Field, offshore Nova Scotia: case study of overpressuring in region of low sedimentation rate; American Association of Petroleum Geologists Bulletin, v. 75, p. 1383-1396.

Osborne, D.A.
1992: Neural networks provide more accurate reservoir permeability; Oil and Gas, Sept. 28, p. 80-83.

Rogers, S., Fang, J.H., Karr, C.L., and Stanley, D.A.
1992: Determination of lithology from well logs using a neural network; American Association of Petroleum Geologists Bulletin, v. 76, p. 731-739.

Pulli, J.J. and Dysart, P.S.
1990: An experiment in the use of trained neural networks for regional seismic event classification; Geophysical Research Letters, v. 17, p. 977-980.

Rumelhart, D.E., Hinton, G.E., and Williams, R.J.
1986: Learning internal representations by error propagation; in Parallel Distributed Processing, v. 1 foundations, D.E. Rumelhart and J.L. McClelland, (ed.); The MIT Press, Cambridge, Massachusetts, p. 318-362.

Schlumberger
1989: Log Interpretation Principles/Applications; Schlumberger Educational Services.

Schmucker, K.J.
1984: Fuzzy Sets, Natural Language Computations, and Risk Analysis; Computer Science Press, 192 p.

Simaan, M. and Aminzadeh, F. (ed.)
1989: Artificial intelligence and expert system in petroleum exploration: advances in geophysical data processing; v. 3, JAI Press Inc., Greenwich, Connecticut.

Stephen, J.J.
1990: Neural network design and the complexity of learning; The MIT Press, Cambridge, Massachusetts, 150 p.

Wang, L.X.
1992: A Neural detector for seismic reflectivity sequences; IEEE Transaction on Neural Networks, v. 3, p. 338-340.

Wendt, W.A., Sakurai, S., and Nelson, P.H.
1986: Permeability prediction from well logs using multiple regression; in Reservoir Characterization, L.W. Lake and H.B. Carroll, Jr. (ed.); Academic Press, San Diego, California. p. 181-221.

Williamson, M.A., Katsube, T.J., Huang, Z., Fowler, M., McAlpine, K.D., Thomas, F.C., and Avery, M.
1993: Hydrocarbon charge history of east coast offshore basins: modelling geological uncertainty; in Current Research, Part E; Geological Survey of Canada, Paper 93-1E, p. 299-306.

Zadeh, L.A.
1965: Fuzzy Sets; Information and Control, v. 8, p. 338-353.

Geological Survey of Canada Project 920058

Relationship between crustal deformation and magmatism in rift zones: modelling approach and applications to the eastern Canadian margin

Marie-Claude Williamson, Robert C. Courtney,
Charlotte E. Keen, and Sonya A. Dehler
Atlantic Geoscience Centre, Dartmouth

Williamson, M.-C., Courtney, R.C., Keen, C.E., and Dehler, S.A., 1994: Relationship between crustal deformation and magmatism in rift zones: modelling approach and applications to the eastern Canadian margin; in Current Research 1994-E; Geological Survey of Canada, p. 251-258.

Abstract: A model of lithospheric stretching and associated mantle melting is described which predicts the geographic distribution, volume, and trace element composition of basaltic magmas generated in rifts. Melt volumes are computed from the post-rift and syn-rift subsidences that account for the thickness of the sedimentary sequence. The concentrations of rare-earth elements (REE) are calculated by applying a sequential melting model to values of the melt fraction vs. depth. The predicted melt volumes and REE concentrations are sensitive to variations in the basal mantle temperature, magnitude of subcrustal stretching, and rifting history. Given moderately high temperatures and large degrees of stretching in the upper mantle, the geochemical model is capable of generating alkaline melts, and predicts the transition from alkaline to tholeiitic magmatism observed in many continental rifts. The model results are currently being constrained with data from the Labrador margin.

Résumé : Les auteurs examinent un modèle de la fusion partielle du manteau et de l'étirement de la lithosphère qui prédit la répartition géographique, le volume et la composition des éléments-traces des magmas basaltiques produits dans les rifts. Le volume de magma est calculé à partir de la subsidence qui a eu lieu pendant et après le rifting. Les concentrations des éléments des terres rares (ETR) sont calculées à partir des valeurs de la fraction de magma en fonction de la profondeur, au moyen d'un modèle séquentiel de fusion particlle. Les valeurs prévues du volume de magma et des concentrations d'ETR sont fonction des variations de la température de la base du manteau, des valeurs de l'étirement subcrustal et de l'histoire du rifting. Étant donné des valeurs modérément élevées de la température mantellique et de l'étirement subcrustal, le modèle géochimique produit un magma alcalin et prévoit la transition au magmatisme tholéiitique observée dans plusieurs rifts continentaux. On compare actuellement les résultats aux données provenant de la marge du Labrador.

INTRODUCTION

The decompression melting model (McKenzie and Bickle, 1988) successfully predicts the average thickness of oceanic crust generated at mid-ocean ridges (White et al., 1992). When combined with chemistry functions, this model is also able to predict the average major element composition of mid-ocean ridge basalts (MORB: see the review by Langmuir et al., 1992). In the uniform stretching model proposed by McKenzie and Bickle (1988), variations in the temperature of the mantle in the order of ~ 200°C can account for differences in the volume of basaltic melts generated at ridges vs. hot spots or volcanic margins (White and McKenzie, 1989).

Igneous activity is common in regions of stretched continental crust and has been explained by decompression melting during extension of the lithosphere (e.g. Keen, 1987). However, unlike their oceanic counterpart, continental rifts are characterized by a wide range of magma types, and a complex association between magmatism, tectonic activity, and the structural development of linked basins through time (e.g. Ebinger, 1989). Studies of magmatism in rift zones generally progress from field and petrochemical studies to one or more petrogenetic models and then to a description of the physical parameters controlling the rifting process (e.g. Perry et al., 1988; Bradshaw et al., 1993). To date, most applications of the decompression melting model have considered a single rifting event when computing melt volumes and chemistry from subsidence analyses (e.g. Ro and Faleide, 1992; Latin and Waters, 1992), whereas the rifting process is undoubtedly more complex and time dependent (Wilson, 1993).

This paper summarizes a modelling approach that includes the history of rifting over time as part of the physical and chemical description of the decompression melting model. This work is part of an interdisciplinary project and contributes to ongoing research on crustal processes at AGC, questioning the creation, subsidence, and tectonomagnetic history of extensional basins. We review the numerical methods used to predict the volume and rare-earth element (REE) abundances of basaltic melts generated during rifting, and describe the results. A comparison of model predictions with observations of the volume and the composition of igneous rocks in several rift basins is underway. Our intention is to include the platinum-group elements (PGE) in the model and to contribute to the study of PGE-enrichment in some ore deposits associated with continental rifting (e.g. Class II of Naldrett, 1981).

MODEL

The following questions define the scope of this project: (1) What are the effects of the rifting history and of two-layer extension on the volumes and composition of melts generated by decompression melting? (2) Can geochemical data on igneous rocks be used to constrain some of the physical models applied to the evolution of rift basins?

Figures 1 and 2 illustrate our basic approach, together with the stretching model used in the calculations. We assume a two-layered lithospheric stretching model in which the crust is stretched by a factor β and the lower lithosphere is stretched by δ (Fig. 2; Keen and Dehler, 1993). Melt thickness and the distribution of melt fraction with depth are calculated using the decompression melting model of McKenzie and Bickle (1988; modified by Keen et al., 1994), and are based on the input parameters and stretching factors derived from subsidence analysis (Fig. 1). As the lithosphere is stretched, mantle rocks are advected adiabatically upward to a new depth determined by the amount of stretching. If the upwelling mantle crosses the solidus, melting occurs (Fig. 2b). The resulting melting column extends from the depth, or pressure, of intersection with the solidus to the final depth where melting occurs. We use an incremental melting model modified after Niu and Batiza (1991) to calculate the concentrations of rare-earth elements. In this model, melting is continuous and polybaric: the melts are extracted in 1% increments, which then accumulate in a reservoir. Each increment is calculated as a non-modal batch melt (Shaw, 1970), and the composition of the pooled melt is the weighted mean of the composition of all the instantaneous melts produced in the column (Klein and Langmuir, 1987). An important assumption is that discrete melt fractions segregate and are chemically isolated from the source region. The mineralogy of the fertile spinel lherzolite source ($Ol_{57}Opx_{25.5}Cpx_{15}Sp_{2.5}$) is taken from Kostopoulos (1991), and converted to garnet peridotite mineralogy using the technique of Kostopoulos and James (1992), at a pressure of 20 kbar.

The FORTRAN program used includes 20 trace elements, 8 of which are the rare-earth elements La, Ce, Nd, Sm, Nd, Tb, Yb, and Lu. Preliminary results demonstrate that

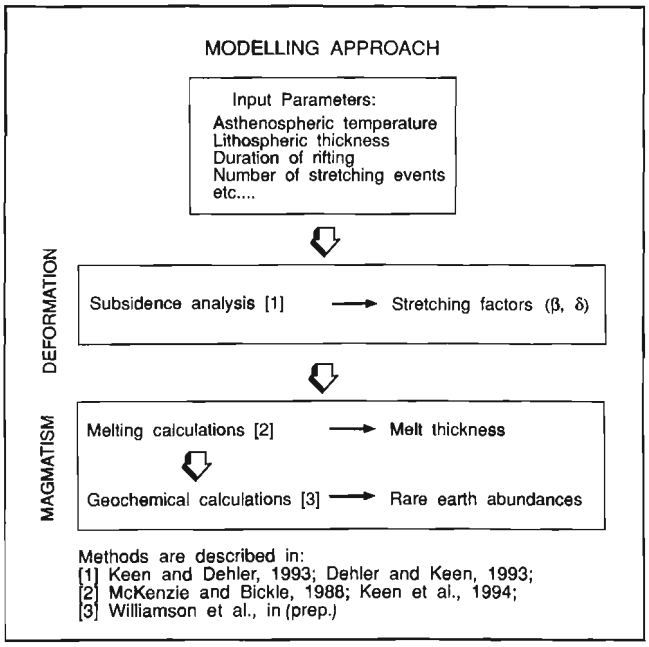

Figure 1. *Sequence of calculations performed in the model.*

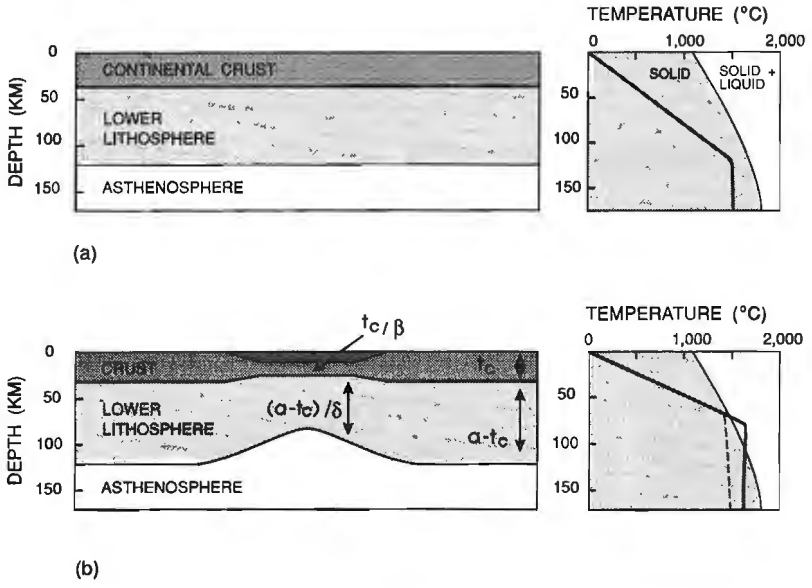

Figure 2.

Cartoons illustrating the two-layer lithospheric stretching model and the effects of extension on the temperature profile through the lithosphere. Figure (a) shows how increasing pressure prevents melting in unstretched lithosphere. In Figure (b), melting only occurs if the temperature profile crosses the solidus (modified from Keen and Dehler, 1993, with profiles from White and McKenzie, 1989).

Table 1. Rare-earth element abundance in source mantle (ppm) and preferred set of partition coefficients.

	La	Ce	Nd	Sm	Eu	Tb	Yb	Lu
C^o_s, PM	0.55	1.40	1.08	0.35	0.13	0.084	0.372	0.057
C^o_s, DM	0.206	0.722	0.815	0.299	0.115	0.077	0.347	0.054
D_{ol}	0.0004	0.0005	0.001	0.0013	0.0016	0.0015	0.0015	0.0015
D_{opx}	0.002	0.003	0.0068	0.01	0.013	0.019	0.049	0.060
D_{cpx}	0.054	0.098	0.21	0.26	0.31	0.31	0.28	0.28
D_{gt}	0.01	0.021	0.087	0.217	0.32	0.75	4.03	5.50
D_{sp}	0.01	0.01	0.01	0.01	0.01	0.01	0.01	0.01

Primitive and depleted mantle: Galer et al. (1989), McKenzie and O'Nions (1991).
Partition coefficients: Irving (1978) and Hanson (1980).

mantle-normalized trace-element diagrams of synthetic melts are useful to characterize large-degree melts (Williamson et al., 1992). However, the modelling of rare-earth elements provides several additional advantages: (1) REEs are relatively unaffected by secondary alteration and weathering processes, so that we can compare calculated and observed abundances with a good degree of confidence. (2) REE abundances vary according to the degree of silica undersaturation of basaltic magmas, and so provide a tool for the classification of tholeiitic and alkaline magma types. (3) Mineral/melt partition coefficients are relatively well known and can be used to calculate the concentrations of REE given the assumption that their activities are linear functions of their concentrations. This allows a number of end-member petrogenetic processes to be tested, including partial melting.

The partition coefficients and initial REE abundances of primitive (PM) and depleted mantle (DM) adopted in this paper are listed in Table 1. The reader is referred to Keen et al. (1994) and Williamson et al. (in prep.) for a list of other physical and chemical input parameters.

RESULTS

Keen et al. (1994) presented a sensitivity study of the physical input parameters and concluded that the predicted melt volumes are most sensitive to the temperature at the base of the lithosphere, the number of stretching events, and the time interval over which rifting occurs. In addition, they found that the effect of mantle stretching, δ, is more important than

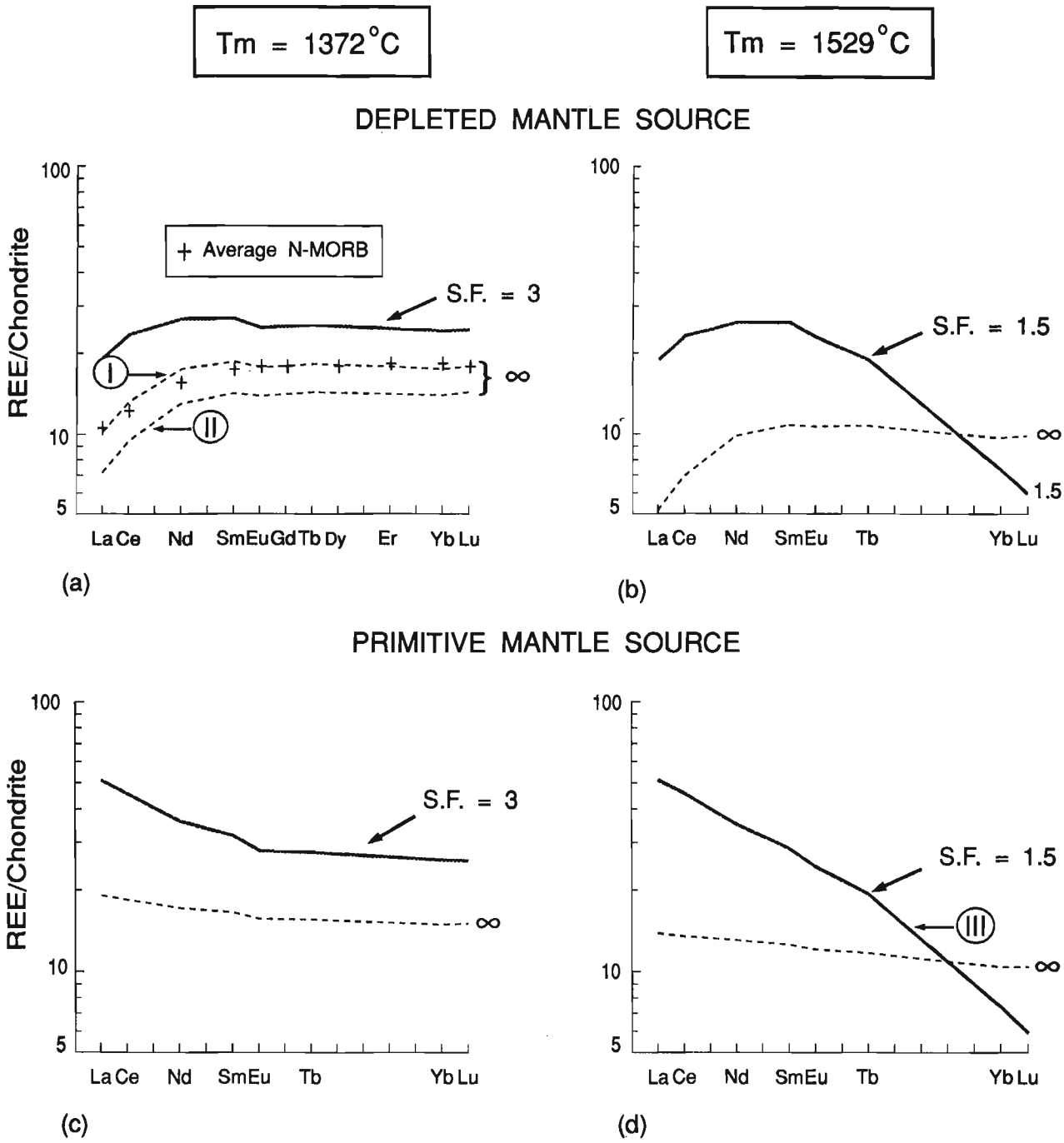

Figure 3. *Chondrite normalized REE patterns of pooled melts calculated by assuming non-modal, incremental batch melting of spinel peridotite during uniform, finite (solid line) and infinite (dashed line) stretching of the lithosphere (β = δ = Stretching Factor, S.F.). Depleted and primitive mantle values are assumed in the upper (**a, b**) and lower (**c, d**) diagrams, respectively. Curves I and II illustrate the overall depletion in REE concentrations, as the basal mantle temperature (Tm) is increased from 1300 to 1372°C, with all other parameters held constant. Curve I compares favourably with the average N-MORB rare-earth data (crosses) of Sun and McDonough (1989), and is a standard of reference in our model. REE patterns typical of alkaline magmas can be generated by small degrees of partial melting of LREE-enriched peridotite, and resemble curve III, in diagram (d). The fractionation of HREE at high temperatures (b, d) is a consequence of melting in the field of garnet peridotite (> 20 kbar pressure).*

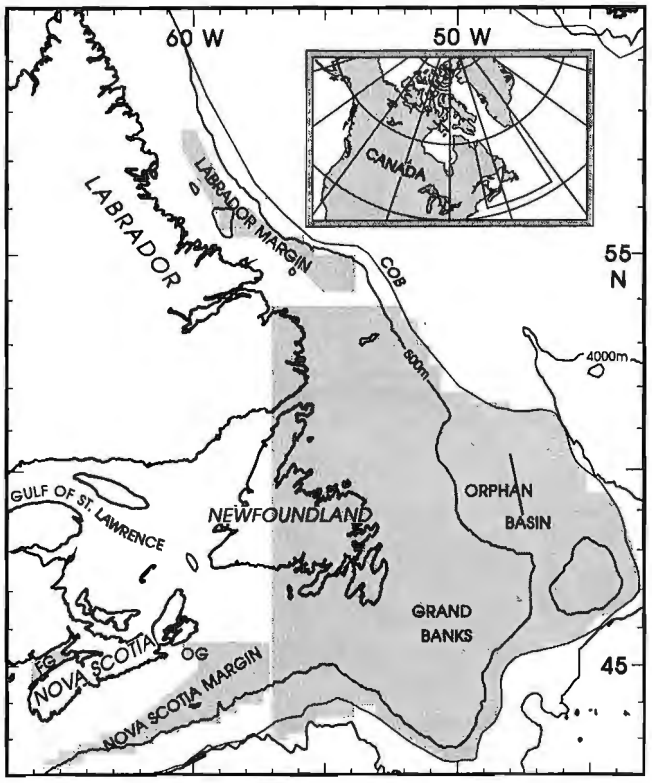

Figure 4. Location map of the eastern Canadian margin showing subsidence data coverage on three segments of the margin. OG = Orpheus graben; FG = Fundy graben (from Keen et al., 1994).

crustal stretching, β, because the magnitude of δ primarily controls the size of the melting region at the base of the lithosphere.

The same controlling parameters apply to the geochemical model, because rare earth abundances become "diluted" as the degree and depth of melting increase, and larger volumes of melt are generated (Williamson et al., in prep.). The effect is an overall decrease in the REE abundances of melts. In our model, this effect can be directly associated with an increase in mantle temperature and/or the degree of lithospheric stretching. For example, curves I and II in Figure 3a were calculated by assuming infinite stretching of the lithosphere and melting of a depleted mantle source. The two curves illustrate an increase in basal mantle temperature (Tm) from 1300 to 1372°C, with all other parameters held constant. In terms of REE abundances, curve I compares satisfactorily with the average composition of 'normal' MORB proposed by Sun and McDonough (1989). Overall, changes in the physical and chemical input parameters show far greater effects on the calculated REE abundances in models of finite lithospheric stretching. For example, a change from depleted to primitive mantle values (Table 1) will result in the production of melts enriched in light rare-earth elements (LREE) at small degrees of stretching (Fig. 3c, d), but this signature is lost as the mean extent of melting increases in the column. Note that the fractionation of heavy rare-earth elements (HREE) in melts generated at higher mantle temperatures (Fig. 3b, d) is a consequence of melting in the field of garnet peridotite (> 20 kbar), and that REE patterns typical of alkali basalts can only be generated by assuming a primitive mantle composition (e.g. curve III, Fig. 3d).

Keen et al. (1994) concluded that multiple stretching events can delay and reduce melt production, depending on the duration of the rifting stage and the amounts of stretching. Given moderately high temperatures and large degrees of stretching in the upper mantle during episodic rifting, the geochemical model is capable of generating alkaline melt with patterns similar to curve III, (Fig. 3d). Depending on the number of stretching events, the model also predicts a transition with time from alkaline to tholeiitic compositions (Williamson et al., in prep.), consistent with the petrological sequence of magmas emplaced in many continental rifts (Giret and Lameyre, 1985).

PREDICTIONS VS. OBSERVATIONS

Considerable petroleum industry activity along the eastern Canadian margin during the seventies and eighties has resulted in a large seismic database, complemented by extensive drilling. As a result, it constitutes one of the most-studied examples of rifted margins in the world. Figure 4 shows three segments of the margin, extending from the southwestern Nova Scotia margin to the northern Labrador Sea, where syn-rift and post-rift sediment thicknesses and subsidence maps are available. Starting in the Early Triassic, rifting and basin development progressed northwards (Fig. 5). With the exception of early Triassic tholeiitic flood basalts and linear composite dykes exposed onshore and present in some of the wells, igneous rocks are predominantly alkaline and Late Jurassic to Early Cretaceous in age (Pe-Piper and Jansa, 1987; Pe-Piper et al., 1992).

Keen et al. (1994) compared the predictions of the decompression model with the observed distribution of igneous rocks sampled in a large number of wells along the margin. They concluded that the Labrador margin is one area where observations on the volume of synextensional basalts are consistent with crustal stretching estimates derived from subsidence analyses (Dehler and Keen, 1993). The Labrador margin is our current area of investigation, because a large geochemical database on igneous rocks from seven offshore wells is available to compare with REE concentrations predicted in our model (Williamson et al., unpub. data). Figure 6 shows the location of these wells and the magnitude of subcrustal stretching factors as computed from the analyses of Dehler and Keen (1993).

Figure 7 shows an example of the geochemical calculations performed for the Roberval K-92 well, using the β and δ values of Dehler and Keen (1993). Some of the input parameters in their model include a basal mantle temperature of 1400°C, an initial lithospheric thickness of 125 km, and 3 stretching events distributed over a period of 45 Ma (N1 to N3, Fig. 5). The calculated REE concentrations of pooled

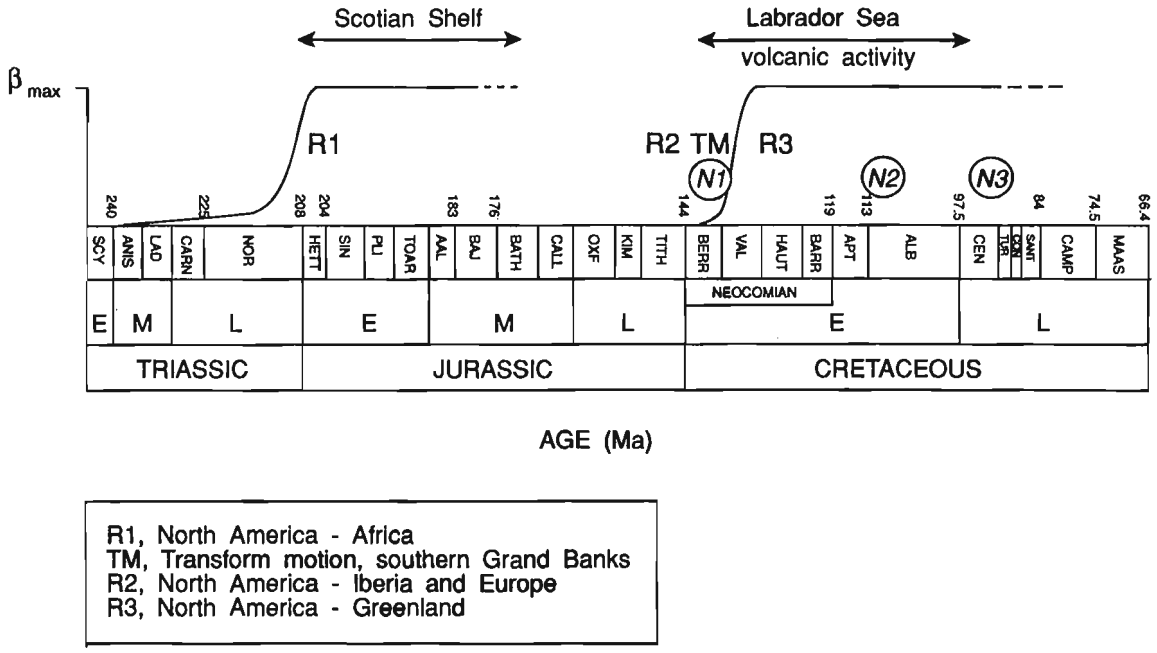

Figure 5. *Schematic representation of the timing of Cretaceous rifting and volcanism in the Labrador Sea, and of earlier rifting and motion along the eastern Canadian margin (DNAG time scale). The dashed line corresponds to the end of the rifting stage and start of seafloor spreading. Keen et al. (1994) assume three episodes of extension during rifting in the Labrador Sea, shown here as N1 to N3.*

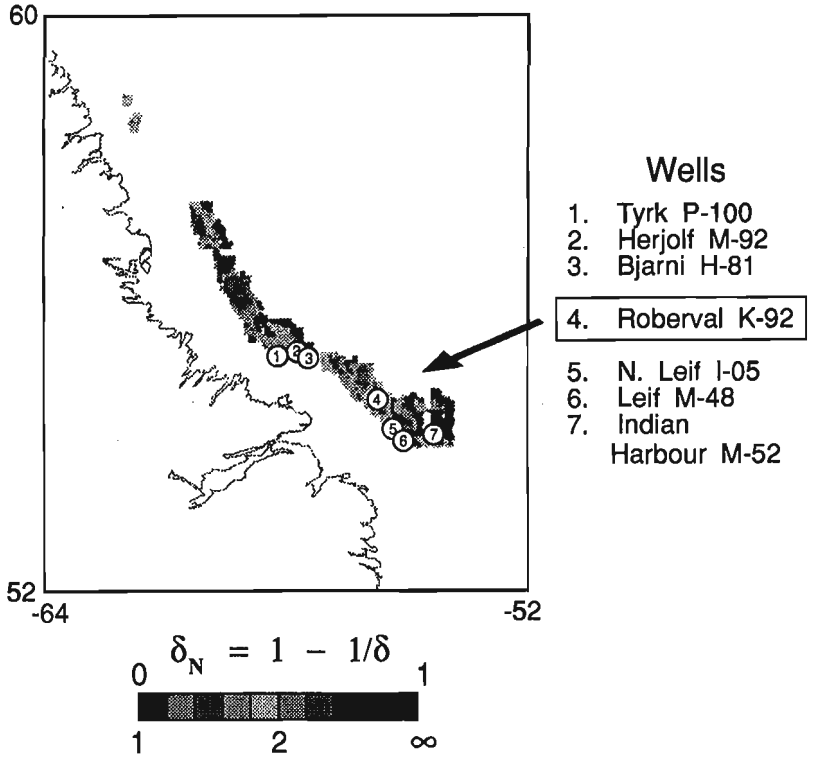

Figure 6.

Deformation map showing variations in the magnitude of subcrustal lithospheric stretching (normalized) along the Labrador margin, and the location of exploration wells where igneous rocks have been recovered (modified from Dehler and Keen, 1993).

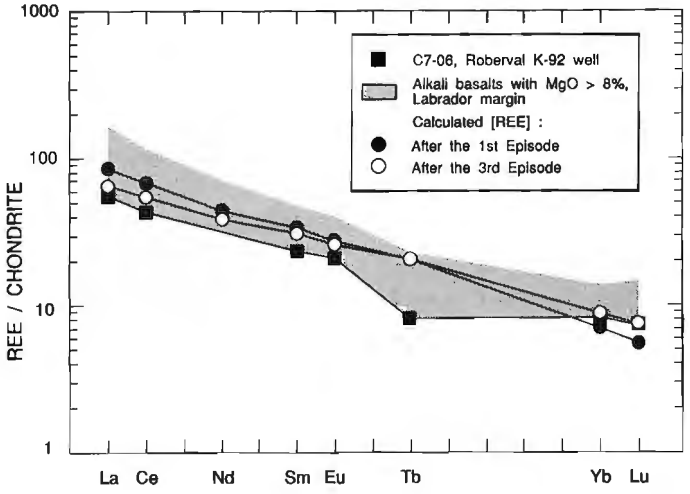

Figure 7. Comparison of chondrite-normalized REE patterns of alkali basalts sampled at the Roberval K-92 well (shown by squares) with abundances calculated by assuming a primitive mantle source, Tm = 1450°C; β = 2 and δ = 10; and three episodes of extension over a period of 45 Ma (all other input parameters in Dehler and Keen, 1993; or Keen et al., 1994). Calculated concentrations do not vary significantly during rifting, as shown by data for the 1st and 3rd stretching episodes (circles; 2nd episode values are intermediate between N1 and N3). The shaded field shows the range of REE abundances in six representative samples of core from other exploration wells (alkali basalts with MgO > 8%; Williamson et al., unpub. data).

melts are typical of alkali basalts (e.g. episodes 1 and 3, Fig. 7) and do not vary significantly during the three melting events, suggesting that alkaline magmatism would persist throughout the rifting history. This is consistent with observations on the composition of igneous rocks recovered in all the wells (Williamson et al., unpub. data). However, the mantle temperature required for alkaline melts to be generated in the geochemical model is higher by 50°C than that used by Keen et al. (1994) in their melting calculations. This discrepancy invites further research on the competing effects of phase changes with depth vs. higher temperatures in the mantle, both of which influence the depth at which melting can take place in the presence of garnet. Finally, the apparent requirement for high values of δ in our models of alkaline melt generation (Williamson et al., in prep.) must be tested with the complete database for Labrador Sea wells, and supported by geophysical and petrological data from other failed rifts. In spite of these outstanding questions, the geochemical calculations provide a good match to the observations and confirm the importance of including the time-dependence of rifting in lithospheric stretching and decompression melting models.

CONCLUSIONS

Preliminary results of modelling the volume and rare-earth concentrations of magmas generated during decompression melting suggest that geochemical data on igneous rocks can be used to evaluate the physical assumptions used in subsidence analyses of rift basins. Studies of model input parameters show that the calculated rare-earth concentrations are most sensitive to temperature and degree of stretching in the upper mantle, and to details of the rifting history. The model is capable of generating alkaline melts, given moderately high mantle temperatures and large amounts of mantle stretching during the rifting stage. A preliminary application of the model to the rifted margin off eastern Canada suggests that these conditions may have existed during rifting in the Labrador Sea.

Our intention was to devise a simple yet flexible numerical approach that would allow us to evaluate the hypotheses proposed for the evolution of rift basins using petrological data. The sensitivity studies and limited applications performed to date suggest that the model is capable of simulating a realistic range of physical and chemical conditions in rifted lithosphere. It may be possible in future to include other trace elements, such as noble metals, that remain geochemically coherent during the partial melting process (e.g. Lorand et al., 1993).

ACKNOWLEDGEMENTS

M-C.W. wishes to acknowledge the late Michael J. Keen for direction and encouragement in formulating this project. We are grateful to D.P. McKenzie for providing us with his program to compute melt volumes, and to D.K. Kostopoulos for discussions early in the project. Comments and suggestions by Kevin C. Coflin, Colin A. Murphy, and Mark A. Williamson of AGC were greatly appreciated.

REFERENCES

Bradshaw, T.K., Hawkesworth, C.J., and Gallagher, K.
1993: Basaltic volcanism in the Southern Basin and Range: no role for a mantle plume; Earth and Planetary Science Letters, v. 116, p. 45-62.

Dehler, S.A. and Keen, C.E.
1993: Effects of rifting and subsidence on thermal evolution of sediments in Canada's east coast basins; Canadian Journal of Earth Sciences, v. 30, p. 1782-1798.

Ebinger, C.J.
1989: Tectonic development of the western branch of the East African rift system; Geological Society of America Bulletin, v. 101, p. 885-903.

Galer, S.J.G., Goldstein, S.L., and O'Nions, R.K.
1989: Limits on chemical and convective isolation in the Earth's interior; Chemical Geology, v. 75, p. 257-290.

Giret, A. and Lameyre, J.
1985: Inverted alkaline-tholeiitic sequences related to lithospheric thickness in the evolution of continental rifts and oceanic islands; Journal of African Earth Sciences, v. 3, p. 261-268.

Hanson, G.N.
1980: Rare earth elements in petrogenetic studies of igneous systems; Annual Review of Earth and Planetary Sciences, v. 8, p. 371-406.
Irving, A.J.
1978: A review of experimental studies of crystal/liquid trace element partitioning; Geochimica et Cosmochimica Acta, v. 43, p. 754-770.
Keen, C.E.
1987: Some important consequences of lithospheric extension; in Continental Extensional Tectonics, (ed.) M.P. Coward, J.F. Dewey, and P.L. Hancock; Geological Society Special Publication, no. 28, p. 67-73.
Keen, C.E. and Dehler, S.A.
1993: Stretching and subsidence: rifting of conjugate margins in the North Atlantic region; Tectonics, v. 12, p. 1209-1229.
Keen, C.E., Courtney, R.C., Dehler, S.A., and Williamson, M-C.
1994: Decompression melting at rifted margins: comparison of model predictions with the distribution of igneous rocks on the eastern Canadian margin; Earth and Planetary Science Letters, v. 121, p. 403-416.
Klein, E.M. and Langmuir, C.H.
1987: Global correlations of ocean ridge basalt chemistry with axial depth and crustal thickness; Journal of Geophysical Research, v. 92, p. 8089-8115.
Kostopoulos, D.K.
1991: Melting of the shallow upper mantle: A new perspective; Journal of Petrology, v. 32, p. 671-699.
Kostopoulos, D.K. and James, S.D.
1992: Parameterization of the melting regime of the shallow upper mantle and the effects of variable lithospheric stretching on mantle modal stratification and trace-element concentrations in magmas; Journal of Petrology, v. 33, p. 665-691.
Langmuir, C.H., Klein, E.M., and Plank, T.
1992: Petrological systematics of mid-ocean ridge basalts: Constraints on melt generation beneath ocean ridges; in Mantle Flow and Melt Generation at Mid-Ocean Ridges, (ed.) J. Phipps Morgan, D.K. Blackman, and J.M. Sinton; American Geophysical Union Monograph, no. 71, p. 183-280.
Latin, D. and Waters, F.G.
1992: Basaltic magmatism in the North Sea and its relationship to lithospheric extension; Tectonophysics, v. 208, p. 77-90.
Lorand, J.P., Keays, R.R., and Bodinier, J.L.
1993: Copper and noble metal enrichments across the lithosphere-asthenosphere boundary of mantle diapirs: Evidence from the Lanzo lherzolite massif; Journal of Petrology, v. 34, p. 1111-1140.
McKenzie, D. and Bickle, M.J.
1988: The volume and composition of melt generated by extension of the lithosphere; Journal of Petrology, v. 29, p. 625-679.
McKenzie, D. and O'Nions, R.K.
1991: Partial melt distributions from inversion of rare earth element concentrations; Journal of Petrology, v. 32, p. 1021-1091
Naldrett, A.J.
1981: Platinum-group element deposits; Canadian Institute of Mining and Metallurgy, Special Issue, no. 23, 197-231.
Niu, Y. and Batiza, R.
1991: An empirical method for calculating melt compositions produced beneath mid-ocean ridges: Application for axis and off-axis (seamounts) melting; Journal of Geophysical Research, v. 96, p. 21 753-21 777.
Pe-Piper, G. and Jansa, L.F.
1987: Geochemistry of Late Jurassic-Early Cretaceous igneous rocks on the eastern North American margin; Geological Society of America Bulletin, v. 99, p. 803-813.
Pe-Piper, G., Jansa, L.F., and Lambert-Robert, St.-J.
1992: Early Mesozoic magmatism on the eastern Canadian margin: Petrogenetic and tectonic significance; Geological Society of America Special Paper, no. 268, p. 13-36.
Perry, F.V., Baldridge, W.S., and DePaolo, D.J.
1988: Chemical and isotopic evidence for lithospheric thinning beneath the Rio Grande rift; Nature, v. 332, p. 432-434.
Ro, H.E. and Faleide, J.I.
1992: A stretching model for the Oslo Rift; Tectonophysics, v. 208, p. 19-36.
Shaw, D.M.
1970: Trace element fractionation during anatexis; Geochimica et Cosmochimica Acta, v. 34, p. 237-243.
Sun, S.-S. and McDonough, W.F.
1989: Chemical and isotopic systematics of oceanic basalts: Implications for mantle composition and processes; in Magmatism in the Ocean Basins, (ed.) A.D. Saunders and M.J. Norry; Geological Society Special Publication, no. 42, p. 313-345.
White, R.S. and McKenzie, D.
1989: Magmatism at rift zones: the generation of volcanic continental margins and flood basalts; Journal of Geophysical Research, v. 94, p. 7685-7,730.
White, R.S., McKenzie, D., and O'Nions, R.K.
1992: Oceanic crustal thickness from seismic measurements and rare earth element inversions; Journal of Geophysical Research, v. 94. p. 19 683-19 715.
Williamson, M-C., Courtney, R.C., Keen, C.E., and Dehler, S.A.
1992: Melt production, composition and emplacement at Atlantic-type margins; Eos, v. 73, no. 43, p. 542.
Wilson, M.
1993: Magmatism and the geodynamics of basin formation; Sedimentary Geology, v. 86, p. 5-29.

Geological Survey of Canada Project 800034

Experiences with concrete pads for calibrating gamma-ray spectrometers

R.L. Grasty
Mineral Resources Division

Grasty, R.L., 1994: Experiences with concrete pads for calibrating gamma-ray spectrometers; in Current Research 1994-E; Geological Survey of Canada, p. 259-263.

Abstract: Experiments have shown that above an energy of about 500 keV, the gamma-ray spectra from small calibration pads 1 m x 1 m x 30 cm accurately represent the spectral shapes from simulated homogeneous infinite sources. Below this energy, the pad spectra lack the downward scattered "skyshine" component. Outdoor portable gamma-ray spectrometer measurements showed that in utilizing the low energy part of spectrum, consideration must also be given to ^{137}Cs gamma-radiation at 662 keV from atomic weapons testing.

Résumé : Des expériences ont révélé qu'au-dessus d'une énergie d'environ 500 keV, les spectres des rayons gamma issus des petits blocs d'étalonnage de 1 m sur 1 m sur 30 cm représentent exactement les formes spectrales associées à des sources homogènes infinies simulées. Au-dessous de cette valeur, les spectres du bloc ne contiennent pas la composante diffusée vers le bas («effet de ciel»). Des mesures effectuées à l'aide d'un spectromètre transportable à rayons gamma ont indiqué que, lorsqu'on utilise la partie des faibles énergies du spectre, on doit également tenir compte des rayons gamma émis par le Cs^{137} à 662 keV lors des essais d'armes atomiques.

INTRODUCTION

The Geological Survey of Canada has been involved with the calibration of ground and airborne gamma-ray spectrometers since it constructed the first calibration facility for airborne spectrometers in 1968 (Grasty and Darnley, 1971). Similar calibration facilities have now been constructed in many countries throughout the world. Airborne facilities, usually four or five large concrete slabs or pads about 8 m x 8 m x 0.5 m thick with known concentrations of potassium, uranium and thorium have been constructed in ten countries. Calibration facilities for portable gamma-ray spectrometers are typically 1 to 3 m across and 0.5 m deep and installed permanently in the ground.

Because of their large size, calibration pads for aircraft are expensive to build. In addition, there are several problems associated with their construction and use. One of the main problems is distributing small amounts of uranium and thorium ores uniformly through the concrete (Corner et al; 1979). Another problem is that many of the uranium pads lose some of their radon with a resultant loss in gamma-ray activity (Løvborg et al; 1978).

The Geological Survey of Canada has recently been experimenting with small transportable pads 1 m x 1 m x 30 cm which weigh approximately 700 kg (Grasty et al; 1991). Because these pads are small, it is easier to make them uniform and their radioelement concentrations can be accurately determined. Consequently, in using these pads, the calibration constants can be measured accurately. Problems of radon loss from the uranium pad have also been overcome by using a uranium-rich slag of calcium silicate which was a byproduct from a phosphorus processing plant.

Experiments with these small pads have shown that they give the same potassium, uranium, and thorium spectral shapes as the much larger aircraft calibration pads (Grasty et al; 1991). Consequently these small transportable pads can be used for calibrating large volume airborne systems as well as portable gamma-ray spectrometers. Small transportable pads are an effective and inexpensive way of calibrating both ground and airborne gamma-ray spectrometers. This paper describes the results of some experiments utilizing these smaller transportable pads which illustrate both their use and limitations in portable gamma-ray spectrometry.

THEORY

From measurements on a calibration pad, the count rates, N_i, in channel i, of a multi channel gamma-ray spectrometer are given by:

$$N_i = S_{Ki} \times K_c + S_{Ui} \times U_c + S_{Ti} \times T_c + B_i \ldots\ldots (1)$$

where K_c, U_c and T_c are the potassium, uranium and thorium concentrations of the pad and B_i is the background count rate of channel i, which arises from cosmic radiation, the radioactivity of the equipment and radon decay products in the air and also radiation from the ground surrounding the pad. The parameters S_{Ki}, S_{Ui} and S_{Ti} are the sensitivities of channel i to unit concentration of each radioelement.

Equation 1 has four unknowns. From measurements on four calibration pads with known concentration of potassium, uranium, and thorium, the three sensitivities, S_{Ki}, S_{Ui} and S_{Ti}, can then be determined.

Figures 1, 2, and 3 show the potassium, uranium and thorium gamma-ray spectra calculated from a series of 1000 second measurements on transportable calibration pads in Ottawa, Canada, using a 256-channel gamma-ray spectrometer manufactured by Exploranium Ltd. of Toronto. The detector was a standard 7.6 x 7.6 cm sodium iodide crystal and each channel covered an energy range of approximately 12 keV. The standard potassium, uranium and thorium windows used to measure the concentrations of potassium, uranium and thorium in the ground are shown in the three figures.

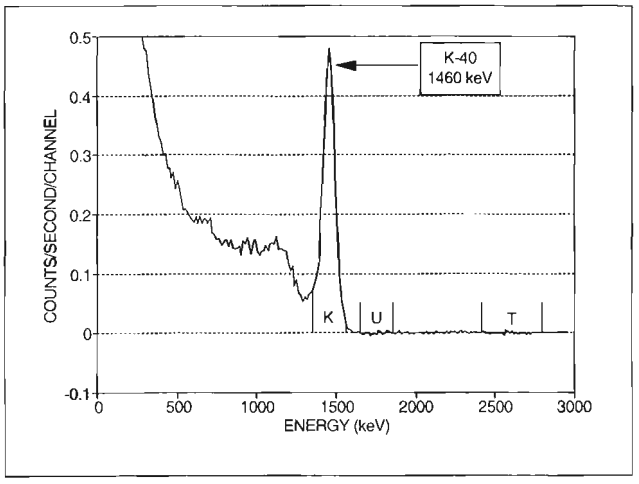

Figure 1. A potassium spectrum for a 7.6 x 7.6 cm detector calculated from measurements on transportable pads.

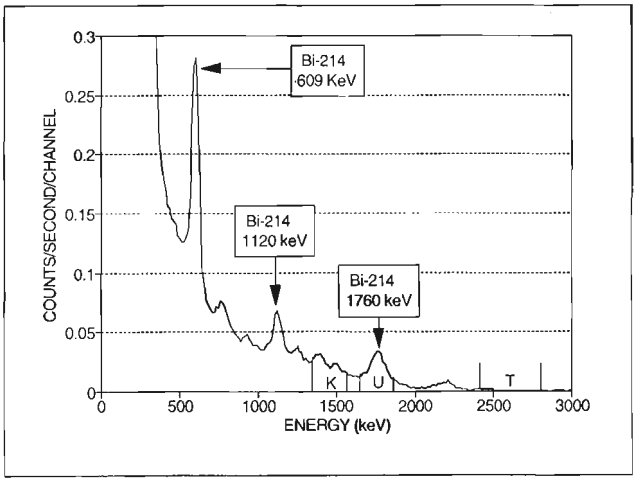

Figure 2. A uranium spectrum for a 7.6 x 7.6 cm detector calculated from measurements on transportable pads.

MEASUREMENT OF SKYSHINE

In any field measurement, some fraction of the total gamma-ray flux originates from gamma-rays emitted from the ground which are Compton scattered in the air and deflected back towards the ground. In the process of scattering, these gamma-rays lose energy. The amount of energy lost is dependent on the angle of scattering and on the initial energy of the gamma ray. ^{208}Tl gamma rays at 2614 keV from the thorium series have the highest energy in the natural spectrum and travel on average about 140 m in the air before suffering a Compton collision. Consequently, the downward scattered flux or "Skyshine" originates from sources in the ground which are several hundred metres from the point of detection. Because of the small size of all calibration pads, virtually no downward scattered flux from the pads can be detected when measurements are made on them.

In the energy range 400 to 2600 keV, Compton scattering is the predominant absorption process occurring in the air. This is also true for materials with low atomic number. A skyshine component can be generated on calibration pads, by placing suitable material over the detector. Gamma rays from the pad will be scattered downwards by the material above the detector and can be measured. The material above the detector simulates a concentrated mass of air, thereby producing a radiation field with the same angular distribution as that obtained over an infinite source.

In the summer of 1991, a series of gamma-ray spectra measurements were made on the four transportable pads in Ottawa using the GR-256 portable gamma-ray spectrometer. The skyshine component was generated using approximately 20 cm of plaster board (essentially calcium sulphate) above the detector as illustrated in Figure 4. Figures 5, 6, and 7 show

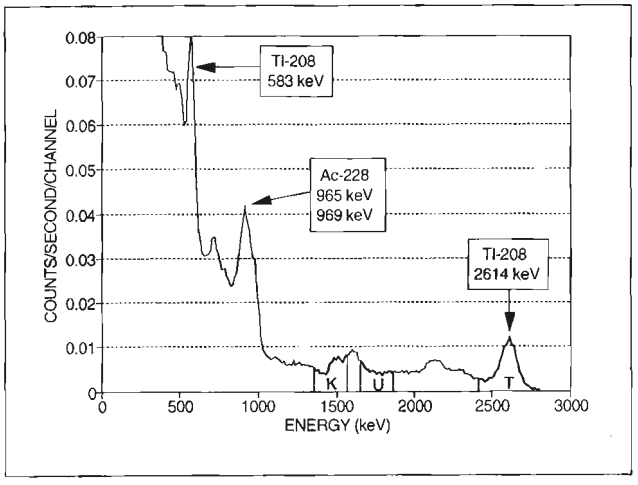

Figure 3. A thorium spectrum for a 7.6 x 7.6 cm detector calculated from measurements on transportable pads.

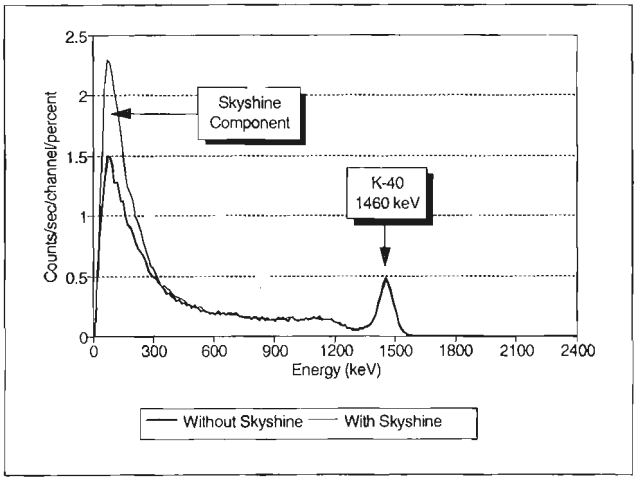

Figure 5. A comparison of potassium spectra with and without skyshine.

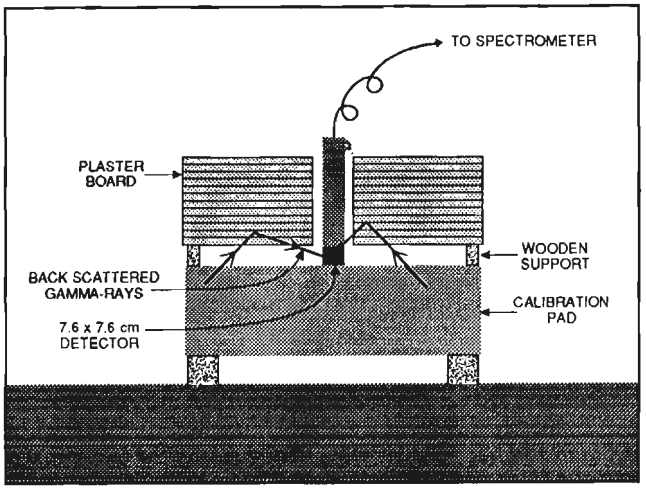

Figure 4. A schematic diagram of the "Skyshine" experiment.

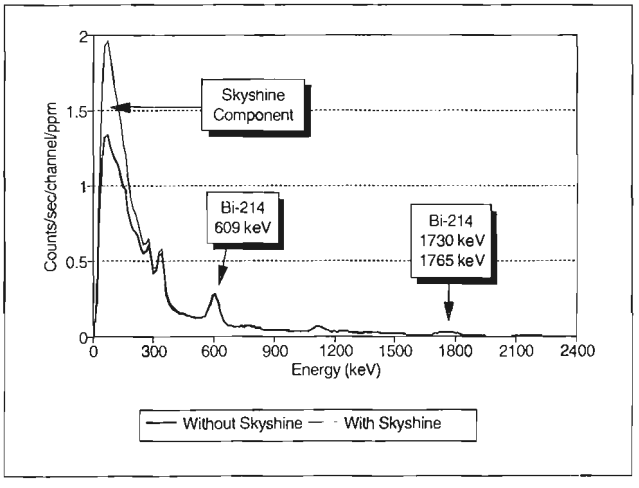

Figure 6. A comparison of uranium spectra with and without skyshine.

the potassium, uranium, and thorium spectra, with and without skyshine. These spectra were calculated using equation (1) from 1000 second measurements on each pad.

Figures 5, 6, and 7 show that the skyshine component only becomes significant below an energy of around 500 keV. Above this energy gamma-ray spectra from the calibration pads should therefore accurately represent the gamma-ray spectra from homogeneous infinite sources of potassium, uranium, and thorium.

COMPARISON OF FIELD AND PAD SPECTRA

In the summer of 1991 a gamma-ray spectrum was recorded outside the Geological Survey of Canada in Ottawa. The spectrum was compared to the potassium, uranium and thorium spectra from the calibration pads shown in Figures 1, 2, and 3. These gamma-ray spectra, and a background contribution measured on the nearby Ottawa River, were fitted to the measured spectrum. The fit was carried out above an energy of 1200 keV.

Figure 8 shows that the measured and fitted natural spectra show good agreement above an energy of around 800 keV. However, below this energy, the fit is poor due to the presence of small amounts of ^{137}Cs originating from atomic weapons fallout. The ^{137}Cs photopeak at 662 keV is shown in Figure 8 and appears on the shoulder of the 609 keV peak of ^{214}Bi.

The fallout spectrum from ^{137}Cs is shown as a difference spectrum in Figure 9 which was obtained by subtracting the measured and fitted natural spectrum. The ^{137}Cs originates from an estimated 2.5 kBq/m^2 of ^{137}Cs and demonstrates the effectiveness of the spectral fitting method in areas of low

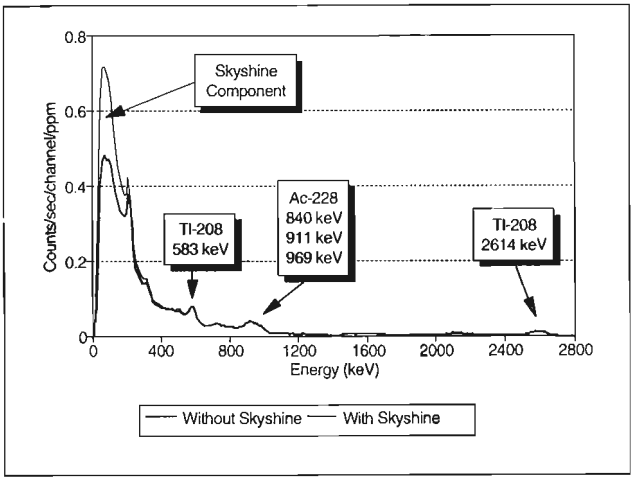

Figure 7. A comparison of thorium spectra with and without skyshine.

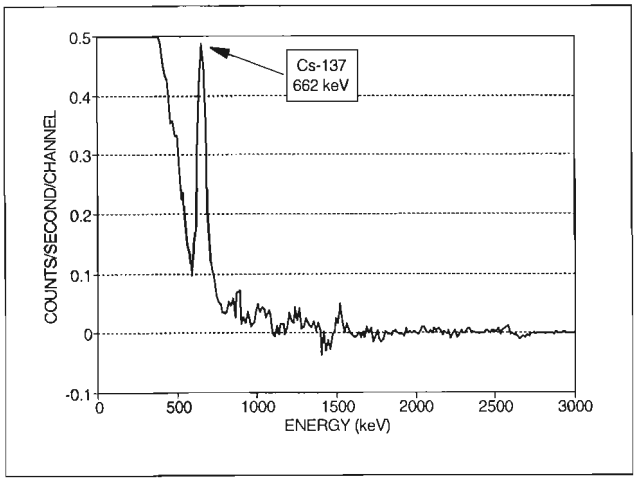

Figure 9. The fallout spectrum obtained by subtracting the natural gamma-ray spectrum from the measured spectrum.

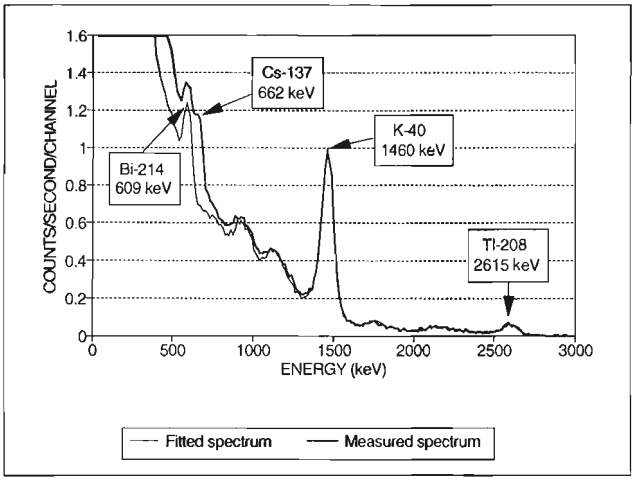

Figure 8. A computer fit above 1200 keV of the potassium, uranium and thorium spectra to a spectrum measured in Canada.

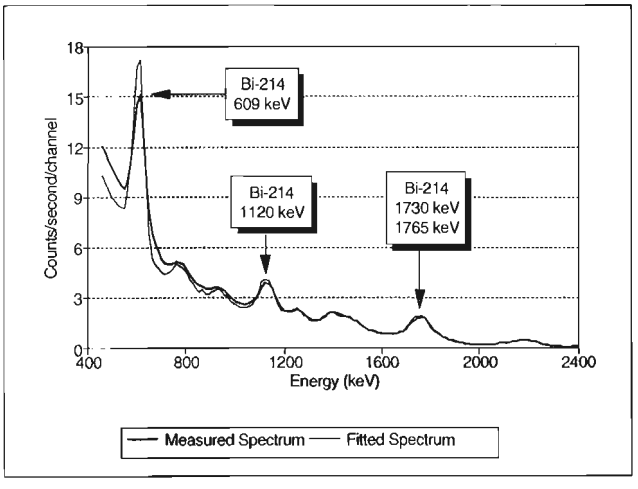

Figure 10. A computer fit of the potassium, uranium and thorium spectra to a spectrum from a buried uranium source.

fallout. The results show that in utilizing the full gamma-ray spectrum, consideration must be given to the small fallout component due to atomic weapons testing.

Measurements were also made over a buried uranium source near Ottawa where the apparent uranium concentration at the surface was measured as several hundred parts per million (ppm). Figure 10 shows a computer fit above 1200 keV of the potassium, uranium, and thorium spectra to the measured spectrum. At the high energy part of the spectra, the fit is extremely good. However, this is not the case at the low energy end, where there is a build-up of scattered gamma radiation from the buried uranium source. The gamma-ray photopeak from the buried uranium source is also somewhat depressed compared to the potassium, uranium, and thorium spectra obtained from the pads.

The results show that there is a greater attenuation of low energy gamma-radiation from the buried source compared to the pad spectra which are effectively uniform sources of radioactivity. There is also a greater build-up of scattered high energy gamma radiation from the buried uranium source compared to a uniform source. The spectral shape can therefore be used to indicate if there is a radioactive source below the ground.

CONCLUSIONS

The following conclusions can be made based on the results of the experiments described:

1. Gamma-ray spectra from calibration pads accurately represent uniformly homogeneous sources above an energy of around 500 keV. Below this energy, the pad spectra lack a downward scattered "skyshine" component and will not represent field gamma-ray measurements.
2. In using the low energy part of the spectrum, consideration must be given to the presence of small amounts of ^{137}Cs from atomic weapons testing.
3. A comparison of the measured spectrum to the spectra obtained from calibration pads can indicate if the measured spectrum originates from a buried source of radioactivity.

REFERENCES

Corner, B., Toens, P.D., Richards, D.J., Van As, D., and Vleggar, C.M.
1979: The Pelindaba facility for calibrating radiometric field instruments; Atomic Energy Board, Pretoria, Report PEL-268, 23p.

Grasty, R.L. and Darnley, A.G.
1971: The calibration of gamma-ray spectrometers for ground and airborne use; Geological Survey of Canada, Paper 71-17, 27 p.

Grasty, R.L., Holman, P.B., and Blanchard, Y.B.
1991: Transportable calibration pads for ground and airborne gamma-ray spectrometers; Geological Survey of Canada, Paper 90-23, 25 p.

Løvborg, L., Bøtter-Jensen, L., and Kirkegaard, P.
1978: Experience with concrete calibration sources for radiometric field instruments; Geophysics, v. 43, p. 543-549.

Geological Survey of Canada Project 880029

Petroleum resource assessments – a fractal approach

Felix C. Lee[1] and P.J. Lee
Institute of Sedimentary and Petroleum Geology, Calgary

Lee, F.C. and Lee, P.J., 1994: Petroleum resource assessments – a fractal approach; in Current Research 1994-E; Geological Survey of Canada, p. 265-270.

Abstract: Possible applications of the property of fractal self-similarity in the petroleum assessments of a single natural population are considered. Among the fractal functions tested, the power function ($Y=X^{\beta}$) is the most versatile. Using this function, one can predict yet-to-be discovered oil and gas pools within a population.

Résumé : La propriété de l'autosimilarité fractale est considérée en vue de son application aux évaluations pétrolières d'une population naturelle unique. Parmi les fonctions fractales testées, la fonction $Y = X^{\beta}$ est la plus versatile. À l'aide de cette fonction, on peut avoir un aperçu des gisements de pétrole et de gaz d'une population qui n'ont pas encore été découverts.

[1] University of Calgary, 2500 University Drive N.W., Calgary, Alberta T2N 1N4

INTRODUCTION

The advantages of fractal geometry include its superior detail and its relative simplicity. Using a fractal function, a simple algorithm can create an entire image that otherwise could not be produced from conventional geometry, unless an array of complex functions were to be applied over a short interval (Barnsley et al., 1988; Devaney and Keen, 1989).

Self-similarity plays a key role in fractal distribution. An object that displays self-similarity appears to be replicated whatever the magnification. Take the form of a fern leaf, for example. When viewed individually, each leaf bears a striking resemblance to the frond as a whole. The principles of fractal geometry allow us to create mathematical replications. To create a model of a self-similar object using the fractal property, the computer needs the following information: (1) the data required to create a model of a self-similar object; (2) the scale at which the part is relative to the whole; and (3) the pattern of arrangement. Thus, fractal geometry can be used to describe complex structures. A comparison of fractal and Euclidean geometry is given in Table 1.

Basic fractal properties are not new. Mathematicians were turning to fractal geometry at the turn of the century to explain observed phenomenon. The von Koch Snowflake curve (Fig. 1) is an excellent example. The figure begins as a straight line (Fig. 1A), which is then divided into three equal sections. An equilateral triangle is then erected in the middle section, and one iteration is completed (Fig. 1B). Usually this sequence is repeated for each line segment until it is impossible to continue (Fig. 1C). Magnifying any section of the figure results in a picture exactly the same as the parent figure (i.e., self-similarity).

Barton et al. (1991) and Scholz and Barton (1991) applied fractals to the analysis of the size and spatial distributions of hydrocarbon deposits. La Pointe (1993) also applied fractal geometry to assessments. Likewise, many natural phenomena in the world exhibit properties that can be described using a fractal paradigm. This paper will attempt to show that fractal properties can be used to predict the missing members of a single naturally occurring population. The method described here can be used to predict a single dimension of the population (e.g., numerical area, volume, or length). In this study, oil and gas pool volumes from the Western Canada Sedimentary Basin are used to examine the behaviour of the fractal properties that may exist.

From his 1992 Canada-wide Science Fair project, the senior author found that some types of geographic data sets obey the self-similarity property. Subsequently, the procedure was tested using more petroleum data sets.

PREDICTION PROCEDURE

The normal course of any prediction procedure is to explain and make predictions from a specific single and natural population. Fractal prediction does not differ in this basic requirement.

Figure 2 explains the property of self-similarity, which consists of the function line y=x and the function y=f(x). The algorithm that may be used to generate the points (X_1, Y_1), (X_2, Y_2), and so on can be summarized in the following equations:

$$\begin{aligned} X_i &= Y_i, \text{ for } i=0, 2, 4, \ldots \\ Y_i &= f(X_i), \text{ for } i=1, 3, 5, \ldots \\ X_{i+1} &= Y_i, \text{ for } i=1, 3, 5, \ldots \end{aligned} \quad (1)$$

Table 1. Comparison of Euclidean and fractal geometry.

Euclidean	Fractal
Traditional (over 2000 years old)	Modern (approx. 10 years old)
Based on characteristic size or scaling	No specific size or scaling
Described by formulas	Recursive algorithm

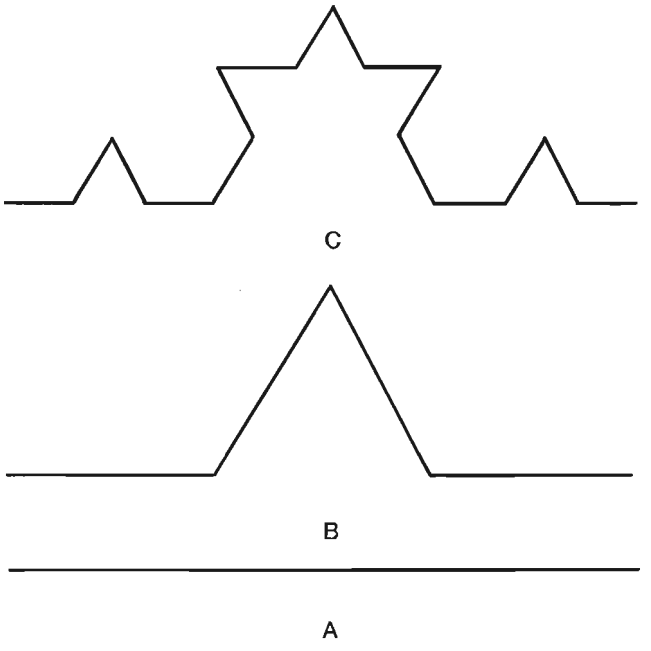

Figure 1. Development of the von Koch Snowflake curve.

If the largest member of population (X_0 , Y_0) is known, then the remaining members of the population may be predicted using the self-similarity property of fractal analysis. The values X_i , where i=2, 4, 6, ..., are the predicted values of the population.

There are a number of functions that have been tested as follows:

$$\text{Power function: } Y=X^{\beta}; \qquad (2)$$

$$\text{Inverse hyperbolic sine: } Y=\sinh^{-1} X;$$

$$\text{Hyperbolic sine: } Y=\sinh X; \text{ and}$$

$$\text{Inverse natural logarithm: } Y=e^{X}.$$

The prediction procedure was executed by a computer program that requires the following input: the type of function; the value of β (for the power function); and the largest value from the population. From this input, a predicted set of values for the population is generated.

The largest value is represented by (X_0 ,Y_0) where X is equal to Y (Fig. 2) and therefore rests on the Y=X line. This value must be known in order to predict the remaining members of the set. The function curve below the Y=X line is determined by the type of function chosen at the start of the program. In the case of the hyperbolic sine and inverse natural logarithm, the function curve is above the Y=X line. The first point to be calculated on the function curve is (X_1 , Y_1). Therefore, $X_1=X_0$ and $Y_1=f(X_1)$. The second point calculated is (X_2 , Y_2), which is also the first predicted member of the set. Further, $X_3=X_2$, and $Y_3=f(X_3)$. This procedure is repeated until all the required predictions have been made.

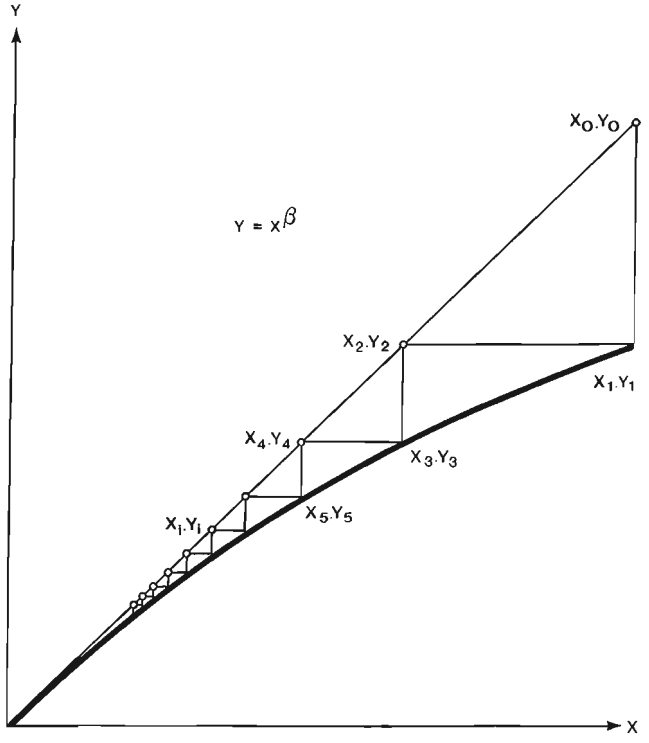

***Figure 2.** Graphic representation of the power function and its application to fractal predictions.*

The hyperbolic sine and inverse natural logarithm differ slightly in that their function curves are above the Y=X line. In these cases, (X_1 ,Y_1) would be calculated as $X_1=X_0$ and $Y_1=X_1$. Further, $Y_2=X_2$ and $X_2=f^{-1}$ (Y_2). Calculations are performed in this order for the remaining members of the set.

The procedure for determining the value of β for the power function is the "trial and error" method. An arbitrary value is assigned to β, and is tested to see whether or not one can predict some of the known members. If not, other β values are tested until a suitable β value is obtained.

THE RATIO PROPERTY

A population consists of N members as follows:

$$X_1 , X_2 , \ldots\ldots X_i , X_{i+1} , \ldots\ldots , X_N . \qquad (3)$$

If the series is arranged in descending order (i.e., $X_i > X_{i+1}$) then there are a number of relationships between two adjacent members.

The power function states that:

$$\frac{X_i}{X_{i\ 2}} = X_0^{\beta^{i/2}\ \ \beta^{(i+2)/2}} \qquad (4)$$

where i=0, 2, 4, 6, 8, ...; and β is constant and is called a fractal dimension. The power function behaves as a lognormal distribution when β tends to zero.

The Pareto distribution states that if the members of the population are grouped into classes, then the ratio between two adjacent classes forms the following relation:

$$N_i / N_{i+1} = C^{\beta}, \qquad (5)$$

where C and β are constants. When C=2, then it becomes a log-geometric distribution. Schuenemeyer and Drew (1983) have suggested that the ratio between two adjacent classes of a log-geometric distribution remains constant throughout the entire population of Denver basin oil fields.

Zipf (1949) counted word frequencies used in storybooks and found that the ratio of the most frequently used word to the second most frequently used word exhibits a definite relationship which can be generalized as follows:

$$X_i / X_{i+1} = [i / (i + 1)]^k \qquad (6)$$

where k is constant. Zipf's relationship is a special case of a Pareto distribution. This relationship has been applied to mineral (Folinsbee, 1977) and petroleum (Coustau, 1980) resource assessments.

Lee and Wang (1983) derived a formula for estimating the r-th largest member without specifying a particular probability distribution as follows:

(7)

$$l_r(x) = \sum_{n=r}^{\infty} \sum_{k=r}^{n} \binom{n}{k} H(x)^k [1-H(x)^{n-k}]\ h(x)\ \frac{P(N=n)}{P(N \geq r)}$$

where h(x) is the pool size density function which can be any type of probability distribution (lognormal assumption is optional), H(x) is the cumulative pool size density function, and P(N) is the number-of-pools distribution.

The expectation of the ratio of ranks $r_1 < r_2$ (Lee and Wang, 1985) is:

(8)

$$g(w) = \int_0^{\infty} \frac{\Gamma(r_2)}{\Gamma(r_2-r_1)\Gamma(r_1)} \frac{[H(x)-H(wx)]^{(r_2-r_1-1)} H(wx)^{r_1-1}]}{H(x)^{r_2-1}}\ x\ h(wx)\ f_{r_2}(x)\ dx$$

where pool rank $r_1 > r_2$, h(x) is the pool size density function which can be any type of distribution (lognormal assumption is optional), and H(x) is the cumulative pool size density function.

The following sections report the results derived from the fractal approach and Lee and Wang's approach.

EXAMPLES

The Leduc-Bashaw oil play

The data set is comprised of oil pools from the Leduc-Bashaw oil play within the Western Canada Sedimentary Basin. From the information given, the fractal model predicts the top ten largest oil pools when the largest pool size is known. In this case, the β value is 0.91. The predictions made by Podruski et al. (1988) and by the fractal approach are listed in Table 2. As one can observe, these two predictions are indeed very similar.

In the case of the Western Canada Sedimentary Basin oil pool data set, fractal predictions were less satisfactory. A possible explanation for this discrepancy is that the combination of distinct oil pools from different natural populations results in an unnatural and heterogenous population. Consequently, the fractal procedure proposed in this paper is restricted to predictions of petroleum or mineral resources in homogenous populations.

The Cranberry gas play

The Cranberry gas play data set, from the Western Canada Sedimentary Basin, was also used for the prediction using the fractal approach and a β value of 0.95 (Table 3). Again, the predictions are very similar to those predicted by Reinson et al. (1993).

Table 2. Comparison of pool sizes predicted from the lognormal and fractal models for the Leduc-Bashaw oil play.

Pool rank	Pool size (10^6 m^3)		
	Original data	Predicted by the lognormal model (0.9 probability)	Predicted by the fractal model
1	19.70	-	-
2	15.00	-	15.06
3	13.10	-	11.80
4	6.39	-	9.45
5	6.19	-	7.72
6	6.15	-	6.42
7	-	3.8 - 6.0	5.43
8	-	3.5 - 4.6	4.67
9	-	3.4 - 4.2	4.06
10	3.00	-	3.58

Table 3. Comparison of pool sizes predicted from the lognormal and fractal models for the Cranberry gas play.

Pool rank	Pool size (10^6 m^3)		
	Original data	Predicted by the lognormal model (0.9 probability)	Predicted by the fractal model
1	14,260	-	-
2	-	3996 - 13,273	8838
3	-	3100 - 9405	5971
4	-	2666 - 6532	4329
5	-	2419 - 4735	3325
6	-	2294 - 3508	2678
7	2276	-	2243
8	-	1704 - 2258	1940
9	-	1539 - 2143	1761
10	-	1444 - 1956	1561

Table 4. Continental area, human population, and river length.

Continent name	Human population (billions)	
	Actual	Predicted
β^=0.62		
Asia	2.7	-
Europe	0.7	0.8
Africa	0.5	0.4
N. America	0.4	0.2
S. America	0.2	0.2
Australia	0.1	0.1
Pacific Is.	0.1	0.1
Continent name	**Area (10^6 km^2)**	
	Actual	**Predicted**
β^=0.6		
Asia	44	-
Africa	30	31
N. America	24	23
S. America	18	17
Antarctica	13	13
Europe	10	11
Australia	8	9
River name	**Length (10^3 km)**	
	Actual	**Predicted**
β^=0.98		
Nile (Africa)	6.7	-
Amazon	6.4	6.4
Yangtze	6.4	6.2
Mississippi	6.0	5.9

Continental area, population, and river length

In addition, the property of self-similarity may exist in other types of data sets. The data sets for human population, continental area, and river length (National Geographic Society, 1981) were also used to test the fractal model. As can be observed from Table 4, the predicted values are very close to the actual values.

SUMMARY

It is possible to predict single and natural populations by employing the fractal self-similarity property. Results of the experiments show that the power function is the most versatile.

The use of the fractal power function, however promising, is not without limitations. These include: (1) not all populations tested have this self-similarity property; (2) the procedure is limited to predicting a single dimension (volume, area, or length); and (3) the number of members that obey a fractal pattern is limited to the top few largest members of the populations tested.

It is interesting to note that Lee (1993) has identified some petroleum populations that may obey power normal distributions that are power functions. This may explain why the predictions are so close between the fractal and the GSC lognormal model.

The power function, which is not distinct from other models, may only be applied to the largest few members of a population. Such other models include: Pareto and log-Pareto distributions (Bettini, 1987); Pareto law (Lee, 1993); and Zipf's law (Coustau et al., 1988).

REFERENCES

Barnsley, M.F., Devaney, R.L., Mandelbrot, B.B., Peitgen, H.-O., Saupe, D., and Voss, R.F.
1988: The Science of Fractal Images; Springer-Verlag, p. 14-27.

Barton, C.C., Scholz, C.H., Schutter, T.A., Herring, P.R., and Thomas, W.J.
1991: Fractal nature of hydrocarbon deposits, 2: spatial distribution; American Association of Petroleum Geologists, 1991 Convention abstract; American Association of Petroleum Geologists Bulletin, v. 75, p. 539.

Bettini, C.
1987: Forecasting populations of undiscovered oil fields with the log-Pareto distribution; Ph.D. dissertation, Stanford University, California, 221 p.

Coustau, H.
1980: Habitat of hydrocarbons and field size distribution: a first step towards ultimate reserve-assessment; in Assessment of undiscovered oil and gas; Issued by CCOP Project Office, UNDP Technical Support for Regional Offshore Prospecting in East Asia, Kuala Lumpur, Malaysia, p. 180-194.

Coustau, H., Lee, P.J., Dupuy, J., and Junca, J.
1988: The Jurassic oil resources of the East Shetland basin, North Sea; Bulletin of Canadian Petroleum Geology, v. 36, p. 177-185.

Devaney, R. and Keen, L. (ed.)
1989: Chaos and Fractals; Proceedings of Symposia in Applied Mathematics, v. 39, p. 41-50.

Folinsbee, R.E.
1977: World's view from Alpha to Zipf; Geological Society of America, v. 88, p. 879-907.

La Pointe, P.
1993: Application of fractal geometry to the assessment and exploration for undiscovered hydrocarbon resources (Abstract); International Association for Mathematical Geology, Silver Anniversary Meeting, Prague, October 10-15, 1993, p. 30.

Lee, P.J.
1993: Lognormal and nonparametric discovery process models - reliable tools in petroleum resource assessment?; American Association of Petroleum Geologists, 1993 Convention abstract; American Association of Petroleum Geologists Bulletin, v. 77, p. 136.

Lee, P.J. and Wang, P.C.C.
1983: Probabilistic formulation of a method for the evaluation of petroleum resources; Mathematical Geology, v. 15, p. 163-181.
1985: Prediction of oil or gas pool sizes when discovery record is available; Mathematical Geology, v. 17, p. 95-113.

National Geographic Society
1981: Geographic Comparisons; National Geographic Atlas of the World, p. 234.

Podruski, J.A., Barclay, J.E., Hamblin, A.P., Lee, P.J., Osadetz, K.G., Procter, R.M., and Taylor, G.C.
1988: Conventional oil resources of Western Canada; Geological Survey of Canada, Paper 87-26, 149 p.

Reinson, G.E., Lee, P.J., Warters, W., Osadetz, K.G., Bell, L.L., Price, P.R., Trollope, F., Campbell, R.I., and Barclay, J.E.
1993: Devonian gas resources of the Western Canada Sedimentary Basin, Part I: Geological play analysis and resource assessments; Geological Survey of Canada, Bulletin 452, 157 p.

Scholz, C.H. and Barton, C.C.
1991: The fractal nature of hydrocarbon deposits 1: Size distribution; American Association of Petroleum Geologists, 1991 Convention abstract; American Association of Petroleum Geologists Bulletin, v. 75, p. 668.

Schuenemeyer, J.H. and Drew, L.J.
1983: A procedure to estimate the parent population of the size of oil and gas fields as revealed by a study of economic truncation; Mathematical Geology, v. 15, p. 145-161.

Zipf, G.K.
1949: Human behaviour and the principle of least effort; Addison-Wesley Press, Inc., 573 p.

Geological Survey of Canada Project 750023

An approach to quantitative interpretation of airborne VLF-EM data

Ajit K. Sinha
Mineral Resources Division

Sinha, A.K., 1994: An approach to quantitative interpretation of airborne VLF-EM data; in Current Research 1994-E; Geological Survey of Canada, p. 271-276.

Abstract: Airborne very low frequency electromagnetic (VLF-EM) methods are frequently used in multiparameter airborne geophysical surveys. In general, the measured total field and the vertical quadrature components of the magnetic field are presented as contours or profiles without any attempts at quantitative interpretation. This paper presents the results of mathematical simulation of the airborne VLF-EM response of two-dimensional tabular conductors located within a host rock of finite resistivity, using a network solution technique. The results are used to prepare characteristic diagrams, which may be used for quantitative interpretation of airborne VLF data acquired with a fixed-wing aircraft or helicopter. The procedure requires prior knowledge of the host rock resistivity, which may be obtained from an independent ground or airborne EM survey. The method also requires that total field values be corrected for temporal and spatial variations, using ground VLF monitors.

Résumé : On utilise fréquemment les levés électromagnétiques myriamétriques (VLF-EM, very low frequency electromagnetic) en mode aéroporté dans les études géophysiques multiparamètres. En général, le champ total mesuré et la composante verticale en quadrature du champ magnétique sont présentés comme des contours ou des profils, sans que l'on en entreprenne une quelconque interprétation quantitative. Dans le présent document, les auteurs présentent les résultats d'une simulation mathématique de la réponse (VLF-EM en mode aéroporté) de conducteurs tabulaires à deux dimensions situés dans une roche hôte de résistivité finie, selon une technique de réseau. On utilise ces résultats pour préparer les diagrammes caractéristiques qui peuvent servir à une interprétation quantitative des données de ce type recueillies à l'aide d'un hélicoptère ou d'un avion. La procédure nécessite la connaissance préalable de la résistivité de la roche hôte, que l'on peut obtenir à partir d'un levé électromagnétique distinct au sol ou à bord d'un aéronef. Cette méthode exige aussi la correction des valeurs du champ total quant aux variations temporelles et spatiales à l'aide de moniteurs myriamétriques au sol.

INTRODUCTION

The very low frequency electromagnetic (VLF-EM) method of exploration is a widely used technique for detection of shallow conductors with application in geological mapping, mineral exploration, and engineering investigations. The method uses signals transmitted by powerful radio transmitters in the VLF frequency band (15-30 kHz), located around the world for communication with submerged submarines. Since the method does not require carrying or energizing a transmitter, the VLF systems are light and less expensive to operate than other EM systems.

The airborne VLF method, developed as an outgrowth of the ground VLF method in late 1960s, reached reliability and sophistication with the introduction of total field measuring systems such as Totem 1-A and Totem 2-A in late 1970s (Herz, 1986). These systems measure the total magnetic field and the quadrature component of the vertical magnetic field at one or two frequencies simultaneously. Although data from airborne geophysical systems, such as magnetics or EM using portable transmitters, are normally processed and interpreted to yield geological models of the ground, VLF data are rarely presented in that manner. For practical reasons and because airborne VLF data are generally recorded only at one second intervals, the total field VLF results are simply levelled to a common base by filtering and presented in contour form. The quadrature component is normally presented in profile form. Hence, interpretation of airborne VLF data is still largely qualitative and best suited for reconnaissance surveys.

It has been suggested recently (Sinha, 1990a; Poikonen, 1990) that a totally digital airborne VLF system capable of measuring orthogonal electric and magnetic field components, in theory, should be capable of mapping the ground resistivity and provide reliable data for quantitative interpretation. Such systems have now been built in Canada and Finland (Sinha and Morrison, 1993) and are being evaluated. This paper, however, does not deal with such systems, but is concerned with developing a method of quantitative interpretation for Totem type VLF systems.

Since the frequencies used in VLF surveys are high (15-30 kHz) in comparison to those normally used in EM surveys (generally less than 5 kHz), the depth penetration achieved by this method is somewhat limited compared to that achieved by other EM methods. Still, the depth penetration can be tens of metres in case of moderately resistive ground, and can be 100 m or more over highly resistive ground, typical of Precambrian plutonic terrane without overburden. Because of the generally large distance between the VLF transmitter and the survey area, the primary field in the VLF method behaves like a uniform plane wave and therefore, the method is suitable for detection of long, but weakly conductive structural features as well as good conductors sought in mineral exploration.

Several papers have been published in the last 15 years on methods for quantitative interpretation of ground VLF data (Kaikkonen, 1979; Saydam, 1981; Sinha, 1990b). However, no equivalent work is available for interpretation of airborne VLF data collected by Totem type systems. The purpose of this study was to examine if a practical method of interpretation of airborne VLF data could be developed using the model of a two-dimensional (2-D) tabular conductor in a host rock of finite resistivity, a model that is valid in many mining and engineering applications. To achieve that, the numerical airborne VLF response of many 2-D conductors in resistive host rocks were obtained during this work using the network solution technique (Swift, 1971; Vozoff, 1971) and interpretation diagrams were prepared to determine the depth and conductance (product of conductivity and thickness) of such conductors from airborne VLF data acquired with a Totem type system.

AIRBORNE VLF RESPONSE

The strength of the primary VLF field at any location depends on several factors, such as its distance from the transmitter, the time of the day, and the presence or absence of any atmospheric storms in the area. The primary field close to the transmitter (less than 800 km from the station) is not uniform due to the rapid drop of the intensity of the ground wave field with distance and the interaction of the ground wave and the sky wave fields, which contributes to interference patterns with rapid changes to the primary field intensity over short distances (Watt, 1967). Hence, the primary field can be considered to be a plane wave with reasonably uniform magnitude only if the survey area is at least 800 km from the transmitter, and the survey avoids periods of severe atmospheric disturbances and sunrise and sunset times. There will be, of course, a slow variation of the field with distance, which can be compensated by the use of data from ground VLF monitors. Vallée et al (1992) have reported that for large scale airborne surveys covering several tens of km, several base station monitors may be needed, say every 20-30 kilometres, to achieve the desired accuracies for quantitative interpretation of airborne VLF data.

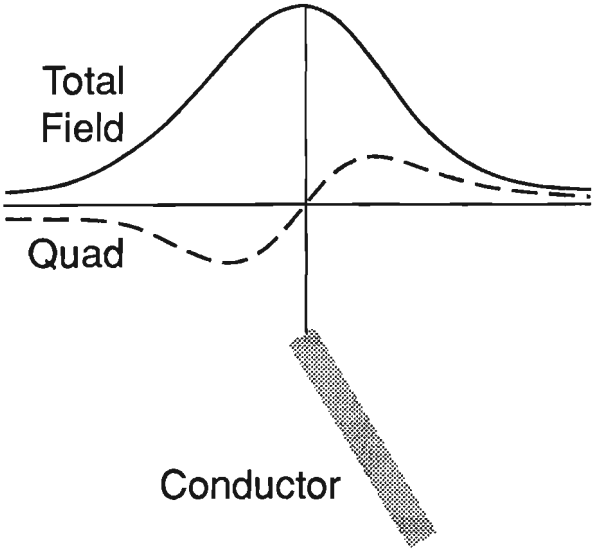

Figure 1. *Airborne VLF-EM anomalies over a 2-D, sheet-like conductor in a total field measuring system.*

Figure 1 shows the nature of airborne VLF response using a total field measuring system over a 2-D, sheet-like, inclined conductor located in a host rock of finite resistivity. The primary VLF field is assumed to be normal to the strike of the conductor. The total field shows a maximum over the conductor, while the vertical quadrature component shows a crossover type response, the crossover point indicating the location of the conductor. The nature of the quadrature response can vary depending on the relative conductivities of the host rock and the conductor, the depth and orientation of the conductor (Sinha, 1990a). For Totem type surveys, the relative strengths of the total field and peak-to-peak quadrature responses are normally presented as percentages of the primary field, which is assumed to be uniform over the survey area. To satisfy this condition for quantitative interpretation of airborne VLF data, the field data must be corrected by transforming the primary field to a uniform value over the entire area by using ground VLF monitors.

VLF MODEL PARAMETERS

The model considered in this study is a 2-D, sheet-like, inclined conductor, located in a host rock of fairly high resistivity, at a finite depth from the ground surface. The assumption about the host rock resistivity is important since if the host rock is conductive, the penetration of VLF energy is severely limited, and a process called "current channelling" dominates over EM induction in the production of VLF anomalies. Presence of conductive overburden in the area can also substantially alter the anomaly and make the application of the VLF method questionable, thereby rendering the interpretation method invalid.

For the modelling, the parameters of the 2-D conductor that are considered are: the depth to the top "d", the dip of the conductor "θ", the depth extent along the dip "ℓ", the conductance "σt", the host rock resistivity "ρ_H", and the altitude of the VLF receiver "H" over the ground. From the computed response, the two primary parameters of the total magnetic field and peak-to-peak vertical quadrature components are normalized by the primary field and expressed as percentages of the primary field. The frequency of the VLF signal was assumed to be 20 kHz for all our modelling.

Numerical modelling was done for two altitudes of the VLF receiver, viz, 120 m and 40 m. An altitude of 120 m is the typical survey altitude of fixed-wing aircrafts like the GSC Skyvan, and 40 m is the average height of the VLF sensor in helicopter installations. Two typical values of the dip of the conductor ($\theta = 90$ and 45 degrees) and three values of the host rock resistivity (ρ_H = 1000, 3000, 10 000 Ω·m) were considered. Five values of the depth to the top of the conductor (d = 0, 10, 20, 30, 50 m) and five values of the conductance of the conductor (σt = 0.5, 1.0, 3.0, 10.0, 20.0 S) were considered in the modelling. The depth extent parameter "ℓ" was taken to be either 10 m or 20 m, since it was observed that its effect on the computed response for values greater than 20 m was small, and often within the noise levels, prevalent in airborne VLF surveys.

Some may consider limiting the value of depth extent to 20 m somewhat restrictive and may wonder how the response would be affected if systems were flown over conductors with greater depth extents (e.g., sulphide ore bodies). Due to high frequencies of VLF systems and consequently limited depth penetration, more so in airborne surveys since the receiver is high above the ground, the anomaly is produced mostly from the top part of the conductor, especially if the depth to the top is finite. Hence, limiting the depth extent to 20 m in airborne VLF modelling is a reasonable and practical assumption.

INTERPRETATION SCHEME

It is obvious that even in the simplest case of a 2-D conductor in a uniform resistive host rock, there are five unknown parameters to be determined, namely, the host rock resistivity, and depth to top, depth extent, conductance, and dip of the conductor. But, there are only two independent parameters (total field and vertical quadrature component) for each frequency of a Totem 2 system. However, a conductor may not even be excited by one of the frequencies because of its orientation, thus reducing the number of known parameters to two. Hence, it is not possible to interpret all unknown parameters without some prior information about the nature

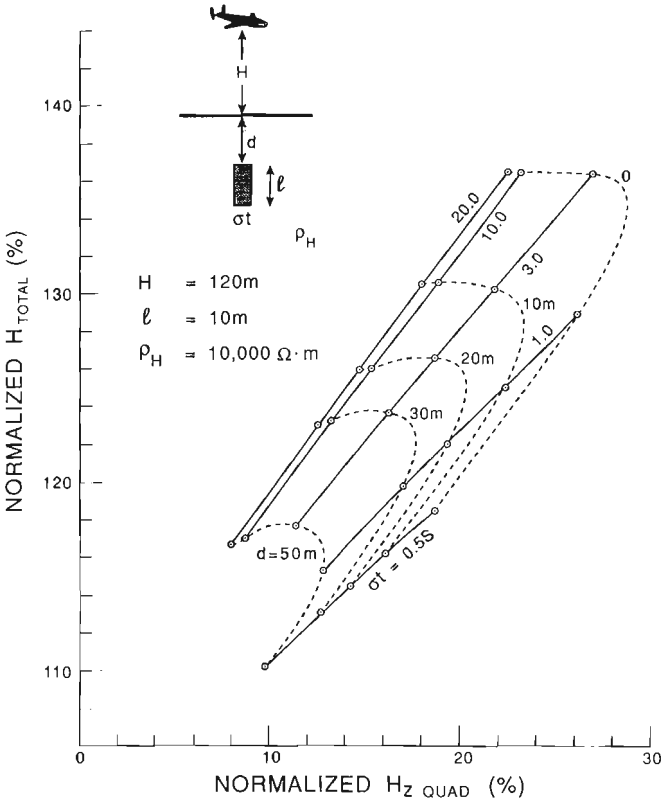

Figure 2. Plot of the normalized total field and vertical quadrature components over a 2-D conductor with a depth extent of 10 m at an altitude of 120 m for a host rock resistivity of 10 000 Ω·m.

of the conductor and the host rock resistivity, which can be obtained from geological information and an independent resistivity survey.

After a few trial runs, it became obvious that the effects of the dip of the conductor on the computed airborne VLF response was very small. This was not surprising, since this effect was rather small even in the case of ground VLF modelling (Sinha, 1990b). In the case of airborne VLF, the receiver is effectively at a greater distance from the conductor, which attenuates and smooths out the response from the conductor, thereby reducing the effect of dip even more. Hence, the effect of dip was not considered further in this study, and the interpretation scheme that follows is applicable to vertical as well as dipping conductors.

Figure 2 shows a plot of the normalized total field and vertical quadrature components expressed as percentages of the primary field over a vertical conductor for a VLF receiver altitude of 120 m to represent a fixed-wing aircraft. The host rock resistivity is assumed to be 10 000 Ω·m, typical of Precambrian granitic terrane without overburden and the depth extent is assumed to be 10 m. Using a diagram like this, one can interpret the depth and conductance of the conductor if its depth extent and host rock resistivity are known. Figure 3 shows a similar plot for a conductor with depth extent of 20 m. The two plots are quite similar. In fact, if one used the plot for 10 m depth extent to interpret field data over a conductor with 20 m depth extent, the error in depth estimation will be less than 5% except for high conductance conductors, but the conductance value will be overestimated by up to 300% for highly conductive conductors. Therefore, if a rough estimate of the depth extent of the conductor is available from borehole or surface geological mapping or from a ground VLF survey, interpretation diagrams such as the ones shown in Figures 2 and 3 can be used effectively.

Some may argue that it is difficult, or even impossible, to estimate the depth extents of conductors in a large survey. But, even if such information is unavailable, one may still use an interpretation diagram, say for ℓ=10 m, to obtain a fairly good estimate of the depth to the top of the conductor and at least a qualitative estimate of its conductance. In a large scale airborne survey, one is more interested in knowing the range of the conductances of the conductors, rather than their absolute values, to distinguish, say, graphitic or sulphide bodies from water-filled fracture and shear zones. Thus, even if the estimates of the conductances are off by 100 or 200% due to incorrect choice of the depth extent parameter, such information can be of great value for follow-up surveys on the ground.

Figures 4 and 5 illustrate interpretation diagrams plotted for two depth extent values of 10 and 20 m respectively, when the altitude of the VLF receiver is 40 m, typical of a helicopter installation. The host rock resistivity is again assumed to be 10 000 Ω·m. Since the receiver is much closer to the conductor, the anomaly amplitudes are significantly higher in this

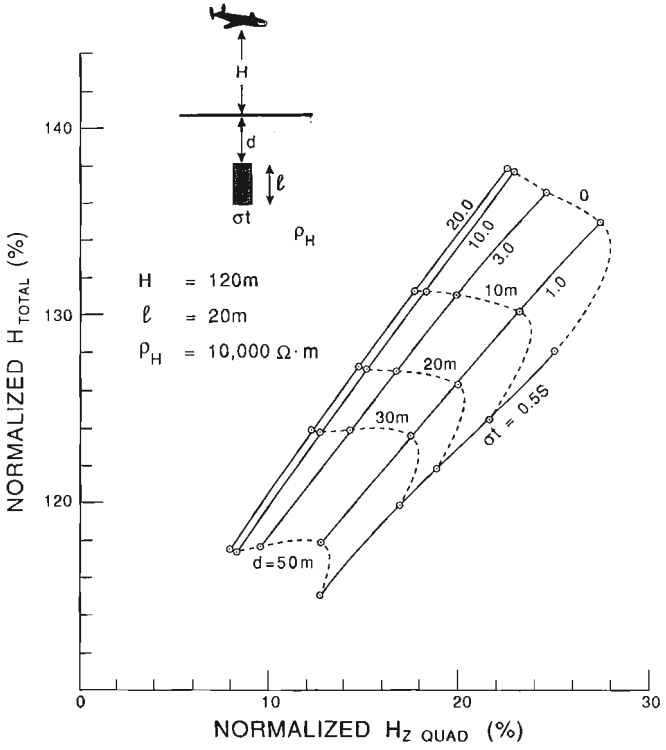

Figure 3. Plot of the normalized total field and vertical quadrature components over a 2-D conductor with a depth extent of 20 m at an altitude of 120 m for a host rock resistivity of 10 000 Ω·m.

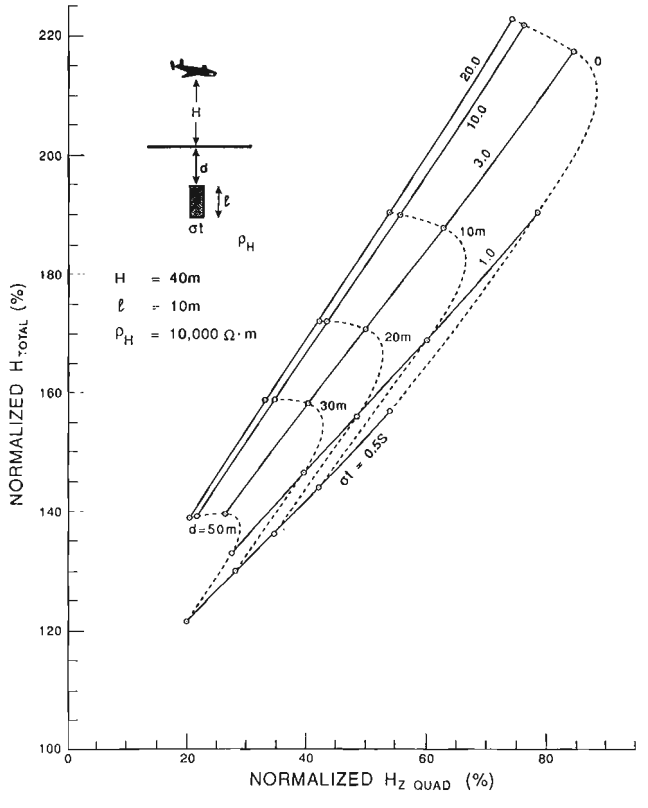

Figure 4. Plot of the normalized total field and vertical quadrature components over a 2-D conductor with a depth extent of 10 m at an altitude of 40 m for a host rock resistivity of 10 000 Ω·m.

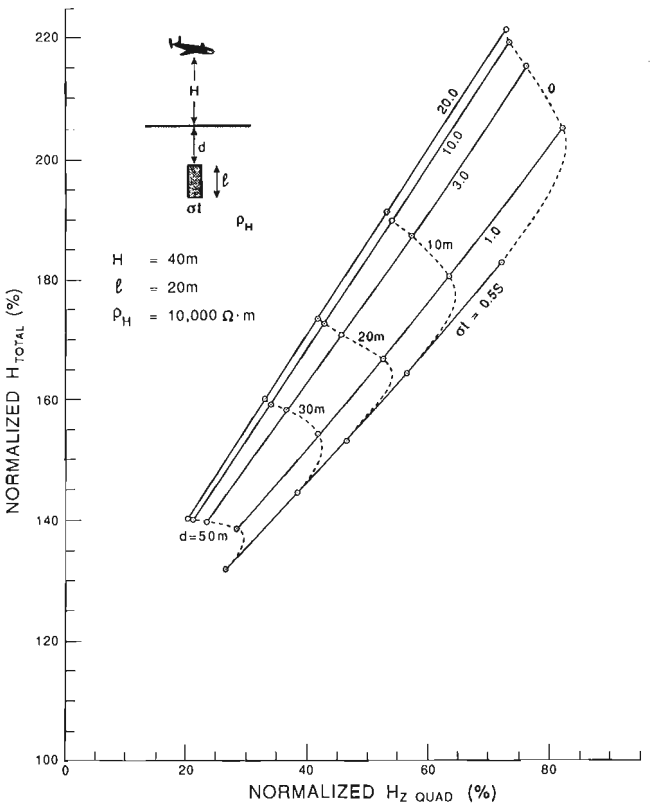

Figure 5. *Plot of the normalized total field and vertical quadrature components over a 2-D conductor with a depth extent of 20 m at an altitude of 40 m for a host rock resistivity of 10 000 Ω·m.*

case. As in the case of 120 m altitude, the interpretation diagrams for either 10 or 20 m depth extent can be used to estimate the depth, except for very low values of depth parameter. The overestimation of the conductance if one used a plot for 10 m depth extent to interpret data where the depth extent is really 20 m will be about 50%. Thus, interpretation of airborne VLF data acquired with a helicopter will be less susceptible to errors if no information about the depth extent of the conductor is available.

CONCLUSIONS

The network solution technique was used to compute the airborne VLF response of 2-D, sheet-like conductors located inside a resistive host rock in order to generate characteristic interpretation diagrams for the quantitative interpretation of airborne VLF-EM data. The method proposed in this paper will work only if the four following conditions are met.

First, the survey area should be at least 800 km from the VLF stations being used, so that the primary fields at the survey area would behave like plane uniform fields.

Second, the assumption of uniformity of the field must be ensured by continuous monitoring of the field data in the entire survey area using one or more ground VLF field monitors. Such monitors should be left on the ground for the duration of the survey, and their data examined periodically to check for field variations and applying necessary corrections for the removal of spatial and temporal variations from the field data.

Third, the host rock resistivity in the area should be known at least approximately. One can make a good estimate of the host rock resistivity over Precambrian terrane with no or thin resistive overburden. A better technique would be to conduct spot ground EM soundings, preferably VLF resistivity soundings at several locations in the area. Data from VLF resistivity methods should be more reliable as they use the same source as the field data.

Fourth, the depth extents of the conductors should be approximately known for complete depth and conductivity interpretation. However, this parameter is not absolutely critical for quantitative interpretation since the depth estimate is not seriously affected by errors in depth extent assumption. The conductance parameter, although more sensitive to it, can still be estimated reasonably well. Even when the estimates of the depth extent are wrong by 50% (values greater than 20 m will produce little field response in airborne VLF surveys), the interpreted conductance values may be useful enough to indicate if the source of an anomaly is a good conductor, such as, a graphitic or a sulphide body, or a weak conductor like a moist, clay-filled shear zone.

Finally, it should be mentioned here that the assumption of a normally incident primary VLF field used in the modelling may not be correct in certain situations (Poikonen and Suppala, 1989), especially when electric field measurements are involved. However, it may be shown that for systems using VLF magnetic fields only, this model is adequate since the magnetic field is independent of the angle of incidence for the aircraft altitudes under consideration.

ACKNOWLEDGMENTS

I am grateful to G.J. Palacky and R.J. Hetu of the Mineral Resources Division (GSC) who critically reviewed the paper and made many comments and suggestions for its improvement.

REFERENCES

Herz, A.
1986: Airborne EM instruments operating at VLF and higher frequencies; in Airborne Resistivity Mapping, G.J. Palacky,(ed); Geological Survey of Canada, Paper 86-22, p. 55-61.

Kaikkonen, P.
1979: Numerical VLF modelling; Geophysical Prospecting, v. 27, p. 815-834.

Poikonen, A.
1990: Development of airborne very low frequency electromagnetic techniques at the Geological Survey of Finland; in Developments and Applications of Modern Airborne Electromagnetic Surveys, D.V. Fitterman,(ed); United States Geological Survey, Bulletin 1925, p. 133-137.

Poikonen, A. and Suppala, I.
1989: On modeling airborne very low frequency measurements; Geophysics, v. 54, p. 1596-1606.

Saydam, A. S.
1981: Very low frequency electromagnetic interpretation using tilt angle and ellipticity measurements; Geophysics, v. 46, p. 1594-1605.
Sinha, A. K.
1990a: Application of airborne very low frequency electromagnetic surveys in geophysical exploration; in Developments and Applications of Modern Airborne Electromagnetic Surveys, D.V. Fitterman,(ed); United States Geological Survey, Bulletin 1925, p. 117-131.
1990b: Interpretation of ground VLF-EM data in terms of inclined sheet-like models; Pure and Applied Geophysics, v. 132, p. 733-756.
Sinha, A. K. and Morrison, E. B.
1993: Promises and prospects of a new airborne VLF-EM system for high resolution mapping (Abstract); International Workshop on Airborne Electromagnetic Methods, Tuscon, September 13-16.
Swift, C. M., Jr.
1971: Theoretical magnetotelluric and Turam responses from two-dimensional inhomogeneities; Geophysics, v. 36, p. 38-52.
Vallée, M. A., Chouteau, M., and Palacky, G. J.
1992: Effect of temporal and spatial variations of the primary signal on VLF total-field surveys; Geophysics, v. 57, p. 97-105.
Vozoff, K.
1971: The effect of overburden on vertical component anomalies in AFMAG and VLF exploration; Geophysics, v. 36, p. 53-57.
Watt, A. D.
1967: VLF radio engineering; Pergamon Press, Inc.

Geological Survey of Canada Project 850058

LANDSAT TM imagery for alteration identification

A. Rencz, J. Harris[1], and S.B. Ballantyne
Mineral Resources Division

Rencz, A., Harris, J., and Ballantyne, S.B., 1994: LANDSAT TM imagery for alteration identification; in Current Research 1994-E; Geological Survey of Canada, p. 277-282.

Abstract: LANDSAT Thematic Mapper (TM) data can be used to map altered rocks given the right geological environment. This paper briefly reviews spectral reflectance theory as it applies to the detection of different minerals and presents an example of how this theory can be applied to LANDSAT TM data. The example is from a Cu-Au porphyry system, the Sulphurets area, located northwest of Stewart, British Columbia. The example illustrates the application of LANDSAT TM data in mapping rocks that have undergone alteration, primarily iron oxidation and clay alteration.

Résumé : Les données saisies par le capteur TM de LANDSAT peuvent servir à cartographier les roches altérées à condition que le milieu géologique soit approprié. Le présent article passe brièvement en revue la théorie sur la réflectance spectrale telle qu'elle est appliquée à la détection de différents minéraux et présente un exemple d'application de cette théorie aux données TM de LANDSAT. L'exemple présenté est celui d'un système de Cu-Au porphyrique, la zone Sulphurets, situé au nord-ouest de Stewart (Colombie-Britannique). Cet exemple illustre la façon dont sont utilisées les données TM de LANDSAT pour cartographier des roches qui ont été altérées, principalement par oxydation du fer et altération de l'argile.

[1] Continental Geoscience Division

INTRODUCTION

Remotely sensed data have been used to investigate spectral changes associated with alteration of rocks caused by hydrothermal fluids (Goetz, 1989). The presence of altered rocks in turn can provide clues to mineralization. The main application of remote sensing technology, related to mapping alteration, has been the identification of various minerals in the visible through the short wavelength infrared portion of the electromagnetic spectrum. In the spectral range of 0.4 μm to 1.1 μm spectral reflectance data have been used to determine the presence of iron oxides and hydroxides such as limonite and goethite. In the 1.0 μm-2.5 μm range, spectral data have been used to identify hydrous minerals such as clay minerals, mica and some sulphates. These spectral ranges are covered by the LANDSAT TM sensor and have been successively used in arid environments (e.g. Abrams et al., 1984; Goetz, 1989; Taranik, 1989).

In arid environments, the spectral signatures of diagnostic minerals are not masked by water or vegetation and the mixing effects of surficial materials caused by glaciation are generally absent. There has only been limited success in the use of LANDSAT TM for alteration detection in Canada and to test these capabilities several test sites have been selected. This report will provide some background information on identification of alteration zones form remotely sensed data and also present a successful test case to illustrate the analytical procedures.

BACKGROUND

Figure 1 illustrates generalized spectral curves for three minerals in the 0.4 μm to the 2.5 μm range (blue light to near infrared). The curves are different and illustrate various absorption features that can be diagnostic for each of the minerals. There are two processes which produce the diagnostic absorption features in the 0.4 μm-2.5 μm range. For wavelengths less than 2 μm, *electronic transitions* occur – changes in the energy state of electrons bound to atoms or molecules or lattices (Goetz, 1989). Above 2 μm, *vibrational transitions* occur – variations in the relative positions of bonded nuclei. These oscillations will stretch molecular bond lengths or bend the interbond angles (Irons et al., 1989). Transitions between vibrational energy states will result in either absorption or emission at specific wavelengths. Each mineral has a specific absorption feature (position along electromagnetic spectrum and depth of absorption curve) that can be used like a fingerprint for identification.

Iron-bearing minerals have a diagnostic absorption at 0.60 μm and around 0.90 μm (Hunt, 1977), corresponding to TM bands 1 and 4, respectively (Fig. 1). The presence of hydroxyl minerals clay-sericite-chlorite is suggested by absorption features in the 2.2 μm-2.5 μm range, which corresponds to TM band 7. Figure 1 also illustrates that carbonate minerals have strong absorption features in the 2.3 μm range, which corresponds to TM band 7. Hunt and Salisbury (1970-1976) and Hunt (1977, 1979) present rock and mineral spectra for a wide range of material.

The TM sensor records electromagnetic energy in seven different band locations (Fig. 1). The width of each band varies but is generally about 0.1 μm. Consequently the scanner is only useful for identifying the presence of clay minerals or Fe-bearing minerals but normally cannot resolve signatures of specific minerals. The identification of specific minerals requires sensors which provide wavelength separation in the order of 0.01 μm (i.e. narrow bandwidth).

ANALYSIS

Based on theoretical spectral curves several techniques have been developed to identify alteration zones. These include principal component analysis, band ratio combinations and various indices (Abrams et al., 1984; Buckingham and Sommer, 1983; Elvidge and Lyon, 1984) In this paper emphasis is placed on several band ratios that have been effective. The other techniques are being investigated.

A ratio of LANDSAT TM 3 / TM 1 will highlight rocks that have been subjected to iron-bearing sulphide oxidation (typically pyrite, chalcopyrite, and bornite in this study area)

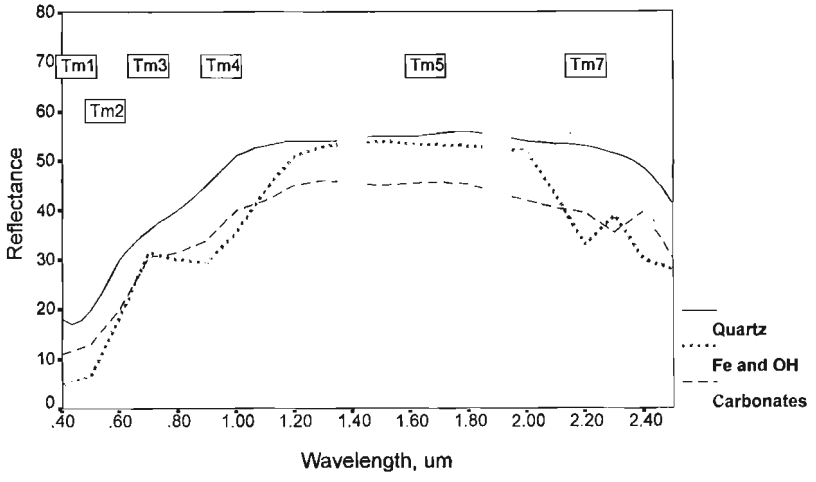

Figure 1.

Generalized reflectance spectra for various minerals (from Abrams et al., 1984).

as altered rocks are more reflective in TM Band 3 and less reflective in TM Band 1 due to iron absorption (see Fig. 1). The ratio image will accentuate the difference between the two bands with higher ratio values (brighter image tones) possibly representing areas of more intense iron sulphide oxidation. Similarly, a ratio of TM 5 / TM 7 will highlight areas of possible clay-sericite-chlorite alteration as altered rocks are highly reflective in Band 5 and will have lower reflectance in Band 7 due in the presence of hydrous minerals (see Fig. 1). A ratio of TM 4 / TM 3 will highlight vegetation and thus can be used to preclude (mask out) these areas from further spectral analysis.

Based on the three ratios described above a variety of colour maps can be produced using image analysis system software to display specific alteration types in specific colours. For example if a three component colour image is composed of the 5/7 ratio in red, the 3/1 ratio in green and the 4/3 ratio as blue the resulting image will indicate the presence

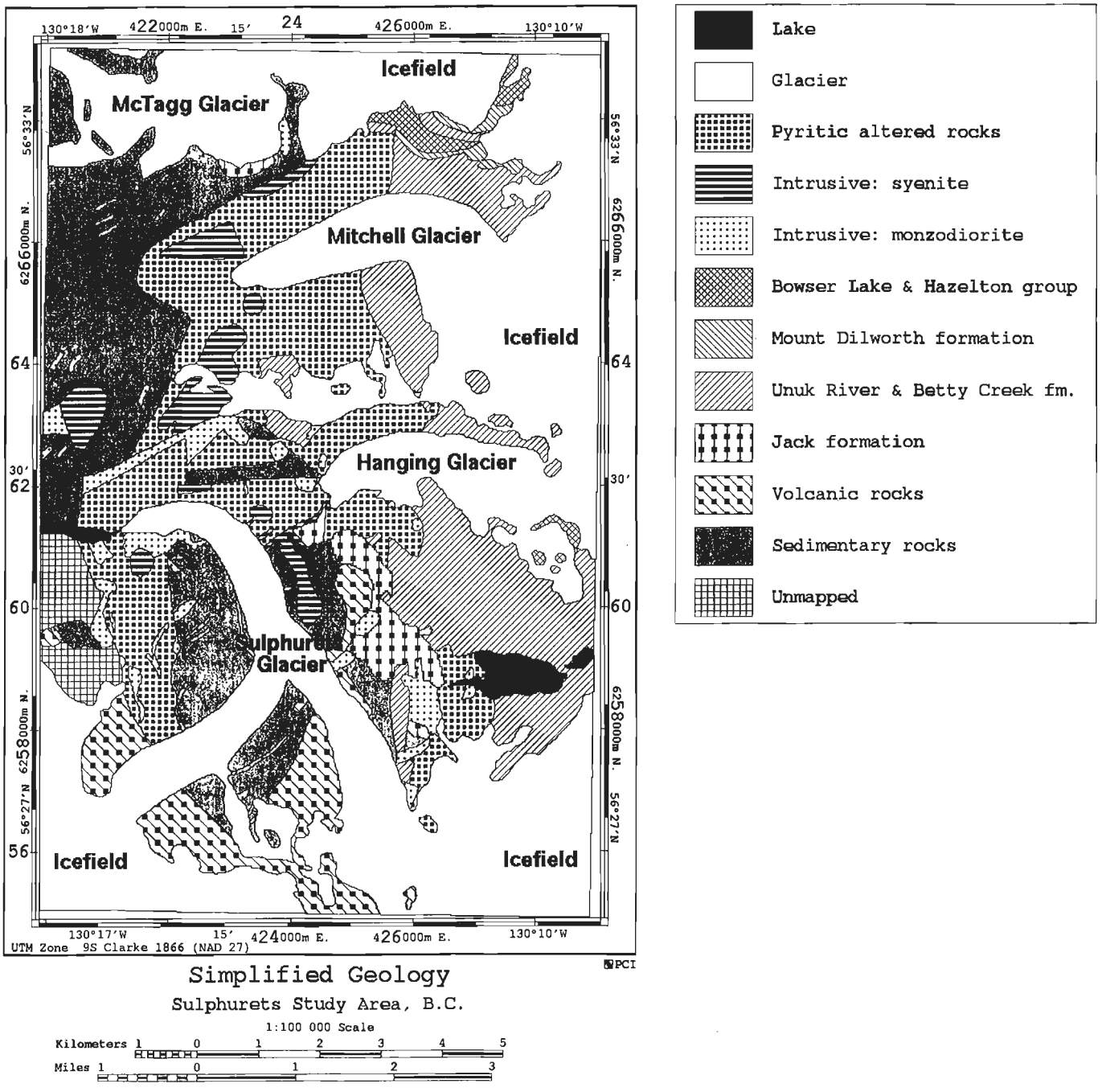

Figure 2. *Geology map of the Sulphurets study area, British Columbia (from R.V. Kirkham, pers. comm.).*

of hydrous minerals in red whereas green will highlight areas of leached and oxidized iron-bearing minerals and yellow (i.e. red plus green) will indicate the occurrence of hydrous minerals plus iron oxidation of sulphides. These ratios and other processing methods have proven effective in other environments (see Elvidge and Lyon, 1984). The three colour combinations (ie red-green-blue) are the preferred output product; however due to colour limitations, only black and white products are included in this report.

EXAMPLE OF ALTERATION DETECTION

Study area

The example is taken from the GSC Sulphurets study area in the Cordilleran of central, northwestern British Columbia where regional scale expressions of Cu-Au porphyry systems are exposed at the present day surface (Ballantyne, 1990; Harris and Ballantyne, 1992). Previous workers have shown that TM mapping is an effective method of exploration in the

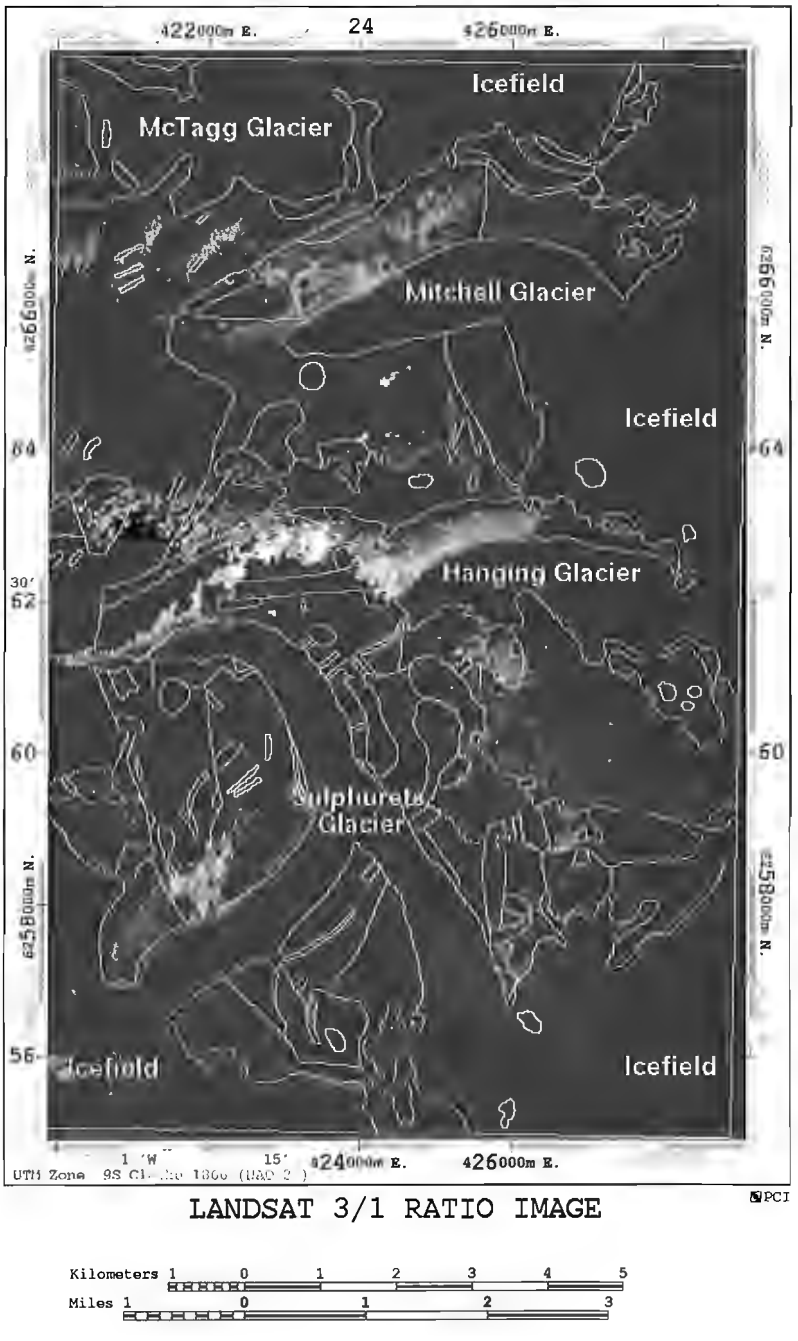

Figure 3. LANDSAT TM 3 / TM 1 map showing hydrated iron sulphide oxidation.

area (Ma et al., 1991; Ballantyne and Ma, 1992). A simplified geology map suitable for TM map interpretation is presented in Figure 2 (R.V. Kirkham, pers. comm., 1992) and further geological details can be found in Kirkham et al., 1990, 1992). The ice field and valley glacier filled study area has relatively steep relief and although lower regions may be vegetated, approximately 20% of the area is bedrock outcrop. Large exposures of outcrop have undergone intense hydrothermal alteration characterized by silicification and pyrite-sericite. Consequently, this site provides the opportunity to investigate the application of LANDSAT TM for detecting hydrothermally altered exposures of bedrock (Ballantyne and Ma, 1992; Ma et al., 1988). It is important to note that with the severe local climate and steep relief, typical for this part of the Cordillera, that there is only limited lichen growth on the rock outcrop. Therefore the reflectance is not masked by a vegetative cover.

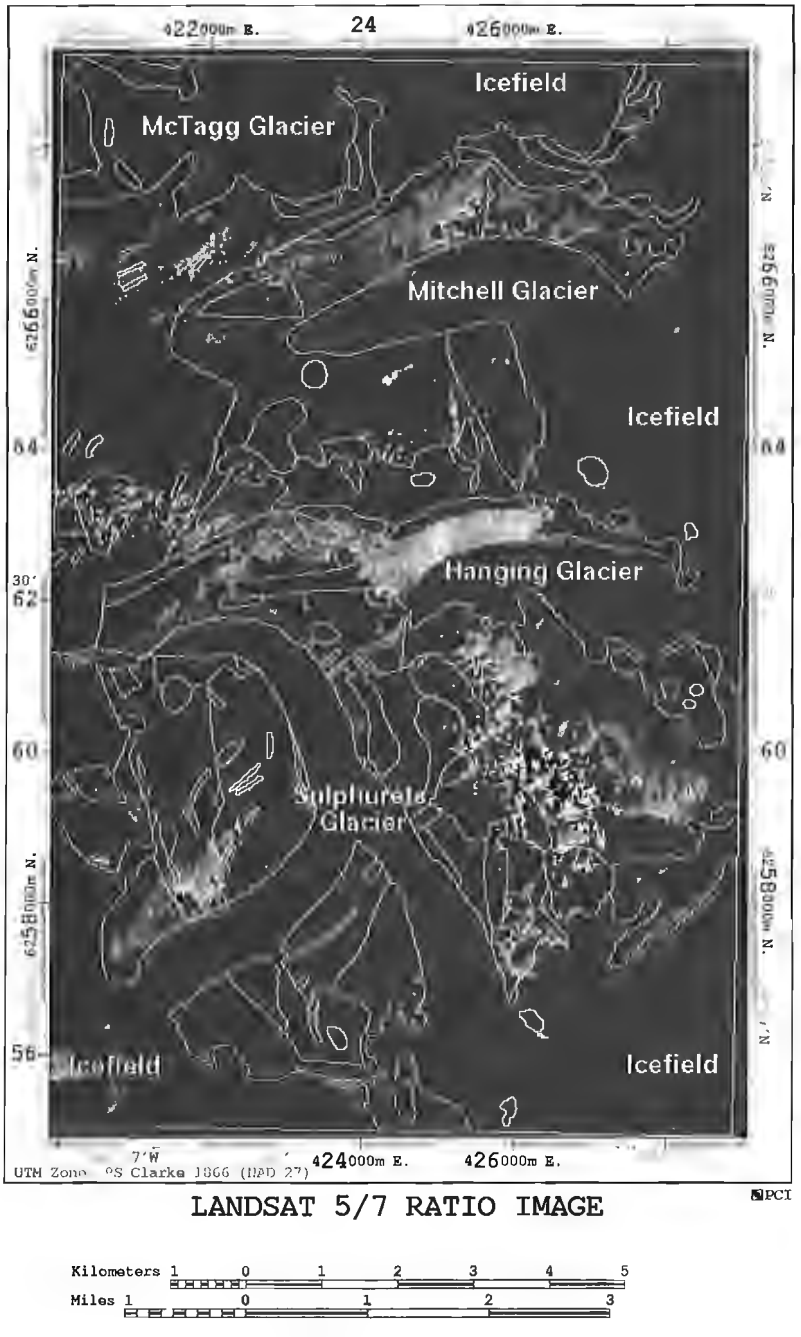

Figure 4. LANDSAT TM 5 / TM 7 map showing clay-sericite alteration.

Method

The technique used in this study was based on the use of the ratios as discussed above. Prior to the calculation of these ratios several preprocessing steps were used to "mask" out certain pixels. These included: areas of ice, snow, shadow and vegetation. The vegetation mask was created by producing a ratio of TM 4 / TM 3 and thresholding this image interactively. The areas of ice, snow, shadow and glacial sediment cover were masked by training on known areas and applying the statistics to classify the remainder of the area. The outcrop (exposed) areas were visually identified on TM Band 5 as they possess the brightest tones on the image. The outcrop mask was integrated with the other land cover masks to identify areas of overlap. These areas were removed from the outcrop mask and all further processing (i.e. calculation of ratios) was restricted to the areas of outcrop.

Discussion

Figure 3 is a TM 3 / TM 1 ratio image which shows areas of iron oxidation. The brighter areas possibly represent areas of more abundant sulphides and therefore areas of limonite staining reflecting iron with Fe sulphide oxidation. Comparison with Figure 2 indicates that much of the outcrop area occurs in the pyritic altered rock map area. Areas of more intense iron limonite staining indicative of pyritic alteration exist west of the Hanging Glacier and to a lesser extent, north of the Mitchell Glacier and west of the Sulphurets Glacier in the southwest portion of the study area. Smaller areas of iron oxidization, as indicated on the TM 3 / TM 1 ratio image occur over areas not appearing as altered at the map scale shown. These occur mostly over sedimentary and volcanic rocks and also over a syenite intrusion in the west-central portion of the study area.

Figure 4 is a TM 5 / TM 7 ratio image which shows areas of possible clay-sericite alteration. The strongest areas of alteration, according to the ratio image, occur just north of the Hanging Glacier within an area mapped as pyritic alteration as well as a broad zone south of the same glacier within the Unuk River and Betty Creek formations.

CONCLUSIONS

In the Sulphurets area ratios of LANDSAT TM data were useful in identifying limonitic and hydrothermal alteration. Further work is progressing to evaluate other analytical procedures with LANDSAT TM data and with the integration of high resolution airborne radiometric survey data. These data are particularily useful in this area because of the relatively large areas of alteration that are not masked by glacial debris or vegetation.

ACKNOWLEDGMENTS

This work is based on earlier findings of J. Ma. Q. Cheng and R. Balma provided the digital data for geological map which incorporates work from R. Kirkham of the GSC. We also appreciate the critical review and comments of D. Wright.

REFERENCES

Abrams, M.J., Conel, J.W., Lang, H.R., and Paley, H.N.
1984: The Joint NASA/Geosat Test Case Project, Final Report; American Association of Petroleum Geologists Bookstore.

Ballantyne, S.B.
1990: Geochemistry of Sulphurets area, British Columbia (abstract); in Program with Abstracts; Geological Survey of Canada, Minerals Colloquium, Ottawa, Jan. 17-18, 1990, p. 14.

Ballantyne, S.B. and Ma, J.
1992: LANDSAT Thematic Mapper with ground truth element, distribution: An example from British Columbia Golden Triangle District (abstract); in Program with Abstracts; Geological Survey of Canada, Forum 92, Ottawa, p. 3.

Buckingham, W.F. and Sommer, S.E.
1983: Mineralogical characteristics of a rock surface formed by hydrothermal alteration and weathering- an application of remote sensing; Economic Geology, v. 78, p. 664-674.

Elvidge, C.D. and Lyon, R.J.P.
1984: Mapping clay alteration in the Virginia Range-Comstock Lode, Nevada with airborne thematic mapper imagery; in International Symposium on Remote Sensing of the Environment, 3rd Thematic Conference for Exploration Geology, p. 61-170.

Goetz, A.F.H.
1989: Spectral Remote Sensing in Geology: Chapter 12; in Theory and Applications of Optical Remote Sensing, G. Asrar (ed.); John Wiley and Sons, p. 491-526.

Harris, D.C. and Ballantyne, S.B.
1992: Ore mineralogy and lithogeochemistry of the Mitchell-Sulphurets District, potassic high-sulphur precious metal system (abstract); in Program with Abstracts; Geological Survey of Canada, Minerals Colloquium, Ottawa, Jan. 22-24, 1992, p. 19.

Hunt, G.R.
1977: Spectral signature of particulate minerals in the visible and near infrared; Geophysics, v. 42(3), p. 501-513.
1979: Near-infrared (1.3-2.4 %m) spectra of alteration minerals- potential for use in remote sensing. Geophysics, v. 44(12), p. 1974-1986.

Hunt, G.R. and Salisbury, J.W.
1970-1976: Visible and near-infrared spectra of minerals and rocks; Modern Geology, Volumes 1-5.

Irons, J.R., Weismiller, R.A., and Petersen, G.W.
1989: Soil Reflectance. Chapter 3; in Theory and Applications of Optical Remote Sensing, G. Asrar (ed.); John Wiley and Sons, p. 66-106.

Kirkham, R.V., Ballantyne, S.B., and Harris, D.C.
1990: Geology, geochemistry and mineralogy of a deformed porphyry copper molybdenum and precious metal system (abstract); in Program with Abstracts; Geological Survey of Canada, Minerals Colloquium, Ottawa, Jan. 22-24, 1992, p. 11.

Kirkham, R.V., Ballantyne, S.B., Harris, D.C., Henderson, J.R., Henderson, M.N., and Wright, T.O.
1992: Lower Jurassic Sulphurets porphyry Cu-Au system Northwest British Columbia (abstract); in Program with Abstracts; Geological Survey of Canada, Minerals Colloquium, Ottawa, Jan. 22-24, 1992, p. 3.

Ma, J., Slaney, V.R., Harris, J., Graham, D., Ballantyne, S.B., and Harris, D.C.
1988: Use of LANDSAT TM data for the mapping of limonitic and altered rocks in the Sulphurets area, central British Columbia; in Proceedings of the 14th Canadian Symposium on Remote Sensing. Calgary, Alberta, p. 419-422.

Taranik, D.
1989: Geologic Exploration of the Earth from Space; Mining Magazine, August, p. 124-128.

Geological Survey of Canada Project 840051

Effect of temperature on drying procedures used in porosity measurements of tight rocks

N. Scromeda and T.J. Katsube
Mineral Resources Division

Scromeda, N. and Katsube, T.J., 1994: Effect of temperature on drying procedures used in porosity measurements of tight rocks; in Current Research 1994-E; Geological Survey of Canada, p. 283-289.

Abstract: Effective porosity measurements of rock samples usually include an oven-drying procedure at temperatures of 93-116°C to evacuate free and adsorbed waters, but leaving structural water intact. However, many laboratories now vacuum-dry their samples at lower temperatures, raising concern of reduced measurement accuracy. One study performed to investigate low temperature effects on drying indicated that although free water may be evacuated at these temperatures, adsorbed water is not, thus implying reduced accuracy. There were also indications that different types of adsorbed waters existed. A similar study was carried out to confirm these results, due to their importance on measurement accuracy.

Results confirmed that free water is evacuated by vacuum oven-drying at low temperatures. They also show trends suggesting that adsorbed water may be divided into more than one component, one evacuated at 80°C and the other at 100°C. However, these trends require confirmation by further investigation.

Résumé : Les mesures de la porosité réelle d'échantillons de roche comportent habituellement un séchage au four à des températures variant entre 93 et 116°C pour évacuer l'eau libre et l'eau adsorbée, mais pas l'eau structurale. Cependant, de nombreux laboratoires recourent à un séchage sous vide de leurs échantillons à des températures plus basses, ce qui soulève la question de l'exactitude des mesures. Une étude réalisée pour analyser les effets des basses températures sur le séchage a indiqué que même si l'eau libre peut être évacuée à ces températures, l'eau adsorbée ne l'est pas, ce qui suppose une réduction de l'exactitude des mesures. Il existerait également différents types d'eau adsorbée. Une étude semblable a été menée pour confirmer ces résultats, étant donné leur importance sur l'exactitude des mesures.

Les résultats ont confirmé que l'eau libre est évacuée par séchage sous vide dans un four à des températures basses. Certaines tendances indiquent en outre que l'eau adsorbée peut être divisée en plus d'une composante, l'une évacuée à 80°C et l'autre à 100°C. Cependant, ces tendances doivent être confirmées par d'autres analyses.

INTRODUCTION

Effective porosity measurements of rock samples usually include an oven-drying procedure at temperatures of 116°C under atmospheric condition or 93°C under vacuum, both following the American Petroleum Institute's recommendations (API, 1960). This is to drive out free and adsorbed waters, but leave structural water intact. However, recently, concern has been raised over possible textural changes occurring for certain clay types (e.g., Soeder, 1986) when drying rocks at temperatures above 50°C. For example, it was suggested that partial expulsion of interlamellar water could occur at these temperatures causing reduced measurement accuracy. For this reason, many laboratories in the petroleum industry now vacuum-dry their samples at temperatures well below 100°C (Katsube et al., 1992). While drying at low temperatures may achieve its objectives in areas of the petroleum industry using conventional petrophysical analysis for reservoir rocks, there was concern as to whether this also applies to petrophysical analysis of rocks (tight and hard rocks) related to other areas, such as hydrocarbon seals, radioactive waste migration and flow of hydrothermal fluids. For this reason, studies are being carried out (Scromeda and Katsube, 1993) to investigate the effect of low temperature vacuum-oven drying on the measurement accuracy of effective porosity for samples representing three tight rock types (granite, gabbro and shale).

The results of one of the studies (Scromeda and Katsube, 1993) indicated that differences between drying under vacuum or atmospheric pressures did not influence the effective porosity values when at temperatures above 100°C. It was also indicated that, although larger fractions of free water may be driven out under vacuum compared to atmospheric conditions at lower temperatures, temperatures above 100°C are required to drive off the adsorbed water, implying that measurements at temperatures below 100°C could be inaccurate. A close examination of the drying data produced by that study suggests that there may be different types of free and adsorbed water which are driven off at different temperatures, and that these waters may provide useful information about the rock. However, the temperature intervals of those data were too coarse to confirm any of these suggestions. Therefore, the present study, with finer temperature intervals, was undertaken to investigate these possibilities.

METHOD OF INVESTIGATION

Samples and sample preparation

Three of the nine samples used in the previous study (Scromeda and Katsube, 1993) were used in this one. They represent rock types of granite (Sample W-2), gabbro (Sample E-2) and shale (Sample V-5), as indicated in Table 1. The granite and the gabbro samples are half-disks with a diameter of 4.10-4.56 cm and a thickness of 0.91-1.05 cm, and the shale sample is a disk with a diameter of 2.54 cm and a thickness of 0.66 cm. Information on their sampling locations and on references to their geological characteristics are listed in Table 1.

Experimental approach

First, the samples are vacuum-saturated to 100%, following the previously used procedure (Scromeda and Katsube, 1993). This is followed by an initial drying, in a vacuum-chamber for time-periods of 500-1500 minutes at room temperature (23°C), until a constant weight, W_{rD}, is reached. A constant weight (W_{rD}) is defined by the sample weight variation being less than 0.1 mg/hour. Following the initial drying, the samples are then placed in a vacuum-oven and dried for periods of 1500-3500 minutes at a series of higher temperatures (50, 60, 64, 70, 75, 83, 90, 95, 100, 108, 116, and 120°C), again until a constant weight is reached. In each case, after the drying is completed at a specific temperature, the sample is re-saturated to 100% before the entire procedure is repeated at the next (higher) temperature. The W_{rD} values are used to determine the constant degree of saturation, S_{rD}, at each temperature. The S_{rD} is determined by

$$S_{rD}=(W_{rD}-W_D)/(W_W-W_D), \quad (1)$$

where W_W is the weight of the fluid saturated rock sample, W_D is that of the dry rock sample, and W_{rD} represents the constant weight at each temperature. The dry weight (W_D) is the constant weight (W_{rD}) at 116°C, and is considered to represent the sample when it is devoid of any free and adsorbed (or bound) water (API, 1960). Finally, the results of the S_{rD} determinations are plotted against drying temperature for analysis and interpretation. The saturating and drying procedures are described in more detail by Scromeda and Katsube (1993).

At the temperatures of 50°C, 70°C, 100°C and 116°C, the state of drying was monitored from the start of the drying process, using the degree of saturation, S_r, which is determined by

$$S_r=(W_r-W_D)/(W_w-W_D), \quad (2)$$

where W_r is the weight of the sample at any given drying time, t_D.

Effective porosity

The effective porosity, ϕ_E, of these samples is derived by the following equation (Scromeda and Katsube, 1993; Katsube et al., 1992):

$$\phi_E = (W_W-W_D)\delta_E/(W_D\delta_W) \quad (3)$$

Table 1. Sample numbers, sampling depth, sampling locations and references to other petrophysical information.

Sample Number	Sampling Depth (m)	Sampling Location	Reference
W-2	564	Lac du Bonnet, Manitoba	[1], [3]
E-2	342	East Bull Lake, Ontario	[2], [3]
V-5	5122	Venture Gas Field, Nova Scotia	[4]

[1]=Katsube and Hume (1987)
[2]=Hume and Katsube (1987)
[3]=Katsube and Scromeda (1991)
[4]=Katsube et al. (1991)

Table 2. Degree of saturation (S_r) variation with vacuum-oven drying time (t_D) at 50°C.

Sample	time(t_D) (min)	W_r (g)	ΔW_r (mg)	S_r (%)
W-2	0	22.3727	6.4	14.5
	150	22.3707	4.4	10.0
	390	22.3706	4.3	9.7
	1410	22.3695	3.2	7.2
	1830	22.3694	3.1	7.0
	2850	22.3694	3.1	7.0
	3240	22.3694	3.1	7.0
E-2	0	20.4537	10.4	44.1
	150	20.4506	7.3	30.9
	390	20.4490	5.7	24.2
	1410	20.4473	4.0	16.9
	1830	20.4473	4.0	16.9
	2850	20.4468	3.5	14.8
	3240	20.4468	3.5	14.8
V-5	0	2.8352	20.2	29.5
	150	2.8281	13.1	19.2
	390	2.8240	9.0	13.2
	1410	2.8217	6.7	9.8
	1830	2.8215	6.5	9.5
	2850	2.8212	6.2	9.1
	3240	2.8210	6.0	8.8

W_r = Weight of specimen at a given time.
ΔW_r = Weight difference between W_r and W_D.

Table 3. Degree of saturation (S_r) variation with vacuum-oven drying time (t_D) at 70°C.

Sample	time (t_D) (min)	W_r (g)	ΔW_r (mg)	S_r (%)
W-2	0	22.3724	6.1	13.8
	150	22.3697	3.4	7.7
	390	22.3695	3.2	7.2
	1410	22.3690	2.7	6.1
	1830	22.3690	2.7	6.1
	2850	22.3687	2.4	5.4
	3240	22.3685	2.2	5.0
E-2	0	20.4544	11.1	47.0
	150	20.4489	5.6	23.7
	390	20.4475	4.2	17.8
	1410	20.4465	3.2	13.6
	1830	20.4459	2.6	11.0
	2850	20.4458	2.5	10.6
	3240	20.4456	2.3	9.7
V-5	0	2.8366	21.6	31.6
	150	2.8224	7.4	10.8
	390	2.8197	4.7	6.9
	1410	2.8186	3.6	5.3
	1830	2.8183	3.3	4.8
	2850	2.8183	3.3	4.8
	3240	2.8182	3.2	4.7

W_r = Weight of specimen at a given time.
ΔW_r = Weight difference between W_r and W_D.

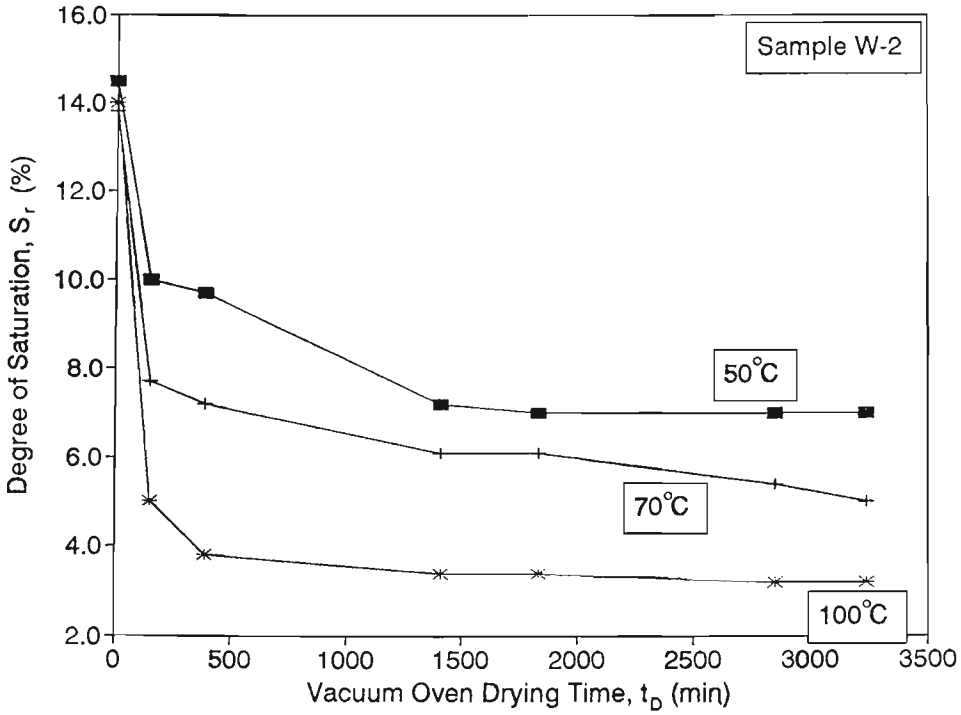

Figure 1.

Degree of saturation (S_r) as a function of vacuum oven-drying time (t_D), for three temperatures of 50°C, 70°C and 100°C, for Sample W-2.

Table 4. Degree of saturation (S_r) variation with vacuum-oven drying time (t_D) at 100°C.

Sample	time (t_D) (min)	W_r (g)	ΔW_r (mg)	S_r (%)
W-2	0	22.3725	6.2	14.0
	150	22.3685	2.2	5.0
	390	22.3680	1.7	3.8
	1410	22.3678	1.5	3.4
	1830	22.3678	1.5	3.4
	2850	22.3677	1.4	3.2
	3240	22.3677	1.4	3.2
E-2	0	20.4549	11.6	49.2
	150	20.4479	4.6	19.5
	390	20.4464	3.1	13.1
	1410	20.4448	1.5	6.4
	1830	20.4448	1.5	6.4
	2850	20.4448	1.5	6.4
	3240	20.4448	1.5	6.4
V-5	0	2.8356	20.6	30.1
	150	2.8186	3.6	5.3
	390	2.8177	2.7	3.9
	1410	2.8168	1.8	2.6
	1830	2.8165	1.5	2.2
	2850	2.8165	1.5	2.2
	3240	2.8165	1.5	2.2

W_r = Weight of specimen at a given time.
ΔW_r = Weight difference between W_r and W_D.

Table 5. Degree of saturation (S_r) variation with vacuum-oven drying time (t_D) at 116°C.

Sample	time (t_D) (min)	W_r (g)	ΔW_r (mg)	S_r (%)
W-2	0	22.3714	5.1	11.5
	150	22.3679	1.6	3.6
	390	22.3671	0.8	1.8
	1410	22.3670	0.7	1.6
	1830	22.3663	0.0	0.0
	2850	22.3663	0.0	0.0
	3240	22.3663	0.0	0.0
E-2	0	20.4527	9.4	39.8
	150	20.4463	3.0	12.7
	390	20.4457	2.4	10.2
	1410	20.4445	1.2	5.1
	1830	20.4439	0.6	2.5
	2850	20.4433	0.0	0.0
	3240	20.4433	0.0	0.0
V-5	0	2.8345	19.5	28.5
	150	2.8177	2.7	3.9
	390	2.8162	1.2	1.8
	1410	2.8161	1.1	1.6
	1830	2.8155	0.5	0.7
	2850	2.8150	0.0	0.0
	3240	2.8150	0.0	0.0

W_r = Weight of specimen at a given time.
ΔW_r = Weight difference between W_r and W_D.

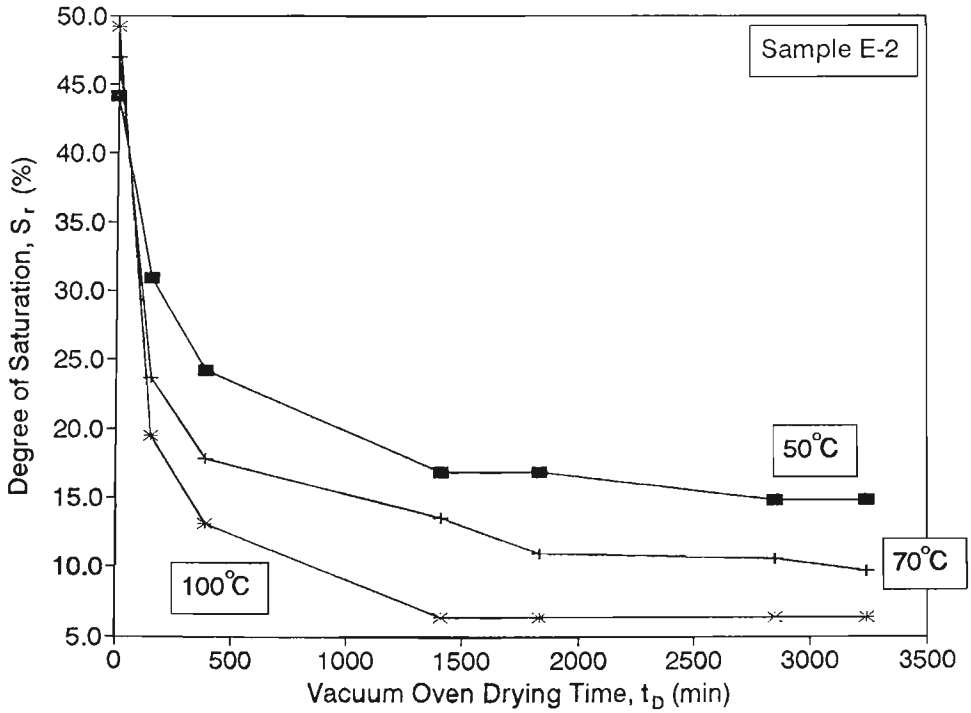

Figure 2.

Degree of saturation (S_r) as a function of vacuum oven-drying time (t_D), for three temperatures of 50°C, 70°C and 100°C, for Sample E-2.

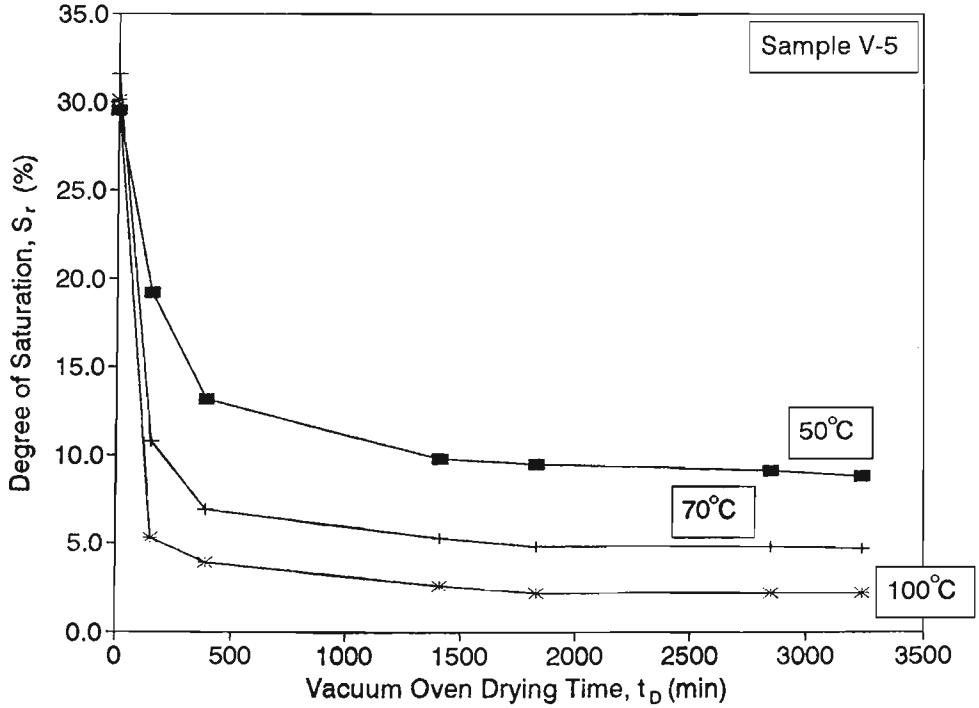

Figure 3. Degree of saturation (S_r) as a function of vacuum oven-drying time (t_D), for three temperatures of 50°C, 70°C and 100°C, for Sample V-5.

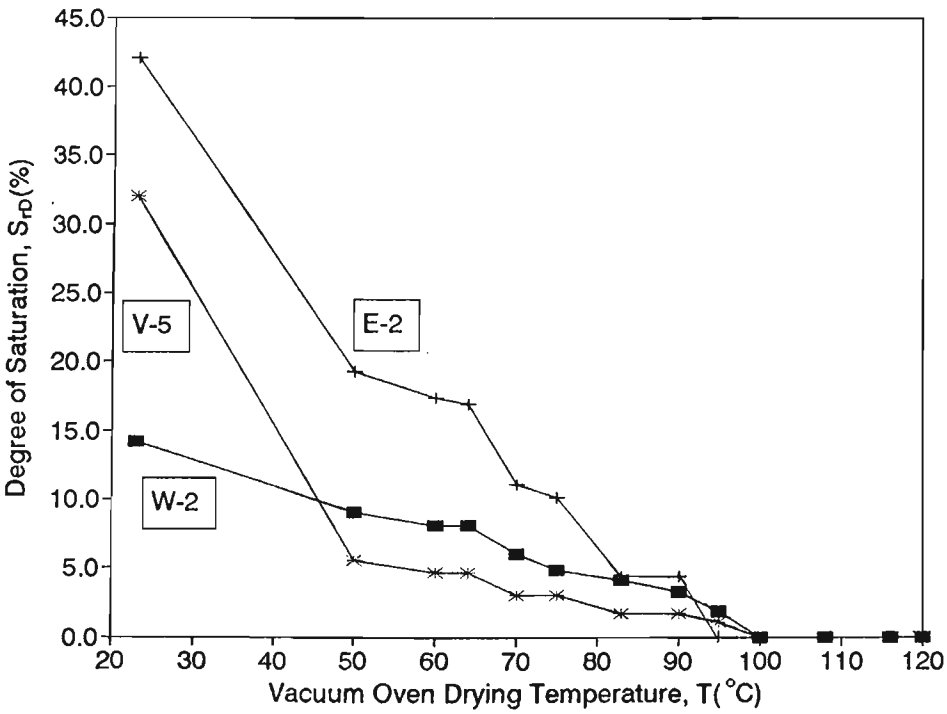

Figure 4. Constant degree of saturation (S_{rD}) as a function of vacuum-oven temperature (T) for the three representative samples W-2, E-2 and V-5.

where δ_E is the bulk density of the rock sample and δ_W is the bulk density of the pore water (usually considered to be unity) saturating the sample.

EXPERIMENTAL RESULTS

Results of monitoring the vacuum drying for the saturated samples at the four temperatures of 50°C, 70°C, 100°C and 116°C are listed in Tables 2 to 5, and are shown in Figures 1 to 3 for the three lower temperatures. The measurement of drying time (t_D) in these tables and figures starts after the drying procedure at room temperature (23°C) is completed, and from the point that drying at the higher temperature is started. Therefore, the S_r values at the beginning ($t_D = 0$) of these figures are the S_{rD} values at room temperature (23°C). Results of vacuum-drying the saturated samples at 23°C, and at all of the other temperatures varying from 50°C to 120°C are listed in Table 6. Previous (Scromeda and Katsube, 1993) S_{rD} values are also listed for comparison. The S_{rD} values at 23°C, for this study, that are listed in Table 6 are averages obtained from the measurements at all temperatures. The relationship between S_{rD} and drying temperature for the three samples is shown in Figure 4. Effective porosities (ϕ_E) derived using equation (3) are listed in Table 7, with previous values (Katsube and Scromeda, 1991; Katsube et al., 1992; Scromeda and Katsube, 1993) also listed for comparison.

The values of ϕ_E are generally very similar to those obtained previously (Table 7) for these samples. Sample V-5 shows the largest deviation of the three with its value being about 10% higher than the previous ones. The S_r shows an initial rapid decrease with drying time (t_D), followed by a levelling off (Fig. 1 to 3) for all three samples. This indicates that the main part of drying is completed, or S_r values close to S_{rD} are attained, for each drying temperature level within 500-1000 minutes of drying at all three temperatures (50, 70 and 100°C). The curves (Fig. 4) for S_{rD} with drying temperature are generally very similar to those of the previous study (Scromeda and Katsube, 1993). However, except for Sample W-2, the absolute values differ to some extent (Table 6). Samples E-2 and V-5 both start out with S_{rD} values higher than those in the previous study (Scromeda and Katsube, 1993), but show considerably lower values in the intermediate temperature range (50-90°C). There are indications of a step-like decrease for the drying curves in Figure 4, a trend not seen previously probably, due to the coarser temperature intervals that were applied. However, this trend requires confirmation by further investigation.

Table 6. Constant degree of saturation (S_{rD}) values recorded at each temperature level.

Sample	Temp (T) (°C)	W_r (g)	ΔW_r (mg)	S_{rD} (%) (I)	S_{rD} (%) (II)
W-2	23	22.3696	6.1	13.5±2.0*	13.4
	50	22.3674	3.9	9.1	8.5
	60	22.3670	3.5	8.1	
	64	22.3670	3.5	8.1	
	70	22.3661	2.6	6.0	6.0
	75	22.3656	2.1	4.9	
	83	22.3653	1.8	4.2	
	90	22.3649	1.4	3.3	4.9
	95	22.3643	0.8	1.9	
	100	22.3635	0.0	0.0	3.6
	108	22.3635	0.0	0.0	
	116	22.3635	0.0	0.0	0.0
	120	22.3635	0.0	0.0	
E-2	23	20.4496	8.7	45.0±5.2*	38.0
	50	20.4449	4.0	19.3	26.2
	60	20.4445	3.6	17.4	
	64	20.4444	3.5	16.9	
	70	20.4432	2.3	11.1	15.8
	75	20.4430	2.1	10.1	
	83	20.4418	0.9	4.4	
	90	20.4418	0.9	4.4	8.6
	95	20.4409	0.0	0.0	
	100	20.4409	0.0	0.0	3.6
	108	20.4409	0.0	0.0	
	116	20.4409	0.0	0.0	0.0
	120	20.4409	0.0	0.0	
V-5	23	2.8368	21.2	30.0±1.6*	25.7
	50	2.8193	3.7	5.6	11.4
	60	2.8187	3.1	4.7	
	64	2.8187	3.1	4.7	
	70	2.8176	2.0	3.0	6.3
	75	2.8176	2.0	3.0	
	83	2.8167	1.1	1.7	
	90	2.8167	1.1	1.7	2.9
	95	2.8163	0.7	1.1	
	100	2.8156	0.0	0.0	1.1
	108	2.8156	0.0	0.0	
	116	2.8156	0.0	0.0	0.0
	120	2.8156	0.0	0.0	

W_r = Weight of specimen at a given time.
ΔW_r = Weight difference between W_r and W_D.
(I) = This study.
(II) = Previous study (Scromeda and Katsube, 1993)
* = Mean of four values from Tables 2 to 5.

Table 7. Results of the effective porosity (ϕ_E) measurements.

Sample	W-2	E-2	V-5
δ_E (g/mL)	2.65	2.88	2.64
W_w (g)	2.8834	20.4669	22.4105
W_D (g)	2.8150	20.4433	22.3663
ΔW (mg)	44.2	23.6	68.4
ϕ_E (%)			
This Study	0.52	0.33	6.4
Previous Studies			
(I) - 1993	0.53	0.31	5.9
(II) - 1991/2	0.51	0.30	5.7

δ_E = bulk density
W_w = wet weight
W_D = dry weight
ΔW = W_w-W_D
ϕ_E = effective porosity
(I)-1993 = Scromeda and Katsube (1993)
(II)-1991/2 = Katsube and Scromeda (1991) for Samples W-2 and E-2, and Katsube et al. (1992) for Sample V-5

DISCUSSION AND CONCLUSIONS

It has been demonstrated by the degree of saturation versus drying time (S_r-t_D) curves (Fig. 1 to 3) that water evacuation from these rock samples can be divided into two stages: the "initial stage" characterized by a rapid decrease in degree of saturation (S_r) with drying time (t_D), and the "later stage" characterized by a small decrease in the degree of saturation (S_r) with drying time (t_D). The later evacuation stage is temperature dependent, but the initial evacuation stage is not. It is reasonable to assume that the "initial stage" represents the evacuation of free water, and the "later stage" represents the evacuation of adsorbed or bound water.

It is, therefore, assumed that the drying curves in Figure 4 represent the evacuation characteristics of the adsorbed water. These constant degrees of saturation versus drying temperature (S_{rD}-T) curves (Fig. 4) indicate that the evacuation of adsorbed water is essentially complete at temperatures above 100°C. The step-like feature is most clear in the S_{rD}-T curve for Sample E-2. However, the starting temperatures (50 and 70°C) of two of these steps are the same as those at which the monitoring of the vacuum-drying process took place (Fig. 1 to 3). This raises questions as to whether the slightly different drying procedure used in the monitoring process had an effect which was different from that of the normal drying procedure and is the cause of these two steps. The step-like feature starting at 80-90°C for samples E-2 and V-5 may be genuine, since it is not related to any of the monitoring temperatures. Although questions of error ranges remain, since differences between these S_{rD} values and those of the previous measurements (Scromeda and Katsube, 1993) are often larger than these steps, the experimental procedures are slightly different so that it is questionable whether this is a fact to be considered. If it is assumed that the step-like feature at 80-90°C is genuine, then these results suggest that the adsorbed water may be divided into two components.

In conclusion, results of this study confirm that free water is evacuated by vacuum oven-drying at low temperatures. They also show trends suggesting that adsorbed water may be divided into more than one component, one evacuated at 80°C and the other at 100°C. However, these trends require confirmation by further investigation.

ACKNOWLEDGMENTS

The authors express their sincere thanks to S.W. Adcock (Geological Survey of Canada, Ottawa) for critically reviewing this paper and for his constructive comments. The authors also thank Q. Bristow (Geological Survey of Canada, Ottawa) for his comments on this work and paper.

REFERENCES

API (American Petroleum Institute)
1960: Recommended practices for core-analysis procedure; API Recommended Practice 40 (RP 40) First Edition, American Petroleum Institute, Washington, D.C., p.55.

Hume, J.P. and Katsube, T.J.
1987: Pore structure characteristics; in Geotechnical Studies at East Bull Lake Research area, (ed.) A.G. Latham; Canada Centre for Mineral and Energy Technology, Report MRL 87-94, p. 39-66.

Katsube, T.J. and Hume, J.P.
1987: Pore structure characteristics of granitic rock samples from Whiteshell research area; in Geotechnical Studies at Whiteshell Research Area (RA-3), CANMET, Report MRL 87-52, p. 111-158.

Katsube, T.J. and Scromeda, N.
1991: Effective porosity measuring procedure for low porosity rocks; in Current Research, Part E; Geological Survey of Canada, Paper 91-E, p. 291-297.

Katsube, T.J., Best, M.E., and Mudford, B.S.
1991: Petrophysical characteristics of shales from the Scotian shelf; Geophysics, v. 56, no. 10.

Katsube, T.J., Scromeda, N., and Williamson, M.
1992: Effective porosity of tight shales from the Venture Gas Field, offshore Nova Scotia; in Current Research, Part D; Geological Survey of Canada, Paper 92-1D, p. 111-119.

Scromeda, N. and Katsube, T.J.
1993: Effect of vacuum-drying and temperature on effective porosity determination for tight rocks; in Current Research, Part E; Geological Survey of Canada, Paper 93-1E, p. 313-319.

Soeder, D.J.
1986: Laboratory drying procedures and the permeability of tight sandstone core; SPE Formation Evaluation, p. 16-22.

Geological Survey of Canada Project 870057

Application of temperature logging to mapping coal seams

C.J. Mwenifumbo
Mineral Resources Division

Mwenifumbo, C.J., 1994: Application of temperature logging to mapping coal seams; in Current Research 1994-E; Geological Survey of Canada, p. 291-298.

Abstract: High precision, high resolution continuous temperature measurements were recorded in shallow holes at the Highvale open pit coal mine, Alberta. The temperature data acquired shortly after drilling provided useful information on the location of permeable zones within sandstones and also detected the coal seams. Higher temperatures were observed within coal seams compared to sedimentary rock formations. Temperature logging done ten to fifteen days after drilling indicated that borehole fluid temperatures were close to equilibrium formation temperatures. Temperature gradient data derived from these quasi-equilibrium borehole temperature measurements accurately defined the depths and thicknesses of coal seams and were successfully used in hole-to-hole correlation of coal seams between several holes separated by up to 2.5 km.

Résumé : Des mesures continues haute précision et haute résolution de la température ont été enregistrées dans des trous peu profonds forés dans la mine de charbon à ciel ouvert Highvale en Alberta. Les données sur la température acquises peu de temps après le forage ont fourni des informations utiles sur l'emplacement des zones perméables au sein des grès et ont permis en outre de détecter les filons de charbon. Les températures étaient plus élevées dans les filons de charbon que dans les formations de roche sédimentaire. Les diagraphies de la température effectuées de dix à quinze jours après le forage ont indiqué que les températures des fluides dans les trous étaient proches des températures de formation d'équilibre. Les données sur les gradients de température établies à partir des mesures des températures des trous en situation de quasi-équilibre ont permis de définir avec exactitude les profondeurs et les épaisseurs des filons de charbon et de corréler avec succès les filons de charbon entre plusieurs trous séparés par une distance allant jusqu'à 2,5 km.

INTRODUCTION

In the oil industry, temperature logs are frequently used to determine the location of cement tops after a recent cementing operation, to delineate zones of lost circulation in a well while drilling is in progress, and to locate fluid entry and exit points in production and injection wells (Peacock, 1965; Bateman, 1985). Other uses of borehole temperature measurements include determining the equilibrium geothermal gradients in terrestrial heat flow studies or studying the transient temperature changes when heat is added to or extracted from the formation. However, temperature gradient logging has been shown to be a potentially useful method in lithostratigraphic correlation (Beck, 1976; Conaway and Beck, 1977; Blackwell and Steele, 1989) and in the identification and evaluation of coal seams (Beck, 1976; Kayal, 1981; Kayal and Christoffel, 1982). Temperature gradient logs were successfully used, in conjunction with electrical resistivity logs, to discriminate between coal seams with high electrical resistivity and high temperature gradients, and resistive sandstones having low temperature gradients. Although temperature gradient measurements reported by Beck (1976) and Kayal (1981) indicated the usefulness of the technique in coal seam mapping, the measurements lacked detail and could not be used to determine accurately the depth and thicknesses of coal seams. The logging was also conducted in fairly deep, cased holes. Deep holes ensure that surface temperature variation effects are minimal. Data obtained in uncased sections of the holes were previously found to be not accurately reproducible (Beck, 1982; Conaway and Beck, 1977).

This paper presents high precision, high resolution temperature measurements acquired at the Highvale open pit coal mine, Alberta. The boreholes were drilled with fresh water as the drilling fluid. These holes were 15 cm in diameter, uncased, and drilled to fairly shallow depths ranging from 60 to 80 m. At these depths, climatic changes can be a major cause of perturbation in the geothermal gradient, especially in high latitude areas. Beck (1982) observed that surface temperature variations may disturb the equilibrium temperatures in boreholes to depths of more than 100 m and it was feared that they would have adverse effects on the use of these measurements in mapping lithology and coal seams. The objective of the temperature logging was to assess the usefulness of these measurements in mapping coal seams.

LOGGING EQUIPMENT AND FIELD PROCEDURE

The temperature logging equipment developed at the Geological Survey of Canada (Bristow and Conaway, 1984) was used in the acquisition of the data. The temperature probe sensor consists of a 10-cm long tip of thermistor beads and has a thermal time constant of less than 2 seconds in stirred water. The thermistor signal is converted in the probe to a square wave, the frequency of which is a function of temperature. The square wave signal is transmitted uphole via a 1 km cable to a mini-computer-based data acquisition system in the logging truck where very accurate period measurements give temperatures with a resolution of better than 0.1 mK. Probe depths are measured with a resolution of 1 mm by an optical shaft encoder on a well head pulley assembly. Details of the logging system are given in Bristow and Conaway (1984).

All temperature data were acquired during a downhole run at a logging speed of 6 m/minute with data sampled every 200 milliseconds giving a measurement approximately every 2 cm. This high spatial resolution is necessary for the determination of accurate temperature gradients with the use of derivative operators (Conaway and Beck, 1977). The deconvolution technique developed by Costain (1970) and Conaway (1977) was used to process and remove the effects of the probe time constant from the temperature measurements. The Savitzky-Golay operator (Madden, 1978) was used to compute the gradients from the temperature data.

The electrical resistivity data presented in this paper were acquired with a 10-cm normal array at a logging speed of 3 m/minute with a sample depth interval of 5 cm. The total count natural gamma-ray log (energy window from 0.1 to 3 MeV) was acquired with a 3.2 cm by 12.7 cm sodium iodide detector. The logging speed for this data set was 3 m/minute with a one second sample time interval (equivalent to a sample depth interval of 5 cm).

GEOLOGY

The lithology above the coal seams consists largely of mudstones, siltstones, and sandstones (Fig. 1). A few of the sandstones are occasionally cemented by calcite. The layer just above the first coal seam is usually mudstone, 3 to 4 m thick with its base frequently consisting of bentonitic clays. The depth to the top of the first of six coal seams ranges from approximately 30 to 60 m. The first and second coal seams are approximately 3 m thick. The other four coal seams range in thickness from 15 cm to 2 m. The coals are sub-bituminous and are characterized by high electrical resistivity, low thermal conductivity, extremely low natural gamma radioactivity, and low density.

TRANSIENT TEMPERATURE LOGGING

Experiments were carried out to investigate the usefulness of transient temperature measurements recorded shortly after drilling in lithological mapping, and in the detection of porous and permeable zones, and also to address the question of how long a hole must be allowed to stand after drilling in order to carry out "quasi-equilibrium" temperature measurements for lithological and coal-seam mapping. Logging was carried out in 15-cm diameter holes which were diamond drilled with fresh water as the drilling fluid.

Short-period transient temperatures disturbances within a borehole may be caused by the addition or extraction of heat from the formation during the circulation of fluids as the borehole is being drilled (Hoang and Somerton, 1981). The process of drilling also causes a disturbance of formation temperatures by the frictional heat generated at the bit

(Lachenbruch and Brewer, 1959; Jaeger, 1961). The heat exchange between the fluid and the formation penetrated either warms or cools the formation depending on the relative temperatures of the drilling fluid and the formation.

Formation temperatures are changed by different amounts in rocks of differing thermal conductivities and permeabilities during the circulation of drilling fluids (Hoang and Somerton, 1981). It has been suggested that transient temperature logging can be used to map sedimentary rock formations such as sandstone, shale, and limestone (Dakhnov, 1959). The borehole fluid around the sandstone formation returns to equilibrium temperatures faster than the shales that have lower thermal conductivities. Within a formation with fairly uniform thermal conductivity but variable permeability, the more permeable zones will be most affected and are often the zones where transitory heat sources or sinks are observed (Drury and Jessop, 1982).

Lithology and coal seam mapping

Figure 1 shows gamma-ray and electrical resistivity logs for hole HV88-427 compared with the temperature log recorded one day after drilling. The coal seams exhibit characteristic high electrical resistivities and extremely low radioactivity. The overall temperatures within the low thermal conductivity coal seams are high compared to the rest of the formations. The individual coal seams are poorly resolved but can be detected from these temperature data. There is a positive correlation between temperature and electrical resistivity data. The inseam mudstone and shale layers exhibit lower temperatures, low electrical resistivities, and high radioactivity. In the upper section of the hole above the coal seams between 25 and 35 m, there is a positive correlation between natural gamma radioactivity and temperature. The sandstone layers with high thermal conductivity are characterized by low gamma radioactivity and low temperatures whereas the bentonitic silty mudstones with lower thermal conductivities exhibit high gamma radioactivity and high temperatures. The electrical resistivity is, however, negatively correlated with both temperature and natural gamma radioactivity. The negative correlation of transient temperature and electrical resistivity within the sandstone layers is a useful characteristic that may aid in distinguishing resistive coal seams from resistive sandstone layers.

Detection of porous and permeable zones

Figure 2 shows the electrical resistivity, self potential, and transient temperature logs acquired in borehole HV88-422. The resistivity log indicates a more resistive zone between 29 and 36 m. Variations in resistivity within this sandstone unit may reflect changes in porosity, higher porosity suggesting

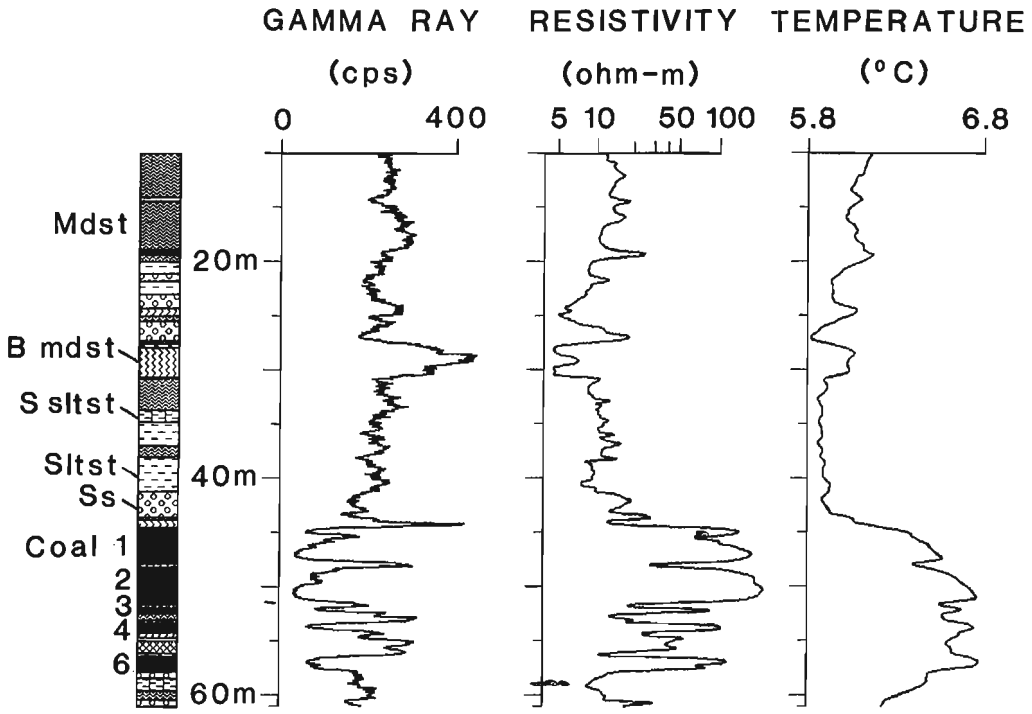

Figure 1. Temperature logs recorded in hole HV88-427 one day after drilling compared with gamma-ray and electrical resistivity logs. The coal seams exhibit characteristic high electrical resistivities and extremely low radioactivity. Temperature and electrical resistivity logs are positively correlated in the coal seams. In the upper section of the hole above the coal seams (between 20 and 35 m), electrical resistivity is negatively correlated with temperature. B mdst - bentonitic mudstone, Mdst - mudstone, S sltst - sandy siltstone, Sltst - siltstone, Ss - sandstone.

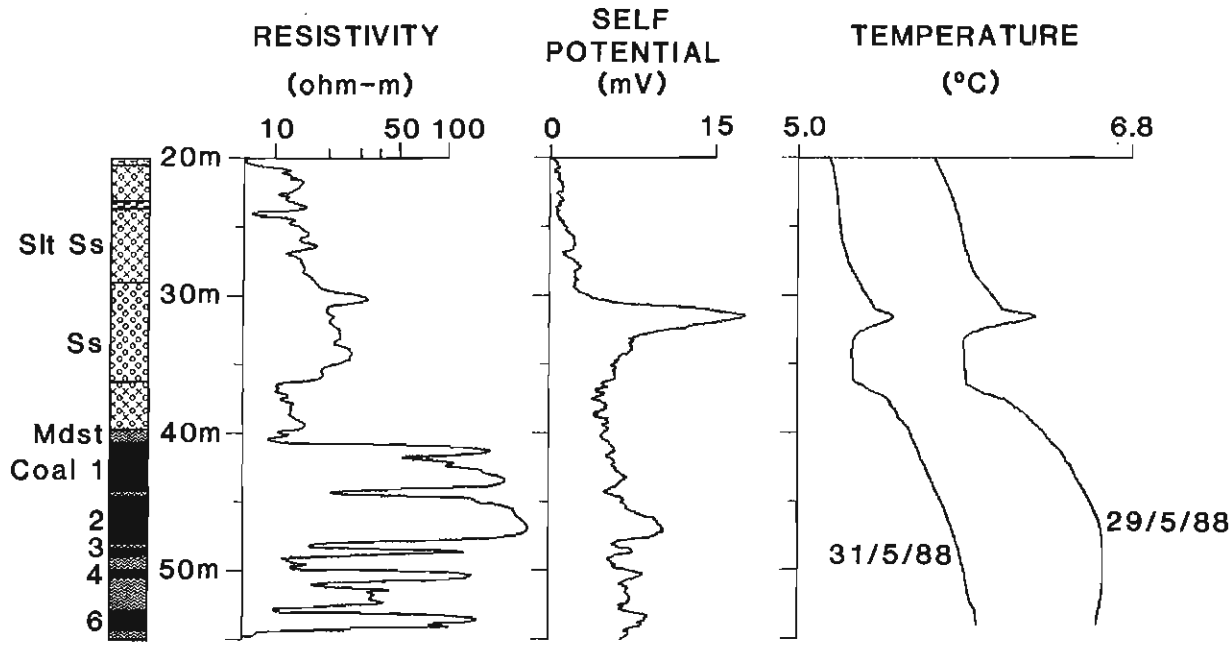

Figure 2. Electrical resistivity, self potential, and transient temperature logs acquired in borehole HV88-422. The prominent peak on the temperature profiles indicates a permeable zone within the sandstone, which is confirmed by a corresponding high SP anomaly and lower resistivity. Temperature measurements were recorded one and three days after drilling. Mdst - mudstone, Slt Ss - silty sandstone, Ss - sandstone.

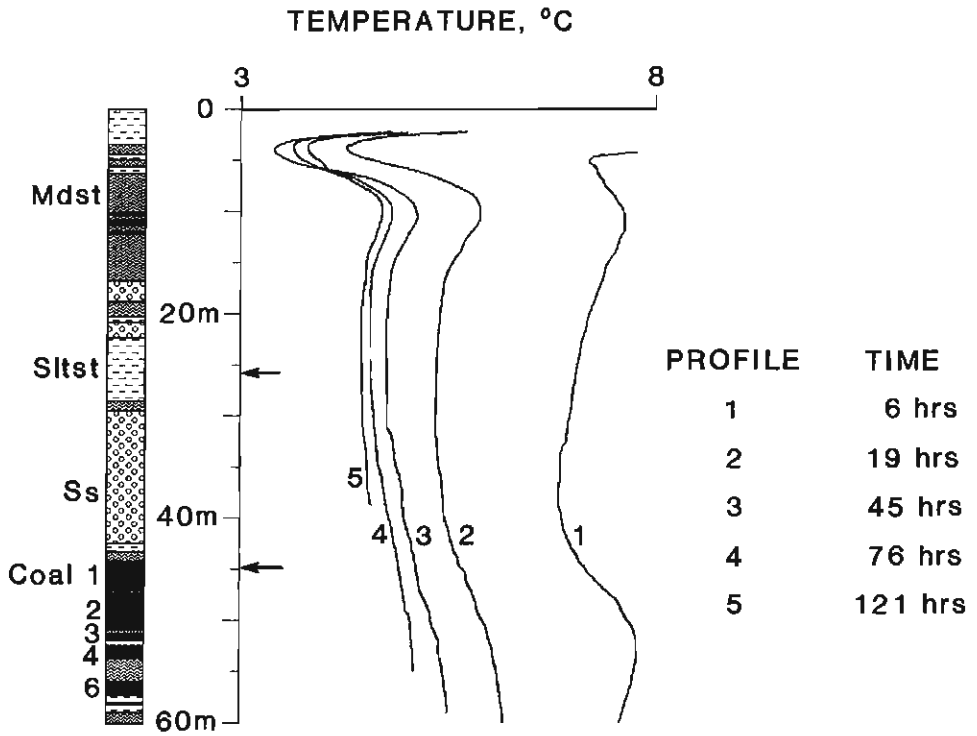

Figure 3. Five temperature logs recorded in hole HV88-424 at approximately the following times after drilling had stopped: 6, 19, 45.5, 76.5, and 121.5 hours. The influence of the drilling fluid, which was warmer than the ambient formation temperatures, is fairly obvious. Mdst - mudstone, Sltst - siltstone, Ss - sandstone.

less cementation. Calcareous cementation is prevalent in a number of sections within the sandstone units in this region. A transient high temperature anomaly is observed around 31.5 m. This anomaly correlates with a self potential anomaly and coincides with a slightly lower resistivity zone within the sandstone. It is interpreted as resulting from the warmer drilling fluids infiltrating a more permeable zone within this sandstone unit creating a transient heat source that decays with time. This may explain the self potential anomaly, which is probably due to filtration of water from the pores into the borehole. SP data have at times been used in detecting porous and permeable zones of the formation surrounding the borehole (Dakhnov, 1959). These measurements indicate that temperature logging shortly after drilling can be used to delineate coal seams, distinguish between mudstone and sandstone, and possibly detect high porosity and high permeability zones.

Return to equilibrium temperatures after drilling

The time required for a borehole to return to equilibrium formation temperatures after drilling will vary depending on the temperature difference between the drilling fluid and formation temperatures, the thermal conductivity of the formation, and the fluid circulation time. Kayal and Christoffel (1982) recorded their temperature measurements three days after drilling and considered this time adequate for equilibrium temperature gradient measurements. The negative gradients observed in their data, however, suggest that the borehole fluid temperatures may not have reached equilibrium with the formation temperatures.

Figure 3 shows five temperature logs carried out in hole HV88-424 to determine the time required after drilling for the borehole to attain quasi-equilibrium temperatures. These logs were recorded at approximately 6, 19, 45.5, 76.5, and 121.5 hours after drilling stopped. The hole collapsed approximately 39 m during the fifth run and measurements were discontinued. The influence of the drilling fluid on the temperature-depth profile is fairly obvious. Unfortunately, the temperature of the drilling fluid was not measured and no detailed evaluation of the data was carried out. The temperatures were raised by more than 4°C from the ambient temperatures. The first log shows increased temperatures between 45 and 60 m due to the low thermal conductivity of the coal seams. Figure 4 shows the approach of the borehole fluid temperatures to equilibrium with time after the circulation of drilling fluid had ceased in borehole HV88-424. The temperatures are plotted for two different locations in the borehole: one within the coal seam at 50 m and the other within the siltstone at approximately 25 m (indicated by arrows in Figure 3). The approach to equilibrium temperatures is roughly exponential. If we assume that the dominant heat transfer process is conduction, then the formation with the highest thermal conductivity will dissipate heat away from the borehole faster than the lower thermal conductivity formations. The rate of return of the borehole fluid temperatures to equilibrium is faster within the mudstone with higher thermal conductivities. After five days the borehole fluid temperatures appear to be approaching equilibrium formation temperatures. Temperature logging in most of holes was done ten to fifteen days after drilling. After this period, reproducible temperature gradients were obtained and no negative gradients were observed.

EQUILIBRIUM TEMPERATURE LOGGING: FIELD RESULTS

In environments where there are no heat sources or sinks, the highest geothermal gradients will be observed in rocks with the lowest thermal conductivity and vice versa. Figure 5 shows the natural gamma-ray and electrical resistivity logs compared with the equilibrium temperature logs for borehole HV88-414. The temperature log was recorded fifteen days after drilling. The water table in this hole was at approximately 6 m and the zero gradient zone or temperature inversion point was fairly shallow, approximately 13 m. Above this point large temperature gradient anomalies exist that are due to surface temperature variations. Below this point, the temperatures are mainly affected by variations in the thermal conductivity of the formation, assuming little or no heat transport by groundwater flow. Temperatures range from 4.5 to 5.5°C. Gross correlations of the temperature log and lithology are apparent. The temperature increases slowly with depth within the siltstone/sandstone/mudstone section from 10 to 35 m. There is an abrupt temperature change at 35 m, and the temperature increases rapidly up to 48 m and flattens thereafter. The region between 35 and 48 m consists of coal seams. The subtle changes in temperature within this section indicate the location of individual coals seams.

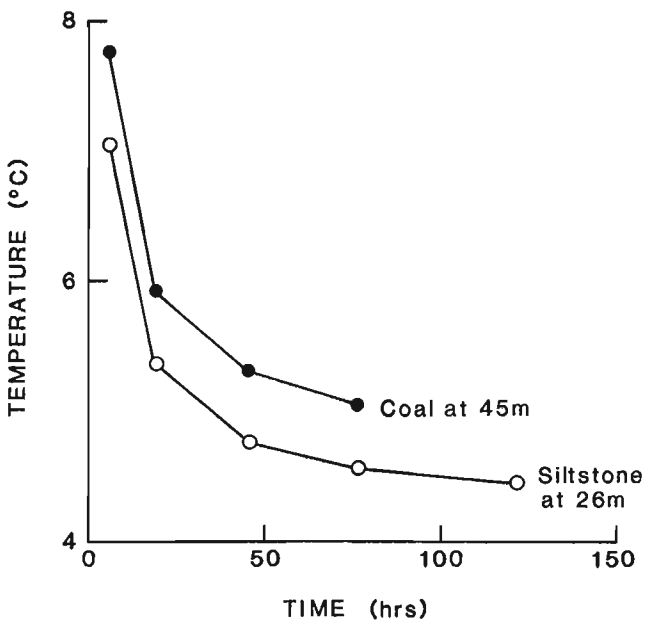

Figure 4. *Temperature-time curves showing the approach of borehole fluid temperatures to equilibrium after circulation of fluid had ceased. The two curves are obtained within siltstone at approximately 25 m and within coal seam no. 1 at 50 m in borehole HV88-424.*

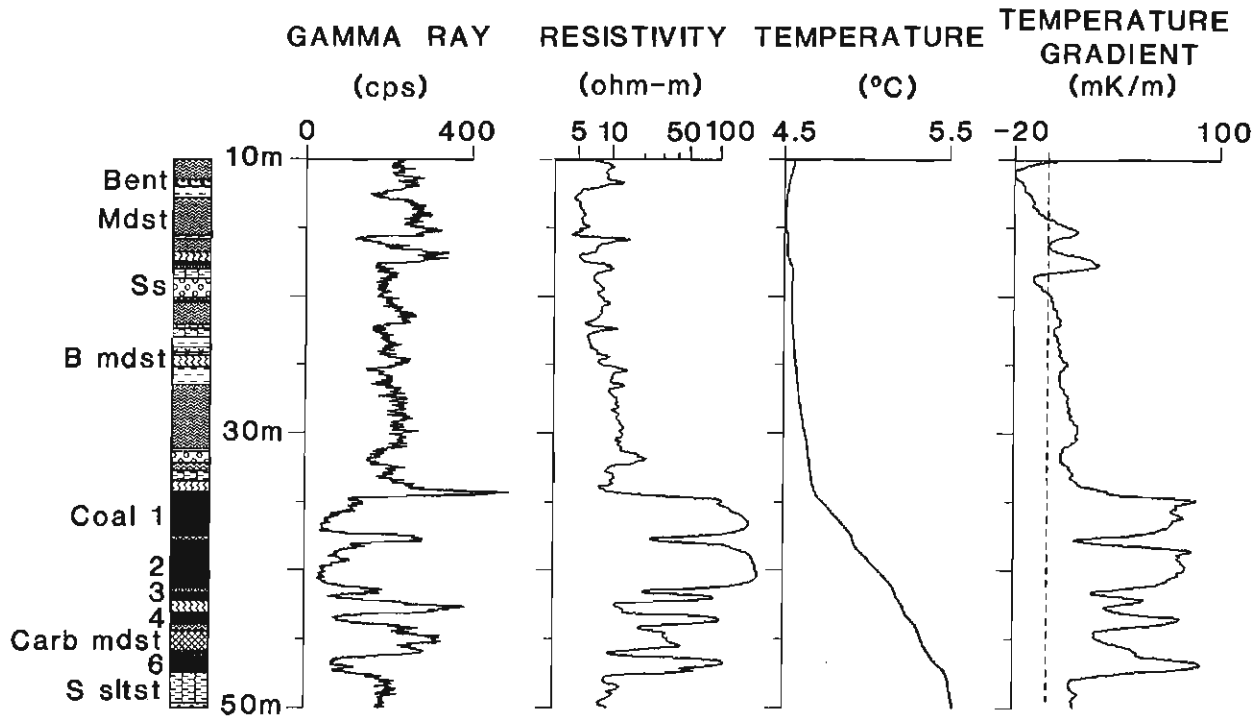

Figure 5. Gamma-ray and electrical resistivity logs compared with equilibrium temperature logs recorded 15 days after drilling in borehole HV88-414. The subtle variations in the smooth temperature profile are transformed into peaks in the temperature gradient profile that correlate well with the location of the coal seams. Bent - bentonite, B mdst - bentonitic mudstone, Mdst - mudstone, Carb mdst - carbonaceous mudstone, S sltst - sandy siltstone, Ss - sandstone.

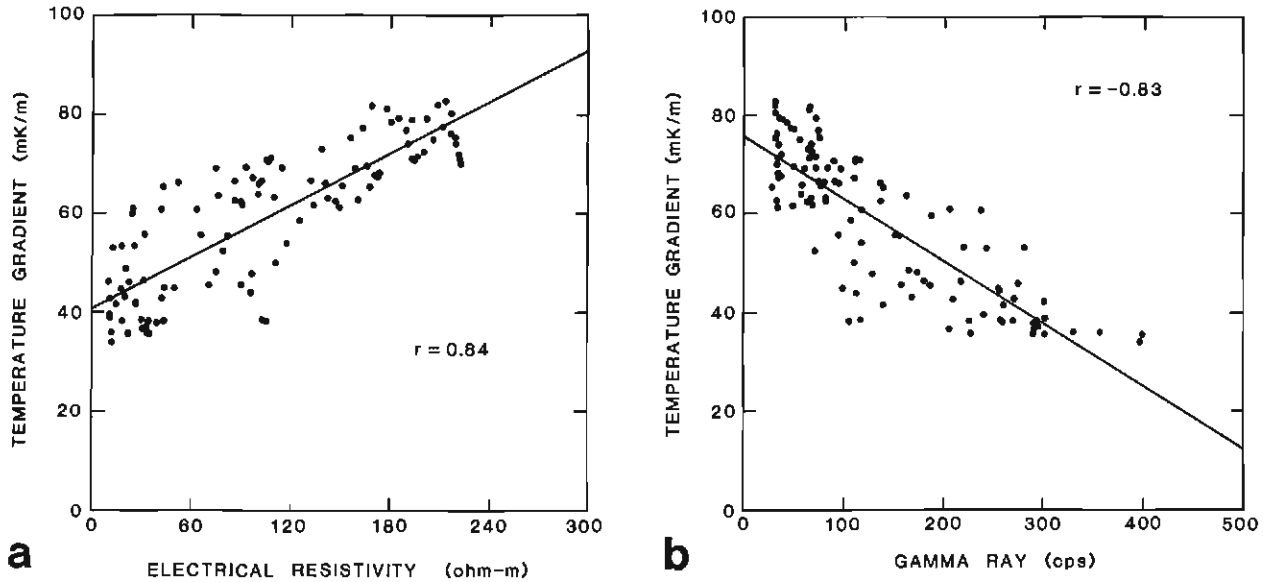

***Figure 6.** Crossplots of electrical resistivity versus temperature gradient, (**a**), and gamma-ray versus temperature gradient, (**b**), for hole HV88-412 within coal seams between 36 and 47 m.*

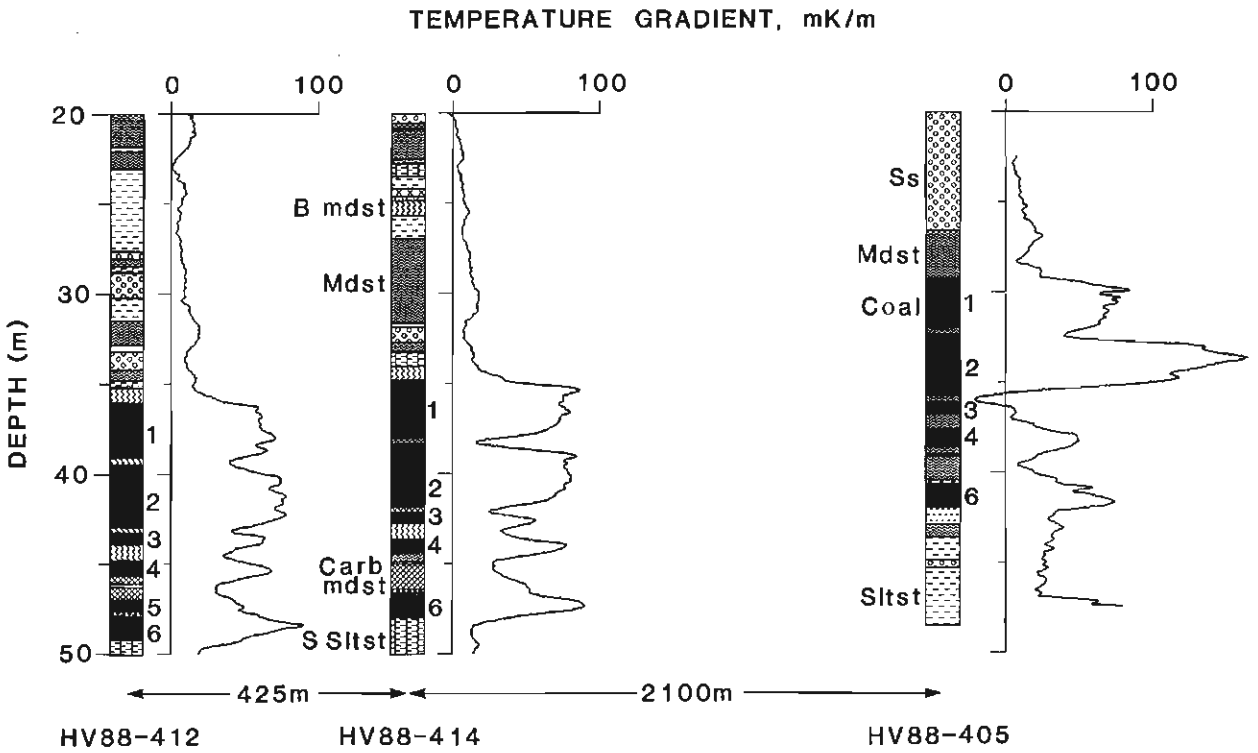

***Figure** 7. Temperature gradient logs in hole-to-hole correlation of coal seams. Hole HV88-405 is more than 2 km from the other two holes and exhibits similar correlation between coal seams and temperature gradient. This makes temperature gradient logging an effective tool for mapping the extent of coal seams. B mdst - bentonitic mudstone, Carb mdst - carbonaceous mudstone, Mdst - mudstone, S Sltst - sandy siltstone, Sltst - siltstone, Ss - sandstone.*

The temperature gradient log shows good correlation with the electrical resistivity log, the gamma-ray log, and the coal seams. All the coal seams are clearly delineated on the temperature gradient log except for coal seam number 5, which is very thin and also poorly defined on the resistivity and gamma-ray logs. The inseam layers of mudstone, siltstone, and carbonaceous shales are clearly identified as high radioactivity, low resistivity, and low temperature gradient zones. Coal seam temperature gradients are approximately 80 mK/m and mudstone gradients are less than 25 mK/m. Variations in the resistivity and natural gamma radioactivity within the coal probably reflect changes in the ash content. Coal seams number 1 and 2 show relatively higher radioactivity and lower resistivities at the top of the seams suggesting an increase in clay content. Therefore, better quality coal is inferred at the bottom of the coal seams (higher resistivities and extremely low radioactivity).

Figures 6a and 6b are crossplots of the electrical resistivity versus temperature gradient and gamma-ray versus temperature gradient for hole HV88-412 within the coal seams. The correlation between these parameters is excellent ($r>0.8$). The temperature gradients decrease with increasing radioactivity.

Figure 7 illustrates the application of temperature gradient logs in hole-to-hole correlation of coal seams. Hole HV88-414 is 425 m from HV88-412 and hole HV88-405 is 2.1 km from HV88-412. Holes HV88-412 and HV88-414 are at approximately the same elevation, and the collar of hole HV88-405 is approximately 12 m higher than the other two. An adjustment has been made to the depths of logs from HV88-405 to reflect this elevation difference. It is clear that temperature gradient logs are an excellent tool for hole-to-hole correlation of coal seams over fairly large distances.

CONCLUSION

It has been shown that both temperature and temperature gradient logs can be successfully used in coal seam and lithological mapping. Coal seams are clearly delineated on the temperature gradient logs and exhibit high gradients, high electrical resistivities, and extremely low natural gamma radioactivity. Accurate depths and thicknesses of the coal seams can be determined from these high spatial resolution temperature data and compare remarkably well with the resistivity logs. There is a negative correlation between temperature gradient and electrical resistivity in sandstone and mudstone. High-resolution temperature measurements in conjunction with electrical resistivity and gamma-ray logs can distinguish between mudstone and sandstone. Temperature logs acquired immediately after drilling may be used to locate more permeable zones within sandstone layers. Since most of the holes drilled in coal environments are not stable,

they often collapse a few days after drilling due to the nature of incompetent rock. Casing the holes would be the most logical way of ensuring that they remain open if logging is contemplated at a later date. Galvanic electrical logs cannot be run in either steel- or plastic-cased holes. Temperature gradient logs in a cased hole offer an alternative parameter to electrical logs as well as providing their own unique response characteristics. The environment at the Highvale coal mine indicates that for fine scale lithological correlation, equilibrium temperature logs should not be recorded until at least ten days after drilling fluid circulation has ceased.

ACKNOWLEDGMENTS

I am indebted to TransAlta Utilities Corporation for permission to carry out these logging measurements in their holes at the Highvale coal mine, Alberta. I am also grateful to Professor A.E. Beck and Dr. J.G. Conaway for reading the manuscript and offering many valuable suggestions. Thanks are due to P.G. Killeen and Q. Bristow for their valuable discussions, to Bill Hyatt and Steven Birk for help in data acquisition, and to Barbara Elliott for help rendered in data processing.

REFERENCES

Bateman, R.M.
1985: Cased-hole log analysis and reservoir performance monitoring; International Human Resources Development Corporation.
1976: The use of thermal resistivity logs in stratigraphic correlation; Geophysics, v. 41, p. 300-309.

Beck, A.E.
1982: Precision logging of temperature gradients and the extraction of past climate; Tectonophysics, v. 83, p. 1-11.

Blackwell, D.D. and Steele, J.
1989: Thermal conductivity of sedimentary rocks: measurement and significance; in Thermal History of Sedimentary Basins: methods and case histories, (ed.) Nancy D. Naeser and Thane H. McCulloh; Springer-Verlag.

Bristow, Q. and Conaway, J.G.
1984: Temperature gradient measurements in boreholes using low noise high resolution digital techniques; in Current Research, Part B; Geological Survey of Canada, Paper 84-1B, p. 101-108.

Conaway, J.G.
1977: Deconvolution of temperature gradient logs; Geophysics, v. 42, p. 823-837.

Conaway, J.G. and Beck, A.E.
1977: Fine-scale correlation between temperature gradient logs and lithology; Geophysics, v. 42, p. 1401-1410.

Costain, J.K.
1970: Probe response and continuous temperature measurements; Journal of Geophysical Research, v. 75, p. 3968-3975.

Dakhnov, V.N.
1959: Geophysical well logging; Quarterly of the Colorado School of Mines, v. 57, no. 2, 1962; translated by G.V. Keller.

Drury, M.J. and Jessop, A.M.
1982: The effect of a fluid-filled fracture on the temperature profile in a borehole; Geothermic, v. 11, p.145-152.

Hoang, V.T. and Somerton, W.H.
1981: Effect of variable thermal conductivity of the formations on the fluid temperature distribution in the wellbore; Transactions, Twenty-Second Annual Logging Symposium, Society of Professional Well Log Analysts, p. L1-L24.

Jaeger, J.C.
1961: The effect of the drilling fluid on temperatures measured in bore holes; Journal of Geophysical Research, v. 66, p. 563-569.

Kayal, J.R.
1981: Correlation of T-log with E-log in coal-bearing formations; Pure and Applied Geophysics, v. 119, p. 349-355.

Kayal, J.R. and Christoffel, D.A.
1982: Relationship between electrical and thermal resistivities for differing grades of coal; Geophysics, v. 47, p. 127-129.

Lachenbruch, A.H. and Brewer, M.C.
1959: Dissipation of the temperature effect of drilling a well in Arctic Alaska; U.S Geological Survey Bulletin 1083-C, p. 73-109.

Madden, H.H.
1978: Comments on the Savitzky-Golay convolution method for least-squares fit smoothing and differentiation of digital data; Analytical Chemistry, v. 50, p. 1383-1386.

Peacock, D.R.
1965: Temperature logging; Transactions, Sixth Annual Logging Symposium, Society of Professional Well Log Analysts, p. F1-F18.

Geological Survey of Canada Project 880030

AUTHOR INDEX

NOTE TO CONTRIBUTORS

Submissions to the Discussion section of Current Research are welcome from both the staff of the Geological Survey of Canada and from the public. Discussions are limited to 6 double-spaced typewritten pages (about 1500 words) and are subject to review by the Chief Scientific Editor. Discussions are restricted to the scientific content of Geological Survey reports. General discussions concerning sector or government policy will not be accepted. All manuscripts must be computer word-processed on an IBM compatible system and must be submitted with a diskette using WordPerfect 5.0 or 5.1. Illustrations will be accepted only if, in the opinion of the editor, they are considered essential. In any case no redrafting will be undertaken and reproducible copy must accompany the original submissions. Discussion is limited to recent reports (not more than 2 years old) and may be in either English or French. Every effort is made to include both Discussion and Reply in the same issue. Current Research is published in January and July. Submissions should be sent to the Chief Scientific Editor, Geological Survey of Canada, 601 Booth Street, Ottawa, Canada, K1A 0E8.

AVIS AUX AUTEURS D'ARTICLES

Nous encourageons tant le personnel de la Commission géologique que le grand public à nous faire parvenir des articles destinés à la section discussion de la publication Recherches en cours. Le texte doit comprendre au plus six pages dactylographiées à double interligne (environ 1500 mots), texte qui peut faire l'objet d'un réexamen par le rédacteur scientifique en chef. Les discussions doivent se limiter au contenu scientifique des rapports de la Commission géologique. Les discussions générales sur le Secteur ou les politiques gouvernementales ne seront pas acceptées. Le texte doit être soumis à un traitement de texte informatisé par un système IBM compatible et enregistré sur disquette WordPerfect 5.0 ou 5.1. Les illustrations ne seront acceptées que dans la mesure où, selon l'opinion du rédacteur, elles seront considérées comme essentielles. Aucune retouche ne sera faite au texte et dans tous les cas, une copie qui puisse être reproduite doit accompagner le texte original. Les discussions en français ou en anglais doivent se limiter aux rapports récents (au plus de 2 ans). On s'efforcera de faire coïncider les articles destinés aux rubriques discussions et réponses dans le même numéro. La publication Recherches en cours paraît en janvier et en juillet. Les articles doivent être envoyés au rédacteur en chef scientifique, Commission géologique du Canada, 601, rue Booth, Ottawa, Canada, K1A 0E8.

The Geological Survey of Canada publishes reports on current field work and laboratory studies twice a year in January and July. The four volumes published in January 1994 (Current Research 1994-A to D) are listed below and can be purchased separately. This volume. Current Research 1994-E, was released in July 1994.

La Commission géologique du Canada publie les résultats de travaux en cours sur le terrain et en laboratoire deux fois par année, soit en janvier et en juillet. Les quatre volumes publiés en janvier 1994 (Recherches en cours 1994-A à D), énumérés ci-dessous, sont vendus séparément. Le présent volume, Recherches en cours 1994-E, a été diffusé en juillet 1994.

1994-A
Cordillera and Pacific Margin
Cordillère et marge du Pacifique

1994-B
Interior Plains and Arctic Canada
Plaines intérieures et région arctique du Canada

1994-C
Canadian Shield
Bouclier canadien

1994-D
Eastern Canada and National and General Programs
Est du Canada et programmes nationaux et généraux

1994-E
(this volume)
(ce volume)